AFCRL-63-457

CONTRACT AF61 -052- 586

PHYSICS OF PLANETS

PROCEEDINGS OF THE
ELEVENTH INTERNATIONAL ASTROPHYSICAL
SYMPOSIUM
LIÈGE, JULY 9-12, 1962

MÉMOIRES
DE LA SOCIÉTÉ ROYALE DES SCIENCES DE LIÈGE
CINQUIÈME SÉRIE
(TOME VII, 1963)

LA PHYSIQUE DES PLANÈTES

COMMUNICATIONS
PRÉSENTÉES AU ONZIÈME
COLLOQUE INTERNATIONAL D'ASTROPHYSIQUE
TENU A LIÈGE
LES 9, 10 ET 11 JUILLET 1962

EXTRAIT DES MÉMOIRES
IN-8° DE LA SOCIÉTÉ ROYALE DES SCIENCES DE LIÈGE
CINQUIÈME SÉRIE
TOME VII
FASCICULE UNIQUE

1963
INSTITUT D'ASTROPHYSIQUE
COINTE-SCLESSIN
BELGIQUE

TABLE DES MATIÈRES

INTRODUCTION

P. SWINGS
Institut d'Astrophysique de Liège

Au cours des vingt ou trente dernières années, l'étude des astres du système solaire a été fort négligée. Bien sûr, elle ne revêtait pas le prestige de certains autres chapitres de l'Astronomie, comme l'étude des nébuleuses extragalactiques, de la structure des atmosphères et intérieurs d'étoiles, de la cosmogonie, de la radio-astronomie ou des sources d'énergie stellaire.

La situation est en train de se modifier. Grâce aux véhicules spatiaux, nous sommes à la veille de découvertes importantes au sujet de la lune, des planètes et de leurs satellites naturels, du milieu interplanétaire et des comètes. Il est indispensable que ces expériences spatiales soient préparées avec le maximum d'efficacité, afin que nous puissions en tirer le plus grand profit scientifique.

Il nous a donc paru utile de consacrer notre onzième colloque à la physique des planètes, afin que nous puissions arriver à une mise au point satisfaisante du problème. Ce projet fut discuté à Berkeley à l'occasion de l'Assemblée Générale de l'U. A. I., lors d'une réunion à laquelle avaient bien voulu assister quelques collègues spécialisés. Il y fut décidé de préciser le sujet et d'éliminer les satellites (y compris la lune), les astéroïdes, les comètes, l'espace interplanétaire, la cosmogonie, les problèmes biologiques, les questions d'orbites. Seuls, les problèmes physiques relatifs aux planètes devaient être envisagés.

Le Professeur M. G. J. Minnaert, Directeur de l'Observatoire de l'Université d'Utrecht, a bien voulu accepter la présidence de

notre 11e Colloque. Pendant toute la préparation, il nous a fait profiter de ses conseils et avis compétents. C'est, pour une large part, à lui qu'est due la réussite du Colloque. Pendant le Congrès lui-même, le Président Minnaert s'est dépensé sans compter. Il termina, d'ailleurs, en beauté en nous résumant, de façon remarquable, les contributions essentielles de la réunion. Qu'il trouve ici l'expression de notre vive gratitude.

Nous remercions aussi cordialement, les auteurs des excellents rapports introductifs, MM. R. Wildt, A. Dollfus, C. H. Mayer, H. C. van de Hulst et W. Irvine. L'auditoire comprenait les personnalités suivantes :

d'Allemagne : W. Lohmann, H. K. Paetzold ;
du Brésil : R. R. de Freitas Mourao ;
du Canada : G. Herzberg ;
du Congo : L. Haser ;
de France : H. Camichel, A. Dollfus, P. Guérin, M. Marin, J. C. Pecker, J. Rösch, G. Wlérick ;
des États-Unis : A. Arking, A. H. Barrett, C. H. Barrow, R. A. Becker, J. C. Brandt, J. W. Chamberlain, R. E. Danielson, W. C. De Marcus, J. B. Douglas, G. de Vaucouleurs, L. Dunkelman, R. Gallet, O. K. Garriott, T. Gehrels, J. S. Goldstein, R. Hide, P. Hodge, G. R. Huguenin, H. C. Ingrao, M. W. Irvine, J. B. Irwin, G. P. Kuiper, B. Leason, E. Levinthal, R. J. Levy, A. J. Masley, C. H. Mayer, D. H. Menzel, Miss B. Middlehurst, R. F. Mlodnosky, D. Morris, G. W. F. Mulders, R. B. Norton, G. Ohring, J. M. Pasachoff, S. I. Rasool, M. S. Roberts, C. Sagan, G. F. Schilling, W. M. Sinton, A. G. Smith, H. J. Smith, H. Spinrad, H. E. Suess, J. Swensson, L. Wallace, J. W. Warwick, R. Wildt, D. Williams, A. T. Young, R. L. Younkin ;
de Grande Bretagne et d'Irlande : R. Beer, E. H. Collinson, G. Fielder, H. A. Gebbie, J. F. Grainger, J. V. Jelley, W. H. McCrea, E. Öpik, B. M. Peek, D. W. N. Stibbs.
de Grèce : J. H. Focas ;

de Hollande : M. G. J. Minnaert, C. J. Schuurmans, H. C. van de Hulst ;

d'Italie : F. Bertola, G. Demottoni, G. Righini ;

du Japon : M. Shimizu ;

de Suisse : E. Miescher ;

de Tchécoslovaquie : F. Link ;

d'U. R. S. S. : M. S. Bobrov, A. D. Kuzmin, D. Y. Martynov, V. V. Sharonov.

de Belgique : S. Arend, Mme D. Bosman-Crespin, A. Boury, R. P. Courtoy, R. Coutrez, F. Dacos, L. Delbouille, A. Delsemme, Mme D. Delsemme-Jehoulet, J. Depireux, J. Dommanget, F. Dossin, R. Duysinx, Mlle L. Gausset, O. Godart, N. Grevesse, Mlle C. Guillaume, L. Houziaux, J. Humblet, A. Koekelenbergh, P. Ledoux, D. Malaise, M. Migeotte, A. Monfils, M. Nicolet, F. Remy, Mme L. Remy-Battiau, H. Robe, Mlle G. Roland, P. Rosen, M. Ruelle, A. Sauval, Mlle M.-J. Sequaris, P. Swings, R. Zander.

Les discussions entre les théoriciens, les expérimentateurs et les observateurs utilisant des méthodes très diverses ont été très fructueuses. Nous les avons résumées comme dans les volumes des colloques antérieurs.

C'est à nouveau Madame D. Bosman-Crespin qui, après avoir été la cheville ouvrière de l'organisation du Colloque, s'est chargée du travail d'édition du présent volume. C'est le neuvième volume publié par ses soins. Nous lui exprimons notre vive reconnaissance.

The 11th International Astrophysical Symposium was sponsored by the University of Liège and by the Cambridge Research Laboratories of the Office of Aerospace Research, United States Air Force, through its European Office. We wish to express to them our most sincere gratitude.

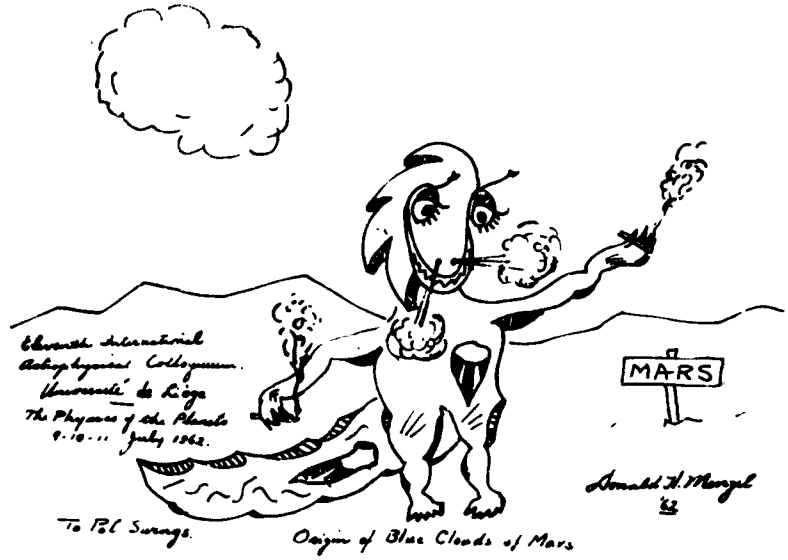
Eleventh International
Astrophysics Colloquium
Université de Liège
The Physics of the Planets
9-10-11 July 1962.
MARS
Arnold H. Mongel
'62
To P.L. Savage.
Origin of Blue Clouds of Mars

SECTION I

THE INTERNAL CONSTITUTION OF THE PLANETS

1. — PLANETARY INTERIORS ; INTRODUCTORY REPORT

RUPERT WILDT
Yale University, U. S. A.

It seems fair to say that astrophysicists, since relegating to the classical astronomer the gravitational aspects of planetary astronomy, have been rather indifferent about the Earth as a planet and its kin, at any rate in so far their internal constitution is concerned. Indeed, what we know of the chemical, thermal, and magnetic state of the Earth's interior we owe to the geodesists, seismologists, and geophysicists, whose strategy has set an example how to attack analogous problems in studying other planets. Nevertheless, among astrophysicists — met for the first time, if I am not mistaken, to consider the physics of the planets — it is fitting to introduce the discussion of planetary interiors by glancing at what the theories of planetary and stellar constitution have in common, and what sets them apart. The common traits are rooted, of course, in the identity of the primary laws of physics ruling the mechanical and thermal equilibrium of masses both of stellar and planetary order of magnitude. Marked differences of secondary nature are due to the less tractable behavior of matter in the solid and liquid state, which we presume to be realized throughout the bulk of planetary matter. Little is known about the properties of wholly gaseous bodies of planetary size, now under investigation by Prof. Öpik, from whom we shall hear later on. Irrespective of their relevance to particular planets, such models and more massive ones, bridging the gap between planets and dark stellar companions, command interest because they would populate a void in the otherwise well-charted domain of stellar configurations.

In order to do justice to the precision attained in measuring the figure and the gravitational potential of some planets, the theory of rotating bodies had to be carried far beyond what as yet is required for application to stars. No loss is incurred by here ignoring these refinements and focusing attention upon the steady-state

characteristics of a slowly rotating planet without internal convection, since the latter will be discussed by Prof. Kopal. A flow diagram descending from the expressions for the pressure and temperature gradient, in the notation familiar from the theory of stellar interiors, affords a condensed representation of the theoretical concepts and empirical data singled out for consideration. Such a graph (Fig. 1) exhibits more clearly than lengthy discourse

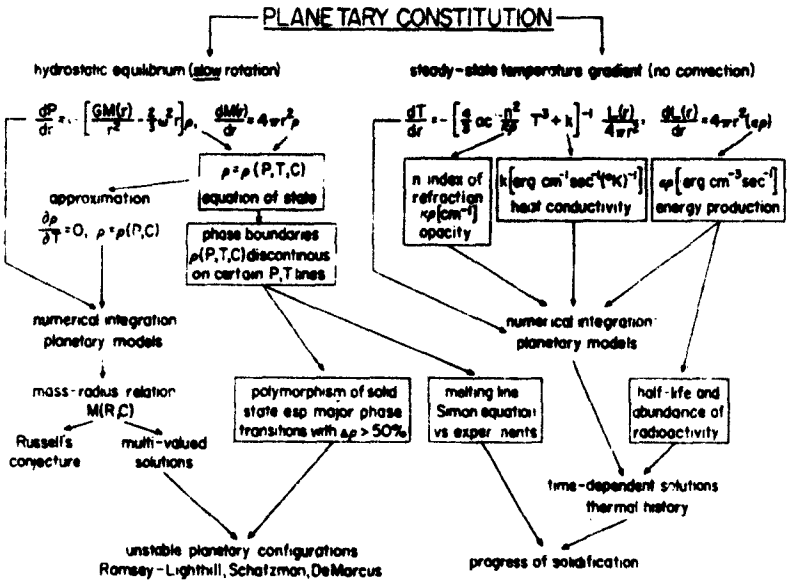

Fig. 1

many ramifications, the diverging lines of argument, and their confluence. The following remarks will supplement my earlier review* by pointing to recent advances. The principal ones are the impressive pertection of the art of experimentation with pressures matching those encountered deep below the surface of the planets, and the recognition of radiative transfer as a possibly

(*) « Planetary Interiors », pp. 159-212, Vol. III of The Solar System, G. P. Kuiper, Editor, University of Chicago Press, 1961. No references listed in the bibliography attached to that chapter will be repeated at the end of this paper.

critical mechanism lowering the internal temperature gradients. I shall conclude with a simple argument, of the type often called dimensional analysis, which bears upon the shape of the asteroids.

Mass-Radius Relation of Planets

If the dependence on temperature of the equation of state is so weak that, in zero-order approximation, it may be neglected, the equations of hydrostatic and thermal equilibrium become

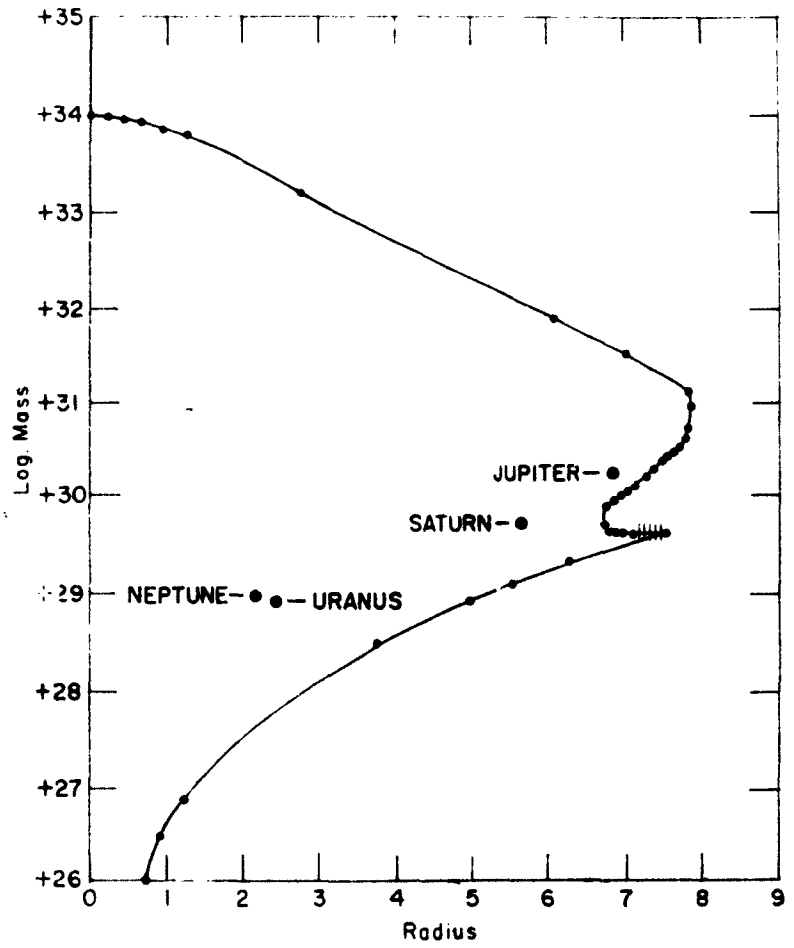

Fig. 2

uncoupled. For any given pressure-density relation $\rho = \rho$ (P, C), where C is a shorthand for the chemical parameters, the equation of hydrostatic equilibrium can then be integrated numerically. The resulting mass-radius relation for spherical configurations of solid pure hydrogen (DeMarcus) is shown in Fig. 2 (scale unit of radii 10^9 cm), which illustrates the existence of a maximum radius for a cold body, often referred to as Russell's conjecture ; the terminal

INSTABILITY OF SMALL CORES OF ROTATING PLANETS

Lighthill(1950) — DeMarcus (1954)

pressure-density relation with single phase transition

$$\rho(P) = \begin{cases} \rho_1(P), & P \le P_c \\ \rho_2(P), & P \ge P_c \end{cases} \qquad \rho_2(P_c) = \lambda \rho_1(P_c)$$

instability criterion

$$\lambda > \tfrac{3}{2} - \frac{\omega^2}{4\pi G \rho_1(P_c)}$$

radius-mass relation triple-valued over a finite mass range

mass $M(R_1) = M(R_2) = M(R_3)$

radius $R_1 < R_2 < R_3$

total energy $E(R_1) < E(R_2) > E(R_3)$

configuration R_1 has core of high pressure phase, R_3 has no core

Fig. 3

point at the upper left side of this graph is the Chandrasekhar limit. In the hatched area of Fig. 2 the course of the mass-radius graph cannot be clearly shown to this scale. In that mass range the hydrostatic equilibrium has triple-valued solutions. This indeterminacy (cf. Fig. 3) is caused by a discontinuity (phase transition) in the adopted pressure-density relation for solid hydrogen. The resulting instability of small planetary cores (Ramsey) has been fully discussed in my earlier review. We shall have a report by

Prof. DeMarcus on the mass-radius relations for configurations of pure helium and for a mixture of heavier elements, called « Mud », which shed some light on the constitution of Uranus and Neptune. Since the mass-radius graph of helium runs far to the left of that of hydrogen, on Fig. 2, the location of the image points of Jupiter and Saturn indicates that these bodies are predominantly composed of hydrogen.

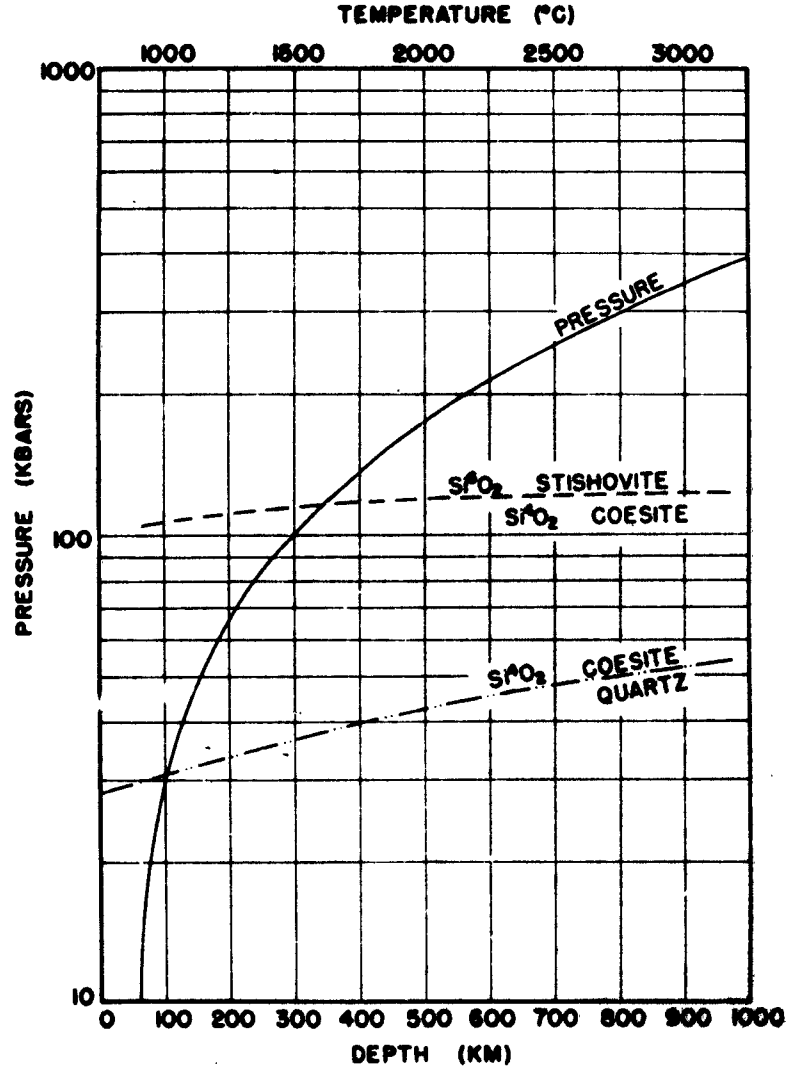

Fig. 4

Polymorphism of Solids

The equation of state of almost any chemically homogeneous solid differs strikingly from that of its gaseous form : the density, as function of pressure and temperature, changes discontinuously across certain P, T-lines that demarcate the fields of thermodynamic stability of what are called the several phases of the solid. These have distinct crystal structures and, under extreme pressure, may even differ in electronic excitation. There are also phase transitions with a discontinuity in the derivative of the density (second-order transitions) instead of the density itself (first-order transitions).

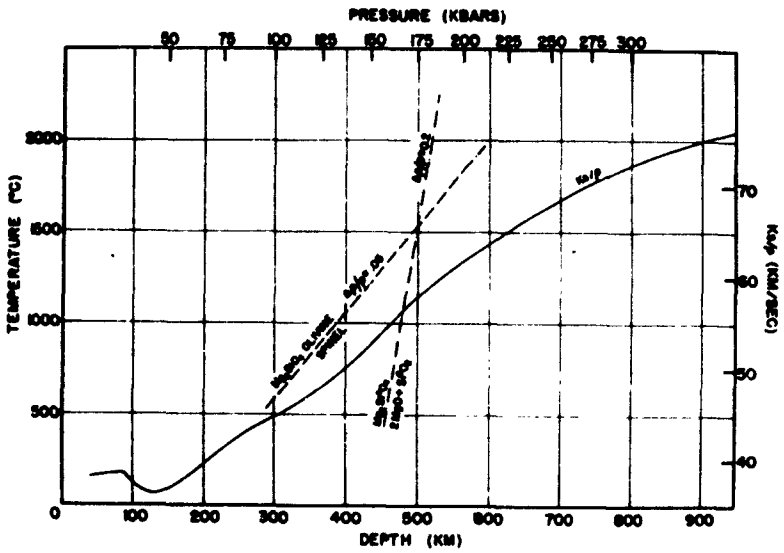

Fig. 5

It is still an open question whether or not progressive pressure ionization is accompanied by first-order phase transitions, the only ones capable of engendering the Ramsey type instability of planetary cores. Examples of phase transitions relevant to the state of the Earth's mantle are given in Fig. 4 and 5 (McDonald 1962). An interesting case, though of no geophysical consequence, is a transition in metallic cerium (Fig. 6), where the coexistent phases

belong to the same crystallographic system, but differ in lattice spacing.

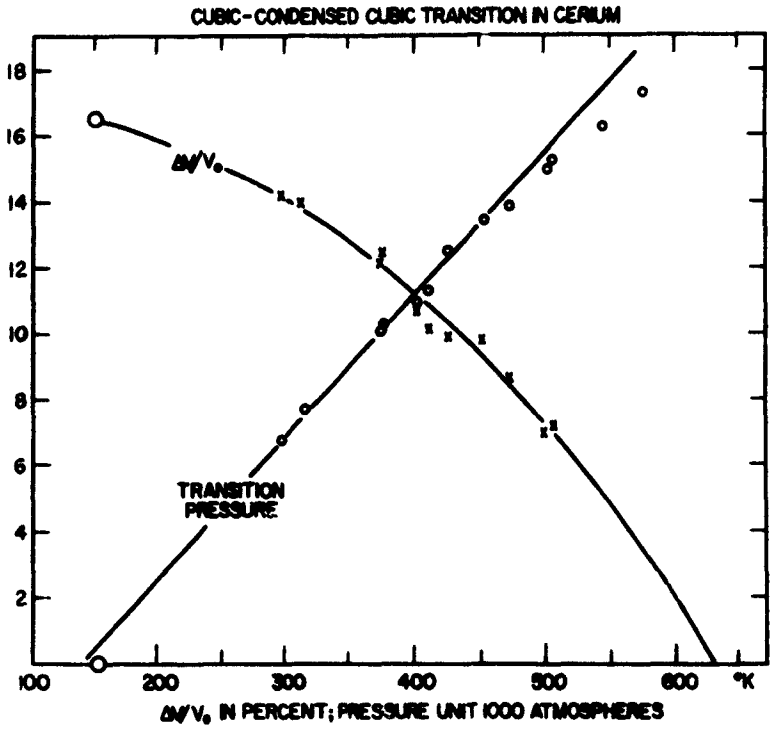

Fig. 6

Liquid Phases and Melting

All phases of a chemically homogeneous solid turn on melting (a first-order phase transition) into the same liquid phase. Immiscible liquid phases are known in chemically inhomogeneous systems, but so far have not been encountered among pure substances. Landau and Zeldovich have surmised that pure liquid metals at high temperatures, close to the critical point liquid-vapor, might undergo a transformation into a dielectric liquid phase (cf. Fig. 7). Liquid conductive cores are required in planets for the generation of magnetic fields, according to the dynamo theory. Moreover liquid

belong to the same crystallographic system, but differ in lattice spacing.

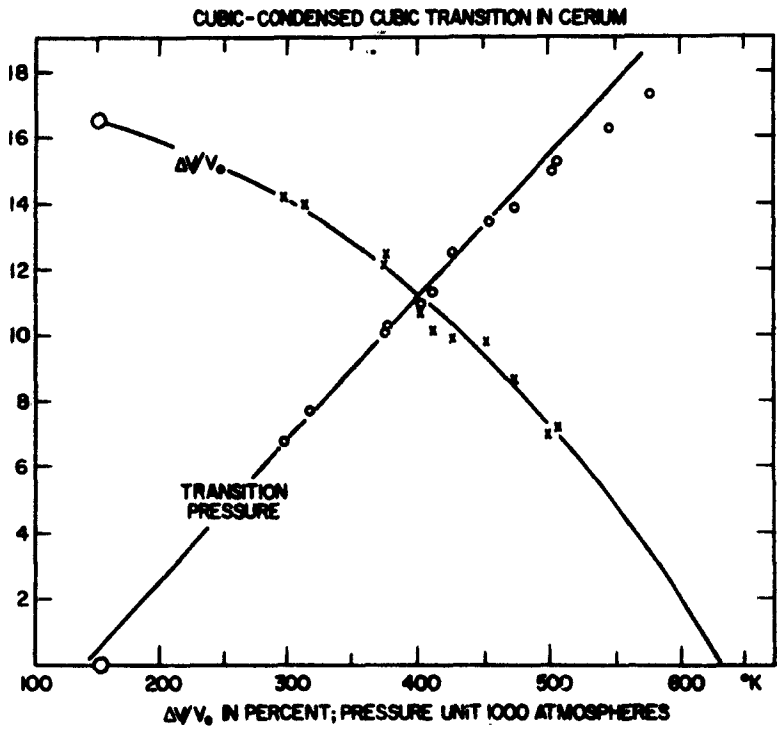

Fig. 6

Liquid Phases and Melting

All phases of a chemically homogeneous solid turn on melting (a first-order phase transition) into the same liquid phase. Immiscible liquid phases are known in chemically inhomogeneous systems, but so far have not been encountered among pure substances. Landau and Zeldovich have surmised that pure liquid metals at high temperatures, close to the critical point liquid-vapor, might undergo a transformation into a dielectric liquid phase (cf. Fig. 7). Liquid conductive cores are required in planets for the generation of magnetic fields, according to the dynamo theory. Moreover liquid

friction affords a much more efficient mode of dissipation of rotational energy than solid friction or other mechanisms. Therefore considerable interest attaches to the variation of the melting temperature in the deep interior of the planets. Simon's semi-

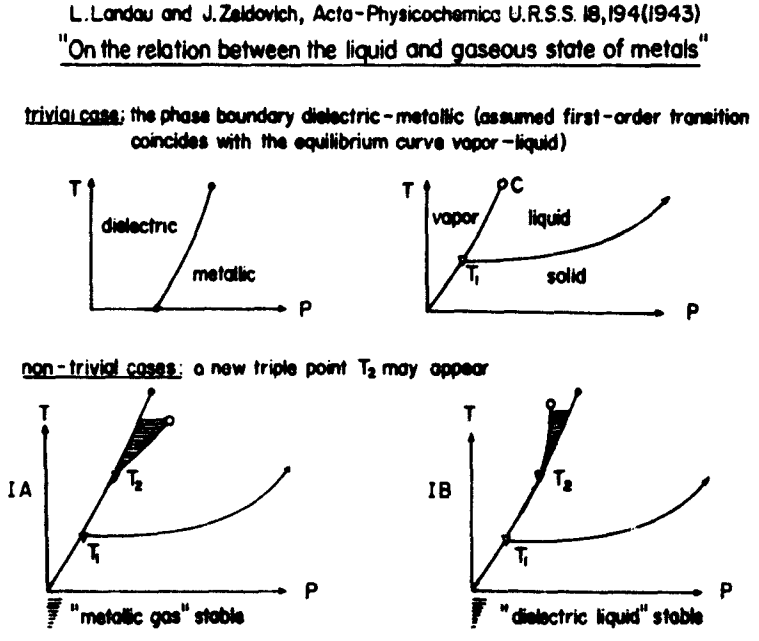

Fig. 7

empirical equation (Fig. 8) has been widely used to extrapolate experimental melting data. Before such were available for iron (Strong 1959, cf. Fig. 9), guesses at the constant c by Simon, and Gilvarry, had led to overestimating the melting temperature of iron at the boundary between mantle and core of the Earth (about 1.4×10^6 atm, marked on Fig. 9). Moreover, Simons' formula *assumes* a monotonic rise of melting temperature with pressure. A startling exception is the melting curve of cesium metal (Kennedy et al. 1962, cf. Fig. 10), which shows two maxima and two cusps.

PRESSURE DEPENDENCE OF MELTING POINT

Simon's equation $T_m = T_0(1+P/a)^{1/c}$

Gilvarry's relation from Debye theory of solids $c = \frac{6\gamma+1}{6\gamma-2}$

Grüneisen ratio $\gamma = -\frac{1}{\rho C_v}\left(\frac{\partial \rho}{\partial T}\right)_P\left(\frac{\partial P}{\partial \rho}\right)_T$

EXPERIMENTAL CONSTANTS	T(°K)	a(atm)	c
He (Dugdale and Simon 1953)	0.992	16.45	0.992
H_2 (DeMarcus 1958)	13.96	242.24	1.83
Fe (Strong 1959)	1805	75,000 (±5,000)	8 (±1)
Ni (Strong 1960)	1726	40,000 (±5,000)	10 (±1)

Fig. 8

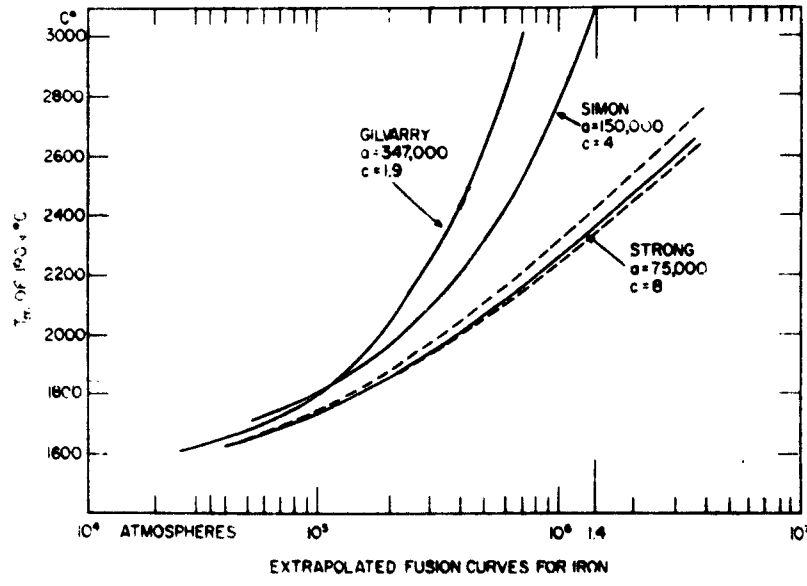

EXTRAPOLATED FUSION CURVES FOR IRON

Fig. 9

At the pressures of the latter solid cesium is known to undergo phase transitions tentatively attributed to changes in the electronic configuration of the atom, which at zero pressure has an incomplete inner shell. Another disturbing case is germanium, which lacks an incomplete inner shell of electrons. The melting temperature of

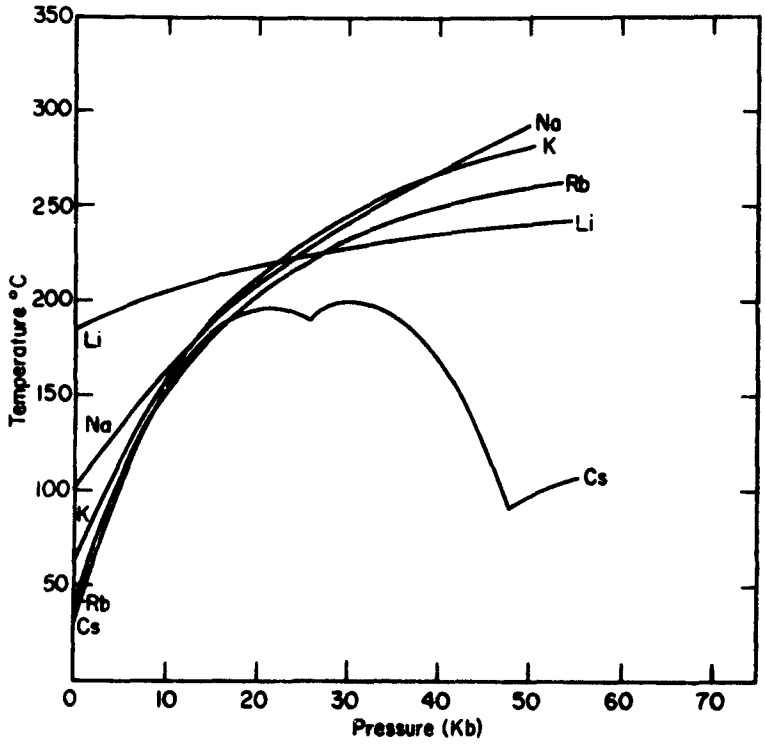

Fig. 10

this metal continues to decrease up to about 170.000 atm. without a new solid phase appearing when the melting temperature begins to rise again. Under these circumstances, one cannot accept without some misgivings the drastic extrapolation of the melting curve of iron. Finally, what remains in doubt is the asymptotic behavior of the melting curve. Does it terminate in a critical point?

Undoubtedly in stellar interiors the transport of heat by conduction is negligible beside that by radiation, but it must not be assumed that the converse regime prevails inside the planets. Following a suggestion of Preston (1956) on the possibility of radiative heat transfer in the Earth's mantle, Clark (1957 a), Lawson and Jamieson (1958), and Lubimova (1958) have concurred

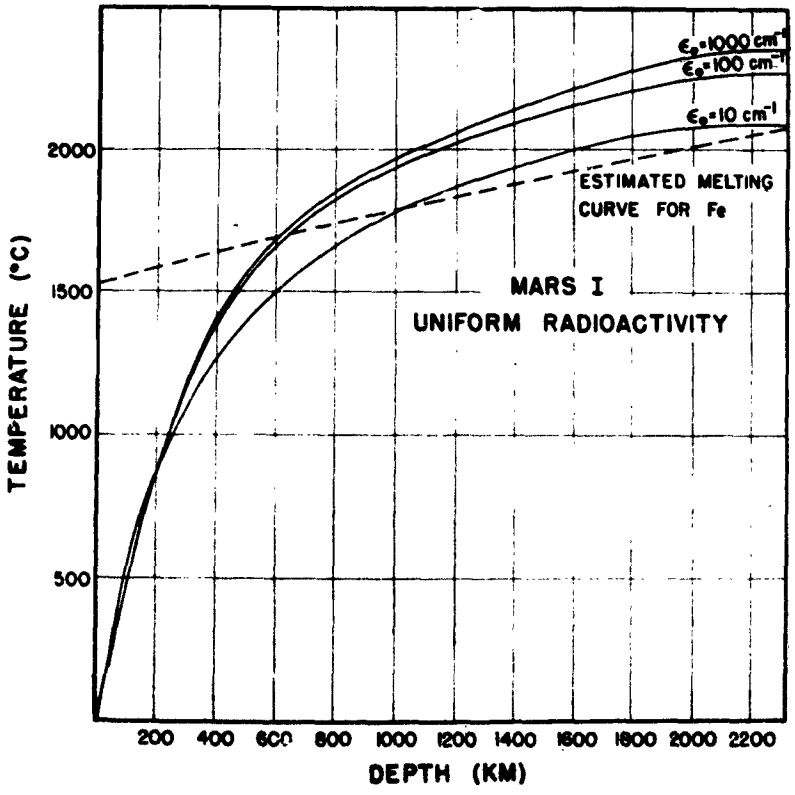

Fig. 11

that this mechanism markedly lowers the temperature gradient, although their numerical results still differ in orders of magnitude. Accordingly, models of planetary temperature distributions and their evolution that do not include the effects of radiative transfer

now stand in need of careful reexamination. Definitive conclusions cannot be reached until the current estimates of the planetary opacity (Rosseland mean) have been replaced by reliable figures. The uncertainty of the index of refraction, whose square appears in the expression for the temperature gradient (cf. Fig. 1) by way of Kirchhoff's law, probably is not serious. Clark (1957b) measured at room temperature a few absorption spectra of silicates presumably occurring in the Earth's mantle; but no corrections for temperature and pressure are available, and the best one can do is

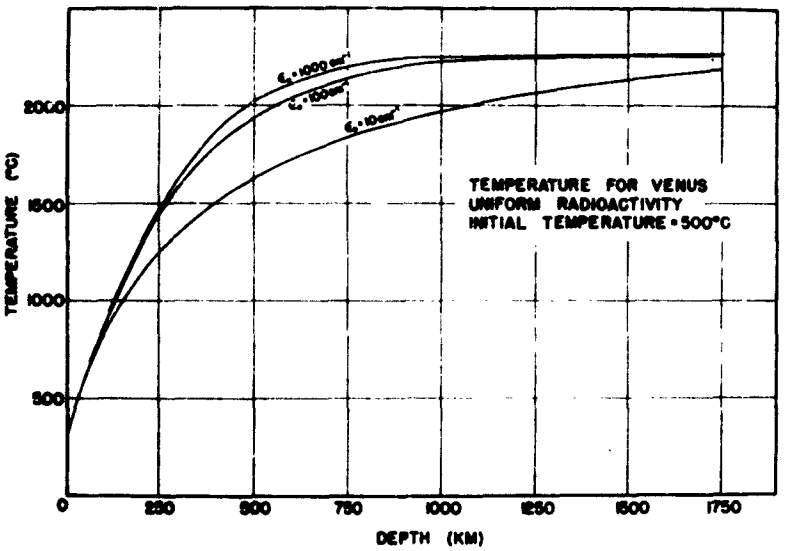

Fig. 12

to fall back on the classical relation between electrical conductivity and optical absorption coefficient. Evidently it will be a long time before the variation of opacity with depth in the planet can properly be taken into account. For the purpose of preliminary orientation it may suffice to put $\varkappa\rho$ = const throughout the planet, a procedure adopted by MacDonald (1962; N. B. ε_0 is used as symbol for the quantity $\varkappa\rho$, in the standard notation of the theory of stellar interiors). He has derived the temperature distributions for numerous models of terrestrial planets, in which ε_0 ranges from

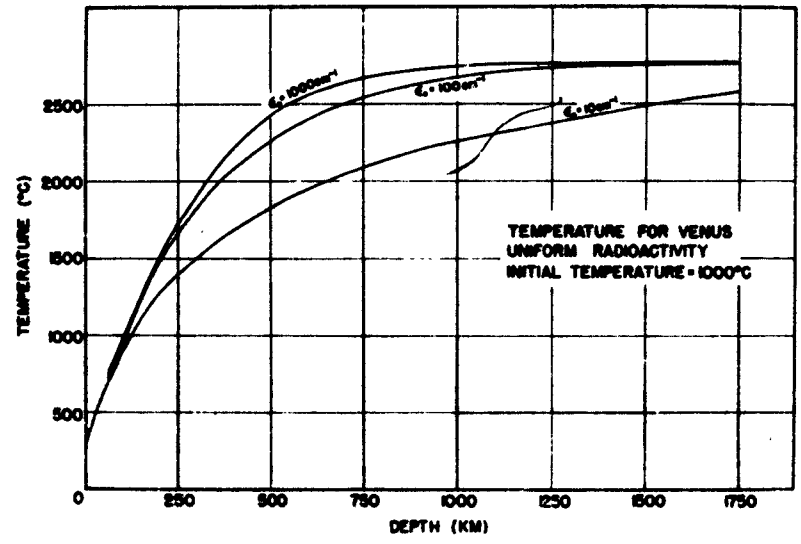

Fig. 13

$1000\ \mathrm{cm}^{-1}$ to 10^{-1}. Fig. 11, 12 and 13, taken from his work, will give some idea of how the temperature gradient is reduced by lowering the opacity (the limiting case of infinite opacity corresponds to ignoring radiative transfer).

Shape of minor Bodies

Obviously self-gravitation of a sufficiently small mass cannot overcome the intrinsic strength of solids. Hence there must be a minimum size of configurations assuming spherical shape under their own gravitation. Now, yield or fracture of materials occurs under a tension or load of

$$S \leqslant 10^9\ \mathrm{g\ cm^{-1}\ sec^{-2}}.$$

If this quantity is matched by the weight of a column of unit cross-section, of density ρ, and length L,

$$S = L\,\rho\,g_{\mathrm{E}},\quad g_{\mathrm{E}} \simeq 10^3\ \mathrm{cm\ sec^{-2}},\quad \rho \geqslant 1\ g\ \mathrm{cm^{-3}},$$

the characteristic length is, on Earth,

$$L \leqslant 10\ \mathrm{km}.$$

Structures exceeding this height, say mountains, would be in danger of yielding under their own weight. On a planet of radius R and mean density $\bar{\rho}$ the acceleration of surface gravity is

$$g(R)/g_E = (R/R_E)\ (\bar{\rho}/\bar{\rho}_E), \quad \bar{\rho}_E = 5.5\ g\ cm^{-3}$$

and the corresponding characteristic length is

$$L(R) = \frac{S}{\rho g(R)} \leqslant [10\ km]\ (R_E/R)\ (\bar{\rho}_E/\bar{\rho}).$$

We now ask : what is the critical radius, say R^*, for which L(R) equals the planetary radius R ? The numerical result is

$$R^* = [250\ km]\ \sqrt{\bar{\rho}_E/\bar{\rho}},$$

or, if the mean density of the planet is that of the denser rocks,

$$R^* \simeq 400\ km,$$

i. e. the very size of the largest asteroids. Thus we find support for another conjecture Henry Norris Russell made many years ago : « In the case of such small bodies the gravitational forces, which compel a large planet to be nearly spherical in form, would be relatively inefficient, and it is not impossible that some of them may be of irregular shape » (Russell 1924).

REFERENCES

Clark, S. P., Jr., *Trans. Amer. Geophys. Union*, **38**, 931-938, 1957a.

— *Amer. Mineralogist*, **42**, 732-742, 1957b.

Kennedy, G. C., et al., *J. Geophys. Res.*, **67**, 2559-2566, 1962.

Lawson, H. W., and Jamieson, J. C., *J. Geol.*, **66**, 540-551, 1958.

Lubimova, H. A., *Geophys. J.*, **1**, 115-134, 1958.

MacDonald, G. J. F., *J. Geophys. Res.*, in press, 1962.

Preston, F. W., *Amer. J. Sci.*, **254**, 754-757, 1956.

Russell, H. N., *Astronomy* (Ginn and Company) 1st edition, p. 353, 1924.

Strong, H. M., *J. Geophys. Res.*, **64**, 653-659, 1959.

2. — THE EFFECTS OF CONVECTION IN THE MANTLE ON THE GRAVITATIONAL FIELD OF THE EARTH

ZDENĚK KOPAL
Department of Astronomy, University of Manchester, England
and
Jet Propulsion Laboratory, California Institute of Technology, U. S. A.

Recent analyses of secular perturbations of artificial Earth satellites (1) have revealed the extent to which the terrestrial globe departs from a figure of equilibrium determined by its axial rotation. In particular, if the internal distribution of density inside the Earth as deduced predominantly by seismic evidence (c. f., e. g., Bullen (2) and other standard sources) is adjusted for the theoretical (equilibrium) coefficient of the dominant second harmonic of polar flattening to agree with the observed perturbations (i. e., the « dynamical ellipticity »), the corresponding equilibrium coefficient of the fourth harmonic of rotational origin is found to be 2.2 times as large as that deduced from the satellite observations (3); and, moreover, all odd harmonics whose presence has been established in the exterior potential of the Earth (4) remain, of course, wholly unaccounted for.

This failure of the equilibrium model to provide for adequate representation of the Earth's external gravitational field suggests the desirability of considering a more general hydrodynamical model for the interior of the terrestrial globe; and the likeliest cause of motion which may significantly affect the distribution of density inside the Earth is *thermal convection* due to radiogenic heating — not only in the core, but also throughout the mantle. The necessary condition for the occurrence of convection — the superadiabatic temperature gradient — appears to obtain even for the minimum estimates of the proportion of radioactive elements (K^{40}, Th^{232}, U^{235} and U^{238}) in the mantle; and even a viscosity as high as 10^{26} g/cm. sec frequently quoted as the upper limit for terrestrial rocks (5) is sufficient (for coefficients of isothermal compression of the order of

10^{-12} cm^2/dyne) for the mantle to behave essentially as a fluid over a much shorter time scale than 10^9 years.

The conditions for the stability of convection characterized by a given spherical-harmonic symmetry (of even as well as odd orders) were recently investigated by Chandrasekhar ([6]) for incompressible flow in liquid spheres (or shells) radioactively heated within ; and several geophysical phenomena — such as anti-symmetric distribution of continents and oceans ([7]), or indications of continental drift ([8]) — suggest that slow convection in the mantle of the Earth may indeed occur ([9]). Let us, therefore, tentatively adopt a hypothesis that the observed coefficients of odd harmonics (as well as the difference between the observed coefficient of the fourth harmonic and one computed on hydrostatic equilibrium) in the gravitational field of the Earth do arise from thermal convection in the Earth's mantle as represented by Chandrasekhar's theory. What is the velocity of convection (or the corresponding variation of density or temperature) necessary to account for the observed characteristics of the external gravitational field of the Earth in this manner?

In order to answer this question, let us recall that, in accordance with Chandrasekhar's theory (and using largely his notations), the radial velocity component U_n of convective motion in a shell of the radii ηR and R, varying as a surface harmonic $S_n^m(\theta, \varphi)$, should be given by

$$U_n = \frac{W_n(r)}{r} S_n^m(\theta, \varphi), \tag{1}$$

where

$$W_n(r) = A_n\{\alpha_1^{-\frac{1}{2}} x^{-\frac{1}{2}} \mathscr{C}_{n+\frac{1}{2}, n+\frac{1}{2}}(\alpha_1 x) + x^n B_1 + x^{n+2} B_2 + x^{-(n+1)} B_3 + x^{-(n-1)} B_4\} ; \tag{2}$$

$x \equiv r/R$ being the fractional radius comprised between η and 1 ; and A_n, the arbitrary scale constants. In this equation,

$$\mathscr{C}_{n+\frac{1}{2}, \nu}(x) = J_{-(n+\frac{1}{2})}(\alpha_1 \eta) J_\nu(x) - J_{n+\frac{1}{2}}(\alpha_1 \eta) J_{-\nu}(x) ; \tag{3}$$

x_1 being first root of the equation

$$\mathscr{C}_{n+1/2,\ n+1/2}(x) = 0\ ; \tag{4}$$

and (provided that the outer boundary of our spherical shell at $x = 1$ is free), the constants B_j on the right-hand side of (2) are obtained by solving the simultaneous set of linear equations

$$B_1 + B_2 + B_3 + B_4 = 0,$$

$$\eta^n B_1 + \eta^{n+2} B_2 + \eta^{-(n+1)} B_3 + \eta^{-(n-1)} B_4 = 0, \tag{5}$$

$$n(n-1)(B_1 + B_4) + (n+1)(n+2)(B_2 + B_3) = -\frac{2\mathscr{C}_{n+1/2,\ n+5/2}(\alpha_1)}{(2n+3)\,\alpha_1^2},$$

and

$$n(n-1)(\eta^{n-2}B_1 + \eta^{-n-2}B_4) + (n+1)(n+2)(\eta^n B_2 + \eta^{-n-2}B_3$$

$$= -\frac{2\mathscr{C}_{n+1/2,\ n+5/2}(\alpha_1\eta)}{(2n+3)\,\alpha_1^2\sqrt{\eta}}$$

if the inner surface at $x = 1$ is free, or

$$n\eta^{n-1}B_1 + (n+2)B_2 - (n+1)\eta^{-n-2}B_3 - (n-1)\eta^{-n}B_4$$

$$= \frac{\sqrt{\eta}\,\mathscr{C}_{n+1/2,\ n+5/2}(\alpha_1\eta)}{(2n+3)\,\alpha_1^2} \tag{7}$$

if it is rigid.

The mean radius R of the Earth is equal to 6371 km ; and the radius of its liquid core $\eta R = 3473$ km leads to $\eta = 0.545$ — approximately half way between $\eta = 0.5$ and 0.6, for which Chandrasekhar and Elbert ([10]) evaluated the roots α_1 of equation (4) for different values of n with the following results :

I. Table of the Roots α_1

	$n = 2$	$n = 3$	$n = 4$	$n = 5$	$n = 6$
$\eta = 0.5$	7.1116	7.8450	8.7168	9.6820	10.7077
$\eta = 0.6$	8.4428	8.9913	9.6717	10.4563	11.3210

The constants B_j ($j = 1, 2, 3$ and 4) as defined by the system of equations (5) and (6) or (7) have been evaluated by Mrs. Natica Greer and Mrs. Gail Lambert of the Division of Space Sciences, J. P. L., and their numerical values are :

II. Table of the Constants B_j

η	$10^5 B_1$	$10^5 B_2$	$10^5 B_3$	$10^5 B_4$
		Free Surface at $x = 1$		
		$n = 2$		
$\eta = 0.5$	—1.6662	4.1301	0.8477	—3.3116
$\eta = 0.6$	—0.7204	1.8591	0.6467	—1.7854
		$n = 3$		
$\eta = 0.5$	1.6022	—2.1931	—0.2080	0.7989
$\eta = 0.6$	0.8076	—1.1705	—0.2210	0.5839
		$n = 4$		
$\eta = 0.5$	—1.0165	1.1716	0.05358	—0.2087
$\eta = 0.6$	—0.5998	0.7299	0.07851	—0.2086
		$n = 5$		
$\eta = 0.5$	0.6016	—0.6441	—0.01447	0.05704
$\eta = 0.6$	0.4065	—0.4549	—0.02857	0.07691
		$n = 6$		
$\eta = 0.5$	—0.3561	0.3683	0.004105	—0.01629
$\eta = 0.6$	—0.2689	0.2872	0.01064	—0.02895
		Rigid Surface at $x = \eta$		
		$n = 2$		
$\eta = 0.5$	5.9491	2.4511	2.5267	—10.9269
$\eta = 0.6$	0.1884	1.5952	0.9106	—2.6942
		$n = 3$		
$\eta = 0.5$	1.4378	—2.1532	—0.2478	0.9633
$\eta = 0.6$	—1.6767	—0.1220	—0.9365	2.7353
		$n = 4$		
$\eta = 0.5$	—0.2487	0.9810	0.2441	—0.9765
$\eta = 0.6$	—2.0079	1.2244	—0.4160	1.1995
		$n = 5$		
$\eta = 0.5$	0.3403	—0.5790	—0.07967	0.3183
$\eta = 0.6$	0.03214	—0.3213	—0.1622	0.4513
		$n = 6$		
$\eta = 0.5$	—0.2659	0.3457	0.02665	—0.1065
$\eta = 0.6$	—0.1110	0.2298	0.06690	—0.1857

With the aid of the foregoing numerical data we can now proceed to compute the absolute values of the expressions (2) for W_n — apart from the multiplicative factors A_n which remain arbitrary. Let us attempt, in what follows, to determine them from known values of the coefficients of the harmonic expansion of the exterior potential V of the Earth, which may be due to this cause. In order to do so, let us recall (cf., e. g. section II-1 of [11] and notations used therein) that the n-th term of the harmonic expansion of V can be theoretically represented by

$$V_n = Gr^{-n-1} \int P_n(\cos\gamma) r'^n dm \tag{8}$$

where G stands for the constant of gravitation,

$$\cos\gamma = \cos\theta \cos\theta' + \sin\theta \sin\theta' \cos(\varphi - \varphi'), \tag{9}$$

and the element of mass

$$dm = \rho' r'^2 \sin\theta \, dr' \, d\theta' \, d\varphi'. \tag{10}$$

In so far as the perturbations ρ' of density are due to thermal convection, then within the framework of Chandrasekhar's theory

$$\left.\begin{aligned} \rho' &= -\alpha\rho_0 \Theta_n(r') S_n^m(\theta', \varphi'), \\ \Theta_n &= \left(\frac{3\mu A_n}{4\pi G \alpha \rho_0^2 R^4}\right) \frac{\mathscr{C}_{n+1/2,\, n+1/2}(\alpha_1 x)}{n(n+1)\sqrt{x}}, \end{aligned}\right\} \tag{11}$$

where ρ_0 denotes the equilibrium density (in the absence of convection) and R, the radius of the Earth ; while α is the coefficient of volume thermal expansion ; and μ, the coefficient of viscosity.

Imposing on (8) the limits of integration appropriate for a shell of thickness $(1 - \eta)$ R we find that

$$V_n = -\frac{\alpha\rho_0 G R^{n+3}}{r^{n+1}} \int_\eta^1 \int_0^\pi \int_0^{2\pi} \Theta(x') P_n(\cos\gamma) S_n^m(\theta', \varphi') x'^{n+2} dx' \sin\theta' d\theta' d\varphi' \tag{12}$$

which by virtue of the orthogonality theorem

$$\int_0^\pi \int_0^{2\pi} P_n(\cos\gamma) S_n^m(\theta', \varphi') \sin\theta' d\theta' d\varphi' = \frac{4\pi}{2n+1} S_n^m(\theta, \varphi) \tag{13}$$

can be simplified to

$$V_n = -\frac{3\mu A_n R^{n+1} S_n^m(\theta, \varphi)}{n(n+1)(2n+1)\rho_0 r^{n+1}} \int_\eta^1 x^{n+3/2} \mathscr{C}_{n+1/2,\, n+1/2}(\alpha_1 x) dx \tag{14}$$

On the other hand, King-Hele and other investigators of the gravitational field of the Earth ([12]) have formally represented its external potential in the form

$$V_n = G\frac{m_\oplus}{r}\left\{1 - \sum_{n=2}^{\infty} J_n\left(\frac{R}{r}\right)^n S_n^m(\theta, \varphi)\right\}, \tag{15}$$

where $m_\oplus = \frac{4}{3}\pi\rho_0 R^3$ is the mass of the Earth, and the J_ns are appropriate coefficients (*) whose values can be deduced from observed secular perturbations of the orbits of artificial satellites. Equating (14) with (15) we find the constants J_n and A_n to be related by

$$J_n = \alpha\varepsilon(\rho_0 R/\varkappa)^2 C_v A_n F_n(\eta), \tag{16}$$

where ε denotes the rate of energy liberation per unit mass ; $\varkappa$, the coefficient of heat conduction of the rocks in the mantle ; C_v, the specific heat of such material at constant volume, and

$$F_n(\eta) = \frac{1}{n(n+1)(2n+1)C_n}\int_\eta^1 x^{n+3/2}\,\mathscr{C}_{n+1/2,\ n+1/2}(\alpha_1 x)dx, \tag{17}$$

where

$$C_n = \frac{4\pi G\rho_0^2\alpha\varepsilon R^6 C_v}{9\varkappa^3\mu} \tag{18}$$

is the nondimensional Rayleigh number characteristic of a flow pattern of the spherical-harmonic symmetry of order n.

According to Chandrasekhar (cf. Table XXII, p. 245 of ([12])) the characteristic values of the Rayleigh numbers C_n are as given in the following tabulation :

III. Table of $10^{-4}C_n$

	$n = 2$	$n = 3$	$n = 4$	$n = 5$	$n = 6$
$\eta = 0.5$	2.181	1.924	2.146	2.673	3.492
$\eta = 0.6$	6.133	4.424	4.076	4.313	4.945

(*) Not to be confused with the Bessel functions $J_\nu(x)$ of equation (3).

and the function $F_n(\eta)$ as defined by equation (17) above has been evaluated by quadratures of Mrs. Patricia Conklin of the Division of Space Sciences, JPL, with the following results :

IV. TABLE OF $10^6 F_n(\eta)$

	$n = 2$	$n = 3$	$n = 4$	$n = 5$	$n = 6$
$\eta = 0.5$	15.94	—5.170	1.799	—0.6893	0.2916
$\eta = 0.6$	3.316	—1.337	0.5625	—0.2448	0.1130

Let us, furthermore, assume for the purpose of our discussion that the behaviour of rocks in the terrestrial mantle is characterized by the following mean values of physical parameters

$$\alpha = 2 \times 10^{-5}\ \text{deg}^{-1},$$
$$C_v = 7 \times 10^6\ \text{erg/g. deg},$$
$$\varkappa = 2 \times 10^5\ \text{erg/cm. sec. deg},$$
$$\varepsilon = 2 \times 10^{-8}\ \text{erg/g. sec.}$$

while the mean density ρ_0 in the mantle is approximately 4 g/cm^3 and, of course, $R = 6.37 \times 10^8$ cm.

On the other hand, according to the authors of references (1) and (4), the most probable values of the coefficients J_n of the potential expansion (15) are :

$$\left.\begin{aligned} 10^6 J_2 &= 1082.2 \pm 0.2, \\ 10^6 J_3 &= -\ 2.4 \pm 0.2, \\ 10^6 J_4 &= -\ 1.4 \pm 0.2, \\ 10^6 J_5 &= -\ 0.2 \pm 0.1, \\ 10^6 J_6 &= \quad 0.9 \pm 0.8, \\ 10^6 J_7 &= -\ 0.3 \pm 0.1, \end{aligned}\right\} \qquad (20)$$

etc. The dominant coefficient J_2 of the second harmonic is preponderantly due to polar flattening of the Earth due to its axial rotation — a cause which is also bound to invoke a second-order contribution to J_4, third-order contribution to J_6, etc. However, it has recently been shown by Kopal and James (3) that the theore-

tical equilibrium value of J_4 appropriate for internal density distribution reproducing the observed value of J_2 is equal to -3.15×10^{-6} — i. e., more than twice as large as the value of J_4 listed in (20) — a fact which leads us to conjecture that the difference $3.2 - 1.4 = 1.8$ may be equal to the actual value of J_4 arising from convection. At any rate, the values of

$$J_3 = -2.4 \times 10^{-6} \text{ and } J_4 = +1.8 \times 10^{-6} \tag{21}$$

lead, by (16), to

$$A_3 = 1.6 \text{ cm}^2/\text{sec. and } A_4 = 3.4 \text{ cm}^2/\text{sec, respectively.} \tag{22}$$

The corresponding radial-velocity component of convective flow then will, in accordance with equations (1) and (2), be clearly of the order of magnitude of

$$\bar{U}_n = \left| \frac{A_n}{\bar{r}\,\alpha_1^4} \right|, \tag{23}$$

where $\bar{r}$ is an appropriate scale length which, for the Earth's mantle, can be approximated by 5×10^8 cm. If so, it follows by a combination of (22) and (23) with the data of Table III that, for

$$\begin{aligned} n = 3 &: \bar{U}_3 = 6 \times 10^{-12} \text{ cm/sec.} \\ n = 4 &: \bar{U}_4 = 1 \times 10^{-11} \text{ cm/sec.} \end{aligned} \tag{24}$$

Velocities of this order of magnitude would correspond to displacement of the order of 10^{-4} cm (i. e. a micron) per year, or a flow length of the order of 10 km during the entire age of the Earth. Velocities so small are all that is required for convection to account for the observed coefficients of higher harmonics in the external gravitational field of the Earth ; but are manifestly quite inadequate to provide motive power for the continental drift or other geophysical phenomena which have been mentioned in this connection ([8,9]). As a corollary, it should also follow from equation (18) that the coefficient μ of viscosity consistent with the physical constants (19) and the Rayleigh numbers characteristic for this type of flow should be of the order of 10^{27} g/cm. sec — i. e., by five orders of magnitude greater than those inferred by other methods ([5]). Only so high a viscosity can retard the convective flow to the low absolute flow velocities (24) quoted above.

Is there any escape from these conclusions, by any admissible variation of the physical constants of the Earth involved in our computations? Of such constants, the values of α as well as of C_p appear to be sufficiently well known for terrestrial rocks that at least their order of magnitude can be considered as fixed. The value of $\varkappa$ is perhaps less firmly established; and that of ε still less so. However, an increase of $\varkappa$ by not less than two orders of magnitude, a diminution of ε by four orders, or a suitable combination of both would be required to harmonize the characteristic Rayleigh numbers C_n with a viscosity of the order of $10^{22} - 10^{23}$ g/cm. sec; and (by increasing the values of A_n for given J_n in equation 16 by the same factor) to obtain a flow velocity of the order of 1 cm/year required for the continental drift. Whether or not so large a change in $\varkappa$ or ε may indeed be supported by other independent evidence, only the future can tell.

Before considering this too seriously, however, we should, at least mention that our present failure to reconcile the consequences of Chandrasekhar's theory of convection in the Earth's mantle with the observed values of J_n for the most probable values of the physical constants based on independent evidence may also go back to the fact that Chandrasekhar used too restricted an equation for the changes in state (at the basis of the Boussinesq approximation). This equation relates the changes of density invoked by convection with the changes of the temperature alone; and the validity of this approximation under conditions prevailing in the Earth's mantle appears to be somewhat questionable ([14]). A consistent development of a more general theory of convection in which the changes of density are related with those of the pressure as well as temperature, remains, however, still a task for the future.

REFERENCES

([1]) Cf. e. g. Y. Kozai, *Smithson. Astr. Obs. Report*, No. 22, 1959; J. O'Keefe, A. Eckels and R. K. Squires, *Astr. Journ.*, **64**, 245, 1959; D. G. King Hele, *Nature*, **187**, 490, 1960; *Geoph. Journ. R. A. S.*, **4**, 3, 1961; D. E. Smith, *Planetary Space Sci.*, **8**, 43, 1961; and others.

(3) K. E. Bullen, *Bull. Seism. Soc. Amer.*, 30, 235, 1940 ; 32, 19, 1942.

(8) Z. Kopal and R. James, *Tech. Summary Report* No. 193, Math. Res. Center, U. S. Army, University of Wisconsin, October, 1960.

(4) Cf. Y. Kozai, O'Keefe et al (op. cit. ante) ; or R. R. Newton, H. S. Hopfield and R. C. Kline, *Nature*, 190, 617, 1961.

(5) Cf. e. g. D. T. Griggs, *Journ. of Geology*, 47, 225, 1939 ; F. Birch, J. R. Schaiber, and H. C. Spicer, *Handbook of Physical Constants*. (Geol. Soc. of Amer. Special Paper No. 36, 1942).

(6) S. Chandrasekhar, *Phil. Mag* (7), 43, 1317, 1952 ; 44, 233 and 1129, 1953 ; or Chapter VI of his *Hydrodynamic and Hydromagnetic Stability*, Oxford Univ. Press, 1961.

(7) A. Prey, *Abh. d. Gesell. d. Wiss.* (Math.-Phys. Klasse) Göttingen, 11,1, 1922.

(8) Cf. e. g., S. K. Runcorn, *Nature*, 193, 311, 1962.

(9) F. A. Vening-Meinesz, *Proc. Kon. Ned. Akad. d. Wet.*, B. 55, 527, 1952.

(10) S. Chandrasekhar and D. Elbert, *Proc. Cambr. Phil. Soc.*, 49, 446, 1953.

(11) Z. Kopal, *Figures of Equilibrium of Celestial Bodies*, Univ. of Wisconsin Press, Madison, 1960.

(12) Cf. Y. Hagihara, *Astr. Journ.*, 67, 108, 1962.

(13) S. Chandrasekhar, *Hydrodynamic and Hydromagnetic Stability*, Oxford Univ. Press, 1961.

(14) Z. Kopal, *Jet Propulsion Laboratory Tech. Report* 32-276, 1962 (in press).

3. — COMPARATIVE ANALYSIS OF THE INTERNAL CONSTITUTION AND DEVELOPMENT OF PLANETS

B. J. LEVIN
O. Schmidt Institute of Physics of the Earth, Acad. Sc. USSR

A comparative analysis of the internal constitution and evolution of planets gives important results for planetary physics as well as for geophysics. The most developed branches of such analysis are a) the comparison of mean densities of related groups of planets and satellites and b) a comparative study of thermal histories of terrestrial planets and the Moon.

I

The analysis of the mean densities of planets consists in the calculation of planetary models with radial distribution of density, which satisfy to the values of mass and radius, and in some cases of the moment of inertia, deduced from observations. The calculations require the knowledge of the equation of state of planetary matter and therefore some assumptions on its chemical composition and on phase transitions are needed. (Wildt, 1961).

For terrestrial planets the analysis of their densities is intimately connected with the important problem of the nature of the dense core of the Earth and of the presence of similar cores in other planets.

The old iron-core hypothesis presents several difficulties :

1. If this hypothesis is admitted the inference of different content of iron in planets, already made by Jeffreys in the thirties, is inevitable. The attempts to ascribe these differences to different fractionation during the formation process (H. C. Urey, 1952, 1954, 1956, 1960 ; A. Ringwood, 1959) cannot be regarded as successful. Insurmountable difficulties remain even within the artificial schemes proposed by these authors.

2. When the cold origin of terrestrial planets was established the formation of the iron core was ascribed to the gravitational differentiation, which began after the radioactive heating and softening of the interior of the Earth and planets. But the possibility of such segregation of iron is doubted by several authors (see f. i. Lyustikh, 1948).

3. Recently the experiments on the shock-wave compression of iron (Altshuler and oth., 1958) showed that at pressure existing in the Earth's core the density of iron is somewhat too great. If we try to obtain a lower density increasing the supposed temperature of the core the unacceptable high temperature is needed. (Zharkov, 1960). We can decrease the density of iron without the increase of temperature, supposing for example the admixture of silicium or magnesium to the core's matter. But this would mean the rejection of analogy with iron meteorites, which is one of the main arguments in favour of the iron core hypothesis.

4. The melting temperatures of iron and silicates at high pressures are such that the iron core hypothesis is unable to combine the solid state of the Earth's mantle with the liquid state of its core, which is needed to explain the magnetic field of the Earth.

The alternative point of view on the nature of the Earth's core is represented by the Ramsey's hypothesis. The analysis of the densities of terrestrial planets based on Ramsey's hypothesis leads to almost common composition of Venus, Earth, Mars and Moon, and all difficulties of the iron core hypothesis mentioned above do not rise (*).

But the real existence of the phase transition in rocks at the pressure of about $1.5.10^6$ atm. has no direct confirmation. Calculations for MgO by Trubitsin (1958) as well as experiments by

(*) The high density of Mercury remains properly unexplained. As was already mentioned (Levin, 1957) it is probably due to the formation of Mercury from particles most heated by the Sun or even condensed under the conditions of higher temperature. Unfortunately a thorough study of the chemical evolution of the protoplanetary cloud remains still lacking.

Altshuler and Kormer (1961) on shock wave compression of dunite failed to give a phase transition at this pressure.

However the present author is not inclined to regard these results as final. Comparing the difficulties of the iron core hypothesis with the merits of Ramsey's hypothesis he continues to support the latter.

The analysis of densities of giant planets shows that with any existing variant of equation of state for hydrogen its content

TABLE 1

	Mass	Mean Diameter k m	Mean Density g/cm³
	Planets :		
Mercury	0,0543	4 800	5,6 ± 0,2
Venus	0,8136	12 200	5,11
Earth	1	12 742	5,516
Mars	0,1069	6 760	3,95
Jupiter	317,38	139 400	1,34
Saturn	95,03	115 400	0,70
Uranus	14,6	48 200	1,48
Neptune	17,2	45 800	2,06
Pluto	0,03 ÷ 0,7	6 400 ÷ 12 700	?
	Satellites :		
Earth : Moon	1	3 476	3,34
Jupiter : I. Io	0,95	3 470	3,2
II. Europa	0,64	3 100	3,0
III. Ganymede	2,09	5 000	2,4
IV. Callisto	1,19	4 700	1,6
Saturn : I. Mimas	$5{,}14.10^{-4}$	500	0,6 ± 0,2
II. Enceladus	$1{,}14.10^{-3}$	570	0,9 ± 0,3
III. Tethys	$8{,}65.10^{-3}$	900	1,7 ± 0,3
IV. Dione	0,015	850	3,4 ± 0,3
V. Rhea	?	1 400	?
VI. Titan	1,886	4 850	2,3
VII. Iapetus	0,025	1 330	1,5
Neptune : I. Triton	1,88	3 770	4,9
II. Nereid	$4{,}7.10^{-4}$	300	2,4

diminues monotonously from Jupiter to Neptune. It is no reason to connect this change with the differences of masses of these planets. Obviously it is due to differences in their distances from the Sun. A tentative explanation was presented some years ago (Levin, 1957).

For the further more refined analysis of densities of planets the most reliable values of their masses and radii must be used. S. Kozlovskaya compiled a review of all determinations and deduced the most probable values, which are given in Table I with corresponding values of the mean density. The full review will be published elsewhere.

II.

In the analysis of thermal histories of planets as in the analysis of their densities a comparative study of related bodies gives much advantages.

For terrestrial planets their internal temperature at the end of their formation was low and was determined mainly by the radiogenic heat, generated during the formation. Only in the more massive planets — Earth and Venus — some additional increase of temperature was caused by the compression of internal parts under the weight of accumulating outer parts. But even for these planets the heat output by the shocks of planetesimals from which they were formed was very small (Safronov, 1959).

Radioactive elements form only nonvolatile compounds, and therefore their content in all terrestial planets must be almost the same. The heating of these planets must be similar (if we neglect the differences in the outflow of heat to the outer space), but nevertheless their thermal histories were different. It is due to the differences in their internal pressures, which cause differences in the melting temperatures.

On fig. 1 the curves of the melting temperature versus radius are drawn for the Earth, Venus, Mars and Moon. The calculations by Uffen (1952) and Zharkov (1959) based on the quantum theory

of solid bodies and on the analysis of seismic velocities give for the Earth's mantle substantially different curves (*). These curves were recalculated for the mantle of Venus and Mars (in the latter the mantle embraces almost the whole planet) assuming that even in the upper mantle of the Earth the curves by Uffen and Zharkov

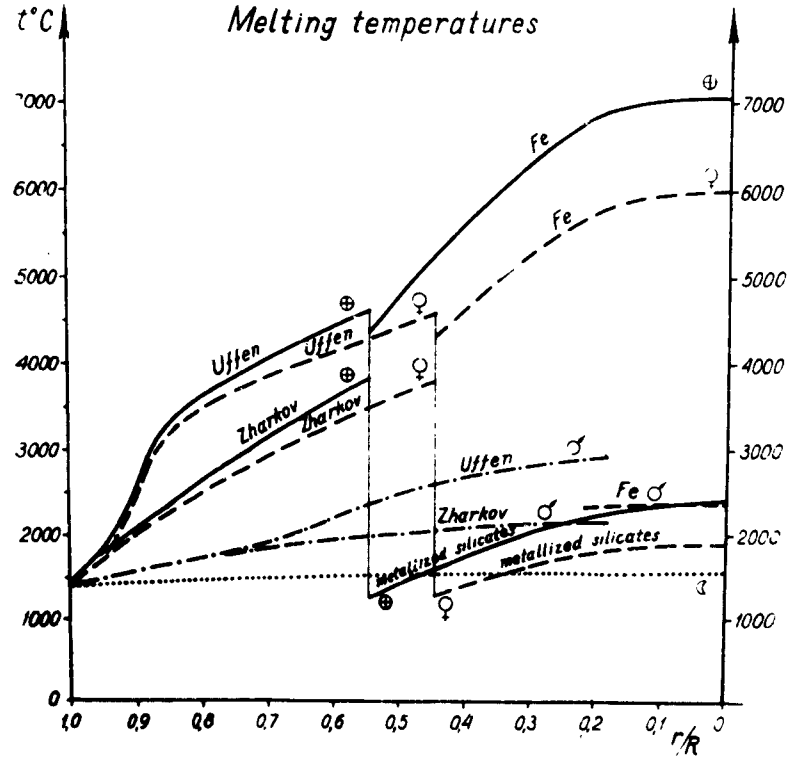

Fig. 1

are determined by changes of pressure and not of chemical composition. The melting curve for the Moon is based on the experimental data for dunite. For the Earth's core the melting curve for iron according to Zharkov (1959) as well as his curve for metallized silicates (Zharkov, 1962) are given. These both curves are recal-

(*) The curve by Uffen was improved by Zharkov and in addition he obtained a new curve using a different method of calculations.

culated also for pressures existing in the core of Venus. For a small Martian core, whose dimensions are badly known, only the melting curve of iron is given.

The calculations of radiogenic heating of the Earth and planets (see, for example, Levin and Majeva, 1961) show that in the internal parts of such great bodies the changes of temperature along the radius are small, i. e. that the internal parts are almost isothermic. The absolute values of the temperature of these parts are determined mainly by the assumed content of radioactive elements.

In the Earth, on the boundary of the core the melting point of iron lies for 600° higher than the melting point of the mantle according to Zharkov and only 200° lower than its melting point according to Uffen. For a molten state of the outer core up to the boundary of the inner core a temperature of about 6000° is needed (for an iron core), but at this temperature the whole mantle would be also molten. However it is not so. In the case of metallized silicates a temperature of about 2000° is enough for a molten state of the outer core and at this temperature the mantle remains solid. Only at the depth of about 0,1 of the Earth's radius the temperature curve turns to be close to the melting temperature, which indeed is needed for a gradual smelting of the crust from the upper mantle. It must be added that such temperature of the Earth's interior corresponds to a most probable content of radioactive elements.

At the temperature of about 2000° the core of Venus, if composed from metallized silicates, must be molten up to the centre. In the upper mantle of Venus the conditions must be similar to those in the Earth and therefore the formation of the outer crust must proceed in a similar way.

For the study of the thermal history of Mars the choice between the two variants of the melting curve for the mantle is of importance : if Uffen's curve is correct then at the temperature of 2000-3000° the central parts of Mars remain solid, but the outer part is molten ; if Zharkov's curve is correct the wholeMartian

interior was sometimes molten and has undergone a physico-chemical and gravitational differentiation similarly to what has probably occurred in the Moon. The melting of the whole interior of Mars, or at least a total melting of its upper mantle must lead to a relatively rapid completion of differentiation, i. e. to the completion of formation of the outer sialic crust similar to the Earth's crust. Since a sialic matter when completely differentiated can amount to 10-15 % of the total mass of silicates (Vinogradov, 1959, a, b) the thickness of Martian crust can reach 40-60 km.

The existence in Mars of a small dense core (Bullen, 1949, 1957) can be most easily explained by the gravitational differentiation of iron. This explanation gives an argument in favour of the melting of the whole interior of Mars, i. e. in favour of Zharkov's melting curve for the mantle. But the data on the melting curves of some minerals are in favour of the curve by Uffen.

In the Earth (and in Venus) the temperature only approaches to the melting curve at the depth of 500-1000 km and therefore the formation of the crust has a long durable character. On the Earth the formation of the crust continues till now at almost constant rate without obvious signes of slackening. The associated tectonic movements and orogenic processes are going on now with about the same intensity as hundreds of millions years ago.

The internal parts of Mars, owing to its smaller dimensions, as compared with the Earth, and greater collection of radio-active elements into the outer crust, must be already cooling, and the formation of the crust has already finished.

Mountain chains of the Earth's type are lacking on Mars and there exist only highlands. Their absence is often explained by an accidental coincidence of the present time with the epoch of temporary slackening of Martian tectonic processes. One refers to the existence of such epochs in the geologic history of the Earth. However the synchronism for the whole Earth of the slackening and resumption of tectonic processes is unproved and even seriously doubted. Another possible explanation for the absence of mountains on Mars can be proposed : climatic conditions on its surface are such

that the weathering proceeds much rapidly than on the Earth and therefore mountains are destroyed before they become high. But the above conclusions on the evolution of Martian interior give good reasons to admit as a most probable cause of flatness of the Martian surface the weakness or a total absence of modern tectonic movements.

Only few can be said on the thermal history of the giant planets. In these planets the gravitational energy liberated in their formation process caused them to be initially hot. (The terrestrial planets rapidly lost this heat into space). This is manifested in the density distribution of the main Jovian satellites, which is similar to the distribution of planetary densities caused by the solar radiation. How high was the initial surface temperature of the giant planets and how did proceed their subsequent cooling require further investigation.

REFERENCES

ALTSHULER L. V. and oth., *J. Exp. Theor. Phys.* (Russian), **34**, 874, 1958.

ALTSHULER L. V. and KORMER S. B., *Izvestia Acad. Sci. USSR*, Ser. geophys., N. 1, 33. 1961.

BULLEN K. E., *M. N.*, **109**, 688, 1949.

BULLEN K. E., *M. N. Geophys. Suppl.*, **7**, N. 5, 271, 1957.

LEVIN B. J., *Mém. Soc. R. Sci. Liège*, IV série, **18**, 186, 1957.

LEVIN B. J. and MAJEVA S. V., *Annali di Geofisica*, **14**, 149, 1961.

LYUSTIKH E. N., *Doklady Acad. Sci. USSR*, **59**, 1417, 1948.

RINGWOOD A. E., *Geochim. Cosmochim. Acta*, **15**, 257, 1959.

SAFRONOV V. S., *Izvestia Acad. Sci. USSR*, ser. geophys. N. 1, 139, 1959.

TRUBITSIN V. P., *J. Exp. Theor. Phys.* (Russian), **34**, 221, 1958

UFFEN R. J., *Trans. Am. Geophys. Un.*, **33**, 893, 1952.

UREY H. C., *The Planets*. (New Haven), 1952.

UREY H. C., *Astroph. J. Suppl.*, ser. 1, N. 6, 147, 1954.

UREY H. C., *Astroph. J.*, **124**, 623, 1956.

UREY H. C., *Geochim. Cosmochim. Acta*, **18**, 151, 1960.

VINOGRADOV A. P., *Izvestia Acad. Sci. USSR*, ser. geol., N. 10,5, 1959a.

VINOGRADOV A. P., *Chemical Evolution of the Earth*. (in Russ.) Moscow, 1959b.

WILDT R., ch. 5 in *The Solar System*, v. III, ed. G. P. Kuiper and B. Middlehurst (Univ. Chicago Press), 1961.

ZHARKOV V. N., *Izvestia Acad. Sci. USSR*, ser. geophys., N. 1,465, 1959.

ZHARKOV V. N., *Doklady Acad. Sci. USSR*, **135**, 1378, 1960.

ZHARKOV V. N., *Trudy Inst. Phys. of the Earth Acad. Sci. USSR*, N. 20 (187), 1962.

4. — JUPITER : CHEMICAL COMPOSITION, STRUCTURE, AND ORIGIN OF A GIANT PLANET (*)

E. J. ÖPIK
Armagh Observatory, Northern Ireland
and
Department of Physics and Astronomy, University of Maryland, U. S. A.

ABSTRACT

A comprehensive analysis is made of the observational and theoretical information regarding the composition, structure, and origin of Jupiter, viewed as a cosmogonic test case of a giant planet.

With a polychromatic radiative-equilibrium temperature of 112 ± 2 °K, based on the radiative properties of ammonia and methane as the chief radiators, the occultation of σ Arietis yields a mean molecular weight of $\mu = 4.3 \pm 0.5$ for Jupiter's atmosphere. The combination of the optical properties of Jupiter's disk with spectroscopically determined abundances of molecular hydrogen, methane and ammonia leads to probable percentages of molecules in Jupiter's observable atmosphere as follows :

Molecule	He	H_2	Ne	CH_4	A	NH_3
%	97.2	2.3	0.39	0.063	0.042	0.0029

This gives another independent value of the mean molecular weight of $\mu = 4.02$, in fair agreement with the occultation value.

Free nitrogen is excluded by considerations of chemical equilibrium. CO_2 must be completely reduced to CH_4 and H_2O, whereas water is snowing out and cannot appear above Jupiter's cloud level. The solid ammonia hypothesis of the clouds is strongly supported. The temperature at cloud top is 156°K, and the probable pressure 11 atmospheres.

(*) This research was supported by the National Aeronautics and Space Administration Grant NsG-58-60. The full paper, about 80 pp., is scheduled for publication in No. 3 of *Icarus*, autumn 1962.

From radiometric observations, as well as from the independent evidence of the temperature of the ammonia clouds, an internal heat supply for Jupiter is indicated, of the order of 1.2×10^4 erg/cm^2. sec or 1.6 ± 0.4 times the solar input. For Saturn the internal heat supply is of the order of 4×10^3 erg/cm^2. sec, almost the double of solar input.

If the bulk of Jupiter's mass is solid hydrogen, its atmospheric composition is very different.

Escape and diffusion processes from a rotating pre-planetary nebular ring, as well as from planetary exospheres are analyzed and numerically evaluated. These processes, of neutral as well as ionized gas, are utterly inadequate to account for any significant differentiation of composition on a cosmic or planetary scale.

It is shown that differentiation by condensation of solid particles, especially snowing-out of hydrogen from the nebular ring, is quantitatively adequate to achieve concentration of hydrogen in the core of a Jovian planet, as well as to lead to the subsequent accretion of a helium atmosphere.

The solid hydrogen-helium model of Jupiter's internal structure is shown to be the only one in harmony with observation and theory.

The alternative of a gaseous sphere of heavier elements (C-N-O) is examined and shown definitely to contradict crucial observational data, especially surface temperature which should then be of the order of 10^4 deg K. Such a sphere would rapidly cool by convection and become a solid-degenerate body of much higher density than that of Jupiter.

The bulk of Jupiter's mass could have originated either directly by accretion of hydrogen snow from the ring, of course vaporizing before reaching the surface of the planet maintained at a temperature of the order of 3000-4000 °K ; or through an intermediate stage of a gasball, contracting through convectional cooling. Cooling by radiative and conductive transfer is far too slow for gasballs of Jupiter's mass.

Principal Conclusions

1. From the combination of the available spectroscopic, radiometric and photometric evidence, including the occultation of σ Arietis, it is concluded that the m 'n constituent of Jupiter's atmosphere is helium, with molecular hydrogen coming next. The mean molecular weight of the atmosphere is close to 4.0.

2. The radiative equilibrium in Jupiter's atmosphere is chiefly governed by ammonia, and to a lesser extent by methane.

3. Radiometric and spectroscopic data consistently indicate an internal heat supply for Jupiter of $(1.2 \pm 0.3) \times 10^4$ erg/cm^2. sec at the planet's surface, or by about 60 per cent greater than the input of solar radiation. The figure follows independently from direct measurements of the infrared radiation, and from the vapor pressure and temperature of the radiating ammonia layer. For Saturn the internal heat supply is $(4.0 \pm 0.4) \times 10^3$ erg/cm^2. sec at the surface.

4. The unusual abundance of helium as compared with hydrogen in Jupiter's atmosphere cannot be due to selective escape, diffusion, or any other atomic (ionic) filtering processes during the planetary or pre-planetary stage. These selective processes are too slow by many orders of magnitude, and can only affect the composition of an unmixed outer atmosphere.

5. Because of the necessity of radiating away the excess energy, neither Jupiter nor any other body of planetary size, of less than 0.03 solar mass (or 30 times Jupiter's mass), could have come into being and acquired its present dense state by condensation or accretion of pure hydrogen, or helium, or any other material in a non-convective gaseous state, during time intervals of less than 10^{10} years. However, convective structures of Jupiter's mass could have cooled off in about 10^6 years.

6. The most direct and plausible way of building up planets of less than 0.03 solar mass appears to be accretion from a cloud of solid particles.

7. Snowing-out of solid hydrogen from a nebular ring of extremely low temperature (4 °K) could account both for the predominantly hydrogenic composition of the bulk of Jupiter's mass, and the predominance of helium in its atmosphere as a later acquisition.

8. The solid hydrogen-helium model of Jupiter is to be regarded as the only plausible structure of this planet, as well as of Saturn.

5. — THE CONSTITUTION OF URANUS AND NEPTUNE

W. C. DEMARCUS and RAY T. REYNOLDS
University of Kentucky
Lexington, Kentucky, U. S. A.

I. INTRODUCTION

The compositions of two of the giant planets, Jupiter and Saturn, seem to be fairly well established if it is assumed that they are cold bodies. (Ramsey and Miles (1952), DeMarcus (1958)) Consequently if the compositions of Uranus and Neptune could also be found, subject to the same assumption that they are cold bodies, a well defined study of the giant planets would be complete.

However it is a conclusion of this paper that results such as those obtained by Ramsey and Miles and by DeMarcus cannot be attained for Uranus and Neptune. The reason for this lies wholly in the fact that these latter planets are much poorer in hydrogen than are Jupiter and Saturn. At low temperatures and a given pressure, densities less than a certain value imply a minimum amount of hydrogen but densities greater than this value can be attained by infinitely many different mixtures of all the elements. All reasonable models of Uranus and Neptune have values of density as a function of pressure which fall in the ambiguous region while the opposite is true for Jupiter and Saturn. As a consequence of this fact the philosophy followed by DeMarcus in his investigation of Jupiter and Saturn has to be modified in order to make any progress at all. DeMarcus sought to avoid the employment of any cosmochemical data in order that his results, whatever they might be worth, might have primary significance. In this paper the requirements of this philosophy have been relaxed to the extent that the relative proportions of all elements more massive than helium are assumed « normal ». By definition « normal » relative abundances are those given by Urey and Suess (1956). This particular mixture

of heavy elements is designated herein by the homely noun, « mud ». The low temperature equations of state of hydrogen, helium and mud are then estimated and the compositions of Uranus and Neptune can be assayed, on the basis of assumed models, to the extent that lines on a tri-linear chart could be marked off near which the compositions of the planets should fall. Before taking up this principal phase of this paper however it was of some interest to see how nearly Neptune and Uranus could be fitted by model planets of pure helium or of pure mud. To these restricted problems we now turn.

II. The Mass-Radius Relation of Helium and Mud Planets

DeMarcus (1959) has given an estimated equation of state of helium by interpolating between the measured results of Stewart (1956) at low pressures and a theoretical calculation at high pressures based on an investigation of divalent metals by Raimes (1952). The 0°K isotherm so derived is reproduced in Table I. On the basis of this pressure-density relation, model planets were constructed with varying central pressure. The results are given in Table II and Figure I.

Table I

The Equation of State of 0°K *Helium*

$p(10^{12}$ dyne/cm$^2)$	ρ(gm/cm^3)
.0002	.234
.0010	.323
.0100	.534
.100	.936
.400	1.40
1.00	1.89
4.00	3.16
10.0	4.56
40.0	8.64
80.0	11.41

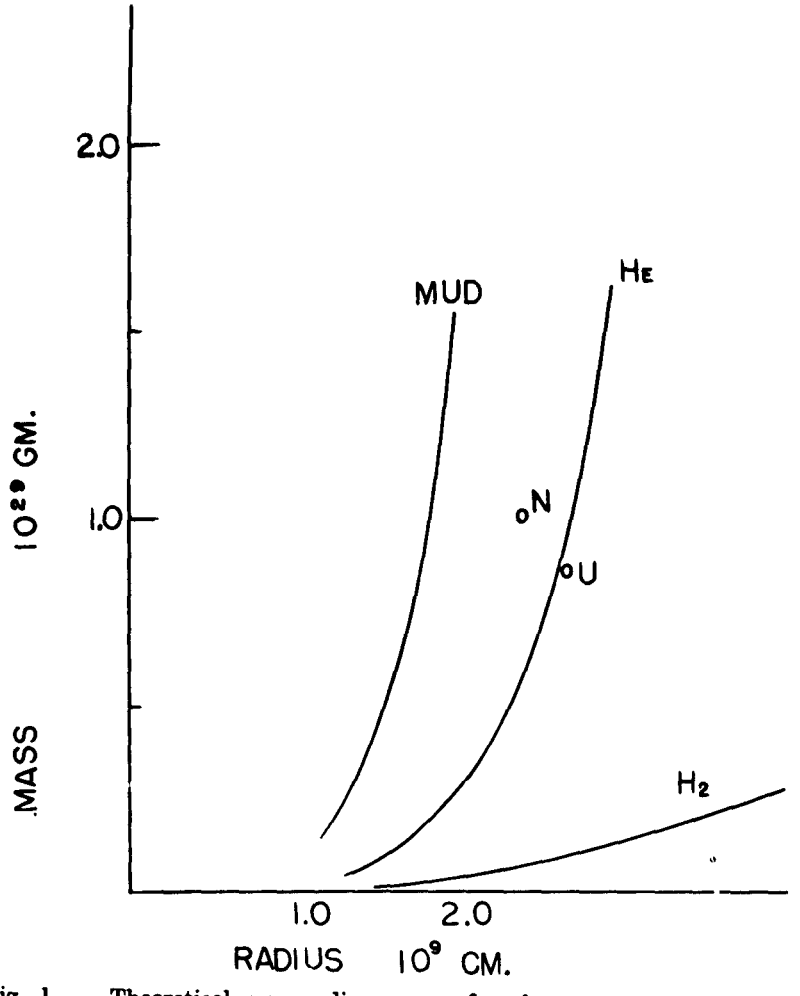

Fig. 1. — Theoretical mass-radius curves for planets composed of pure hydrogen, helium or mud. The small circles correspond to the empirical values for Uranus and Neptune

TABLE II

Mass-Radius Relation for Cold Helium Planets

Mass (10^{27} gm)	Radius (10^9 cm)
55.8	2.12
101.2	2.40
166	2.63
194	2.71
303	2.92
392	3.04
461	3.10

Mud is considered to be a mixture in the proportions by numbers of atoms given in Table III.

TABLE III

Composition of Mud

Element	Relative Abundance
C	3.5
N	6.6
O	21.5
Ne	8.6
Si	1.0
Fe	0.60

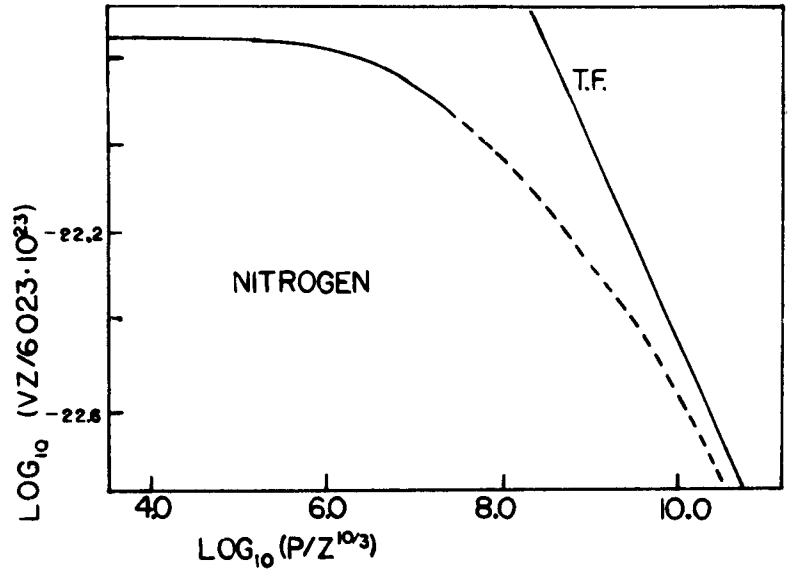

Fig. 2. — Illustrating the extrapolation of pressure density relations. The curve T. F. is the equation of state of nitrogen calculated by the Thomas-Fermi method. The main curve represents measured values of volume as function of pressure in its solid portion while the dashed portion is the extrapolation used in this paper. The units of volume and pressure are those appropriate to the Thomas-Fermi method for atomic number Z.

The densities of the pure individual elements were obtained by interpolating between the experimental results of Bridgman or Stewart and the Thomas-Fermi Equation of state. Figure II illustrates the interpolated equation of state for nitrogen. Assuming that the molar volumes are additive, the density ρ_m of cold mud at any pressure is then given by

$$\frac{1}{\rho_m} = \sum \frac{w_i}{\rho_i}$$

wherein w_i is the mass fraction of the i^{th} constituent and ρ_i is the density of the i^{th} constituent at the given pressure. The equation of state so estimated is displayed in Table IV.

TABLE IV

Equation of State of Cold Mud

$p(10^{12}$ dynes/cm$^2)$	ρ(gm/cm^3)
0.01	1.97
0.04	2.18
0.10	2.49
0.40	3.29
1.00	3.99
4.00	5.87
10.00	7.89

The densities of Mud as a function of pressure are fairly well fitted by the equation

$$\rho^3 = 6.85 + 50\,p$$

where ρ is in units of gm cm^{-3} if p is in units of 10^{12} dynes/cm^2. Consequently the mass-radius diagram of mud planets can be deduced from the Emden Polytrope of index 0.5 (For details on the procedure see DeMarcus 1959, p. 422). The mass radius relation of mud planets thus obtained is also displayed in Table V and Fig. I. Figure I also contains points representing the masses and radii of Uranus and Neptune. From the figure it can be seen that

TABLE V

Mass-Radius Relation of « Mud » Planets

Radius (10^9 cm)	Mass (10^{27} gm)
.655	2.77
.856	7.21
1.08	17.9
1.28	36.2
1.74	148.2

a model planet of Uranus can be constructed of almost pure helium but that Neptune requires at least a sizeable admixture of mud. Of course, as will be shown below, Uranus could equally well be fitted by a model made up of a mixture of mud and hydrogen since the density of helium can always be matched by a mixture of mud and hydrogen.

III. Model Planets of Uranus and Neptune

The values adopted for the physical parameters of Uranus and Neptune are given in Table VI. The quantity I/MR^2 is the ratio of the mean moment of inertia to the product of mass and

TABLE VI

Mechanical Data for Uranus and Neptune

	Uranus	Neptune
Mass (10^{27} gm)	86.0	102.8
Mean radius (km)	23,700	21,500
Mean density (gm/cm^3)	1.56	2.47
Ellipticity	0.06	0.017
Period (hr)	10.8	15.7
I/MR^2	0.34	0.30
J		.0074

Sources : Masses and Radii, Kuiper (1952) ; dynamic ellipticity and J for Neptune, Brouwer and Clemence (1961) ; rotational periods and visual ellipticity for Uranus, Allen (1955) ; I/MR^2 estimated from Radau-Darwin approximation.

squared radius of the planet and would be 0.40 if the planets were homogeneous. The quantity J is a measure of the departure of the external gravitational potential of the planet from spherical symmetry. Explicitly the external gravitational potential is assumed to be

$$V = -\frac{GM}{r}\left[1 - \left(\frac{2}{3}\right)\left(\frac{Ja^2}{r^2}\right) P_2(\cos\varphi) + \ldots\right]$$

where G is the gravitational constant, M the mass of the planet, a the equational radius of the planet, r the distance from the center of mass of the planet, φ is the co-latitude and $P_2(\mu)$ is the Legendre polynomial of order 2 normalized so that $P_2(1) = 1$.

The ellipticity ε of the surface, $(a - b)/a$) (where b is the polar radius), is given by numerous authors, for example Spencer-Jones (1954) as

$$\varepsilon = J + \tfrac{1}{2} m$$

with

$$m = \frac{3\omega^2}{4\pi G\rho}$$

Here ρ is the mean density of the planet and ω is its angular speed of rotation The moment of inertia can then be estimated from the Radau-Darwin approximation

$$\frac{I}{MR^2} = \frac{2}{3} - \frac{4}{15}\sqrt{\frac{5m}{2\varepsilon} - 1}$$

A possible model of Uranus or Neptune must have a density distribution $p(r)$ defined for $0 \leqq r \leqq R$ where r is the planetary radius and moreover must satisfy the two conditions

$$M = 4\pi\int_0^R r^2\rho(r)dr$$

$$I = \frac{8\pi}{3}\int_0^R r^4\rho(r)dr$$

It is also customary to add the extremely plausible condition that $d\rho/dr \leqslant 0$ for $0 \leqq r \leqq R$ i. e. the density must not increase with radius. These three conditions are not enough to determine the

density distribution completely but the combination does markedly decrease the flexibility of choice from the case where the mass alone is given.

In this paper, four models of each planet have been considered. These are two and three shell models plus a Laplace model and another model, recently discovered by DeMarcus, which shares with the Laplace model the welcome circumstance that Clairaut's equation for the ellipticity can be integrated in closed form.

A. Two Shell Models.

These models have only two different values of the density $\rho(r) = \rho_c$ if $0 < r < \beta R$ and $\rho = \rho_m$ if $\beta R < r < R$ with $0 < \beta < 1$. The mass is given by

$$M = \frac{4\pi}{3} R^3[\rho_m + \beta^3(\rho_c - \rho_m)]$$

and their moment of inertia by

$$I = \frac{8\pi}{15} R^5[\rho_m + \beta^5(\rho_c - \rho_m)]$$

The mass and moment of inertia thus serve to fix only two of the necessary three parameters. In this investigation we have arbitrarly set $\rho_m = 1$ gm/cm^3 in order to obtain definite models. The pressure $p(r)$ as a function of radius is then obtained by integrating

$$dp/dr = -g(r)\,\rho(r)$$

where $g(r)$ is the local acceleration of gravity at the surface of mean radius r.

B. Three Shell Models

These are defined by $\rho(r) = \rho_1$ if $0 < r < \beta_1 R$, $\rho(r) = \rho_2$ if $\beta_1 R < r < \beta_2 R$ and $\rho(r) = \rho_3$ if $\beta_2 R < r < R$ for which

$$M_1 = \frac{4\pi}{3} R^3[\rho_3 + \beta_2^3(\rho_2 - \rho_3) + \beta_1^3(\rho_1 - \rho_2)]$$

$$I = \frac{8\pi}{15} R^5[\rho_3 + \beta_2^5(\rho_2 - \rho_3) + \beta_1^5(\rho_1 - \rho_2)]$$

All five parameters are determined from the two preceding relations by arbitrarily setting $\rho_s = 25$ gm/cm^3, $\beta_1 = .20$ and $\rho_1 = 1$ gm/cm^3. The pressure is determined as before and the somewhat cumbersome expressions are not reproduced here.

C. The Laplace Models.

These are defined by assuming

$$\rho(r) = \rho_c(\sin kr/kr)$$

which has two adjustable parameters, the central density ρ_c and the parameter k which is a reciprocal length.

Consequently fixing the mass and moment of inertia uniquely defines a density distribution for a model planet and again the pressure can be calculated at every level.

D. D(β) Models.

In this paragraph let $r = \beta R$, $\rho(r) = \bar{\rho}_0 \delta(\beta)$ where $\bar{\rho}_0$ is the mean density of the planet to be modeled and R is its radius. Then these models have densities given by

$$\delta(\beta) = \frac{(1+a)^{5/2} \exp\left\{\frac{1}{4} a(1-\beta^2)\right\}\left[1 - \frac{a\beta^2}{6} - \frac{a^2\beta^4}{6}\right]}{(1+a\beta^2)^{5/2}}$$

The pressure is then found to be given by

$$p = \frac{4\pi}{3} G\bar{\rho}_0^2 R^4 [\varphi(1, a) - \varphi(\beta, a)]$$

with

$$\varphi(\beta, a) = \frac{\beta^3}{6}\left(\frac{1+a}{1+\beta^2 a}\right)^3 \exp\left\{\frac{1}{2} a(1-\beta^2)\right\}$$

$$+ \frac{1}{3}\frac{(1+a)^3}{a} \exp\left\{\frac{1}{2}(1+a)\right\}\left[E_3\left(\frac{1}{2}\right) - \frac{E_3\left(\frac{1+a\beta^2}{2}\right)}{(1+a\beta^2)^3}\right]$$

In the preceding expression, $E_3(x)$ is the usual exponential integral defined via

$$E_N(x) = \int_1^\infty \frac{e^{-xu}}{u^N}\, du$$

With the exception of the three-shell model, the preceding models all share the happy circumstance that the ellipticities they would assume when rotating with angular speed ω can be worked out in closed form. For the two shell model and the Laplace model, the relevant formulae can be found in Darwin (1877, 1900). For the D(β) model one of us has recently found

$$\epsilon = \frac{\frac{5}{2}m}{2 + a}$$

with

$$m = \frac{3\omega^2}{4\pi G\bar{\rho}_0}$$

$\bar{\rho}_0$ being the mean density of the planet. The parameter a should not exceed 2 numerically for a meaningful model since densities at some values of β would be negative.

IV. Estimation of Compositions

The employment of one of the preceding models furnishes an estimate of the pressure and density at every point within the planets Uranus and Neptune. Bounds on the compositions at every point in the planet may now be computed under the following assumptions :

(a) The relevant mechanical data for the Uranus and Neptune as given above in Table VI are correct.

(b) The heavier elements of the planet have the same relative abundances as our « mud ».

(c) The equations of state of helium, hydrogen and mud are correct at 0°K as given in the paper.

(d) The planets are cold i. e. have the same densities at the pressures in question that they would have if cooled to the absolute zero of temperature.

(e) Partial molar volumes of a mixture of hydrogen, helium and mud are additive.

(f) Hydrostatic equilibrium holds throughout each planet.

At a given point in the planetary model where the density is ρ and the pressure p the following relation then holds

$$\frac{1}{\rho} = \frac{w_1}{\rho_H} + \frac{w_2}{\rho_{He}} + \frac{w_3}{\rho_m}$$

where w_1, w_2 and w_3 are respectively the fractions by mass of hydrogen, helium and mud and ρ_H, ρ_{He}, ρ_m are the densities of hydrogen, helium and mud at the pressure p. Naturally this relation makes sense only if $\rho_H < \rho < \rho_m$ which is the case for the models considered herein. A second relation for the mass fractions follows from their definition

$$w_1 + w_2 + w_3 = 1$$

These two relations between the mass fractions are not sufficient to determine them. However limits can be set on the mass fractions. For example w_1 cannot exceed

$$\max w_1 = \frac{\rho_H}{\rho}\left(\frac{\rho_m - \rho}{\rho_m - \rho_H}\right)$$

which is obtained by setting $w_2 = 0$. Also w_1 cannot be less than the larger of the two numbers 0 and

$$\frac{\rho_H}{\rho}\left(\frac{\rho_{He} - \rho}{\rho_{He} - \rho_H}\right)$$

Consequently, a minimum and a maximum value of w_1 can be obtained at every level and the corresponding minimum or maximum value for the total mass fraction of the whole planet is obtainable by summing over all levels in the planet. The minimum value of w_2 is 0, for helium can always be simulated by an appropriate mixture of hydrogen and mud. The maximum possible value of w_2 is

$$\max w_2 = \frac{\rho_{He}(\rho_m - \rho)}{\rho(\rho_m - \rho_{He})} \qquad \rho > \rho_{He}$$

or

$$\max w_2 = \frac{\rho_{H_e}(\rho - \rho_H)}{\rho(\rho_{H_e} - \rho_H)} \qquad \rho < \rho_{H_e}$$

The results obtained in this way by using the model planets described in this paper are given in Table VII and Table VIII.

TABLE VII

Extreme Hydrogen Mass Fractions

Uranus			Neptune		
Model	Max w_H	Min w_H	Model	Max w_H	Min w_H
2 Shell	.235	.060	2 Shell	.137	.038
3 Shell	.250	.101	3 Shell	.158	.031
Laplace	.232	.035	Laplace	.140	.000
D(β)	.231	031	D(β)	.142	.000

TABLE VIII

Maximum Helium Mass Fraction

Max w_{H_e}

Model	Uranus	Neptune
2 Shell	.810	.432
3 Shell	.710	.550
Laplace	.949	.616
D(β)	.926	.637

We thus conclude, on the basis of the stated assumptions, that Uranus and Neptune have a much smaller fraction of their mass attributable to hydrogen than do Jupiter and Saturn. In fact it would seem that Uranus cannot be more than about 23 % hydrogen by mass while Neptune cannot be more than about 14 % hydrogen by mass.

V. Discussion of Errors

To give some idea of the importance of the assumptions which have been made, re-evaluation of $(w_H)_{max}$ has been done when some of the assumptions were changed. Table IX below shows the effects of these changes on the maximum hydrogen mass fraction.

Table IX

Changes in the Maximum Mass Fraction of Hydrogen Due to Changes in the Fundamental Assumptions

Change in Assumptions	Change in (w_H) max	
	Uranus	Neptune
Densities of hydrogen assumed 5 % smaller than values given by DeMarcus	—.013	—.007
Density of helium assumed 5 % larger than given in Table I	0.0	0.0
Density of mud assumed 20 % larger than given in Table IV	.023	.033
Radius of planet assumed 1 % smaller than given in Table VI	—.006	—.007
Moment of Inertia assumed to be 0.25 MR^2	—.0	
Moment of Inertia assumed to be 0.40 MR^2		.030

The reader may infer the effects of some other errors not mentioned explicitly in the Table above. For example the fact that the temperatures are not absolute zero lowers all densities from the absolute zero values assumed. But estimates of the effects of the density changes are given above and the reader may form his own opinion as to the magnitude of the temperature error. A similar set of calculations has been made for the changes in the maximum helium abundance following changes in the assumptions. Except for the change in the densities of helium itself, the effects are all much smaller than in the case of the hydrogen abundances. If the density of helium is raised 5 % with respect to the values given in

Table I, the respective change in of maximum helium abundances are —.004 and +.047 for Uranus and Neptune respectively.

REFERENCES

ALLEN, C. W., *Astrophysical Quantities*, The Athlone Press, 1955.

BROUWER, D. and CLEMENCE, G. M., *Planets and Satellites*, University of Chicago (Chapter 3), 1961.

DEMARCUS, W. C., *Astronomical Journal*, **63**, 2, 1958.

DEMARCUS, W. C., *Handbuch der Physik*, Springer Verlag, Vol. LII, **444**, 1959.

KUIPER, G. P., *The Atmospheres of the Earth and Planets*, University of Chicago, p. 308, 1951.

RAIMES, S., *Philosophical Magazine* (7), **43**, 327, 1952.

RAMSEY, W. H. and MILES, B., *Monthly Notices Roy. Astronom. Soc. London*, **112**, 234, 1952.

SPENCER-JONES, Sir HAROLD, *The Earth as a Planet*, University of Chicago, p. 9, 1954.

STEWART, J. W., *Journal of Phys. Chem. Solids*, **1**, 146, 1956.

UREY, H. C. and SUESS, H. C., *Rev. Mod. Phys.*, **28**, 53, 1956.

DISCUSSION DES COMMUNICATIONS 1 à 5.

J. C. Pecker (2). — J'ai lu voici quelques années le travail de Parker expliquant une importante fraction du géomagnétisme par les mouvements convectifs dans le noyau terrestre. Que faut-il aujourd'hui en penser à la lumière des calculs de Kopal?

H. Robe (2). — Mr. Kopal a étudié la convection dans le manteau et non dans le noyau ; de plus, il s'agit uniquement de convection due à une instabilité thermique et l'influence du champ magnétique n'a pas été considérée.

J. C. Pecker (2). — Comment pourrait-on envisager que ces convections affectent le moment d'inertie de la Terre? Par ailleurs est-il possible qu'une action corpusculaire solaire puisse freiner le manteau sans freiner le noyau? Ces questions se posent naturellement à qui veut tenter d'interpréter la relation étroite entre rotation terrestre et activité solaire mise en évidence par Danjon.

H. Robe (2). — L'existence de courants de convection (matière moins dense) et descendants (matière plus dense) affecte la distribution de densité dans le manteau et modifie donc les moments d'inertie de la terre ; il est toutefois difficile dans l'état actuel de la théorie de définir les cellules de convection les plus stables pour déterminer l'ordre des moments modifiés par la convection.

W. C. De Marcus (2). — Many people think the earth is chemically inhomogeneous from depth 413 Km down to approximately 900 Km. Does not this possibility throw grave doubt on the significance of the equations you have used?

H. Robe (2). — Dr. Kopal does not mention any question concerning this fine structure of the mantle ; certainly, it would be difficult to discuss rigorously the influence of such an inhomogenuity.

H. E. Suess (4). — One of the basic questions of Dr. Öpik's, and also Dr. DeMarcus' talk is the mechanism of separation of hydrogen from helium. We observe in meteorites a separation of He from Ne and Ne from Ar etc. that at least in part cannot have been caused by chemical processes. Is it possible that this separation of the rare gases from each other could have been caused by a similar process as that which led to a separation of hydrogen from helium in the outer planets? In the case of the meteorites slow temperature condensation cannot be an explanation because of the observed isotope fractionation in Ne and Ar.

E. J. Öpik (4). — Differentiation of noble gases and their isotopes in meteorites may have been achieved by escape and diffusion processes in a residual interplanetary nebula, of the order of 10^{-6} to 10^{-12} of a planetary mass. It could not have taken place at an early stage when the mass of a nebular ring was of planetary order.

H. Spinrad (4). — We now may make crude spectroscopic estimates of the H_2 atmosphere, and presumably H_2/H_e ratio by number in the Jovian atmosphere. The partial pressure of molecular hydrogen is compared to total pressures derived from the line widths of the NH_3 and CH_4 lines in the red region of the spectrum. If the H_2 and CH_4 and NH_3 absorptions are at comparable optical depths, then the H_2/atmos. ratio $\geqslant 3$ %. This estimate will be improved shortly.

E. J. Öpik (4). — Dr. Spinrad's estimate is in reasonable agreement with mine, made by a different method, which gave 2.3 % H_2.

C. Sagan (4). — Your conclusion that Jupiter has an internal source of radiation energy depends on an estimate of the fraction of solar energy absorbed. But the bolometric albedo of Jupiter is very poorly known. If there is substantial absorption by Jupiter in the near infrared, might the radiative output and input then be equal?

E. J. Öpik (4). — The bolometric albedo of Jupiter is somewhat uncertain on account of the near infrared. This covers about 40 per cent of the solar energy spectrum and the uncertainty in albedo must be less than this. The excess of 160 per cent over solar input cannot be accounted for in this manner, and much greater is the excess of radiation for Saturn. Both the giant planets must possess significant energy sources of their own.

J. Rösch. — A propos de cette session, je signale le résultat récent obtenu par H. Camichel et moi-même par la discussion de nos observations lors du passage de Mercure devant le Soleil le 7 novembre 1960. Nous concluons aux valeurs suivantes : *diamètre apparent à la distance unité* : $6''75 \pm 0''02$; *densité* : $5{,}30 \pm 0{,}04$, soit un peu moins que la Terre.

SECTION II

THE SURFACES AND ATMOSPHERES

6. — COOPÉRATIONS INTERNATIONALES POUR L'ÉTUDE DES PLANÈTES : RAPPORT INTRODUCTIF

AUDOUIN DOLLFUS
Observatoire de Paris, France

Les diverses communications exposées durant ce colloque résument les travaux originaux effectués par leurs auteurs. Chaque groupe de travail fait usage de ses propres ressources et progresse dans sa propre spécialité. Par suite, un sérieux besoin de coopération s'est fait sentir entre les différents Observatoires et groupes de recherches. Pour tirer tout le parti des efforts individuels, il apparaît désirable de mettre sur pied des coordinations, des nomenclatures unifiées, des programmes d'observation collectifs, des centres de documentation.

Les problèmes posés par de telles coopérations sont particulièrement délicats. Ils doivent procéder d'une équitable justice, tenir compte des divergences d'opinions, des conséquences politiques, etc. D'autres écueils sont la stérilité par excès de procédure ou de discussions, sur-organisation ou influences trop prépondérantes. Seul un corps constitué international, de très haut niveau, universellement reconnu et expérimenté par une longue pratique est à même d'entreprendre une telle tâche avec une efficacité suffisante. Cet organisme supérieur dont l'autorité et l'expérience remontent déjà à plus de quarante deux ans est évidemment l'*Union Astronomique Internationale*. De façon plus particulière, les problèmes de coordination dans l'étude des planètes sont assumés par la Commission 16 de l'U.A.I. « Étude Physique des Planètes et Satellites ».

Consciente du très rapide développement des recherches planétaires au cours des dernières années, la Commission 16 de l'U.A.I. apporte tout son soin à faire face aux besoins croissants, à préparer les problèmes futurs, à éviter toute rupture ou crise

et à rester disponible pour toutes questions nouvelles qui se poseraient à elle.

Avant d'exposer les projets internationaux développés actuellement sous les auspices de l'Union Astronomique Internationale, je me propose de résumer sommairement quelques-uns des travaux réalisés ces dernières années par cette Commission.

Les problèmes de *nomenclature* surgirent pour la première fois en 1955 à propos de la planète Mars. Une Sous-Commission particulière a été constitué dans le but d'établir une nomenclature martienne internationalement unifiée. Le travail a été achevé en 1958 par la publication de cartes, listes de noms et recommandations, disponibles pour tous les observateurs, et devenues actuellement d'un emploi courant.

Les problèmes de nomenclature et de cartographie se posèrent de nouveau en 1960 pour la Lune à la suite du développement considérable des recherches lunaires et des dangers inhérents au manque de coordination. Vers la même époque, la découverte de nouveaux territoires sur la face arrière de la Lune posa un nouveau problème de nomenclature fort intéressant. Ces questions ont été résolues grâce aux travaux de l'U.A.I. à l'Assemblée Générale de Berkeley en 1961. Un comité a été également constitué pour préparer le chemin vers les importants développements prévus dans l'exploration lunaire à venir.

Des programmes internationaux d'observations ont également été proposés. En particulier, une importante campagne d'observation de la planète Mars a été coordonnée à l'occasion des oppositions périhéliques de 1954, 1956 et 1958. Grâce aux contributions financières du Comité Exécutif et de plusieurs autres organismes, une coopération a pu s'établir entre différents Observatoires, particulièrement aux États-Unis, en France, en Grèce, en Italie, au Japon et en Afrique du Sud. Plusieurs centaines de photographies de Mars ont été recueillies et groupées. Plusieurs milliers de mesures de polarisation ont été relevées sur Mars ainsi que des mesures photométriques et des déterminations photométriques précises. Les

résultats obtenus par ce gros effort international ont déjà fait l'objet de plusieurs publications ; quelques conclusions nouvelles seront également données au cours de ce colloque et d'autres résultats de cette large coopération seront encore publiés prochainement.

Un phénomène astronomique s'est présenté le 7 novembre 1960 comme circonstance particulièrement propice à des observations coordonnées. A cette date, la planète Mercure se projeta devant le disque solaire. Ce passage fournissait une occasion exceptionnelle de déterminer de façon précise le diamètre du globe de Mercure primitivement très mal connu. La planète se présentait alors comme un disque noir sur fond brillant de la photosphère solaire. Trois procédés de mesures ont été recommandés à la Commission : avec micromètre à fils — avec micromètre à double image — par photométrie à travers un diaphragme circulaire dont le diamètre est légèrement supérieur à celui de la planète, alternativement centré sur l'image et la planète ou sur une région voisine du disque solaire.

Dix observatoires participèrent à ces observations. Six d'entre eux ont pu recueillir des données, les quatre autres ayant eu un ciel couvert. Le résultat des mesures donne pour le diamètre de Mercure la valeur 6''63 $\pm$ 0''07 ; la précision atteint 1 %. Les observations antérieures présentaient des désaccords d'au moins 5 %. Ces résultats seront communiqués dans l'un des prochains numéros de la revue « Icarus ».

Un autre objet de coopération fut la découverte en avril 1960 d'une tache brillante sur le disque de Saturne à la latitude élevée de + 55°. Ce phénomène est très rare. La circonstance imprévue fournit la première possibilité d'une détermination précise de la période de rotation de la planète à cette latitude élevée. La Commission a demandé, par l'intermédiaire des Circulaires de l'U.A.I., que des observations de passage au méridien soient relevées. Au moins neuf Observatoires ont envoyé des mesures utilisables et la période de rotation résultante a été trouvée de 10 h 39^{m}, 9. La

manière dont la tache brillante s'est désagrégée a pu également être précisée.

L'un des buts d'un organe de coopération internationale doit être aussi de recommander des *instruments d'observation nouveaux* et de les rendre accessibles aux observateurs disponibles pour participer aux programmes collectifs.

Deux appareils ont été spécialement étudiés dans ce but par la Commission pour l'Étude Physique des Planètes de l'U.A.I.

Le premier est un *polarimètre visuel de Lyot*. Cet instrument a pour but de recueillir visuellement des mesures polarimétriques avec une précision aussi élevée que 1/1000, sur de petites régions de la surface du disque des planètes. Le disque planétaire apparaît strié par des franges d'interférence ; l'observateur égalise le contraste de ces franges sur la région du disque qu'il a choisi, pour deux positions alternatives d'une manette. Ces polarimètres sont construits par la société française Jobin & Yvon. Les Observatoires dont voici la liste sont pourvus de tels instruments ou le seront très prochainement et peuvent de la sorte participer à des programmes collectifs : Meudon (France) — Athènes (Grèce) — Naini Tal (Indes) — Kwasan (Japon) — Gênes (Italie) — Harvard (U.S A.) — Tucson, Arizona (U.S.A.) — Jet Propulsion Laboratory, Californie (U.S.A.).

Le second instrument est un *micromètre biréfringent*. Cet appareil est basé sur un principe nouveau étudié à l'Observatoire de Meudon ; il est reproduit en plusieurs exemplaires par la Société R. Danger. Quatre instruments sont actuellement en usage. Le but est de permettre l'utilisation de la technique de la double image avec des télescopes de grand diamètre et pour des séparations angulaires importantes. Par suite, le micromètre biréfringent est capable de donner des mesures de diamètres planétaires en plusieurs longueurs d'ondes, avec une précision voisine de quelques millièmes seulement. Des déterminations de diamètres ont été réalisées au Pic du Midi depuis déjà dix ans avec le prototype de cet instrument, la sensibilité avoisinait 3/1000. Des observations plus nombreuses

seraient encore nécessaires et pourront être recueillies dans différentes autres stations.

Nous allons maintenant examiner les programmes collectifs d'*observations photographiques de Vénus en lumière ultra-violette* actuellement en cours de réalisation entre le 1er mai et le 1er août 1962. L'objet de cette coopération est l'étude de la formation, du mouvement et de l'évolution des nuages brillants que l'on peut déceler dans l'atmosphère de la planète en utilisant la lumière ultra-violette. Une limite inférieure de la période de rotation du globe pourra également être obtenue ; les lois qui président aux mouvements convectifs dans l'atmosphère de la planète pourront peut-être être précisées.

Les photographies recueillies chaque jour dans un seul observatoire ne permettent pas de résoudre un tel problème ; l'évolution des structures atmosphériques est si rapide que l'on ne peut généralement pas reconnaître les formations d'un jour à l'autre. Par contre, la coopération entre des Observatoires répartis sous différentes longitudes permet une telle tâche ; elle entraîne un programme collectif international.

Depuis plusieurs années, un début de coopération a été développé entre l'Observatoire du Pic du Midi (France), la station privée de Brazzaville (Congo), l'Observatoire de l'Université de New-Mexico (U.S.A.). Ces campagnes d'observation ont permis de trouver à plusieurs reprises trois ou quatre journées consécutives durant lesquelles des photographies furent recueillies à des intervalles d'environ douze heures. Ces documents seront reproduits dans la prochaine publication des Transactions de l'U.A.I. Il apparaît avec évidence sur ces images que des formations nuageuses peuvent être bien reconnues après un intervalle de douze heures ; par contre, elles le sont très rarement après vingt quatre heures. Cependant, les clichés recueillis sont encore insuffisants pour permettre de résoudre les problèmes proposés.

Une nouvelle campagne d'observation beaucoup plus complète se déroule actuellement. Voici la liste, relevée dans l'ordre des

longitudes décroissantes, des Observatoires qui participent actuellement à ce programme et qui ont accepté de prendre des photographies ultra-violettes de Vénus chaque soirée de beau temps : Observatoire Lick (U.S.A.) — Observatoire Lowell (U.S.A.) — Station du New-Mexico (U.S.A.) — Observatoire du Pic du Midi (France) — Observatoire de Milan (Italie) — Station privée de Brazzaville (Congo) — Observatoire National d'Athènes (Grèce) — les Observatoires du Concile Astronomique de l'Académie des Sciences (U.R.S.S.) — Observatoire Kwasan (Japon).

J'ai le plaisir de pouvoir préciser maintenant que cet effort international s'annonce déjà comme un succès. Lorsque j'ai quitté la France pour assister à ce colloque, j'étais déjà informé qu'au moins 80 clichés ont été réalisés depuis le 1er mai. Au moins 54 clichés couvrent la période du mois de mai seulement. Une première étude des dates et heures relatives à chaque observation révèle que plusieurs périodes d'au moins trois journées consécutives sont couvertes par trois images quotidiennes au moins. Par suite, cette coopération permettra probablement de résoudre plusieurs des problèmes encore inconnus de la circulation atmosphérique de Vénus et de sa rotation.

La dernière partie de ce rapport sera consacrée aux *Centres Internationaux de Documentation sur les photographies planétaires.*

Depuis plusieurs années, le désir a été exprimé fortement et fréquemment que soient groupées dans des Centres de Documentation les très nombreuses photographies planétaires obtenues depuis le début du siècle dans les endroits les plus divers et actuellement réparties dans le monde entier. Les études synoptiques des planètes concernant de nombreuses années sont presque impossibles à entreprendre si la documentation n'est pas disponible dans un même lieu de travail. De plus, des collections de photographies de toute première valeur, recueillies par les meilleurs spécialistes à la suite de très longues et très patientes observations nocturnes, resteront complètement perdues pour les études planétaires aussi longtemps qu'elles demeureront des collections de néga-

tifs inconnus déposés dans les archives des Observatoires où elles furent prises.

Le projet très important de grouper les collections de photographies planétaires a été discuté avec beaucoup de soin durant la dernière Assemblée Générale de l'U.A.I. ; un Comité spécial a été désigné dans ce but. Une résolution a été adoptée pour aider la constitution d'au moins deux Centres de Documentation, dont l'un serait situé en Europe et l'autre aux États-Unis.

J'ai le plaisir de pouvoir faire connaître officiellement aujourd'hui que l'emplacement des deux Centres de données de l'Union Astronomique Internationale est maintenant désigné. L'un des Centres sera à l'*Observatoire Lowell*, Flagstaff, Arizona (U.S.A.), et l'autre à l'*Observatoire de Meudon* (France).

Le Dr. J. HALL, Directeur de l'Observatoire Lowell, m'a écrit que son personnel entreprend actuellement la tâche considérable de reproduire le très grand nombre de photographies planétaires qui ont été recueillies depuis un demi-siècle dans cette station afin de les rendre immédiatement disponibles à la consultation de toute personne intéressée par les recherches planétaires.

Je désire aussi donner ici des informations directes sur le travail actuellement développé au Centre de Meudon avec l'assistance de mes collaborateurs, et plus particulièrement de Monsieur MARIN. Nous avons entrepris de grouper et reproduire tout d'abord les photographies consacrées à la planète Mars. 1.108 clichés de Mars sont actuellement réunis à Meudon et facilement consultables. 740 clichés sont reproduits en diapositifs sur verre, 368 clichés sont provisoirement reproduits sur papier. Cette très importante collection provient des Observatoires dont voici la liste :

— *Observatoire du Pic du Midi* (France)	: 659 clichés reproduits sur verre
— *Observatoire Lick* (U.S.A.)	: 130 clichés sur papier
— *Observatoire de Johannesburg*	: 76 clichés reproduits sur verre
— *Observatoire Lowell* (U.S.A.)	: 63 clichés sur papier

— *Steward Observatory* (U.S.A.) : 50 clichés sur papier
— *Observatoire Kwasan* (Japon) : 54 clichés sur papier
— *Observatoire Bloemfountein* (Union Sud Africaine) : 24 clichés sur papier
— *Observatoire Mont Wilson et Palomar* (U.S.A.) : 21 clichés sur papier
— *Observatoire de Haute-Provence* (France) : 5 clichés reproduits sur verre
7 clichés sur papier
— Observatoires *Yerkes* (U.S.A.), *Mc Donald* (U.S.A.), *de Stalingrad* (URSS) *The National Science of Tokyo* (Japon) : 19 clichés sur papier

Tous les clichés diapositifs sur verre sont classés et ordonnés dans des casiers à double entrée. Une même rangée de boîtes contient les documents montrant la planète au cours d'une même opposition, chaque boîte successive groupant tous les clichés relatifs à un même intervalle de longitude du méridien central croissant de 30° en 30° d'une boîte à la suivante. Les rangées perpendiculaires montrent la planète aux oppositions successives. Il est facile de la sorte de comparer une même région martienne d'une année à la suivante.

Un catalogue détaillé de cette documentation est disponible. Chaque cliché reporté dans ce catalogue peut être reproduit et envoyé sur demande. Les chercheurs qui désireraient consulter cette documentation internationale sont les bienvenus à l'Observatoire de Meudon pour tirer parti de cette collection.

Malheureusement, cette importante collection présente encore des lacunes. Plusieurs séries de photographies martiennes n'ont pu encore être rendues accessibles et reproduites. En raison de l'importance de ce travail, nous cherchons à compléter ces lacunes aussi rapidement qu'il nous est possible. Bien entendu, le travail photographique de copies de nombreux clichés reste important et coûteux ; il représente une charge évidente pour l'Observatoire

concerné. Quoi qu'il en soit, nous espérons que les Directeurs de ces Observatoires comprendront l'importance du problème et pourront apporter leur concours, soit en rendant disponibles pour l'Union Astronomique Internationale les collections de clichés originaux négatifs recueillis dans leur établissement, soit même en contribuant au travail photographique de leur reproduction.

Je me permets de solliciter ces contributions parce que le groupement de tous les documents photographiques planétaires existants prend une importance particulière à l'époque critique actuelle où s'ouvre l'exploration directe du système solaire et aussi parce que tout document manquant ne peut que réduire la valeur des études synoptiques sur les planètes déjà si difficiles à entreprendre.

7. — GENERAL REPORT ON RADIATION TRANSFER IN PLANETS : SCATTERING IN MODEL PLANETARY ATMOSPHERES

H. C. VAN DE HULST and W. M. IRVINE
Leiden Observatory, Leiden, Netherlands

I. INTRODUCTION

There is a vast literature on radiative transfer theory. Chandrasekhar's book in 1950 was very comprehensive, but work has continued, and by now we may examine besides numerous papers and reports at least five books for further detailed methods and results ([1]) ([2]) ([9]) ([19]) ([25]). The work of Ueno, consisting of about 20 papers, might also be considered as a book (see for instance ([27])).

In front of this pile of achieved work we have asked the simple question : *To what extent is this work helpful in interpreting present (or future) observations of planets*? To our surprise the answer to this question is still disappointing. There are still many simple questions to which one would like to have a simple answer, which just is not available. It turns out that either the question has never been raised in that form, or the answer has been obtained in principle, but nobody has gotten around to computing the values of the required functions.

We feel that there often has been undue emphasis on mathematical method and form of presentation, even in the work of the professed astrophysicists. In our opinion, a proof of existence or of convergence may be avoided whenever it is possible to refer to the perfectly definite physical meaning of the quantities involved. We think this is legitimate in a study of models aimed at application to astrophysics. And more emphasis could still be placed on graphs and tables as end products, rather than formulae. Much has been done in this direction for finite plane-parallel atmospheres both with isotropic and with Rayleigh scattering, but even for these relatively simple phase functions there still is an uncomfortable

gap for optical thicknesses in the range $1 \leqslant \tau_1 < \infty$. Transfer problems of direct physical importance, say, referring to the radiation balance and the greenhouse effect, or to polarization of light diffusely reflected from clouds, have often been made with the crudest mathematics. This could be remedied fairly easily.

In reviewing the data now available we have taken an earlier review ([16]) in 1949 as a convenient starting point. In the present paper, however, our aim has been confined to reviewing the properties of simple models. We omit a critical discussion of observational data and any discussion of the physical theory of pressure and temperature distribution.

The review is grouped under five headings :

II. Nearly isotropic scattering,

III. The scattering diagram of large drops,

IV. The method of successive scattering,

V. Absorption bands,

VI. Variations on the standard problem.

II. Nearly isotropic scattering

We include isotropic scattering and Rayleigh scattering in this section because they both have been used rather extensively in transfer theory and because Rayleigh scattering is not vastly different from isotropic. In particular, we define the *asymmetry factor* g for a given particle phase function $\Phi(\cos\alpha)$ as the weighted mean of the cosine of the scattering angle with the phase function as weighting function. That is,

$$g = \overline{\cos\alpha} = \frac{1}{2}\int_{-1}^{1} d(\cos\alpha)\ \cos\alpha\ \Phi(\cos\alpha) \tag{1}$$

(when necessary, an average over polarizations must be included). Then g is zero in both these cases. This means that in many model calculations not involving polarization the results for isotropic scattering and Rayleigh scattering may be expected to be roughly similar.

Two further phase functions have been employed, namely

a. The Rayleigh phase function (Rayleigh scattering ignoring polarization)

$$\Phi(\alpha) = \frac{1}{2}(1 + \cos^2 \alpha)$$

We can forget about this possibility now that better data on actual Rayleigh scattering are available.

b. The phase function

$$\Phi(\alpha) = 1 + x \cos \alpha$$

This has been used by several authors ([11]) ([12]) ([25]) as a test case for asymmetric phase functions. This is quite suitable for small asymmetries. However, the asymmetry factor belonging to this phase function is

$$g = x/3$$

Since x can be at most 1 (then the backscatter becomes 0), g can be at most 1/3, which is too small to serve as a test case for scattering by droplets. For this reason we suggest in section III a phase function in which g can go all the way from 0 to 1.

About the isotropic scattering itself nothing new of great importance can be reported. Since the appearance of Chandrasekhar's book the X- and Y- functions for finite plane-parallel atmospheres with $\tau_1 = 0.05$ to 1 and various albedo values have been tabulated ([3]) ([5]). In addition, values of these functions are available for selected values of the albedo a (less than 1) for τ_1 in the range $1 \leqslant \tau_1 \leqslant 10$ ([22]).

Reference should also be made to the very thorough numerical results for the H- functions (semi-infinite atmosphere) given by Stibbs and Weir ([26]), which includes the approximation by polynomials of the complete set of H- functions

$$(0 \leqslant a \leqslant 1, \mu = 0\,(0.05)\,1).$$

Further, a good deal has been done about the firmer mathematical foundation of the methods used (Busbridge's book), as well as about new methods or new variations on old methods

(e. g., Sobolev's and Ueno's work). These latter authors consider radiative transfer as a problem in stochastic theory. None of this is of particular relevance in the present context.

The transfer of radiation in an atmosphere with Rayleigh scattering has always been considered as a master problem. In it the mathematical complexities arising from anisotropic scattering and from polarization are combined, and a direct test can be found in the blue daylight sky.

A complete solution was first given by Chandrasekhar in several papers in 1946-47 and repeated in his book *Radiative Transfer*. Theoretical novelties since that time are Lenoble and Sekera's discussion of the correction for curvature in a spherical Rayleigh atmosphere ([20]) and Mullikin's more careful evaluation of the restraints to be placed on the solutions of the integral equations ([29]). Full tables concerning the illumination and polarization of the sunlit sky by Chandrasekhar and Elbert appeared in 1954 ([4]).

Further numerical tables based on the same formulae had in the mean time been computed under the direction of Z. Sekera in various reports and papers. Sekera's handbook paper ([23]) gives full details. More complete tables by Coulson, Dave and Sekera have recently appeared ([8]). This book gives equally extensive tables on the light emerging from the top of the (planetary) atmosphere, as it gives on the light visible at the bottom of the (earth) atmosphere. Surface albedos adopted are $A = 0$, 0.25 and 0.8 ; optical depths are $\tau_1 = 0.02$, 0.05, 0.10, 0.15, 0.25, 0.50, 1.00. Several results from these latter calculations have been presented with comments and graphical illustrations by Coulson in two papers in 1959 ([6]) ([7]). A very useful presentation of these results in the form of maps has been given in a separate report ([24]), from which we reproduce for illustration figure 1.

As a further illustration, which has a direct interest in the interpretation of now available data, we present figure 2. Here the degree of polarization has been plotted for a planet in exact

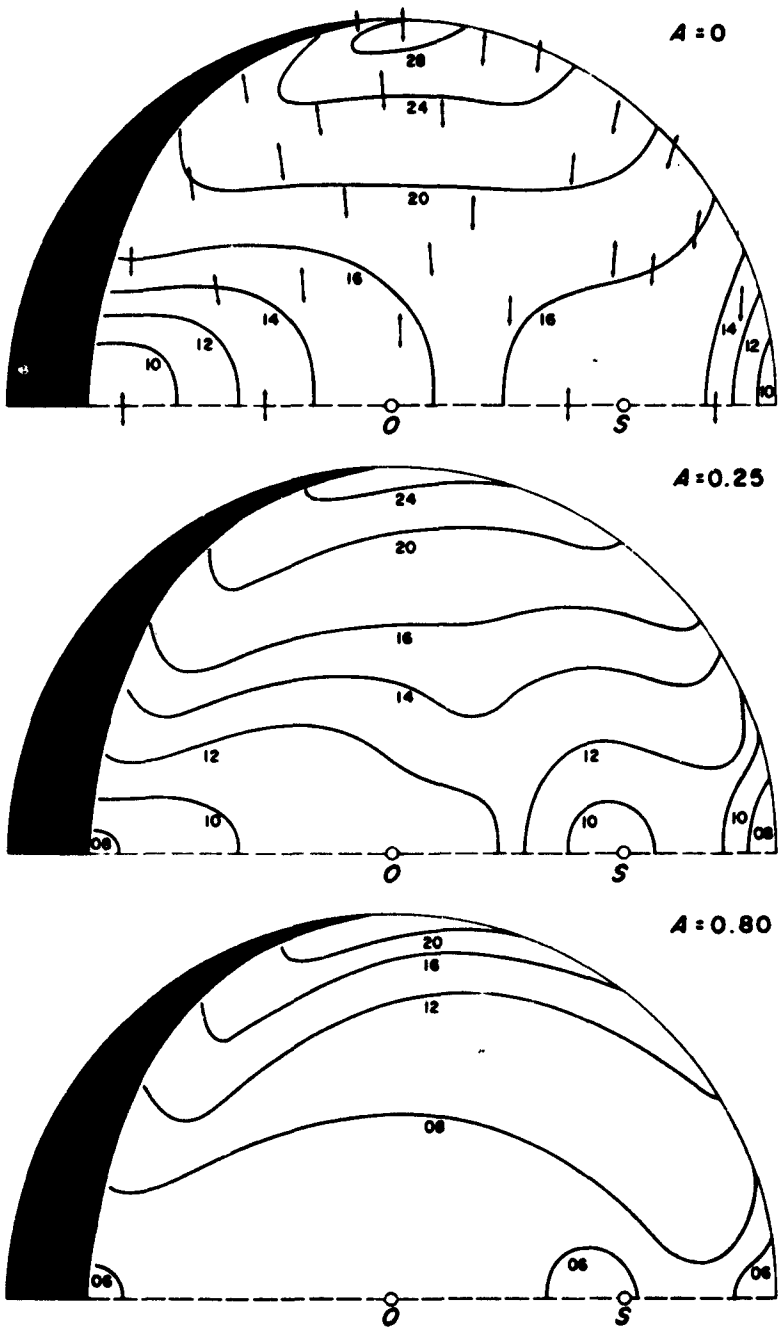

Fig. 1. — Degree of polarization of a planet covered with a Rayleigh atmosphere with optical depth 1.0 for three different values of the surface albedo. The angle of incidence is 36.90 degrees (from ([34])).

opposition. The abscissa is $r/r_e = \sqrt{1 - \cos^2 (\text{angle of incidence})}$. All polarizations are negative, which means that the plane of electric vibration is in the prime meridian (in the plane containing the normal and the direction of incidence). That this must be so can readily be seen for a thin atmosphere above a black surface (A = 0) viewed in an oblique direction — the primary scattered radiation has $p = 0$, but the illumination leading to secondary scattering comes predominantly from directions giving negative p.

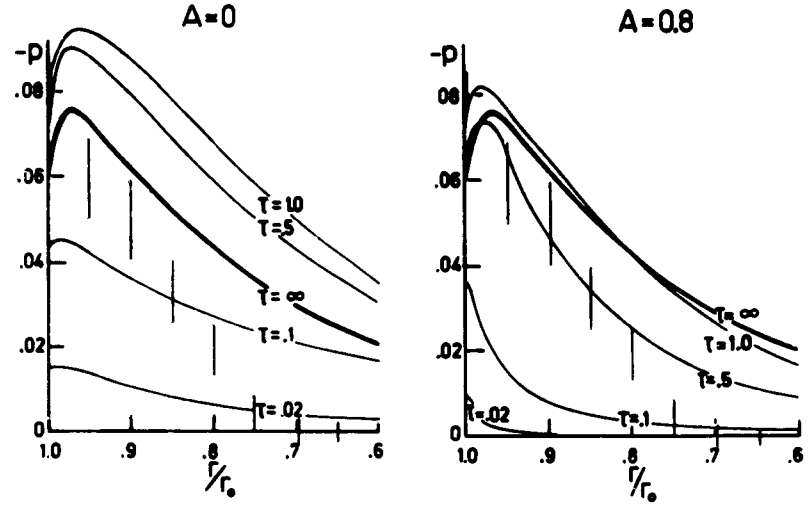

Fig. 2. — Degree of polarization near the limb of a planet in opposition covered by a Rayleigh atmosphere. Calculations for two values of the surface albedo A and five values of the optical depth. Observations (vertical hatching) by Lyot for polar areas of Jupiter.

The full curves in the left and right figures ($\tau_1 = \infty$) are the same as the curve given in Figure 35 of the 1949 review paper ([16]). The observed data show the approximate position of Lyot's polarization measurements for Jupiter's polar areas ([21]).(*) The curves for finite τ_1 were constructed from the new tables of Coulson

(*) These correspond to the range of polarization displayed by the four illustrative examples in Lyot's Figure 14 ; his table X shows that these were typical. We are grateful to Dr. T. Gehrels for pointing out that Lyot's data were incorrectly plotted (factor of 2 in the abscissa) in Figure 35 of ([16]).

et al. ([8]). It is to be noted that the polarization for $\tau_1 = 0.5$ and 1.0 exceeds that for a semi-infinite atmosphere if there is no reflection from the surface. Since the observed albedo of Jupiter is about 0.73, the curves appear to confirm the tentative explanation given in ([16]). The polar areas seem to be covered by a fairly thick Rayleigh atmosphere ($0.5 < \tau_1 \lesssim 1$). Farther from the limb ($r/r_0 < 0.8$) this atmosphere is considerably thinner, indicating that the underlying clouds are relatively higher as we approach the equatorial zone.

The observations suggest a tendency for the polarization to become positive for $r/r_0 < 0.7$. A tendency for positive polarization might arise from two effects.

a. If the opposition is not exact, the primary scattered radiation is positively polarized. An angle of 170° instead of 180° would give $p = 0.004$ for the primary scattering ; hence this effect is small.

b. If the surface does not reflect according to Lambert's law (as assumed by Coulson et al.) but shows limb darkening as seen from a point within the atmosphere, the radiation which is scattered once *after* reflection from the surface is again positively polarized. This effect may be more substantial.

III. Scattering diagram of large drops

The actual scattering diagram of a cloud droplet or aerosol particle is very complex, even when a distribution of particle sizes is assumed so that the fiercest intensity peaks are smoothed out. Nonetheless, we believe that a great deal of useful information could be obtained by approximating such a scattering diagram by means of the simple phase function first introduced by Henyey and Greenstein ([10]),

$$\Phi(\cos\alpha) = \frac{1 - g^2}{(1 + g^2 - 2\,g\cos\alpha)^{3/2}}. \qquad (2)$$

g is for this phase function just the asymmetry factor defined by eq. 1. The g may range all the way from 0 for isotropic scattering to 1 for an infinitely narrow forward beam (g may also take negative values if predominantly backward scattering is considered, such as occurs for small spheres with a very large refractive index m).

The quantity $\overline{\cos \alpha}$ can, of course, also be defined for the true particle scattering diagram. It is closely related to the radiation pressure exerted on the scattering particle, and is in fact given by

$$\overline{\cos \alpha} = \frac{C_{ext} - C_{pr}}{C_{sca}},$$

where C_{ext}, C_{sca} and C_{pr} are the cross sections of the particle for extinction, scattering, and radiation pressure ([17]).

The value of $\overline{\cos \alpha}$ corresponding to the actual scattering diagrams of particles has been discussed by van de Hulst ([17]) ([16]). A formula expressing $\overline{\cos \alpha}$ in terms of a series involving the Mie coefficients and valid for spheres of arbitrary size and complex refractive index is given in sec. 9.32 of reference ([18]), as are some approximate results for special cases of this formula. Numerical results are given for totally reflecting spheres and for very large dielectric spheres. These last results, which were taken from a paper by Debye, are reproduced in Table 1.

TABLE I

Weighted mean of the cosine of the scattering angle for spheres large compared to the wave length

refr. index m	$\overline{\cos \alpha}$ with diffraction	γ without diffraction
1.00	1.00	1.00
1.1	0.96	0.92
1.333	0.87	0.74
1.5	0.82	0.64
2.00	0.70	0.40
3.00	0.55	0.10
4.00	0.52	0.04
∞	0.50	0
1.27-1.32i	0.78	0.14

For these large spheres half of the scattered light is in the form of a narrow forward-directed diffraction cone and the question naturally arises whether this diffraction should be included and, therefore, which of the two quantities γ and $\overline{\cos\alpha}$ from Table 1 should be used in the Henyey-Greenstein phase function (2). In some cases it may be best to choose $g = \gamma$ at the same time taking the scattering cross-section as that due to reflection and refraction alone thus treating the diffracted light as though it were unscattered.

The last line of Table 1 shows the effect of absorption in a large sphere (sec. 14.23 of reference 17). The absorption cuts out the refracted light, which greatly affects the value of γ whereas $\overline{\cos\alpha}$ is diminished only slightly as compared to the value for $m = 1.27$.

With diminishing size of the spheres, the diffraction pattern widens and cannot be distinguished any longer from the reflected

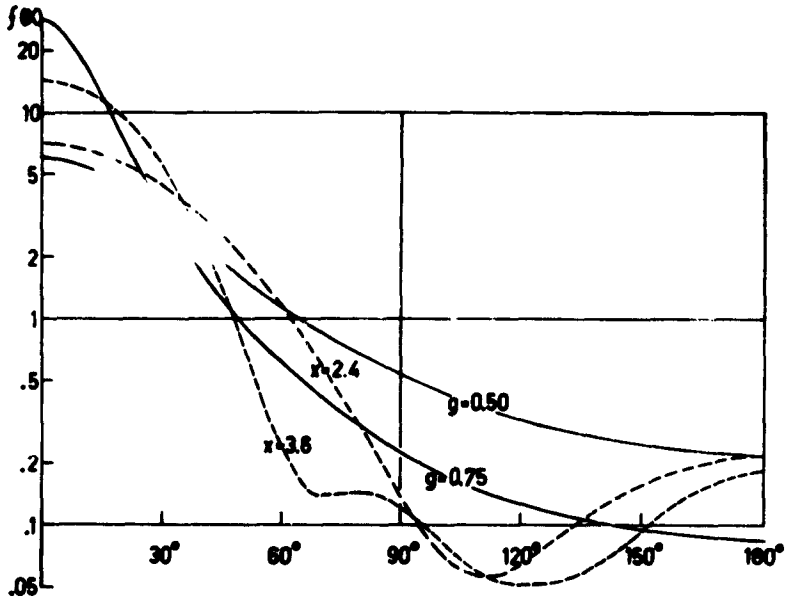

Fig. 3. — Dashed curves : Total intensity scattering diagram for droplets with $m = 1.33$ and two values of the size parameter $x = 2\pi a/\lambda$. Solid curves : Henyey-Greenstein phase function for $g = 0.5$ and 0.75.

and refracted light. In these circumstances it is necessary to use $g = \overline{\cos \alpha}$. Numerical data could easily be computed from the Mie formulae. They are indeed available in the literature, for g is 1/3 of the coefficient A_1 tabulated in (30) and unpublished reports by the same authors.

In figure 3 we compare the scattering diagram of spherical water droplets for two values of the size parameter $x = 2\pi a/\lambda$ (a = radius) with the Henyey-Greenstein phase function for $g = 0.5$ and 0.75. It would seem that a value of g slightly less than 0.75 would provide a reasonable approximation to the actual curves (we have not calculated $\overline{\cos \alpha}$ or γ directly from the droplet scattering diagrams). We have also drawn similar curves (not shown) for a distribution of sizes around the given values of x, based on the work of Houziaux and Battiau ([13]). These were not greatly different from the curves for a single size.

The agreement shown in Figure 3 is by no means excellent. It is obvious that this could be improved by using a more-parameter formula. For the moment, however, a qualitative exploration of the effects of asymmetry by the formula (2) with one parameter only seems preferable.

IV. Method of Successive Scattering

It is well known ([15]) that in the case of isotropic scattering the intensity of radiation in a plane-parallel, homogeneous layer may be developed as an infinite series, the n-th term of which represents radiation which has been scattered just n-times. Exactly the same thing may be done in the case of anisotropic scattering according to the phase function (2). Once the incident intensity I_0 is given, we may proceed in order to find S_1 (the source function for once-scattered light), I_1, S_2, etc. We wish to point out particularly two facts in connection with this *method of successive scattering* which seem to have escaped prior notice.

First, let the resulting intensity of the n-times scattered

radiation in the absence of absorption and for an optical depth τ_1 be denoted by I_n, so that the total intensity is

$$I = \sum_n I_n.$$

Now let us introduce an arbitrary albedo a for the scattering particles, and in addition immerse these particles in a homogeneous absorbing, but non-scattering, gas. The extinction coefficient for the atmosphere will then be the sum of three terms : σ, the scattering coefficient caused by the particles ; $\varkappa$, the absorption coefficient caused by the particles ; and $\varkappa_g$, the absorption coefficient caused by the gas molecules. Each coefficient may be defined to have the dimension length^{-1} (number density times cross section). We set the ratio of particle extinction to total extinction equal to p, so that

$$a = \frac{\sigma}{\sigma + \varkappa}, \tag{3}$$

$$p = \frac{\sigma + \varkappa}{\sigma + \varkappa + \varkappa_g}. \tag{4}$$

If we now choose the geometric thickness of the atmosphere such that the optical depth is still τ_1, we find that the total intensity is given by

$$I = \sum_n (ap)^n I_n, \tag{5}$$

where I_n still represents the functions found for the conservative case ($a = p = 1$). That is, we may express the solution for arbitrary particle albedo and absorption coefficient of the gas in terms of the solution in the absence of absorption, if we use the same *total* optical depth τ_1 in both cases. It should be noted that this is not the situation encountered inside and outside a gas absorption line, where the *total* optical depth will be greater inside the line.

We also observe that only the product ap, which may be called the effective albedo, enters the equation (5).

The usefulness of this method depends on the rapidity of

convergence of the infinite series, and the accuracy with which terms of higher order may be approximated.

Our second point of emphasis is the expectation on physical grounds that as $n \to \infty$, the ratio of successive terms, I_{n+1} / I_n or S_{n+1} / S_n, approaches a constant η that is independent of angle, depth in the atmosphere, and of the original source of the radiation (incident radiation or sources within the layer). η is in fact an eigenvalue defined by just the equation which determines in neutron transport theory the critical chemical composition of a medium for it to have a self-substaining neutron flux (cf. (9)). In the present case η^{-1} is that value, greater than one, which the particle albedo would have to assume in order for the newly generated energy to compensate exactly the losses of radiation taking place at both surfaces of the layer.

If our intuition is correct, then the factor η is a function of g and τ_1. It should be relatively easy for computational purposes to check when I_{n+1} / I_n becomes sufficiently independent of angle and optical depth in the layer so that it repeats at the next n. From that value of n on, the sum of the series in the method of successive scattering may be replaced by $I_n / (1 - \eta)$, the sum of a geometric series.

We have recently made some preliminary machine calculations based on the method of successive scattering, both in the case of parallel radiation incident on a finite atmosphere and for a homogeneous distribution of sources within the atmosphere. In all cases the expectation expressed above has been confirmed. Earlier desk computations by van de Hulst and Davis (18) for a homogeneous source distribution also found a rapid approach to a geometric series. In figure 4 we illustrate all the values of η that, to our knowledge, have been found for various g and τ_1. The results for $\tau_1 = 0.8$ and 0.5 are taken from (18), and the other points are new.

If we assume that the η factor exists, then, when the scattering is isotropic, approximative formulae may be found fairly simply. Figure 5 is based on such formulae. The lower curve was found by

taking the ratio of the first to the zeroth order source function, each averaged over optical depth in the layer τ, for the case of a homogeneous distribution of sources in the medium and no incident radiation. The upper curve was obtained on the assumption that near the top and bottom surface of an optically thick atmosphere with such a distribution of sources, the source function would be approximately that of a semi-infinite atmosphere with a constant net flux.

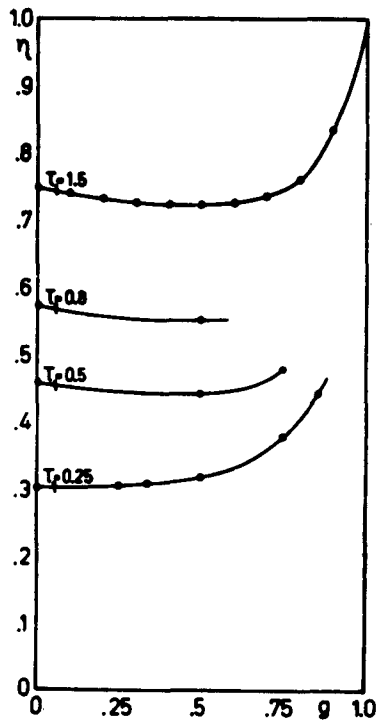

Fig. 4. — Ratio η between successive scatterings as a function of optical depth τ_1 and asymmetry index g. Only the points indicated have been computed.

Figure 6 and figure 7 give some results from our new calculations for the integrated intensity reflected from a Henyey-Greenstein atmosphere illuminated by parallel radiation incident normally.

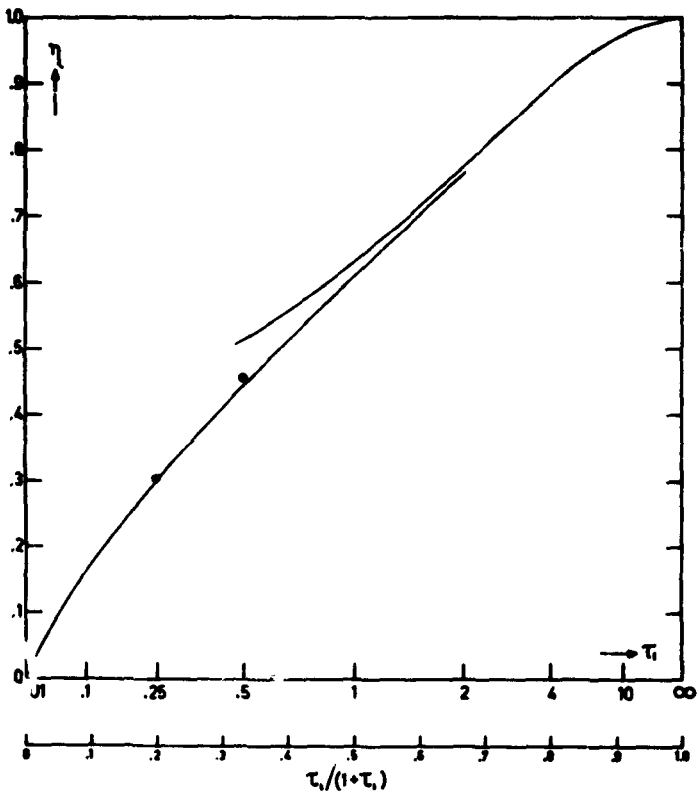

Fig. 5. — Ratio η between successive scatterings for isotropic scattering. Approximations valid for small τ_1 and for large τ_1 are shown, as well as two points exactly computed. The abscissa corresponds to a linear scale of $\tau_1/(1 + \tau_1)$.

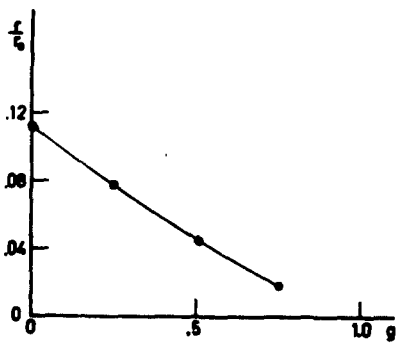

Fig. 6. — Reflectivity of a Henyey-Greenstein atmosphere of optical depth $\tau_1 = 0.25$ for normal incidence and unit particle albedo as a function of the asymmetry factor g (Calculated points $g = 0$, 0.25, 0.50, 0.75).

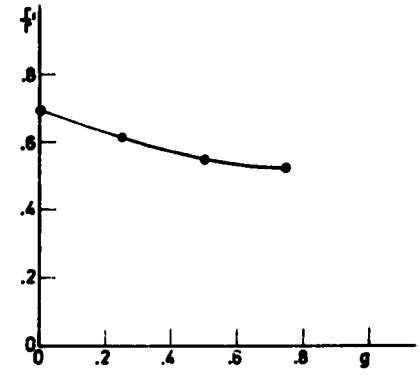

Fig. 7. — Proportion of once-scattered light in the integrated flux reflected from a Henyey-Greenstein atmosphere of optical depth $\tau_1 = 0.25$ for normal incidence and unit particle albedo as a function of g.

V. Absorption bands

For a wavelength interval in which the atmospheric parameters a, g, p, and τ_1 are constant, the inclusion of absorption in the problem is accomplished very simply (eq. 5). Within an absorption band, however, these parameters will in general vary so rapidly that their values at a given frequency cannot be seperately measured or computed. Only certain averages characteristic of the band as a whole will be known, and the previous analysis does not apply.

The effect of absorption will be dependent on the length of path travelled by a beam of light, so that we are led to consider $P_n(l)\,dl$, *the probability in the absence of absorption that a photon contributing to* I_n *has travelled on optical path for scattering between* l *and* $l + dl$. If, in addition to this probability the average transmittance $\psi(\xi)$ for a geometric path ξ at the particular wavelength interval is sought, the final intensity will again be given by an infinite series. Each term of the series will be a product of the intensity of the n-times scattered light in the absence of absorption I_n, times a factor depending on the transmittance ψ and the probability for a given path length P_n. This last factor represents the

attenuation due to absorption. Indicating explicitly the dependence of the intensity on optical thickness of the atmosphere τ_1 and optical depth within the atmosphere τ, we find for the desired intensity

$$I(\tau, \tau_1) = \sum_n I_n(\sigma z, \sigma h) \int_0^\infty dl\, P_n(l)\, \psi(l/\sigma). \tag{6}$$

z is the geometric depth of the point of interest and h is the geometric thickness of the layer. Observe that, in contrast to eq. 5, I and I_n are here evaluated for different optical depths, but for the same z and h.

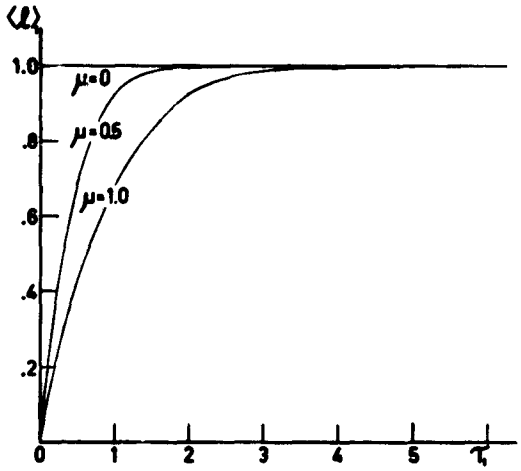

Fig. 8. — Mean optical path travelled by once scattered light reflected from a Henyey-Greenstein atmosphere of optical depth τ_1 and unit particle albedo for angle of incidence = angle of reflection = Arc cos μ.

If the probability $P_n(l)$ is known, we may also find

$$\langle \xi \rangle_n = \frac{1}{\sigma} \int_0^\infty dl\, l\, P_n(l) \tag{7}$$

and

$$\langle \xi \rangle = \sum_n \langle \xi_n \rangle I_n \Big/ \sum_m I_m, \tag{8}$$

the mean geometric path travelled by light scattered n times and this mean for the total intensity, respectively. The latter quantity

is important in any attempt to determine abundances of molecular species by comparison of observed absorption lines with laboratory spectra formed for a known path length.

In order to find the probability of a given optical path $P_n(l)$, we subdivide the intensities and source functions from the method of successive scattering into contributions corresponding to various l so that

$$I_n = \int_0^\infty dl\, W_n(l)$$

and

$$S_n = \int_0^\infty dl\, J_n(l)$$

$P_n(l)$ is then obviously given by the ratio

$$P_n(l) = \frac{W_n(l)}{I_n} \tag{9}$$

The successive terms $W_n(l)$ may also be found by the method of successive scattering. In this way we have obtained for reflected light

$$P_1(l) = \begin{cases} \dfrac{e^{-l}}{e^{-\tau s'} - e^{-\tau_1 s' + (\tau - \tau_1)s}} & \tau s' < l < \tau_1 s' + s(\tau_1 - \tau) \\ 0 & \text{otherwise} \end{cases} \tag{10}$$

where

$s' = \sec$ (angle of incidence) > 0,

$s = \sec$ (angle of reflection) > 0.

From eq. (10) may be found $\langle l \rangle_1 = \sigma \langle \xi \rangle_1$, the mean optical path travelled by once-scattered radiation reflected from a conservative atmosphere. In figure 8 $\langle l \rangle_1$ is plotted as a function of optical depth for the case (angle of incidence) = (angle of reflection). It is seen to be independent of the asymmetry factor g and of azimuth.

$\langle l \rangle_1$ approaches unity as $\tau_1 \to \infty$ or as we approach grazing incidence.

For light reflected from a semi-infinite atmosphere a general

expression for $P_n(l)$ may be found by equating (5) and (6) at a given infinitely narrow wavelength interval. The result is extremely simple,

$$P_n(l) = \frac{e^{-l} l^{n-1}}{(n-1)!}, \tag{11}$$

which is independent of angle and of the particle phase function in all orders of scattering. From this result it follows that

$$\langle l \rangle_n = n$$

for reflection from a semi-infinite atmosphere.

VI. Variations on the standard problem

Up to this point we have been considering primarily the following idealized *standard problem.* A plane-parallel, homogeneous gas, is illuminated obliquely from above by monochromatic radiation from a distant source. The intensity of radiation $I(\tau, \theta, \varphi)$ is sought as a function of optical depth from the top of the layer to the point considered and of two angular coordinates. This intensity will also depend upon the angle of incidence θ_0 and the parameters characterizing the atmosphere, g, τ_1, and the product $a\,p$.

For an interpretation of phenomena in planetary atmospheres several additional variations and complications should be introduced; the manner to cope with these may be judged after the standard problem has been solved. Among these added complications we mention :

a. *A diffusely reflecting surface below the atmosphere.* This does not introduce much of a difficulty, compare ([15]) or ([2]).

b. *Different scattering patterns for different polarizations.* If these could be introduced without appreciably complicating the form of the expression (2), the work might be approximately multiplied by a factor 4 (four Stokes parameters). However, it is questionable whether this could indeed be accomplished.

c. *Scattering patterns corresponding to actual particles or droplets.* Even if a mixture of sizes is assumed so that the fiercest peaks in intensity and polarization are smoothed out, the problem would still seem extremely difficult (compare ([17])).

d. *Broad-band molecular absorption.* See section V.

e. *Inhomogeneous atmospheres.* Variations of particle size or composition, particle density, and the ratio of molecular absorption to particle extinction will occur in most practical applications. They can be introduced in any solution method at the expense of more numerical work. A theoretical treatment of this question has been given by Yanovitskii ([28]), who, however, includes no numerical results.

f. *Curvature of the atmosphere.* This complication may not often occur together with the need to consider strongly anisotropic scattering.

g. *Local illumination or shadow.* If the incident light differs in any way from a parallel, infinitely extended beam, the radiation field depends not only on the depth but on two further coordinates of position in the atmosphere. Such problems occur, for example, upon illumination by a narrow search light beam, by a point source close to the atmosphere, or in cases where integration over the solar disk is required. The solution is bound to be more complex than that of the standard problem. If such problems are solved, other questions for instance, regarding the visibility of surface details and the sharpness of the shadow of a natural or artificial satellite above the atmosphere, may be answered with ease.

h. *Time dependent problems.* A beginning in this direction has been made by Sobolev ([25]). Much more has been done in the literature on neutron diffusion.

VII. Acknowledgements

The authors are grateful to Dr. A. Ollongren and the staff of the Centraal Reken-Instituut, Leiden, for their time and assistance in the numerical calculations.

One of us (W. I.) has the pleasure of thanking Professor J. H. Oort for the hospitality extended to him during a year's stay in Leiden, and the North Atlantic Treaty Organization for financial assistance in the form of a NATO Postdoctoral Fellowship.

REFERENCES

(1) I. W. Busbridge, *The Mathematics of Radiative Transfer*, Cambridge Univ. Press, 1960.

(2) S. Chandrasekhar, *Radiative Transfer*, Oxford Univ. Press, 1950.

(3) S. Chandrasekhar and D. Elbert, *Ap. J.*, **115**, 269, 1952.

(4) S. Chandrasekhar and D. Elbert, *Trans. Am. Phil. Soc.*, **44**, 643, 1954.

(5) S. Chandrasekhar, D. Elbert and A. Franklin, *Ap. J.*, **115**, 244, 1952.

(6) K. L. Coulson, *Planet Space Sci.*, **1**, 265, 1959.

(7) K. L. Coulson, *Planet Space Sci.*, **1**, 277, 1959.

(8) K. L. Coulson, J. V. Dave and Z. Sekera, *Tables Related to Radiation Emerging from a Planetary Atmosphere with Rayleigh Scattering*, Univ. of Calif. Press, 1960.

(9) B. Davison and J. B. Sykes, *Neutron Transport Theory*, Oxford Univ. Press, 1957.

(10) L. C. Henyey and J. L. Greenstein, *Ap. J.*, **93**, 70, 1941.

(11) H. G. Horak, *Ap. J.*, **116**, 477, 1952.

(12) H. G. Horak and C. A. Lundquist, *Ap. J.*, **119**, 42, 1954.

(13) L. Houziaux and L. Battiau, *Mém. Acad. Roy. Belg. (Cl. Scien.)*, Ser. 2, XIV, fasc. 4, 1958.

(14) H. C. van de Hulst, *Thesis*, Utrecht, 1946.

(15) H. C. van de Hulst, *Ap. J.*, **107**, 220, 1948.

(16) H. C. van de Hulst, Chap. 3 in *The Atmospheres of the Earth and Planets* (G. P. Kuiper, ed.) Univ. Chicago Press, 1949, and 1953, second ed., this chapter unchanged.

(17) H. C. van de Hulst, *Light Scattering by Small Particles*, New York, John Wiley, 1953.

(18) H. C. van de Hulst and M. Davis, *Proc. Kon. Ned. Akad. Wet. Series* B, **64**, 220, 1961.

(19) V. Kourganoff, *Basic Methods in Transfer Problems*, Oxford Univ. Press, 1952.

(20) J. Lenoble and Z. Sekera, *Proc. Nat. Acad. Sci.*, **47**, 372, 1961.

(21) B. LYOT, *Ann. Observ. Paris* (*Meudon*) 8, fasc. 1, 1929.

(22) D. F. MAYERS, *M. N.*, 123, 471, 1962.

(23) Z. SEKERA, *Handbuch der Physik*, 48, 288, 1956.

(24) Z. SEKERA and W. VIEZEE, *Distribution of the Intensity and Polarization of the Diffusely Reflected Light over a Planetary Disk*, U. S. Air Force Project Rand Report R-389-PR, 1961.

(25) V. V. SOBOLEV, *Transfer of Radiative Energy in the Atmospheres of Stars and Planets* (In Russian) Moscow, 1956.

(26) D. W. N. STIBBS and R. E. WEIR, *M. N.*, 119, 512, 1959.

(27) S. UENO, *Ann. Astrophys.*, 24, 352, 1961.

(28) E. G. YANOVITSKII, *Astron. Zh.*, 38, 912, 1961. English trans. in *Soviet A. J.*, 5, 697, 1962.

(29) T. W. MULLIKIN, Paper presented at « Interdisciplinary Conference on Electromagnetic Scattering », Potsdam, New York, August 1962.

(30) G. C. CLARK, C. M. CHU, and S. W. CHURCHILL, *J. Opt. Soc. Amer.*, 47, 81, 1957.

8. — GENERAL REPORT ON PLANETARY RADIO ASTRONOMY

CORNELL H. MAYER
Radio Astronomy Branch
U. S. Naval Research Laboratory
Washington, D. C., U. S. A.

Some results of the radio observations of the planets which have been made over the past few years are well known. For example, the centimeter wavelength radiation from Venus with a thermal-like spectrum which suggests a temperature in excess of 550° K at the solid surface ; the very intense, burstlike decameter radiation from Jupiter which appears to come from localized regions which rotate with a period slightly shorter than the system II period ; and the partially linearly polarized decimeter radiation which comes from an extended region in the equatorial plane of Jupiter and which seems to be the radiation of electrons trapped in the magnetic field. The evidence leading to these results is probably not so well known, and in the short time available it may be most useful to mention some of the evidence as well as some of the questions which need to be answered.

MERCURY, MARS, AND SATURN

First, the few reported observations of the very weak radio radiation from Mercury, Mars, and Saturn are summarized in Figure 1. These are the only planets other than Venus and Jupiter from which radio radiation has been observed. The observations of Mercury were especially difficult because of the very low intensity of the planetary radiation and because of the interference from the much more intense solar radio radiation which was picked up by the minor lobes of the antenna reception pattern. The observers, Howard, Barrett, and Haddock, have derived a value for the temperature of the subsolar point of about 1000° K from the measurement

which is higher than the temperature expected from solar heating and the temperature of 610°K derived by Pettit and Nicholson from infrared observations. The discrepancy is, however, comparable with the uncertainty in the radio measurement.

RADIO OBSERVATIONS OF MERCURY, MARS, AND SATURN

	λ cm	T_A °K	T_{BB} °K	
MERCURY	3.45, 3.75	0.05	350	Howard, Barrett and Haddock 85-foot Reflector, 1960-61.
MARS	3.15	0.24	218 ± 50	Mayer, McCullough, and Sloanaker 50-foot Reflector, 1956.
MARS	3.14	0.08	211 ± 20	Giordmaine, Alsop, Townes, and Mayer, 50-foot Reflector, 1958.
SATURN	3.75	~0.04	- - - -	Drake and Ewen 28-foot Reflector, 1957.
SATURN	3.45	0.10	106 ± 21	Cook, Cross, Bair, and Arnold 85-foot Reflector, 1960

Fig. 1

The observations of Mars were made near favorable oppositions, and the observed blackbody disk temperatures at about 3 cm wavelength are not much different from the estimated average temperature over the planet. For example, the average radiation temperature computed by Kuiper is 217°K. This close comparison supports the interpretation that these waves penetrate the atmosphere and some distance into the crust of Mars, although the present data are insufficient for a definite interpretation. The measured 3 cm radio emission of Saturn again seems consistent with thermal radiation from the body of the planet, although the measurements are sparse.

Venus

The observed radio radiation from Venus shows several outstanding characteristics which can best be seen from illustrations, and the data plotted in Figure 2 summarize the results of the obser-

vations. At wavelengths near 3 cm, 10 cm, and 21 cm the observed intensity is nearly twice that which was predicted for the thermal radiation of the surface of Venus. In spite of this, the observed dependence of the measured flux density on the inverse square of the wavelength corresponds to a nearly constant brightness temperature under the assumption that the size of the radiating region does not depend on wavelength. The millimeter wavelength radiation, however, gives a different result. As was originally discovered by Gibson and McEwan working at 8.6 mm, the intensity

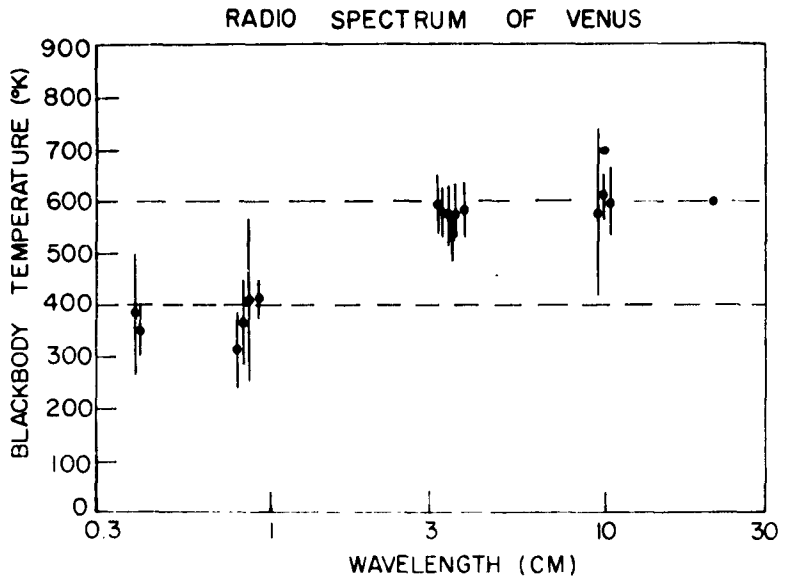

Fig. 2

measured at wavelengths near 8 mm and 4 mm is more nearly that to be expected of a blackbody having the angular size of Venus and a temperature of 350 or 400°K. The measurements plotted here are published values or reliable unpublished values from The Lebedev Physical Institute at 4 mm, 8 mm, 3.3 cm, and 9.6 cm ; The Naval Research Laboratory in Washington at 4.3 mm, 8.6 mm, 3.15 cm, 3.37 cm, 3.4 cm, 9.4 cm, and 10.2 cm ; The National Radio Astro-

nomy Observatory in Green Bank at 3.75 cm, and 10 cm ; and the Harvard College Observatory at 21 cm.

Another important characteristic of the observed radio radiation from Venus is the apparent minimum of emission which has been observed near inferior conjunction and which suggests a dependence of the radio emission on the phase of solar illumination. An indication of such an effect was noted in the earliest observations in 1956, and indications have appeared in most of the more recent series of observations which have covered a sufficient phase interval. It has proved difficult, though, to definitely establish the existence of a phase effect for several reasons. The intensity of the radiation reaching the earth falls of rapidly on either side of inferior conjunction because of the increasing distance of Venus, and accurate observations can be made for only a limited time centered on inferior conjunction. Further, systematic errors become serious over long time intervals and limit the accuracy of fitting together measurements made at different times and possibly with different apparatus.

The most complete published evidence for a phase effect is shown in Figure 3. This is the result of a long series of observations which were made in 1961 at 10 cm wavelength by F. D. Drake using the 85 foot reflector at Green Bank. During these observations a special effort was made to maintain constant calibration and to minimize systematic errors. These observations indicate a small minimum in the emission at about 17 degrees after inferior conjunction and a variation from a minimum blackbody disk temperature of 583°K to an extrapolated maximum of 661°K. The occurrence of the minimum after inferior conjunction can be interpreted as an indication of retrograde rotation of Venus.

In addition to the evidence shown here, the observations of Kuzmin and Salomonovich at 8 mm in 1959 suggested a much larger phase effect, and the observations made at the Naval Research Laboratory, Washington near 3 and 10 cm between 1956 and 1959 also suggested a larger effect. Venus was observed extensively during 1961 at both the Lebedev Institute and at the Naval

Research Laboratory and the results will be presented at this meeting.

At this time there is no evidence for long term variations in the radio radiation from Venus which are not connected with the phase of solar illumination and which might indicate seasonal or rotational

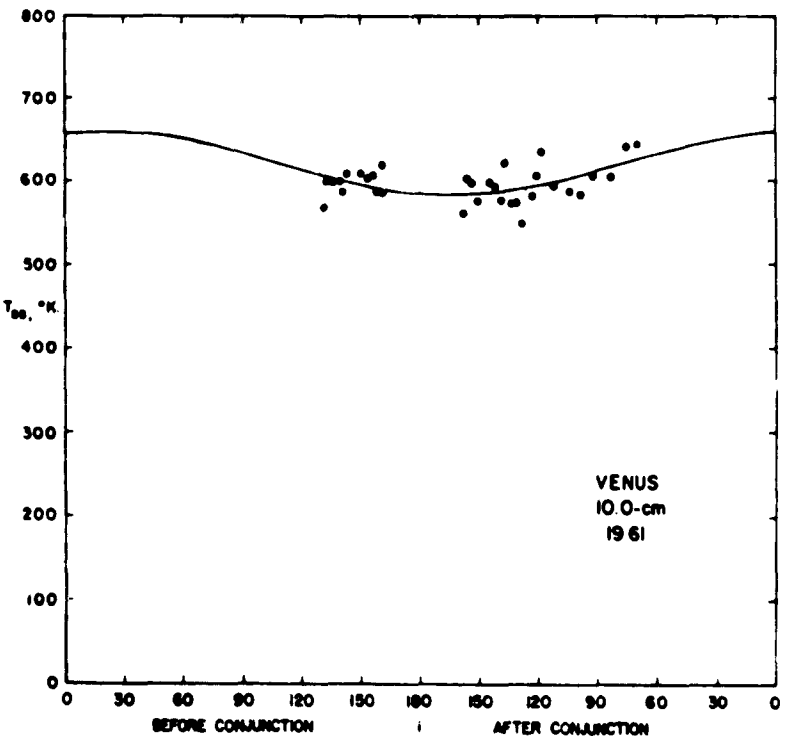

Observed mean daily values of T_{BB} plotted as a function of phase angle i.

FROM:
F. D. DRAKE
PUBL. N.R.A.O., Vol. 1, No. 11, 1962.

Fig 3.

effects. The possibility of short time fluctuations has however been suggested. Most observers have felt that the variability in their measured intensities of Venus did not differ significantly from the expected experimental scatter. Recently, though, the observers at

the Lebedev Institute have raised the possibility that their measurements of the 9.6 cm radiation from Venus made in 1961 show greater scatter than they would expect from experimental effects, and they suggest that such variability may indicate the existence of an ionospheric component of the radiation. On the other hand, the measurements of Drake at 10 cm which were shown were made over the same period of time in 1961 and apparently show no evidence for variability, at least not of more than a few percent above the expected experimental scatter.

A fair amount of observational information on the radio emission of Venus has now been accumulated, and several of the general characteristics which were inferred from the earlier and less complete results have now been verified. The observed spectrum at wavelengths between 3 cm and 21 cm is consistent with the thermal radiation of opaque material. The disk of Venus radiating as a black body at a temperature of between 550°K and about 600°K would explain the observed intensity of radiation from the dark hemisphere. The corresponding value for the sunlit hemisphere can only be estimated from extrapolations of observations at large phase angles to be about 660°K at 10 cm and perhaps 50°K greater than this at 3 cm wavelength. The emission apparently drops suddenly between 3 cm and 8.6 mm. The observed spectrum between 4 mm and 8.6 mm is again consistent with thermal radiation from opaque material, but this time the blackbody disk temperature is 350 to 400°K near inferior conjunction.

This spectrum could be produced either by thermal radiation of material at or near a hot solid surface beneath a cooler atmosphere which is transparent at centimeter wavelengths but only partly transparent at millimeter wavelengths ; or of a very extensive ionized atmosphere with a high effective temperature which is opaque at wavelengths longer than about 3 cm, but transparent to the radiation of a relatively cool solid surface at millimeter wavelengths. The main difficulty with the hot surface hypothesis is to find a way to maintain such a high temperature. Two possibilities

have been given serious consideration ; the greenhouse mechanism considered mainly by Dr. Sagan and the aeolosphere model of Professor Opik. The recent work of Dr. Spinrad gives other evidence of high temperature in the atmosphere of Venus which lends additional support to the hypothesis that at least a large part of the observed radio radiation is the thermal emission of a hot solid surface.

The main difficulty with the ionosphere hypothesis is to find a way to maintain an ionized region dense enough to be opaque to such a short wavelength as 3 cm. Densities of the order of 10^9 cm^{-3} are required. The results of the recent radar observations are also difficult to reconcile with such an ionosphere. The possibility of non-thermal emission has also been considered. The radiation of electrons trapped in the magnetic field of Venus does not seem at all promising as an explanation of the observed spectrum, and attempts to detect a linearly polarized component of the radiation have given negative results. A suggestion has recently appeared in the literature that the conversion of energy incident on Venus to radio radiation through discharges between charged particles about 1 mm in diameter could account for the observed radio radiation. It appears that much more work is necessary before this suggestion can be evaluated.

It is hoped that space probe measurements will soon help to answer the questions about Venus, but in any case radio observations from the earth should be able to settle the question of variability, determine the phase effect, fill in the spectrum particularly the important transition region between 8 mm and 3 cm, and search at longer wavelengths for evidence of non-thermal radiation and effects of the ionosphere of Venus. With these questions answered the explanation of the radio emission of Venus should be much less difficult.

JUPITER

The observations of Jupiter in the decimeter wavelength region have produced spectacular results in the few years since 1958 when Sloanaker's observation of an unexpectedly high intensity at 10.3 cm stimulated interest in the radiation at these wavelengths. The identification of a non-thermal component of the

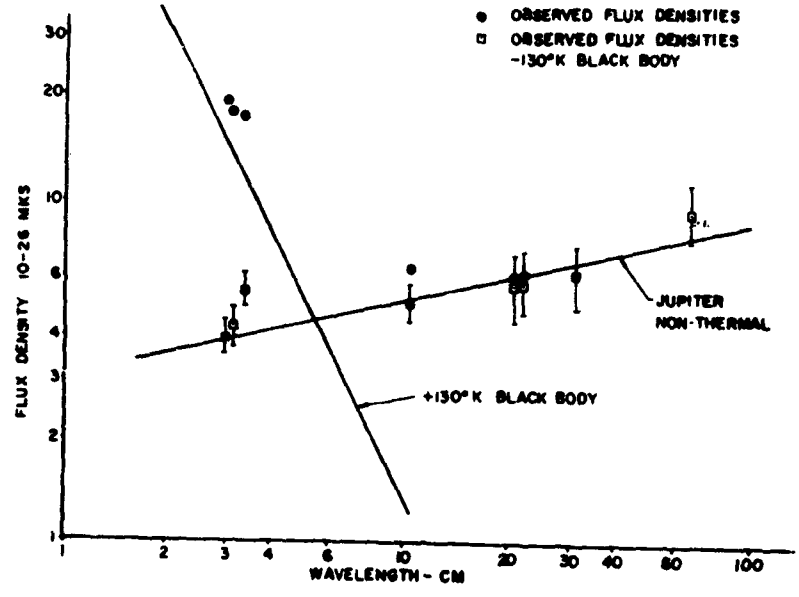

MICROWAVE SPECTRUM OF JUPITER

FROM: F. D. DRAKE
PHYSICS TODAY, APRIL, 1961

Fig. 4

decimeter radiation followed, and the spectrum in Figure 4 illustrates a possible separation of the thermal and non-thermal components based on the assumption of thermal radiation at 130°K at all wavelengths. The observations at wavelengths between 3 cm and 4 cm, where the radiation is thought to be predominantly thermal, give blackbody disk temperatures between 140°K and

JUPITER

The observations of Jupiter in the decimeter wavelength region have produced spectacular results in the few years since 1958 when Sloanaker's observation of an unexpectedly high intensity at 10.3 cm stimulated interest in the radiation at these wavelengths. The identification of a non-thermal component of the

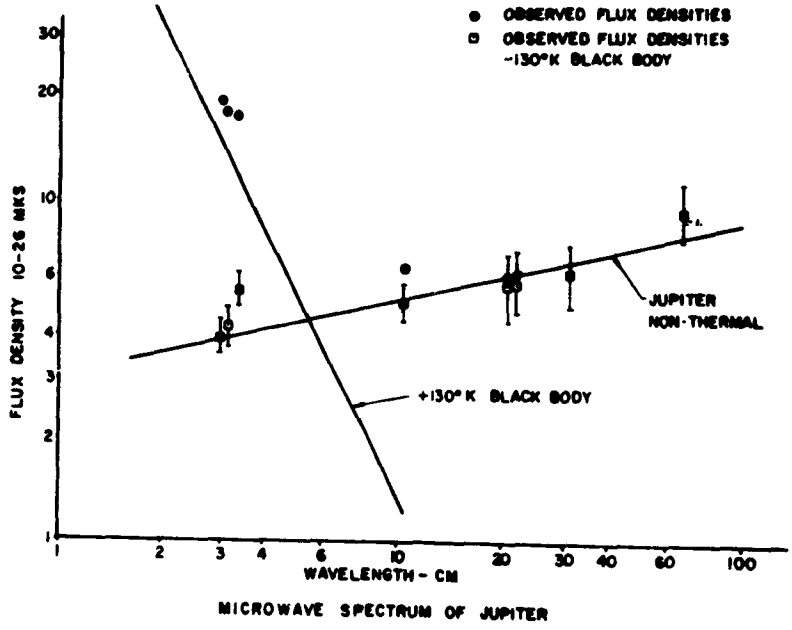

MICROWAVE SPECTRUM OF JUPITER

FROM: F. D. DRAKE
PHYSICS TODAY, APRIL, 1961

Fig. 4

decimeter radiation followed, and the spectrum in Figure 4 illustrates a possible separation of the thermal and non-thermal components based on the assumption of thermal radiation at 130°K at all wavelengths. The observations at wavelengths between 3 cm and 4 cm, where the radiation is thought to be predominantly thermal, give blackbody disk temperatures between 140°K and

about 200°K so that the assumed value of 130°K used here is probably somewhat low, but this is not important to the general meaning of the diagram. It was on the basis of this kind of spectrum that F. D. Drake proposed that the decimeter radiation was of non-thermal origin and was due to electrons trapped in the magnetic field of Jupiter in analogy with the van Allen belts of the earth. Although the different observers were in general agreement on the relative wavelength independence of the Jupiter decimeter radiation there was not agreement with regard to the variability of the radiation. Some observers found evidence for variations with the rotation of Jupiter or with time, or both, while others found no variation. Among the early observations the strongest evidence for a variation of the measured intensity with the rotation of Jupiter was found by McClain, Nichols, and Waak who observed a variation of about 30 % at 21 cm wavelength at the System II (or for this short interval also System III) period.

The very important observations of Jupiter made using the twin 90 foot reflector interferometer of the Owens Valley Radio Observatory first by Radhakrishnan and Roberts and more recently by Morris and Berge have supplied several crucial results. The measurements show that the Jupiter decimeter radiation is partially linearly polarized with a degree of polarization of about 30 percent and with the electric vector approximately parallel to the equator at both 22 cm and 31 cm ; that the equatorial diameter of the radio source is about 3 times the visible diameter at both wavelengths ; and that the polar diameter is about the same as the visible diameter. The failure to observe a strong wavelength dependence in the polarization and source size is taken as evidence favoring synchrotron radiation where each electron radiates over a range of wavelengths. Morris and Berge also made the important observation that variations in the direction of the polarization with the rotation of Jupiter indicate that the magnetic axis is inclined by about 9 degrees to the axis of rotation and that the magnetic poles are at longitudes of about 20 degrees and 200 degrees in

System III. They suggest that the tilt of the magnetic axis causes variations in the measured radio intensity with rotation of Jupiter both because of the change of polarization with respect to the antenna and because of the varying tilt of the plane of maximum radiation at the magnetic equator toward or away from the earth, and that the latter cause may account for the dependence on rotation found in the 21 cm observations of McClain, Nichols, and Waak made in 1959. Recent 21 cm observations made at NRL by Miller and Gary using conventional single-antenna techniques appear to confirm the polarization of the radiation and the tilt of the magnetic axis.

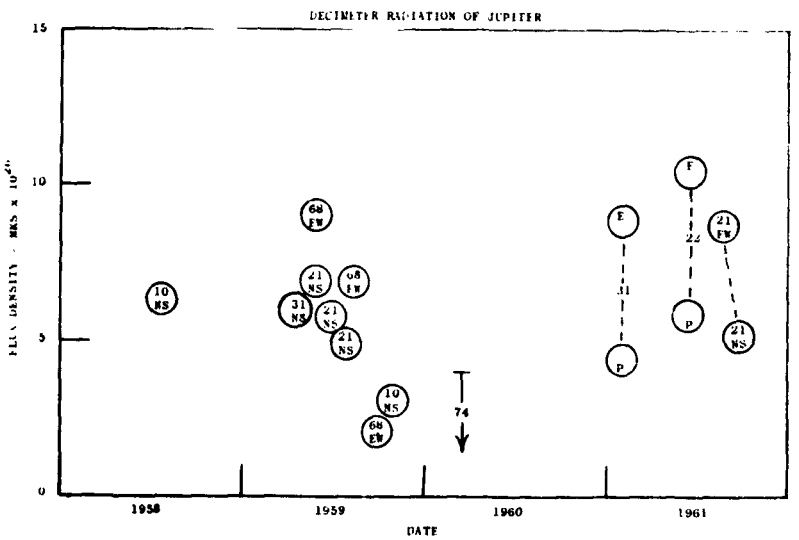

Fig. 5

Several observers have reported what appear to be significant changes in the decimeter emission of Jupiter with time, and some of the observations are summarized in Figure 5. The observed emission at 10.3 cm according to Sloanaker and Boland ; at 21 cm according to McClain, Nichols, and Waak ; and at 68 cm according to Drake and Hvatum apparently decreased greatly during 1959. Elsmore and Long confirm a low level of emission at 74 cm in

March 1960 by their inability to detect Jupiter. The intensities measured by Morris and Berge at 22 cm and 31 cm in 1961, and by Miller and Gary at 21 cm in 1961 suggest a level of emission near that in 1959, when it is taken into account that the earlier observations, with the exception of those at 68 cm, were taken with a North-South polarization which is unfavorable for the polarized component. The observations in 1961 were made with adjustable polarization and indicate the amount by which the measured intensity can be changed by changes of the antenna polarization. It seems unlikely that changes in the polarization of the Jupiter radiation with respect to the antenna can explain the large apparent decrease in emission at 10 cm, although there is more uncertainty at 68 cm where the Faraday rotation in the earth's ionosphere may be important.

These observations leave the question of the variability of the decimeter emission of Jupiter in an unsatisfactory state, but the interesting new results of Roberts and Huguenin of the Harvard Observatory which will be reported at this meeting provide additional information on variability and suggest a possible connection between the radiating particles and the sun.

To skip now to the intense, sporadic decameter radiation of Jupiter which was discovered by Burke and Franklin in 1955, the observations now extend over a period of more than ten years including pre-detection observations, and have established that the active source regions are stable and rotate with a steady period which is about 11 seconds shorter than the System II period. It has been suggested that the radio sources may be connected with the solid body of Jupiter or with the magnetic field ; for example, J. W. Warwick has proposed that the radiation is generated by the precipitation of particles into an auroral zone of Jupiter.

It is interesting that the low frequency end of the observed spectrum has decreased along with the decrease of the ionospheric cutoff frequency as the solar activity minimum approaches so that this radiation is not restricted to such a narrow frequency range as

previously supposed. There have been many interesting and significant results of the recent intensive work on the low frequency radiation of Jupiter which I believe will be covered at this symposium. Attempts to identify similar low frequency outbursts from other planets have produced negative or inconclusive results.

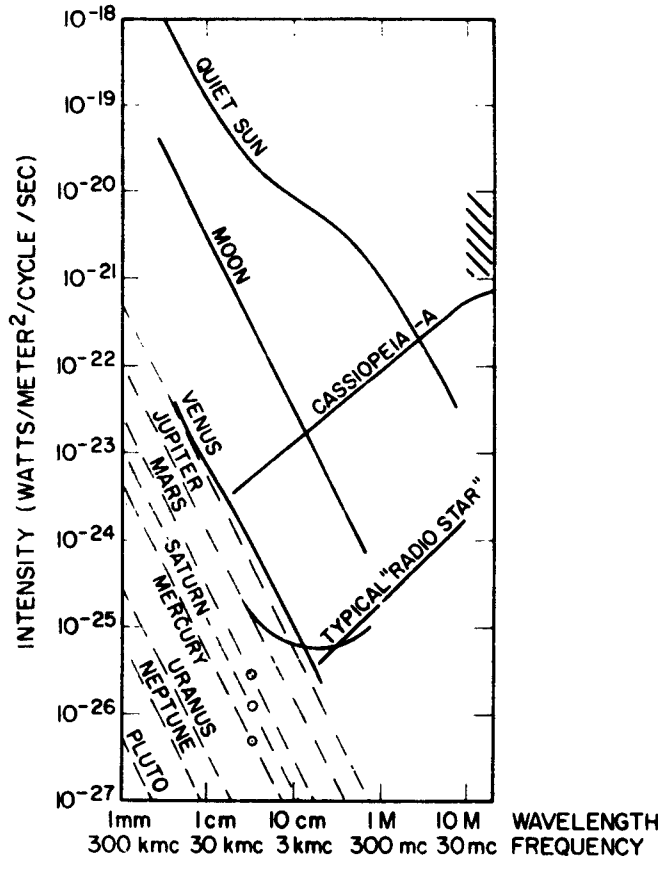

Fig. 6

The recent results for both the decimeter and decameter radiation of Jupiter have brightened the prospects for understanding Jupiter as a source of radio waves and in so doing to gain valuable physical information about the planet and its surroundings. There is hope that the thermal radiation of Jupiter,

which has been all but forgotten in the excitement over the more prominent non-thermal radiation, can be identified and can provide additional physical information about the atmosphere of Jupiter.

In closing, it may be of general interest to see where the planets fit in with the other discrete sources of radio emission. The general relationship of the predicted thermal intensities of the planets at closest approach and the measured intensities at different wavelengths to the spectra of the quiet sun, Cassiopeia-A, and a typical radio source are illustrated in Figure 6. The cross-hatched region is a crude indication of the low frequency sporadic radiation of Jupiter.

A. GENERAL PAPERS

9. — A NEW PROGRAM OF PLANETARY PHOTOGRAPHY

D. H. MENZEL
Harvard College Observatory
Cambridge 38, *Mass., U. S. A.*

Harvard College Observatory, under NASA sponsorship, has initiated a three-year program for multicolor photometry of the Moon, Mars, Venus, and other planets. The studies are being undertaken with a new 16-inch Cassegrain reflector at Boyden Observatory in South Africa and with the 12-inch reflector at the Le Houga Observatory in Southern France. Observations started July 1 at the Le Houga Observatory and are scheduled to start at the Boyden Observatory in early August.

The photometer used for the project contains a number of special features. Dr. Harold Johnson designed it for us. The photometer permits measures in thirteen spectral regions from 3200 A to more than 1 micron. The two photocells are of the « end-on » type, a Farnsworth IR 118 tube and an EMI tube. The photocells are cooled with dry ice. A rapid switching arrangement simplifies the operation. The 13 filters are held in a rotating disk. We have selected about three dozen comparison stars, some of zero color index, some of index + 1, and others of solar type, scattered along the ecliptic. A special lens gives an image of the moon on a scale roughly matching that of the planets.

Dr. Gerard de Vaucouleurs has been a consultant and collaborator in the project. Dr. Andrew Young has been actively in charge of the instrumental and observing program.

Perhaps I should note that our original plans included measures of polarization as well as of brightness, but this refinement has unfortunately proved impossible at this time.

This research is sponsored by the National Aeronautics and Space Administration under NASA Grant NsG89-60 with Harvard University.

10. — THE WAVELENGTH DEPENDENCE OF POLARIZATION OF PLANETARY ATMOSPHERES

THOMAS GEHRELS
University of Arizona, U. S. A.

The polarization of the Jupiter poles, discovered by Lyot in 1922, was observed with six filters, 3250 — 9900 A. The observations were made, in April 1960 with the McDonald 82-inch reflector, on regions of 4 seconds-of-arc in diameter. Strong wavelength dependence is found. The polarization of the total disc of Venus was observed over the 30° — 150° range of phase, 1959-1961, and strong waveler gth and phase dependence is found. A description of the program, of the instrumentation, and of preliminary results (also for Mars, the moon, and the blue sky) will be published shortly (Gehrels and Teska 1963).

RÉFÉRENCES

T. GEHRELS and T. M. TESKA, *Applied Optics*, Vol **2**, January issue, 1963.

11. — THE RED BANDS OF CH_3 AND THEIR POSSIBLE IMPORTANCE IN THE SPECTRA OF THE MAJOR PLANETS

G. HERZBERG and J. W. C. JOHNS
Division of Pure Physics
National Research Council
Ottawa, Canada

The main features of the spectra of the outer planets are very well understood as being due to CH_4 and NH_3. There are, however, some minor features like the Kuiper bands of Uranus (Kuiper 1949) which have not yet been satisfactorily explained. In addition, it appears probable that, as higher resolution is applied to these spectra, additional fine line features will be observed. Recently Kiess, Corliss and Kiess (1961), by using somewhat higher resolution than previously available, have established the presence of the quadrupole lines of H_2 in the spectrum of Jupiter, and Spinrad and Münch (1962) in this symposium report two such lines in the spectrum of Saturn. Previous to these observations, H_2 had been established as a major constituent only in Uranus by its pressure induced line at 8270 Å (Herzberg 1952). The importance of high resolution for the observation of fine weak lines cannot be overemphasized. As an example, it may be mentioned that recently Rank, Rao, Slomba, Sitaram and Wiggins (1962) observed in the laboratory the quadrupole lines of H_2 with less than one-tenth tha path length used in the original work of Herzberg (1950) because they had available a much higher resolution. Since higher resolution will undoubtedly become available for the spectra of the outer planets, it may be of interest to consider some other spectra that may reasonably be expected, given that the main constituents are H_2, CH_4 and NH_3.

As in the earth's atmosphere, many photochemical reactions must take place in the upper layers of the atmospheres of the major planets. Two primary reactions are clearly

$$CH_4 + h\nu \rightarrow CH_3 + H \qquad (1)$$

$$NH_3 + h\nu \rightarrow NH_2 + H \qquad (2)$$

The first reaction requires light of a wavelength less than 1450 Å, the second less than 2100 Å. The lifetimes of the radicals CH_3 and NH_2 formed in this way depend greatly on the physical and chemical conditions of the atmosphere. In view of the uncertainty of the lifetime, it is impossible to predict what the concentration of CH_3 and NH_2 might be, but some small concentration must exist. The absorption spectrum of NH_2 is well known, thanks to the work of Dressler and Ramsay (1959). It consists of a large number of very fine lines lying in a convenient region (8000 — 5000 Å). The most prominent lines have been listed by Ramsay (1957) in a contribution to a previous Liège colloquium, but no evidence for NH_2 in the spectra of the major planets has yet been found.

The absorption spectrum of CH_3 is also well known (Herzberg 1961), but the first known absorption lies at 2160 Å, and its detection in the major planets will have to await observations from outside the earth's atmosphere. However, the 2160 Å CH_3 band is diffuse, indicating that nearly every light quantum absorbed by CH_3 leads to its dissociation according to

$$CH_3 + h\nu \rightarrow CH_2 + H \qquad (3)$$

and thus to the formation of CH_2. This radical may also be formed directly by the photodissociation of CH_4 according to the reaction

$$CH_4 + h\nu \rightarrow CH_2 + H_2 \qquad (4)$$

In addition, there may be various secondary reactions that lead to the formation of CH_2.

Recent work in our laboratory has established the existence of two modifications of CH_2 : linear CH_2 with a $^3\Sigma_g^-$ ground state, and bent CH_2 with a $^1A_1$ ground state (Herzberg 1961). Of the two modifications, the first has slightly lower energy. The known absorption spectrum of linear CH_2 lies entirely in the vacuum ultraviolet, but a strong absorption of bent CH_2 lies in the red and yellow region of the spectrum (9000 — 5000 Å). It is similar in character to the NH_2 absorption, consisting of a large number of sharp lines.

The primary dissociation (4) of CH_4 can only yield singlet (bent) CH_2 on account of the spin conservation rule, since both CH_4 and H_2 are in singlet states. The predissociation of CH_2, as far as spin conservation is concerned, could give either triplet or singlet CH_2. However, the upper state of the 2160 Å band of CH_2 is a $^2A_1'$ state, and the state causing the predissociation must also be of this type. A $^2A_1'$ state cannot arise from $^3\Sigma_g^- + {}^3S$, but can arise from $^1A_1 + {}^3S$. We therefore conclude that the predissociation of CH_2 also leads in the primary process to singlet (bent) CH_2.

Bent CH_2 is transformed by collisions into linear CH_2, but according to laboratory experiments, this transformation is considerably slowed down at low temperatures. Again it is impossible to estimate the lifetime of CH_2 under the conditions of the atmospheres of the outer planets and therefore to estimate the stationary concentration.

Extensive spectra of CH_2 in the visible and near infra-red regions were obtained by the flash photolysis of diazomethane (CH_2N_2) mixed with N_2 in the ratio 1 : 100 in an absorption tube of 2 m length, through which, by means of a White mirror system, the light from the source of continuous background was passed 24 times, that is, the absorbing path was 48 m. The partial pressure of CH_2N_2 varied from 0.01 to 0.04 mm. Thus, even assuming that all the CH_2N_2 was decomposed giving CH_2, and all the CH_2 formed was present at the same time, its partial pressure was less than 0.04 mm. Probably it was less by a factor of the order of 10. The strongest lines appear fairly strongly with a path length of 2 m. Therefore, it appears not unlikely that the CH_2 singlet absorption could be observed in the major planets if sufficiently high resolution is applied.

In Table 1 we present the wavelengths of all the stronger lines measured in the region 5300 — 8700 Å. The majority of these lines, but not all, have been classified. The assignments are given in the third and fourth columns of Table 1. A few lines that are weak on our spectrograms have been included because they involve

TABLE 1

Prominent Lines in the Red System of CH_2

λ_{air} (Å)	I	v_1', v_2', v_3'	$J'_{K_aK_c}$—$J''_{K_aK_c}$	Excitation Energy of Lower State above J = 0 in cm^{-1}
5367.387	w	0, 14, 0	2_{02}—1_{10}	31
5375.529	vs	0, 14, 0	2_{02}—2_{12} ; 4_{04}—4_{14}	59, 170
5381.084	m	0, 14, 0	0_{00}—1_{10}	31
5433.488	m	0, 14, 0	4_{22}—4_{14}	170
5480.714	m	0, 14, 0	2_{20}—3_{20}	208
5570.952	ms	0, 14, 0	4_{40}—3_{30}	208
5629.819	m	0, 13, 0	2_{11}—1_{01}	18
5635.718	w	0, 13, 0	1_{10}—0_{00}	0
5640.387	mw	0, 13, 0	1_{11}—1_{01}	18
5646.606	ms	0, 13, 0	3_{13}—3_{03}	105
5647.933	ms	—	—	
5666.048	w	—	—	
5674.651	m	—	—	
5728.755	m	0, 13, 0	5_{23}—4_{23}	226
5739.622	m	0, 13, 0	3_{21}—2_{21}	98
5892.074	ms	0, 12, 0	4_{04}—3_{13}	132
5895.396	w	0, 12, 0	2_{02}—1_{10}	31
5901.897	m	0, 12, 0	6_{06}—6_{16}	340
5905.272	s	0, 12, 0	2_{02}—2_{12}	59
5905.460	s	0, 12, 0	4_{04}—4_{14}	170
5912.236	ms	0, 12, 0	0_{00}—1_{10}	31
5930.625	m	0, 12, 0	2_{02}—3_{13}	132
5931.444	m	—	—	
5952.575	ms	0, 12, 0	4_{04}—5_{14}	304
5956.558	m	0, 12, 0	2_{20}—1_{10}	31
6020.216	m	0, 12, 0	2_{20}—3_{30}	208
6030.312	ms	0, 12, 0	3_{22}—4_{23} ; 3_{21}—4_{21}	283, 284
6068.697	m	1, 8, 0	4_{04}—4_{14}	170
6123.992	m	—	—	
6200.658	m	0, 11, 0	4_{13}—3_{03}	105
6210.214	ms	0, 11, 0	2_{11}—1_{01}	18
6216.098	w	0, 11, 0	1_{10}—0_{00}	0
6221.635	vs	0, 11, 0	7_{17}—7_{07}	445
6223.207	s	0, 11, 0	1_{11}—1_{01}	18
6225.591	vs	0, 11, 0	3_{13}—3_{03}	105
6254.432	m	0, 11, 0	1_{11}—2_{21}	98
6264.760	m	0, 11, 0	2_{11}—3_{21}	158
6265.384	m	—	—	
6272.877	m	0, 11, 0	3_{13}—4_{23}	226
6292.520	m	0, 11, 0	4_{13}—5_{23}	341

λ_{air} (Å)	I	v_1', v_2', v_3'	$J'_{K_aK_c}$—$J''_{K_aK_c}$	Excitation Energy of Lower State above J = 0 (cm^{-1})
6307.687	m	0, 11, 0	3_{21}—2_{21}	98
6310.896	m	0, 11, 0	7_{17}—8_{27}	672
6312.079	m	—	—	
6405.003	m	—	—	
6411.847	m	0, 11, 0	3_{21}—4_{41}	356
6515.312	ms	0, 10, 0	4_{04}—3_{13}	132
6522.062	m	—	—	
6531.684	vs	0, 10, 0	2_{02}—2_{12}, 4_{04}—4_{14}	59, 170
6539.562	m	0, 10, 0	0_{00}—1_{10}	31
6540.375	m	0, 11, 0	3_{22}—2_{12}	59
6548.296	s	—	—	
6562.714	ms	0, 10, 0	2_{02}—3_{13}	132
6589.360	ms	0, 10, 0	4_{04}—5_{14}	304
6616.661	m	(1, 6, 0)	3_{22}—2_{12}	59
6626.916	m	(1, 6, 0)	2_{20}—1_{1}	31
6627.083	m	0, 10, 0	2_{20}—3_{30}	208
6631.597	ms	—	—	
6749.379	m	—	—	
6857.759	m	1, 5, 0	1_{11}—1_{01}	18
6950.827	m	—	—	
6951.431	m	0, 9, 0	3_{13}—3_{03}	105
6985.129	m	0, 10, 0	5_{42}—4_{32}	283
7009.377	ms	0, 9, 0	3_{21}—2_{21}	98
7010.424	ms	0, 9, 0	3_{13}—4_{23}	226
7034.406	m	0, 9, 0	4_{13}—5_{23}	340
7218.983	m	1, 4, 0	2_{02}—1_{10}; 5_{05}—4_{13}	31, 210
7233.750	m	1, 4, 0	2_{02}—2_{12}	59
7236.075	m	1, 4, 0	4_{04}—4_{14}	170
7242.045	m	0, 9, 0	5_{23}—4_{23}	226
7250.843	m	0, 9, 0	4_{31}—3_{31}	158
7254.253	m	0, 9, 0	3_{21}—2_{21}	98
7294.671	ms	0, 8, 0	4_{04}—3_{13}	132
7300.825	mw	0, 8, 0	2_{02}—1_{10}	31
7315.233	ms	0, 8, 0	1_{11}—1_{11} 4_{04}—4_{14};	18, 170
7315.934	ms	0, 8, 0	2_{02}—2_{12}; 1_{01}—1_{11}	59, 18
7322.412	s	—	—	
7325.809	m	0, 8, 0	0_{00}—1_{10}	31
7327.994	s	—	—	
7338.699	m	—	—	
7354.913	ms	0, 8, 0	2_{02}—3_{13}	132
7392.341	ms	0, 9, 0	3_{21}—4_{41}	356
7595.215	s	—	—	

λ_{air} (Å)	I	v_1', v_2', v_3'	$J'_{K_aK_c}$—$J''_{K_aK_c}$	Excitation Energy of Lower State above J = 0 (cm^{-1})
7596.410	s	—	—	
7689.351	s	0, 7, 0	2_{11}—1_{01}	18
7696.051	w	0, 7, 0	1_{10}—0_{00}	0
7705.775	s	0, 7, 0	3_{13}—3_{03}	105
7707.925	m	0, 7, 0	1_{11}—1_{01}	18
7714.283	s	—	—	
7755.920	mw	0, 7, 0	1_{11}—2_{21}	98
7760.128	m	—	—	
7773.222	m	0, 7, 0	2_{11}-3_{21}	158
7786.305	m	—	—	
7864.537	ms	—	—	
7887.457	s	—	—	
7892.595	ms	0, 8, 0	5_{42}—4_{32}	283
7896.248	s	0, 8, 0	4_{40}—3_{30}	208
7904.164	m	(1, 3, 0)	3_{13}—3_{03}	105
7911.032	mw	(1, 3, 0)	1_{11}—1_{01}	18
8053.920	mw	(1, 2, 0)	4_{04}—4_{14}	170
8110.083	m	0, 8, 0	4_{40}—5_{50}	542
8166.041	ms	0, 6, 0	4_{04}—3_{13}	132
8166.388	ms	0, 6, 0	5_{05}—4_{13}	209
8171.187	w	0, 6, 0	2_{02}—1_{10}	31
8178.079	m	0, 7, 0	3_{21}—2_{21}	98
8190.071	vs	0, 6, 0	2_{02}—2_{12}	59
8191.742	vs	0, 6, 0	4_{04}—4_{14}	170
8202.355	s	0, 6, 0	0_{00}—1_{10}	31
8219.248	s	0, 6, 0	1_{01}—2_{11}	70
8238.993	s	0, 6, 0	2_{02}—3_{12}	132
8282.693	ms	0, 6, 0	4_{04}—5_{14}	304
8354.066	m	0, 7, 0	3_{21}—4_{31}	356
8378.845	m	—	—	
8499.888	mw	0, 6, 0	3_{22}—2_{12}	59
8503.430	mw	0, 6, 0	4_{22}—3_{12}	132
8515.352	m	0, 6, 0	2_{20}—1_{10}	31
8519.547	m	—	—	
8531-339	m	0, 6, 0	4_{22}—4_{14}	170
8535.841	m	0, 6, 0	2_{20}—2_{12}	59
8541.880	m	—	—	
8552.541	mw	0, 6, 0	3_{22}—3_{12}	132
8569.865	mw	0, 6, 0	5_{24}—5_{14}	
8646.034	m	0, 6, 0	2_{20}—3_{30}	208
8690.121	s	—	—	

Note : Vibrational assigments in parentheses have not been confirmed.

the lowest rotational levels of the ground state, and may therefore be more prominent at very low temperature.

In the last column of Table 1 is given the energy (in cm^{-1}) of the lower state above the $J = 0$ state for all the assigned lines. This may serve as a guide for the relative intensities of the lines at temperatures other than 300°K, at which our spectrograms were taken. A second absorption system of singlet CH_2 occurs near 3400 Å; but since it is very much weaker than the red system, we need not consider it here.

The width of the CH_2 lines in our experiments is determined entirely by the Doppler effect, which under our laboratory conditions was about 0.02 Å (at 6000 Å). It was always smaller than the instrumental width, the actually attained resolving power being 70,000. Only if it were possible to obtain planetary spectra with a resolution surpassing that of our laboratory spectra could one reach the detection limit of CH_2 (and similarly NH_2). It is unlikely that this limit would be made less favourable because of turbulence or high temperature in the upper atmospheric layers in which CH_2 is produced.

The weak absorption band at 7500 Å observed by Kuiper in the spectra of Uranus and Neptune, does not coincide with any of the CH_2 features. As shown by Table 1, there are no strong features between 7392 and 7595 Å, but even for the weaker features not listed in Table 1 there is no agreement. Kuiper's band therefore remains unidentified. It does not seem entirely impossible that it may yet be due to CH_4 even though laboratory spectra with long paths do not show it. The weak features in planetary spectra correspond to much greater absorbing depths in the atmosphere than the stronger features, as has recently been again demonstrated by Spinrad (1962) in the spectrum of Venus. On the other hand, it must be emphasized that the structure of Kuiper's band with a spacing of 50 cm^{-1} of the principal features, does not fit well with the assumption that it is due to CH_4.

In view of the strong occurrence of CH and CH^+ in cometary

spectra, it is probable that the CH_2 bands here under discussion will occur in comets. However, a preliminary search by Swings (unpublished) has not led to any definite identification.

Even if there were no collisions, CH_2 molecules in the lower $^1A_1$ state of the red bands would eventually go over by radiative transitions to the $^3\Sigma_g^-$ ground state (in which the molecule is linear). To be sure, this transition is not only forbidden by the spin conservation rule, which is fairly strict for such a light molecule, but in addition, there is in all probability a considerable potential barrier between the bent and the linear state. Nevertheless, one must assume that all CH_2 molecules present in the interstellar medium are in the real ground state ($^3\Sigma_g^-$) and that therefore the lines with lower state J = 0 of Table 1, will not be found in interstellar absorption. In the interstellar medium, CH_2 is therefore only detectible by the strong absorption at 1415 Å, which will become accessible when satellite observatories start operating.

We are greatly indebted to Dr. A. E. Douglas for a critical reading of this manuscript.

REFERENCES

DRESSLER, K. and RAMSAY, D. A., *Phil. Trans.*, **251A**, 553, 1959.

HERZBERG, G., *Can. J. Res.*, **28A**, 144, 1950.

HERZBERG, G., *Astrophys. J.*, **115**, 337, 1952.

HERZBERG, G., *Proc. Roy. Soc.*, **262A**, 291, 1961.

KIESS, C. C., CORLISS, C. H., and KIESS, H. K., *Astrophys. J.*, **132**, 221, 1960.

KUIPER, G. P., *Astrophys. J.*, **109**, 540, 1949.

RAMSAY, D. A., *Mém. Soc. R. Sci. Liège*, **18**, 471, 1957.

RANK, D. H., RAO, B. S., SLOMBA, A. F., SITARAM, P., and WIGGINS, T. A., *Nature*, **194**. 1267, 1962 ; *J. Opt. Soc. Am.*, **52**, 1004, 1962.

SPINRAD, H., This symposium.

SPINRAD, H. and MÜNCH, G., This symposium.

12. — SPECTRAL ENERGY DISTRIBUTIONS OF THE MAJOR PLANETS

ROBERT L. YOUNKIN
Jet Propulsion Laboratory
California Institute of Technology
Pasadena, California, U. S. A.

and

GUIDO MÜNCH
California Institute of Technology
Pasadena, California, U. S. A.

1. INTRODUCTION

Color photometry of the major planets, particularly Jupiter and Saturn, has been carried out by a number of authors during the last thirty-five years. The bulk of the work has been photographic, with some photoelectric measurements in recent years.

The nature of the energy distribution curve of the planets may be determined in a general way from such measurements. However the filter band passes used have been many hundreds of Angstroms wide, and the curves obtained consist of points separated by one thousand Angstroms or more.

The logical extension of these measurements is to repeat them with greatly improved spectral resolution. Such a program is being carried out at the Mt. Wilson and Palomar Observatories with a scanning monochromator. A nominal resolution of ten Angstroms in the second order may be obtained with this instrument. This program does not include measurement of the absolute value of the energy, but rather of the relative energy per unit wavelength interval as a function of wavelength.

Preliminary results of the program will be presented here.

2. Instrumentation

The procedure for obtaining and recording the spectral scans is given in Figure 1.

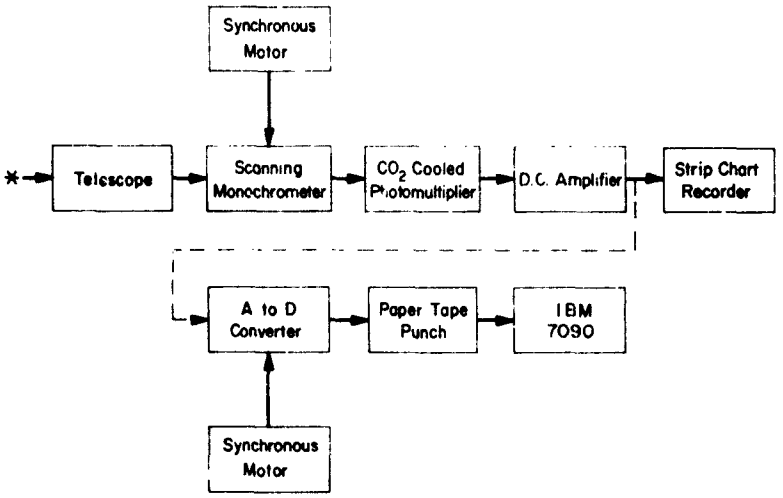

Fig. 1. — Block Diagram of the Instrumentation

The original measurements were made in 1961 with an existing system consisting of the boxes on the first horizontal line. The raw data then consisted of curves on the strip chart recorder. To increase the accuracy of the measurements as well as speed the data reduction, the second row of boxes was added for measurements subsequent to May 1962. The digital information now serves as the primary data source, with the strip chart recorder used only as an immediate check on the data at the time of observation.

All measurements to date have been carried out using the 60-inch telescope at Mt. Wilson. The scanning monochromator used is the Mt. Wilson scanner developed by Code. This is an Ebert monochromator, used with a 600 l/mm, grating blazed for maximum energy at about λ 4000 in the second order.

The spectrum is scanned in two sections. An RCA 1P21 is used to scan from λ 3300 to λ 5200 in the second order. An RCA 7265 is used to scan from λ 4800 to λ 8000 in the first order. Both photo-

multipliers are cooled to dry ice temperature, but mounted in separate cold boxes so it is not feasible to change rapidly from one to the other. In practice the two spectral regions are usually scanned on different nights.

The D. C. amplifier is a General Radio Model 1230 A, and the strip chart recorder a Brown instrument, with a one-second time constant.

The analogue to digital converter for the modified data recording system is a Packard-Bell Model M1. This obtains a binary reading of the voltage, which is punched on the paper tape by a Teletype Model DRPE-2.

The A to D converter has an accuracy of one part in a thousand, full scale, and the sampling rate is currently limited by the tape punch. The spectrum is usually scanned at a rate of 200 A/minute for the second order, and double this for the first. The digital readout is obtained at a nominal rate of one per Angstrom. The sampling rate is controlled by a synchronous motor as is the grating drive of the monochromator. This has eliminated a small uncertainty in wavelength which was previously present when it was necessary to assume uniformity of the chart drive speed.

3. Examples of Planetary Scans

A scan of Jupiter with the 1P21 is shown in Figure 2. At the discontinuity in wavelength, a gain change occurs. A filter to block third order UV was removed near λ 4400.

A scan of Jupiter with the 7265 is shown in Figure 3. The cut-off on the short wavelength side is due to a filter to block second order UV.

In both Figures the wavelength scale is approximate. This scanner does not have a sine drive so the wavelength scale is non-linear.

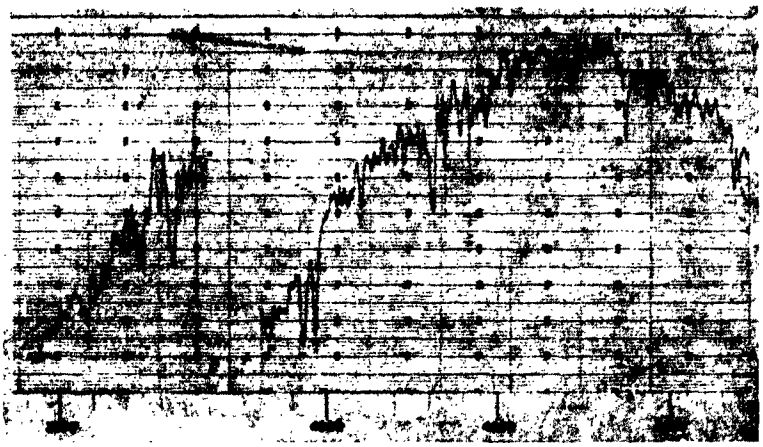

Fig. 2. — Second Order Scan of Jupiter

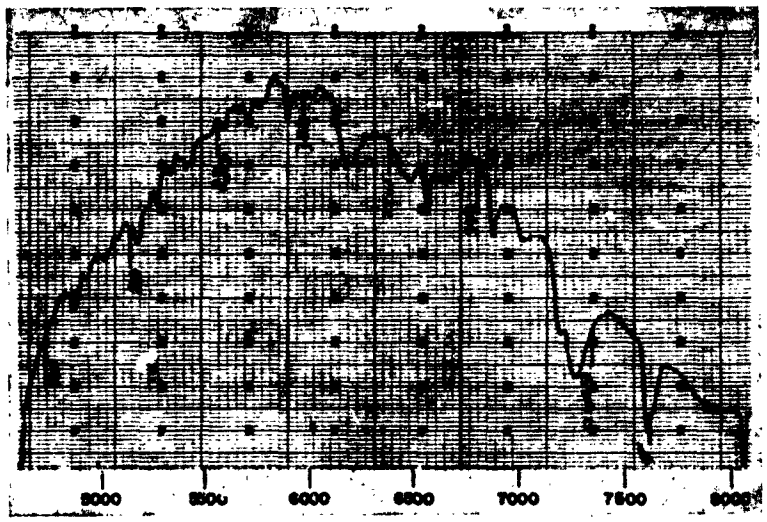

Fig. 3. — First Order Scan of Jupiter

4. Reduction of Data

No provision has been made to carry out an absolute calibration to determine the color sensitivity of the telescope-photomultiplier system. Instead, the star α Lyr has been adopted here

as a primary standard. The energy distribution of this star has been determined relative to laboratory black-body sources by several authors. The mean curve of Code ([1]) has been adopted for these calculations, with the modification of Oke ([2]) near the Balmer limit.

Oke ([2]), using the same scanner used here on the planets, has determined the energy distribution relative to α Lyr of six other stars of spectral classes B7 to A0 for the spectral range λ 3390 to λ 5882. This group of stars has recently been enlarged to twelve, and the wavelength range extended to λ 11000. They have been used as secondary standards for the major planet program.

These standards have relatively smooth continua, except for hydrogen absorption. To determine the color response of this system, on nights that the planets are scanned, scans are also made of α Lyr and the secondary standard closest to each planet. A smooth curve is then drawn across the hydrogen lines of the standards, except in the region λ 4000 down to the Balmer limit. Here the Balmer lines are crowded so close together it is not possible to determine the continuum level. For this region a smooth curve is drawn for the difference $(\alpha\ \mathrm{Lyr}_{\mathrm{Code}} - \alpha\ \mathrm{Lyr}_{\mathrm{Mt.\,W.}})$ or $(\mathrm{Star}^{\blacksquare}_{\mathrm{Oke}} - \mathrm{Star}_{\mathrm{Mt.\,W.}})$.

It is planned to reduce the data for each planet against this secondary standard. The measurements by Oke of the secondary standards are still in progress, so the curves at the end of this paper have been obtained by the use of α Lyr only. This procedure will of course neglect possible spacial inhomogeneities in the atmosphere.

For removal of the atmospheric extinction from the measured curves, an extinction of the following form has been assumed

$$\exp\left[-(A_0 + A_1\lambda^{-4})\sec z - A_2(\lambda)\right]$$

where $A_2(\lambda)$ is extinction due to absorption bands which may exhibit a curve of growth. It has been assumed the product of A_0 times the change in sec z is small compared to the Rayleigh term. The Rayleigh extinction has been removed by means of a standard

Rayleigh atmosphere. The coefficient A_1 has been determined experimentally at Mt. Wilson by Oke ([3]).

Extinction due to telluric absorption has been removed for the λ 6870, λ 7200, and λ 7600 O_2 bands. Where these bands are clearly defined in the planetary scan, they are removed by drawing a smooth curve across the band. For those cases where absorption in the planetary atmosphere obliterates the shape of the O_2 band, correction is made by interpolation to the proper air mass from a curve of absorption vs. air mass for those planets and stars for which the shape of the band is clearly defined.

5. Spectral Energy Distributions of the Major Planets

Measurements of the spectral energy distributions are still in progress. Nevertheless, in the complete absence of any such « high » resolution data in the literature, examples of the reduced curves will be presented here. These may be considered as provisional energy distributions. The 7090 program is not yet completed, so these curves have been obtained by planimetering the data in 100 Angstrom intervals between wavelengths of even hundred Angstroms.

The curve for each planet is obtained by fitting together the first and second order curves, which overlap from λ 4800 to λ 5200.

Figure 4 gives the energy distribution for Jupiter, and Figure 5 for Saturn. In the case of Jupiter the slit covered an area near the center of the image of the planet, for Saturn, half way between the inside edge of the ring in front of the planet, and the upper edge of the planet.

The large dip in these curves with minimum at λ 7200-λ 7300 is methane absorption, as is the smaller one from λ 6100-λ 6300. It may be seen from these points that methane absorption is greater for Saturn, in accordance with the finding of previous authors.

The relative maximum for Jupiter occurs over the region λ 5500 to λ 6100 and for Saturn, λ 5500 to λ 6500. These are in con-

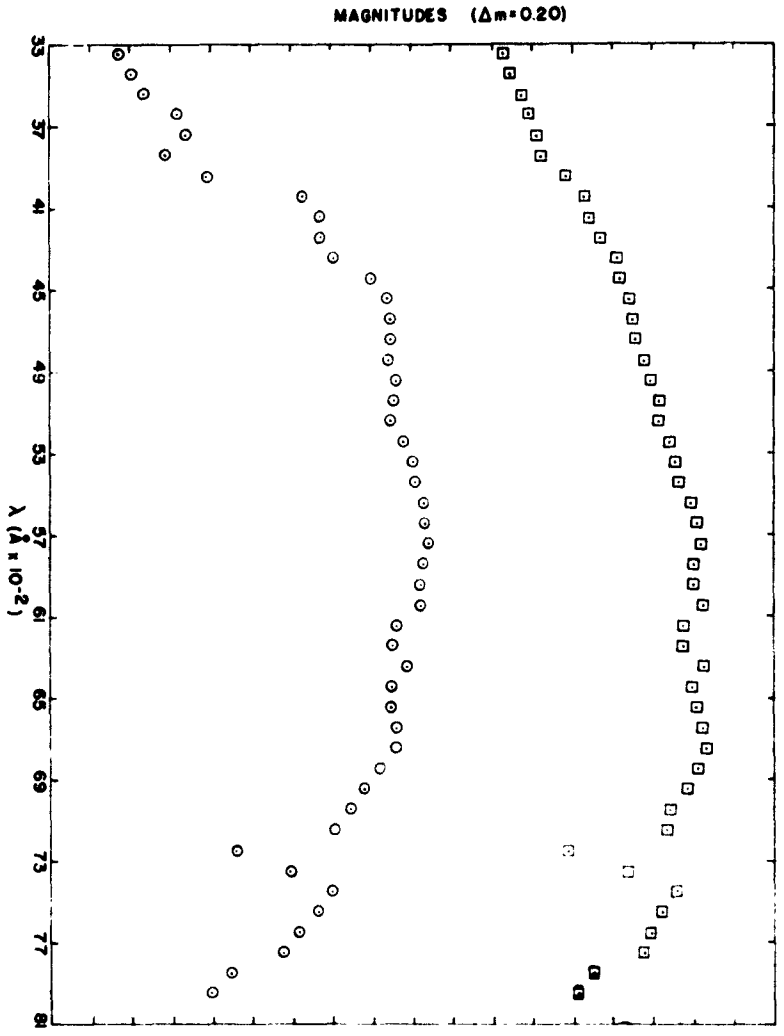

Fig. 4. — Jupiter. ⊙ — Spectral Energy Distribution. ⊡ — Reflectivity.

trast with the solar energy distribution which exhibits a maximum from λ 4500 to λ 4900.

Detailed comparison of the energy distributions is difficult unless the two curves agree over a substantial region of the spectrum. The curves for Jupiter and Saturn do not. It does appear however that Saturn's energy falls off more rapidly shortward of at least λ 4900, followed by the unique minimum near λ 3850.

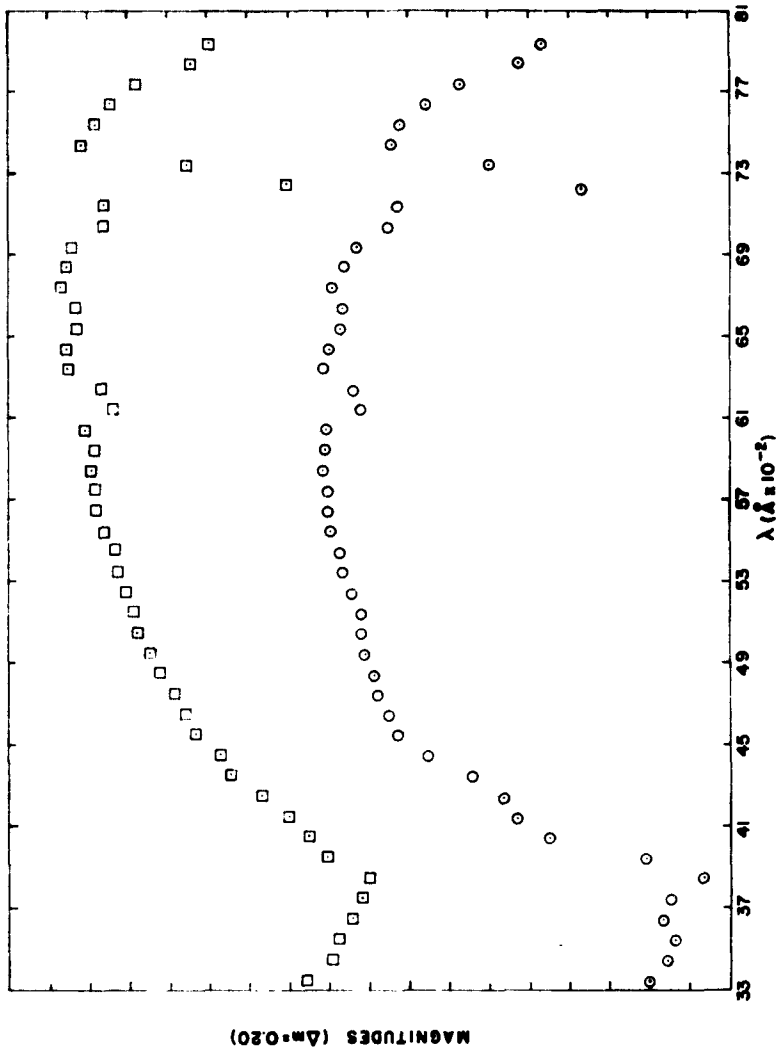

Fig. 5. — Saturn. ⊙ — Spectral Energy Distribution. ⊡ — Reflectivity.

Figure 6 gives the energy distribution for Uranus and Figure 7 for Neptune. For these two planets slitless spectroscopy of the whole disk was used.

For Neptune and to a lesser degree Uranus, in order to receive sufficient energy on the photomultiplier at the resolutions used, it is necessary to increase the amplifier gain to a point where dark current pulses become troublesome. The Neptune curve has there-

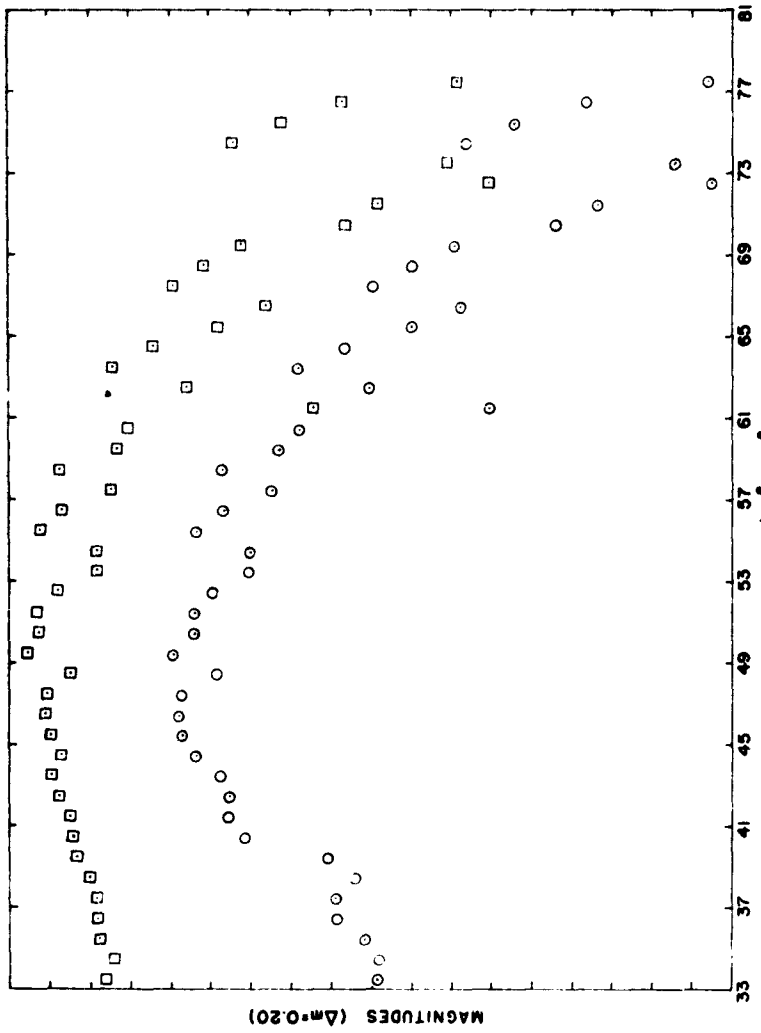

Fig. 6. — Uranus : ⊙ — Spectral Energy Distribution. ⊡ — Reflectivity.

fore been cut-off at λ 7000 and Uranus at λ 7800 pending further analysis of the data.

For these two planets, longward of approximately λ 5000 the spectra are dominated by a continuous series of methane bands which make it impossible to determine the true continuum level with this resolution.

Comparison of the energy distributions of the four planets

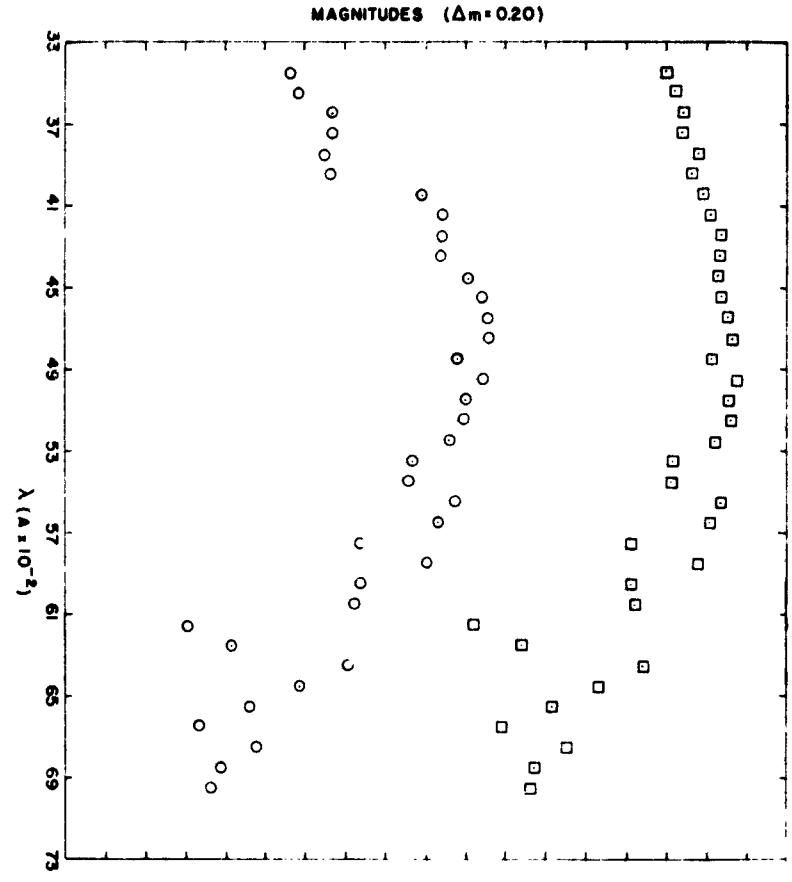

Fig. 7. — Neptune : ⊙ — Spectral Energy Distribution. ⊡ — Reflectivity.

shows the great similarity between Uranus and Neptune, and between Jupiter and Saturn, compared to differences between the two groups. This is exhibited particularly by the methane dominance mentioned above and to a lesser degree by the slope in the blue and UV region. In this latter region the Uranus and Neptune curves are very similar while Jupiter and Saturn both show markedly greater slopes although differing somewhat.

6. Planetary Reflectivities

It is not possible to make direct measurements of the solar

spectrum with this instrument. Instead, a standard solar curve has been adopted from the work of other observers.

The most extensive work on the solar energy distribution was done by observers at the Smithsonian Institution. Their results were slightly modified by Johnson ([4]) and his values were used here from λ 4100 to λ 8000. Below λ 4000 the solar absorptions cause greater local fluctuations in the energy distribution curve. However the Smithsonian resolution was considerably less than that used here and in this region Johnson's values do not smooth out the fluctuations in the planetary values.

Dunkelman and Scolnik ([5]) have recently remeasured the solar spectral irradiance to λ 6500. Their resolution more nearly approximates that used here, although still somewhat less. Their integrated curve compares closely with the Smithsonian data. Their values have been fitted to the Smithsonian data and are used for $\lambda < 4100$ A.

Planetary reflectivities have been calculated with the use of this composite solar curve and are shown in Figures 4-7. This net effect is to raise both ends of the curves and to smooth out regions where there are no planetary absorptions. The energy of all four planets still falls off steadily toward the UV, Jupiter and Saturn from maxima which now have moved out to λ 6750.

7. Concluding Remarks

A formal averaging process of the reduced curves for a given planet has been reserved for a later publication primarily because certain refinements in the instrumentation are still being made which will decrease the probable errors. In general the curves reduced to date repeat quite well and it is anticipated that changes from these provisional curves will be small, less than $\Delta m = \pm 0.03$ in local regions. Modifications between UV regions and curve maxima may exceed this because of the standard atmosphere assumed to date.

REFERENCES

(1) CODE, A. D., *Stellar Atmospheres*, edited by J. L. Greenstein, The University of Chicago Press, p. 50, 1960.

(2) OKE, J. B., *Ap. J.*, **131**, 358, 1960.

(3) OKE, J. B., Private Communication.

(4) JOHNSON, F. S., *J. Meteorology*, **11**, 431, 1954.

(5) DUNKELMAN, L., and SCOLNIK, R., *JOSA*, **49**, 356, 1959.

13. — HYDROGEN AND HELIUM RESONANCE RADIATION FROM THE PLANETS

JOHN C. BRANDT
Berkeley Astronomical Department
University of California, U. S. A.

1. VENUS AND MARS

The diffuse Lyman-α radiation in the night sky discovered by Kupperian, Byram, Chubb, and Friedman (1958, 1959) has been interpreted as solar Lyman-α radiation scattered by a cloud of terrestrial hydrogen (Brandt 1961 a, b). It is natural, then, to inquire about the possibility of similar hydrogen (and helium) emissions from other planets such as Venus and Mars. As on the earth, the existence of appreciable amounts of neutral hydrogen on Venus and Mars depends on a production process ; we assume that the process is the same as in the terrestrial atmosphere, namely, the photodissociation of water vapor. Since the amount of water in these planetary atmospheres may be relatively small compared to the amount in the terrestrial atmosphere, the relative amount of neutral hydrogen may also be smaller (see Kellogg and Sagan, 1961).

An observer looking down on the day side of the earth would see the diffuse reflection of solar Lyman-α from a conservative, isotropic scattering atmosphere of approximately unit opacity. The emission rate is given by (Chandrasekhar 1960, p. 211 and p. 218).

$$4\pi I_\nu (0, \mu) = (\pi F_\nu) \frac{\mu_0}{\mu + \mu_0} [X^*(\mu) X^*(\mu_0) - Y^*(\mu) Y^*(\mu_0)], \quad (1)$$

where the notation is standard and the functions $X^*(\mu)$ and $Y^*(\mu)$ have been tabulated (Chandrasekhar and Elbert 1952). To obtain the total line intensity, one then integrates equation (1) over the full Doppler width of the atmosphere (taken as due to a temperature of 300-400°K for the earth).

We adopt a flux in Lyman-α of 6 ergs/cm^2-sec and a width of

1A (Purcell and Tousey 1960). The day emission rate for the earth then becomes

$$4\pi I_{\oplus}\ (\lambda\ 1215) \approx 10\ k\mathrm{R}. \tag{2}$$

One rayleigh(R) corresponds to an apparent emission rate of $4\pi I = 10^9$ photons/cm^2-sec (column). By simply scaling the incident solar flux, we may compute upper limits to the day intensity of diffuse Lyman-α on Venus and Mars. These values are

$$4\pi I_{\varphi}\ (\lambda 1215) \lesssim 25\ k\mathrm{R}, \tag{3}$$

and

$$4\pi I_{\sigma}\ (\lambda 1215) \lesssim 5\ k\mathrm{R}. \tag{4}$$

Observations of the day intensity of diffuse Lyman-α radiation from close approaches could yield valuable information concerning the abundance of hydrogen, the scale height and the temperature in the outer layers, the abundance and photochemistry of water vapor, and the rate of escape of planetary atmosphere (see also Chamberlain 1961).

The day problem for reflection of $\lambda 584$ by neutral helium in the terrestrial atmosphere has been treated (Brandt 1961c). The terrestrial atmosphere is thought to be optically thick over the full Doppler width of the atmosphere. The intensity is given by (Chandrasekhar 1960, p. 124)

$$4\pi I_{\nu} = (\pi F_{\nu}) \frac{\mu_0}{\mu + \mu_0} H(\mu)\, H\ (\mu_0), \tag{5}$$

where the H-functions have been tabulated (Chandrasekhar 1960, p. 125). We adopt the same parameters as before (Brandt 1961c) to obtain

$$4\pi I_{\oplus}\ (\lambda 584) \approx 1000\ \mathrm{R}. \tag{6}$$

When the fluxes are changed for Mars and Venus, we find

$$4\pi I_{\sigma}\ (\lambda 584) \lesssim 400\ \mathrm{R}, \tag{7}$$

and

$$4\pi I_{\varphi}\ (\lambda 584) \approx 2000\ \mathrm{R}. \tag{8}$$

The scaling receives some justification from the fact that the densities of the earth, Mars, and Venus are similar, and because

helium is produced in the earth's crust by the radioactive decay of thorium and uranium. The inequality has been placed in equation(7) as Mars has a mass approximately 1/10 that of the earth. There is some expectation that Mars has undergone less geological differentiation than the Earth, that less crustal concentration of U and Th has occured, and that, consequently, the abundance of radiogenic He is smaller on Mars (Sagan, 1962 a).

Observations of the λ584 radiation from Mars and Venus could yield valuable information concerning the composition of the crust and rate of escape of helium in addition to the abundance and scale height of helium. The expected terrestrial day intensity of λ304 is small (Brandt 1961*c*), and we will not consider this line here.

2. Jupiter and Saturn

In a recent study, Zabriskie (1962) has determined the column density of molecular hydrogen above the cloud tops in the Jovian atmosphere and finds $N(H_2) = 1.25 \times 10^{25}/cm^2$. This value and the appropriate cross section for Rayleigh scattering by H_2 (e. g., Vardya 1962) give an opacity above the cloud tops of about 5 at λ1215. Thus, there is the possibility that the far ultraviolet spectrum of Jupiter may be largely the solar spectrum diffusely reflected by a conservative, Rayleigh scattering atmosphere (which we approximate as scattering according to Rayleigh's phase function, $p(\Theta) = 3/4\,(1 + \cos^2\Theta)$, where Θ is the scattering angle).

For observations of Jupiter at opposition from the earth, $\mu \doteq \mu_0$, $\varphi \doteq \varphi_0$, and the diffusely reflected intensity from a conservative atmosphere scattering on Rayleigh's phase function can be written (Chandrasekhar 1960, p. 143) as

$$\frac{4\pi I(\mu)}{(\mu F_\odot)} = 3/16\,\{1/3\,\psi^2(\mu) + 8/3\varphi^2(\mu) - [2\mu\,(1-\mu^2)^{1/2}H^{(1)}(\mu)]^2 + [(1-\mu^2)\,H^{(2)}(\mu)]^2\} = R(\mu). \tag{9}$$

The functions $\psi(\mu)$, $\varphi(\mu)$, $2\mu(1-\mu^2)^{1/2}\,H^{(1)}(\mu)$, and $(1-\mu^2)\,H^{(2)}(\mu)$ have been tabulated by Chandrasekhar (1960, p. 145, Table XXI). The flux from an atmosphere scattering on Rayleigh's phase function is readily calculated and is

$$(\pi F) = \frac{(\pi F_\odot)}{2}\left(\frac{r}{d}\right)^2 \int_0^1 \mu R(\mu) d\mu \qquad (10)$$

Here r is the radius of the planet under observation and d is the distance. The integral in equation (10) has the value 1.37.

The only observations available to test the hypothesis of Rayleigh scattering are the observations of Boggess and Dunkelman (1959). These rocket observations at 2700A give a flux from Jupiter of 1.65×10^{-7} ergs/cm^2-sec-100A. The same quantity can be calculated from equation (10) with the aid of known solar fluxes (Hinteregger 1961) and we obtain 8.2×10^{-7} ergs/cm^2-sec-100A. Thus, the observed flux is about 20 percent of the computed flux, and hence, an absorbing process must be important at 2700 A. This behavior is roughly consistent with ground based photometry (Harris 1961). The fact that only 20 percent of the « expected » flux at 2700A is observed should not be surprising. The atmosphere is far from optically thick in Rayleigh scattering by H_2 above the cloud tops as the opacity is only 1/5. Hence, the absorption could be caused by constituents in the clouds. We note also that the observations at 2700A could be influenced by the dissociation continuum of H_2. On the basis of the ultraviolet photometry (λ3500, see Harris 1961) we would favor absorption in the clouds (see also, Sagan, 1962b). The region near λ1215 is optically thick above the cloud tops and away from the H_2 dissociation limit. Hence, calculations of the Lyman-α intensity on the basis of an optically thick, conservative, Rayleigh scattering atmosphere may be reasonable. In any event, these numbers may be regarded as upper limits.

From equation (9), we may calculate the intensity at any point on the disk of Jupiter, e. g.,

$$4\pi I_{2\downarrow}\ (\lambda 1215 : \text{disk-center}) \approx 60\, k\mathrm{R}, \qquad (11)$$

and

$$4\pi I_{2\downarrow}\ (\lambda 1215 : \text{limb}) \approx 10kR. \tag{12}$$

The flux from Jupiter at the earth can be computed from equation (10) and is

$$\pi F_{2\downarrow}\ (\lambda 1215 : \text{opposition}) \approx 2 \times 10^{-9}\ \text{ergs/cm}^2\text{-sec}. \tag{13}$$

Such fluxes are measurable with present day techniques. It is simply necessary to use a sufficiently small field of view to reduce the contamination due to terrestrial hydrogen (Friedman 1962).

The analogous quantities for the helium lines from Jupiter are easily computed from Hinteregger's (1961) data. For λ584, the flux is 3×10^{-11} ergs/cm²-sec and the emission rate (disk-center) is 500 R. For λ304, the flux is 8×10^{-11} ergs/cm²-sec and the emission rate (disk-center) is 650R.

The quantities for Lyman-α from Saturn follow from equations (9) and (10) and are :

$$4\pi I_{\hbar}\ (\lambda 1215 : \text{disk-center}) \approx 20\ kR\ ; \tag{14}$$

$$4\pi I_{\hbar}\ (\lambda 1215 : \text{limb}) \approx 3\ kR\ ; \tag{15}$$

and

$$\pi F_{\hbar}\ (\lambda 1215 : \text{opposition}) \approx 1 \times 10^{-10}\ \text{ergs/cm}^2\text{-sec} \tag{16}$$

For λ 584, the flux is 2×10^{-12} ergs/cm²-sec and the emission rate (disk-center) is 150 R. For λ 304, the flux is 4×10^{-12} ergs/cm²-sec and the emission rate (disk-center) is 200 R.

Observations of the hydrogen and helium resonance lines from Jupiter and Saturn could provide us with clues concerning the scattering mechanism and the presence of absorbing media in these atmospheres.

3. Conclusions

It appears that Lyman-α radiation can be observed with present day techniques from Venus, Mars, Jupiter, and Saturn if the intensities are near the estimates given in this paper. It is clear that much valuable information concerning the particular atmosphere would be obtainable from such observations. Observations of the

Raman band (Q-branch) near 1280A (Herzberg 1950, p. 62 and p. 114) due to Lyman-α may also be of some value in the study of the atmospheres of Jupiter and Saturn.

Valuable information concerning the crusts (and possibly the interior) of Mars and Venus may be obtainable from observations of the helium line λ 584.

I am indebted to Drs. H. Friedman and C. Sagan for helpful communications.

REFERENCES

Boggess, A. and Dunkelman, L., *Ap. J.*, **129**, 236, 1959.

Brandt, J. C., *Ap. J.*, **134**, 394, 1961a.

— *Space Research II*, edited by H. C. van de Hulst, C. de Jager, and A. F. Moore, p. 624, North-Holland Publishing Co., Amsterdam, 1961b.

— *Ap. J.*, **134**, 975, 1961c.

Chamberlain, J. W. in *The Atmospheres of Mars and Venus*, ed. W. W. Kellogg and C. Sagan, National Academy of Sciences-National Research Council Publication 944, Washington, p. 147, 1961.

Chandrasekhar, S., *Radiative Transfer*, Dover, New York, 1960.

Chandrasekhar, S. and Elbert, D., *Ap. J.*, **115**, 269, 1952.

Friedman, H., private communication, 1962.

Harris, D. L., *Planets and Satellites*, ed. G. P. Kuiper and B. M. Middlehurst, University of Chicago Press, Chicago, 1961.

Herzberg, G., *Spectra of Diatomic Molecules*, 2nd ed., D. Van Nostrand Co., New York, 1950.

Hinteregger, H. E., *J. Geophys. Res.*, **66**, 2367, 1961.

Kellogg, W. W. and Sagan, C., *The Atmospheres of Mars and Venus*, National Academy of Sciences, National Research Council Publication 944, Washington, 1961.

Kupperian, J. E., Byram, E. T., Chubb, T. A., and Friedman, H., *Ann. Geophys.*, **14**, 329, 1958.

— *Planet. Space Sci.*, **1**, 7, 1959.

Purcell, J. D. and Tousey, R. J., *J. Geophys. Res.*, **65**, 370, 1960.

Sagan, C., private communication, 1962a.

— to be published, 1962b.

Vardya, M. S., *Ap. J.*, **135**, 303, 1962.

Zabriskie F. R., *A. J.*, **67**, 168, 1962.

14. — NUMERICAL SOLUTIONS OF THE AUXILIARY EQUATION FOR AN INHOMOGENEOUS PLANETARY ATMOSPHERE (*)

J. S. GOLDSTEIN

Brandeis University
Waltham, Mass.
and
Baird Atomic, Inc.
Cambridge, Mass., U. S. A.

I. Introduction

The problem of scattering in a planetary atmosphere has been considered by Chandrasekhar (1950) and others. We wish to extend this treatment to the case of an atmosphere in which, for one of several reasons, the ratio of the local mass scattering coefficient to the local mass extinction coefficient may vary. This ratio, which is termed the local albedo, will be considered in this note to vary only with depth in the atmosphere.

There are two distinct reasons why the local albedo may be a function of depth in a planetary atmosphere. The more obvious reason is a variation in chemical composition with depth, leading to a change in absorptivity with a non-compensating change in the mass scattering coefficient. Examples of this phenomenon are to be expected in all planetary atmospheres ; thus, in the terrestrial atmosphere, the highest levels contain dissociated oxygen and nitrogen ; at lower levels, the molecular forms predominate, and in the ozonosphere, the O_3 molecule contributes a large absorptivity at about 9 microns. In the atmosphere of Mars, according to the model of Chamberlain (1962), the upper levels are rich in the molecule CO ; at an altitude of about 130 km., there is a transition to the CO_2 molecule, together with a thin layer of O_2.

In the infrared portion of the spectrum, there is an additional reason why, even in a chemically homogeneous atmosphere, the local albedo may vary with depth, and this effect is due to pressure

(*) Suported in part by U. S. Air Force Cambridge Research Laboratory, Office of Aerospace Research, under Contract AF 19(604)-7283.

broadening of spectral lines. If an absorption line is completely contained within the slit width of the detector, and if the path length is long enough so that the line center begins to saturate in absorption, then an increase in line width due to pressure broadening will lead to an increase in the observed absorption as seen by the detector. For a detector of finite slit width, the observed absorptivity usually consists of an average over many spectral lines. This effect leads to a significant departure from the usual exponential attenuation law, and also leads to an effective absorption coefficient which is dependent on the pressure. This case has been considered by Goldstein (1960), where a solution of the scattering problem is obtained as an expansion in the number of scatterings.

II. The Equation for the Reflectivity

The general equation for the reflectivity of an atmosphere for which the local albedo is a function of depth has been derived by Bellman (1956) and by Goldstein (1960). The assumptions which are made are the following :

a) The atmosphere is considered to be stratified in planes of constant z, that is, all atmospheric parameters such as density, etc., are functions of z only ;

b) The atmosphere is considered to be infinitely thick, although this restriction can ultimately be removed ;

c) At the wavelength considered the atmosphere is sufficiently cold to permit the neglect of self-emission (*).

(*) The solution for the case when emission cannot be neglected is in any case based on the solution for no emission. The case for no emission leads to an equation (e. g., eq. (3)) which is termed the « auxiliary equation » by Busbridge (1960).

Assumption (a) permits the definition of the optical thickness τ:

$$\tau(z) = \int_z^\infty \rho(z')k(z')dz' \tag{1}$$

where $\rho(z)$ is the density, and $k(z)$ is the total extinction coefficient at the wavelength in question (the dependence of various parameters on wavelength will not be indicated explicitly). In equation (1) the positive direction of τ is taken inwards ; that is, $\tau = 0$ corresponds to a point outside the atmosphere.

The outward and inward radiative intensities are denoted by I_+, I_- respectively. These quantities are functions of the variable τ and of the directions, denoted by (μ, φ). Here φ is the azimuthal angle, and μ is defined as the cosine of the acute angle between the beam and z- direction. By convention, $0 \leqslant \mu \leqslant 1$.

The reflectivity may then be defined by the equation

$$I_+(\tau, \mu, \varphi) = \frac{1}{\mu}\int_0^1 d\mu' \int_0^{2\pi} d\varphi' \, S(\tau ; \mu, \varphi ; \mu', \varphi') \; I_-(\tau, \mu', \varphi') \tag{2}$$

and it follows directly from the equation of radiative transfer that the reflectivity, S, satisfies the following nonlinear integral equation (where the symbol Ω stands for (μ, φ)) :

$$S(\tau, \Omega, \Omega_0) = \frac{1}{4\pi}\int_\tau^\infty \omega(\tau')e^{-\left(\frac{1}{\mu}+\frac{1}{\mu_0}\right)(\tau'-\tau)} d\tau' \{ \gamma(\Omega, \Omega_0)$$

$$+\int_0^1 \frac{d\mu'}{\mu'}\int_0^{2\pi} d\varphi'[S(\tau', \Omega, \Omega')\gamma(\Omega', \Omega_0) + \gamma(\Omega, \Omega')S(\tau', \Omega', \Omega_0)] \tag{3}$$

$$+\int_0^1 \frac{d\mu'}{\mu'}\int_0^{2\pi} d\varphi' \int_0^1 \frac{d\mu''}{\mu''}\int_0^{2\pi} d\varphi'' \, S(\tau', \Omega, \Omega') \, \gamma(\Omega', \Omega'') \, S(\tau', \Omega'', \Omega_0)\}$$

This equation is to be understood as follows : the quantity $\omega(\tau)$ is what we have called the local albedo ; if σ is taken as the local mass scattering coefficient, we have

$$\omega(\tau) = \sigma(\tau)/k(\tau) \tag{4}$$

where the z-dependence of σ and k has been replaced by a τ-dependence. The quantity $\gamma(\Omega, \Omega_0)$ is the scattering phase function,

representing the probability of scattering from direction Ω_0 into direction Ω. This function is normalized to 4π, i. e.

$$\int_{-1}^{1} d\mu \int_{0}^{2\pi} d\varphi\, \gamma(\Omega, \Omega_0) = 4\pi \tag{5}$$

The phase function is always a function only of the cosine of the angle between the two directions. We shall be concerned principally with the case of isotropic scattering, characterized by $\gamma = 1$. Rayleigh scattering, with $\gamma = 3/4(1 + \cos^2\theta)$, will also be discussed, and we shall make some comments regarding other phase functions. The full derivation of eq. (3) may be found in the paper by Bellman or that of Goldstein. The problem of variable local albedo has also been considered by Case (1957).

III. Isotropic Scattering

We consider now approximate methods for the solution of eq. (3). A case of particular interest, owing to its relative simplicity, is the case of isotropic scattering, $\gamma = 1$. This case is characterized by a relatively slow convergence of the iteration process previously mentioned. We, therefore, seek a more suitable procedure.

For $\gamma = 1$, the reflectivity is independent of the azimuthal angle φ. Eq. (3) then assumes the form

$$S(\tau, \mu, \mu_0) = \frac{1}{4\pi} \int_{\tau}^{\infty} \omega(\tau') e^{-\left(\frac{1}{\mu} + \frac{1}{\mu_0}\right)(\tau' - \tau)} d\tau'$$

$$\left[1 + 2\pi \int_0^1 \frac{d\mu'}{\mu'} S(\tau', \mu, \mu')\right] \left[1 + 2\pi \int_0^1 \frac{d\mu'}{\mu'} S(\tau', \mu', \mu_0)\right] \tag{6}$$

It is readily seen that $S(\tau, \mu, \mu_0)$ is symmetric in the arguments μ, μ_0. Following the approach used by Chandrasekhar when $\omega =$ constant, we define

$$\mathscr{H}(\tau, \mu) = 1 + 2\pi \int_0^1 \frac{d\mu'}{\mu'} S(\tau, \mu, \mu') \tag{7}$$

from which it follows at once that $\mathscr{H}(\tau, \mu)$ satisfies the following non-linear equation :

$$\mathscr{H}(\tau, \mu)=1+\tfrac{1}{2}\int_0^1 \frac{d\mu'}{\mu'}\int_\tau^\infty \omega(\tau')e^{-\left(\frac{1}{\mu}+\frac{1}{\mu'}\right)(\tau'-\tau)}\,\mathscr{H}(\tau', \mu')\mathscr{H}(\tau', \mu)d\tau' \quad (8)$$

In the event $\omega(\tau) =$ constant, the $\mathscr{H}$-functions may be assumed to be independent of τ. In that case, the τ' integration may be carried out at once, and the familiar equation for the Chandrasekhar H-function is obtained.

For general $\omega(\tau)$, the manipulations used by Chandrasekhar cannot be used ; in particular, the moment integrals cannot be obtained. While we hope eventually to compute the function $H(\tau, \mu)$ exactly, for the present work we have used an approximation method which is presented below.

We introduce the notation $H_\omega(\mu)$ for the Chandrasekhar H-function appropriate to the constant albedo ω. Let us then assume that eq. (8) may be solved approximately by such a function for an albedo ϖ which may depend on τ, but not on τ'. Thus, we assume

$$H_\varpi(\mu) \approx 1 + \tfrac{1}{2}\int_0^1 \frac{d\mu'}{\mu'}\int_\tau^\infty \omega(\tau')e^{-\left(\frac{1}{\mu}+\frac{1}{\mu'}\right)(\tau'-\tau)}\,H_\varpi(\mu')\,H_\varpi(\mu)d\tau' \quad (9)$$

The parameter ϖ must now be determined to make the error as small as possible.

We expand $\omega(\tau')$ in a power series about $\tau' = \tau$

$$\omega(\tau') = \omega(\tau) + (\tau' - \tau)\omega'(\tau) + \ldots \quad (10)$$

The exponential factor ensures that we do not have to consider values of $(\tau' - \tau)$ much in excess of $\left(\frac{1}{\mu}+\frac{1}{\mu'}\right)^{-1} < \frac{1}{2}$. We obtain then

$$H_\varpi(\mu) \approx 1 + \frac{\omega(\tau)}{2}\int_0^1 \frac{d\mu'}{\mu'}\int_\tau^\infty e^{-\left(\frac{1}{\mu}+\frac{1}{\mu'}\right)(\tau'-\tau)}\,H_\varpi(\mu')\,H_\varpi(\mu)\,d\tau' \quad (11)$$

$$+ \frac{\omega'(\tau)}{2}\int_0^1 \frac{d\mu'}{\mu'}\int_\tau^\infty (\tau' - \tau)e^{-\left(\frac{1}{\mu}+\frac{1}{\mu'}\right)(\tau'-\tau)}\,H_\varpi(\mu')\,H_\varpi(\mu)\,d\tau' + \ldots$$

The Chandrasekhar H-functions satisfy eq. (9), with $\omega(\tau') = \varpi$;

consequently the integrals in (11) are easily evaluated, and we obtain the following equation for ϖ :

$$H_{\varpi}(\mu) \approx 1 + \frac{\omega(\tau)}{\varpi}[H_{\varpi}(\mu) - 1] + \frac{\omega'(\tau)}{\varpi}\mu^2 \frac{H'_{\varpi}(\mu)}{H_{\varpi}(\mu)} + \ldots \quad (12)$$

As might have been expected, when $\omega'(\tau)$ is small, a reasonable solution of this equation is

$$\varpi = \omega(\tau) \quad (13)$$

If we introduce this approximation, the last term in eq. (12) represents the error ; dividing that term by $H_{\omega(\tau)}(\mu)$, we obtain the fractional error, which we denote by δ :

$$\delta = \frac{\omega'(\tau)}{\omega(\tau)}\mu^2 \frac{H'_{\omega(\tau)}(\mu)}{H^2_{\omega(\tau)}(\mu)} \quad (14)$$

Under this approximation, the reflectivity S may now be written

$$S(\tau, \mu, \mu_0) \approx \frac{1}{4\pi}\int_{\tau}^{\infty} \omega(\tau') e^{-\left(\frac{1}{\mu}+\frac{1}{\mu_0}\right)(\tau'-\tau)} H_{\omega(\tau')}(\mu) H_{\omega(\tau')}(\mu_0) \quad (15)$$

This function has been calculated for three different functional variations of $\omega(\tau)$, which may be expected to be of physical significance. It should be noted that in the event δ is not very small, an improved approximation to ϖ can be obtained by iterating eq. (12) one or more times, in which case ϖ becomes a function of μ as well as of τ.

IV. Numerical Evaluation of $S(\tau, \mu, \mu_0)$ for the Isotropic Case

The local albedo, $\omega(\tau)$, defined by eq. (4) can in some cases be represented as

$$\omega(\tau) = \sigma/(\sigma + \varkappa_\lambda p(\tau)/p_0) \quad (16)$$

where σ is the mass-scattering coefficient, and $\varkappa_\lambda$ is the mass-absorption coefficient for λ-radiation. The ratio $p(\tau)/p_0$ is introduced to account for the effective change in absorption path length

due to pressure broadening. (The effects of temperature broadening, which ought also to be included, have been neglected on the grounds that this is in general a smaller effect).

If one assumes an exponential isothermal atmosphere, in which the density is given by

$$\rho(z) = \rho_0 e^{-z/H} \; ; \; p(z) = p_0 e^{-z/H} \tag{17}$$

then τ, the optical thickness, may be written

$$\tau = \int_{\tau}^{\infty} [\sigma + \varkappa_\lambda p(z)/p_0], \; \rho(z)dz = \sigma H \rho_0 e^{-z/H} + \frac{\varkappa_\lambda H \rho_0}{2} e^{-2z/H} \tag{18}$$

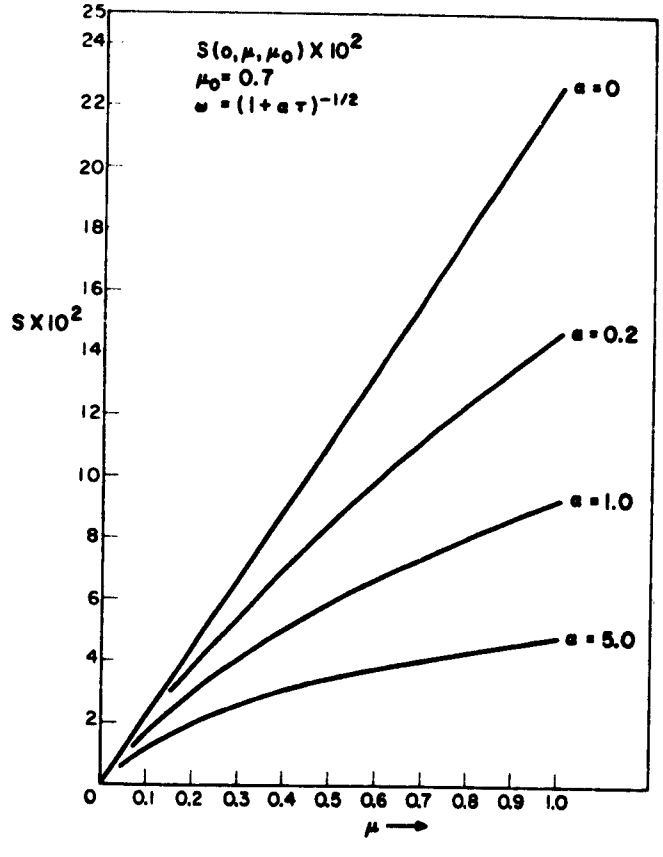

Fig. 1

TABLE I

μ_0 \ μ	0.1	0.2	0.3	0.4	0.5	0.6	0.7	0.8	0.9	1.0
0.1	0.61911	0.95976	1.2228	1.4527	1.665	1.8668	2.0620	2.2524	2.4395	2.6240
0.2		1.6738	2.2747	2.8149	3.3186	3.7983	4.2620	4.7138	5.1569	5.5932
0.3			3.2203	4.0989	4.9328	5.7356	6.5162	7.2797	8.0304	8.7708
0.4				5.3259	6.5112	7.6655	8.7967	9.9093	11.0076	12.0940
0.5					8.0599	9.5846	11.0907	12.5807	14.0583	15.5251
0.6						11.4927	13.3916	15.2812	17.1635	19.0389
0.7							15.6971	18.0034	20.3118	22.6195
0.8								20.7419	23.4926	26.2525
0.9									26.7004	29.9296
1.0										33.6425

Reflectivity, $S(0, \mu, \mu_0)$, for Isotropic Scattering, $\times 10^2$

Conservative Case ($\omega = 1$)

TABLE II

μ_0 \ μ	0.1	0.2	0.3	0.4	0.5	0.6	0.7	0.8	0.9	1.0
0.1	0.619	0.959	1.222	1.452	1.665	1.866	2.062	2.252	2.439	2.624
0.2		1.673	2.185	2.652	3.054	3.428	3.781	4.116	4.437	4.747
0.3			2.969	3.656	4.286	4.870	5.418	5.934	6.425	6.895
0.4				4.583	5.438	6.233	6.979	7.681	8.348	8.983
0.5					6.510	7.511	8.452	9.340	10.183	10.985
0.6						8.711	9.842	10.912	11.928	12.895
0.7							11.157	12.403	13.589	14.717
0.8								13.820	15.169	16.456
0.9									16.678	18.118
1.0										19.707

Reflectivity, $S(0, \mu, \mu_0)$, for Isotropic Scattering, $\times 10^2$

$\omega = (1 + 0.2\tau)^{-1/2}$

TABLE III

μ_0 \ μ	0.1	0.2	0.3	0.4	0.5	0.6	0.7	0.8	0.9	1.0
0.1	0.568	0.851	1.052	1.228	1.366	1.493	1.609	1.717	1.819	1.915
0.2		1.412	1.825	2.162	2.451	2.706	2.940	3.146	3.341	3.522
0.3			2.425	2.925	3.357	3.737	4.079	4.390	4.676	4.941
0.4				3.573	4.136	4.635	5.085	5.494	5.868	6.214
0.5					4.821	5.431	5.981	6.481	6.939	7.363
0.6						6.143	6.786	7.371	7.908	8.404
0.7							7.514	8.179	8.789	9.353
0.8								8.917	9.596	10.223
0.9									10.338	11.025
1.0										11.768

Reflectivi J, μ, μ_0), for Isotropic Scattering, $\times 10^2$

$\omega = (1 + 1.0\tau)^{-1/2}$

TABLE IV

μ_0 \ μ	0.1	0.2	0.3	0.4	0.5	0.6	0.7	0.8	0.9	1.0
0.1	0.304	0.518	0.725	0.935	1.04	1.122	1.187	1.246	1.300	1.349
0.2		1.099	1.359	1.558	1.719	1.857	1.975	2.080	2.175	2.598
0.3			1.720	2.003	2.234	2.429	2.597	2.744	2.875	2.993
0.4				2.356	2.646	2.890	3.100	3.284	3.447	3.593
0.5					2.985	3.271	3.518	3.733	3.924	4.095
0.6						3.594	3.871	4.115	4.332	4.526
0.7							4.177	4.447	4.687	4.903
0.8								4.739	5.002	5.238
0.9									5.284	5.540
1.0										5.815

Reflectivity, $S(0, \mu, \mu_0)$, for Isotropic Scattering, $\times 10^2$

$\omega = (1 + 5.0\tau)^{-1/2}$

Hence the pressure correction factor, p/p_0 is given by

$$p/p_0 = e^{-z/H} = \frac{1}{\varkappa_\lambda}\left[\left(\sigma^2 + \frac{2\varkappa_\lambda\tau}{H}\right)^{1/2} - \sigma\right] \tag{19}$$

and the local albedo reduces to

$$\omega(\tau) = (1 + \alpha\tau)^{-1/2} \tag{20}$$

where $\alpha = 2\varkappa_\lambda/\sigma^2 H\rho_0$. When $\alpha = 0$, we have the case of conservative scattering ($\omega = 1$). The approximate reflectivity has been calculated for $\alpha = 0.0$, 0.2, 1.0 and 5.0. In all cases, the error, as given by eq. (14), is of the order of 5 % or less. (The error is greatest for μ, $\mu_0 \sim 1$, and α large). The results are tabulated in tables 1-4. Sample results are shown in figure 1.

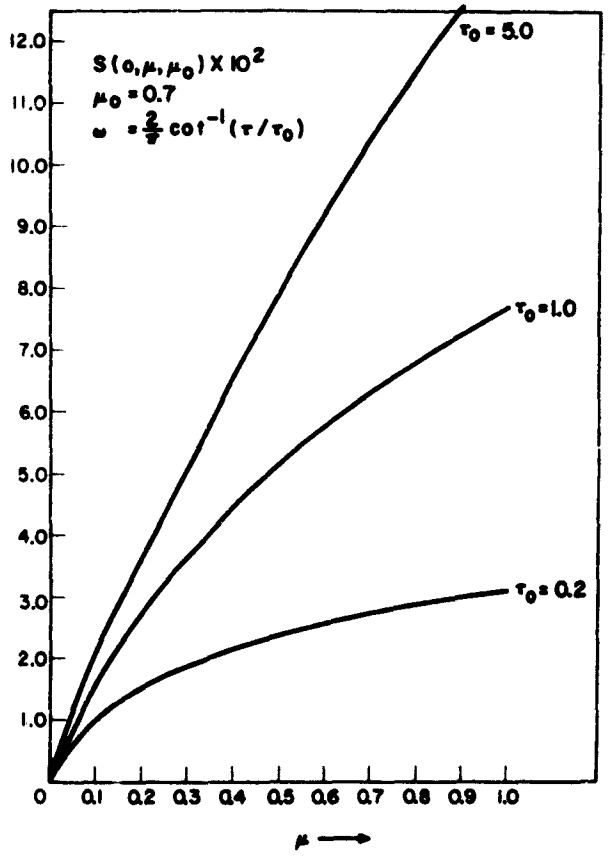

Fig. 2

A more rapid variation of ω with τ is given by the function

$$\omega(\tau) = \frac{2}{\pi} \cot^{-1}\tau/\tau_0 \tag{21}$$

which was selected only for its ease in programming, rather than from any physical significance. These results are tabulated in tables 5-7, and sample results are plotted figure 2.

Finally, we have attempted to represent the case of a transition occurring at some depth τ_0 in the atmosphere, by choosing a function of the form

$$\omega(\tau) = a + \frac{b}{1 + (\tau/\tau_0)^4} \tag{22}$$

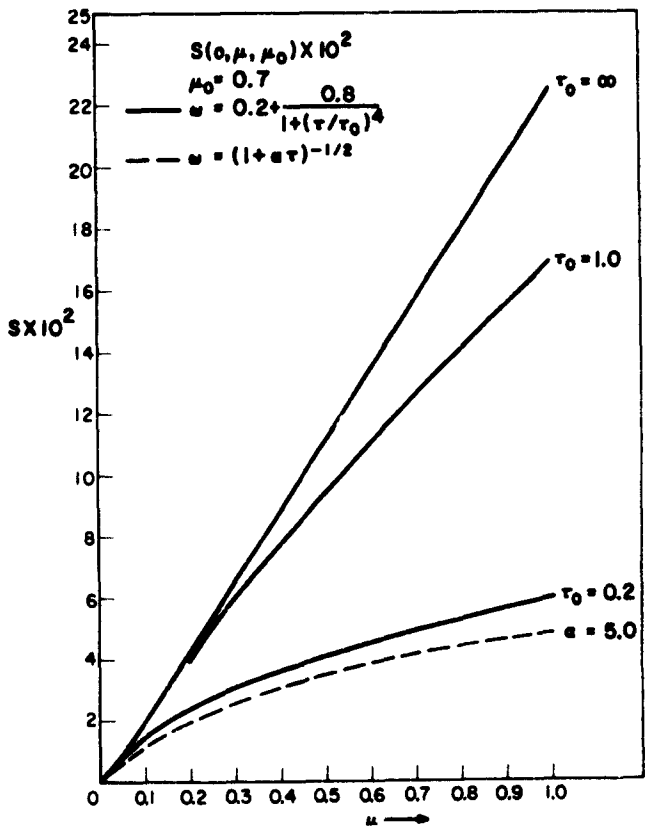

Fig. 3

These results have been obtained for $a = 0.2$, $b = 0.8$, and for three values of τ_0; the results are presented in tables 8-10, and typical results shown in figure 3. We have included in that figure one of the curves from figure 1 ($\omega = (1 + \alpha\tau)^{-1/2}$), for the sake of comparison. The three functional forms of $\omega(\tau)$ are plotted in figure 4.

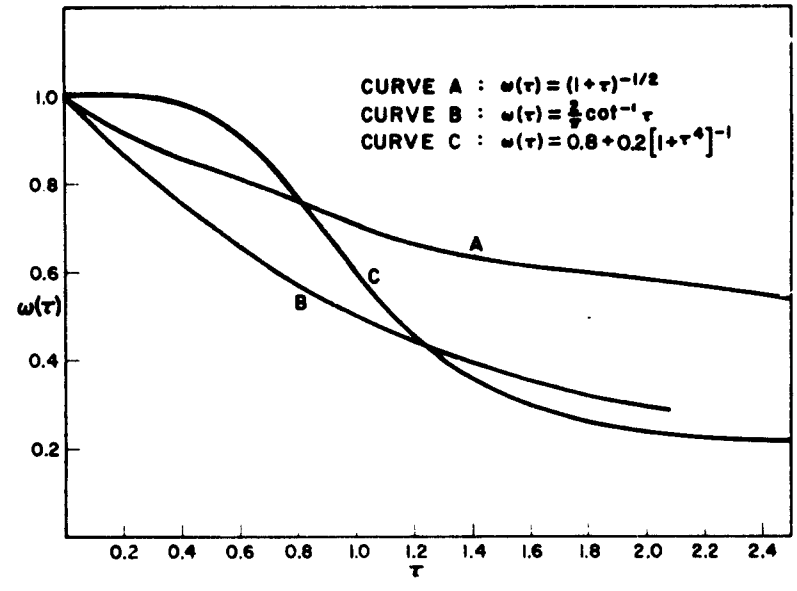

Fig. 4. — $\omega(\tau)$ *vs* τ

It will be seen from the figures 1,2 and 3 that it is extremely difficult to distinguish one functional form of $\omega(\tau)$ from another, insofar as the limb darkening is affected. Although our calculation is only approximate, the errors are estimated to be only of order 5%, so that we expect this conclusion to be more generally true.

This result is to be understood by recognizing that the principle dependence of $S(0, \mu, \mu_0)$ on angles is contained in the exponential term in the integral of eq. (15), which is common to all ω-functions. The H-functions themselves do not vary strongly over the interval of τ which contributes to the integral; for many of the integrations, particularly at large values of zenith angle, all of the contribution comes from values of τ such that $\omega(\tau) \approx 1$.

TABLE V

μ_0 \ μ	0.1	0.2	0.3	0.4	0.5	0.6	0.7	0.8	0.9	1.0
0.1	0.4669	0.6416	0.7510	0.8331	0.8999	0.9570	1.007	1.052	1.093	1.131
0.2		.9327	1.120	1.258	1.368	1.460	1.539	1.609	1.671	1.728
0.3			1.362	1.541	1.684	1.802	1.904	1.992	2.071	2.142
0.4				1.752	1.920	2.060	2.179	2.284	2.377	2.460
0.5					2.110	2.267	2.403	2.521	2.626	2.720
0.6						2.441	2.589	2.720	2.835	2.940
0.7							2.750	2.891	3.017	3.130
0.8								3.042	3.177	3.298
0.9									3.319	3.448
1.0										3.583

Reflectivity, $S(0, \mu, \mu_0)$, for Isotropic Scattering, $\times 10^2$

$$\omega = \frac{2}{\pi} \cot^{-1}(\tau/0.2)$$

TABLE VI

μ_0 \ μ	0.1	0.2	0.3	0.4	0.5	0.6	0.7	0.8	0.9	1.0
0.1	0.5688	0.8390	1.027	1.178	1.308	1.423	1.529	1.626	1.717	1.803
0.2		1.352	1.728	2.030	2.285	2.508	2.707	2.888	3.054	3.209
0.3			2.263	2.698	3.067	3.388	3.673	3.830	4.165	4.381
0.4				3.249	3.717	4.126	4.488	4.814	5.111	5.384
0.5					4.273	4.760	5.182	5.581	5.934	6.258
0.6						5.316	5.811	6.256	6.660	7.031
0.7							6.362	6.857	7.309	7.722
0.8								7.401	7.895	8.348
0.9									8.429	8.918
1.0										9.441

Reflectivity, $S(0, \mu, \mu_0)$, for Isotropic Scattering, $\times 10^3$

$$\omega = \frac{2}{\pi} \cot^{-1}\tau$$

TABLE VII

μ_0 \ μ	0.1	0.2	0,3	0.4	0.5	0.6	0.7	0.8	0.9	1.0
0.1	0.6190	0.9598	1.222	1.453	1.665	1.867	2.060	2.252	2.439	2.624
0.2		1.632	2.123	2.553	2.940	3.295	3.627	3.941	4.239	4.525
0.3			2.871	3.534	4.134	4.683	5.194	5.672	6.124	6.554
0.4				4.419	5.224	5.965	6.654	7.299	7.907	8.482
0.5					6.225	7.150	8.012	8.820	9.581	10.301
0.6						8.251	9.280	10.245	11.156	12.017
0.7							10.047	11.584	12.638	13.635
0.8								12.845	14.037	15.165
0.9									15.359	16.661
1.0										17.989

Reflectivity, $S(0, \mu, \mu_0)$, for Isotropic Scattering, $\times 10^2$

$$\omega = \frac{2}{\pi} \cot^{-1}(\tau/5.0)$$

TABLE VIII

μ_0 \ μ	0.1	0.2	0.3	0.4	0.5	0.6	0.7	0.8	0.9	1.0
0.1	0.619	0.959	1.222	1.452	1.665	1.866	2.05	2.204	2.349	2.490
0.2		1.202	1.508	1.761	1.983	2.184	2.370	2.546	2.712	2.871
0.3			1.915	2.250	2.543	2.806	3.048	3.275	3.488	3.692
0.4				2.654	3.005	3.321	3.611	3.882	4.137	4.378
0.5					3.408	3.771	4.104	4.414	4.706	4.982
0.6						4.177	4.549	4.895	5.221	5.530
0.7							4.957	5.338	5.696	6.035
0.8								5.750	6.138	6.506
0.9									6.555	6.950
1.0										7.371

Reflectivity, $S(0, \mu, \mu_0)$, for Isotropic Scattering, $\times 10^2$

$\omega = 0.2 + 0.8\,[1 + (\tau/0.2)^4]^{-1}$

TABLE IX

μ_0 \ μ	0.1	0.2	0.3	0.4	0.5	0.6	0.7	0.8	0.9	1.0
0.1	0.619	0.959	1.222	1.452	1.665	1.866	2.062	2.252	2.439	2.623
0.2		1.659	2.231	2.741	3.212	3.659	4.089	4.506	4.913	5.313
0.3			3.106	3.899	4.637	5.337	6.007	6.656	7.288	7.907
0.4				4.963	5.957	6.900	7.803	8.676	9.524	10.035
0.5					7.195	8.370	9.496	10.581	11.635	12.663
0.6						9.766	11.104	12.383	13.644	14.862
0.7							12.644	14.129	15.569	16.970
0.8								15.802	17.423	19.000
0.9									19.220	20.968
1.0										22.881

Reflectivity, $S(0, \mu, \mu_0)$, for Isotropic Scattering, $\times 10^2$

$\omega = 0.2 + 0.8\,[1 + \tau^4]^{-1}$

TABLE X

μ_0 \ μ	0.1	0.2	0.3	0.4	0.5	0.6	0.7	0.8	0.9	1.0
0.1	0.619	0.959	1.223	1.453	1.665	1.867	2.062	2.252	2.439	2.623
0.2		1.672	2.274	2.814	3.318	3.792	4.259	4.712	5.154	5.590
0.3			3.220	4.098	4.932	5.735	6.515	7.277	8.027	8.766
0.4				5.325	6.509	7.660	8.789	9.898	10.994	12.077
0.5					8.053	9.573	11.073	12.556	14.026	15.484
0.6						11.472	13.360	15.236	17.102	18.959
0.7							15.647	17.930	20.210	22.485
0.8								20.631	23.337	26.044
0.9									26.478	29.629
1.0										33.230

Reflectivity, $S(0, \mu, \mu_0)$, for Isotropic Scattering, $\times 10^4$

$\omega = 0.2 + 0.8[1 + (\tau/5.0)^4]^{-1}$

V. Rayleigh Scattering

Although the calculation for Rayleigh scattering is not yet complete, we indicate here the nature of the problem, and how we will proceed, guided by the solution for the isotropic case.

Rayleigh scattering is characterized by a phase function of the form (neglecting polarization phenomena) :

$$\gamma(\cos\theta) = \frac{3}{4}(1 + \cos^2\theta) \tag{23}$$

or, in terms of normalized spherical harmonics

$$\gamma(\cos\theta) = 1 + \sqrt{\frac{\pi}{5}}\, Y_{2,0}(\theta, \varphi) \tag{24}$$

We assume that $S(\tau, \Omega, \Omega_0)$ can be written in the form

$$S(\tau, \Omega, \Omega_0) = \sum_{m=-2}^{2} S_m(\tau, \mu, \mu_0) e^{im(\varphi - \varphi_0)} \tag{25}$$

where, since $\gamma(\Omega, \Omega_0)$ is an even function of $(\varphi - \varphi_0)$, we may assume $S_{-m} = S_m$.

If eqs. (24) and (25) are substituted into eq. (3), and use is made of the addition theorem for spherical harmonics, the following equations are obtained :

$$S_0(\tau,\mu,\mu_0) = \frac{1}{4\pi}\int_\tau^\infty \omega(\tau') e^{-\left(\frac{1}{\mu}+\frac{1}{\mu_0}\right)(\tau'-\tau)} \{\Phi(\tau', \mu)\Phi(\tau', \mu_0) + \chi(\tau', \mu)\chi(\tau', \mu_0)\} d\tau' \tag{26}$$

where

$$\Phi(\tau, \mu) = 1 + \frac{1}{2}\int_0^1 \frac{d\mu'}{\mu'}\int_\tau^\infty e^{-\left(\frac{1}{\mu}+\frac{1}{\mu'}\right)(\tau-\tau')} \omega(\tau') [\Phi(\tau', \mu')\, \Phi(\tau', \mu) + \chi(\tau', \mu')\chi(\tau', \mu)]\, d\tau' \tag{27}$$

and

$$\chi(\tau, \mu) = \frac{1}{\sqrt{5}}[\bar{P}_2(\mu) + \frac{1}{2}\int_0^1 \frac{d\mu'}{\mu'}\, \bar{P}_2(\mu')\int_\tau^\infty e^{-\left(\frac{1}{\mu}+\frac{1}{\mu'}\right)(\tau'-\tau)} \omega(\tau') d\tau' \times [\Phi(\tau', \mu')\, \Phi(\tau', \mu) + \chi(\tau', \mu')\chi(\tau', \mu)]$$

(Here $\bar{P}_2$ is the normalized Legendre polynomial).

We also obtain equations for S_1 and S_2, which are

$$S_j(\tau, \mu, \mu_0) = \frac{1}{4\pi} \int_\tau^\infty d\tau' \, \omega(\tau') e^{-\left(\frac{1}{\mu}+\frac{1}{\mu_0}\right)(\tau'-\tau)} \chi_j(\tau', \mu) \chi_j(\tau', \mu_0) \qquad (29)$$

where

$$\chi_j(\tau, \mu) = \frac{1}{\sqrt{5}}$$

$$[\bar{P}_2^j(\mu) + \frac{1}{2}\int_0^1 \frac{d\mu'}{\mu'} P_2^j(\mu') \int_\tau^\infty e^{-\left(\frac{1}{\mu}+\frac{1}{\mu'}\right)(\tau'-\tau)} \omega(\tau') \chi_j(\tau', \mu') \chi_j(\tau', \mu) d\tau'] \quad (30)$$

Chandrasekhar has shown that in the case $\omega(\tau) =$ constant, separate equations may be obtained for the Φ- and χ-functions; they are simply related to a more general class of H-functions. In the present instance, the separation does not appear to be possible, and eqs. (27) and (28) must be solved as a coupled set.

It is our intention to deal with these equations in the same approximation already introduced for isotropic scattering; namely, to compute a set of functions for constant ω, e. g., $\Phi_\omega(\mu)$, $\chi_\omega(\mu)$; and then to assume in eq. (26), for example, that

$$\Phi(\tau, \mu) \approx \Phi_{\omega(\tau)}(\mu)$$
$$\chi(\tau, \mu) \approx \chi_{\omega(\tau)}(\mu) \qquad (31)$$

with similar assumptions for eq. (29).

Insofar as one may predict a result not yet calculated, we anticipate that the results will show a general insensitivity to atmospheric structure, just as in the isotropic case. Nevertheless, it is felt that the stronger dependence on angle which occurs in the Rayleigh case makes it worth while to pursue the calculation.

VI. Solution by Series

It has been shown by the author (1960) that an iterative solution to eq. (3) may be constructed in which each term represents the contribution of a single order of scattering; that is, the first term represents single scattering, the second, double scattering, and so on. We shall not develop the procedure, since it is outlined

in the author's earlier paper, but we shall merely indicate the nature of the results up to triple scattering. In the following, S_1 and S_2 represent the contributions to the reflectivity of single and double scattering :

$$S_1(0, \Omega, \Omega_0) = \frac{1}{4\pi}\gamma(\Omega, \Omega_0)\int_0^\infty \omega(\tau)e^{-\left(\frac{1}{\mu}+\frac{1}{\mu_0}\right)\tau} \tag{32a}$$

$$S_2(0, \Omega, \Omega_0) = \frac{1}{16\pi^2}\int_+ \gamma(\Omega, \Omega')\gamma(\Omega', \Omega_0)\frac{d\Omega'}{\mu'} \int_0^\infty \omega(\tau')e^{-\left(\frac{1}{\mu}+\frac{1}{\mu_0}\right)\tau'} d\tau' \int_{\tau'}^\infty d\tau''\omega(\tau'')e^{-\left(\frac{1}{\mu_0}+\frac{1}{\mu'}\right)(\tau''-\tau')}$$

$$+ \frac{1}{16\pi^2}\int_+ \gamma(\Omega, \Omega')\gamma(\Omega', \Omega_0)\frac{d\Omega'}{\mu'} \int_0^\infty \omega(\tau')e^{-\left(\frac{1}{\mu}+\frac{1}{\mu_0}\right)\tau'} d\tau' \int_{\tau'}^\infty d\tau''\omega(\tau'')e^{-\left(\frac{1}{\mu_0}+\frac{1}{\mu'}\right)(\tau''-\tau')} \tag{32b}$$

The expression for triple scattering involves five separate integrals, each of the form

$$S_3^i = \left(\frac{1}{4\pi}\right)^3 \int_0^\infty \omega(\tau)e^{-\left(\frac{1}{\mu}+\frac{1}{\mu_0}\right)\tau} d\tau \int_\tau^\infty \omega(\tau')d\tau' \int_{\tau'}^\infty \omega(\tau'')d\tau'' \int_+ \frac{d\Omega'}{\mu'}\frac{d\Omega''}{\mu''}$$

$$\times e^{-\left(\frac{1}{\mu}+\frac{1}{\mu'}\right)(\tau'-\tau)} e^{-\left(\frac{1}{\mu}+\frac{1}{\mu''}\right)(\tau''-\tau)} \gamma(\Omega, \Omega')\gamma(\Omega', \Omega'')\,\gamma\,(\Omega'', \Omega_0) \tag{32c}$$

It is clear that the labor of computation increases very rapidly with the order of iteration, so that unless very rapid convergence can be expected, the method of iteration seems impractical.

There are two cases, however, where the convergence appears rapid enough for practical use. It is easily seen that under quite general conditions on $\omega(\tau)$ the effective expansion parameter is no larger than

$$\varepsilon = \int_0^\infty \omega(\tau)e^{-\tau}d\tau \tag{33}$$

(representing the coefficient of γ in eq. (32a) when μ and μ_0 assume their maximum values). If this quantity ε is sufficiently small,

suitable results can be obtained, although to obtain reasonable accuracy with a two-term expansion, it is necessary for ε to be $o(0.1)$. The question of convergence and the rate of convergence has been considered in more detail by Gross (1962).

A second case of interest occurs when the scattering phase function has a strong forward peak. In that case, as long as $\omega(\tau)$ is not identically equal to unity (conservative scattering) the series can be shown to converge rapidly except at angles near grazing. As an example of this, calculations have been made of S_1 and S_2, using a scattering function due to Deirmendjian (1962), suitable for calculation of 3.01 micron radiation by water droplets. This phase function is shown in figure 5 and typical results for S_1 and S_2 are plotted in figure 6, for an albedo function given by eq. (20)

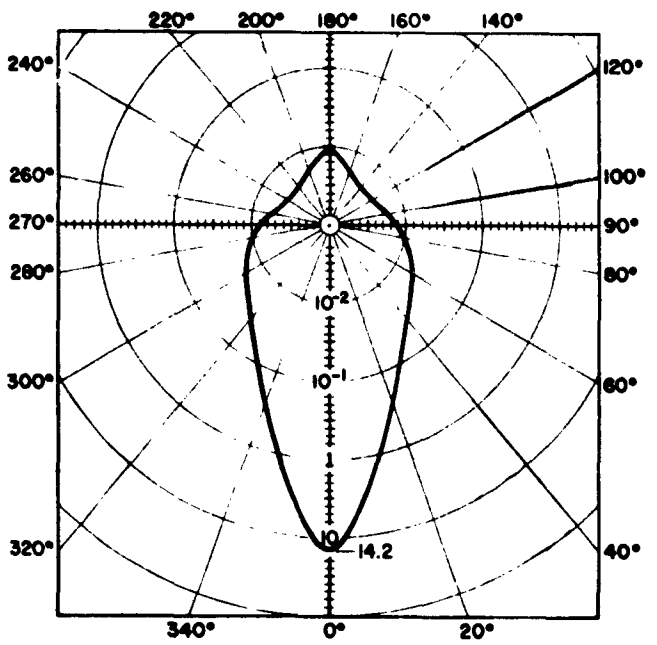

Fig. 5. — Phase function [$\gamma(\cos\theta)$] due to Deirmendjian

Although the iteration procedure becomes extremely difficult to calculate for orders of scattering greater than three, it remains

the only procedure that displays the reflectivity explicitly as a function of $\omega(\tau)$. This is extremely important if the infrared region is to be considered, for only in this case can suitable wavelength averages be taken. The procedure for making such averages in terms of the measured extinction function is outlined in the author's previous paper (1960).

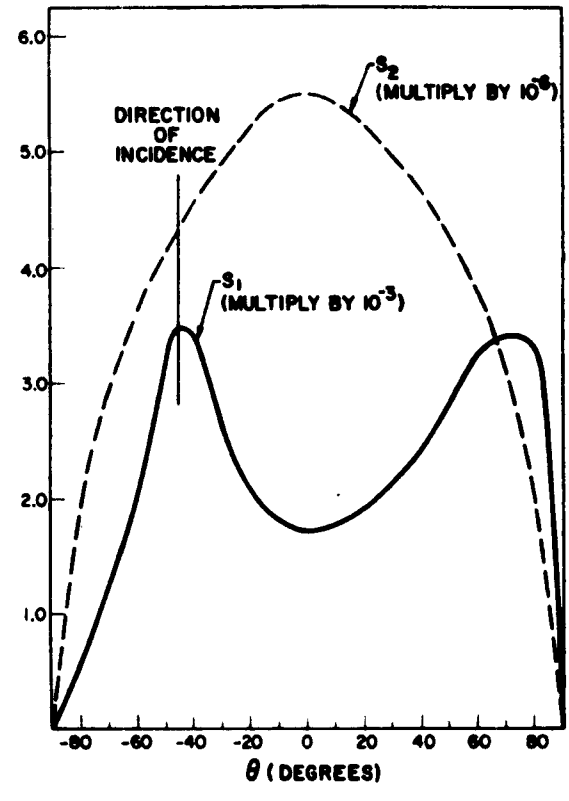

Fig. 6. — Single and double scattering ; Deirmendjian's phase function ($\omega = 1$; $\theta = 45°$; Meridional plane)

VII. Summary and Conclusions

An approximate method has been derived for the calculation of the reflectivity of a planetary atmosphere for the case of an albedo varying with optical depth. The method is restricted by

the condition that $\omega'(\tau)/\omega(\tau)$ not be too large, but in other respects seems relatively unrestricted. The method can, in principle, be used whenever the scattering phase function can be expanded in a finite series of Legendre polynomials. Numerical results have thus far been obtained only for isotropic scattering. The case of Rayleigh scattering is presently being calculated.

The results for isotropic scattering indicate a marked insensitivity to atmospheric structure. In order to test whether this insensitivity also characterizes a more physical case, the following problems will be investigated :

a) The case of Rayleigh scattering.

b) The case in which not only ω is a function of τ, but also γ. It is felt that the method can be extended to cover this case, although the approximations will have to be somewhat different.

The author would like to thank Dr. M. Baker and Mr. M. Turoff, for extensive help with the computations. He would also like to express his gratitude to Baird-Atomic, Inc., Cambridge, Mass., for making possible the presentation of this paper at the 11th International Astrophysical Colloquium.

REFERENCES

BELLMAN, R., *Proc. Nat. Acad. Sci.*, **42**, 629, 1956.

BUSBRIDGE, I., *The Mathematics of Radiative Transfer* (Cambridge : University Press), 1960.

CASE, K., *Rev. Mod. Phys.*, **29**, 651, 1957.

CHAMBERLAIN, J. W., *Upper Atmospheres of the Planets*, preprint, to be published, 1962.

CHANDRASEKHAR, S., *Radiative Transfer* (London : Oxford University Press), 1950.

DEIRMENDJIAN, D., Paper presented at the International Symposium on Radiation, Rad. Com. of IARAP of IUGG, Vienna, Aug. 1961, and private communication, 1961.

GOLDSTEIN, J., *Ap. J.*, **132**, 473, 1960.

GROSS, K., *J. Math. Phys.*, **41**, 53, 1962.

15. — SCATTERING FUNCTIONS FOR PLANETARY ATMOSPHERES

D. W. N. STIBBS
University Observatory, St Andrews, Gt Britain

Introduction

Detailed numerical application of the theory of radiative transfer in planetary atmospheres depends largely upon the availability of certain scattering functions in tabular form. This paper is concerned with the calculation of two such functions : Chandrasekhar's H-functions for arguments greater than unity, and the coupled H-functions originally introduced by Busbridge and Stibbs ([1]) in the theory of interlocked multiplet lines. These functions are required for calculations on the greenhouse effect in planetary atmospheres and for work on diffuse reflection by planetary atmospheres with fluorescent scattering involving coupling among transitions. Although the physical problems are quite distinct, the calculations are related by the fact that the H-functions are required for arguments greater than unity.

1. Greenhouse effect

At the Nantucket Meeting of the American Astronomical Society held in June, 1961, Dr Wildt ([2]) drew attention to the fact that the solution obtained by Hopf in 1934 for a semi-infinite planetary atmosphere in strict radiative equilibrium could be applied to the problem of the greenhouse effect. Wildt's generalization of Hopf's solution applies to a planetary atmosphere with a grey absorption coefficient $\varkappa_s$ for the solar radiation and a different absorption coefficient $\varkappa_p$ for the planetary infra-red radiation, the ratio $\varkappa_s/\varkappa_p = n$ of the two absorption coefficients being constant with depth. Dr Wildt pointed out that although this is

not a good model for familiar planetary atmospheres, it is nevertheless the only model for which the exact mathematical solution is known.

The solution for the planetary source function is comprised of two terms, one arising from the emergent flux of planetary heat, and another from the insolating flux of solar radiation. In the absence of planetary heat, the solution for the temperature distribution in L. T. E. involves Hopf's q-function, and Chandrasekhar's H-function in the conservative case $\tilde{\omega} = 1$ for the argument μ_0/n, where $\cos^{-1}\mu_0$ is the angle of incidence of the solar radiation. Since $n \leqslant 1$, the detailed numerical application of the solution will depend upon the availability of the H-function for conservative isotropic scattering for values of the argument greater than unity.

1. 1. *Calculation from the integral equation for the H-function.*— Consider the case of isotropic scattering with a particle albedo $\tilde{\omega}$,and let us suppose that $H(\mu', \tilde{\omega})$ is known for $0 \leqslant \mu' \leqslant 1$. The function $H(\mu, \tilde{\omega})$ for $\mu \geqslant 1$ may then be obtained directly by quadrature in Ambartsumian's integral equation

$$H(\mu, \tilde{\omega}) = 1 + \tfrac{1}{2}\tilde{\omega}\mu H(\mu, \tilde{\omega}) \int_0^1 \frac{H(\mu', \tilde{\omega})}{\mu + \mu'} d\mu' \qquad \ldots (1)$$

Since $\partial H(\mu', \tilde{\omega}) / \partial\mu'$ has a logarithmic singularity at $\mu' = 0$, it is necessary to remove the effect of this singularity on the quadrature over μ' by subtracting the function

$$F(\mu', \tilde{\omega}) = 1 - \tfrac{1}{2}\tilde{\omega}\mu' ln\mu' \qquad \ldots (2)$$

from $H(\mu', \tilde{\omega})$ before performing the quadrature. From equation (1) we thus obtain

$$\frac{1}{H(\mu, \tilde{\omega})} = 1 - \tfrac{1}{2}\tilde{\omega}\mu \int_0^1 \frac{H(\mu', \tilde{\omega}) - F(\mu', \tilde{\omega})}{\mu + \mu'} d\mu'$$
$$- \tfrac{1}{2}\tilde{\omega}\mu ln \frac{1+\mu}{\mu} - \tfrac{1}{4}\tilde{\omega}^2\left(\frac{1}{4} - \frac{1}{9\mu} + \frac{1}{16\mu^2} - \ldots\right) \qquad \ldots (3)$$

Now when $\mu = 1$, the series in the second of the correction terms in equation (3) is the Riemann-Zeta function for argument

TABLE I

The H-Function in the Conservative Case
$\tilde{\omega} = 1.0$ *and for* μ *greater than unity*

μ	H(μ)	μ	H(μ)	μ	H(μ)	μ	H(μ)
1.0	2.9078	25.5	45.386	50.5	88.680	75.5	131.973
1.5	3.7872	26.0	46.252	51.0	89.546	76.0	132.839
2.0	4.6613	26.5	47.118	51.5	90.412	76.5	133.704
2.5	5.5327	27.0	47.984	52.0	91.278	77.0	134.571
3.0	6.4025	27.5	48.850	52.5	92.143	77.5	135.436
3.5	7.2713	28.0	49.716	53.0	93.009	78.0	136.302
4.0	8.1394	28.5	50.582	53.5	93.875	78.5	137.168
4.5	9.0071	29.0	51.447	54.0	94.741	79.0	138.034
5.0	9.8745	29.5	52.313	54.5	95.607	79.5	138.900
5.5	10.7416	30.0	53.179	55.0	96.473	80.0	139.765
6.0	11.6086	30.5	54.045	55.5	97.339	80.5	140.631
6.5	12.4754	31.0	54.911	56.0	98.204	81.0	141.497
7.0	13.3420	31.5	55.777	56.5	99.070	81.5	142.363
7.5	14.2086	32.0	56.643	57.0	99.936	82.0	143.229
8.0	15.0751	32.5	57.509	57.5	100.802	82.5	144.095
8.5	15.9415	33.0	58.375	58.0	101.668	83.0	144.960
9.0	16.8078	33.5	59.240	58.5	102.534	83.5	145.826
9.5	17.6741	34.0	60.106	59.0	103.399	84.0	146.692
10.0	18.5403	34.5	60.972	59.5	104.266	84.5	147.558
10.5	19.4065	35.0	61.838	60.0	105.131	85.0	148.424
11.0	20.2727	35.5	62.704	60.5	105.997	85.5	149.290
11.5	21.1388	36.0	63.570	61.0	106.863	86.0	150.156
12.0	22.0050	36.5	64.436	61.5	107.729	86.5	151.021
12.5	22.8711	37.0	65.302	62.0	108.595	87.0	151.887
13.0	23.7371	37.5	66.168	62.5	109.461	87.5	152.753
13.5	24.6032	38.0	67.033	63.0	110.326	88.0	153.619
14.0	25.4692	38.5	67.899	63.5	111.192	88.5	154.485
14.5	26.3353	39.0	68.765	64.0	112.058	89.0	155.351
15.0	27.2013	39.5	69.631	64.5	112.924	89.5	156.216
15.5	28.0673	40.0	70.497	65.0	113.790	90.0	157.082
16.0	28.9334	40.5	71.363	65.5	114.656	90.5	157.948
16.5	29.7993	41.0	72.229	66.0	115.521	91.0	158.814
17.0	30.6653	41.5	73.094	66.5	116.387	91.5	159.680
17.5	31.5313	42.0	73.960	67.0	117.253	92.0	160.546
18.0	32.3973	42.5	74.826	67.5	118.119	92.5	161.412
18.5	33.2632	43.0	75.692	68.0	118.985	93.0	162.277
19.0	34.1292	43.5	76.558	68.5	119.851	93.5	163.143
19.5	34.9951	44.0	77.424	69.0	120.717	94.0	164.009
20.0	35.8610	44.5	78.290	69.5	121.583	94.5	164.875
20.5	36.7270	45.0	79.155	70.0	122.449	95.0	165.741
21.0	37.5929	45.5	80.021	70.5	123.314	95.5	166.607
21.5	38.4588	46.0	80.887	71.0	124.180	96.0	167.473
22.0	39.3248	46.5	81.753	71.5	125.046	96.5	168.339
22.5	40.1907	47.0	82.619	72.0	125.912	97.0	169.204
23.0	41.0566	47.5	83.485	72.5	126.778	97.5	170.070
23.5	41.9226	48.0	84.351	73.0	127.644	98.0	170.936
24.0	42.7885	48.5	85.217	73.5	128.509	98.5	171.802
24.5	43.6544	49.0	86.083	74.0	129.375	99.0	172.668
25.0	44.5203	49.5	86.948	74.5	130.241	99.5	173.534
25.5	45.3861	50.0	87.814	75.0	131.107	100.0	174.399

two. This series is very slowly convergent and the series for μ near unity will be likewise slowly convergent. In order to achieve high numerical accuracy, it would be necessary in such circumstances to improve the convergence of the alternating series by means of Euler's method.

In this way, calculations based upon equation (3) will yield values of $H(\mu, \tilde{\omega})$ for $\mu > 1$ with an accuracy limited only by the accuracy of $H(\mu', \tilde{\omega})$ for $0 \leqslant \mu' \leqslant 1$. Since $H(\mu', \tilde{\omega})$ has been tabulated accurately to six decimal places by Stibbs and Weir [3] for values of the particle albedo in the range

$$\tilde{\omega} = 0(.05)0.900(.025)0.950(.010)0.980(.005)0.990(.0025)1.0,$$

values of the $H(\mu, \tilde{\omega})$ for $\mu > 1$ can be calculated with comparable accuracy. For values of $\tilde{\omega}$ other than those tabulated, $H(\mu', \tilde{\omega})$ can be readily obtained from the Chebychev polynomial approximations given by Stibbs and Weir which give the required H-function accurately to four decimal places.

1. 2. *Calculations based upon the complex integral for* $H(\mu, \tilde{\omega})$. — There is an alternative method of calculation which was the original basis of the work by Stibbs and Weir [3]. The method makes use of the fact that the solution of equation (1) can be represented as a complex integral which can be readily transformed into a real integral to give

$$H(\mu, \tilde{\omega}) = \exp\left\{-\frac{\mu}{\pi}\int_0^{\frac{\pi}{2}} \frac{ln\,(1 - \tilde{\omega}\theta\cot\theta)}{\cos^2\theta + \mu^2\sin^2\theta}\,d\theta\right\} \quad \ldots (4).$$

It is possible to calculate the required H-function for all μ by a suitable quadrature of this integral form. Table 1 gives the H-function for $\tilde{\omega} = 1$ and $\mu = 1.0(.5)100.0$ calculated from equation (4) using a flexible programme written for the IBM 7090 computer.

2. Fluorescent scattering in planetary atmospheres

The computer programme used for the calculation of the H-functions is flexible in the sense that solutions are obtained for

the coupled H-functions which arose in the work by Busbridge and Stibbs [1] on interlocked multiplet lines with a common upper state, Chandrasekhar's H-function being a special case of these more general functions. Since the problem of line formation in a semi-infinite atmosphere with no incident radiation is intimately related to the problem of diffuse reflection by way of the principles of invariance, the same scattering functions and the associated H-functions considered in detail by Busbridge and Stibbs are directly applicable to the problem of fluorescent scattering in planetary atmospheres in which there is a similar coupling among the transitions. Some aspects of this problem in planetary atmospheres have been considered recently by Chamberlain and Sobouti [4,5]. However, detailed application of the theory awaits the accurate calculation of the coupled H-functions.

2.1. *Calculation of the coupled H-functions.* — It has been shown by Busbridge and Stibbs [1] that the H-functions for coupled transitions involving a common upper state satisfy the simultaneous integral equations

$$\mathrm{H}_i(\mu) = 1 + \tfrac{1}{2}\mu \mathrm{H}_i(\mu) \sum_{p=1}^{k} \tilde{\omega}_p \varkappa_p \int^1 \frac{\mathrm{H}_p(\mu')\, d\mu'}{\varkappa_p \mu + \varkappa_i \mu'}, \qquad \ldots (5)$$

$$i = 1, 2, \ldots, k$$

k being the number of lower states, $\tilde{\omega}_p$ the albedo for the transition and $\varkappa_p$ the corresponding absorption coefficient. It was also shown that the H-functions satisfy the relation

$$\mathrm{H}_1(\mu) = \mathrm{H}_2(\mu\varkappa_2/\varkappa_1) = \mathrm{H}_3(\mu\varkappa_3/\varkappa_1) = \ldots \qquad \ldots (6)$$

If the absorption coefficient for the strongest transition is $\varkappa_1$, all the functions $\mathrm{H}_i(\mu')$ for $0 \leqslant \mu' \leqslant 1$ may be calculated from the function $\mathrm{H}_1(\mu)$ for values of μ in the range $0 \leqslant \mu \leqslant \varkappa_1/\varkappa_i$. Since $\varkappa_1 > \varkappa_i$, it is thus necessary to consider once again the calculation of an H-function for arguments greater than unity.

Let us first consider an approximate solution of equation (5) by replacing $\mathrm{H}_p(\mu')$ under the integral sign by Chandrasekhar's

H-function for albedo $\Sigma\tilde{\omega}_p$ denoted by $H(\mu', \Sigma\tilde{\omega}_p)$. Dividing by $H_i(\mu)$ and integrating, we obtain

$$\frac{\Sigma\tilde{\omega}_p}{H_i(\mu)} = \sum_{p=1}^{k} \frac{\tilde{\omega}_p}{H(\mu x_p/x_i, \Sigma\tilde{\omega}_p)} \qquad \ldots (7)$$

It is readily seen that the approximate function $H_i(\mu)$ given by equation (7) satisfies the fundamental relation (6). The calculation of these approximate functions will require the further calculation of some ordinary H-functions for arguments $\mu x_p/x_i$ which will be greater than unity for terms in the summation in equation (7) for which $\mu > x_i/x_p$. These may be calculated in the manner described in Section 1.

Busbridge and Stibbs have shown that the complex integral representation of the solution of the simultaneous integral equations (5) can be transformed into the following real integral

$$H_i(\mu) = \exp\left\{-\frac{\mu}{\pi}\int_0^{\pi/2} \frac{ln\left[1-\Sigma\tilde{\omega}_p \frac{x_p}{x_i}\cot\theta\cot^{-1}\left(\frac{x_p}{x_i}\cot\theta\right)\right]}{\cos^2\theta + \mu^2\sin^2\theta} d\theta\right\} \ldots (8)$$

In the special case when $k = 1$ and there is only one term in the summation under the [illegible] sign, equation (8) reduces to equation (4) for the ordinary [illegible]ion.

2.2. *Calculation of diffuse reflection.* — The intensity of diffuse reflection follows from the generalized form of the law of diffuse reflection given by Stibbs (6) and applied by Busbridge and Stibbs (1) to the problem of interlocked lines. The emergent intensity in the μ-direction is

$$I_i(0, \mu) = \tfrac{1}{4} F\tilde{\omega}_i H_i(\mu) \sum_{p=1}^{k} \frac{\mu_0 x_p H_p(\mu_0)}{x_p\mu + x_i\mu_0}, \qquad (9)$$

where μ_0 is the angle of incidence of the insolating radiation, and πF is the intrinsic flux in the monodirectional incident beam.

It follows from equation (9) that the intensity of diffuse

reflection satisfies a relation similar to equation (6) for the H-functions, namely

$$I_1(0,\mu) = I_2(0,\mu x_2/x_1) = I_3(0,\mu x_3/x_1) = \ldots \quad \ldots (10)$$

In this case, however it is necessary to use the fact that the ratio of the albedo for transitions with a common upper state is equal to the ratio of the absorption coefficients.

2.3. *An example of fluorescent scattering.* — Although fluorescent scattering in the Lyman-Birge-Hopfield bands of nitrogen is a more interesting example, the numerical application in this paper has been limited to the case of fluorescent scattering in a semi-infinite atmosphere of sodium in order to compare the exact H-functions and intensities of diffuse reflection with the approximate calculations obtained for the same example by Sobouti [5].

The case considered is the hyperfine doublet of the sodium D_1 line which arises from the hyperfine splitting of the ground state $3s^2S_{1/2}$. Neglecting the hyperfine splitting of the upper state $3p^2P^0_{1/2}$, the coupled transitions give rise to a doublet which may be conveniently designated as the a and b-components of the D_1 line. For these transitions we have $\tilde{\omega}_a = 5/8$, $\tilde{\omega}_b = 3/8$, and $x_a/x_b = 5/3$.

Table 2 gives the exact H-functions and the intensities of diffuse reflection for each component of the hyperfine doublet of sodium calculated from equations (8) and (9) with $\mu_0 = 0.6$ and $F = 1$. A comparison is then made in Table 3 between these exact H-functions and the approximate H-functions given by equation (7) as well as a comparison between the exact and approximate intensities of diffuse reflection. The table also gives the corresponding results calculated from a formula for the H-functions derived by Sobouti by replacing the functions $H_i(\mu)$ and $H_p(\mu')$ in the right-hand side of equation (5) by Chandrasekhar's H-function $H(\mu, \Sigma\tilde{\omega}_p)$. This multiple substitution is not only unnecessary but it destroys the fundamental relations (6) and (10) which the approximate H-functions and diffuse intensities would satisfy if the substitution

TABLE II

Exact H-functions and intensities of diffuse reflection for the hyperfine doublet components of the D_1 line

μ	$H_a(\mu)$	$H_b(\mu)$	$I_a(0, \mu)$	$I_b(0, \mu)$
0	1.000000	1.000000	0.548570	0.548570
0.05	1.115898	1.178891	0.572874	0.578827
0.10	1.208877	1.322808	0.583427	0.591470
0.15	1.295029	1.457081	0.589865	0.597000
0.20	1.377330	1.586139	0.594109	0.599978
0.25	1.457081	1.711857	0.596999	0.601559
0.30	1.534993	1.835238	0.599002	0.602314
0.35	1.611510	1.956888	0.600381	0.602559
0.40	1.686925	2.077205	0.601321	0.602478
0.45	1.761450	2.196465	0.601938	0.602188
0.50	1.835238	2.314869	0.602315	0.601763
0.55	1.908407	2.432567	0.602507	0.601250
0.60	1.981048	2.549672	0.602563	0.600684
0.65	2.053233	2.666275	0.602512	0.600088
0.70	2.125023	2.782447	0.602382	0.599474
0.75	2.196465	2.898248	0.602189	0.598857
0.80	2.267600	3.013724	0.601947	0.598242
0.85	2.338461	3.128914	0.601667	0.597634
0.90	2.409078	3.243853	0.601358	0.597039
0.95	2.479474	3.358568	0.601030	0.596456
1.00	2.549672	3.473083	0.600685	0.595889

were limited to $H_p(\mu')$. The table shows the extent to which Sobouti's results depart from the exact relationship whereas the results from the approximate H-functions given by equations (7) satisfy the relationship exactly.

The complete results of the calculations are shown in Fig. 1 which is self explanatory. Of particular interest is the behaviour of the exact solution for the uncoupled case, that is when the hyperfine splitting of the ground state is neglected. The solution in the uncoupled case is so close to the solution when the coupling is taken into account that it would appear unwise to use rough approximations to the H-functions for problems in fluorescent scattering

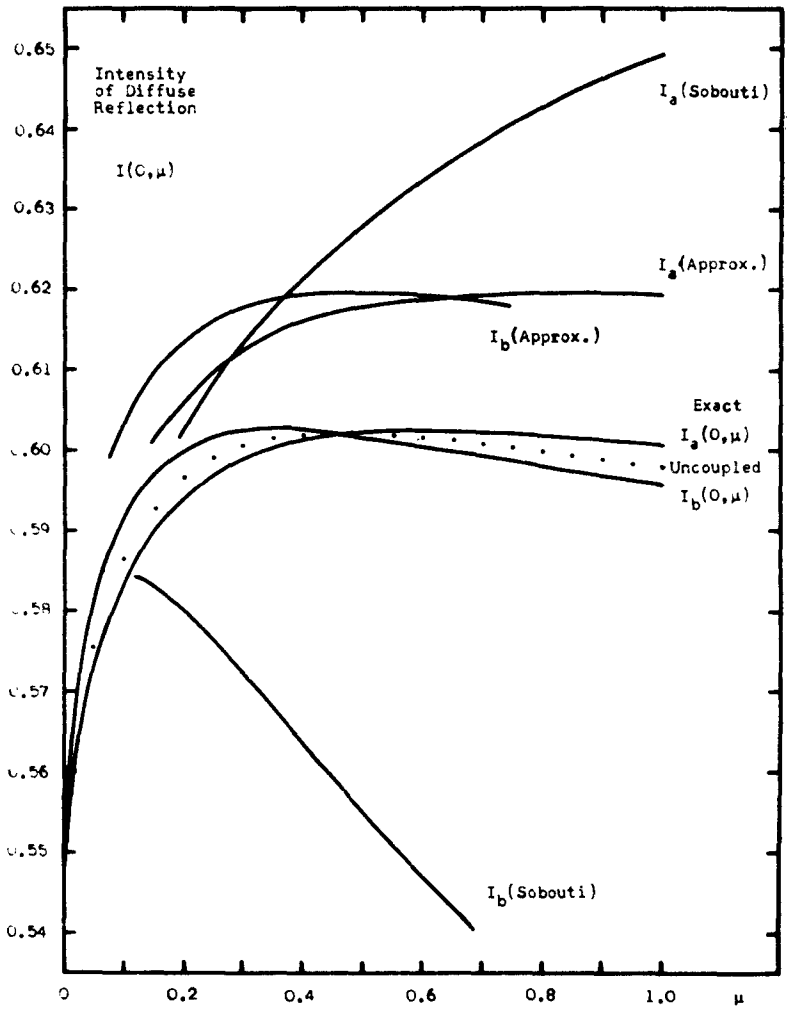

Fig. 1. — The intensity of diffuse reflection from a semi-infinite plane-parallel atmosphere of sodium illuminated by a parallel beam of radiation containing unit intrinsic flux and incident upon the atmosphere at an angle of $\cos^{-1} 0.6$. The curves show exact and approximate intensities for the *a* and *b*-components of the hyperfine doublet of the D_1 line. A solution for the intensities which neglects the coupling between the levels is indicated by dots in the figure.

since the errors thus introduced may be much greater than those produced by neglecting the coupling between the levels.

TABLE III

Comparison between exact and approximate H-functions and intensities of diffuse reflection

Function	$H_a(\mu)$	$H_b(\mu)$	$I_a(0, \mu)$	$I_b(0, \mu)$
μ	0.25	0.15	0.25	0.15
Exact	1.4571	1.4571	0.5970	0.5970
Approx.	1.4673	1.4673	0.6098	0.6098
Sobouti	1.4928	1.4302	0.6086	0.5831
μ	0.50	0.30	0.50	0.30
Exact	1.8352	1.8352	0.6023	0.6023
Approx.	1.8559	1.8559	0.6179	0.6179
Sobouti	1.9282	1.7575	0.6281	0.5725
μ	0.60	0.36	0.60	0.36
Exact	1.9810	1.9810	0.6026	0.6026
Approx.	2.0059	2.0059	0.6190	0.6190
Sobouti	2.1003	1.8801	0.6335	0.5671
μ	0.75	0.45	0.75	0.45
Exact	2.1965	2.1965	0.6022	0.6022
Approx.	2.2277	2.2277	0.6196	0.6196
Sobouti	2.3576	2.0589	0.6404	0.5592
μ	1.0	0.6	1.0	0.6
Exact	2.5497	2.5497	0.6007	0.6007
Approx.	2.5917	2.5917	0.6195	0.6195
Sobouti	2.7858	2.3475	0.6494	0.5472

CONCLUSION

This paper has been concerned mainly with the accurate calculation of H-functions for the greenhouse effect and fluorescent scattering in planetary atmospheres, the computational features in common being that the functions are required for arguments greater than unity, and that the IBM 7090 computer programme

calculates both the ordinary H-functions and the coupled H-functions not from the integral equations of the problem but from an equivalent integral form.

Attention has been paid in the paper to the accuracy of approximate solutions for the H-functions and the intensity of diffuse reflection. It is of some importance to make a detailed study of the errors of the approximate solutions since the functions which occur in the problem of diffuse reflection by fluorescent scattering can only be calculated readily and accurately in the case of semi-infinite atmospheres. For a finite atmosphere, it does not appear possible to represent the solution of the coupled equations as a complex integral, and it is consequently necessary to revert to the method of solution of the equations by iteration. If such a solution cannot be readily achieved, there is some consolation in the knowledge that a solution which neglects the coupling altogether could be more accurate than an approximate solution of the coupled problem.

Acknowledgment. — I should like to acknowledge with gratitude the assistance of Mr R. E. Weir who wrote the computer programme, and Dr T. R. Carson whose comments on some of the numerical analysis aspects of the problem were particularly valuable.

REFERENCES

(1) I. W. Busbridge and D. W. N. Stibbs, *M. N.*, **114**, 1, 1954 ; Comm. Univ. Obs., Oxford, No. 42.

(2) R. Wildt, *A. J.*, **66**, 298, 1961.

(3) D. W. N. Stibbs and R. E. Weir, *M. N.*, **119**, 512, 1959.

(4) J. Chamberlain and Y. Sobouti, *Ap. J.*, **135**, 925, 1962.

(5) Y. Sobouti, *A. J.*, **135**, 938, 1962.

(6) D. W. N. Stibbs, *M. N.*, **113**, 493, 1953 ; Comm. Univ. Obs., Oxford, No. 40.

16. — NON-GREY CONVECTIVE PLANETARY ATMOSPHERES

ALBERT ARKING
Goddard Space Flight Center
Institute for Space Studies
New York 27, N. Y., U. S. A.

INTRODUCTION

The recent advances in infra-red spectrophotometry are leading to more measurements, with greater precision, of the surface conditions and atmospheres of planets. To interpret these measurements and to translate them into unique models it has become necessary to develop more accurate methods for treating the problem of heat transfer in planetary atmospheres and for better understanding of the effects of commonly used approximations. The purpose of the present investigation is to develop some highly simplified models of planetary atmospheres in which the radiative transfer equations are solved numerically *without approximation*. The effect of the atmosphere having only finite extent, the effect of a convection zone, and the effect of a frequency dependent absorption coefficient are three effects whose bearing on the solution to the radiative transfer equations we wish to consider.

Our highly simplified model is a plane parallel atmosphere with cylindrical symmetry around the vertical. A distinction is made between *solar radiation*, to which it is assumed the atmosphere is completely transparent and the *infra-red radiation*, which can be emitted and absorbed in the atmosphere. The surface of the planet (i. e. the ground) partially absorbs and partially reflects the solar radiation ; it emits, however, only in the infra-red under conditions of local thermodynamic equilibrium. The conditions of local thermodynamic equilibrium are assumed to hold throughout the atmosphere.

In the absence of internal heat sources the planet will be

in over-all equilibrium so that the solar flux absorbed by the ground will be equal to the infra-red flux radiated from the planet, which we set equal to σT_e^4, thus defining the effective temperature T_e.

In the radiative region the temperature is determined by satisfying the equations of radiative equilibrium, whereas in the convective region the temperature is determined by the adiabatic temperature gradient, β_a.

The infra-red absorption is assumed to decrease exponentially with increasing altitude. In units of reciprocal length the absorption as a function of altitude is given by

$$\varkappa(z)\,\rho(z) = \varkappa_0\,\rho_0\,e^{-z/H_A}$$

where z is the height above the ground and H_A is a characteristic length called the « absorptive scale height ».

For some arbitrary reference frequency, the optical depth, τ, is defined so that $\tau = 0$ corresponds to the position of the ground, $z = 0$

$$\tau(z) = \int_0^z \varkappa(z)\,\rho(z)\,dz$$

$$= \tau_0\,(1 - e^{-z/H_A}),$$

where $\tau_0 = \varkappa_0\rho_0 H_A$ is the total optical depth of the atmosphere at the reference frequency. The inverse of the function $\tau(z)$ is

$$z(\tau) = H_A\,ln\,\frac{\tau_0}{\tau_0 - \tau}.$$

The Finite optical Thickness

First we consider grey models without convection. The solution is obtained by the same iteration method used in the solution of the Milne problem (i. e. the infinite atmosphere).

The results show that when the total optical depth of the atmosphere is greater than 3 or 4 the temperature profile follows that for the infinitely thick atmosphere to within 1 or 2 % — the greatest deviation, of course, occurring at the ground. For optical depths ~ 1 or less, the deviations can be greater than 10 %.

The grey convective Model

To add a convection zone to the grey model, the atmosphere is divided into two regions.

1. Below the tropopause (corresponding to optical depth τ_c) the atmosphere is in *convective equilibrium* and the temperature is determined by extrapolation from the value at the tropopause along the adiabatic gradient. Therefore, in the *convective region* ($0 \leqslant \tau \leqslant \tau_c$)

$$T(\tau) = T(\tau_c) - \beta a\,[z(\tau_c) - z(\tau)].$$

2. Above the tropopause the atmosphere is in radiative equilibrium. This leads to the following integral equation that the temperature must satisfy in the *radiative region* ($\tau_c \leqslant \tau \leqslant \tau_0$)

$$T^4(\tau) = \tfrac{1}{2}\,T^4(0)\,E_2(\tau) + \tfrac{1}{2}\int_0^{\tau_0} T^4(t)\,E_1(|\tau - t|)\,dt,$$

where $E_n(x)$ is the exponential integral

$$E_n(t) = \int_1^\infty \frac{e^{-xt}}{x^n}\,dt$$

The value of τ_c, corresponding to the tropopause height, is chosen so that the infra-red flux emanating from the top of the atmosphere

$$F(\tau_0) = 2\sigma T^4(0)\,E_3(\tau_0) + 2\sigma\int_0^{\tau_0} T^4(t)\,E_2(\tau_0 - t)\,dt.$$

is equal to the solar flux absorbed by the planet, σT_e^4. (If τ_c is chosen too small then $F(\tau_0) < \sigma T_e^4$; if too large, then $F(\tau_0) > \sigma T_e^4$). This method [1] of choosing τ_c is equivalent to the requirement that the radiative flux leaving the convective region match the constant flux that passes through the radiative region.

The solution to the above equations is obtained numerically by iteration on an IBM 7090.

A model atmosphere based upon this method is shown in Figure 1. With the intent of approximating a possible situation on Mars, the effective temperature, the adiabatic gradient, and the

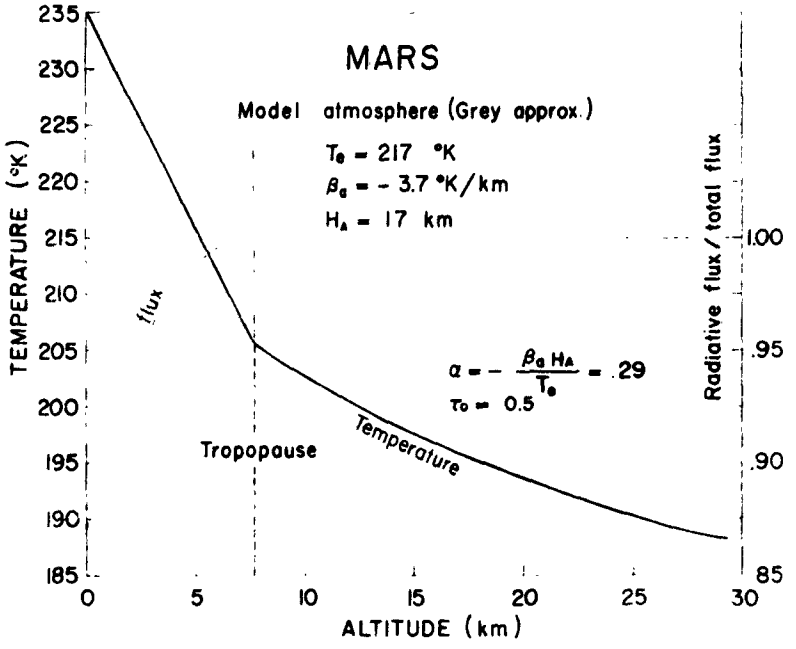

Fig. 1. — A grey model atmosphere for which the effective temperature T_e, the adiabatic gradient β_a and the absorptive scale height H_A are chosen to approximate possible conditions on Mars. Temperature as function of altitude is given by the solid line with ordinate scale on the left. The radiative flux is given by the dashed line with ordinate scale on the right.

absorptive scale height were chosen as shown. There are only two independent parameters that specify a profile : τ_0, the total optical depth, and α, the negative of the adiabatic temperature gradient in units of the effective temperature and the absorptive scale height :

$$\alpha = -\frac{\beta_a H_A}{T_e}.$$

The choice of $\tau_0 = 0.5$ was made to obtain a ground temperature of 235°K in agreement with the average of observations. The dependence of ground temperature on τ_0 is shown in Figure 2.

The radiative flux divided by the total flux is given by the dashed curve in Figure 1. It is seen that convection never carries more than 13 % of the total flux in this case.

Whereas the treatment of the problem in the radiative region

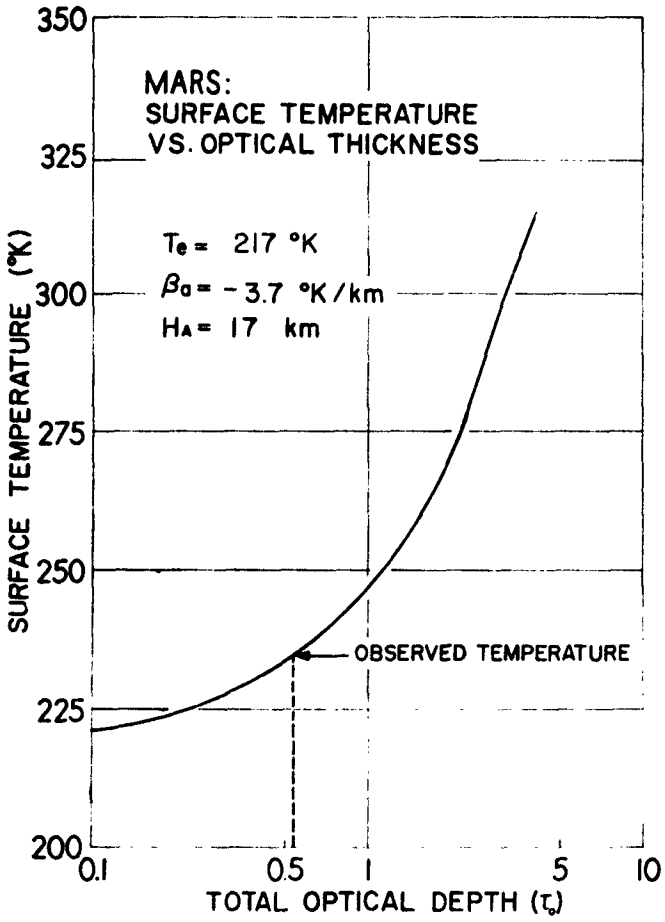

Fig. 2. — Using models like those in Figure 1, the ground temperature is shown as a function of the total optical depth of the atmosphere. The arrow indicates the optical depth for which the ground temperature agrees with the average observed temperature.

is absolutely rigorous, the convective region is treated in the limit of perfect efficiency for convective transfer. Thus, the temperature gradient is never greater than the adiabatic gradient and is in fact equal to it throughout the convective region.

The resulting temperature profile, therefore, is somewhat artificial in the vicinity of two portions of the atmosphere :

1. At the tropopause there is a discontinuity in the temperature

gradient. If one took into account the penetration of convection into the stable region above the tropopause then there would be a smooth transition.

2. Near the ground the temperature gradient remains adiabatic. One would expect the efficiency of convective heat transfer to decrease with height above ground so that the gradient should be super-adiabatic very close to the ground.

The latter effect can usually be neglected in planetary atmospheres. Using a mixing length theory for convection one can show that above a few tens of meters above the ground the gradient is already very close to adiabatic so that the ground temperature will not be changed by more than a few degrees.

The situation at the tropopause is a little more complicated because penetration convection is not well understood. However, if the optical thickness of the transition region $\Delta\tau \ll 1$, then it is not necessary to know the temperature accurately in this region, since the flux entering the radiative region comes primarily from a region extending to $\Delta\tau \approx 1$.

The non-grey Model

Molecular absorption is characterized by deep windows and tall bands and the simplest non-grey case to consider is a constant absorption coefficient with one window in it.

The optical depth, τ, refers to the optical depth outside the window and we denote the ratio of the absorption coefficient inside the window to that outside by w. Thus, at any optical depth τ the optical depth within the window is actually $w\tau$.

The equation for the temperature in the convective region is the same as in the grey case. In the radiative region the integral equation is now written in terms of partial integrals of the Planck distribution,

$$\overline{B}_\lambda(T) = \frac{2hc^2}{\pi} \frac{1}{\lambda^5} \frac{1}{e^{hc/\lambda kT} - 1}.$$

If the wavelength limits of the window are λ_1 and λ_2 then the relevant partial integrals are :

inside the window

$$B^w(\tau) = \int_{\lambda_1}^{\lambda_2} \bar{B}_\lambda (T(\tau))d\lambda$$

outside the window

$$B^o(\tau) = \frac{\sigma}{\pi} T^4(\tau) - B^w(\tau).$$

Given T one can compute B^w and B^0 ; conversely given B^w or B^o one can readily compute T. Thus, the determination of $B^w(\tau)$ or $B^o(\tau)$ is equivalent to the determination of the sought function $T(\tau)$.

The equation that must be satisfied in the *radiative region* ($\tau_c \leqslant \tau \leqslant \tau_0$) is

$$B^o(\tau) + wB^w(\tau) = \tfrac{1}{2} B^o(0) E_2(\tau) + \tfrac{1}{2} wB^w(0) E_2(w\tau)$$
$$+ \tfrac{1}{2} \int_0^{\tau_0} [B^o(t) E_1(|\tau - t|) + w^2 B^w(t) E_1(w|\tau - t|)]\, dt,$$

and the value of τ_c is determined as in the grey case, by requiring the flux at the top of the atmosphere

$$F(\tau_0) = 2B^o(0) E_3(\tau) + 2B^w(0) E_3(w\tau) + 2\int_0^{\tau_0} [B^o(t) E_2(\tau_0 - t)\, dt$$
$$+ wB^w(t) E_2(w|\tau_0 - t|)]\, dt$$
$$= \sigma T_e^4.$$

The solutions are obtained numerically by iteration.

The window was set between 7μ and 9μ, as suggested by a rough calculation ([2]) of the absorption coefficient for an atmosphere of CO_2 and water, shown in Figure 3.

The effect of the window on a non-convective atmosphere with optical depth $\tau_0 = 30$ and effective temperature 230°K (corresponding to Venus) is shown in Figure 4, where the temperature at the ground is plotted as a function of w. As the relative depth of the window decreases below about $w = .3$, the cooling effect on the ground becomes very large.

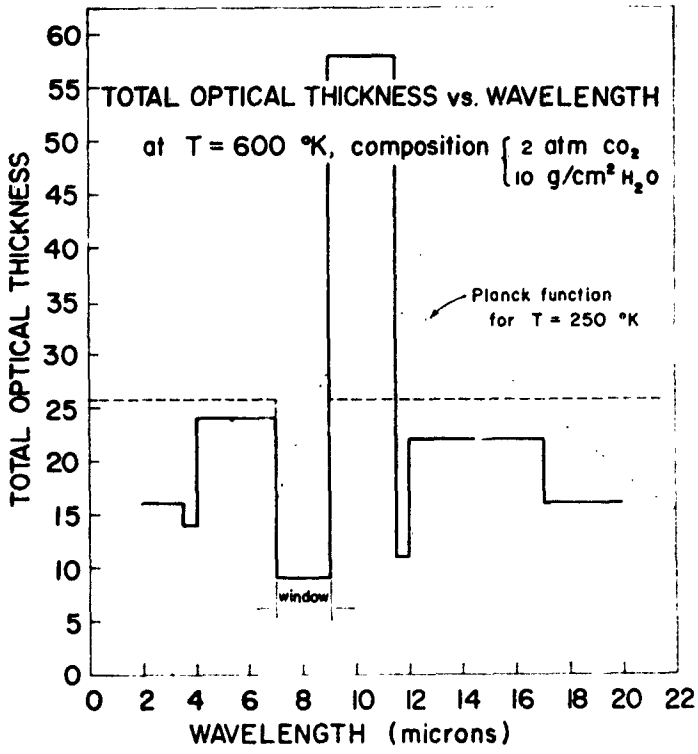

Fig. 3. — The step function indicated by the solid line gives the total optical thickness of an atmosphere composed of CO_2 and water as a function of frequency (adapted from a table in reference 2). The dashed line — which gives the average optical thickness outside the window plus a window, as shown, with arbitrary depth — was the basis for our non-grey calculations. The dotted curve shows the Planck distribution for T = 250°K in relation to the chosen window.

It is clear that one cannot compensate for the cooling effect of the window by a band of equal size in another portion of the spectrum. In other words, making the absorption coefficient dependent upon frequency without changing the Planck mean will still have a cooling effect. This can be seen in Figure 5 where w was allowed to become greater than one. Raising the absorption coefficient somewhere in the spectrum has a much smaller effect than lowering it.

In comparing the curve in Figure 4 (for $\tau_0 = 30$) with the curve

in Figure 5 (for $\tau_0 = 2$)), it is seen that the non-grey cooling effect is much more important the thicker the atmosphere.

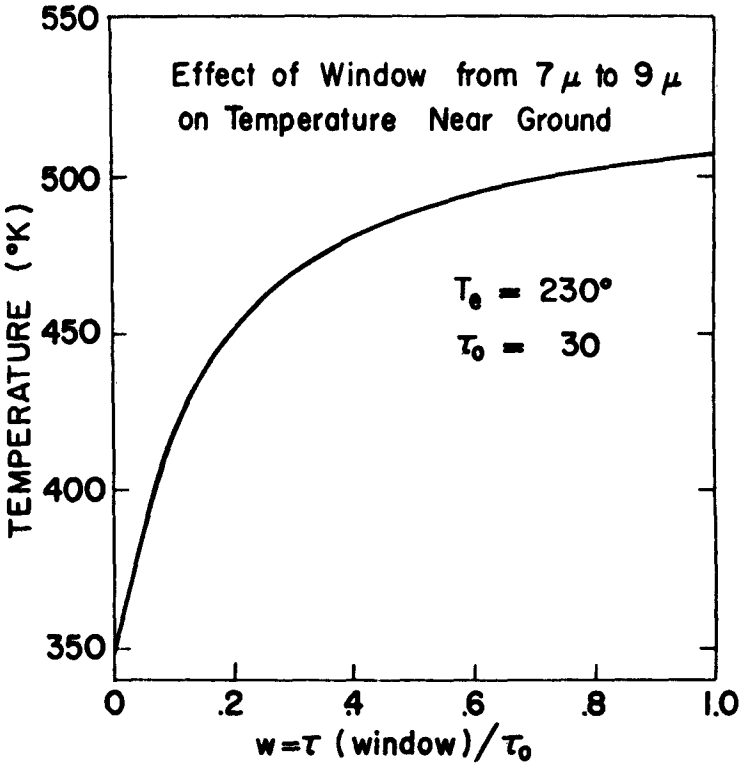

Fig. 4. — The ground temperature as a function of the ratio of the optical thickness inside the window to that outside the window is shown for a non-convective model whose effective temperature is taken from observations of Venus and for which a large optical thickness ($\tau_0 = 30$) is chosen.

This method for treating the non-grey atmosphere is exact and quite general. By inserting any number of windows and bands with arbitrary widths and heights into the equation, we can treat the case of an absorption coefficient with arbitrary dependence upon frequency.

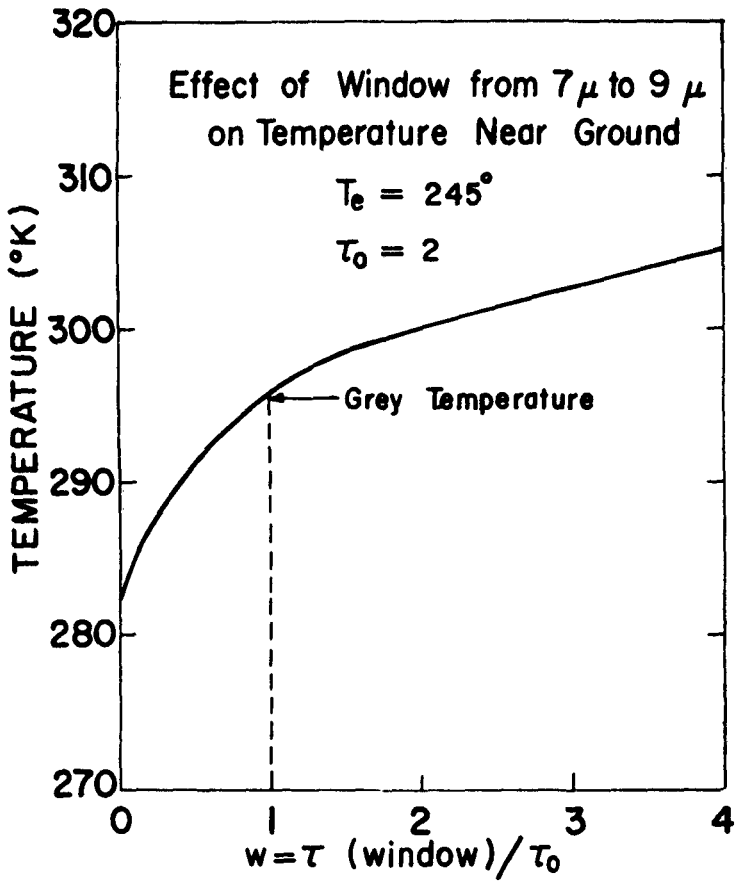

Fig. 5. — Similar to Figure 4 except that T_r and τ_e are chosen to approximate conditions for the earth. The relative optical depth was permitted to go above one, making the « window » an « absorption band ».

ACKNOWLEDGMENT

It is a pleasure to acknowledge the help of Kenneth Grossman in carrying out the numerical computations on the IBM 7090. In addition, I would like to thank Professor R. Wildt, R. Goody and R. Jastrow for interesting discussions related to this problem.

REFERENCES

(1) Based upon the method used by R. M. GOODY (private communication).

(2) R. JASTROW and S. I. RASOOL, *Space Research III*, Proceedings of COSPAR Symposium, May 1962, Washington, D. C.

17. — DIFFUSION DANS LES ATMOSPHÈRES PLANÉTAIRES

MARCEL NICOLET
Centre National de Recherches de l'Espace,
Bruxelles, Belgique

Si on considère l'équation générale de la diffusion des gaz dans le champ de la pesanteur déterminée par Chapman et Cowling (*), (1939, 1952), on peut déduire une expression simple du transport par diffusion dans une atmosphère planétaire si on considère que l'équation de la statique s'applique :

$$\frac{\partial p}{\partial r} = -g\rho \tag{1}$$

Dans cette équation, p est la pression, g est l'accélération de la pesanteur et ρ la densité à la distance r du centre de la planète. Si l'équation des gaz parfaits est utilisée, c'est-à-dire

$$p = nk\mathrm{T} \tag{2}$$

où n est la concentration, T est la température absolue et k la constante de Boltzmann, on décrit en toute généralité (1),

$$\frac{dp}{p} = \frac{dn}{n} + \frac{d\mathrm{T}}{\mathrm{T}} = \frac{d\rho}{\rho} + \frac{d\mathrm{T}}{\mathrm{T}} - \frac{dm}{m} = -\frac{dz}{\mathrm{H}} \tag{3}$$

où H est la hauteur d'échelle définie par

$$\mathrm{H} = k\mathrm{T}/mg, \tag{4}$$

m étant la masse moléculaire moyenne.

L'équation de Chapman s'écrit pour un mélange de deux gaz sous la forme suivante :

$$w_1 - w_2 = -\mathrm{D}_{12}\left\{\frac{n^2}{n_1 n_2}\frac{\partial(n_1/n)}{\partial r} - \frac{m_1 - m_2}{m}\frac{1}{p}\frac{\partial p}{\partial r} + \alpha_\mathrm{T}\frac{1}{\mathrm{T}}\frac{\partial \mathrm{T}}{\partial r}\right\} \tag{5}$$

où α_T est la facteur de diffusion thermique et D_{12} le coefficient de

(*) The Mathematical Theory of Non-Uniform Gases, Cambridge, University Press, 1939, 1952, 1960.

diffusion. Dans cette équation, le flux vertical à un niveau d'altitude z se traduit par le bilan

$$n_1 w_1 + n_2 w_2 = 0 \tag{6}$$

c'est-à-dire que les molécules considérées ont des flux de diffusion égaux et opposés. On voit que la vitesse de diffusion w_1 des particules de masse m_1 et de concentration n_1 est donnée par

$$w_1 = -D_{12}\left\{\frac{1}{n_1/n}\frac{\partial n_1/n}{\partial r} + \frac{n_2(m_2 - m_1)}{nm}\frac{1}{p}\frac{\partial p}{\partial r} + \alpha_T \frac{n_2}{n}\frac{1}{T}\frac{\partial T}{\partial z}\right\} \tag{7}$$

L'équation (7) indique que la vitesse de diffusion d'un constituant de concentration n_1 et de masse m_1 dépend des trois gradients de concentration, de pression et de température.

L'introduction de la relation (3) dans (7) peut s'effectuer aisément si on considère que le gradient de la hauteur d'échelle H donné par

$$\beta = d\mathrm{H}/dz \tag{8}$$

conduit aux relations générales

$$\frac{1}{n}\frac{\partial n}{\partial r} = -\frac{1 + \beta - 2\mathrm{H}/r}{\mathrm{H}} \tag{9a}$$

et

$$\frac{1}{T}\frac{\partial T}{\partial r} = \frac{\beta - 2\mathrm{H}/r}{\mathrm{H}} \tag{9b}$$

L'utilisation de (3) dans (7) exprime le fait que l'on néglige devant l'accélération de la pesanteur les accélérations dues à la diffusion.

Ainsi, l'équation exprimant la vitesse de diffusion w_1 s'écrit

$$w_1 = -D_{12}\left\{\frac{1}{n_1}\frac{\partial n_1}{\partial r} + \frac{1}{\mathrm{H}}\left[\frac{m_1}{m} + \left(\beta - \frac{2\mathrm{H}}{r}\right)\left(1 + \alpha_T \frac{n_2}{n}\right)\right]\right\} \tag{10}$$

En considérant l'expression (9a) de la distribution verticale de la concentration totale, on peut admettre que la distribution verticale du constituant de concentration n_1 s'écrit

$$\frac{1}{n_1}\frac{\partial n_1}{\partial z} = -\frac{\mathrm{X}}{\mathrm{H}}\left(1 + \beta - \frac{2\mathrm{H}}{r}\right) \tag{11}$$

où X est considéré comme le facteur de la distribution verticale d'un constituant de masse m_1 et de concentration n_1.

Ainsi, on a, au lieu de (10),

$$w_1 = \frac{D_{12}}{H}\left[\left(X - \frac{m_1}{m}\right) + \left(\beta - \frac{2H}{r}\right)\left(X - 1 - \alpha_T \frac{n_2}{n}\right)\right] \quad (12)$$

Cette équation indique quelle est la nature du transport vertical par diffusion. Dans une atmosphère isotherme,

$$\beta = \frac{2H}{r} \quad (13)$$

et l'équation (12) se réduit à

$$w_1 = \frac{D_{12}}{H}\left(X - \frac{m_1}{m}\right) \quad (14)$$

De plus, si les constituants sont en mélange parfait,

$$X = 1 \quad (15)$$

et (14) devient

$$w_1 = \frac{D}{H}\left(1 - \frac{m_1}{m}\right) \quad (16)$$

Dans ce cas, le transport par diffusion s'effectue vers le haut si la masse $m_1 < m$ et l'inverse apparaît si $m_1 > m$. Lorsque l'atmosphère n'est pas isotherme, il convient de considérer l'effet du facteur de diffusion thermique α_T. Il est généralement négligeable pour des constituants dont les masses ne diffèrent pas beaucoup. Mais, pour un élément léger diffusant dans un gaz lourd, $\alpha_T \simeq -0{,}4$ et n'est donc pas négligeable devant l'unité, surtout lorsque l'élément léger est un constituant secondaire ($n_2 \simeq n$).

L'intérêt de l'équation de diffusion écrite sous la forme (12) réside dans le fait que, dans bien des cas, il est certain que le facteur de distribution verticale est très différent de l'unité. C'est le cas, par exemple, lorsque la dissociation intervient ou lorsque des réactions chimiques modifient la distribution verticale de constituants secondaires. Afin d'obtenir des valeurs numériques, il suffit d'introduire dans (12) l'expression du coefficient de diffusion D_{12}. Il peut s'écrire

$$D_{12} = \frac{3}{8}\frac{f}{\pi\sigma_{12}^2}\left(\frac{m_1 + m_2}{m_1}\right)^{1/2}\left(\frac{\pi kT}{2m_2}\right)^{1/2}\frac{1}{n} \quad (17)$$

où $\pi\,\sigma_{12}^2$ est la section efficace de collision pour des sphères élastiques rigides de diamètre σ_1 et σ_2, c'est-à-dire

$$\sigma_{12} = \frac{1}{2}(\sigma_1 + \sigma_2) \tag{18}$$

et où f est un facteur de correction qui tient compte du fait que la section efficace peut dépendre de la température. Dans ce cas, D_{12} n'est pas directement proportionnel à $T^{1/2}$.

En introduisant (17) dans l'expression (12), on obtient pour le flux de particules de masse m_1, $F(m_1)$:

$$F(m_1) = \frac{3}{8}\frac{fg}{\pi\sigma_{12}^2}\left(1+\frac{m_2}{m_1}\right)^{1/2}\left(\frac{\pi m^2}{2m_2kT}\right)^{1/2}\frac{n_1}{n}$$
$$\left[\left(X-\frac{m_1}{m}\right)+\left(\beta-\frac{2H}{r}\right)\left(X-1-\alpha_T\frac{n_2}{n}\right)\right] \tag{19}$$

Si le constituant de masse m_1 est un constituant secondaire, c'est-à-dire si $n_1 \ll n_2$, l'expression (19) devient

$$F(m_1) = \frac{3}{8}\frac{fg}{\pi\sigma_{12}^2}\left(1+\frac{m_2}{m_1}\right)^{1/2}\left(\frac{\pi m_2}{2kT}\right)^{1/2}\frac{n_1}{n_2}$$
$$\left[\left(X-\frac{m_1}{m_2}\right)+\left(\beta_2-\frac{2H_2}{r}\right)(X-1-\alpha_T)\right] \tag{20}$$

En vue de déterminer des conditions pratiques, nous adoptons une section efficace moyenne $2{,}8 \times 10^{-15}$ cm^2 correspondant à un diamètre de collision $\sigma_1 = \sigma_2$ de 3A. Ainsi, la section efficace de diffusion n'est pas surestimée. Introduisant, en outre, les masses physiques, c'est-à-dire $M(O) = 16$, le flux de diffusion est donné par $F(M_1)$ cm^{-2} sec^{-1}

$$F(M_1) = 1{,}823 \times 10^{11}\, g_0\left(\frac{r_0}{r}\right)^2\left(1+\frac{M_2}{M_1}\right)^{1/2}\left(\frac{M_2}{T}\right)^{1/2}\frac{n_1}{n_2}$$
$$\left[\left(X-\frac{m_1}{m_2}\right)+\left(\beta_2-\frac{2H_2}{r}\right)(X-1-\alpha_T)\right] \tag{21a}$$

On voit donc que, dans l'homosphère, c'est-à-dire dans la partie de

l'atmosphère où les constituants principaux sont dans les mêmes proportions, on a

$$F(M_1) = 1{,}823 \times 10^{11}\, g_0 \left(\frac{r_0}{r}\right)^2 \left(1 + \frac{M_2}{M_1}\right)^{1/2} \left(\frac{M_2}{T}\right)^{1/2} \frac{n_1}{n_2} \left[\left(1 - \frac{m_1}{m_2}\right) - \alpha_T\left(\beta_2 - \frac{2H_2}{r}\right)\right] \quad (21b)$$

Cette expression montre que le flux de diffusion dans l'homosphère ne varie pas beaucoup en fonction de l'altitude, car il dépend essentiellement du rapport $(r_0/r)^2$ et de la variation de $T^{-1/2}$. En simplifiant, on adopte une altitude de l'ordre de 100 km correspondant à $(r/r_0) = 0{,}985$, une température de 200°K et un faible gradient. Ainsi, on a, dans le cas de l'atmosphère terrestre,

$$F(m_1) = 1{,}7 \times 10^{13} \left(1 + \frac{M_2}{M_1}\right)^{1/2} \left(\frac{M_2}{T}\right)^{1/2} \left(1 - \frac{M_1}{M_2}\right) \frac{n_1}{n_2} \quad (22)$$

Pour les diverses planètes, l'expression (22) est applicable si le facteur numérique est multiplié par les valeurs suivantes :

Mercure	Vénus	Mars	Jupiter	Lune	Titan
0,36	0,858	0,40	2,64	0,165	0,176

Si on adopte comme constituant principal l'azote moléculaire M = 28, on approche très souvent des conditions réelles. On obtient ainsi, à partir de (22), les flux de diffusion suivants :

Hydrogène : $F(H) = 3{,}4 \times 10^{13}\,[n(H)/n_2]$ cm^{-2} sec^{-1} (23)

Deutérium : $F(D) = 2{,}3 \times 10^{13}\,[n(D)/n_2]$ cm^{-2} sec^{-1} (24)

Hélium-3 : $F(He^3) = 1{,}9 \times 10^{13}\,[n(He^3)/n_2]$ cm^{-2} sec^{-1} (25)

Hélium-4 : $F(He^4) = 1{,}6 \times 10^{13}\,[n(He^4)/n_2]$ cm^{-2} sec^{-1} (26)

Oxygène-16 : $F(O) = 4{,}6 \times 10^{13}\,[n(O)/n_2]$ cm^{-2} sec^{-1} (27)

Oxygène-32 : $F(O_2) = -7{,}6 \times 10^{13}\,[n(O_2)/n_2]$ cm^{-2} sec^{-1} (28)

La conclusion est que dans l'atmosphère terrestre, l'ordre de grandeur du flux de diffusion est donné par

$$F \simeq 10^{13}(n_1/n_2) \text{ cm}^{-2} \text{ sec}^{-1} \quad (29)$$

On doit néanmoins se rendre compte qu'il ne faut qu'un léger changement des conditions physiques pour modifier le sens du flux de

diffusion. Prenons comme exemple la molécule d'oxygène. La formule (21b) conduit à

$$F(O_2) = 8{,}8 \times 10^{13} \frac{n(O_2)}{n_s} [(X - 1{,}14) + \beta(X - 1)] \qquad (30)$$

Le transport a lieu vers les hautes altitudes si le terme entre crochets est positif, c'est-à-dire si

$$X > 1 + 0{,}14 \frac{\beta}{1 + \beta} \qquad (31)$$

ou avec un gradient $\beta = 0{,}2$,

$$H > 1{,}12\, H(O_2) \qquad (32)$$

Donc, il suffit que la hauteur d'échelle de l'oxygène moléculaire devienne inférieure à 1,12 fois celle de l'atmosphère pour que la diffusion provoque un transport vers le haut. En particulier, si on admettait un équilibre photochimique on aurait :

$$F(O_2) = 2 \times 10^{13}\, n(O_2)/n_s \text{ cm}^{-2} \text{ sec}^{-1} \qquad (33)$$

c'est-à-dire un flux qui compense aisément la photodissociation. En d'autres termes, il existe un flux vertical de molécules qui peut compenser les molécules photodissociées dans le champ du rayonnement du soleil.

D'autre part, si on considère un constituant apparaissant dans l'hétérosphère comme résultat d'une dissociation, un maximum de concentration apparaît. Au niveau de ce maximum, il existe toujours un transport vers le bas dont le flux s'obtient à partir de (20) où $X = 0$. En particulier, pour l'oxygène atomique dans l'azote, on trouve :

$$F(O) = -6 \times 10^{13}\, n(O)/n_s \text{ cm}^{-2} \text{ sec}^{-1} \qquad (34)$$

c'est-à-dire encore une fois un flux très important qui doit influencer les conditions photochimiques. Ceci est d'autant plus important qu'il s'agit d'un transport vers le bas que ne contrecarre pas le brassage de l'air dû à la turbulence ou à tout autre mouvement atmosphérique.

Ces exemples montrent combien l'étude de la structure des

atmosphères supérieures planétaires ne peut se déterminer dans le cadre élémentaire des équilibres de photodissociation ou de photoionisation. Le transport par diffusion modifie l'équilibre de dissociation par suite du transport vers le haut des molécules. Il faudrait que les processus de dissociation soient extrêmement rapides pour que le processus de diffusion ne domine pas. Dans le cas de la distribution des atomes, il s'agit de comparer les temps de recombinaison et de diffusion. Lorsque la recombinaison est due à une collision triple, le maximum de concentration sera toujours déplacé vers le bas par rapport aux conditions d'équilibre et il y aura un transport vers le bas des atomes produits par dissociation ou ionisation. Des réactions rapides sont nécessaires pour éviter un tel processus.

En bref, on ne peut fixer les conditions physiques des atmosphères planétaires en considérant uniquement les processus photochimiques. Il faut tenir compte de l'effet de diffusion dans le champ de la pesanteur. Cet effet, à partir des conditions photochimiques, se traduit par des transports des atomes ou des molécules dans le sens opposé au transport résultant du passage du mélange parfait à l'équilibre de diffusion.

18. — MICROWAVE SPECTRAL LINES AS PROBES OF PLANETARY ATMOSPHERES

ALAN H. BARRETT
Research Laboratory of Electronics
Massachusetts Institute of Technology
Cambridge, Massachusetts, U. S. A.

1. INTRODUCTION

It has been seven years since radio emission was detected from Jupiter, and during this time radio emission from Mercury, Venus, Mars, and Saturn has also been detected. For the planets Mercury, Mars and Saturn, the detection has been limited to single observations at wavelengths between 3-4 cm, hence no information is available about their radio spectra, but the intensity of the received radiation is in good agreement, within the observational uncertainties, with that to be expected by thermal emission from the planetary surfaces and/or atmospheres. However, the intensity of the emission from Venus and Jupiter was wholly unexpected and has stimulated considerable research, both theoretical and experimental, on these planets and their environment. Needless to say, the possibility of obtaining data on the planets from close range by means of space probes has also served to heighten the interest in planetary phenomena.

Because of extensive cloud cover on Venus and Jupiter, their surfaces have eluded direct study by ground-based observations at all wavelengths shorter than the radio wavelengths. The great value of the radio observations is that they afford a means of studying the physical conditions below the cloud layers and, at the moment, this appears to be the only method by which this can be accomplished from ground-based observations, with perhaps a few isolated exceptions. However, it should not be construed a priori that the clouds have a negligible effect at all radio wavelengths and hence can be dropped from further consideration of the radio data. It is equally dangerous to assume that the radio observations auto-

matically refer to the surface and lower atmosphere of the planet. In fact, a strong case can be built for explaining the bulk of the microwave radiation from Jupiter as originating in an intense radiation belt surrounding the planet at distances of several planetary radii. Also, a dense ionosphere about a planet could render the surface totally unobservable by radio methods, although the requirements imposed upon the ionosphere appear to be quite severe.

The hindrances imposed by either a planetary radiation belt or a dense ionosphere can be circumvented, at least partially, by radio observations made at short centimeter and millimeter wavelengths. The clouds, however, will play a larger role at these wavelengths than at longer wavelengths in determining the radio spectra. Another factor also becomes important at the short centimeter and millimeter wavelengths. The spectral lines of molecules resulting from their rotational or fine-structure energy are predominantly found at wavelengths shorter than 3 cm and these can be expected to be vitally important in defining the planetary microwave spectra. This fact alone opens up the possibility of detecting molecular species in planetary atmospheres which might be undetectable, at present, by other methods. For example, molecular constituents whose electronic or vibrational spectra lie in a region of the spectrum obscured by the terrestrial atmosphere might be detected by their microwave spectra, or a constituent distributed predominantly in the lower atmosphere of the planet could produce a detectable resonance in the radio region and have escaped detection by other techniques. In any event, as radio observations are extended into the millimeter spectrum it will become increasingly important to know the microwave properties that can be expected of the molecular species to guide the interpretation of the millimeter data.

II. Microwave Spectra of Planetary Constituents

Several authors have discussed the possibilities of detecting atomic and molecular spectral lines of astrophysical interest by

radio techniques, but such discussions have usually been concerned with detection possibilities in the interstellar medium and thus are not entirely appropriate for the present discussion [1-7]. In this section the subject will be re-examined from the point of view of planetary atmospheres and this will require a consideration of many more molecular species, generally of a more complex nature, than would be expected in the interstellar medium.

Needless to say, the first question to be considered is : What atoms and molecules are known to exist, or might be expected to exist, in the atmospheres of the planets? The answer to this question must be supplied, at least partially, by the observations of planetary spectra which have been made. The atoms and molecules that have been identified in the atmospheres of Venus, Mars, and Jupiter are given in Table I-a. The constituents of the Earth's atmosphere are also listed, in order of decreasing abundance. Also presented in this table in parentheses are those molecules that are present in the terrestrial atmosphere and might be expected to occur in the atmospheres of the planets indicated. (Only Venus, Mars, and Jupiter will be considered, as they are sufficiently representative.) Table I-a clearly illustrates the contrast between

TABLE Ia

Molecular constituents of planetary atmospheres

Planet	*Molecules*
Venus	CO_2, H_2O (?), (N_2, N_2O, NO_2, CO, CH_4, A, O_2, O_3).
Earth	N_2, O_2, H_2O, A, CO_2, Ne, He, CH_4, Kr, N_2O, H_2, O_3, CO, SO_2, OH.
Mars	CO_2 (N_2, A, O_2, O_3, H_2O, CO, N_2O, NO_2, CH_4).
Jupiter	H_2, CH_4, NH_3 (He, Ne, A, H_2O).

the number of identified atoms and molecules in the Earth's atmosphere as compared with the neighboring planets. It is to be expected that many of the suspected molecules actually do exist in the atmospheres of the other planets, but their abundance is such that they have escaped detection by present spectroscopic techniques.

Our present knowledge of planetary atmospheres is such that a list of possible molecular constituents should include more than just those found in the terrestrial atmosphere. Therefore, in addition to considering the microwave properties of all of the molecules in Table I-a, the molecules listed in Table I-b will also be considered. Note that the bulk of the molecules in Table I-b are organic compounds involving the astrophysically abundant atoms H, C, N, and O. Molecules containing six or more atoms are excluded. The organic compounds may prove to be very important in planetary physics, particularly with reference to Venus.

TABLE Ib

Other possible molecular constituents

CH_2O	C_2H_2	HCNO
CH_2O_2	C_2H_4O	H_2O_2
CNSH	C_2N_2	H_2S
CS	C_2HN	NO
CS_2	HCN	OCS

Having selected a fairly large and representative group of molecules, the next question to ask is : What are the microwave properties, if any, of these molecules? The answer to this question is unfortunate. Many of the most abundant molecules in the planetary atmospheres do not have any microwave resonance spectra. This is a consequence of the fact that practically all symmetric molecules, of which the homonuclear molecules are an obvious example, do not have any permanent dipole moment and, therefore, do not exhibit any microwave resonance lines. Thus H_2, N_2, CO_2, and CH_4, for example, are unobservable by microwave techniques. The molecule O_2 is a familiar exception to this group because it has

a permanent magnetic dipole moment, even though its electric dipole moment is zero. In Table II the molecules of Table I are separated into those having no microwave spectra, and those that do, and it is this latter group that will be considered.

TABLE II

Microwave properties of atomic and molecular constituents

Lacking microwave resonance spectra	*Having microwave resonance spectra*	
A	CH_2O	H_2S
CH_4	CH_2O_2	NH_3
CO_2	CO	NO
CS_2	CS	NO_2
C_2H_2	C_2H_4O	N_2O
C_2N_2	C_2HN	OCS
H_2	HCN	OH
He	HNCO	O_2
Kr	HNCS	O_3
N_2	H_2O	SO_2
Ne	H_2O_2	

The molecules in Table II are relatively simple molecules and, for the most part, were among the first to be studied by the techniques of microwave spectroscopy. Therefore a large body of data has been accumulated from which we can evaluate their microwave properties under circumstances that are of interest to us ([8]). Of particular importance is the fact that measured frequencies of most of the principal transitions have been published or may be accurately calculated from the molecular parameters evaluated from measurements at other frequencies. A compilation of these frequencies is given in Appendix I for those molecules listed in Table II that have resonance spectra. Included also are the available quantum numbers of the transitions. Very often calculated intensities are published but these usually refer to a temperature of 300°K, low pressure, and no foreign gas broadening. Under these

circumstances the calculated intensities can be more misleading than helpful for considerations of planetary atmospheres and have been omitted.

We have dropped from consideration those molecules that have no permanent dipole moment. However, it should not be assumed that these molecules have no effect upon microwave propagation under all circumstances. During a molecular collision a molecule may have an induced dipole moment that gives rise to nonresonant interaction with microwave radiation. In situations of high pressure, the effect of the induced dipole may be appreciable because the molecule will spend a larger fraction of its time in collision. This process has been used to explain the high-pressure nonresonant absorption exhibited by CO_2, N_2, C_2H_4, for example ([9, 10]). In fact, the collision-induced dipole absorption by CO_2 formed the basis of the interpretation of the Venus radio observations that indicated that the surface pressure of Venus might be very much higher than was previously supposed ([11]). For future interpretations of the Jupiter radio observations, it should be noted that the collision-induced dipole effect is very small for both H_2 and CH_4 for pressures up to 100 atm. ([10]).

III. Dependence of microwave properties on Planetary Environment

The basic parameters of any spectral line are its frequency, intensity, and line shape, but all of these quantities are dependent upon the particular circumstances of observation. In this section we shall show how the parameters are influenced, or altered, by the conditions within the planetary atmosphere, as this will be important in dictating equipment design, planning an observing program, or interpreting the observations.

The resonance frequency of a transition is defined by the spacing of the energy levels within the molecule and, under many circumstances, may be considered to be independent of external

interactions on the molecule. However, if a molecule does experience external interactions such as collisions, the resonant frequency will be shifted when the average energy of interaction is comparable with the energy separation of the levels. This effect is important for molecules in high-pressure environments, and may be very important for considerations involving Venus and Jupiter microwave spectra. Unfortunately, very little experimental data are available about this effect for polar molecules, although NH_3 has been thoroughly studied ([12-14]). It has been found that for pressures of 1 atm of pure NH_3 the observed absorption at wavelengths of approximately 1 cm can be explained only by assuming that the resonance frequency has a value less than its low-pressure value, and for pressures of 2 atm, or higher, one must take the resonance frequency to be zero. This result is in agreement with theoretical predictions ([15, 16]). Data on high-pressure effects for other polar molecules appear to be limited to a study of NO, carried out at frequencies of 9 KMc/s and 23KMc/s over a range of pressures of 3-27 atm ([17]). It has been found that NO, which has a small dipole moment, showed no irregular high-pressure effects until approximately 15 atm, and rather slight effects above this value. High-pressure effects have also been studied experimentally and theoretically for O_2 ([18, 19]). For pressures greater than 20 atm, the observed results can only be fitted to the usual line shape theories if one assumes that the resonance frequencies decrease rapidly to zero when the pressure exceeds 20 atm.

We expect that all molecules will exhibit a shift of their resonance frequencies under conditions of high pressure, for in the limit of very high pressures the resonance absorption, which is typical of the gaseous state, must approach the nonresonance absorption characteristic of a liquid. Quantitatively, the frequency-dependent portion of the absorption coefficient α for a single line of frequency ν_0 is given by ([8, 20])

$$\alpha \sim \nu^2 \left\{ \frac{\Delta\nu}{(\nu - \nu_0)^2 + \Delta\nu^2} + \frac{\Delta\nu}{(\nu + \nu_0)^2 + \Delta\nu^2} \right\}, \qquad (1)$$

where $\Delta\nu$ is the halfwidth of the line. When ν_0 becomes zero this expression gives

$$\alpha \sim \frac{2}{\Delta\nu} \frac{\nu^2}{1 + \left(\frac{\nu}{\Delta\nu}\right)^2}, \tag{2}$$

which is the form of the familiar Debye absorption for liquids. The question of when the pressure shift of ν_0 sets in is dependent upon the dipole moments of the molecules in collision and the force law acting between them. For example, a molecule with a large dipole moment will have a large effective collision diameter ; hence it will require fewer collisions per unit time to shift its frequency than a molecule with a very small dipole moment. Therefore, not only must each case be treated separately, but it must be treated with particular reference to the molecular environment. In general, the transition to zero frequency appears to be important when $(\Delta\nu)p$ is of the same order as ν_0, where $\Delta\nu$ is the halfwidth at low pressures ([18]).

The question of linewidth of a spectral line is closely associated with the frequency shift because both result from external interactions of identical nature. For planetary atmospheres, the mechanism dominating the linewidth will be pressure broadening, with the possible exception of the extreme upper atmosphere in which Doppler broadening may become comparable with pressure broadening. Microwave spectroscopic measurements of linewidths are usually made at low pressures, less than 1 mm Hg, and the extrapolation of these measurements to pressures of 1 atm or greater must be considered hazardous. At pressures for which multiple collisions become important, the linewidth predicted on the basis of low-pressure results will give an erroneous value. Again, when this becomes important depends on the dipole moments of the colliding molecules and the force law. Another complication is that linewidths are usually determined for broadening by collisions of one molecule with another of the same species, that is, self-broadening, but in planetary atmospheres the broadening will be

by collisions with several types of molecules, each with its own interaction potential. Formally, the resultant linewidth may be computed from the expression ([8])

$$\Delta\nu_1 = \sum_{i=1}^{i} x_i \, \Delta\nu_{1i}, \tag{3}$$

where x_i is the fractional abundance of molecule i, and $\Delta\nu_{1i}$ is the linewidth of the absorption line of molecule 1 if it were broadened only by molecule i. Unfortunately, experimental data on foreign gas broadening are meager, although the relative importance of some species can be judged by their effect in broadening the NH_3 resonances ([3]). As might be expected, molecules with large dipole moments produce the largest pressure broadening. Even fewer data are available for application to high-pressure situations ([21]).

Although the linewidth is an important parameter of spectral lines, the question of the over-all line shape is equally vital when we consider observations throughout an entire atmosphere of a planet. Because the path of observation is through a medium of continually changing temperature, pressure, and, perhaps, molecular composition, the resultant line shape will be drastically altered from that obtained in laboratory spectroscopy. The width of the overall line will dictate the required frequency resolution of the observing equipment and, furthermore, will be a contributing factor in the resultant intensity of the line. In addition, the intensity of the line will depend directly upon the vertical distribution of the molecular species and the temperature profile of the atmosphere. Both the intensity and shape of the line may be computed from the equations ([22])

$$T_B = T_S \, e^{-\tau_m} + \int_0^{\tau_m} T \, e^{-\tau} \, d\tau, \tag{4}$$

$$\tau = \int_x^{\infty} \alpha \, dx', \tag{5}$$

where T_S is the effective radiation temperature of the surface, T is the temperature of the atmosphere, T_B is the brightness tempera-

ture of the emergent ray in the direction in which x is measured, and τ_∞ is the optical depth integrated from the surface throughout the atmosphere. In writing these equations, the usual Rayleigh-Jeans approximation to the Planck radiation law is assumed, hence intensity can be expressed as a temperature. The general expression for the absorption coefficient α has been given by Van Vleck and Weisskopf ([10])

$$\alpha = \frac{4\pi^2 N\nu \sum_i \sum_j |\mu_{ij}|^2 \nu_{ij} f(\nu, \nu_{ij}) e^{-E_j/kT}}{3ckT \sum_j e^{-E_j/kT}} \tag{6}$$

$$f(\nu, \nu_{ij}) = \frac{\nu}{\nu_{ij}} \left[\frac{\Delta\nu}{(\nu - \nu_{ij})^2 + \Delta\nu^2} + \frac{\Delta\nu}{(\nu + \nu_{ij})^2 + \Delta\nu^2} \right], \tag{7}$$

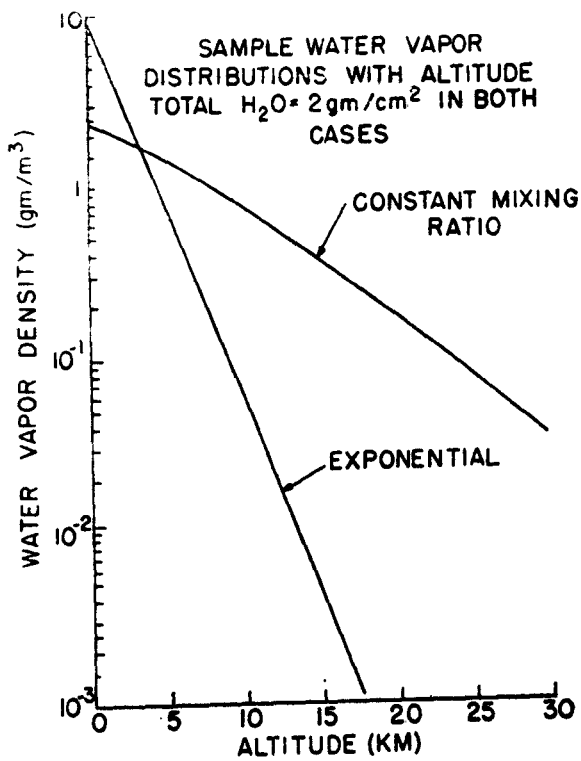

Fig. 1. — Sample vertical distributions of H_2O.

where N is the number density of molecules of a particular species, ν_{ij} are the resonance frequencies, E_j is the energy of level j, and μ_{ij} is the dipole matrix element between levels i and j. The frequency dependence of the line is largely contained in the « shape factor » $f(\nu, \nu_{ij})$, therefore the line shape will be dictated by Eqs. (3) and (7), the vertical distribution of the molecular species, and the total pressure, since the total pressure will determine the linewidth $\Delta\nu$.

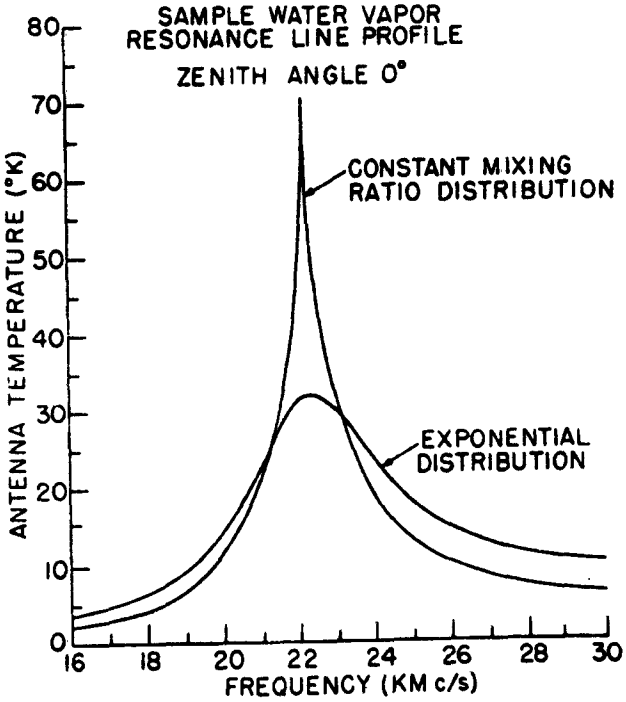

Fig. 2. — H_2O line shape as seen from the surface of the Earth computed using the distributions of Fig. 1.

As an illustration of how the line shape and intensity are influenced by the vertical distribution of the molecules the resonance profiles of a single isolated line have been computed for the hypothetical distributions shown in Fig. 1. The resultant line profiles are shown in Fig. 2. These figures are applicable to the H_2O line in the terrestrial atmosphere, as viewed from the Earth's

surface, but they illustrate how important the effect of the vertical distribution is in determining the line profile ([23]). The total H_2O is the same in the two cases, so the difference in the profiles results entirely from the manner in which the H_2O is distributed in height. The increased intensity and narrow profile of the constant mixing ratio case is due solely to the fact that more H_2O is distributed at higher altitudes where line broadening is less because of the reduced pressure. Figure 2 was computed from the equations

$$T_B = \int_0^\infty T\, e^{-\tau}\, d\tau, \quad \tau = \int_0^s \alpha\, dx', \tag{8}$$

which are appropriate for observations made from the surface of a planet. These equations are analogous to Eqs. (4) and (5) which apply to observations made from outside a planetary atmosphere. Figure 2 demonstrates that microwave observations, taken in sufficient detail to define the line shape, can be used to give information about the vertical distribution of planetary atmospheric molecules. However, it should be mentioned that a unique determination of the molecular distribution would be dependent upon a knowledge of the temperature and pressure distribution throughout the atmosphere. The microwave observations could also be used to monitor the resonance frequency and give information concerning temporal variations in the abundance and/or the distribution.

Observations made from a planetary surface require a means of placing and orienting the equipment on the surface of the planet. Of more immediate interest, perhaps, is the effect of a microwave resonance line as viewed from outside the planetary atmosphere, either from a space craft or from a groundbased site. Unfortunately, the effect of the resonance may not be as pronounced in this case, and therefore its utility is more limited. For example, if the total optical depth is small, as is the case for the terrestrial H_2O line at 1.35 cm, the effect of the resonance line is largely compensated for by the emission from the surface. This can be seen clearly by comparing Figs. 2 and 3 ; the latter has been computed

by using Eqs. (4) and (5) for the exponential distribution of H_2O in the terrestrial atmosphere. Note that the total effect of the resonance line is an order of magnitude less when viewed in absorption against the terrestrial surface than when viewed from the surface looking into cold space. It should be emphasized that the intensity of the resultant line depends critically upon the effective radiation temperature T_s of the background. In computing Fig. 3

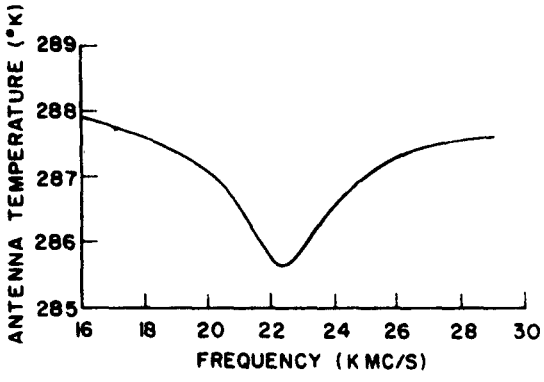

Fig. 3 — H_2O line shape as seen from above the atmosphere. Computations were made for an exponential distribution, and assuming a radiation temperature of 288°K for the Earth's surface.

the value used for T_s corresponded to that of the atmosphere at ground level, an assumption that is equivalent to assuming that the emissivity of the surface is unity and that the surface and lower atmosphere are at identical temperatures. On the other hand, consider the case of ocean surfaces in which the radiating temperature T_s may depart appreciably from the groundlevel atmospheric temperatures because of the low emissivity (high reflectivity). In this case, the resultant temperature in the center of the line may exceed that of the background and the line would appear as an emission line, characteristic of observations from the surface. Such a case is shown in Fig. 4, which has been computed for the terrestrial H_2O as seen over ocean areas that have an assumed effective temperature of 165°K.

The examples above have been computed by using parameters that are typical of the Earth and are representative of an atmospheric H_2O distribution to illustrate the various possibilities here. It should be emphasized, however, that the examples apply to a single resonance line for which the total optical depth is small

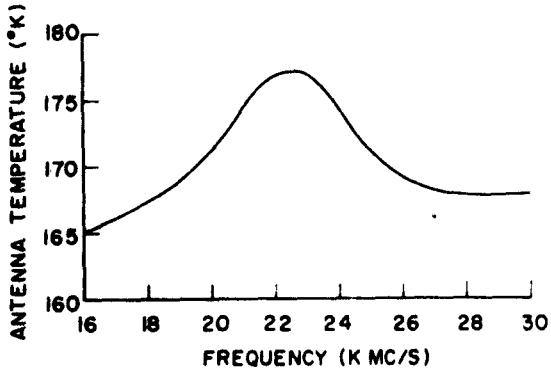

Fig. 4. — H_2O line shape as seen from above the atmosphere. Computations were made for an exponential distribution, and assuming a radiation temperature of 165°K for the Earth.

compared with unity. For the case of large optical depth and many closely spaced lines, the resultant profiles will be more dependent on the temperature distribution in the atmosphere. In fact, the question of whether a line will be seen in absorption or emission, when viewed from outside the atmosphere, will depend on the optical depth at frequencies near a particular line and the distribution of temperature in the atmosphere. An example illustrating this case is the complex of O_2 lines at 5-mm wavelength in the terrestrial atmosphere where the optical depth is so large that the radiation from the Earth's surface is totally absorbed in the center of the line complex, therefore, even though the lines are generated in the upper atmosphere they will be seen in emission because of the temperature distribution ([14]).

Our knowledge of planetary atmospheres, other than that of the Earth, is so meager that detailed calculations are not justified unless a molecule has been identified, or is strongly suspected, in an

atmosphere. As shown in Table Ia, the only molecules with microwave resonance spectra which are likely possibilities are H_2O on Venus and NH_3 on Jupiter, and both have been investigated theoretically to determine their effect on the microwave spectra of

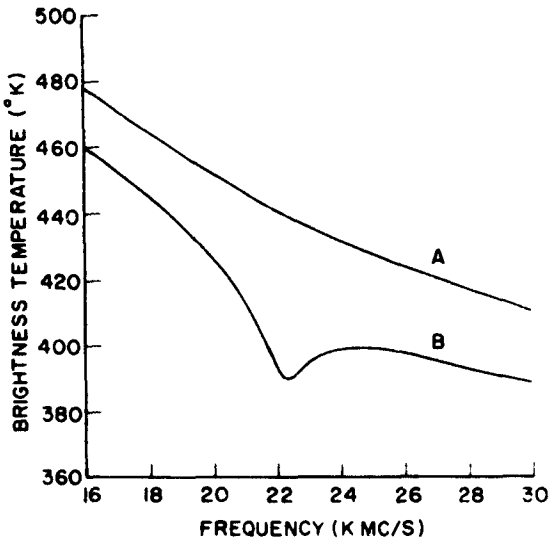

Fig. 5. — Theoretical microwave spectra of Venus computed assuming an atmosphere of CO_2, N_2, and H_2O, a surface temperature of 580°K and a surface pressure of 30 atm. Curve A assumes an H_2O mixing ratio of 10^{-3} at the surface and decreasing linearly to zero at 33 km. Curve B assumes an H_2O mixing ratio of 10^{-3} to be uniform throughout the atmosphere.

these planets ([11, 25, 26]). In both cases the analyses are replete with assumptions about the physical characteristics of the planetary atmosphere and surface and the results are dependent, of course, on the nature of the assumptions. As an example, Fig. 5 shows a portion of the Venus microwave spectra as influenced by the presence of H_2O computed for different assumed altitude distributions and total H_2O content ([26]). These curves illustrate how critical the actual distribution is in determining the resultant effect on the spectrum and, as already mentioned, how the observation of a line profile can give information relative to the physical structure of the atmosphere. These curves also point out the fact

that it may be very difficult to identify a resonance with a particular molecular species. The resonance is likely to be quite broad, making it difficult to determine accurately the center frequency. As can be seen from Appendix I, the spectrum for wavelengths less than 3 cm is rich in spectral lines and only by an accurate measurement of the resonance frequency could other molecules be excluded. Therefore, while the detection of a resonance requires observations over a broad range of frequencies, the identification of the resonance would be greatly increased by observations over a narrow band of frequencies near the resonance frequency. This is especially true if there is an abundance of molecules in the upper atmosphere of the planet because the frequency dependence of the spectrum would then be rather sharp near resonance, and the limits of error on the center frequency reduced accordingly.

IV. Determination of Atmospheric Properties by a Microwave Experiment

As has been discussed above, observations from ground-based sites might possibly detect a molecular resonance in the spectrum of a planet and, by its shape, deduce the gross characteristics of the vertical distribution. Observations from close range such as are afforded by planetary fly-by spacecrafts would greatly increase the spatial resolution so that local areas could be examined, longitudinal effects determined, equatorial and polar differences detected, and day-night effects studied. However, it will be difficult to determine the physical structure of the atmosphere, such as temperature, pressure, and abundance distributions, by microwave measurements alone, without supporting data.

Many of these uncertainties can be removed by a spacecraft experiment in which the vehicle passes through the atmosphere and impacts on the planet. Consider two fixed-frequency radiometers, one directed toward the surface of the planet, and the other oppositely directed, i. e., into cold space. Assume that the frequency is

chosen so that the total optical depth through the atmosphere is not small. Then, for the radiometer directed toward the surface, Eqs. (4) and (5) are applicable, and, for the radiometer directed toward space, Eqs. (8) apply. The radiometer outputs will continually change, of course, as the vehicle falls through the atmosphere, and, supposedly both radiometer outputs will be increasing. At the moment before impact, one radiometer will register the effective radiation temperature of the surface, while the other will give the effective temperature of the atmosphere as seen from the surface, or very close to it. At a height h_1 in the atmosphere, which is presumed to be known from altimeter data, the output of radiometer 1, T_{A1}, directed toward the surface, will be

$$T_{A1}'(h_1) = T_S e^{-\tau(h_1)} + T_g(h_1)[1 - e^{-\tau(h_1)}], \tag{9}$$

where $T_g(h_1)$ is the average gas temperature over the height interval h_1, and $\tau(h_1)$ is the optical depth of the layer of thickness h_1. On the other hand, the output of radiometer 2, T_{A2}, directed toward space will be

$$T_{A2}(h_1) = \int_{h_1}^{\infty} T_g e^{-\tau} d\tau, \tag{10}$$

which is simply the integrated effect of all of the atmosphere above h_1. At the surface of the planet, i. e., $h = 0$, the outputs of the radiometers will be

$$T_{A1}(0) \doteq T_S \tag{11}$$

$$T_{A2}(0) = T_g(h_1)[1 - e^{-\tau(h_1)}] + e^{-\tau(h_1)} \int_{h_1}^{\infty} T_g e^{-\tau} d\tau \tag{12}$$

By using Eqs. (10) and (11), it is possible to solve Eqs. (9) and (12) for $T_g(h_1)$ and $\tau(h_1)$. By a similar procedure for other heights, it is possible to obtain the temperature distribution with height and the variation of the optical depth with height throughout the atmosphere. The vertical resolution afforded by this method, i. e., the size of the increments of h, will depend entirely upon the sensitivity of the equipment, the value of $\tau(h_1)$, and the temperature gradient in the atmosphere. Note that if $\tau(h_1)$ is large, then both radiometers will measure simply the gas temperature as a function

of height and no information will be gained about the optical depth.

The experiment outlined above can determine the temperature gradient, but further information about the atmosphere is contained in the optical depth determination as a function of height. The mechanism of absorption has not been specified. In particular, the experiment is not dependent upon a microwave resonance line for its success, since a nonresonance absorption such as is exhibited by CO_2 under high pressure ([9]) would suffice. Needless to say, the interpretation of the optical depth data would depend on the mechanism of absorption and the choice of operating frequency, but, for purposes of illustration, suppose that the absorption is due to a resonance line and the observing frequency is on the center of the resonance. Then, for an isolated line, the optical depth can be written

$$\tau(h_1) = K \frac{N h_1}{T \Delta\nu}, \tag{12}$$

where K is evaluated from Eqs. (6) and (7). If it can be assumed that the linewidth $\Delta\nu$ is proportional to the total pressure and that the number density of the particular molecule N is proportional to a fraction e of the total pressure, then it follows from Eq. (13) that $\tau(h_1)$ is proportional to e and independent of the total pressure. Therefore, a determination of the optical depth in increments of h_1 can be interpreted in terms of the fractional abundance of the molecule throughout the atmosphere.

Many versions of this experiment can be proposed. For example, it might be more feasible to have two radiometers, both looking toward the surface, tuned to different frequencies in the line, or to accomplish the same thing with one radiometer but to time-share the frequencies. The details of any experiment will depend on the type of information sought, constraints imposed by the spacecraft, state-of-the-art techniques, etc., but microwave techniques may afford a means of probing planetary atmospheres that is competitive with, or superior to, other methods.

V. Acknowledgements

The author is indebted to Dr. M. L. Meeks, of Lincoln Laboratory, M. I. T., for permission to use his unpublished computations of the O_2 frequencies in the Appendix, and to Mr V. K. Chung for assistance with the computations and preparation of the figures. All computations were done at the Computation Center, M. I. T. This work was supported in part by the U. S. Army Signal Corps, the Air Force Office of Scientific Research, and the Office of Naval Research, and in part by the National Aeronautics and Space Administration (Contract NaSr — 101 and Grant NsG-250-62).

REFERENCES

(1) I. S. Shklovsky, *Astron. Zhur, USSR*, **26**, 10, 1949.

(2) J. P. Wild, *Ap. J.*, **115**, 206, 1952.

(3) E. M. Purcell, *Proc. Ame. Acad. Arts and Sci.*, **82**, 347, 1953.

(4) I. S. Shklovsky, *Dok. Akad. Nauk USSR*, **92**, 25, 1953.

(5) C. H. Townes, IAU Symposium No. 4, *Radio Astronomy*, edited by H. C. van de Hulst, Cambridge University Press, London, 1957.

(6) A. H. Barrett, *Proc. IRE*, **46**, 250, 1958.

(7) I. S. Shklovsky, *Cosmic Radio Waves* (Harvard University Press, Cambridge, Mass., 1960).

(8) C. H. Townes and A. L. Schawlow, *Microwave Spectroscopy* (McGraw-Hill Book Co., Inc., New York, N. Y., 1955).

(9) A. A. Maryott and G. Birnbaum, *J. Chem. Phys.*, **36**, 2026, 1962.

(10) A. A. Maryott and G. Birnbaum, *J. Chem. Phys.*, **36**, 2032, 1962.

(11) A. H. Barrett, *Ap. J.*, **133**, 281, 1961.

(12) B. Bleaney and J. H. W. Loubser, *Proc. Phys. Soc.* (*London*), **A63**, 483, 1950.

(13) D. F. Smith, *Phys. Rev.*, **74**, 506, 1948.

(14) I. R. Weingarten, *Ph. D. thesis*, Columbia University, 1949.

(15) P. W. Anderson, *Phys. Rev.*, **75**, 1450, 1949.

(16) H. Margenau, *Phys. Rev.*, **76**, 1423, 1949.

(17) A. A. Maryott and S. J. Kryder, *J. Chem. Phys.*, **31**, 617, 1959.

(18) A. A. Maryott and G. Birnbaum, *J. Chem. Phys.*, **32**, 686, 1960.

(19) M. Mizushima, *J. Chem. Phys.*, **32**, 691, 1960.

(20) J. H. Van Vleck and V. F. Weisskopf, *Rev. Mod. Phys.*, **17**, 227, 1945.

(21) G. Birnbaum and A. A. Maryott, *Phys. Rev.*, **95**, 622, 1954.

(23) S. CHANDRASEKHAR, *Radiative Transfer* (Dover Publications, New York, N. Y., 1960).

(24) A. H. BARRETT and V. K. CHUNG, *J. Geophys. Res.*, **67**, 4259, 1962.

(25) M. L. MEEKS, *J. Geophys. Res.*, **66**, 3749, 1961.

(26) G. B. FIELD, *J. Geophys. Res.*, **64**, 1169, 1959.

(27) V. K. CHUNG, *M. S. thesis*, Massachusetts Institute of Technology, 1962.

(28) T. NISHIKAWA and K. SHIMODA, *J. Phys. Soc. Japan*, **10**, 89, 1955.

(29) G. ERLANDSSON, *J. Chem. Phys.*, **28**, 71, 1958.

(30) R. TRAMBARULO, A. CLARK and C. HEARNS, *J. Chem.. Phys.*, **28**, 736, 1958.

APPENDIX

Microwave resonance lines of selected molecules

All frequencies are in Mc/s. Lines designated by (*) are calculated frequencies; all other frequencies have been measured in the laboratory. Identifications of transitions by their quantum numbers, where available, are those reported in the original publications.

CH_2O (H_2CO, Formaldehyde)

Transition		*Frequency*	*Transition*		*Frequency*
$12_{3,10}$ →	$12_{2,9}$	3,225.58	$25_{4,22}$ →	$25_{4,22}$	19,595.23
$20_{4,17}$	$20_{4,16}$	3,518.85	$9_{2,8}$	$9_{2,7}$	22,965.71
$1_{1,1}$	$1_{1,0}$	4,829.73	$17_{3,15}$	$17_{3,14}$	24,068.31
$6_{2,5}$	$6_{2,4}$	4,954.79	$35_{5,31}$	$35_{5,30}$	24,730.40
$13_{3,11}$	$13_{3,10}$	5,136.58	$26_{4,23}$	$26_{4,22}$	26,358.82
$21_{4,18}$	$21_{4,17}$	5,138,57	$3_{1,2}$	$3_{1,2}$	28,974.85
$22_{4,19}$	$22_{4,18}$	7,362.60	$18_{3,16}$	$18_{3,15}$	33,270.80
$31_{5,27}$	$31_{5,26}$	7,833.20	$10_{2,9}$	$10_{2,8}$	34,100.32
$14_{3,12}$	$14_{3,11}$	7,892.03	$27_{4,24}$	$27_{4,23}$	34,982.80
$7_{2,6}$	$7_{2,5}$	8,884.87	$19_{3,17}$	$19_{3,16}$	45,063.10
$23_{4,20}$	$23_{4,19}$	10,366.51	$28_{4,25}$	$28_{4,24}$	45,835.58
$32_{5,28}$	$32_{5,27}$	10,608.74	$4_{1,4}$	$4_{1,3}$	48,284.60
$15_{3,13}$	$15_{3,12}$	11,753.13	$11_{2,10}$	$11_{2,9}$	48,612.70
$33_{5,29}$	$33_{5,28}$	14,211.68	$29_{4,26}$	$29_{4,25}$	
$24_{4,21}$	$24_{4,20}$	14,361.54	$20_{3,18}$	$20_{3,17}$	
$2_{1,2}$	$2_{1,1}$	14,488.65	$12_{2,11}$	$12_{2,10}$	
$8_{2,7}$	$8_{2,6}$	14,726.74	$5_{1,5}$	$5_{1,4}$	72,409.35
$16_{3,14}$	$16_{3,13}$	17,027.60	$0_{0,0}$	$1_{0,1}$	72,838.14
$34_{5,30}$	$34_{5,29}$	18,841.20	$30_{4,27}$	$30_{4,26}$	

CH_2O_2 ($HCOOH$, Formic acid)

Eighty-nine lines between 16 KMc/s and 203 KMc/s have been identified and accurately measured. (See ref. 28 and 29.)

CO (Carbon monoxide)

Transition		Frequency
J = 0 →	1	115,271.20
J = 1	2	230,537.97
J = 2	3	345,795.90

C_2H_2O (H_2C_2O, Ketene)

Transition		Frequency
$6_{1,6}$ →	$6_{1,5}$	7,925.18
$27_{2,26}$	$27_{2,25}$	9,188.20
$28_{2,27}$	$28_{2,26}$	10,588.88
$9_{1,8}$	$9_{1,8}$	16,980.97
$0_{0,0}$	$1_{0,1}$	20,209.20
$10_{1,10}$	$10_{1,9}$	20,753.90
$11_{1,11}$	$11_{1,10}$	24,903.53
$12_{1,12}$	$12_{1,11}$	29,430.02
$12_{1,12}$	$13_{1,12}$	34,333.14

C_3HN (CHCCN, Cyanoacetylene)

Transition		Frequency
J = 1 →	2	18,196.6
J = 2	3	27,294.7

HCN (Hydrogen cyanide)

Transition		Frequency
Δ J = 0,	J = 3	2,693.35
	J = 4	4,488.50
	J = 5	6,731.95
	J = 6	9.460
	J = 7	12,562.46
	J = 8	16,147.67
	J = 9	20,181.39
	J = 10	24,660.40
	J = 11	29,585.12
	J = 12	35,043.24
J = 0 → 1		88,631.4

HNCO (Isocyanic acid)

Transition		Frequency
$0_{0,0}$ →	$1_{0,1}$	21,981.7

CS (Carbon monosulfide)

Transition		Frequency
J = 0 →	1, $v = 0$	48,991.00
J = 0	1, $v = 1$	48,635.91
J = 1	2, v = 0	97,982*

Transition		Frequency
$14_{1,14}$ →	$14_{1,13}$	39,612.55
$1_{1,1}$	$2_{1,2}$	40,038.80
$1_{0,1}$	$2_{0,2}$	40,417.90
$1_{1,0}$	$2_{1,1}$	40,793.62
$2_{1,2}$	$3_{1,3}$	60,057.92
$2_{2,1}$	$3_{2,2}$	60,615.88
$2_{2,0}$	$3_{2,1}$	60,617.30
$2_{0,2}$	$3_{0,3}$	60,625.68
$2_{1,1}$	$3_{1,2}$	61,190.24

HNCS (Isothiocyanic acid)

Transition		Frequency
$1_{1,1}$ →	$2_{1,2}$	23,499.5

H_2O (Water)

Transition		Frequency
$5_{2,3}$ →	$6_{1,6}$	22,235.22
$2_{2,0}$	$3_{1,2}$	183.311

H_2O_2(Hydrogen peroxide)

Frequency	
11,072	37,518
14,829	39,033
22,054	39,495
27,639	39,760
35,916	

H_2S (Hydrogen sulfide)

Transition		Frequency
$1_{0,1}$ →	$1_{1,0}$	168,762.51
$2_{1,1}$	$2_{2,0}$	216,710.42

NH_3 (Ammonia)

Between 11,947 Mc/s and 39,942 Mc/s there are 91 lines whose frequencies have been measured. (See ref. 8 and 27). For pressures of approximately 1 atm, the spectrum is equivalent to a single line at approximately 27,000 Mc/s.

NO (*Nitric oxide*)

$^2\Pi_{1/2}$, J = 1/2	→	3/2	150,210 ± 35 (5 lines)
			150,510 ± 150 (5 lines)
$^2\Pi_{1/2}$, J = 3/2		5/2	250,460 ± 23 (5 lines)
			250,760 ± 55 (5 lines)
$^2\Pi_{3/2}$, J = 3/2		5/2	257,790 ± 40 (6 lines)
			257,890 ± 40 (6 lines)

Each line is split by magnetic hyperfine structure into several lines covering the frequency range shown.

NO_2 (*Nitrogen dioxide*)

Transition		*Frequency*
$8_{0,8}$ →	$7_{1,7}$	15,290 ± 360 (10 lines)
$40_{2,38}$	$39_{2,37}$	16,020 ± 12 (6 lines)
$23_{2,22}$	$24_{1,23}$	26,630 ± 66 (8 lines)
$22_{1,21}$	$21_{2,20}$	39,150 ± 95 (6 lines)
$9_{1,9}$	$10_{0,10}$	40,820 ± 160 (6 lines)

Each rotational line is split by magnetic fine structure into several lines covering the frequency range shown.

N_2O (*Nitrous oxide*)

Transition		*Frequency*
J = 0 →	1	25,123.25
J = 1	2	50,246.03
J = 2	3	75,370*
J = 3	4	100,491.76
J = 4	5	125,613.68

OCS (*Carbonyl sulfide*)

Transition		*Frequency*
J = 0 →	1, $v = 0$	12,162.9*
J = 1	2, $v = 0$	24,325.9
J = 2	3, $v = 0$	36,488.8
J = 3	4, $v = 0$	48,651.6
J = 4	5, $v = 0$	60,814.1
J = 35	36, $v = 0$	486,184.2
J = 41	42, $v = 0$	510,457.3

OH (*Hydroxyl radical*)

	Transition	*Frequency*
$^2\Pi_{3/2}$,	J = 3/2	1,666 ± 1
	J = 5/2	6,033 ± 2
	J = 7/2	13,438 ± 3
	J = 9/2	23,824 ± 4

OH	*Transition*	*Frequency*
	J = 11/2	36,988 ± 5
$^2\Pi_{1/2}$,	J = 3/2	7,790 ± 30
	J = 5/2	8,160 ± 25

Frequency range shown includes only the two strong hyperfine transitions.

O_2 (*Oxygen*)

N	*N*+	*N*—
1	56,265.2	118,745.5
3	58,446.6	62,486.2
5	59,591.0	60,306.0
7	60,434.8	59,164.2
9	61,150.6	58,323.9
11	61,800.2	57,612.3
13	62,411.2	56,968.7
15	62,997.8*	56,363.2*
17	63,568.5	55,784.1
19	64,127.6	55,220.8
21	64,678.9	54,672.5
23	65,224.1	54,130.0
25	65,761.6*	53,597.6*
27	66,297.8*	53,069.5*
29	66,831.3*	52,545.8*

31	67,362.7*	52,025.9*
33	67,892.3*	51,509.1*
35	68,420.5*	50,994.9*
37	68,947.8*	50,483.0*
39	69,474.1*	49,973.0*
41	69,999.8*	49,464.8*
43	70,524.9*	48,958.2*
45	71,049.7*	48,453.0*
47	71,574.3*	47,949.2*
49	72,098.6*	47,446.5*

* Frequencies calculated by M. L. Meeks.

O_3 (*Ozone*)

Transition			Frequency
$21_{2,20}$	→	$20_{3,17}$	9,201
$9_{2,8}$		$10_{1,9}$	10,226
$3_{1,3}$		$4_{0,4}$	11,073
$24_{3,21}$		$23_{4,20}$	15,116
$26_{4,23}$		$27_{3,25}$	16,413
$19_{3,16}$		$18_{3,15}$	23,861
$46_{6,40}$		$45_{7,39}$	25,300
$39_{5,35}$		$38_{6,33}$	25,511
$17_{1,17}$		$16_{2,14}$	25,649
$40_{6,34}$		$41_{5,37}$	27,862
$25_{3,23}$		$24_{4,20}$	28,960
$16_{2,14}$		$15_{3,13}$	30,052
$15_{1,15}$		$14_{2,13}$	30,181
$19_{1,19}$		$18_{2,16}$	30,525
$22_{3,19}$		$23_{2,21}$	36,023
$17_{3,15}$		$18_{2,16}$	37,832
$2_{0,2}$		$1_{1,1}$	42,833
$13_{1,13}$		$12_{2,10}$	43,654
$2_{0,2}$		$2_{1,1}$	96,229
$4_{0,4}$		$4_{1,3}$	101,737
$0_{0,0}$		$1_{1,1}$	118,364

SO_2 (*Sulfur dioxide*)

Transition			Frequency
$1_{1,1}$	→	$2_{1,2}$	18,580.2
$1_{0,1}$		$2_{0,2}$	19,126.4
$1_{1,0}$		$2_{1,1}$	19,684.3
$13_{2,12}$		$12_{3,9}$	20,335.47
$23_{1,22}$		$24_{4,20}$	22,482.51
$6_{1,6}$		$5_{2,4}$	23,414.30
$22_{4,18}$		$21_{5,17}$	24,039.50
$9_{1,9}$		$8_{2,6}$	24,083.39
$34_{7,27}$		$35_{6,30}$	25,049.13
$7_{2,6}$		$8_{1,7}$	25,392.80
$24_{5,19}$		$25_{4,21}$	26,777.20
$2_{1,2}$		$3_{1,3}$	27,867.0
$2_{0,2}$		$3_{0,3}$	28,674.3
$2_{2,1}$		$3_{2,2}$	28,699.3
$2_{2,0}$		$3_{2,1}$	28,723.4
$16_{2,15}$		$17_{3,15}$	28,858.11
$3_{1,3}$		$4_{0,4}$	29,321.22
$2_{1,1}$		$3_{1,3}$	29,522.8
$3_{1,3}$		$4_{1,4}$	37,149.0
$3_{0,3}$		$4_{0,4}$	38,203.0
$3_{2,2}$		$4_{2,3}$	38,260.9
$3_{2,0}$		$4_{2,3}$	38,279.1
$3_{2,1}$		$4_{2,3}$	
$3_{2,1}$		$4_{2,3}$	38,322.3
$3_{1,3}$		$4_{1,3}$	39,356.2
$2_{0,2}$		$2_{1,1}$	53,529.16
$4_{0,4}$		$4_{1,3}$	59,225.00
$0_{0,0}$		$1_{1,1}$	69,576.06

19. — NON-THERMAL NOISE MEASUREMENTS NEAR PLANETS (*)

R. F. MLODNOSKY, D. L. CARPENTER, R. A. HELLIWELL
Radioscience Laboratory, Stanford University
Stanford, California, U. S. A.

SUMMARY

It is proposed to study planetary ionization and magnetic fields by the interpretation of measurements of non-thermal radio noise made near planets on a fly-by space probe. The noises to be considered are (a) noises which are external to a planet such as cosmic noise, and solar and Jovian noise bursts, and (b) noises which might be expected to be local to a planet such as atmospheric noise and whistlers (originating with lighting discharges), and VLF emissions whose origin is currently believed to be related to streams of charged solar particles and such generation mechanisms as Cerenkov or Cyclotron radiation and perhaps traveling-wave amplification effects. It is assumed that the measurements could be made at a distance close enough to the planet so that the probe would pass through the planetary magnetosphere. It is expected that the local plasma frequencies would be greater than the local electron gyro-frequencies and that the electron density would decrease with radial distance from the planet.

The measurements would be made by receivers also functioning for propagation measurements of man-made radio transmissions, which are another class of experiments adaptable to the study of planetary atmospheres. While noise measurements near a planet would be of great value in determining the noise environment of the planets and in extending knowledge of the noises themselves, emphasis here is on the information about the planetary *ionization* and magnetic fields which may be obtained.

(*) This work was supported by the National Aeronautics and Space Administration under Grant NsG 174-61 to Stanford University.

Magneto-ionic theory suggests that the spectrum of noise which may be observed at the probe will consist of (*a*) an upper frequency range whose lowest frequency will be the plasma frequency local to the probe, and in which range the noise will reach the probe via conventional ionospheric propagation ; and (b) a lower frequency range whose highest frequency will be the electron gyro-frequency local to the probe, and in which range the noise can reach the probe by propagating in the whistler-mode, or, for the extremely low frequencies, in various hydromagnetic modes (which will not be considered here).

From the high frequency noise measurements :

(1) The local plasma frequency along the trajectory may be obtained by noting the lower-frequency-cutoff in the cosmic noise (assuming cosmic noise sources are isotropic).

(2) An estimate can be made of the variation of outer ionization density with radial distance by combining the cosmic-noise-cutoff measurement with the somewhat greater lower-cutoff-frequency of the enhanced noise intensity which should be observed from strong discrete sources such as the sun and Jupiter. Ray path considerations show that, for frequencies lower than some critical value, the probe will be within an occulted zone relative to the discrete source. The discrete noise lower cutoff frequency will be a function of probe-planet distance, planet-source angle, and planetary electron density variation. Simple considerations show that the ratio of enhanced discrete noise cutoff to cosmic noise cutoff frequencies is greatest and most sensitive to the variation of planetary electron density for small planet-source angles. A minimum number of discrete events would provide useful information. Should more than one discrete source be present coincidentally, the interpretation is more complicated but still possible.

(3) An estimate of the maximum plasma frequency of the planetary ionosphere may be obtained from noting the cutoff in

the spectra of atmospheric noise (if present) which is able to penetrate the planetary ionosphere.

For the low frequency noise, whistlers and VLF emissions are of the greatest significance. If no magnetic field exists, no VLF noise will be observed ; a fact of importance in itself. If a magnetic field exists, and there is planetary atmospheric lightning, whistlers should be observed. From the low frequency measurements :

(4) An estimate of the minimum electron gyro-frequency along the whistler propagation path (approximately along a magnetic field line) may be obtained from the determination of whistler nose frequency, that is, the frequency of minimum time delay.

(5) An estimate of the integrated electron density along the whistler path may be obtained from a measurement of time delay at the nose frequency.

(6) An estimate of the electron temperature in the exosphere may be obtained by noting the upper cutoff frequency of the whistler spectrum. This interpretation is based on Landau damping.

(7) The approximate height of the lower ionosphere may be obtained by noting the lower cutoff frequency of whistler spectra for those whistlers which have propagated between the planet and the ionosphere for some distance before penetrating the ionosphere. This phenomenon is analogous to a waveguide-cutoff effect and is observed in terrestrial whistlers.

If a planetary magnetic field exists, VLF emissions should be observed. The theory of the many types of VLF emissions is not very well advanced, compared to whistler theory, and consequently the information which can be obtained from their observation is limited. When the emission is discrete and periodic, it can be assumed that the emission is echoing along a field line in the whistler mode. In this case, approximate information on the minimum electron gyro-frequency along the path may be obtained from a measurement of the upper cutoff frequency of the spectrum, and

information on integrated electron density along the path may be obtained from measurements of the echo period.

The proposed measurements require the determination of cutoff frequencies and time delays or echoing intervals. The accuracy with which the various parameters may be determined, depends upon resolution in time and frequency. In general, for deep space probes, the instrumentation would consist of many fixed-frequency receivers whose outputs would be digitally sampled. The number of receivers and the sampling rate would be limited primarily by the telemetry system data transmission rate. Specific instrumentation could be designed to investigate some of the outstanding questions of particular planets.

The data on ionization and magnetic fields that would be obtained from the interpretation of noise measurements are of an indirect nature, and the noise measurements are here proposed to supplement more direct measurements as might be made by devices such as magnetometers, Langmuir probes, ion traps, etc. Noise measurements would increase the probability of overall success of a planetary probe without resorting to redundant instrumentation. It is therefore felt that non-thermal measurements should be included among the experiments to be performed on the first probes designed to study planetary atmospheres.

20. — INSTRUMENTATION FOR OBSERVATIONS OF PLANETS IN THE FAR INFRARED

HECTOR C. INGRAO and DONALD H. MENZEL
Harvard College Observatory
Cambridge, Massachusetts, U. S. A.

INFRARED DETECTORS

When we reduce the available data of the various IR detectors for intercomparison, we generally find two difficulties : either the data is not expressed in homogeneous representative parameters, or all the necessary information is not provided. The following set of representative parameters (1) (2) for the IR detectors was chosen in order to make the intercomparison possible.

Detector Temperature T_d : the operation temperature of the detector expressed in °K.

Responsive Area A : the area over which the detector is more or less equally responsive expressed in cm^2 or mm^2.

Noise Bandwidth Δ_f : the bandwidth of the noise effective in NEP measurements, expressed in cps.

Responsivity R_f : the responsivity defined as the ratio of the *rms* power incident upon the detector at a modulating frequency *f*. The units will depend upon the type of output. Generally, in detectors with electrical output, the responsivity will be expressed in volt $watt^{-1}$.

Responsivity R_0 : the responsivity defined as the ratio of the *rms* output to the *rms* power incident upon the detector at zero frequency. In detectors with electrical output it will be expressed in volt $watt^{-1}$.

Time Constant τ : defined, if the responsivity varies in accordance with the following relation as

$$R_f = R_0 / [1 + (2\pi f\tau)^2]^{1/2},$$

where R_f and R_0 are defined as above ; f is the modulating frequency and τ the time constant.

The following figures of merit were chosen :

Noise Equivalent Power NEP or P_n : the *rms* noise at the detector output, expressed in terms of the detector input given in watts.

Noise Equivalent Power Density NEPD : the *rms* noise in the detector output expressed in terms of the power density at the input and given in watt cm^{-2}.

Normalized Detectivity D* : the reciprocal of the NEP measured with a bandwidth of one *cps* and reduced to a responsive area of one cm^2. D* (pronounced « dee-star ») is expressed by the following relation :

$$D^* = (A\,\Delta f)^{1/2}\,(NEP)^{-1},$$

and is given in cm $(cps)^{1/2}$ $watt^{-1}$.

To examine the effect on D* by the field of view subtended by the detector Jones ([3]) has introduced the figure of merit D** (pronounced « dee-double-star ») defined as

$$D^{**} = (\Omega/\pi)^{1/2}\,D^*,$$

where Ω is the solid angle view by the detector. Moreover, since the response will be proportional to the convolution of the spectral radiant emittance of the source and the spectral response of the detector or the spectral transmittance of the window in a thermal detector, the temperature of the source should be defined for the measurement of D*. Furthermore, because of the noise power spectrum of the detector, the modulating frequency and the noise bandwidth also should be specified.

In general and for a certain operating point of the detector, D* is expressed as D* (T, f, Δf), where T is the temperature of the source, f the chopping frequency and Δf the bandwidth used for the measurement. In the case of quantum detectors D^*_λ, the normalized detectivity function of the radiation wavelength, or $D^*_{\lambda m}$ the normalized detectivity at maximum response is often given.

TABLE I

Characteristics of single thermal detectors

Detector	NEP μμw	B cps	Time Const. msec	Resp. v/w	Resist. ohm	Sensit. Area mm × mm	Mod. Freq. cps	Ref.
Thermocouples								
Bi—51.7%Sb+48.3% Cd, evacuated			6000	500μv/°C	8	10×0.5		(1)
Bi—Sb evacuated			2500	500μv/°C	30	7.5*		(1)
Bi—Sb sputtered thin film				30-80μv/°C				(2)
97%Bi+3%Sb—95%Bi+5%Sn (1 junction)	50		36	4.4	5	0.5*	5	(3)
97%Bi+3%Sb—95%Bi+5%Sn (2 junctions)	70		36	4.4	10	1.0*	5	(3)
97%Bi+3%Sb—95%Bi+5%Sn (4 junctions)	140		41	3.1	12.5	4.0*	5	(3)
Bi—Te sputtered thin film	10				1.5×10^5		1	(4)
Bi—Sb evaporated, evacuated	200		50		20-50		1	(5)
Hilger—Schwartz, semi-conductor alloyed Cu, Ag, Te, Se, S-alloyed Ag2S, Ag2Se	46	1	55	38.5	43	2×0.2	5	(6)
Bi—Bi+Sn alloyed	200	1				2×0.3	10	(7)
Au foil, Evacuated	200-300	1		2	10	2×0.2	13	(8)
Farrand (selected)	40	1	15	20	15	.75×.75		**
(standard)	50	1	5	6	5	.75×.75		**
Thermopile								
Bi—Sb «Folded» evaporated, 50 junctions	«a few» tens		equiv. to 10	0.4—0.52	70	11* (active area)	1	(9)

* mm^2

** Personal communication from Dr. Nolan from Farrand Optical Company. Inc.

Detector	NEP μμw	B cps	Time Const. msec	Resp. v/w	Resist. ohm	Sensit. Area mm × mm	Mod. Freq. cps	Ref.
Bolometers								
Ni Evaporated strip	33,000	100	4		100	1 × 6	30	[10,11]
Pt			4	1	20		120	[12]
Au evaporated, evacuated	350	1	7	1.5	15	2.6 × 0.2	10	[13]
Thermistor	100	1	5	500	2×10^6	3 × 0.2	15	[14]
Thermistor (saphire backed)	440	10	2.2	1,400	2.24×10^6 (25°C)	.3 × .3	15	[15]
Thermistor (copper backed)	1,110	10	1.0	810	2.24×10^6 (25°C)	.5 × .5	15	[15]
Thermistor (copper backed)	50	10	6.5	11,200	2.59×10^6 (25°C)	.1 × .1	15	[15]
Thermistor (experimental)						.05 × .05		[15]
Superconductor	45		1.2	3.8	0.73	1.2*	360	[16]
Superconductor	32		0.33	7.3	0.8	0.8*	360	[17]
Superconductor	21		0.5	13.5	0.2	1.0*	360	[18]
Low temperature carbon core, $T_d = 5°K$	11	1	10	14,000	1.2×10^6	19*		[19]
Ge:Ga, $T_d = 2.1°K$	5×10^{-1}	1	0.4	4,500	1.2×10^4	15*	200	[20]
Thermal Linear Expansion								
Constantan, thin strip, ** $T_d = 300°K$	5 (theor. value) 15 (measured)	1				1 × 1 (0.1μ thick)		[21]
Pneumatic								
O.N.E.R.A., *** $T_d = 300°K$	110	1	25			16*		[22]
Golay Cell, **** $T_d = 300°K$	150	0.1				6.3*	10	[23]

* mm^2.

** The output signal is measured by an optical lever and photoelectric amplifier.

*** The output signal is measured by the variation of the membrane capacitor.

**** The ouput signal is measured by the deflection of the membrane and by a Photoelectric amplifier.

REFERENCES — Table I

(1) R. V. JONES, « The Design and Construction of Thermoelectric Cells », *J. Sci. Instr.*, **11**, 247, 1934.

(2) E. A. JOHNSON and L. HARRIS, « Thermoelectric Force of Thin Films », *Phys. Rev*,. **44**, 944, 1933.

(3) D. HORNIG and J. O'KEEFE, « The Design of Fast Thermopiles and the Ultimate Sensitivity of Thermal Detectors », *Rev. Sci. Inst.*, **18**, 474, 1947.

(4) L. HARRIS and E. A. JOHNSON, « The Technique of Sputtering Sensitive Thermocouples », *Rev. Sci. Inst.*, **5**, 153, 1934.

(5) L. C. ROESS and E. N. DACUS, « The Design and Construction of Rapid-Response Thermocouples for Use as Radiation Detectors in Infrared Spectrographs », *Rev. Sci. Inst.*, **16**, 164, 1945.

(6) D. A. H. BROWN, R. P. CHASMAR, and P. B. FELLGETT, « Construction of Radiation Thermocouples Using Semi-Conducting Thermoelectric Materials », *J. Sci. Inst.*, **30**, 195, 1953.

(7) H. CARY and K. P. GEORGE, « Sensitive High Speed Thermocouple », abstracted in *Phys. Rev.*, **71**, 276, 1947.

(8) R. DEWAARD and E. M. WORMSER, « Description and Properties of Various Thermal Detectors », *Proc. Inst. Radio Engrs.*, **47**, 1508, 1959.

(9) L. HARRIS, « Rapid Response Thermopiles », *J. Opt. Soc. Am.*, **36**, 597, 1946.

(10) B. H. BILLINGS, W. L. HYDE, and E. E. BARR, « An Investigation of the Properties of Evaporated Metal Bolometers », *J. Opt. Soc. Am.*, **37**, 123, 1947.

(11) B. H. BILLINGS, W. L. HYDE, and E. E. BARR, « Construction and Characteristics of Evaporated Nickel Bolometers », *Rev. Sci. Inst.*, **18**, 429, 1947.

(12) W. G. LANGDON, « A Fast Sensitive Metal Bolometer », *J. Opt. Soc. Am.*, **36**, 1946.

(13) E. ARCHBOLD, « An Evaporated Gold Bolometer », *J. Sci. Instr.*, **34**, 240, 1947.

(14) J. A. BECKER and H. R. MOORE, « Thermistor Bolometer Detecting System for Infrared Spectrometers », abstracted in *J. Opt. Soc. Am.*, **36**, 354, 1946.

(15) R. DEWAARD and E. M. WORMSER, « Thermistor Infrared Detectors », Part I, *NAVORD*, **5495**, 30, 34, 35, 1958.

(16) N. FULSON, « The Infrared Sensitivity of Superconducting Bolometers », *J. Opt. Soc. Am.*, **38**, 845, 1948.

(17) R. M. MILTON, « Report of International Conference on Low Temperatures », Cambridge, 1946.

(18) D. H. ANDREWS, « Report of International Conference on Low Temperatures », Cambridge, 1946.

(19) W. S. BOYLE and K. F. RODGERS, Jr., « Performance Characteristics of a New Low-temperature Bolometer », *J. Opt. Soc. Am.*, **49**, 66, 1959.

(20) FRANK LOW, « Low-Temperature Bolometer », *J. Opt. Soc. Am.*, **51**, 1300, 1961.

(21) R. V. JONES, « The Detection of Thermal Radiation Using Linear Expansion », Fifth Meeting and Conference of the ICO, Stockholm, 24-30 August, 1959.

(22) A. GIRARD, « Recepteur Pneumatique de Rayonnement », Fifth Meeting and Conference of the ICO, Stockholm, 24-30 August, 1959.

(23) Data provided by Eppley Laboratory for the Golay cell with Ge coated window purchased by Harvard College Observatory, 1960.

TABLE II

Characteristics of single quantum detectors

Detector	Long cut-off μ	NEP μμw	Time Const. μ sec	B cps	Mod. Freq. cps	Source Temp °K	Imped ohm	D* × 10^{-9} cm cps $^{1}/_{2}$ w^{-1}	Resp. v/w	Sensit. Area mm × mm	Ref.
Photoconductive (Cooled)											
PbTe, T_d = 80°K	6	42	15	1	900	500	3.2×10^7	2.4		1 × 1	(1)
PbTe, T_d = 80°K	6	22	15	1	900	500	1.5×10^6	5.6		0.5 × 3	(1)
Ge:Au, T_d = 77°K	9.5	49	1	1	900	500	1.0×10^6	4.3		2.1 × 2.1	(1)
Ge:Au, Sb, T_d = 300°K	6	220	40	1	900	500	1.0×10^6	1.8		4 × 4	(1)
Ge:Zn, T_d = 4°K	40		0.01	1	800	500	3.0×10^5	4		2 × 2	(2)
(Ge-Si):AuI (11% Si) T_d = 60°K	12		> 1	1		500	5.0×10^5	5			(3)
(Ge-Si):ZnII (4% Si), T_d = 50°K	13		> 1	1		500	3.0×10^7	7		225*	(3)
InSb, T_d = 300°K	5.6	26	0.4	1			1.8×10^3		400		(4)
InSb, T_d = 300°K	5.6	70	0.4	1			2.0×10^4		1,300		(4)
Te at 3.4μ, T_d = 77°K		0.31		5	5,000						(5)
Photovoltaic (Cooled)											
InSb, T_d = 78°K	5.5	100	1	1	800	500	50—200	2		4—5*	(6)
InSb at 5μ, T_d = 78°K	5.7	2	1	1			1×10^3—4×10^4	5		0.1 × 0.1	(7)
Photoelectromagnetic (PEM)											
InSb at 6.6μ, T_d = 300°K	7.5	2100	0.6	1	400	200		0.04		0.71*	(8)
InSb, T_d = 300°K	7.5	2000—6000	1	1	400	200		0.011		0.1—0.3*	(9)
InSb, T_d = 300°K	6	500	1	1		500	5—10	0.14		1 × 0.5	(9)

* mm^2

REFERENCES — Table II

(1) W. Beyen, P. Bratt, H. Davis, L. Johnson, H. Lewinstein, A. MacRae, « Cooled Photoconductive Infrared Detector », *J. Opt. Soc. Am.*, **49**, 686, 1959

(2) Perkin-Elmer Corp., Norwalk, Conn., Model PE 536-1 Detector.

(3) W. L. Eisenman and A. B. Naugle : NOLC Report 527, August 1960.

(4) D. W. Goodwin, « Cooled Photoconductive Detectors Using Indium Antimonide », *J. Sci. Instr.*, **34**, 367, 1957.

(5) D. F. Edwards and M. Mercado, « Ultimate Sensitivity and Practical Performance of the Tellurium Photoconductive Detector », *Infrared Physics*, **1**, 17, 1961.

(6) M. E. Lasser, P. Cholet, E. C. Wurst, Jr., « High-Sensitivity Crystal Infrared Detectors », *J. Opt. Soc. Am.*, **48**, 468, 1958.

(7) News and New Products, *Proc. Inst. Radio Engrs.*, **134A**, July, 1960.

(8) P. W. Kruse, « Indium Antimonide Photoelectromagnetic Infrared Detector », *J. Appl. Phys.*, **30**, 770, 1959.

(9) Radiation Electronics Co., Div. of Comptometer Corp., Chicago, I, 11, Thermotek Detector.

Our group has thoroughly investigated the literature in the field of single detectors. The available detectors that have any interest for our program are listed in Tables I and II.

Table I lists the single thermal detectors and Table II lists the single quantum detectors that have a spectral response in the range, or close to the wavelength of the atmospheric window 8μ — 14μ. The thermal linear expansion detector was included in Table I for comparison purposes and not for any potential astronomical application.

The choice of an infrared detector for astronomical purposes should depend on the spectral response, NEP, time constant, and responsive area, but other factors that finally will affect the performance of the equipment are linearity, characteristics independent of time, sensitivity to vibration and stray fields.

Having evaluated the list in Table I, we believe that for an uncooled thermal detector of a small responsive area the right choices are a selected thermocouple produced by Farrand ($D^* = 1.5 \times 10^9$), or one similar, or a good thermistor bolometer.

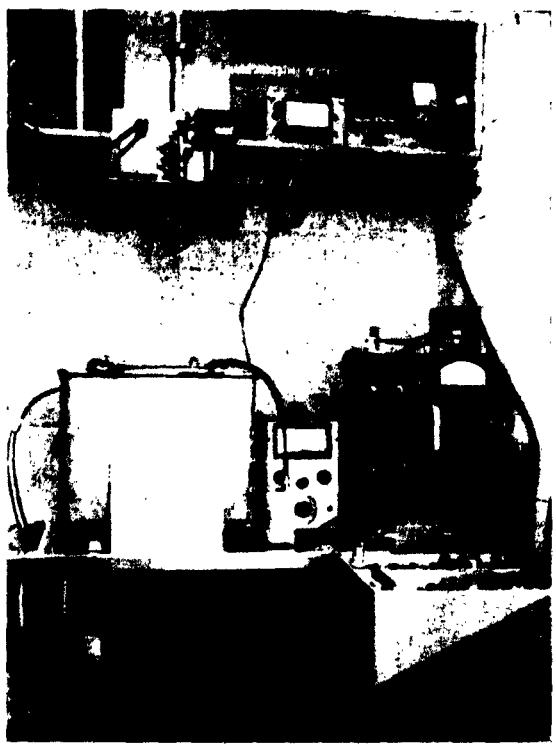

Fig. 1. — Laboratory setup at Harvard College Observatory for testing the ferroelectric bolometers.

When a larger or « adjustable » responsive area is needed, a pneumatic detector, such as a selected Golay or ONERA cell ($D^* = 4 \times 10^9$), would be advisable.

Quantum detectors from Table II should be chosen on the basis of each specific application. We should point out in this Table that the Te detector has a NEP of 3.1×10^{-13} watt at 3.4 μ operating at 77°K and for a bandpass of 5 *cps* at 5,000 *cps* modulating frequency. This detector operates practically background limited.

Ferroelectric Bolometer

In an effort to develop a thermal image-forming system of simultaneous read-in for lunar observations, our laboratory has built and tested several single thermal detectors using the combined pyroelectric and dielectric variations of (Ba, Sr)TiO_3 solid solutions as a function of the temperature near the Curie point. When we began our program in 1960, we did not know that other laboratories were engaged in work in this field.

Hanel ([4]) has shown theoretically that a good single crystal of $BaTiO_3$ used as a temperature-sensitive capacitance can achieve temperature noise-limited operation under certain conditions. Cooper ([5]) has extended the analysis to the pyroelectric effect of $BaTiO_3$ single crystal and has shown that under certain operating conditions the bolometer could be limited only by temperature fluctuations. Both the above calculations make rather optimistic assumptions and use values for the thermal and electrical parameters of the detector material without analyzing the simultaneous pyroelectric and dielectric variations as a function of temperature for DC operation.

Mattes and Perals ([6]) have made a pyroelectric transducer of $BaTiO_3$ ceramic for measuring large temperature changes of tens of degrees. Lang ([7]), by using pyroelectric phenomena in a rod of $BaTiO_3$ ceramic reported detection of temperature changes of 2×10^{-7}°C.

The first ceramic for the bolometer made in our laboratory ([8]) used a solid solution of 25 mole % $SrTiO_3$ and 75 mole % $BaTiO_3$, ground to a size 2 mm × 2 mm × 0.5 mm. The two square surfaces have been metallized, a 0.001 in. platinum wire has been bonded to each of these metallized sides by a conductive cement. The detector is suspended by these wires from two pins of a 7-pin tube base. On one side of the detector a blackbody layer (camphor suit or Glyptal paint) is deposited to receive the incoming radiation. At first, although the shorter milling time in the preparation of the ceramic avoided introducing impurities during the milling process, the two constituents failed to form a solid solution. As a result the Curie points of the crystallites varied over a range from 0° to 25°C, so that the dielectric constant varied quite smoothly with temperature. For this ceramic at 25°C the relative permittivity is $K' = 2740$, the temperature coefficient of the permittivity is $\alpha = 0.1\ \%/°C$, and the tangent of loss angle is $\delta = 0.01$.

The detectors made with this material operated in open air and were mounted in an aluminum cavity with heavy walls and placed in a water bath for close temperature control. The infrared signals were fed from a blackbody cavity through a hole in the aluminum cavity. Figure 1 gives a general view of the experimental setup.

The hysteresis losses of the detector were measured at 50 *cps* calculating the area of the hysteresis curve, electrostatic charge *vs* voltage, for a large signal level comparable with the coercive field E_c. Below the Curie point T_c the losses were of the order of 10 microwatts, while above the transition temperature they were immeasurably small. This is to be expected since above T_c the domains and their associated reversal losses disappear. Losses for a small signal level (0.01 E_c) were immeasurably small for all T. However, according to the cube law for (Ba, Sr)TiO_3 the small signal losses should be about $10^{-5}\ (0.01)^3 = 10^{-11}$ watt at 50 cps. These figures compare with the julean heating in thermistor of the order of 10^{-2} watt.

For the second series of ferroelectric bolometers a ceramic with the characteristics shown in Figure 2 was used. In this case T_c is around 8°C, the DC resistivity close to 10^{12} ohm-cm, and the thermal coeficient $\alpha = 4.85\ \%/°C$ at the point of operation. The bolometers are 2 mm × 2 mm in size and 0.2 mm in thickness, have platinum lead 0.0005 in. diameter, and are enclosed in a vacuum enclosure at 1×10^{-6} mm Hg of pressure. In addition, the enclosures are provided with a BaF_2 window. These bolometers have a capacitance $C_d = 800$ pf and an equivalent leakage resistor $R_b = 1 \times 10^{12}$ *ohm*.

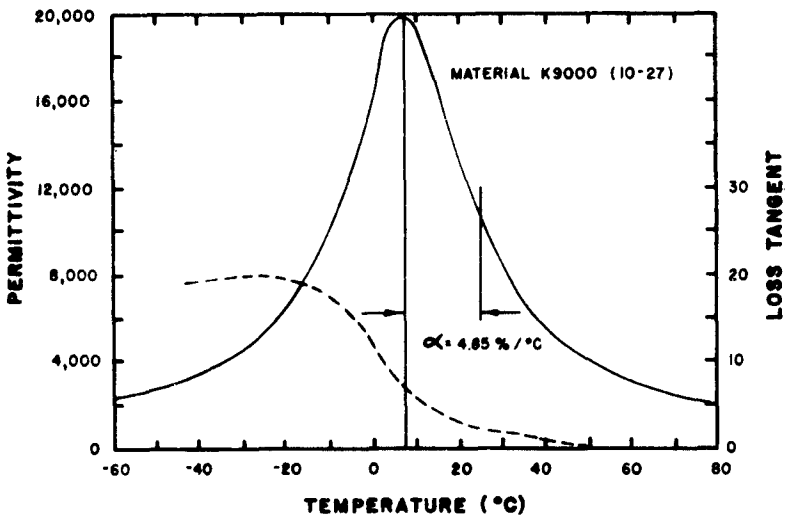

Fig. 2. — Permittivity of (Ba, Sr)TiO_3 and loss tangents as a function of temperature. DC resistivity of the ceramic close to 10^{12} ohm-cm. (Measurement by Gulton Industries, Inc., New Jersey, USA.).

To measure the responsivity, the detectors were connected in series with a mercury battery of 30 volts to the preamplifier input. The preamplifier uses as a first stage a Crystalonics C-624* field-effect transistor, which is a new type of transistor that gives a low noise operation at very high input impedance. This stage is fol-

(*) Crystalonics, Inc., Cambridge, Massachusetts, USA.

lowed by two 2 N 2049 Fairchild transistors. The point of operation of the first transistor gave an equivalent input resistance of $R_i = 3 \times 10^{10}$ ohm and an input capacitance of $C_i = 180\ pf$. With these values the second bolometer (G 22) to be prepared gave a responsivity of 480 volts per watt at a modulating frequency of 3 *cps*.

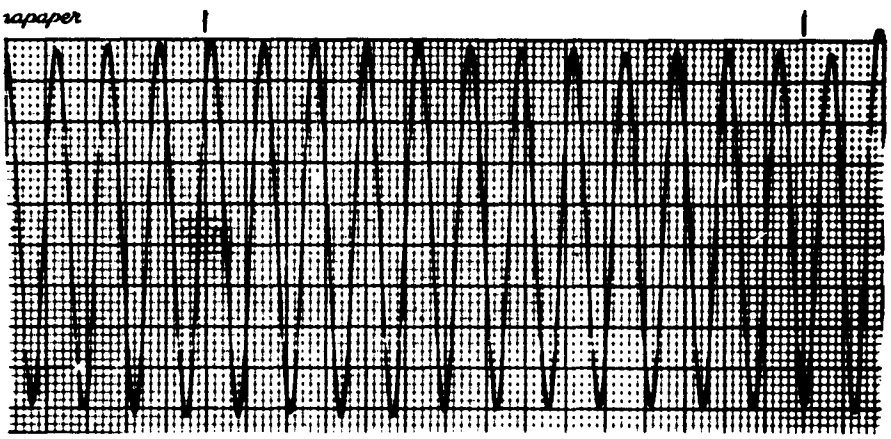

Fig. 3. — Output of the ferroelectric bolometer G-22, 2 mm × 2 mm in size ; infrared signal approximately 7×10^{-8} watt peak to peak, chopped at 3cps and a bandwidth $\Delta f = 0.25$ cps.

Figure 3 shows a record with this detector at room temperature (23°C) of a signal level of the order of $7 \times 10^{-8}/(*)$ watt peak to peak at a modulating frequency of 3 *cps* and a $\Delta f = 0.25$ *cps* at a chart speed of 20 mm s^{-1}. The noise present on the record comes almost entirely from the electronics and not from the detector. Hence, we cannot yet quote a measured NEP for this bolometer.

At present, we are improving the electronics to achieve detector noise operation and measure the detector parameters. We have also started to prepare ferroelectric bolometers 1 mm × 1 mm in size and 0.2 mm in thickness.

(*) The radiation slide rule from General Electric was used.

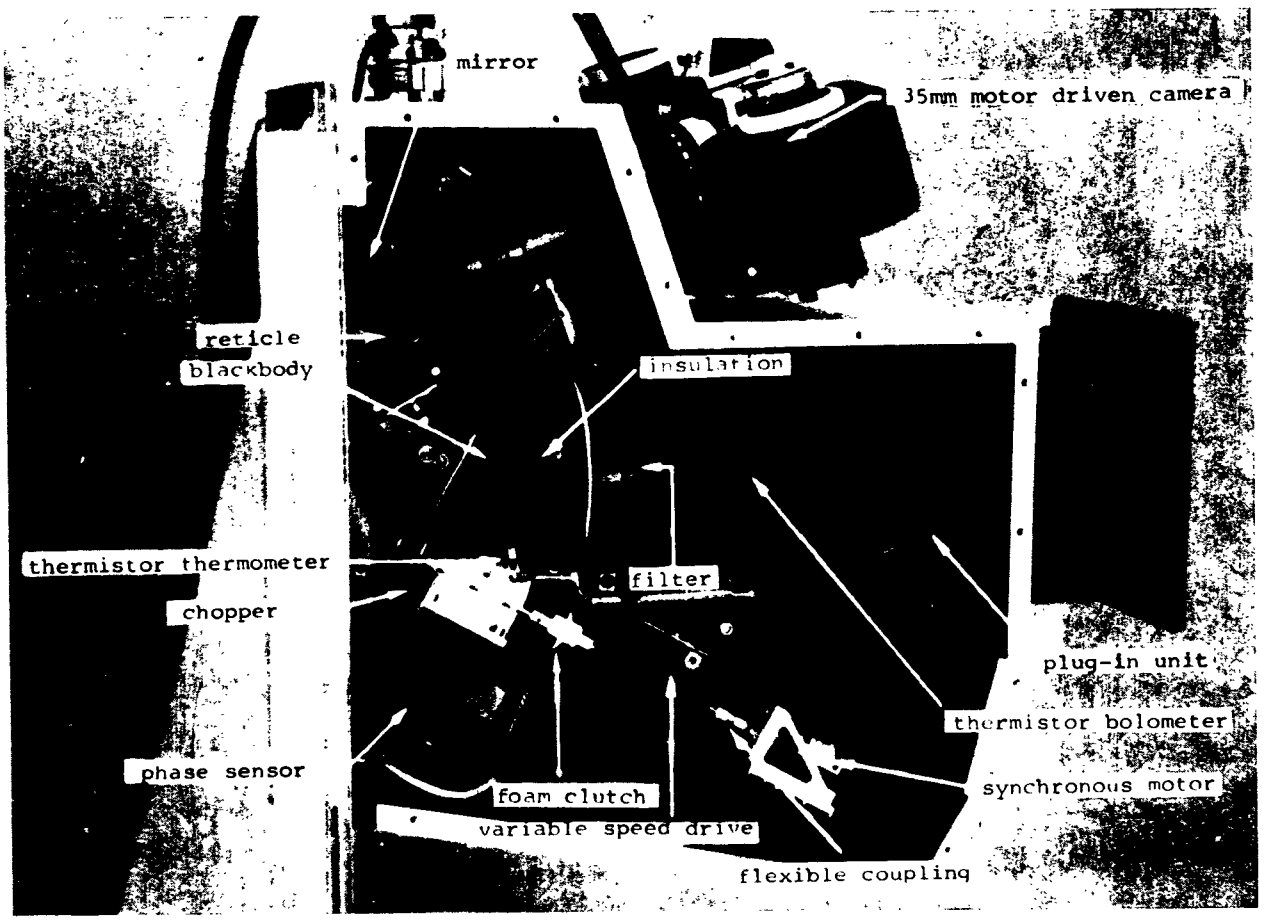

Fig. 4. — Side view of the radiation pyrometer head, Model 1-B.

Radiation Pyrometer

To obtain thermal scannings of the Moon, we are constructing in our model shop a radiation pyrometer labeled Model I-B. A view of the radiation pyrometer head is given in Figure 4. This head has been designed to operate with optical systems between $f/3$ and $f/6$. The chopper 5-inch diameter double blade is made of pyrex, 3/32 inches in thickness. One side has a good optical finish and is aluminized ; the side facing the detector has a gold evaporated film (reflectivity 99 % at 10 μ). The chopper shaft uses three high-precision-instrument, angular, contact ball bearings, preloaded with 4 *lb.* to remove any axial play. The shaft is coupled to the driving mechanism by a foam-clutch coupling.

The drive consists of a miniature hysteresis synchronous motor operating at 1800 *rpm* and coupled to a friction-type variable-speed drive by means of a flexible coupling. The ratios range from 5 : 1 to 1 : 5, giving a chopping frequency from 12 *cps* to 300 *cps*, and thus allow for operation of different time constants of the system and consequently at different scanning speeds.

The phase sensor for the coherent rectification has a Ge photodiode and a miniature light bulb. The adjustment of the phase sensor is 90° (geometrical).

The thermal detector is mounted in a plug-in unit where the preamplifier, power, and bias supply are located. The unit is all magnetically shielded inside with « Co-Netic ».*

When the plug-in is in place, the detector is at one end of the blackbody. This blackbody is made of steel with interior milled grooves of 15° aperture to give an equivalent emissivity that is practically independent of the emissivity of the steel. Moreover, the blackbody is completely insulated with styrofoam to increase the thermal time constant due to temperature variation in the environment. The temperature is monitored continuously by means of a thermistor thermometer. The filter holder is located in the same blackbody with space for three filters.

(*) Perfection Mica Co., Illinois, USA.

The Model I-B pyrometer has been designed for use with different detectors. At present we have a thermistor bolometer, an immersed thermistor bolometer, and a Golay cell. The first has a size 0.1 mm × 0.1 mm and a 6.2 millisecond time constant and is housed in an evacuated chamber having a Ge window with a spectral transmittance given in Figure 5-a. For this thermistor the resistance is 2.42×10^6 ohm at 25°C ; the responsivity is 13,300 volt RMS per watt average* at 40 volt bias, provided that the thermal sink is at 25° C and the signal from the blackbody at 470°K is square modulated at 15 *cps*. Furthermore, the NEP is 1.6×10^{-10} watt for a bandpass of 40 *cps* (computed). This detector at the newtonian focus of the 100-inch reflector at Mount Wilson ($f/5$; $s =$ 16.2″/mm) will have a field of view of 1.6″ × 1.6″ and thus would be comparable with the atmospheric seeing. At the prime focus of the 82-inch reflector at McDonald ($f/4$; $s = 25.4''$/mm), the detector will have a field of view of 2.5″ × 2.5″.

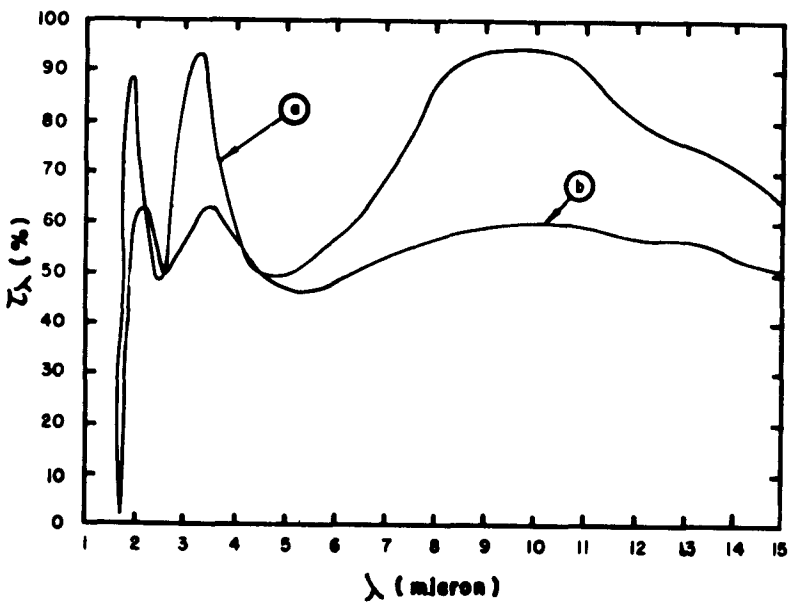

Fig. 5. — Spectral transmittance of : *a*. Ge immersion lens coated λ/4 at 10.4 μ on one side ; *b*. Ge window coated λ/4 at 10 μ on both sides. Window diameter .250 in. and .040 in. thick.

The immersed thermistor bolometer has a size of 0.1 mm × 0.1 mm, 5 millisecond time constant and is housed also in an evacuated chamber with a hemisphere Ge lens mounted on. Figure 5*b* gives the spectral transmittance of the lens. The resistance for this thermistor is 2.39×10^6 ohm at 25°C ; the responsivity is 12,500 volts RMS per watt average* at 45-volt bias provided that the thermal sink is at 25°C ; moreover, the NEP is 2×10^{-10} watt for a bandpass of 50 *cps* (computed). This detector for the telescopes given in the previous examples will subtend fields of view of 6.4″ × 6.4″ and 10.0″ × 10.0″, respectively.

When the chopper blade uncovers the blackbody front opening, the detector exchanges radiation with the target through the telescope optics ; when the chopper closes the front opening, the detector exchanges radiation with the blackbody cavity. When the opening is closed, the reflexion on the other side of the mirror chopper brings the focal plane on the reticle. The following optical train and the 35 mm camera can photograph an area of 5′ × 7.5′ of the field of view superimposed on the reticle, for a telescope scale 25″/mm.

The reticle has been lined up previously so that the intersection of the reticle coincides with the position of the detector, respective to the image. A worm-gear arrangement allows adjustment of the reticle along the optical axis.

The camera is a 35 mm type, holds 50 feet (420 frames) of film, and is operated by an electric motor. Every time a picture is secured, an electric pulse from the shutter is recorded on the paper chart for future identification of the area under measurement. The calibration is obtained by means of another blackbody that can be mounted on the front of the pyrometer ; it is not shown in the Figure. Moreover, the temperature of this blackbody is raised by a heater, and the temperature measure, by another thermistor thermometer.

We have mounted in the pyrometer a bandpass filter 8.5 μ-

(*) Bolometer bridge output is half this value.

12.8 μ (between half points) and another bandpass interference filter 8.4 μ-9.3 μ (between half points). The 8.5 μ-12.8 μ filter consists of a long wavelength pass filter with Ge substrate .040 in. thick in a series with a BaF_2 window giving a peak transmittance of 80 % at 9.0 μ and 10.4 μ as Figure 6b shows.

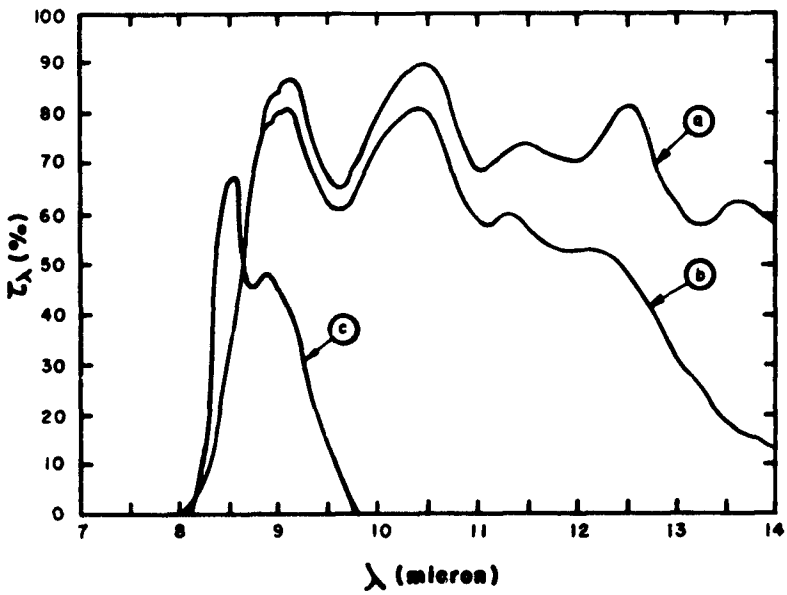

Fig. 6. — Spectral transmittance of : *a*. long wave pass filter. Ge substrate .040 in. thick ; *b*. the same in series with BaF_2 window (Mfg. Optical Coating Lab., Inc., Calif., USA) ; *c*. bandpass interference filter, Irtran-II with a deposition of a series of dielectric and semiconductor layers, approximately in the order of fifty (Infrared Industries, Inc., Massachusetts, USA).

The 8.4 μ — 9.3 μ bandpass filter with an Irtran-II* substrate .040 thick and a deposition of approximately 50 dielectric and semiconductor layers gives a peak transmittance of 68 % at 8.5 μ as Figure 6c shows. The short and long wavelengths of this filter are at 8.1 μ and 9.8 μ, respectively.

When the thermistor is used, a preamplifier will follow with a

(*) Irtran-II, zinc sulfide, developed by Eastman Kodak Co., Rochester, N. Y.

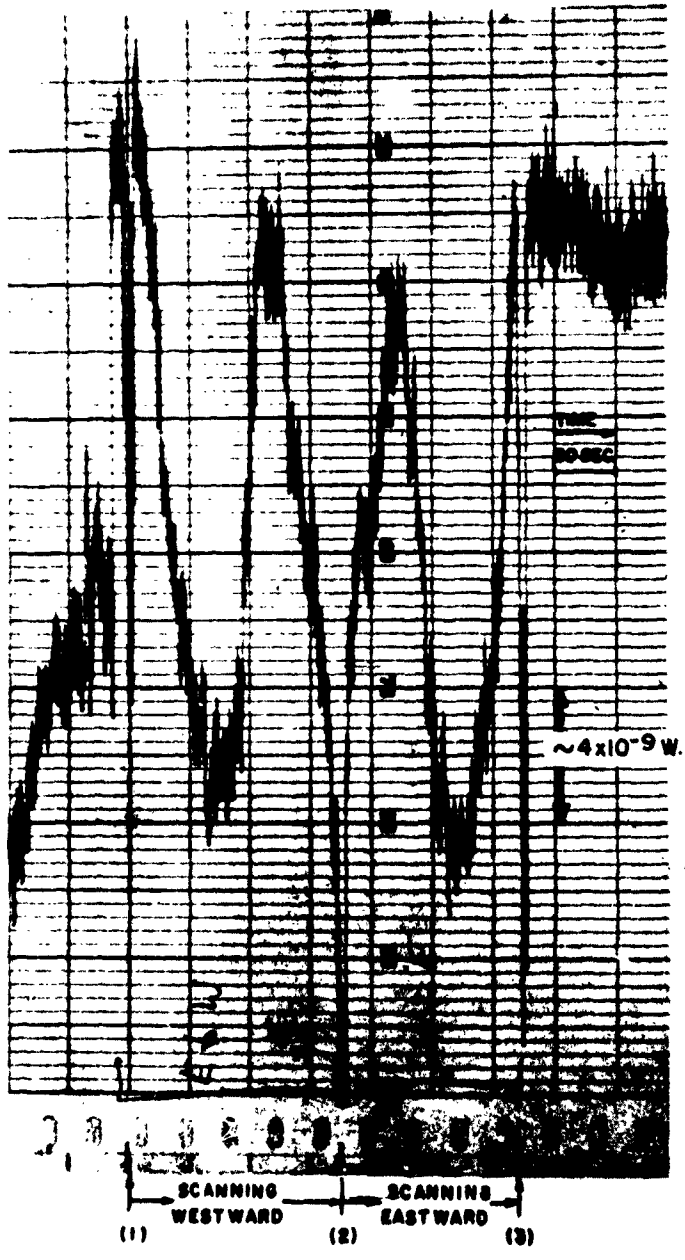

Fig. 7. Scan across the crater Hercules using the radiation pyrometer model 1-A at the Newtonian focus of the 61-inch telescope (Agassiz Station). The scan was obtained to check the pyrometer.

field-effect transistor as a first stage. After an attenuator the signal will be fed to a synchronous rectifier (transistorized) which will also receive the reference signal from a photodiode. This stage will be followed by a DC vacuum tube voltmeter, an integrator, and finally a Sanborn recorder.

The signal from the attenuator can also be fed to an AC vacuum tube voltmeter followed by the Sanborn recorder. Provisions are made to feed the output signal instead to the paper chart recorder to a magnetic tape recorder with a rather wide bandpass for more flexible data reduction. The electronics are being completed.

An experimental pyrometer labeled Model 1-A using a Golay cell as a detector and a Ge filter has been the basis of the design of the equipment described above. Mr. Anthony Burke secured several lunar scannings. A scan of the crater Hercules was secured with this pyrometer on September 26, 1961 (see Figure 7). This scan was obtained at the newtonian focus of the 61-inch telescope at Agassiz Station for the purposes of checking the equipment. The recording was not reduced at the time because of lack of good optical filtering and because of the high amount of precipitate water in the path.

This work was sponsored by the National Aeronautical and Space Administration under Grant N°. 64-60. The authors wish to thank Mr. N. W. Cunningham, Acting Head, Lunar Sciences, NASA, for his continued encouragement throughout the development of the program. Acknowledgment is also due to Mr. Anthony Burke, Mr. Michael Harris, Mr. Jay Passachoff, Mr. Frank Murphy, and Mr. Dieter Froehling who participated directly in this part of the project.

BIBLIOGRAPHY

(1) R. Clark Jones, « Quantum Efficiency of Detectors for Visible and IR Radiation », *Advances in Electronics and Electron Physics*, Vol. XI, Academy Press, 1959.

(2) R. Clark Jones, « Phenomenological Description of the Response and Detecting Ability of Radiation Detectors », *Proc. Inst. Radio Engrs.*, p. 1495, 1959.

(3) R. Clark Jones, « Proposal of the Detectivity D** for Detectors Limited by Radiation Noise ». *J. Opt. Soc. Am.*, **50**, 1058, 1960.

(4) R. A. Hanel, « Dielectric Bolometer, A New Type of Thermal Radiation Detector », *J. Opt. Soc. Am.*, **51**, 2,220, 1961.

(5) J. Cooper, « Minimum Detectable Power of a Pyroelectric Thermal Receiver », *Rev. Sci. Instr.*, **33**, 1, 92, 1962.

(6) B. L. Mattes and T. A. Perals, « Transducer for the Measurement of Thermal Power », *Rev. Sci. Instr.*, **32**, 3, 332, 1961.

(7) S. B. Lang, « Temperature, Its Measurement and Control in Science and Industry », 27-31 March 1961, Fourth Symposium on Temperature, Columbus, Ohio.

(8) H. C. Ingrao and D. H. Menzel, « Infrared Work at Harvard College Observatory », Informal Infrared Astronomy Symposium, Nov. 1[illegible], 1961, Lab. of Astrophysics and Physical Meteorology, The Johns Hopkins University, Baltimore, Maryland.

21. — PLANS FOR PLANETARY OBSERVATIONS WITH STRATOSCOPE II

ROBERT E. DANIELSON
Princeton University Observatory
Princeton, New Jersey, U. S. A.

Stratoscope II is a balloon-borne telescope which will have high resolution photography of the planets as one of its goals. A model of this instrument is shown in figure 1. The height of the instrument is about 25 feet and its weight is about 3 tons. The primary optical element is a 36-inch fused silica mirror.

Since the theoretical resolution of this mirror is nearly 0.1 second of arc, it is clear that the pointing system must have an accuracy which is considerably better than 0.1 second of arc in order to fully utilize the capabilities of the mirror. The pointing will take place in two stages. First, the entire telescope (the L shaped part consisting of the main tube and the side arm) will be pointed with an accuracy of one or two seconds of arc by a three-axis pointing system. One of these axes, the azimuth axis, turns on a mercury float bearing ; the entire telescope floats on a layer of mercury about a millimeter thick in order to eliminate much of the friction present in ordinary bearings. The other two axes are orthogonal and turn, over a limited range of $\pm$ 5°, on flexure bearings. When these flexure bearings reach the end of their range, the telescope is turned on ordinary bearings until the flexure bearings are centered. A shutter temporarily interrupts the exposure during this centering. Second, the final pointing is accomplished by an image stabilization system (see figure 2) which is designed to keep the image fixed on the photographic plate to better than 0.03 seconds of arc.

The signals for the pointing system are provided by two guide stars located within 25 minutes of arc of the region to be photographed. These (9th magnitude or brighter) guide stars are detected by the two retrodividers located in the $f/50$ plane. Each retrodivider

splits the light of one of the guide stars into four parts and reflects this light on to four photomultiplier tubes. (Only one set of photomultiplier tubes is shown in figure 2 for simplicity.) The amount of signal on each of the four photomultiplier tubes depends on how well the guide star is centered on the retrodivider. One of the retrodividers, the translational retrodivider, provides the signals for the transfer lens. If the translational guide star is not centered on its retrodivider, then the transfer lens will move so as to center it. The frequency response of the transfer lens is about 20 c/sec. The average displacement of the transfer lens from its neutral position and the miscentering of the rotational guide star on the rotational retrodivider provide the signals for the main servo system which points the entire telescope.

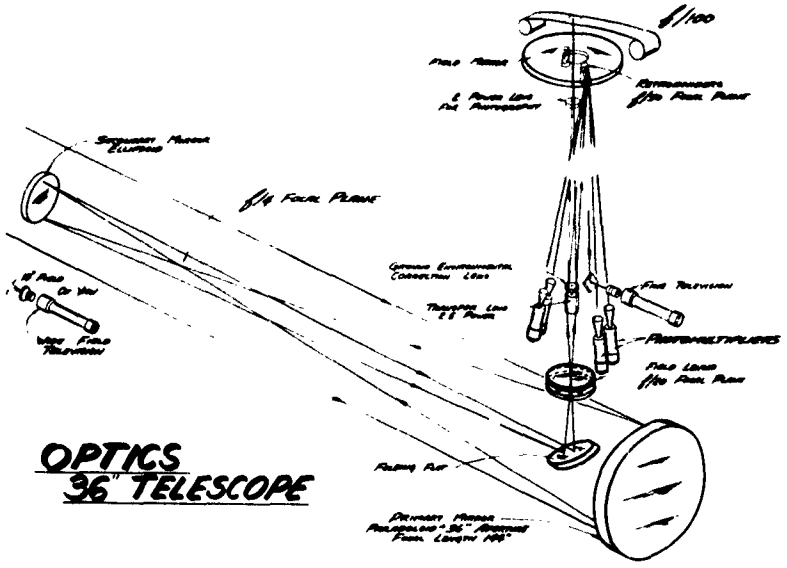

Fig. 2. — The Optical System of Stratoscope II

Stratoscope II, like Stratoscope I, will be operated at altitude by means of television, telemetry, and radio command (Wissinger 1961). Two RCA image orthicon television cameras are used to find the region of interest and to lock the servo system on to the

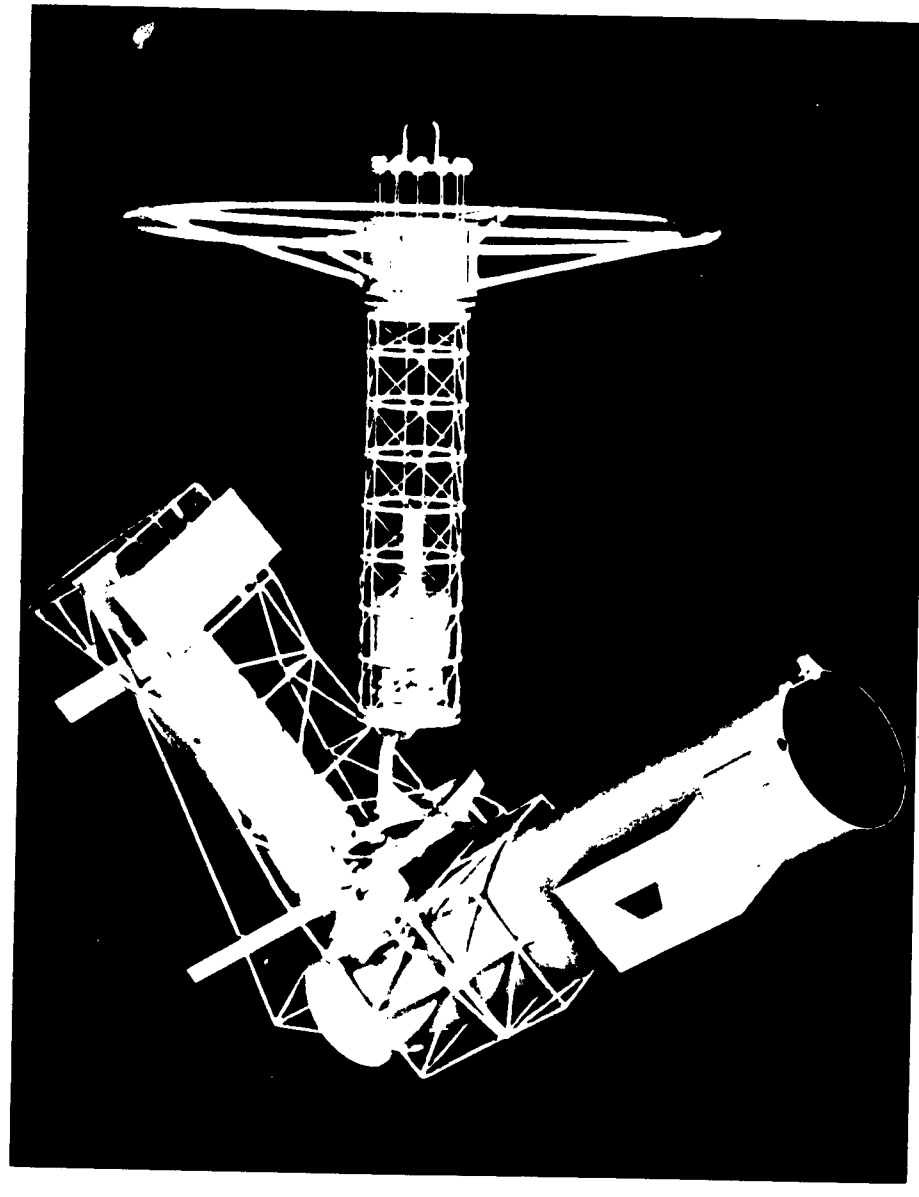

Fig. 1. A Model of Stratoscope II

guide stars. One of these cameras, having a field of view of 10° in diameter, will be used in conjunction with a magnetic compass reading to locate the region of the sky where the object to be photographed is located. The other television camera (the fine television — see figure 2) looks through the entire optical system of the telescope at the 50 minute of arc diameter field of view containing the retrodividers.

The region to be photographed is the central portion of this 50 minute of arc diameter field of view. This region is 2 minutes of arc square which, at f/100, corresponds to a 50 mm square photograph. An *f* ratio as large as 100 is necessary so that the resolving power of the telescope is not lost in the grain of the photographic plate. Seventy millimeter 103aG film will be used.

Planets will be the first photographic objects attempted because their exposure times at f/100 are relatively short — of the order of a second. Four different filters will be available by radio command. This will make it possible to photograph the planets in B and V colors as well as in the entire 4000 Å — 6000 Å wavelength interval in which the optics are corrected. Furthermore, it will be possible to obtain photographs in polarized light by commanding a polaroid filter.

When this very complicated instrument is perfected, it will allow photographs of planetary details on a scale which, up to the present, has only been glimpsed by visual observers. Indeed, when one considers detail of low contrast, it is possible that Stratoscope II will eventually photograph details which have not been seen visually. Besides the obvious gains of higher resolution on the bright planets, many other objects of the solar system will come within photographic resolution. These include Uranus, Neptune, Pluto, the larger asteroids, and several of the satellites of the Major Planets. Time sequences up to 8 hours (a night's flight) will be possible.

It is clear that Stratoscope II has capabilities for infra-red spectroscopy as well as high resolution optical photography. The

reason is, of course, that it is a relatively large instrument which, at altitude, will be above all but about 0.03 of the carbon dioxide and about 0.001 of the water vapor in the earth's atmosphere.

At Princeton, we (Dr. Schwarzschild — the project director, Dr. Bahng, Dr. Woolf, and myself) had plans to make infra-red observations with Stratoscope II after a few successful optical flights. These plans were, however, greatly accelerated as a result of a proposal from Dr. Weaver and Dr. Sagan of the University of California at Berkeley. They essentially proposed that Stratoscope II be used at the next (February 1963) opposition of Mars for infra-red observations similar to those planned for the 1964 Mars flyby and that they provide the infra-red equipment.

Basically this infra-red equipment consists of a calcium fluoride prism spectrograph (Littrow mounting) operating between 1 μ and 7.5 μ. The resolution varies with wavelength, a typical value is 0.04 μ at 5 μ. A new highly sensitive bolometer (Low 1961) will be operated at 2°K which is the temperature of liquid helium at the balloon altitude of 24 km. At this temperature, the detectors and associated electronics produce a signal to noise ratio of unity if an infra-red power of $2 \cdot 10^{-13}$ watts is integrated for one second. It appears that most of the noise does not come from the detector but rather from the detector pre-amplifier. This preamplifier noise is about an order of magnitude greater than the background radiation noise. With this sensitivity, signal to noise ratios in excess of 20 are expected on Mars during each 20 minute scan of the 1 μ – 7.5 μ wavelength interval.

A measurement of the amount of water vapor on Mars is the minimum goal of the first infra-red flight. The present upper limit for water vapor is 3.5×10^{-2} gm/cm^2 (Sagan 1961). The water vapor abundance in the earth's atmosphere above 24 km is believed to be of the order of 10^{-3} gm/cm^2 (Murcray, Murcray, and Williams 1962). Since 10^{-3} gm/cm^2 of water vapor on Mars would cause an absorption of several per cent in the 6 μ region, it should be possible to detect water vapor abundances of this magnitude.

Comparison spectra of the sky near Mars and of the Moon will be taken to help eliminate effects of terrestrial water vapor.

Other goals of this infra-red flight will be to search for evidence of organic matter on Mars similar to the features near 3.5 μ which Sinton (1959) has identified as C-H vibration absorptions. Related emissions from other organic bonds should be detected in the 6 μ region if the amount of Martian water vapor is not too high (Sagan 1961). Further goals are searching for minor constituents in Mars' atmosphere and checking the carbon dioxide abundance.

At the time of this writing (July 1962), Stratoscope II has been assembled at the Perkin-Elmer Corporation and is in the process of alignment and testing. Reassembly of the instrument will begin on about October 1 at the NCAR balloon launching center at Palestine, Texas in preparation for the Mars infra-red flight.

Hence the first Stratoscope II flight will not be an optical flight. This has the advantage that it is not necessary to pre-cool the primary mirror since neither the figure of the primary mirror nor the local disturbance in seeing caused by the instrument is critical. Also, the image stabilization portion of the pointing system is not needed. Thus the infra-red flight offers the opportunity to test Stratoscope II under considerably simpler requirements than an optical flight and still have a good opportunity to obtain extremely valuable observations. The main complication which the infra-red equipment produces is the necessity to fly liquid helium.

One should be reminded, however, that Stratoscope II is an extremely complicated instrument incorporating many new engineering features. The size and weight of the instrument is such as to require the development of new ballooning techniques. Hence it is possible that the initial difficulties will be more severe than with Stratoscope I. However, the observational results which can be obtained when Stratoscope II is perfected are so important as to warrant these additional difficulties.

Project Stratoscope of Princeton University is sponsored by

the following United States Agencies : The Office of Naval Research, The National Science Foundation, and the National Aeronautics and Space Administration.

BIBLIOGRAPHY

LOW, F. G., *J. Opt. Soc. Am.*, **51**, 1300, 1961.

MURCRAY, D. G., MURCRAY, F. H. and WILLIAMS, W. J., *J. Geophys. Res.*, **67**, 759, 1962.

SINTON, W. M., *Science*, **130**, 1234, 1959.

SAGAN, C., *Astron. J.*, **66**, 52, 1961.

WISSINGER, A. B., *Astronautics*, **6**, No. 5, 38, May 1961.

NOTE ADDED IN PROOF

At the time of this proof (Dec. 26, 1962), Stratoscope II has been reassembled at Palestine, Texas and the infra-red equipment has been integrated into the telescope. An infra-red spectrum of a test source has been obtained while the telescope pointed at the source. Infra-red observations of Mars from the ground will be made during January in preparation for the actual balloon flight in February.

DISCUSSION DES COMMUNICATIONS 6 à 22.

J. Rösch (6). — Dollfus indique 6″,63 ± 0,07 comme moyenne des mesures du diamètre de Mercure le 7 novembre 1960. Cette moyenne comprend des mesures faites au micromètre à double image. Dans la discussion de nos mesures faites par la méthode photométrique de Hertzprung, nous indiquerons pourquoi nous pensons que la valeur plus élevée que nous trouvons nous paraît devoir être retenue.

S. I. Rasool (6). — Avez-vous déjà analysé les photographies de Venus en ultraviolet afin de déterminer les vitesses de mouvement des nuages ?

A. Dollfus (6). — Avec les quelques clichés dont nous disposons je ne peux pas vous donner un chiffre. Ce travail est en cours et nous espérons avoir des résultats très bientôt.

F. Link (6). — En ce qui concerne la collaboration internationale dans le domaine de la Commission 16 (Planètes) de l'U.A.I., il serait souhaitable d'organiser des observations de la Lune à l'occasion de prochaines tentatives d'atteindre notre satellite. Il faudrait préparer le programme d'observation qui serait déclenché automatiquement par l'annonce du lancement, à la Radio.

A. Dollfus (6). — Avant d'organiser une telle coopération, il serait désirable de faire un sondage pour connaître le nombre d'observateurs qui désireraient participer à un tel programme. Si le Professeur Link veut bien se charger d'une telle tâche, il serait alors plus facile ensuite d'organiser cette coopération.

J. C. Pecker (7). — How is it possible to disentangle the depth-variation from the anisotropic properties of particles, in observed phenomena (such as limb-darkening) ?

W. M. Irvine (7). — For a homogeneous atmosphere a variation of optical thickness can produce photometric effects similar to those arising from a variation of asymmetry factor. Ideally these effects could be separated by an examination of the limb darkening curve, but in practice it may be difficult. We have not yet computed enough examples for large asymmetries to be able to make a definite statement. Fortunately, spectroscopic and polarimetric data may often provide clues to supplement the photometric results.

A variation with depth of the structure of the atmosphere (Section VI, e), as will generally occur in actual cases, makes the situation even more complicated. We have not examined this problem, but I believe Dr. Goldstein will have something to say on the subject tomorrow.

E. J. Öpik (10). — Opik's value for the optical depth of Rayleigh scattering above Jupiter's clouds, $\tau = 0.25$, refers to 3900 Å and, with λ^{-4}, is almost exactly equivalent to $\tau = 0.06$ assigned by Gehrels for the equa-

torial belt at 5600 Å. Öpik considered τ to be very large in the dark bands, which also would agree with the value given by Gehrels for the dark polar caps.

E. J. Öpik (11). — Triple collisions $CH_2 + H_2 + Z \rightarrow CH_4 + Z$ would prevent CH_2 from accumulating except in the uppermost atmospheric layers. Its total amount may be too small in the atmospheres of the giant planets to be detectable.

L. Dunkelman (12). — In determining the « monochromatic reflectivities » of the four planets (Jupiter, Saturn, Uranus and Neptune) from the observed respective « monochromatic spectral energy distributions », it would be preferable to use a solar energy distribution with a spectral resolution comparable to what was observed with the Mt. Wilson 60-inch telescope planetary measurements. It is recommended that, particularly from 4000 Å to 3000 Å, the Mt. Lemmon Solar data be used instead of the Smithsonian. Refer to L. Dunkelman and R. Scolnik, *J. Opt. Soc. Am.* **49**, 356 (1959).

C. Sagan (13). — Dr. Brandt's conclusion that a source of true absorption exists at 2800 Å on Jupiter is most interesting. The presently detected constituents of the Jovian atmosphere — hydrogen, helium, methane and ammonia — are all transparent in the gaseous phase at this wavelength. Experiments have been performed in which energy is supplied to a mixture of such gases in a simulated Jovian atmosphere ; the major products include hydrogen cyanide, methyl cyanide, acetylene, ethane and ethylene (C. Sagan and S. L. Miller, *Astronomical Journal*, **65**, 499, 1960). None of these molecules have absorption features in the gaseous state at 2800 Å. Molecules which are capable of absorbing at this wavelength, such as aldehydes and ketones, require water as a photochemical precursor — but water is not a constituent of the Jovian atmosphere above the cloud deck. Therefore, the possibility arises that the infrared absorption exists in the cloud layer itself.

The most likely composition of the clouds is ammonia cirrus. (G. P. Kuiper, *Atmospheres of the Earth and Planets*, revised edition, University of Chicago Press, Chicago, Chapter 12, 1952). It has been known for many years that absorption of gaseous ammonia on a variety of substrates shifts its photolytic threshold to longer wavelengths. (See, for example, K. Kassparov and A. Terenin, *Acta. Phys. Chim. U.R.S.S.*, **15**, 348, 1941). It may therefore be that the absorption at 2800 Å inferred by Brandt arises from gases absorbed in the Jovian clouds.

G. F. Schilling (17). — In applying your diffusion flux equation to Mars, how would you define the altitude of the mesopause? Where photodissociation and heating begin to occur?

M. Nicolet (17). — In the equation, two parameters depend on the altitude : $(r/r_0)^2$ and $T^{1/2}$. Therefore, it is not necessary to know exactly the altitude of the mesopause. If $0.95 \leq (r/r_0)^2$ and $T = 200°K$, no large error is involved. Photodissociation and heating must begin above the mesopause.

B. SPECIAL PAPERS ON THE SUCCESSIVE PLANETS

22. — PARTICULATE MATTER IN THE ATMOSPHERES OF THE TERRESTRIAL PLANETS

MICHAEL H. BRIGGS
Department of Geology, Victoria University of Wellington, New Zealand

In this paper the term « particulate matter » is applied to any non-gaseous atmospheric constituent.

INTRODUCTION

Atmospheric hazes have been reliably reported to obscure surface features of all the inner planets. In this paper a discussion will be presented on the available evidence for the composition of the hazes of each of the inner planets, and it will be shown that it is exceedingly likely that each planet has a variety of different hazes and that there are few in common.

It is apparent that the hazes of the terrestrial atmosphere are the most easily investigated and a comparison of the properties of these with the hazes of the other planets seems a profitable approach. It will also be shown that a knowledge of the hazes of other planets can afford valuable evidence concerning the origin of terrestrial hazes.

TERRESTRIAL ATMOSPHERIC HAZES

A surprisingly large number of different types of particulate matter occur in the atmosphere of Earth. The most abundant of these are, of course, water and ice clouds. However, there are numerous others ; for example, it has often been reliably reported that over large uninhabited tracts of the Earth's surface, which possess dense vegetation, abundant blue hazes commonly can be seen. The nature of these hazes has been the subject of some discussion, but it now appears (Went, 1960) that the hazes are composed of volatile essential plant oils, probably largely terpenes or other isoprene

derivatives. Hence, the low-lying hazes over some terrestrial regions are biogenic in origin and estimates on the amount of these volatile oils released annually into the Earth's atmosphere give values of about 10 tons. It is apparent, therefore, that if vegetation similar to Earth's occurs on other planets, blue hazes composed of biogenic hydro-carbons are likely to occur.

There is considerable special evidence of the presence of metals in appreciable quantities in the Earth's upper atmosphere. There is good evidence (Bates, 1960) of free sodium, lithium and ionized calcium and magnesium. The sodium appears to be confined to a thin layer about 14 kilometres thick at an altitude of approximately 85 kilometers. The total amount of sodium atoms above 70 kms is of the order of 10^9 atoms per centimetre^2. Moreover, this is a minimal value representing only the neutral atomic fraction. The total amount of sodium in the Earth's entire atmosphere is probably of the order of several tons. The origin of this material, however, is still obscure and possible sources are salt from the oceans, dust from volcanoes or meteors. In a recent paper, Junge, *et al.* (1962) have discussed this problem and conclude that meteors and micrometeorites are the most likely sources. It will consequently be of great interest to determine whether sodium occurs in similar amounts in the atmospheres of any of the other inner planets. The absence of sodium in the Martian atmosphere, for example, would be strong evidence against an extraterrestrial origin.

Lithium is present also in a broad layer of mean height approximately 85 kilometres (Delannoy and Weill, 1958); the concentration, however, is considerably less than that of sodium and estimates put the total Earth's atmospheric lithium at about 500 grams (see Gadsden and Salmon, 1958). Again, there is no certainty concerning the origin of this material, which could equally have arisen from any of the sources suggested for sodium, though there is the alternative possibility that it is a relic of nuclear explosions, as lithium was not reliably reported in the Earth's atmosphere before 1957.

The calcium-containing layer of the Earth's atmosphere is considerably higher than that for the two other metals, being above 135 kilometres. Estimates of the total abundance (Jones, 1958) gave values of approximately 200 kilograms of ionized calcium in the entire atmosphere. Considering the height of the layer, it seems likely that the calcium is of meteoric origin, for it is known to increase considerably when the Earth passes through meteor swarms. However, it is also possible that some is derived from intense solar flares. It seems extremely likely that the ionized calcium is in equilibrium with CaO, which presumably is continually deposited on the Earth's surface.

Evidence for ionized magnesium comes from mass spectrographic data from high altitude rockets. The height of the layer was 100 to 110 km., and the total number of ions was 7×10^9 cm^{-2} column (Istomin, 1961).

There is also the possibility of minor hazes of the Earth due to nitrogen oxides. The Earth's atmosphere contains several oxides of nitrogen ; nitrous oxide is probably a permanent atmospheric constituent present to an extent of about .5 parts per million and it may arise through either interactions of nitrogen-free radicals with nitrogen dioxide ($N + NO_2 \rightarrow N_2O + O$), or be a product of soil micro-organisms. While a gaseous constituent, nitrous oxide probably influences the concentration of other oxides which are not. Nitrogen dioxide is now known to be formed continually in the dark hemisphere of the Earth from nitric oxide (Harteck, 1957), the day-time concentration of nitric oxide having been estimated (Kistiakowsky and Volpi, 1958) at about 10^4 molecules per centimetre^3 at an altitude of 85 kilometres. This value is somewhat less than that estimated by earlier workers (e. g. Nicolet, 1949). Nitrogen dioxide has a m. p. of — 9°C and a b. p. of + 21°C. It is consequently a particulate constituent of the upper atmosphere.

Other terrestrial hazes are produced by weathering of the Earth's solid surface. There is now considerable evidence of the continuous presence of large quantities of dust particles (see Hulst,

1952) which are probably largely of silicate composition. Hazes close to the surface are, of course, formed frequently by dust and sand storms.

It is apparent, therefore, that the Earth possesses a wide variety of chemically different atmospheric particulate materials. In summary, these are : — water and ice, biogenic hydro-carbons, free metals, nitrogen dioxide, the products of silicate weathering.

Mercury

Examinations of the spectrum of Mercury taken at Mt. Wilson by Adams and Dunham (1932), both of the 8000 Å region and in the blue, were unable to detect any absorption bands or lines due to an atmosphere. Consequently it is a reasonable conclusion, taking into account the low surface gravity and high temperature, that there is no permanent abundant atmosphere round Mercury. However, several observers of the planet have occasionally reliably reported (Antoniadi, 1932) temporary obscurations of the permanent surface markings. The nature of the hazes causing these obsc ances is still completely unknown. Moreover, there have been no accurate measurements of their physical properties. Urey and Brewer (1957) have suggested that, under certain circumstances, accumulations of various free radicals could occur over the Mercurial surface and account for the hazes. This is certainly a likely possibility — however, there are undoubtedly alternatives. For example, the presence of active volcanoes on the Mercurial surface is not impossible, and this could lead to the production of volcanic out-gassings containing sulphur compounds which could form a temporary atmosphere and, moreover, would give rise to hazes, possibly due to the interaction of reduced and oxidised sulphur compounds, to form minute sulphur particles. A further alternative is that radio-active heating produced in the Mercurial crust by heterogenous distribution of radio-active elements such as potassium or uranium could give rise to local heating and decomposition

of materials which would be released occasionally as a small explosion, in which case some of the reported hazes could be fragmented surface materials.

On the whole, however, it seems most likely that the Mercurial hazes are fluorescent-free radicals or volcanic sulphur.

Venus

The atmosphere of Venus is completely opaque and no surface features have ever been reliably observed. Estimates of the height of the clouds have been made by a variety of methods (Sagan, 1961), and it would appear that there are two distinct cloud layers, on at about 100 kilometres from the surface and second, denser layer at 30-40 kilometres.

The upper atmospheric haze is certainly of different physical and chemical composition to the lower. Attempts to investigate its nature have proved largely unsuccessful, and possibly the suggestion of Kuiper (1957) that it is composed of polymerised carbon sub-oxide formed from atmospheric carbon dioxide, which is known to be present in large quantities, is the most likely. A new suggestion is that of Hayden *et al.* (1959) who have reported the presence of a broad continuum in the near UV spectrum of Venus, which they ascribe to nitrogen tetroxide. They have consequently suggested that this material is the major component of the upper atmosphere haze. However, this suggestion seems extremely unlikely as nitrogen tetroxide is readily dissociated by radiation of wavelength less than 3000 Å, with the liberation of free oxygen. As this gas is undetectable in the Venusian atmosphere, the presence of nitrogen tetroxide seems most improbable, and the spectral features must arise from some still unidentified substance.

The lower atmosphere clouds have been the subject of considerable controversy. The only agreement at present is that they are slightly yellow in colour and probably are present in an atmosphere of mean temperature about 250°K. However, there is now strong

evidence from micro-wave determinations (Sagan, 1961) that the surface temperature of Venus is approximately 600°K and consequently it seems exceedingly likely that any satisfactory hypothesis of the lower cloud layer (composition) must account for this high surface temperature.

The materials suggested as the major constituents of these clouds are as follows : polymerised formaldehyde (Wildt, 1937), ammonium nitrite (Dauvillier, 1958), volatile hydrocarbons (Hoyle, 1955), high molecular weight hydrocarbon polymers (Wilson, 1960), micro-organisms (Kozyrev, 1956), water droplets (Menzel and Whipple, 1955), silica particles (Kuiper, 1952), sodium and magnesium chlorides (Suess, quoted by Kuiper, 1952), calcium and magnesium carbonates (Opik, 1961), volatile low molecular weight organic compounds (Briggs, 1959).

To decide between these alternate hypotheses is not easy on the slender experimental evidence available ; however, it is fairly apparent that some volatile material must be involved. This could be water, but the lack of major absorption lines due to water vapour in the spectrum of Venus must be accounted for. The traces detected by Strong, *et al.* (1960) are obviously insufficient to account for the clouds. Moreover, Kozyrev (1954) has reported the presence of several absorption bands, including ones at 4372 and 4120 A, that are probably due to components of the clouds. In a recent paper, Opik (1961) has argued that the high surface temperature of Venus cannot be entirely accounted for in terms of a « radiative glasshouse » effect, and must be due mainly to frictional heating arising from interaction of the clouds with the surface. Consequently, he concludes from the CO_2 content and optical properties that only calcium and magnesium carbonates are likely major components. These materials, however, are involatile, nor could they give rise to the reported absorption bands in the spectrum. If Opik's approach is valid, possibly the most likely materials are a mixture of finely-ground inorganic salts with adsorbed volatile low-molecular weight organic materials.

The origin of the organic matter is abiogenic. It seems likely that the Venusian atmosphere has undergone as marked chemical changes from its original state as has Earth's. As the primitive atmospheres of all the inner planets were presumably of similar composition, i. e., methane, ammonia, water vapour, etc. (Urey, 1952) it seems probable that these gases were converted on all planets to a mixture of organic compounds by the action of solar radiation and electrical discharges. On Earth these compounds were the precursors of life, but on Venus, with a high surface temperature, the materials would simply volatilise and recondense in colder regions, and could well form permanent layers in the atmosphere.

The presence of two distinct hazes in the atmosphere of Venus is well-established, but the chemical composition of either is very much in doubt and, with the present lack of data on the physical and chemical constituents of the planet's atmosphere, it is only possible to construct hypothetical model systems, such as the one outlined above.

Mars

The composition of the Martian atmosphere is still largely in doubt. The possible extreme ranges of atmospheric conditions have been summarized recently by Schilling (1962). The probable composition of the atmosphere has been recently reviewed (Briggs and Revill, 1960). The only gas for which there is conclusive evidence is carbon-dioxide ; however, it is likely that nitrogen is the other major constituent. A mixture of 95-96 % nitrogen, 4-5 % argon and 0.03 % carbon dioxide, possibly with traces of other gases, provides a model atmosphere that agrees closely with the observed properties such as scattering power, polarization, etc. Consequently, the recent report that the reflection spectrum of Mars shows details characteristic of nitrogen tetroxide (Kiess *et al.*, 1960) should be viewed with some scepticism as, similar to the case

of Venus, there is no detectable free oxygen in the Martian atmosphere as would follow from the presence of this substance.

The reported hazes of the Martian atmosphere fall into three distinct types. The first, which is yellow in telescopic appearance, forms close to the surface and is almost certainly due to dust storms of some sort, formed by local turbulence. There is an excellent account of the appearance of such clouds in 1956 (Mars Section Report, 1958). However, as wind speeds on Mars are low, the dust cannot be raised by widespread winds, but is probably the result of local turbulence.

The second cloud type is fairly rare, but has been reliably reported by several observers (Dollfus, 1948) and polarization studies have been made. From this work it seems reasonable to assume that the clouds are of ice crystals, possibly in equilibrium with water in the liquid phase. The average height of the white clouds has been estimated at about 20 kilometres above the surface.

The most controversial haze of the Martian atmosphere is the so-called « blue haze » or « violet layer ». This appears to be situated some 30-35 kilometres above the surface and is several kilometres thick. From its appearance it is entirely composed of particles of average diameter less than 0.1 micron. The chemical composition, however, has been the subject of considerable debate (see Hess, 1958). The most obvious choice, ice crystals, is unlikely as the particles absorb slightly in the blue and near UV ; this evidence also discounts the possibility that the particles are solidified carbon dioxide. An alternate hypothesis that has recently received some discussion is particles of elemental carbon, formed by an interaction of carbon dioxide and carbon monoxide ; the latter gas being formed in the upper atmosphere by irradiation of the dioxide (Rosen, 1953). It is exceedingly difficult to discount this hypothesis, though the observed absorption properties of the haze do not seem to fit well with particles of this composition.

A further alternative (Briggs, 1962) is that the haze is similar

to the blue haze of the Earth's atmosphere and is composed of hydrocarbons, possibly of biogenic origin.

Conclusions

It is apparent that very little is known of the hazes present in the atmospheres of the inner planets. Their observed properties, however, suggest that they belong to several very different chemical categories and, in fact, several may have no terrestrial analogues. Nevertheless, an investigation of the nature of these hazes in a more direct manner by interplanetary instrument capsules should answer many problems concerning the origin of the Earth's atmospheric hazes.

References

Adams, W. S. and Dunham, T., Jr., *Publ. Astron. Soc. Pacific*, **44**, 380, 1932.

Antoniadi, E. M., « *La planète Mercure* », Masson, Paris, 1932.

Briggs, M. H., *The Observatory*, **79**, 20, 1959.

Briggs, M. H. and Revill, J. P., *J. Brit. Interplanet. Soc.*, **17**, 391, 1960.

Briggs, M. H., « *Scientist Speculates* », I. J. Good (editor), Heinemann, London, 1962.

Dauvillier, A., « *L'Origine Photochimique de la Vie* ». Masson, Paris, 1958.

Delannoy, J. and Weill, G., *C. R. Acad. Sci., Paris*, **247**, 806, 1958.

Dollfus, A., *C. R. Acad. Sci., Paris*, **227**, 383, 1948.

Gadsden, M. and Salmon, K., *Nature*, **182**, 1598, 1958.

Harteck, P., « *Threshold of Space* ». M. Zelikoff (editor). Pergamon Press, New York.

Hess, S. L., *Astrophys. J.*, **127**, 743, 1958.

Heyden, F. J., Kiess, C. C., and Kiess, H. K., *Science*, **130**, 1195, 1959.

Hoyle, F., « *Frontiers of Astronomy* ». Heinemann, London, 1955.

Hulst, H. C. van de, « *Atmospheres of the Earth and Planets* ». G. P. Kuiper (editor). University of Chicago-Press, 1952.

Istomin, V. G., *Doklady, Akad. Nauk USSR*, **136**, 1066, 1961.

Jones, A. V., *Ann. Geophys.*, **14**, 179, 1958.

Junge, C. E., Oldenberg, O. and Wasson, J. T., *J. Geophys. Res.*, **67**, 1027, 1962.

Kiess, C. C., Corliss, C. H., and Kiess, H. K., *Science*, **131**, 1319, 1960.

Kistiakowsky, G. B. and Volpi, G. G., *J. chem. Phys.*, **28**, 665, 1958.

Kozyrev, N. A., *Bull. Crimean Astrophys. Observ.*, **12**, 169, 1954.

Kozyrev, N. A., *Akad. Nauk, USSR Astron. Circ.*, **175**, 26, 1956.

KUIPER, G. P. « *Threshold of Space* ». M. Zelikoff (editor). Pergamon Press, New York, 1957.

Mars Section Report, *J. Brit. Astron. Assoc.*, **68**, 142, 1958.

MENZEL, D. H. and WHIPPLE, F. L., *Publ. Astron. Soc. Pacific*, **67**, 161, 1955.

NICOLET, M., *J. Geophys. Res.*, **54**, 373, 1949.

OPIK, E. J., Paper presented to 42nd Ann. Meeting Amer. Geophys. Union, Washington D. C., April 18-21, 1961.

ROSEN, B., *Ann. Astrophys.*, **16**, 288, 1953.

SAGAN, C., *Science*, **133**, 849, 1961.

SCHILLING, G. F., *J. Geophys. Res.*, **67**, 1170, 1962.

STRONG, J., ROSS, M. D., and MOORE, C. B., *J. Geophys. Res.*, **65**, 2526, 1960.

UREY, H. C., « *The Planets* ». Yale University Press, 1952.

UREY, H. C. and BREWER, A. W., *Proc. Roy. Soc.*, A, **241**, 37, 1957.

WENT, F., *Proc. Nat. Acad. Sci., U. S.*, **46**, 212, 1960.

WILDT, R., *Astrophys. J.*, **86**, 321, 1937.

WILSON, A. T., *Nature*, **188**, 1007, 1960.

23. — INTERACTIONS OF THE PLANET MERCURY WITH INTERPLANETARY MATERIAL

PAUL HODGE
Berkeley Astronomical Department
University of California, U. S. A.

INTRODUCTION

Meteoritic erosion of minor bodies of the solar system is an important effect, as Whipple has shown for the case of erosion of small particles by small particles (1962). Erosion of this sort is no doubt important also in the case of asteroids, satellites, and comets. The majority of the planets, however, do not suffer meteoritic erosion, because of the way in which their atmospheres protect them from the constantly bombarding meteoroids. Only the planet Mercury has an atmosphere too thin to afford it much protection. Its lack of appreciable atmosphere is not the only thing that makes Mercury especially susceptible to meteoritic erosion ; its nearness to the sun means that both the density of interplanetary material and the velocities of encounter are much higher than for other planets, so that erosion is greatly more effective. In the following discussion, we evaluate as accurately as possible the rate of erosion of Mercury's surface due to meteoritic encounters. The atmosphere of Mercury is assumed to be negligible, but at the end of the discussion the effect of a possible atmosphere is considered.

THE AMOUNT OF INTERPLANETARY MATERIAL

The space density of interplanetary dust can be determined in very direct ways for the earth's distance from the sun. The most direct measures are those of satellites and space probes (La Gow and Alexander, 1960 ; Komissarov, Nazarova, Neugodov, Poloskov, and Rusakov, 1959 ; Dubin, 1960 ; Mc Cracken, 1960 ; Cohen, 1960 ; Soberman and Della Lucca, 1961 ; Mc Cracken, 1962). Other direct

23. — INTERACTIONS OF THE PLANET MERCURY WITH INTERPLANETARY MATERIAL

PAUL HODGE
Berkeley Astronomical Department
University of California, U. S. A.

INTRODUCTION

Meteoritic erosion of minor bodies of the solar system is an important effect, as Whipple has shown for the case of erosion of small particles by small particles (1962). Erosion of this sort is no doubt important also in the case of asteroids, satellites, and comets. The majority of the planets, however, do not suffer meteoritic erosion, because of the way in which their atmospheres protect them from the constantly bombarding meteoroids. Only the planet Mercury has an atmosphere too thin to afford it much protection. Its lack of appreciable atmosphere is not the only thing that makes Mercury especially susceptible to meteoritic erosion ; its nearness to the sun means that both the density of interplanetary material and the velocities of encounter are much higher than for other planets, so that erosion is greatly more effective. In the following discussion, we evaluate as accurately as possible the rate of erosion of Mercury's surface due to meteoritic encounters. The atmosphere of Mercury is assumed to be negligible, but at the end of the discussion the effect of a possible atmosphere is considered.

THE AMOUNT OF INTERPLANETARY MATERIAL

The space density of interplanetary dust can be determined in very direct ways for the earth's distance from the sun. The most direct measures are those of satellites and space probes (La Gow and Alexander, 1960 ; Komissarov, Nazarova, Neugodov, Poloskov, and Rusakov, 1959 ; Dubin, 1960 ; Mc Cracken, 1960 ; Cohen, 1960 ; Soberman and Della Lucca, 1961 ; Mc Cracken, 1962). Other direct

methods include rocket experiments (Mc Cracken, 1960 ; Soberman and Hemenway, 1961), meteor observations (Hawkins and Upton, 1958 ; Millman and Burland, 1957), and collections of dust from the high atmosphere (Hodge and Wright, 1962), the ocean sediments (Laevastu and Mellis, 1955), fossil lake sediments (Crozier, 1960), arctic ice sediments (Thiel and Schmidt, 1961), and at the surface of the earth (Crozier, 1961 ; Hodge and Wildt, 1958). Results from these methods are often given in the form of an accretion rate for material incident on the earth. At least a value as large as 3×10^3 gm/sec is necessary to explain the number of tiny magnetite spherules found in the high atmosphere, the arctic, and the ocean floors. These make up only a fraction of the incident material, so that the total accretion is certainly much larger than this value. From a variety of such sources, Whipple (1962) has adopted a value of 3×10^4 gm/sec for the earth's accretion rate for all particles. This is in reasonable agreement with practically all available data except some of those computed from space vehicle experiments.

The accretion rate computed from rocket and satellite measures is much larger, unless we accept the presence of a dense belt of particles surrounding the earth (Whipple, 1961 ; Hibbs, 1961). Explorer I (satellite 1958 α), for instance, encountered 10^3 more particles than was predicted. The encounters of Sputnik III (1958 δ) and Vanguard III (1959 η) were a little more than 10^2 times the predicted number. Such anomalies are fairly easily explained by the earth dust cloud hypothesis of Whipple and Hibbs. However, Dubin (1961) has questioned this hypothesis ; if we do not accept it, and use a mean value for the space density from all satellite data, we are led to an accretion rate for the earth of roughly 10^6 gm/sec, an improbably high value.

There are also less direct means for determining the space density of dust at the earth's solar distance. One of these is presented by the observations of the zodiacal cloud. A recent very careful study by Ingham (1961) has given probable values for the local space density of dust as derived from Ingham and Blackwell's

observations of the zodiacal light from high in the Peruvian Andes. He finds that if reasonable assumptions are made about the size distribution and density of the dust the observations indicate a spacial density of approximately 500 particles/km^3 at one A. U. This includes all particles greater in radius than 0.4 μ, the limit below which radiation pressure blows the dust away (if its density is roughly 2 gm/cm^3). The total mass density is of the order of 10^{-24} gm/cm^3 at 1 A. U. Another determination of the spacial density of dust at the earth's distance from the sun is that by Briggs (1962), based on considerations of supply of dust by comets and depletion by the Poynting-Robertson effect. Briggs finds a space density at 1 A. U. of 165 particles/km^3.

Both of these determinations are in reasonable agreement with Whipple's accretion rate for the earth of 3×10^4 gm/sec, though comparison requires assumptions as to size distribution and physical properties of the particles. We adopt this value as a lower limit and most probable value, keeping in mind that a value of 10^6 gm/sec is possible in view of satellite measures.

The space density normally is assumed to vary as $r^{-\alpha}$, where r is the distance from the sun and α is a constant near unity in value. Following Briggs, we adopt $\alpha = 1$. Thus the space density of material at Mercury's distance from the sun is a little more than 3 times that at 1 A. U.

The Orientations of the Orbits

In order to estimate the distribution of the velocities of impact on Mercury's surface, it is necessary to know something of the orientations of the orbits. We know that they are not random in inclination, as the zodiacal cloud shows for the small particles and the meteor observations show for the larger particles. There is some indication, from the comparison of these two sources, that the smaller particles have smaller inclinations than the larger (meteor particles), and we know that the most massive (meteorite

particles) have again very small inclinations. Properly, we should discuss a variety of different distributions of orbital parameters, as a function of the size and nature of the particles. However, it would be fruitless to attempt to do so with the presently available knowledge, and therefore, we must adopt a simple model which approximates the probable situation.

The characteristic angular distance from the ecliptic of meteor orbit planes has been found to be roughly 10° for sporadic meteors (Whipple 1959) and a minority of the meteors are retrograde. We adopt below a model in which all particles at 0.3 A. U. have small inclinations and $\sim 1/3$ of them are retrograde. The distribution of impact velocities derived from this model should not differ greatly from that based on a more complicated model, which would in any case be premature at this time.

Impact Velocities

If the impact velocity of a particle which collides with Mercury is v_c, then the geometry of a collision leads to the equation,

$$v_c = v_s + v_m \cos \alpha + \mathrm{K}\,(\alpha)\, v_{\mathrm{E}} \text{ for } 0^\circ \leqslant \alpha \leqslant 90^\circ$$

and

$$v_c = v_s - v_m \cos \alpha + \mathrm{K}\,(\alpha)\, v_{\mathrm{E}} \text{ for } 90^\circ \leqslant \alpha \leqslant 180^\circ$$

where v_s is the particle's spacial velocity, v_m is Mercury's velocity, α is the angle between the forward direction of Mercury's motion and that of the particle, v_{E} is the velocity of escape from Mercury (3.6 km/sec) and K (α) is a function of α and varies from approximately 0.5 for $\alpha = 0^\circ$ to 0.1 for $\alpha = 180^\circ$. For orbits in the zodiacal plane ($i = 0$), the space velocities are approximately

$$v_s = 48 + 20 \cos \alpha.$$

For moderate values of i the value of v_s is only slightly altered, according to the inclination and eccentricity of the orbit. If we adopt

the above expression then we find that the velocity of collision is approximated by

$$v_c = 48 + 68 \cos \alpha, \text{ for } 0^o \leqslant \alpha \leqslant 90^o$$

and

$$v_c = 48 - 28 \cos \alpha, \text{ for } 90^o \leqslant \alpha \leqslant 180^o$$

For the sake of simplicity we adopt a model of the orbital characteristics of particles near 0.3 A. U. such that the orbits are primarily of low inclination, low eccentricity, and primarily direct, 1/3 being retrograde. Such circumstances no doubt are reasonably close to the truth.

The Amount of Displaced Material

Öpik (1958) has worked out a theory for high-speed impact cratering in which the mass of material displaced by the impact is proportional to the momentum of the incoming particle. Whipple (1962) has compared Öpik's theory with experimental determinations of cratering properties and concludes that the theory is probably applicable to meteoritic problems. Öpik finds

$$M = kmv_c (\rho/S)^{1/2}$$

where M is the displaced mass, m is the mass of the projectile, k is a constant depending on the density of the projectile ($k \approx 4.3$ for a stone particle hitting an iron surface), ρ is the density of the surface hit, v_c is the velocity of impact, and S is the compressive strength of the material struck. For rock on rock, we adopt values of 4 for k, 10^9 dyn/cm^2 for S, and 3 gm/cm^3 for ρ. Thus

$$M \approx 20\, mv_c,$$

if v_c is given in km/sec. and m in grams.

We find that the mass displaced by a collision per gram of incident material is

$$\int \frac{M}{m} d\alpha \approx 1000.$$

Our adopted value for the mass of incident material on the earth is 3×10^4 gm/sec. Mercury would have approximately

0.11 times that of the earth, because of its smaller diameter and smaller mass. However, the space density of particles is about three times as great at Mercury's distance from the sun, so we find an incident mass of approximately 10^4 gm/sec. Thus the displaced mass is 10^7 gm/sec. The surface of Mercury has been severely eroded by interplanetary material, probably as fully as the earth's surface has been changed constantly by weather. Furthermore, since meteoritic erosion has the almost irreversible effect of making material increasingly smaller in size, we expect the surface of Mercury to be largely dust-covered. The principle source of non-dusty material is probably volcanic activity. We expect that extrusions from Mercury's reservoir of molten rock push up and flow out over the dusty land, only to be slowly weathered away by meteoritic erosion.

Pettit (1961) has pointed out that optical evidence suggests that the side of Mercury presented at western elongation is considerably rougher on the surface than the side presented at eastern elongation. This seems a reasonable confirmation of the importance of meteoritic erosion at the surface of the planet. The observed rough side faces in the direction of Mercury's motion, so that this side is expected to be the more seriously eroded.

Ejected Material

Some of the mass of material displaced by meteoritic collisions is possibly ejected from Mercury with velocity greater than the escape velocity. Just how much is so ejected is very difficult to evaluate at the present. We know that even with the dense atmosphere and the high mass of the earth, material is thrown to very great heights by impressive explosions such as those of the Tunguska meteorite, Krakatoa, and nuclear bombs. However, for a quantitative theory of ejection, we are left with very little pertinent data. For a rough approximation, we follow the arguments of Whipple (1959), who suggests that the mass of material ejected

from the moon equals that incident upon it. In Mercury's case, the velocity of escape is somewhat larger, and the velocity of impact is also larger, so that the ratio of ejected to incident is probably very similar to that for the moon. Accepting this leads to a value of roughly 10^4 gm/sec of dust ejected from the planet. Most of this dust will be of very small dimensions, much of it in the range (0.1 μ to a few microns in diameter) of size which is acted upon by radiation pressure. This material should form a faint tail opposite the sun, analogous to comets' dust tails. The remainder of the ejected material will disperse ; that larger than a few microns will spiral inward under the Poynting-Robertson effect, and will in itself suffer gradual meteoritic erosion.

The Problem of an Atmosphere

The above discussion assumes that Mercury has no appreciable atmosphere. There is some evidence (Dollfus 1961) that a small atmosphere on the bright side is detected by polarization measures. The erosion rate on this side would be unaffected by an atmosphere of less than about 0.1 mb pressure, which is approximately the pressure at the level at which meteoroids are decelerated by the earth's atmosphere. An atmosphere 10^{-4} the earth's is the maximum allowable if Mercury's sunward surface is extensively eroded meteoritically. Dollfus' value of 3×10^{-3} earth atmospheres is so great that most meteoroids would never reach Mercury's sunward surface. On the dark side, where any atmosphere would immediately freeze out, the erosion rate should be as estimated above.

REFERENCES

R. Briggs, *Astron. J.*, in press, 1962.

H. Cohen, *G. R. D. Research Notes*, **28**, USAF, 1960.

W. Crozier, *J. Geophys. Res.*, **65**, 2971, 1960.

— ibid, **66**, 2793, 1961.

A. Dollfus, in *Planets and Satellites*, (ed. Kuiper), U. of Chicago, 1961.

M. Dubin, *Planet Space Sci.*, **2**, 121, 1960.

— *J. Geophys. Res.*, **66**, 2592, 1961.

G. Hawkins and E. Upton, *Astrophys. J.*, **128**, 727, 1958.

A. Hibbs, *J. Geophys. Res.*, **66**, 371, 1961.

P. Hodge and R. Wildt, *Geochim et Cosmochim Acta*, **14**, 126, 1958.

— and F. Wright, *Nature*, **195**, 269, 1962.

O. Komissarov, T. Nazarova, L. Neugodov, S. Poloskov, and L. Rusakov. *J. Amer. Rocket Soc.*, **29**, 742, 1959.

T. Laevastu and O. Mellis, *J. Geophys. Res.*, **66**, 2507, 1961.

H. La Gow and W. Alexander, *NASA Technical Notes*, D-**488**, 1960.

C. Mc Cracken, *Res. Found.*, Oklahoma Univ., **2**, 65, 1960.

P. Millman and M. Burland, *Sky and Tel.*, **16**, 222, 1957.

E. Öpik, *Irish Astron. J.*, **5**, 14, 1958.

E. Pettit, in *Planets and Satellites* (ed. Kuiper), U. of Chicago, 1961.

R. Soberman and L. Della Lucca, *GRD Research Notes*, **72**, USAF, 1961.

— and C. Hemenway, ibid, **71**, 1961.

E. Thiel and R. Schmidt, *J. Geophys. Res.*, **66**, 307, 1961.

F. Whipple, *Vistas in Astronautics*, vol. II, Pergamon Press, 1959.

— *Nature*, **189**, 127, 1961.

— « Meteoritic Erosion in Space », in press, 1962.

24. — PHOTOMETRY OF THE INFRARED SPECTRUM OF VENUS, 1-2.5 MICRONS (*)

GERARD P. KUIPER
The University of Arizona, Tucson, Arizona, U. S. A.

1. INTRODUCTION

The spectrum of Venus beyond the photographic range has been investigated with resolutions of about 250 up to 1.8 μ (Kuiper, 1948), 80 up to 2.5 μ (Kuiper, 1947), and about 30 for the range 8-14 μ (Sinton, 1962). Recently Gebbie, Delbouille, and Roland (1962) recorded the region 1.2-2.5 μ with an interferometer and obtained a spectral resolution similar to that used by Kuiper. Some inconsistencies are apparent between these provisional interferometer results and the earlier direct tracings.

From time to time during the past decade, the writer had attempted to improve on his 1948 results with the prism spectrometer but no distinct progress was made until a grating spectrometer was built which allowed increased resolution without undue loss of light. With it, the Venus spectrum in the region 1.0-2.5 μ has been recorded in two series, one obtained with the 36-inch telescope of the Kitt Peak National Observatory in June 1962 (resolutions about 700 and 250) ; and one with the 82-inch telescope of the McDonald Observatory in August 1962 (resolutions about 1500 and 800). The Kitt Peak series was supplemented with matching solar comparison runs, so that precise photometric determinations of the Venus absorptions could be made. The McDonald series was calibrated with lunar spectra for the regions 1.1-1.4 and 2.0-2.5 μ, and stellar spectra for the remaining regions ; these spectra by their nature do not have the highest precision for defining the continuous spectrum. The wavelengths of the telluric

(*) A somewhat expanded version of this paper will be published as *Communications of the Lunar and Planetary Laboratory No. 15.*

absorptions were taken from the McMath-Hulbert Observatory Atlas (1950).

The spectral records obtained are photometric since the intensity scales are known to be strictly linear. The absorption depths and equivalent widths could therefore be taken directly from the spectra.

Nearly forty absorption bands were found in the Venus spectrum between 1.0-2.5 μ. All of these without exception could be attributed to CO_2. A survey of possible CO_2 bands showed that all bands up to a certain intensity that should be present in the Venus spectrum are indeed present. Several bands due to $^{13}CO_2$ have been identified as well as a number of « hot » CO_2 bands. Some weaker features shown in both the laboratory spectra and in Venus and apparently due to CO_2, have been left unidentified. One fairly strong band, at $\lambda = 2.15$ μ, appeared to be outside the scheme of permitted transitions of $^{12}CO_2$, and is attributed, not to the $2\nu_3$ band of $^{12}C^{16}O^{16}O$, which is forbidden, but to its heavy oxygen, ^{18}O, isotopic companion, $^{12}C^{18}O^{16}O$. which is permitted. Because the principal band is forbidden the isotopic band can be observed with unusual freedom from interference.

2. The Kitt Peak Spectra

Some of the original records obtained, with wavelength marks added, are reproduced photographically in Figures 1-3.

The resolution of the spectra is not the same for the two intervals 1.0-1.8 μ and 1.9-2.5 μ. In each case the spectrometer was used in slitless form to minimize intensity fluctuations due to seeing or guiding. The planetary disk was about 0.80 illuminated, with the narrow dimension 10″ in width. The spectrometer was turned such that this narrow dimension served as the entrance slit. With the Kitt Peak 36-inch telescope, f/15 Cassegrain, this means that the equivalent slit was 2/3 mm, or actually slightly less because of the curvature of the planet and the uneven illumination of the

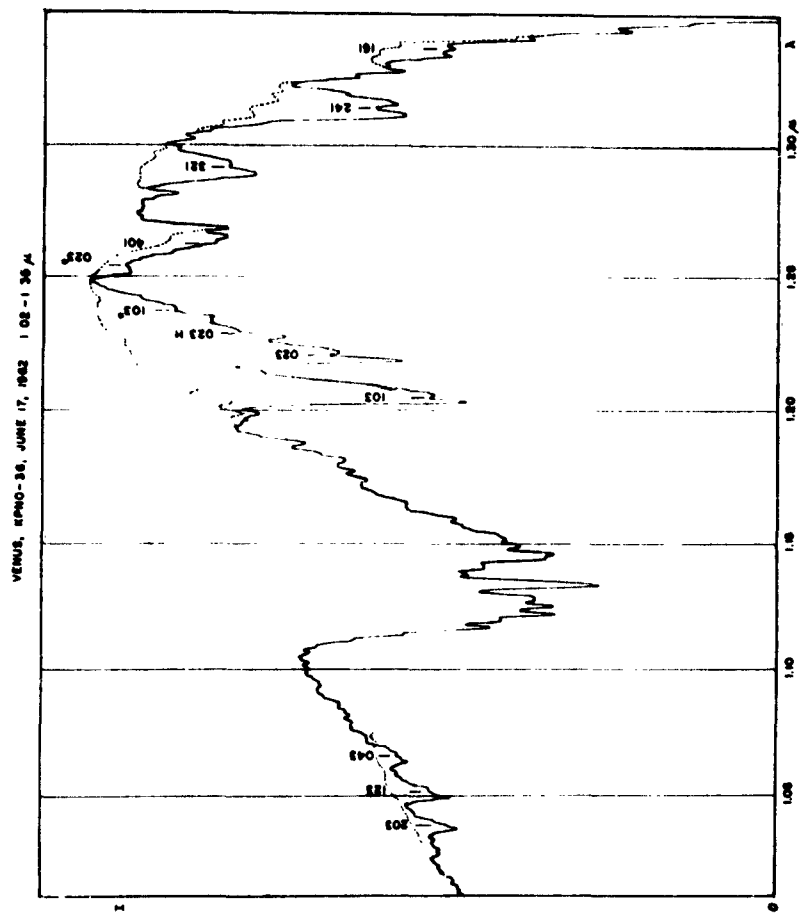

Fig. 1. - Venus Spectrum, Kitt Peak National Observatory, 1.02--1.35 μ. Upper curve outlines solar comparison spectrum where it differs from the Venus spectrum. Classification of CO_2 bands follows Table 1, with short lines marking band origins (not heads); *H* designates « hot » bands; asterisks, isotopic $^{13}CO_2$ bands. Grating 1.6 μ, filter Corning 2540 ($\lambda > 1.0\,\mu$), cell width 0.25 mm, slitless spectrum, time constant (τ) 12 seconds. Declination of Venus + 21°49′, hour angle 1^h49^m — 2^h44^mW (in all spectral records the time runs from *right* to *left*).

disk. The cell width used for 1.0-1.8 μ was 0.25 mm, so that the resolution in the spectrum was about $\sqrt{(2/3)^2 + (0.25)^2} = 0.7$ mm, that is, $\lambda/\Delta\lambda \cong 700$ at 1.6 μ, giving $\Delta\lambda \cong 25$ Å. From 1.9-2.5 μ a 1.0 mm cell was used to improve the signal/noise ratio. This means

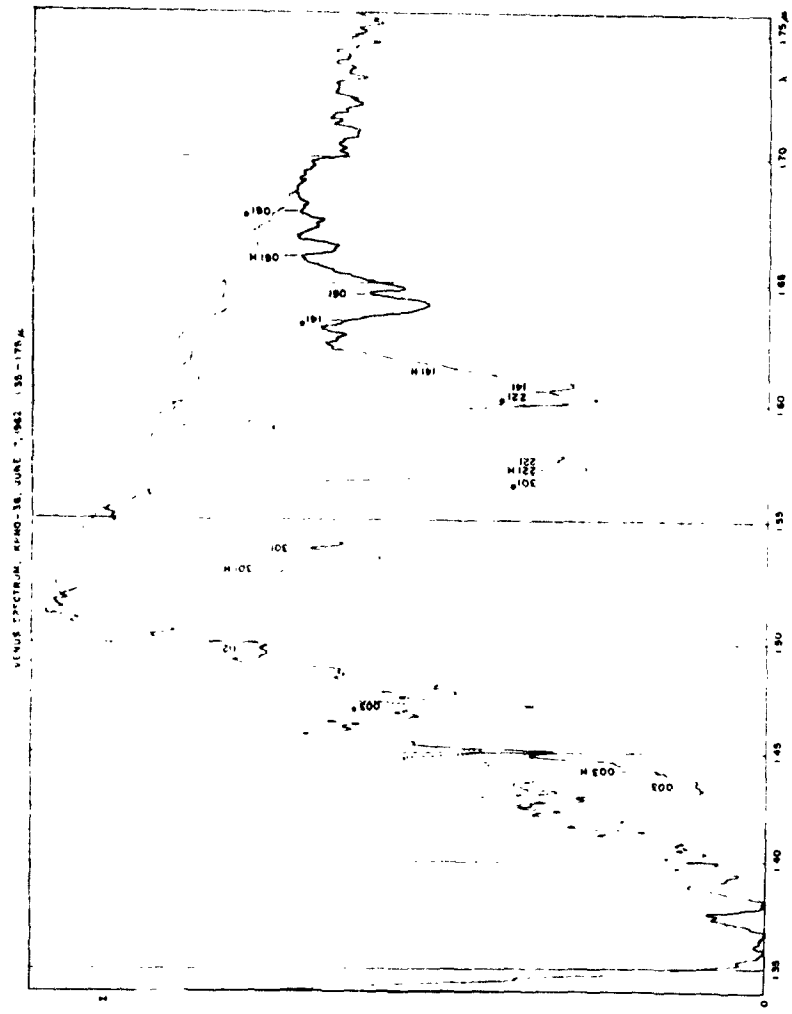

Fig. 2. — Venus Spectrum, 1.35 – 1.75 μ. Upper curve is solar comparison spectrum. CO_2 bands as in Table 1. Same parameters as Figure 1 except H. A. 0^h27^m – 1^h40^mW.

that the spectral resolution there was about $\sqrt{(2/3)^2 + 1} = 1.2$ mm ; and because the dispersion with the 2 μ grating is only 0.4 times that of the 1.6 μ grating, the overall spectral resolution was $(1.2/0.7)/0.4 = 4.3$ times poorer ; i. e., about 100 Å or $\lambda/\Delta\lambda = 200$ at 2.2 μ.

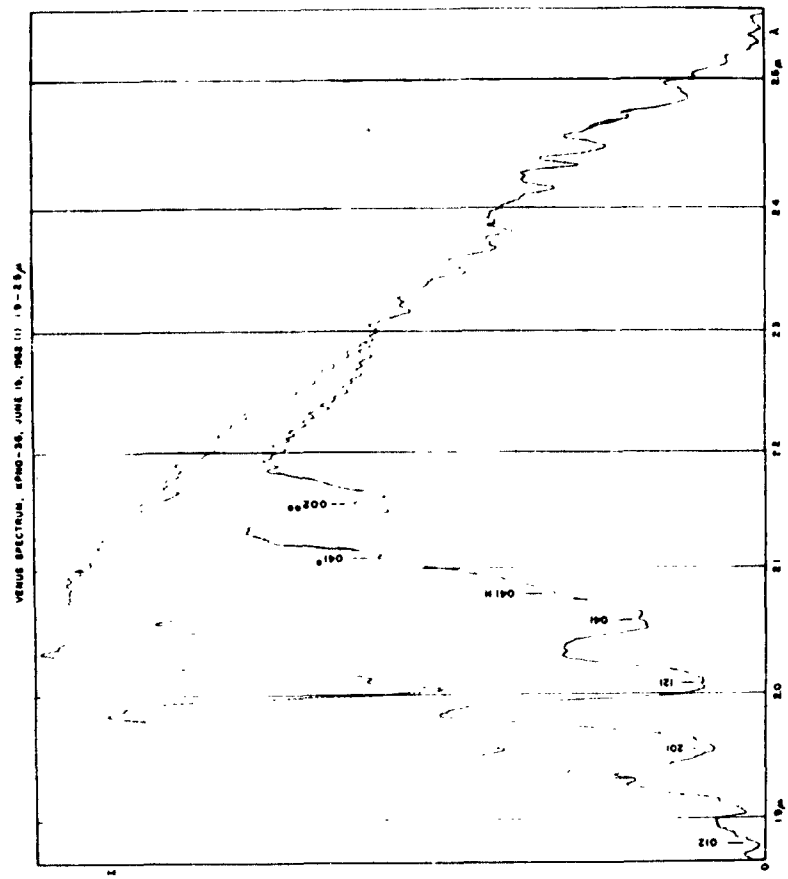

Fig. 3. – Venus Spectrum, 1.87 – 2.55 μ. Upper curve is solar comparison. Grating 2 μ, filter λ > 1.9 μ, cell 1.0 mm, slitless, τ = 6 seconds. Decl. –22°20′, H. A. 0^{h}46^m – 1^{h}11^{m}W.

The chief interest of the spectra is, of course, to obtain a listing and identification of the planetary absorptions. The Kitt Peak records are clear for all but a few of the CO_2 bands marked. These marginal cases are recognized more easily with the increased resolution obtained in the McDonald spectra. There is no evidence for an absorption between 2.3 and 2.4 μ which could be attributed to CO. Between 2.2-2.3 μ there is in Figure 3 a feature which, if real, indicates a local color difference between Venus and the Sun, attributable to the Venus cloud cover. The question arises whether

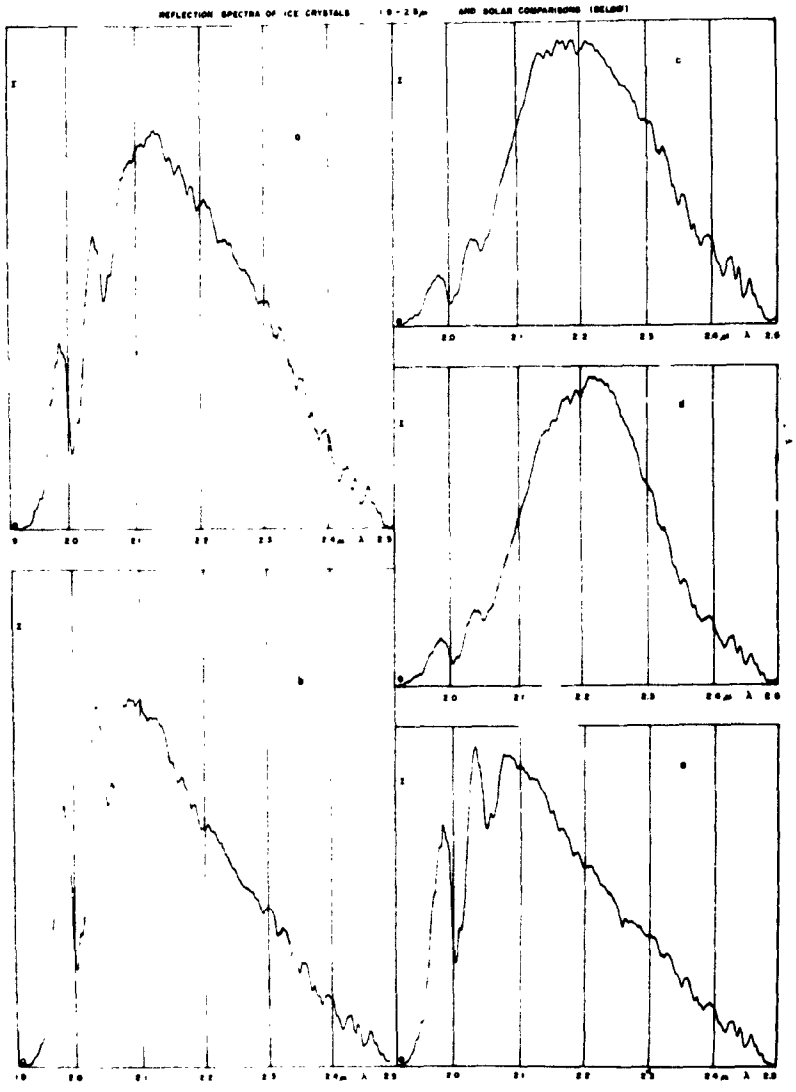

Fig. 4*a*. — Spectra 1.9 — 2.5 μ of sunlight reflected by a layer of small H_2O crystals formed on a dark metal plate cooled by contact with a block of frozen CO_2. Tucson, September 11, 1962, early afternoon ; (*a*) crystal layer about 1 mm thick ; (*b*) solar comparison as reflected by MgO block ; (*c*) frost layer about 3 mm thick ; (*d*) frost layer about 4 mm thick ; (*e*) second solar comparison.

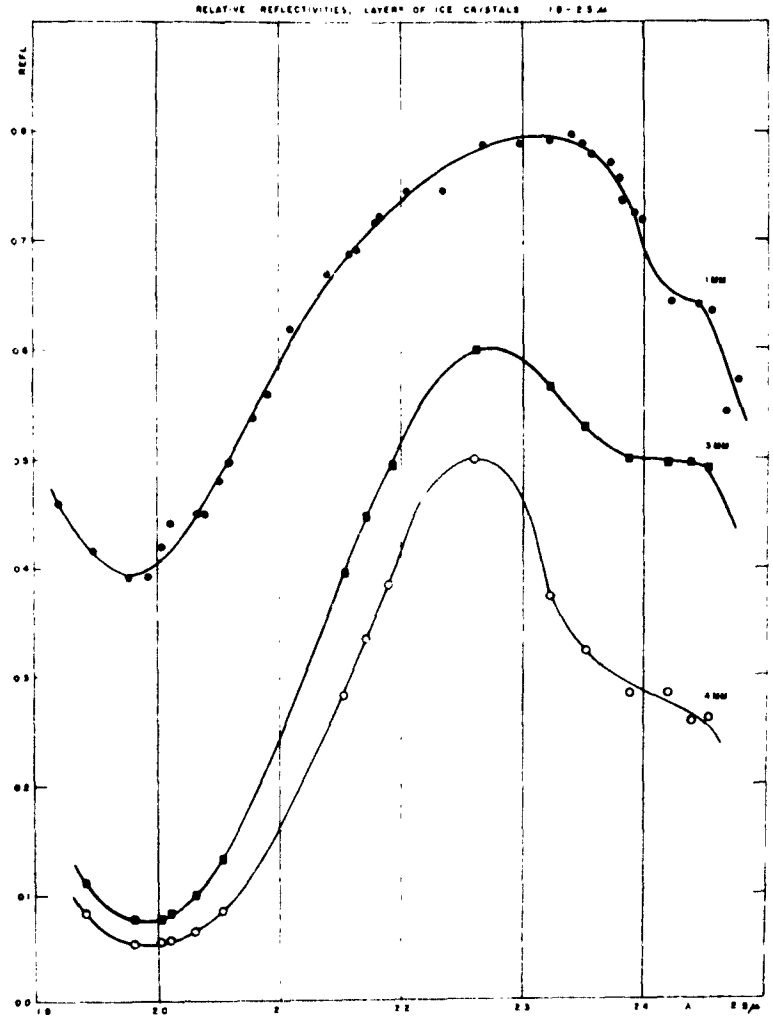

Fig. 4*b*. — Reflectivities of layers of ice crystals 1 mm, 3 mm, and 4 mm thick, derived from Figure 4*a*. The *shapes* of the curves are fixed by the ratios measured from Figure 4*a* ; the scales of the ordinates cannot be found from the measures and have been chosen somewhat arbitrarily.

this feature could be due to small ice crystals in the Venus atmosphere. To check this, reflection spectra were obtained of sunlight shining on small H_2O crystals formed on a dark metal plate in contact with a block of frozen CO_2 and matched with the solar

spectrum reflected from a MgO block. The records are reproduced in Figure 4*a*, and the ratios between the ordinates measured at identifiable wavelengths are plotted in Figure 4*b*. It is seen that the ice causes a wide absorption band from 1.9-2.1 μ, and another one beyond 2.4 μ, increasing in strength with increasing depth of the layer; but that the absorption is least between 2.2-2.3 μ, where the suspected Venus absorption occurs. The ice band is displaced from the corresponding vapor band by about + 0.1 μ, in accordance with previous laboratory work. It is seen from Figure 3 that the Venus spectrum from 1.88-1.93 μ and the peak at 1.98 μ are incompatible with the ice band at 2.0 μ shown in Figure 4*b*.

3. The McDonald Spectra

A 0.1 mm cell was used throughout so that the equivalent spectral resolution was 0.32 mm making $\lambda/\Delta\lambda \cong 1500$ at 1.6 μ, or $\Delta\lambda \simeq 10$ Å. Inspection of the spectral records confirms this value. For 1.9-2.5 μ the 2 μ grating was used again but with the same narrow cell and slit as used at 1.6 μ; the resolution was thus about 25 Å and $\lambda/\Delta\lambda$ about 800-1000. However, the smaller ratio signal/noise in this region caused some loss of effective resolution which could be recaptured only by the use of a longer time constant and a slower scanning rate.

Because solar comparison runs with the spectrometer on or off the 82-inch telescope could not be made during a full-time night program, the calibration of the McDonald spectra on Venus had to be left somewhat incomplete. Nighttime lunar spectra were taken for the 1.18-1.35 and 1.9-2.5 μ regions, which served as a first approximation. They were obtained by throwing the lunar image on the spectrometer slit far out of focus so that the unavoidable drift of the image would cause only comparatively small and smooth spurious intensity changes in the recorded spectrum. Stellar spectra served as additional checks on the strengths of the telluric absorptions.

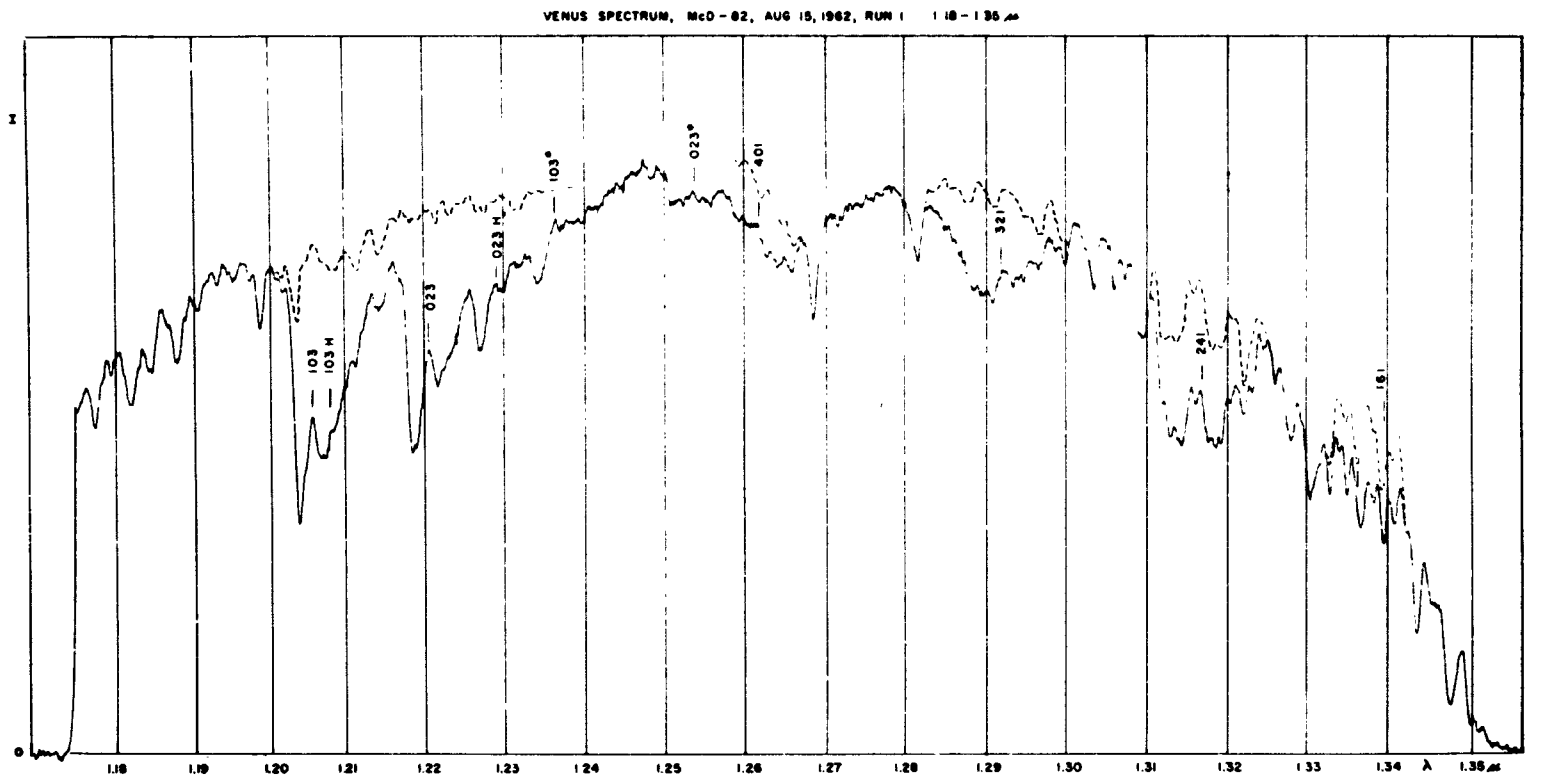

Fig. 5. — Venus Spectrum, McDonald Observatory, 1.18 — 1.35 μ. Dashes outline lunar comparison spectrum (which was somewhat disturbed from 1.24 — 1.26 μ by relocation of the lunar image). CO_2 bands as in Figure 1. Grating 1.6 μ, filter Corning 2540, cell 0.25 mm, slit 0.3 mm, τ = 3 seconds. Decl. — 3°39′, H. A. 0^h34^mE — 0^h01^mW. Dome temperature (T) 23°C, humidity (H) 36 %.

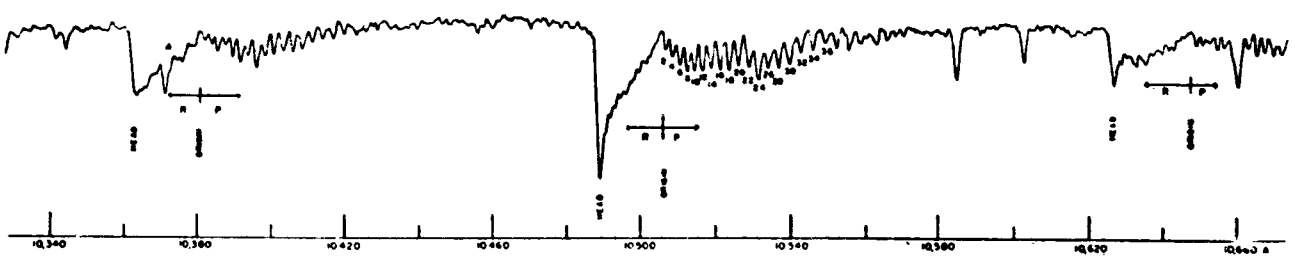

Fig. 6. — Microphotometer tracing of the (043, 123, 203) bands of CO_2 in Venus (Chamberlain and Kuiper, 1956).

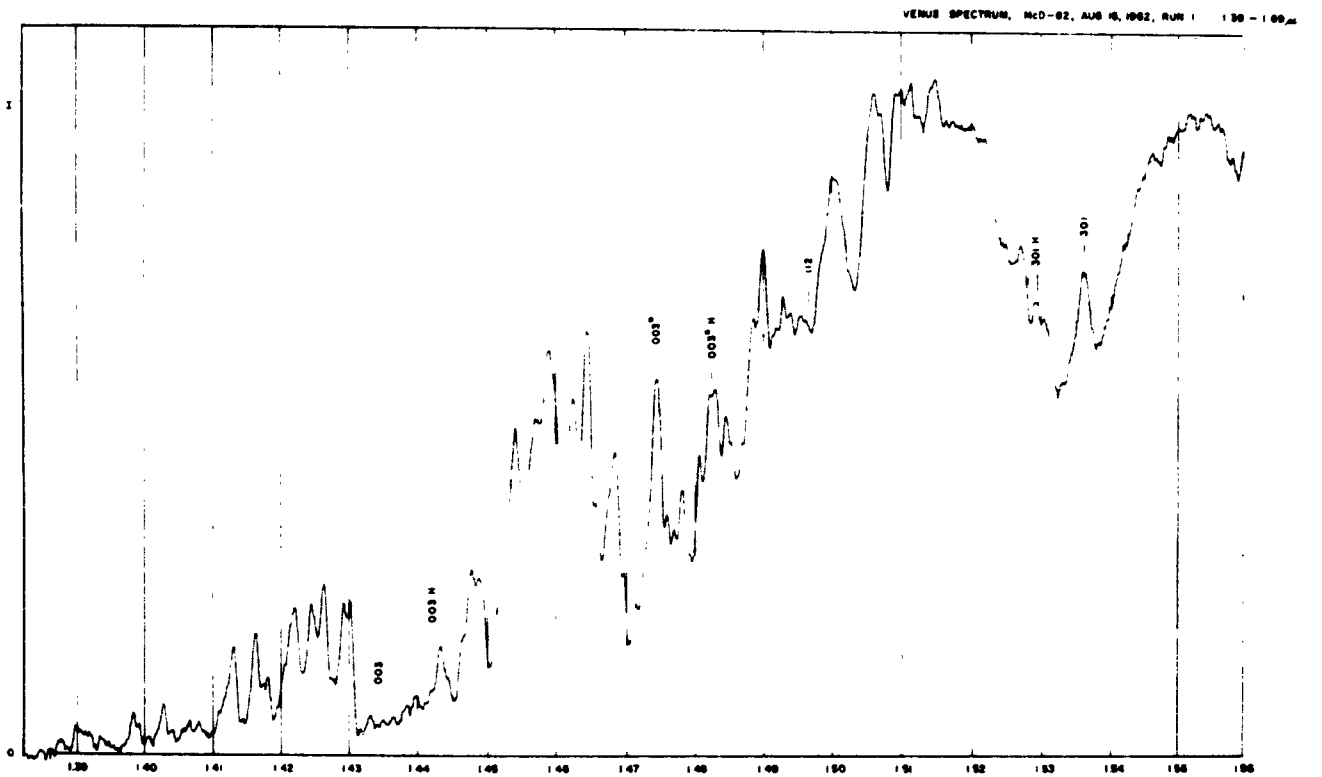

Fig. 7*a*. — Venus Spectrum, 1.39 — 1.69 μ. Part 1. The CO_2 bands are the same as marked in Figure 2. Grating 1.6 μ, filter 2540, cell width 0.10 mm, spectrometer slit 0.3 mm, τ = 6 seconds. Decl. — 3°41′, H. A. 0^h39^m — 1^h40^m W. T = 24°C, H = 34 %.

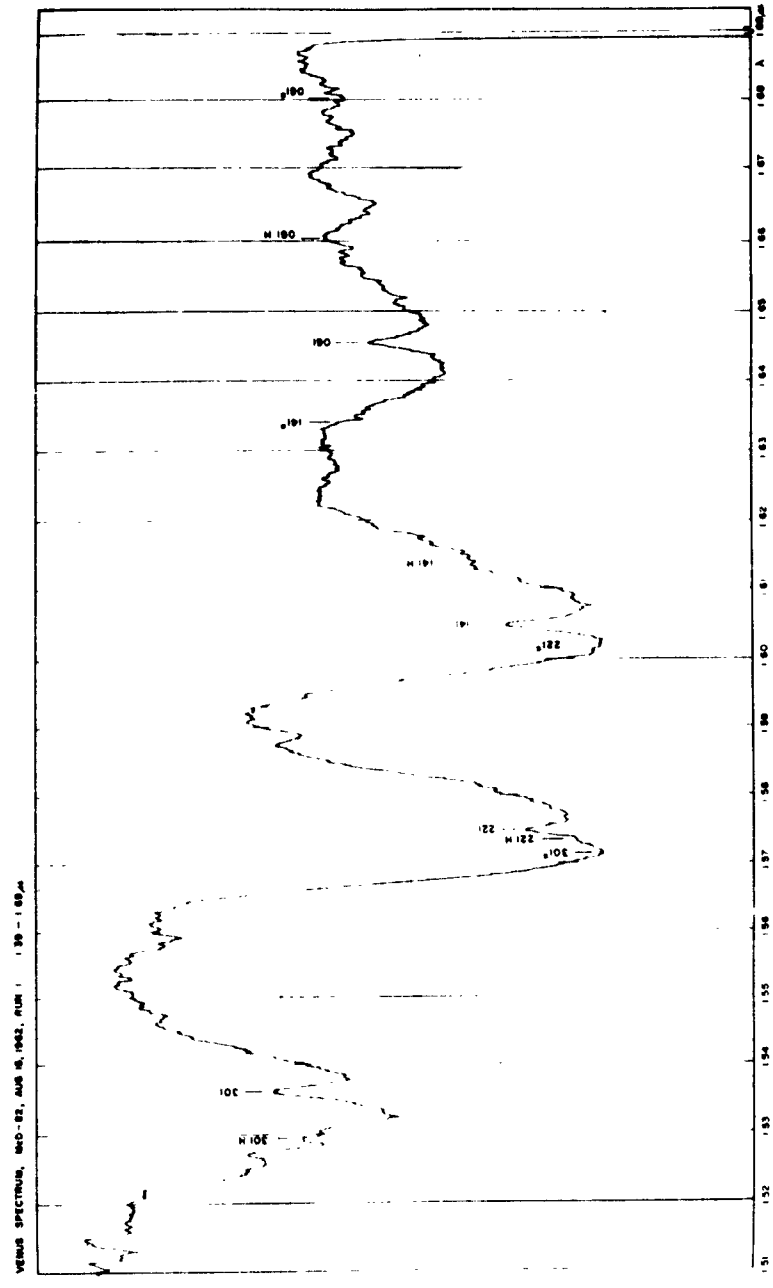

Fig. 7*b*. — Venus Spectrum, 1.39 — 1.69 μ, Part 2.

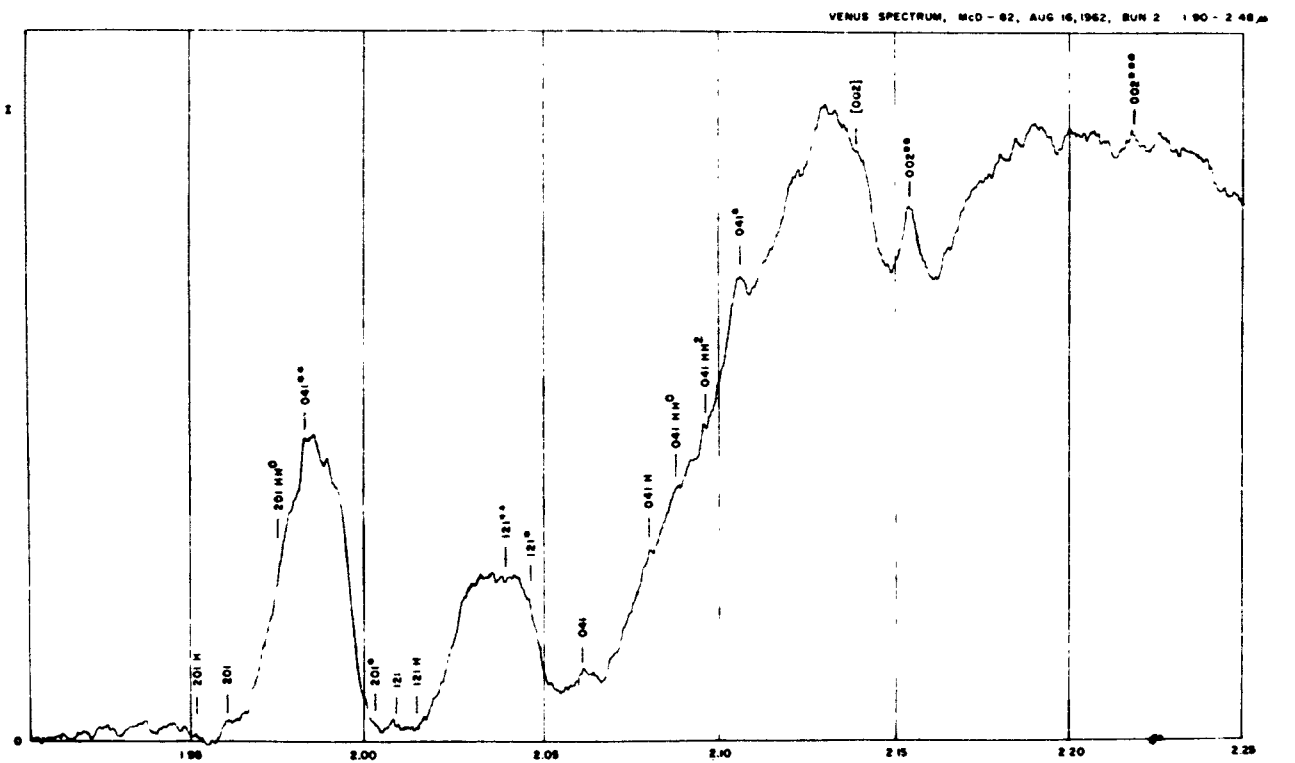

Fig. 8. — Venus Spectrum, 1.90 — 2.48 μ. The CO_2 bands are the same as marked in Figure 3. Grating 2 μ, filter > 1.9 μ, cell 0.1 mm, slit 0.3 mm, τ = 12 seconds. Decl. — 4°10′, H.A. 1^h08^m — 2^h02^mW. T = 23°C, H = 38 %.

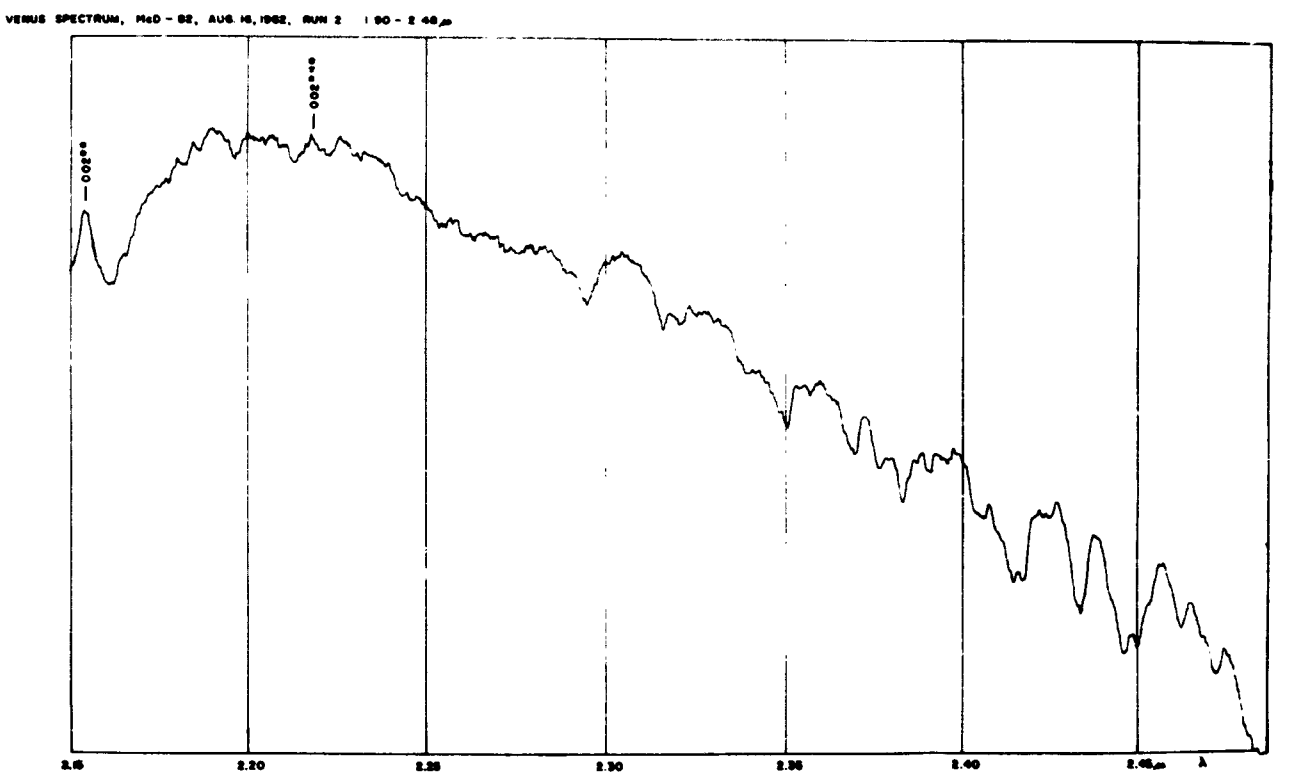
VENUS SPECTRUM, McD - 82, AUG. 16, 1962, RUN 2 1.90 - 2.48μ
2.00
2.20
2.30
2.40
λ

Fig. 8*b*

The comparatively high summertime humidity of the McDonald atmosphere is apparent from the strong telluric absorptions. Additional spectral runs of Venus must be made in a dry winter atmosphere. Nevertheless, the present McDonald spectra add information on the wavelengths of the new bands, and are therefore included here.

Figure 5 shows one of two consecutive runs on the region 1.18-1.35 μ. For the sake of completeness an earlier microphotometer tracing of the three bands between 1.0 and 1.1 μ is added in Figure 6. This tracing also clarifies the characteristic band shape for the Σ-Σ transitions in the IR tracings, such as the depths and widths of the R and P branches and the position of the origin, the point indicated in the tracings.

Comparison of Figures 5 and 1 shows that the added resolution has clarified, e. g., the location of the band heads near 1.23 μ. A small difference exists in the shapes of the (401) band where it merges with the telluric O_2 band at 1.268 μ. An earlier record with the same resolution but higher noise level than Figure 1 was available. On that record the (401) band has intermediate strength.

Figure 7 covers the region 1.39-1.69 μ. The structure of slopes of the strong CO_2 bands is now more clearly brought out, allowing more certain identification (Sec. 4).

The region 1.9-2.5 μ was recorded in two consecutive runs on August 16, 1962, with different time constants, one of which is reproduced in Figure 8. It is found that the three CO_2 bands marked in this region by Gebbie, *et al.* (1962) are not real.

4. Interpretation and Laboratory Spectra

Several prominent absorption bands in the Venus spectrum have been known to be due to CO_2. They arise from the ground state and contain the *odd* overtones of ν_3, namely ν_3, $3\nu_3$ and $5\nu_3$, with various combinations of ν_1 and ν_2 in Fermi resonance, leading to the formation of diades, triades, tetrades, pentades, etc. These

transitions are of the type $\Sigma_u^+ \leftarrow \Sigma_g^+$, not involving a change in the azimuthal quantum number, l, and have two branches, R and P, which are resolved in our spectra, though the finer rotational structure is not. In addition, there are much weaker permitted transitions from the ground state of the type $\Pi_u \leftarrow \Sigma_g^+$, involving the *even* overtones of ν_3 and such combinations of ν_1 and ν_2 making $(v_2 + v_3)$ odd, even combinations of $(v_2 + v_3)$ being forbidden. These transitions involve a change by l of the azimuthal quantum number and cause the presence of a Q branch, which on our spectra makes the band look like a narrow feature with a pointed minimum.

A list of the permitted transitions from the ground state was constructed on the basis of the energy diagram given by Herzberg and Herzberg (1953, p. 1041). Comparison of this list with the very detailed laboratory investigations by Courtoy (1957, 1959) showed that additional bands must be present in the Venus spectrum arising from the Π_u (01^10) level and possibly even the higher levels, Σ_g^+ 02^00, Σ_u^- 10^00 and Δ_g 02^20. These bands, conveniently called the «hot» and «doubly-hot» bands, are of interest in connection with a possible determination of the temperature of the Venus atmosphere.

Accordingly, we have collected in Table 1 all transitions for $\lambda < 2.5\ \mu$ that seemed relevant or promising, including the strongest isotopic bands of $^{13}CO_2$ and $^{12}C^{18}O^{16}O$. The latter were taken from the laboratory studies by Courtoy (1959), as were the wavelengths of all other relevant bands listed by him. Some permitted bands, such as 212, were dropped when no evidence for their presence was found in Venus or the laboratory.

The complexity of the CO_2 spectrum is sufficient to prevent the classification of the weaker bands without laboratory spectra showing the rotational structure. In particular, the hot bands and the isotopic bands appear as satellites of the principal bands arising from the ground state of the $^{12}CO_2$ molecule, often present as disturbing features in the wings. Thus $\nu_2 + 3\nu_3 - \nu_2$ at $\lambda = 1.442\ \mu$ occurs in the P branch of $3\nu_3$; and the triade 201, 121, 041 at $\lambda = 1.961$, 2.009, and 2.060 μ has the companion bands $2\nu_1 + \nu_2 +$

TABLE 1

CO_2 *Bands observed in Venus and Laboratory*

(λ and ν_0 of band origin)

$\lambda(\mu_0)$ (vac.)	λ (Head) (Air)	ν_0	Transition*	Symbol Used In Figures
0.7165	0.7158	13957	12^05	125
0.7828	0.7820	12774.7	10^05	105
0.7891	0.7883	12672.3	02^05	025
0.8698	0.8689	11496.4	00^05	005
0.8749	0.8736	11430	01^15-01^10	005H
0.9267 :		10790.4 :	14^03	143
0.9244 :		10817.2 :	22^03	223
1.0383	1.0362	9631.4	20^03	203
1.0508	1.0488	9517.0	12^03	123
1.0651	1.0627	9389.0	04^03	043
1.2055	1.2030	8294.0	10^03	103
1.2082	1.2055	8276.8	11^13-01^10	103H
1.2206	1.2177	8192.6	02^03	023
1.2291	1.2262	8136.0	03^13-01^10	023H
1.2364		8089.0	$10^03(^{13}C)$	103*
1.2530		7981.2	$02^03(^{13}C)$	023*
1.2606		7932.9	21^12	212
1.2625		7920.5	40^01	401
1.2929		7734.3	32^01	321
1.294		7730	33^11-01^10	321H
1.3116		7624.0	25^11-01^10	241H
1.3169		7593.5	24^01	241
1.3367		7481.3	$24^01(^{13}C)$	241*
1.3404		7460.4	16^01	161
1.3729		7284.0	08^01	081
1.4342		6972.5	00^03	003
1.4420		6935.0	01^13-01^10	003H
1.444		6925	$00^03(^1O)$	003**
1.4749		6780.1	$00^03(^{13}C)$	003*
1.4826		6745.0	01^13-$01^10(^{13}C)$	003*H
1.497		6681	11^12	112
1.507 :		6636 :	03^12	032

$\lambda(\mu_0)$ (vac.)	λ (Head) (Air)	ν_0	Transition*	Symbol Used In Figures
1.5299		6536.4	$31^{1}1\text{-}01^{1}0$	301H
1.5377		6503.0	301	301
1.5714		6363.6	$301(^{13}C)$	301*
1.5733		6356.2	$23^{1}1\text{-}01^{1}0$	221H
1.5753		6347.8	$22^{0}1$	221
1.6021		6241.9	$22^{0}1(^{13}C)$	221*
1.6057		6227.9	$14^{0}1$	141
1.6139		6196.1	$15^{1}1\text{-}01^{1}0$	141H
1.6341		6119.6	$14^{0}1(^{13}C)$	141*
1.6458		6075.9	$06^{0}1$	061
1.6609		6020.8	$07^{1}1\text{-}01^{1}0$	061H
1.6802		5951.5	$06^{0}1(^{13}C)$	061*
1.8812		5315.7	$01^{1}2$	012
1.8900		5291.1	$02^{2}2\text{-}01^{1}0$	012H
1.9348		5168.6	$01^{1}2(^{13}C)$	012*
1.9457		5139.4	$22^{2}1\text{-}02^{2}0$	$201HH^{2}$
1.9519		5123.2	$21^{1}1\text{-}01^{1}0$	201H
1.9609		5099.6	$20^{0}1$	201
1.9754		5062.4	$22^{0}1\text{-}02^{0}0$	$201HH^{0}$
1.9831		5042.5	$04^{0}1(^{18}O)$	041**
2.0035		4991.3	$20^{0}1(^{13}C)$	201*
2.0089		4977.8	$12^{0}1$	121
2.0140		4965.3	$13^{1}1\text{-}01^{1}0$	121H
2.0388		4904.8	$12^{0}1(^{18}O)$	121**
2.0461		4887.3	$12^{0}1(^{13}C)$	121*
2.0603		4853.6	$04^{0}1$	041
2.0800		4807.7	$05^{1}1\text{-}01^{1}0$	041H
2.0872		4791.2	$20^{0}1\ ^{18}O)$	201**
2.0875		4790.5	$06^{0}1\text{-}02^{0}0$	$041HH^{0}$
2.0971		4768.5	$06^{2}1\text{-}02^{2}0$	$041HH^{2}$
2.1061		4748.0	$04^{0}1(^{13}C)$	041*
2.1238		4708.5	$05^{1}1\text{-}01^{1}0(^{13}C)$	041*H
2.1341		4685.7	$06^{0}1\text{-}02^{0}0(^{13}C)$	$041*HH^{0}$
2.1397		4673.6	$06^{2}1\text{-}02^{2}0(^{13}C)$	$041*HH^{2}$
2.140		4673	$[00^{0}2]$	[002]
2.1556		4639	$00^{0}2(^{18}O)$	002**
2.220		4505	$00^{0}2(^{18}O,^{13}C)$	002***
...		...	$01^{1}2\text{-}01^{1}0(^{18}O)$	002**H

(*) From ground state Σ_g^+ $00^{0}0$ unless stated otherwise.

$\nu_3 - \nu_2$, $\nu_1 + 3\nu_2 + \nu_3 - \nu_2$, and $5\nu_2 + \nu_3 - \nu_2$, at $\lambda = 1.952\,\mu$, $2.014\,\mu$, and $2.080\,\mu$, respectively. To bring out this correspondence we have used the symbols 201 H, 121 H, and 041 H for these companions in Table 1 and in the figures. Doubly-hot companions are indicated by HH^0 or HH^2, depending on the quantum number l of the lower state.

The isotopic bands are marked by asterisks. Since the $^{12}C/^{13}C$ ratio on the Earth is 89, and the $^{16}O/^{18}O$ ratio about 500, a single asterisk was used for ^{13}C isotopes and a double asterisk for ^{18}O isotopes. The equivalent intensity of single-asterisk bands may therefore be down by two orders of magnitude, the intensity of the double asterisk bands by nearly three. On the assumption that the strength of the hot bands on Venus is down by one order of magnitude or more, the combination *H was retained, but not **H or *HH.

As Courtoy has found and as may be seen from Table 1, the positions of the ^{18}O isotopic bands with respect to the ^{16}O bands are irregular, unlike the positions of the ^{13}C or $^{18}O^{18}O$ isotopes, where nearly constant ratios with the wavelengths of the principal bands are maintained.

The symbols in the last column of Table 1 have been transferred to the figures where this appeared warranted. It is found that the Venus absorption can be satisfactorily accounted for by the permitted transitions listed in Table 1 with one major exception, the band at $2.15\,\mu$. In addition, a few minor features remain unexplained. Both the $2.15\,\mu$ band and the minor features are present in the laboratory spectra of CO_2, reproduced in Figures 9-11, and are therefore attributed to CO_2.

No permitted $^{12}CO_2$ or $^{13}CO_2$ transition appears to fit the $\lambda = 2.15\,\mu$ band. Accordingly, the possibility of its being a pressure-induced dipole or a quadrupole transition of $^{12}CO_2$ was examined. The forbidden $2\nu_2$ transition from the ground state fits the observed position $\nu_0 = 4643 \pm 5$ rather closely, but not precisely, the computed position being $\nu_0 = 4673$. Dr. Herzberg suggested to the

writer that the observed band may rather be identified as the $^{12}C^{18}O^{16}O$ isotopic $2\nu_3$ band, which is permitted because of the asymmetry of the molecule. The writer had already estimated that the observed band was roughly 10^3 times weaker than expected from a fully permitted $2\nu_3$ band. This ratio is of the same order of magnitude as the $^{18}O/^{16}O$ ratio. Dr. Herzberg has computed the position of this isotopic band at $\nu_0 = 4639$, in full accord with the observations. This identification is of special interest because the unhampered observation of what would be normally a very weak isotopic companion is made possible because the principal band is forbidden and the isotopic $2\nu_3$ transition exceptionally strong.

The minor CO_2 features in the 1.6 μ region will be examined in greater detail in future laboratory investigations. It will also be attempted to resolve the rotational structure of the isotopic $2\nu_3$ band to settle the identification.

The Venus spectra give information on (a) the CO_2 abundance on Venus ; (b) the $^{13}C/^{12}C$ ratio ; (c) the $^{18}O/^{16}O$ ratio ; (d) the hot bands.

(a) The CO_2 abundance is found from the relation between Venus band strength and laboratory band strength. The discussion is limited to bands of the type $\Sigma_g^+ - \Sigma_u^+$ (i. e., the ν_3, $3\nu_3$, and $5\nu_3$ series) in the spectral region 1.20-1.66 μ for which the Venus photometry (Figures 1 and 2) is satisfactory and the range of available band intensities suitable. So far only the laboratory spectrum reproduced in Figure 9 was used for the comparison. The equivalent width of twelve $^{12}CO_2$ bands and one $^{13}CO_2$ band were determined from planimeter measures on the original tracings, with allowance for the mean ordinate of the interpolated continuum at each absorption band.

The equivalent widths of the CO_2 bands, in Angstrom units and divided by λ^2, are recorded in Table 2 and plotted in Figure 12. It is noted that the strong bands are stronger in the laboratory spectrum while the reverse is true for the weaker bands. This is explained by the reduced penetration into the Venus atmosphere

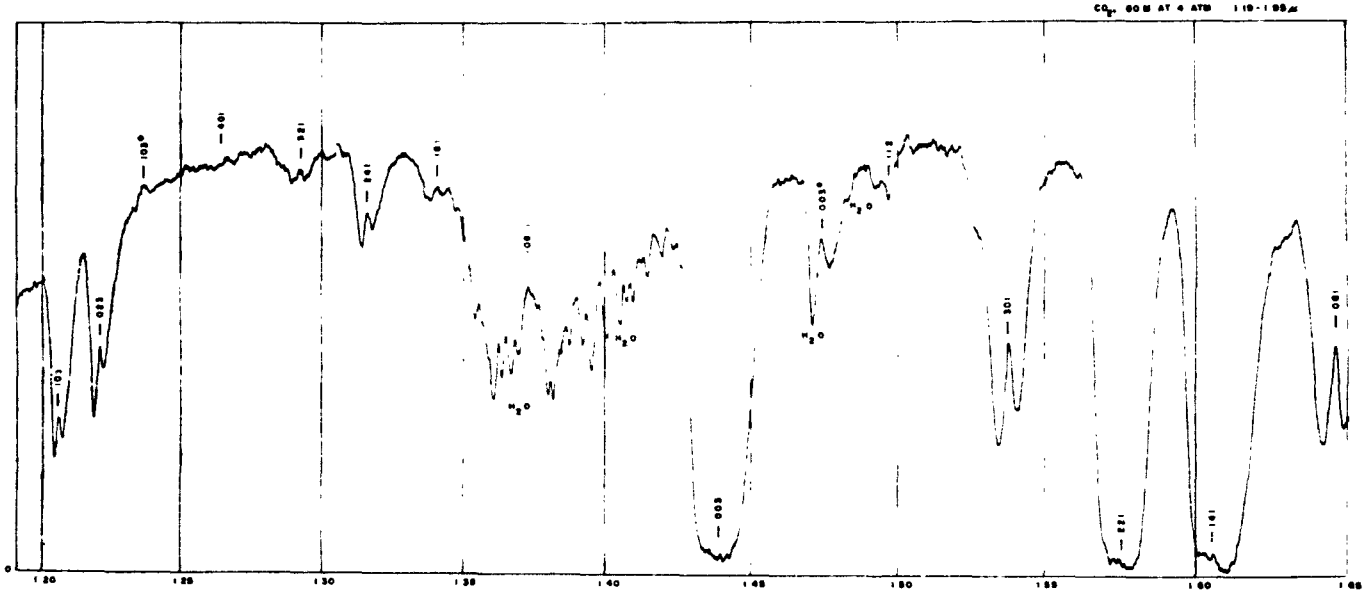

Fig. 9. — CO_2 Spectrum, 80 meter path at 4 atm., 1.19—1.95 μ, grating 1.6 μ, filter 2540, cell 0.25, slit 0.3 mm, $\tau = 6$ seconds. The CO_2 is contaminated with water vapor. The zero level 1.85 — 1.95 μ is raised by second-order 0.92 — 0.97 μ passing the 2540 filter.

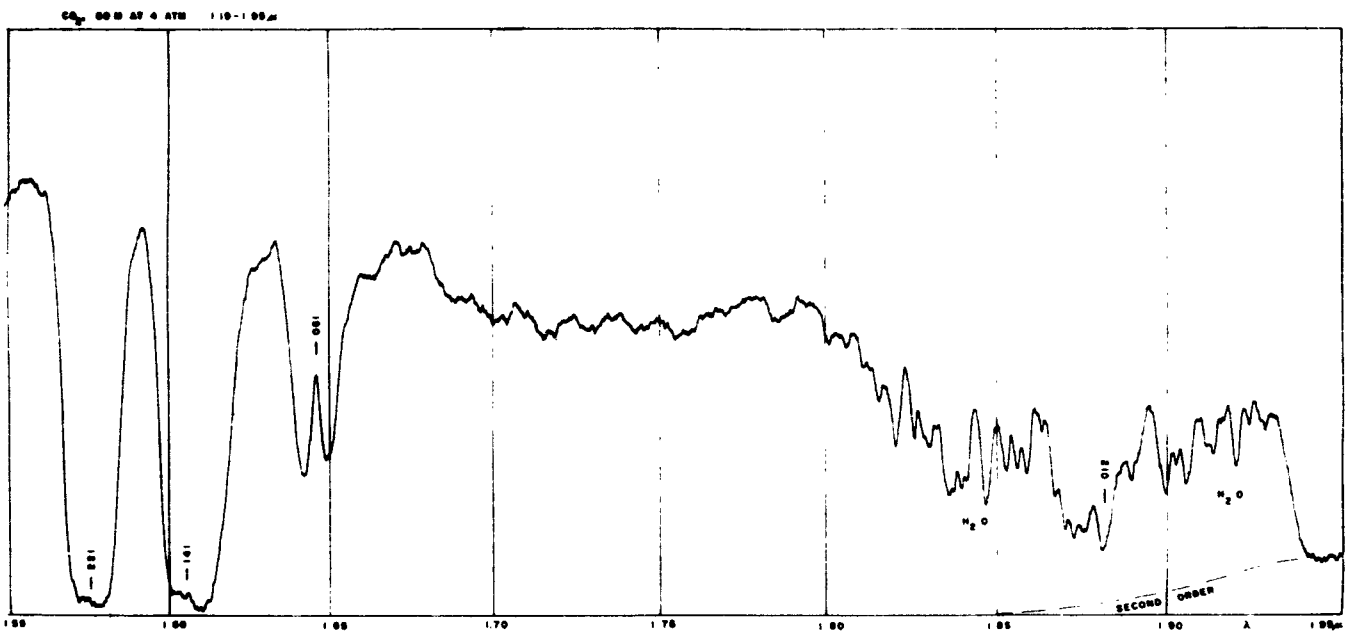
201
101
100
H_2O
010
H_2O
SECOND ORDER
1.55
1.60
1.65
1.70
1.75
1.80
1.85
1.90
λ

Fig. 9b

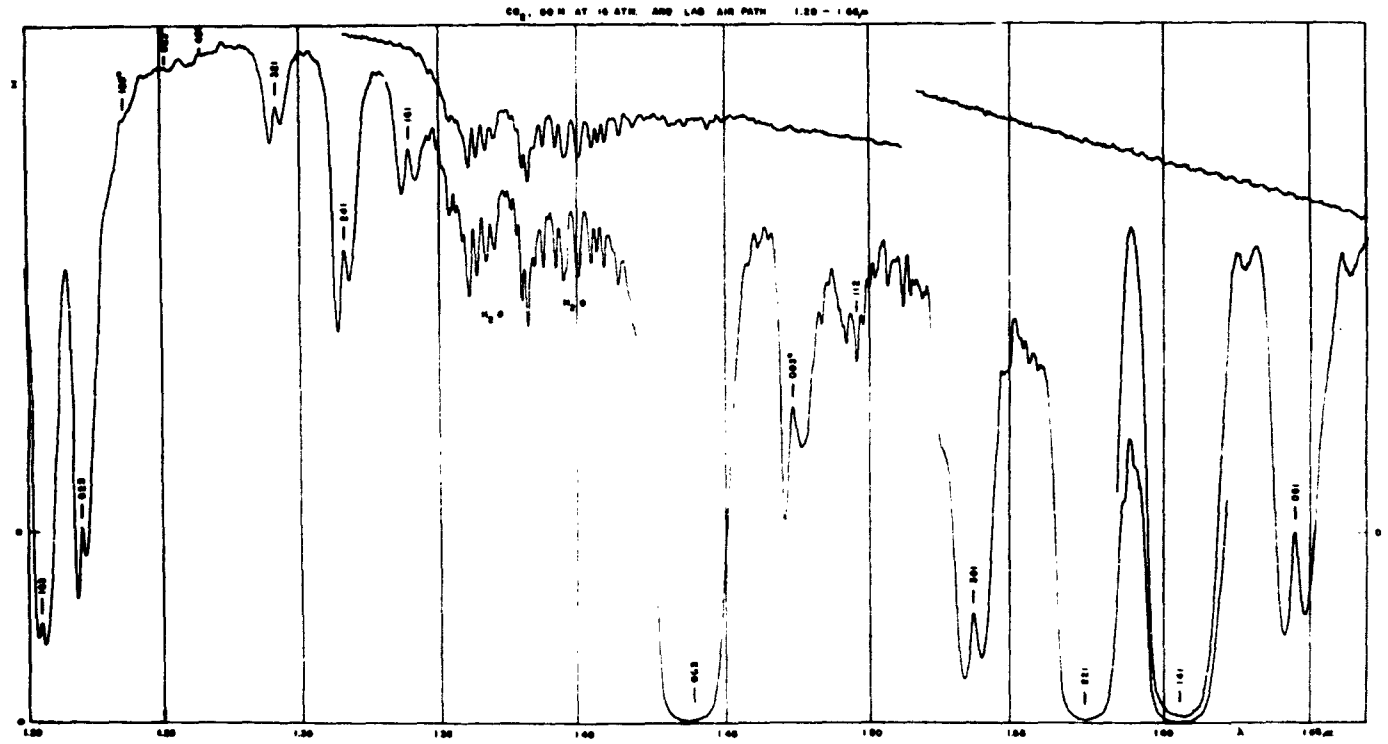

Fig. 10. — CO_2 Spectrum, 80 meter path at 16 atm., 1.20 — 1.66 μ, grating 1.6 μ, filter 2540, cell 0.25, slit 0.25 mm, $\tau = 2\,^1/_2$ seconds. The CO_2 has a small H_2O content, but much less than in Figure 9. The H_2O absorption contributed by the $4\,^1/_2$ meter air path in the laboratory and the spectrometer is shown in the upper curve. The zero intensity level of the air path spectrum is different from the bottom line for the interval 1.20 — 1.51 μ only, and is indicated in the margins.

TABLE 2

Equivalent Widths in Wavelength and Frequency Units of CO_2 Bands in Venus and Laboratory Spectra

Band	EW (Venus) (A)	EW/λ^2 (A/μ^2)	EW (Lab.) (A)	EW/λ^2 (A/μ^2)
103	42	29	43	30
023	30.3	20	33	22
401	6.7	4.2	1	0.7
321	16	9.6	8	5
241	27	15.6	18	10.4
161	15	8.4	5	2.8
003	129	63	204	99
003*	34	16	33	15
301	61	26	87	37
221	122	49	180	72
141	154	60	235	91
061	72.5	27	103	38
002**	77	16.5	59	12.7

with increasing band strength. The limiting penetration for very weak bands may be used to define the observable depth of the Venus atmosphere. The curve must pass through the origin and is presumably not tangent to the y-axis since the opacity of the Venus atmosphere in red and infrared light between the CO_2 bands is not due to Rayleigh scattering but to a diffuse cloud of particles, so that, as seen in the weakest bands, the cloud layer on Venus limits the penetration. The slope of the curve near the origin is about 6, so that for weak bands the Venus spectrum corresponds to about 6 $\times$ 80 meters $\times$ 4 atm. of CO_2 or about 2 km atm. of CO_2. Since the line absorptions must add linearly for very weak bands, this result should be independent of pressure. However, since the strength of the CO_2 absorption on Venus is variable, both with phase and from day to day, and even region to region on the planet (Kuiper, 1952), the amount of CO_2 found only applies to the date of observation. A somewhat improved value of the CO_2

abundance may be found from comparison with Figure 10, which has 4 times the CO_2 equivalent of Figure 9. The weakest bands in Venus are still somewhat stronger than in Figure 10, indicating a pathlength of about 2 km atm. for Venus.

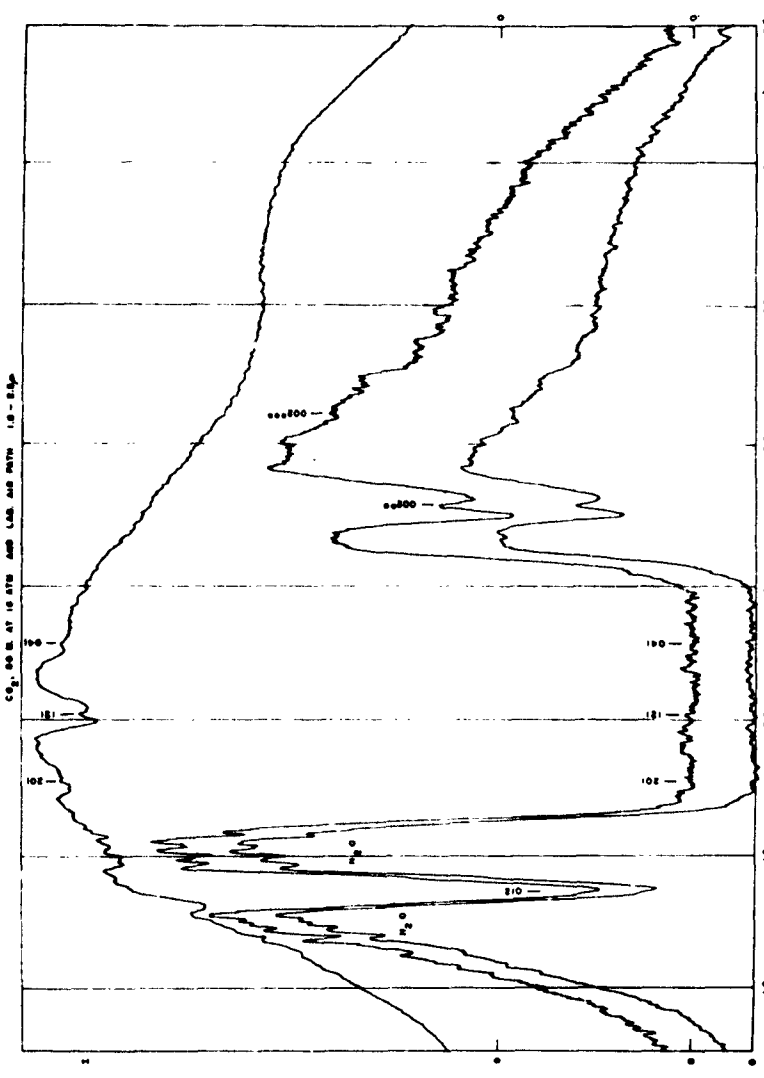

Fig. 11. —CO_2 Spectrum, 80 meter path at 16 atm., 1.8 — 2.5 μ, Grating 2 μ, filter $\lambda > 1.8$ μ, cell 0.25 mm, slit 0.28 mm, $\tau = 6$ seconds. The H_2O and CO_2 absorptions contributed by the 4½ meter air path in the laboratory and the spectrometer is shown in the upper curve. The zero intensity levels are indicated in the margins.

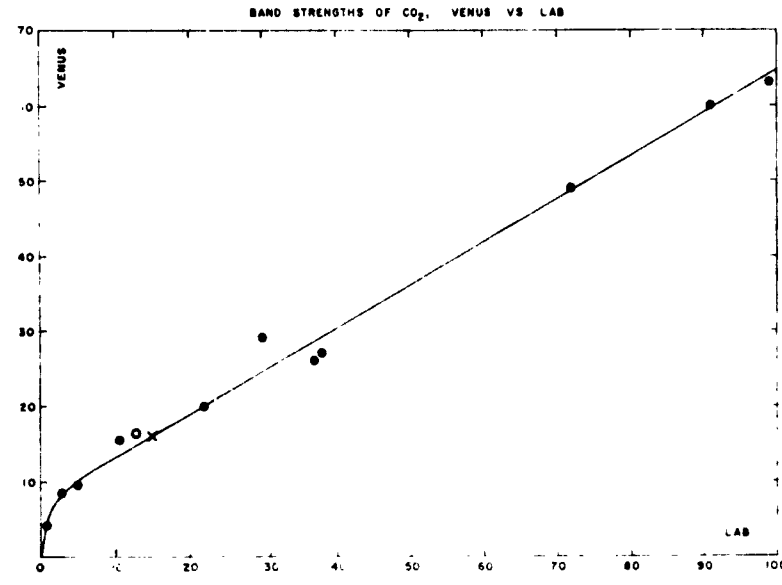

Fig. 12. — Relation between CO_2 band strength in the Venus spectrum (June 17, 1962) and a laboratory spectrum similar to that reproduced in Figure 9. Data taken from Table 2. Each band is represented by a dot. The isotopic band $3\nu_3$ of $^{13}CO_2$ is shown as a cross ; the $2\nu_3$ band of $^{12}C^{18}O^{16}O$ is shown as an open circle.

(b) Considerable interest attaches to the abundance ratio $^{13}C/^{12}C$ on Venus. On the Earth this ratio is 1/89 and in some R stars it reaches a value as high as 1/5, and in some N stars 1/2 (McKellar, 1960). The equilibrium ratio attained if the carbon-nitrogen cycle of nuclear energy production were operative to the exclusion of other processes is 1/4 if the H abundance is greater than the C abundance (Caughlan and Fowler, 1962). Fowler, Greenstein, and Hoyle (1962) attribute the terrestrial isotope ratio to an incomplete nuclear process occurring in the T Tauri stage of the solar nebula. On this basis the isotope ratio on Venus might be higher, owing to the greater proximity to the sun.

The $3\nu_3$ isotopic band at $\lambda = 1.47\ \mu$ is the strongest available for measurement and was included in Table 2 and Figure 12. Laboratory spectra with increased pathlengths and improved defi-

nition will allow an extension of the discussion to other isotopic bands shown in Venus, particularly 103, 023, 061, and 041.

The determination of the isotope ratio from direct comparisons between the two $3\nu_3$ bands is difficult since the equivalent pathlength in the Venus atmosphere depends on the band strength itself. This is not true for laboratory spectra since the pathlength traversed is necessarily the same for both weak and strong bands. However, if the isotopic band fits the relationship of Figure 12, it means that the isotope ratio is the same on Venus as on the Earth. If not, the equivalent laboratory intensity of the isotopic Venus band may be found and the abundance ratio determined from laboratory tests with different pathlengths.

It is seen that the $3\nu_3$ isotopic band falls closely to the curve of Figure 12. The estimated precision of the Venus measure is $\pm$ 10 per cent, corresponding to $\pm$ 20 per cent in equivalent width in the laboratory intensity, as found from the local slope of the curve. Within this precision, the isotope ratio of $^{13}C/^{12}C$ is the same on Venus and on the Earth. Better precision should be obtainable in a very dry winter atmosphere.

(c) The oxygen isotope ratio $^{18}O/^{16}O$ can, at present, be determined from one band only, $2\nu_3$, the other bands being too badly blended (cf. Table 1 and the spectral records reproduced). The method used is the same as for the carbon isotope ratio, i. e., differentially, Earth vs. Venus. The equivalent width of the band has been measured on Venus spectrum Figure 3 and a laboratory spectrum taken under similar conditions as Figure 9. The resulting data have been entered in Table 2 and Figure 12. It is seen that the isotope ratio is equal to that on the Earth within the error of measurement.

(d) The hot bands arising from the ν_2 level Π_u (01^10) are quite prominent in the Venus spectrum wherever they are relatively free from blending. The best case is 023 H, observed in the laboratory by Herzberg and Herzberg (1953, p. 1038), and well shown in the

Venus spectrum on our Figures 1 and 5. It is better separated from the corresponding cold band than its twin member of the diade, 103, also well shown in the spectral plate reproduced by Herzberg and Herzberg. A separate laboratory study will be made to calibrate the Venus 023 H band in terms of temperature. It is seen by comparison with Figures 9 and 10 that the Venus temperature is

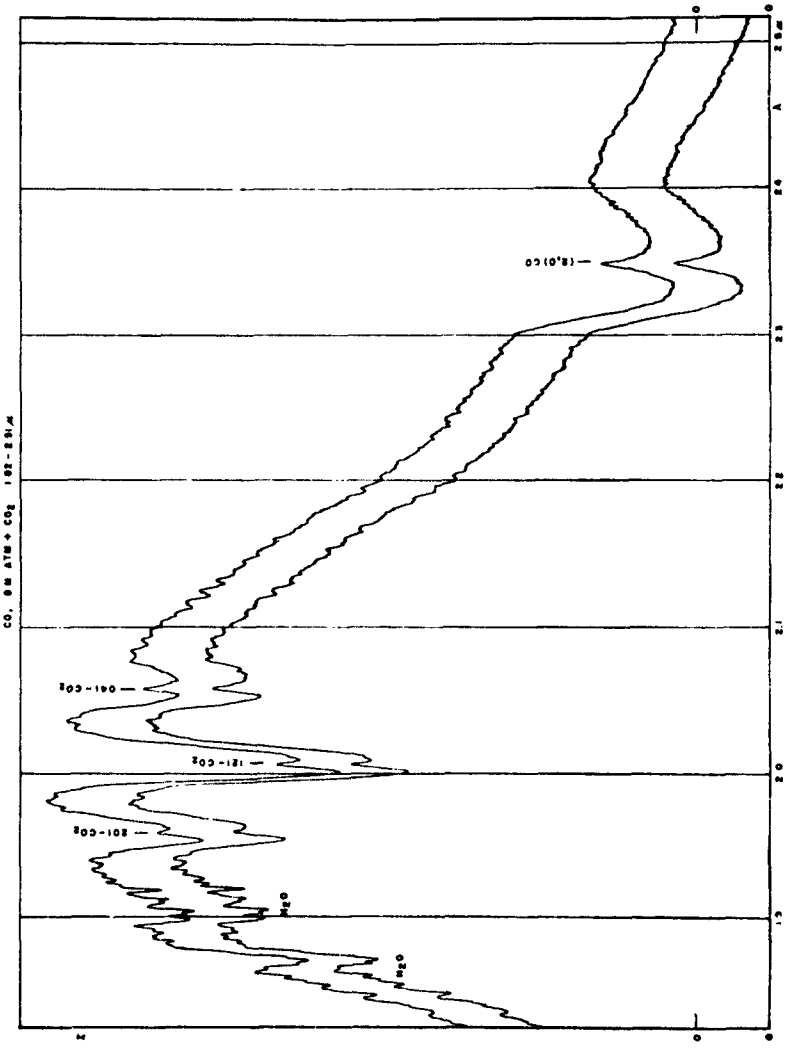

Fig. 13. — Two consecutive runs, $CO + CO_2$, pathlength 8 meters, pressure 1 atm., 1.82 — 2.51 μ, grating 2 μ, filter $\lambda > 1.8$ μ, cell 0.25 mm, slit 0.3 mm, $\tau = 3$ seconds. The CO is contaminated with CO_2 and water vapor.

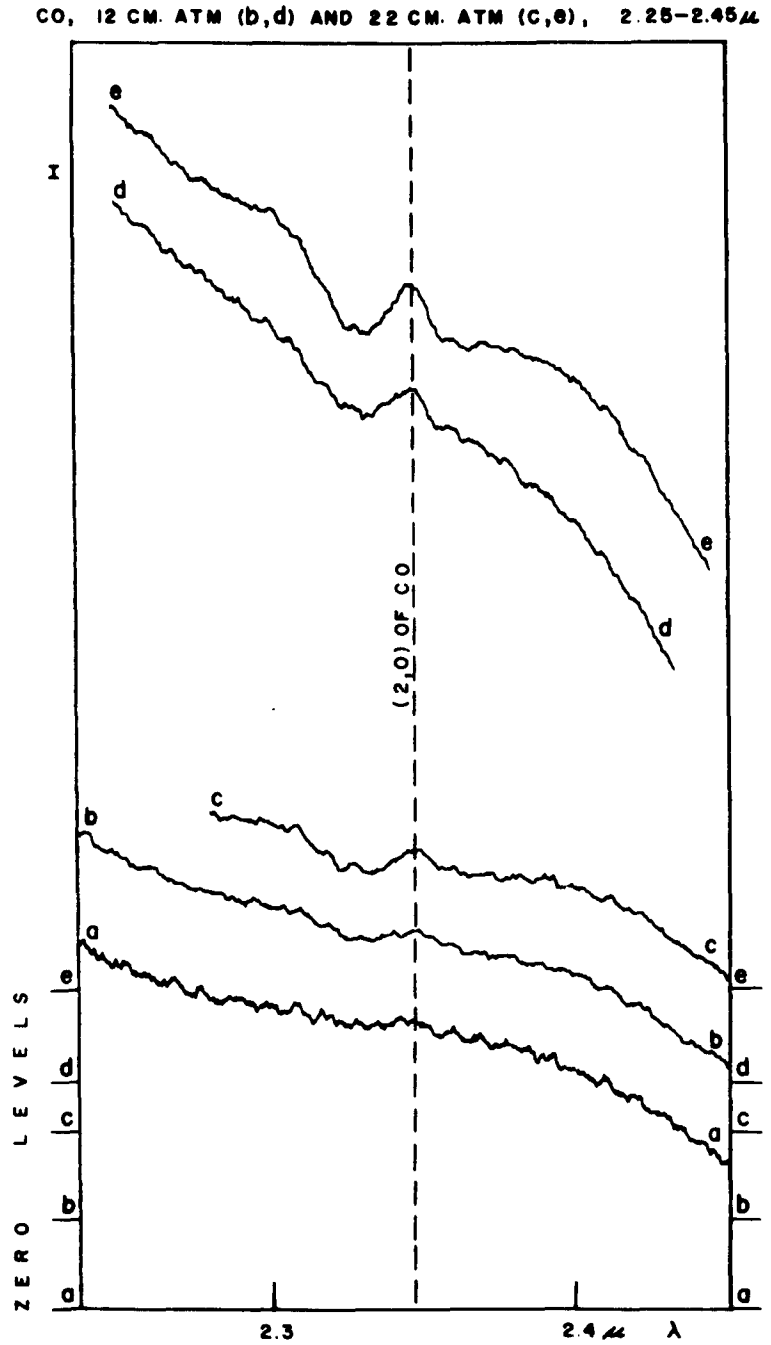

Fig. 14. — Laboratory spectra of CO at 1 atm., 2.25 — 2.45 μ, 2 μ grating, filter 0.3 mm, slit 0.25 mm cell. Same scale as Figure 13. (*a*) blank run ; (*b*) 12 cm, $\tau = 6$ sec. ; (*c*) 22 cm, $\tau = 6$ sec. ; (*d*) 12 cm, $\tau = 12$ sec. ; (*e*) 22 cm, $\tau = 12$ sec.

considerably higher than the laboratory temperature of about 300° K.

(e) Of interest also is the determination of the maximum CO content in the Venus atmosphere, consistent with the spectra here reproduced. The necessary laboratory comparisons are given in Figures 13 and 14. From the observed strength of the $\lambda = 2.35\ \mu$ band of CO, the upper limit of 10 cm atm. NPT is found, implying an approximate upper limit of one-fourth of this amount for a vertical column in the Venus atmosphere. The (3,0) band of CO was also observed in the laboratory but it is an order of magnitude weaker than the (2,0) band and has, moreover, the same wavelength as the ($22^0 1$) band of CO_2 at 1.575 μ. It is therefore unsuitable for the determination of the CO content of Venus. The upper limit of about 3 cm for the Venus atmosphere represents an advance of about 30 x in the threshold limit compared to the author's 1948 result.

In the more extensive publication referred to (*Communications of the Lunar and Planetary Laboratory No. 15*) the related problem is considered of the relative efficiency of a one-channel infrared spectrometer as used here and a Michelson-type interferometer. It is shown that the advantages claimed for the interferometer for stellar sources are not real.

Acknowledgments. — The writer is much indebted to the administration of the Kitt Peak National Observatory for the use of the 36-inch telescope for several short observing runs culminating in the June, 1962, run; and to the Director of the McDonald Observatory for the generous use of the 82-inch telescope during several recent sessions, particularly the August, 1962, run. Dr. G. Herzberg, Head of the Division of Physics, National Research Council of Canada, greatly assisted our program by the loan of the 2-meter multiple-path absorption tube (used in the work by Courtoy referred to); and suggested the identification of the $\lambda = 2.15\ \mu$ band of CO_2. Messrs. Binder and Cruikshank assisted

in the Kitt Peak runs and in obtaining the laboratory spectra and Mr. Binder also in the two-week McDonald run. Mrs. Fabe and Mrs. Scheer prepared the spectra records for reproduction. I am indebted to Dr. A. B. Meinel for a discussion on the energy diagram of CO_2 and to Mr. T. Owen, who made the installation of the Herzberg absorption tube and developed the accessories ; he also assisted in the laboratory runs. The earlier phases of this work were carried out under Air Force Contract No. AF 19(604)7260 ; the later phases were sponsored by the National Aeronautics and Space Administration (NsG 161-61).

REFERENCES

CAUGHLAN, G. R., and FOWLER, W. A., *Ap. J.*, **136**, 453, 1962.

COURTOY, C.-P., *Can. J. Phys.*, **35**, 608, 1957.

COURTOY, C.-P., *Ann. Soc. Sci. de Bruxelles*, **73**, 5-203, 1959.

FOWLER, W. A., GREENSTEIN, J. L. and HOYLE, F., *Geophys. J.*, **6**, 148, 1962.

GEBBIE, H. A., DELBOUILLE, L. and ROLAND, G., *M. N.*, **123**, 497, 1962.

GEBBIE, H. A., ROLAND, G. and DELBOUILLE, L., *Nature*, **191**, 264, 1961.

HERZBERG, G. and HERZBERG, L., *J. Opt. Soc. America*, **43**, 1037-1044, 1953.

KUIPER, G. P., *Ap. J.*, **106**, 252, Figs. 3 and 4, 1947.

KUIPER, G. P., *The Atmospheres of the Earth and Planets*, ed. G. P. Kuiper (1st ed. ; Chicago : University of Chicago Press), p. 331, 1948.

KUIPER, G. P., *ibid.*, 2d ed., pp. 370-371, 1952.

MCKELLAR, A., *Stellar Atmospheres*, ed. J. L. Greenstein (Chicago : University of Chicago Press), p. 579, 1960.

PLYLER, E. K., TIDWELL, E. D. and BENEDICT, W. S., *J. Opt. Soc. America*, **52**, 1017, 1962.

SINTON, W. M., *Planets and Satellites* (Chicago : University of Chicago Press), p. 433, Fig. 3 and references given there, 1961.

25. — INFRARED OBSERVATIONS OF VENUS

WILLIAM M. SINTON
Lowell Observatory, U. S. A.

This paper presents most of the infrared observations of Venus made by the author since 1958. They have been made within most of the transparent atmospheric « windows » between 1 and 13 μ. All observations have been made with the 42-inch Lowell reflector.

SPECTROSCOPIC STUDIES, 1 — 4 μ

The lithium fluoride prism spectrometer with liquid-nitrogen-cooled lead sulfide detector which has already been described [1, 2] has been used for spectra of the nearer planets. The spectrum of the Sun (Fig. 1) which was obtained by using an aluminum scatter plate [1], is useful for comparison with the spectrum of Venus for it represents the radiation impinging on a planet as well as giving ready reference to location and strengths of absorption bands imposed by the terrestrial atmosphere The radiation of Venus in the 1—4 μ region appears to be primarily reflected sunlight modified by absorption bands in the Venus atmosphere. One may obtain the absorptions characteristic of the planetary atmosphere merely by dividing the spectrum of Venus by the Sun's spectrum, both being taken with identical conditions such as air mass, atmospheric water vapor, and instrumental slit width.

Many bands of carbon dioxide designated by circles in Figure 2 are apparent in this region and have previously been discussed by Kuiper [3]. The band at 1.47 μ Figure 2 is worthy of note, in that it is produced by $C^{13}O_2$. It may eventually be possible to determine the C^{12} to C^{13} ratio from this band and the C^{12} bands when spectra of higher resolution are obtained. It is not possible now because of the severe interference by water-vapor absorption at 1.47 μ.

Carbon monoxide if present on Venus should produce absorp-

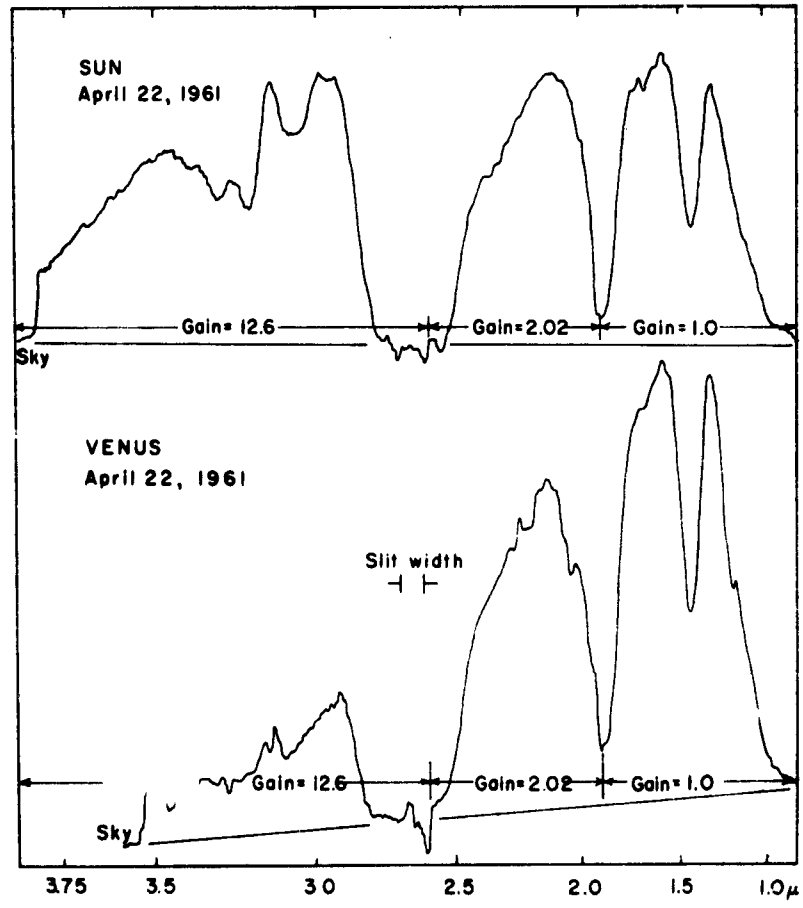

Fig. 1. — Spectra of Venus and the sun, which were obtained at low resolution in order to ascertain the spectrum of Venus relative to that of the sun.

tion in its 2 — 0 band at 2.345 μ. I have taken a number of spectra covering the region of the 2.345-μ band in an effort to determine the amount of CO present. Figures 2 and 3 show spectra of Venus having a resolution equal to 0.008 μ (15 cm^{-1}) at the wavelength of this band. The band, resolved into its P and R branches, appears to be present in these spectra. Figure 4 shows at the top the mean of 6 spectra of Venus which were obtained with a resolution of 0.013 μ and better signal-to-noise ratio. The lower curves of Figure 4 are laboratory spectra with 79 cm-atmo of CO at a pressure of 7.1 cm

of Mercury introduced into the path. There is some indication of the P and R branches of this band in the Venus spectrum, but the shape of the band agrees only poorly with the laboratory spectra. Though it seems definite that something is absorbing at this wavelength, it is not certain that it is carbon monoxide. The observations were made on February 24, 1961 when Venus had a phase angle, $i = 108^{\circ}$ and the slit during these observations approximately traversed the center of this crescent at 90°.

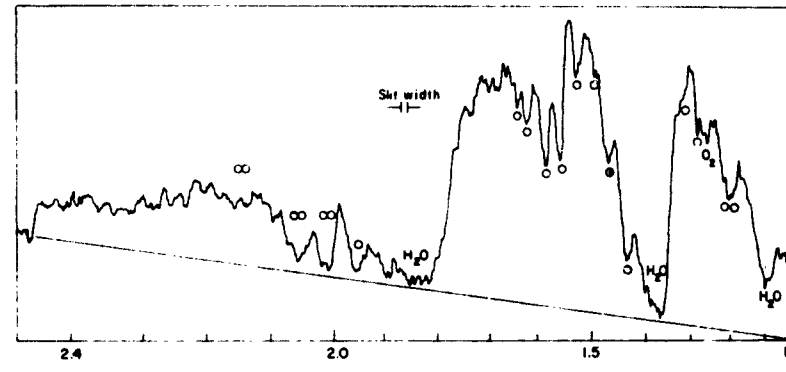

Fig. 2. — A spectrum of Venus obtained at high resolution and which illustrates the many CO_2 bands, indicated by circles, which are found.

At the time of the inferior conjunction of Venus with the Sun in 1961 it was possible to measure the effective temperature on the dark hemisphere of Venus by measuring the emission at 3.75 μ. The spectrometer was set at this wavelength and the slit's width and effective length were 1 mm, which corresponds to a square 35.3 seconds of arc on a side at the scale at the slit of the spectrometer. The observed effective temperatures of Venus and Mercury are given in Table I. Calibration was made by the difference in emission of a blackbody source at 35° C and the ambient temperature of the spectrometer (about 10° C). But during the first measurements on April 12, the calibration devices were not prepared and the reference measurements were made to the emission from my finger (assumed to be 28° C). Though this method of calibration may seem quite rough, it is emphasized that a 50 % error in the observed

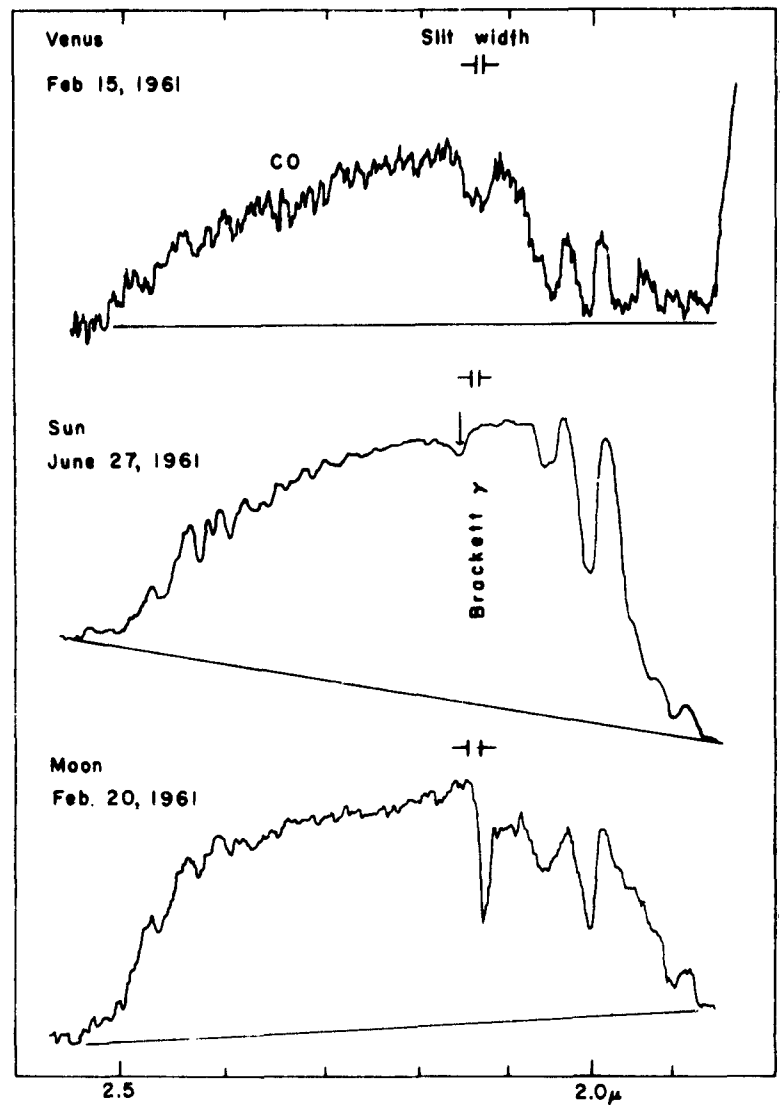

Fig. 3. — Spectra of Venus, sun, and the moon. The spectrum of Venus shows a band which may be produced by carbon monoxide. The sharp dip in the lunar spectrum was due to a guiding error.

Venus deflection or in the calibration deflection produces only a 5° error in the temperature of Venus.

The observed Mercury temperatures have been reduced to

subsolar temperatures by the method used by Pettit and Nicholson ([4]) and later by Strong and Sinton ([5]). This method of determining the subsolar temperature from the effective temperature for the entire disk assumes that the incident solar radiation is distributed over the surface according to the cosine of the angle between

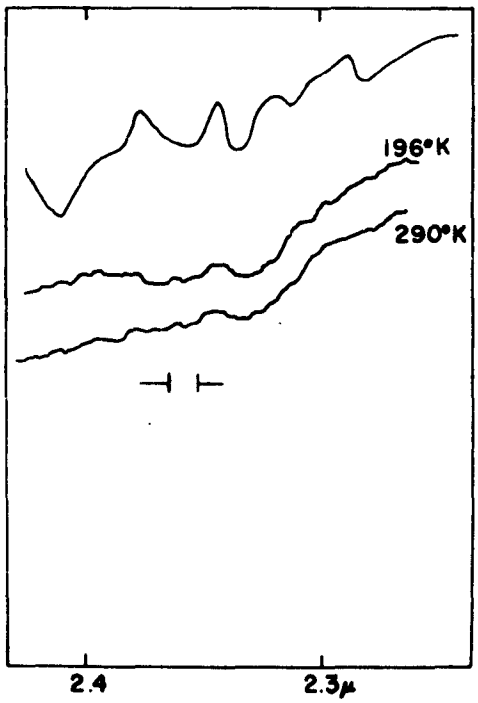

Fig. 4. — The mean of six Venus spectra after division by the spectrum of the moon. There is perhaps an indication of the CO band but the agreement in shape with the two laboratory CO spectra beneath it is poor. The laboratory spectra were made of a 8.5 meter path of CO at a total pressure of 7.1 cm of mercury and at the temperatures indicated. In the Venus spectrum the dip at 2.42 μ may be a real feature.

the surface normal and the direction to the sun. It is then assumed that the total heat radiation at any point on the surface will have the same distribution. Since the 3.75 μ measurement is in no way a measurement of total radiation, this reduction is not correct. However, a calculation for the case $i = 0$ indicates that it is not

grossly in error but only by 10°. The subsolar temperatures have also been corrected to Mercury-Sun distance of 0.387 A. U.

The mean of the Venus temperatures in Table I is 236°K. This is within experimental error of the 8 — 13 μ temperatures determined by Pettit and Nicholson ([6]) and Strong and Sinton ([5]).

TABLE I

Temperatures of Venus and Mercury Measured at 3.7 μ

Date U. T.	Venus (dark hemisphere)	Mercury (effective temperature)	Mercury (Calculated subsolar temperature at 0.387 A.U.)
April 12	227° K	457° K	582° K
April 15	242	474	580
April 17	238	487	580

TABLE II

λ	Fraction of Solar Energy, f	Albedo, A	$f \times A$
0-3500 A	0.070	(0.40)	0.028
3500-4000 (U)	0.053	0.53	0.028
4000-5000 (B)	0.126	0.78	0.098
5000-6000 (V)	0.129	0.87	0.112
6000-12000	0.428	(0.87)	0.372
12000-15000	0.074	(0.75)	0.056
15000-19000	0.053	(0.52)	0.028
19000-27000	0.040	(0.40)	0.016
27000-	0.027	(0.15)	0.004
		Total Albedo	0.734

TEMPERATURE DETERMINATIONS

The infrared pyrometer. which has been previously described([7]) has been employed for a series of measurements of the effective

temperature of the entire disk of Venus. In this series a focal-plane aperture was used that, depending on the apparent diameter of the planet, was large enough to pass the whole image including seeing excursions. Thus during the series the aperture size varied between 11″2 and 58″3. The aperture used for observing the comparison blackbodies was usually the next smaller aperture size in order that it was more nearly the actual size of the Venus image. The measurements were made with the setting first in one and then in the other of two apertures of the instrument. Usually about 10 pairs of readings in this manner were taken and readings on the blackbodies were made at the beginning and the end of the series of readings. The whole extent of a day's measurements was about one hour which was generally with the planet close to the meridian. Observations were made on 70 days in the period 1958-1961 with the majority concentrated in 1959.

Unfortunately many of these observations were afflicted by an instability in the pyrometer that was subsequently discovered ([8]). The observations that were so affected have been corrected where possible by adjusting the scale so that the temperature of the subsolar point of the Moon or other established lunar temperatures came to their established values if such lunar observations were made on the same day. Other uncorrected observations were rejected. The fault in the pyrometer was corrected in September 1959 and all observations made subsequent to this time have been retained. Of the 27 observations that were retained 15 were made in a 1.5 μ band at 8.8 μ while the remainder were made in a similar band at 11.9 μ. The mean temperature for the series is 235.1°K. The standard deviation of an observation on a single day from the mean is 6.8°K.

One deviation was outstanding — that of September 29, 1960 when a temperature of 257°K was found. This deviation is more than 3 times the standard deviation and if it is eliminated the mean temperature is 234.3°, and the standard deviation for one observation becomes 5.4°K. That there was no substantial syste-

matic error in the observation on September 29, 1960 is shown by the fact that essentially normal temperatures for Mercury, Moon, Mars, Jupiter, and Saturn were obtained on the same day. It is believed that this observation offers evidence of a real variation of the effective radiating temperature of Venus. Another example of a probably real variation is in the published observations of Pettit and Nicholson and Coblentz and Lampland. The highest temperature found by Pettit and Nicholson ([8]) was 257°K observed on August 29, 1924, while 4 days earlier Coblentz and Lampland ([9]) found 330° K. An inspection of Lampland's observing books shows that he found in later observations water-cell transmissions and therefore temperatures in agreement with those observed by Pettit and Nicholson. Lampland has referred to the variability in emission from Venus ([10]).

The remainder of the 70 days of observation, which are not included in Table II, do not show large variations from the included ones. We may conclude that Venus generally has quite constant effective radiating temperature but occasionally may have substantial variation.

Discussion

The spectra of Figure 1 may be used to evaluate the dependence of the Venus albedo on wave length. In Figure 5 the spectrum of Venus has been divided by the spectrum of the Sun. From the wave length variation of reflectivity obtained from Figure 5 it is possible to make an estimate of the albedo for the solar energy curve. The albedos from UBV photometry found by Knuckles, Sinton, and Sinton ([11]) are used as the basis. They found $A_U = 0.53$, $A_B = 0.78$, and $A_V = 0.87$ for the observations through the U, B, and V filters respectively. The albedo in the region 6000 — 12000 A is assumed to be identical to the albedo found for the V filter. From this datum and the spectra presented in Figure 5 the albedos are then weighted according to the solar energy distribution. The calculations are made in Table II.

From the derived solar albedo, 0.73, the effective radiation temperature of the planet may be derived with the formula $T_{eff} = 394 \frac{(1 - A_s)^{1/4}}{(2r)^{1/2}}$ °K where A_s is the solar albedo and r is the Venus-Sun distance in A. U. From this formula one finds $T_{eff} = 234°$ K in exact agreement with the observed mean radiometric temperature.

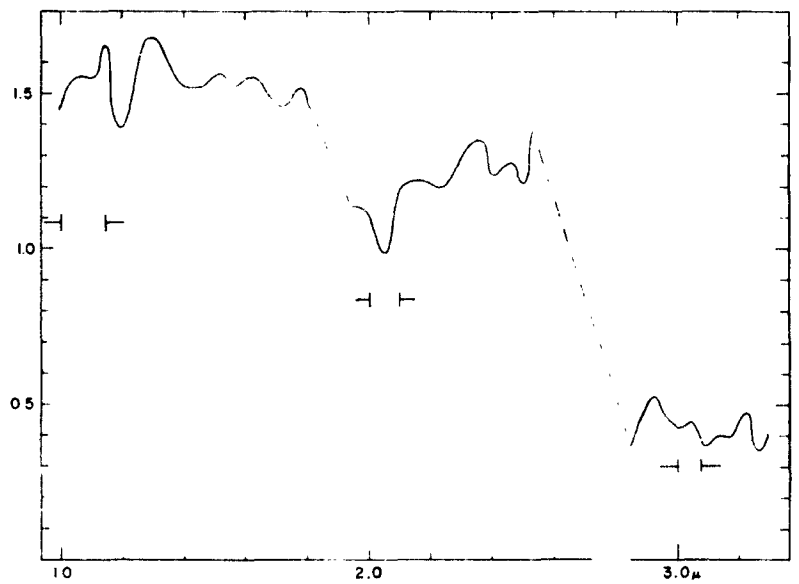

Fig. 5. — The Venus spectrum of Fig. 1 divided by the solar spectrum. The dashed portions were not determined because of the presence of strong atmospheric bands.

The agreement of the theoretical temperatures with that observed in the 8 — 13 μ region means that in the unobserved region beyond 13 μ to about 30 or 40 μ the effective radiating temperature is the same as that which applies in the short wave length region ; otherwise an imbalance of the heat budget would have to occur.

The more-or-less stepwise decrease of albedo in the infrared region suggests the possibility that water in the form of ice crystals

is present in the atmosphere. In ice the near infrared bands of the H_2O molecule are found to be shifted to longer wave length and perhaps to be broadened. Because observations cannot be made sufficiently accurately within the terrestrial water bands a step wise appearance to the reflection spectrum may result. The absorption coefficient of ice at 3.08 μ (the same band that shows up at 2.7 μ in the vapor form) is 3000 cm^{-1}. Thus scattering from 3 μ particles is expected to be much reduced compared to shorter wave lengths where the absorption coefficient is less, thus partly explaining the low albedo which is found beyond 2.7 μ. A difficulty with this interpretation of the stepwise decrease of albedo as due to ice is that at 3.4 μ, where the albedo is still low, ice may not have sufficient absorption.

If clouds are responsible for the atmospheric opacity at 10 μ and also at 3.75 μ, we may make an estimate of the cloud cover. For the sake of argument it is assumed that radiation from beneath the clouds is equivalent to a blackbody at 400°K. We neglect the contribution of the gaps in the clouds to the radiation at 10 μ and consider only their contribution at 3.75 μ. At this wave length the flux from a 400° source is 1200 times that from a 236° source. If the observed temperature is increased by 5°, the observed flux is nearly doubled. Thus gaps in the cloud cover must have an area less than 0.1 %. On the other hand, to increase the radiation observed at 11.9 μ to that corresponding to 257°K as found on September 29, 1960 gaps in the cloud cover amounting to 5 % would be required.

This research has for the most part been supported by Contract AF 19(606)-5874 with the Air Force Cambridge Research Laboratories, Bedford, Massachusetts.

REFERENCES

(1) SINTON, W. M., *Science*, **130**, 1234, 1959.

(2) SINTON, W. M., *Applied Optics*, **1**, 105, 1962.

(3) KUIPER, G. P., « *The Atmosphere of the Earth and Planets* », p. 351, Univ. of Chicago Press, 1952.

(4) PETTIT, E. and NICHOLSON, S. B., *Ap. J.*, **83**, 84, 1936.

(5) SINTON, W. M. and STRONG, J., *Ap. J.*, **131**, 470, 1960.

(6) PETTIT, E. and NICHOLSON, S. B., *P. A. S. P.*, **67**, 293, 1955.

(7) SINTON, W. M., *Low. Obs. Bull.*, **4**, 260, 1959.

(8) GEOFFRION, A. R., KORNER, M. and SINTON, W. M., *Low. Obs. Bull.*, **5**, 1, 1959.

(9) MENZEL, D. H., COBLENTZ, W. W. and LAMPLAND, C. O., *Ap. J.*, **63**, 177, 1926.

(10) LAMPLAND, C. O., *Ap. J.*, **93**, 401, 1941.

(11) KNUCKLES, C. F., SINTON, M. K. and SINTON, W. M., *Low. Obs. Bull.*, **5**, 153, 1960.

26. — ON THE QUESTION OF THE PRESENCE OF OXYGEN IN THE ATMOSPHERE OF VENUS

V. K. PROKOFJEV and N. N. PETROVA
Crimean Astrophysical Observatory, U.S.S.R.

There were several attempts to find absorption bands of the molecular oxygen O_2 in the Venus spectrum with the dispersions of the spectrum 3Å/mm (1), 5.5Å/mm (2) and 1.7-2.5Å/mm (3) using α —, B — and A — bands near 6300 A, 6900 A and 7600 A respectively.

The Doppler shifts in the Venus spectra were sufficient to separate absorption bands of Venus oxygen from telluric bands, but no absorption was found out.

The following circumstances must be taken into account when considering the question of spectroscopic discovering of Venus oxygen.

I. Only upper part of the Venus atmosphere which is above the cloud layer is available to optical observations ; so the possible amount of oxygen must not be large, and only weak absorption band is to be awaited.

2. Telluric absorption bands of oxygen differ greatly in their absorption coefficients. It is equal to 1 : 2.5 : 35 (4) for α —, B — and A — bands respectively. So the bands A — and B — have large wings and α — bands on the contrary are very narrow and often are used for investigation of apparate function of the Solar spectrographs.

3. For discovering weak absorption bands (with small equivalent width) very essential are the width of the slit of the spectrograph, the linear dispersion of the spectrograph and the resolving power of the used photographic plate. When the slit is too wide, the weak absorption band may disappear among fluctuations of the grain of the photoemulsion. These circumstances were taken into account in the present investigation.

During the year 1961 the spectra of Venus were taken using echelle spectrograph of the Solar tower of the Crimean Astrophysical Observatory ([5]).

This spectrograph had linear dispersion of 1Å/mm in the region of oxygen α — bands. Table 1 gives conditions of photographing, spectral width of the slit of the spectrograph and the value of the Doppler shift calculated from change of the heliocentric distance and measured on the spectra.

TABLE 1

Date 1961	δλ Å	Exposure time	Δλ Å		Plate
			Calc.	Measur.	
26,02	0,17	3^h00^m	—0,251	—0,252	103aF
16,08	0,17	1^h35^m	—0,237	—	103aE
20,08	0,12	2^h10^m	+0,233	+0,231	—»—
22,08	0,08	2^h10^m	+0,230	+0,233	—»—
23,08	0,08	2^h25^m			—»—
20.10	0,08	1^h30^m			
21.10	0,08	1^h30^m	+0,147	—	—»—

In February only one spectrum available for photometric measures was taken because of weather conditions.

The same sort of photographic plates was used for taking Solar spectrum on the height of 15° above the horizon, the spectral width of the slit being 0.17 and 0.08A and exposure time 0.2. The intensity scale was taken with the same exposure times for the Venus and Solar spectra.

10 lines of P-branch of α — band of the oxygen chosen for the detailed photometry are given in the table 2. In the same table the complete list of the solar and atmospheric lines which are near the oxygen lines is given according to Revision of Rowland preliminary table and ([6]).

The work ([6]) presents the complete list of atmospheric bands of

water vapor observed in Solar spectrum when the sun is low above the horizon.

The intensities of lines taken from ([6]) and reduced to the Rowland's intensity scale are taken in brackets as not very certain.

During the photometer measures the densities were taken with the step of 0.01 Å and converted into intensities using respective characteristic curves ; then the profiles of each two pairs of oxygen lines were traced. On these tracings the places of atmospheric and Solar lines were marked. For each profile of telluric oxygen line the centers were determined and all profiles were reduced to the same depth taken as a unity. Then according to the centers the profiles were laid on each other so that an average profile was obtained ; the same method was used in ([7]) for B-bands

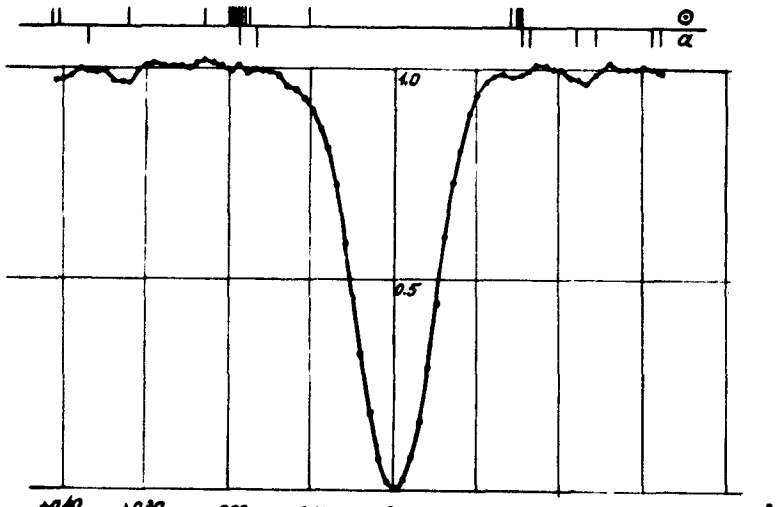

Fig. 1

when attempting to find out Martian oxygen. Such kind of operation, minimizing fluctuation of the photographic grain and averaging all Solar and atmospheric lines which are on different distances from the lines of telluric oxygen does not weaken the lines of Venus oxygen whose place is caused by the same Doppler shift for each line.

TABLE 2

N°N°	O_2 Å	λ Å	Ident.	I	N°N°	O_2 Å	λ Å	Ident.	I
1	2	3	4	5	6	7	8	9	10
		6307,885		—2N			6296,511	V ; H_2O	—3
		558	$O_{16}O_{18}$	—3N			378		—3
		07	$O_{16}O_{18}$				156	Ce^+	—3
		6306,745	$O_{16}O_{18}$	—3	5	6295,966		O_2	3
1	6306,575		O_2	2			6295,818		—3
		6306,414	$O_{16}O_{18}$; H_2O	—3			657	H_2O	—3N
		225	$O_{16}O_{18}$; H_2O	—3			387		
							290	Ti	—3
		05			6	6295,186		O_2	3
		6305,996	Sc	—3			6295,039		—3
2	6305,819		O_2	2			6294,672	H_2O	—3
		6305,674	Sc	—3			180	H_2O	(—3)
		321	H_2O	—2N			6293,952		—1
		6304,866		—3N			905	H_2O	(0)
		578	H_2O	(—3)			436	H_2O	(—3)

		440	H_2O	(0)			167		—3
		341		—2N	7	6292,967		O_2	3
		6303,774	Ti	—2N			6292,827		—2
		496		—2N			622	H_2O	—3
		6302,995		—3			369		—3
	6302,771		O_2	2	8	6292,170		O_2	2
		6302,508	Fr	5			6291,931	H_2O	(—3)
		197	Ce_+	—3			775	H_2O	(—3)
	6302,005		O_2	2			062	H_2O	(—3)
		6301,852		—3			6290,981	Fe	4
		517	Fe	7			850	H_2O	(—2)
		6300,700	Sc^+	—2			547	Fe	— 2N
		331		—2	9	6290,224		O_2	2
		003	H_2O	(—3)			6289,903	H_2O	—3
		6299,601	H_2O	0			587		—3
		421	H_2O	—2	10	6289,403		O_2	1
3	6299,231		O_2	—3			6289,181	H_2O	—2
		6298,800	H_2O	(—3)			6288,752		—3
		650	V	—3			688	H_2O	(—3)
4	6298,462		O_2	2			636		—3
		6298,309	H_2O	—3			554	H_2O	(—3)
		091	Ti	—3			327		—2
		627,808	Fe	5					
		313		—3					
		267	H_2O	—3					
		6296,67	Ti	—3 (Sp)					

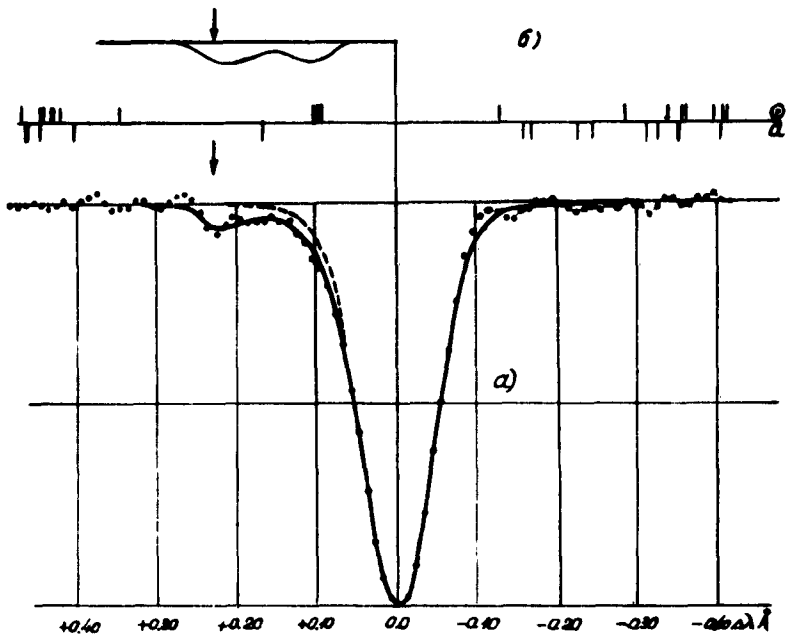
б)
а)
+0.40
+0.30
+0.20
+0.10
0.0
-0.10
-0.20
-0.30
-0.40 Å

Fig 2.

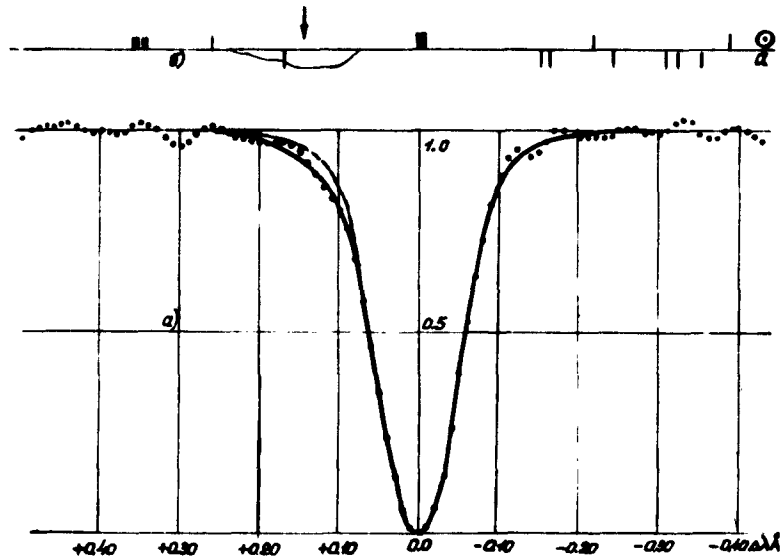
б)
а)
1.0
0.5
+0.40
+0.30
+0.20
+0.10
0.0
-0.10
-0.20
-0.30
-0.40 Å

Fig 3

The separate lines of the P-branch of oxygen α — band are presented as the doublets with the distance of 0.75-0.82 Å. So when their profiles were laid on each other one could not obtain the wings of the average profile farther than 0.4 A from its center.

Fig. I shows the average profile of the lines 1-10 (see table 2) for the Solar spectrum. Ordinate is the distance $\Delta\lambda$ from the center of the line in Å, + meaning red side of the spectrum. On the top of the Fig. 1, the places of the Solar ($\odot$) and atmospheric (a) lines in the neighbourhood of the telluric lines are marked.

As one could expect ([4]) the profile thus obtained is essentially symmetrical. Some fluctuations of the *phone* in the wings may be caused by the close groups of weak Solar and atmospheric lines, but they may also be the residual fluctuations of grains of the photo-emulsion.

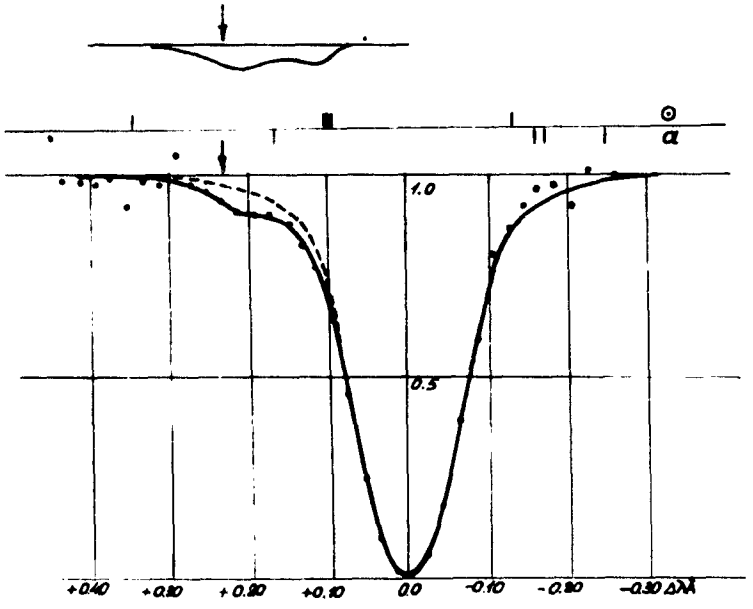

Fig. 4

Figs. 2-4 show average profiles of the telluric lines 1, 2, 4-10 (in Fig. 2 and 3) and 1-4, 6-8 (Fig. 4).

Fig. 2. is the mean from the spectra taken 22 and 23 August, Fig. 3 — for October 20 and 21, Fig. 3 — for August 20. On the tops of the figures the position of the Solar and atmospheric lines is shown, taking into account Doppler shifts for the Solar lines. As well as for the profile on the Fig. 1, there is no blending lines in the middles of the profiles on the Fig. 2 and 4. So the profile must be symmetrical.

Dashed line is the symmetrically traced profile according to its short-wave side ; it is obvious that the red wing of the profile has a distinct depression. The calculated difference between observed and symmetrically traced profiles is presented in the top of the drawing. This depression has two maxima.

The first is on the distance of $\Delta\lambda = + 0.10$ A and may be caused by the close group of 4 weak Solar lines with Rowland intensities — 3 (three of the lines) and — 2. Only the atmospheric line of oxygen isotope $O_{16}O_{18}$ with $\Delta\lambda = + 0.16$ A is near the second maximum. The concentration of this isotope in the earth atmosphere is 1/600 (see (⁶) and (⁸)). Besides that this line is weakened by averaging. The only possible explanation remains : as this maximum is near $\Delta\lambda = + 0.23$ A which corresponds to Doppler shift (see the arrow) of Venus spectrum in the time of observation, one may suppose that this maximum is caused by the weak absorption band of Venus oxygen.

Fig. 3 corresponds to another value of Doppler shift, and the location of Solar lines (⊙) is another.

The group of 4 Solar lines is close to the middle of the profile and only makes it a little deeper without disturbing its symmetry. One may notice a certain depression in the red side of the line in comparison with its symmetrical shape (dashed line). This depression is presented in the top of the drawing as the difference between observed and symmetrical profile. The above mentioned line of the isotope of earth oxygen as well as in the cases of figures 2 and 4 cannot cause this depression. The location of maximum of this depression corresponds to Doppler shift $\Delta\lambda = + 0.15$ A in the

Venus spectrum for October 20 and 21. So in this case the observed depression may be also explained as the O_2 absorption in the Venus atmosphere.

Observed displacement of the maximum of the depression from + 0.23 A to + 0.15 A confirms the suggestion about the presence in the spectrum of Venus weak absorption band of oxygen.

It is of interest to confront considered profiles with the profile for February 26, when the Doppler shift is negative. But it may be only qualitative comparison. First of all, we have only one spectrum, then it is taken by the large width of the slit (0.17 Å) that makes impossible its comparison with the profiles on Fig. 2-4 ; only the spectrum of August 16 taken with the same slit width is suitable for such comparison.

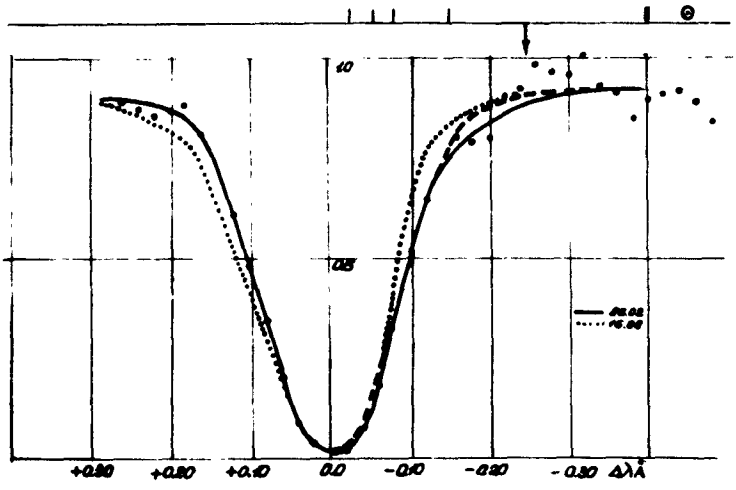

Fig. 5

Besides that, there are 6 water vapor lines on the short-wave side of the averaged profile that prevents from the identification of depression if it is discovered on this side of the profile.

However one may carry out a certain very approximate comparison. The averaging of the profile for February 26 was made with the exception of all oxygen lines which have water vapor bands on the short wave sides of their profiles ; the remaining lines (2, 6, 7)

were averaged (See table 2). It is evident that such averaging of 3 lines cannot considerably minimize the role of granulating of photoemulsion.

On the fig. 5 the comparison of average profiles for August 16 (lines 1-8) and February 26 (lines 2, 6, 7). The noticeable asymmetry on the short wave side of the profile for February 26 (the symmetrical profile according to the red side is traced with the dashed line) is caused with the location of the four Solar lines ; three of them are of the intensity — 3 according to Rowland and the fourth-2 N ; another cause of the depression may be the presence of absorption band in the Venus atmosphere corresponding to the Doppler shift of $\Delta\lambda = -0.25$ Å. The profile for August 16 is traced with the dot line.

The comparison of these two profiles makes evident the displacement of the depression from long-wave wing of the profile of August 16 to the short-wave wing of the profile for February 26.

That may qualitatively confirm suggestion about the presence of the weak oxygen absorption in the Venus spectrum.

The supposition remains that the mentioned asymmetry located according to the Doppler shift of Venus spectrum may be connected with the presence of lines of Solar spectrum which are exactly behind the lines of telluric oxygen and appear when the Solar spectrum is shifted by reflection from moving body.

To verify this suggestion the spectra of eastern and western Solar limbs were taken using the IV order of diffraction grating providing the dispersion of 0.25 A/mm with the spectral width of the slit 0.017 A. The detailed examination of the profiles did not show any noticeable asymmetry in the wings of the lines of telluric oxygen.

Thus, the observed effect in the spectrum of Venus must be due to absorption in its atmosphere. The quantitative estimate of the amount of oxygen in the Cyterian atmosphere would be premature : it is necessary to continue the investigations in the short-

wave side of the telluric lines during the time of approaching of Venus to the Earth.

The authors are very grateful to Professor A. B. Severny, who was the initiator of the present work, for his constant attention and useful discussions. We want also to thank Mrs N. E. Orlova for her assistance in observations and measurements.

REFERENCES

(1) Ch. E. S. John and S. B. Nichilson, *Ap. J.*, **56**, 380, 1922.

(2) W. S. Adams and Th. Dunham, *P. A. S. P.*, **44**, 243, 1932.

(3) F. J. Heyden, C. C. Kiess and H. K. Kiess, *Sci.*, **130**, 3383, 1195, 1959.

(4) C. W. Allen, *Ap. J.*, **85**, 156, 1937.

(5) A. B. Severy, N. V. Steshenko, V. L. Chochlova., *Astron. Journ.*, **37**, N 1, 23, 1960.

(6) D. I. Eropkin and V. N. Kondratiev. *Bull. de la Commis. pour les recherches du Soleil.* VII, VIII, 1934.

(7) W. S. Adams and T. Dunham, *Ap. J.*, **79**, 308, 1934.

(8) R. Mecke and W. H. J. Childs, *Zs. f. Phys.*, **68**, 362, 1931.

27. — SPECTROSCOPIC TEMPERATURE AND PRESSURE MEASUREMENTS FOR THE VENUS ATMOSPHERE

HYRON SPINRAD
Division of the Space Sciences
Jet Propulsion Laboratory, U. S. A.

ABSTRACT

The rotation-vibration band of carbon dioxide at λ 7820 has been analyzed on ten Mount Wilson spectrograms of Venus. The spectroscopic data covers the phase interval from 51° to 113°. The rotational temperatures are derived in the usual way by use of the Boltzman equation : T_{rot} varies from about + 220°K to 440°K.

Total pressures in the Venus atmosphere have been derived by means of the measurement of line profiles for individual rotational lines in the λ 7820 CO_2 band. The derived pressures are the first direct measurements of pressure in the lower Cytherean atmosphere ; they are considerably higher than other recent pressure estimates for the 'reflecting cloud' level. The pressures derived from the small J rotational lines average about 2 atmospheres and increase with larger J values to about 5 atmospheres. This result is to be expected in a region of increasing temperature and pressure with decreasing altitude.

There is a good correlation between the « effective » mean temperatures and the « effective » pressures, in the sense that high temperatures go with high pressures and vice versa. This statement implies a high pressure and a high temperature for the Cytherean surface.

A comparison of the Venus spectra and laboratory CO_2 spectra, kindly loaned by G. Herzberg, indicates that the λ 7820 band CO_2 abundance on Venus may be about 2 km-atm above the reflecting surface. This amount of carbon dioxide is compatible with an atmospheric composition of about 5 % CO_2 by mass.

28. — THE STRUCTURE OF THE VENUS ATMOSPHERE

L. D. KAPLAN
Space Sciences Division
Jet Propulsion Laboratory
California Institute of Technology, U. S. A.

ABSTRACT

Spinrad's analysis of the Adams and Dunham spectrograms indicates very high temperatures deep in the Venus atmosphere, in agreement with an interpretation of the centimeter emission as originating from a hot ground surface. Closer examination of the spectrograms substantiates this interpretation in a spectacular fashion. Inspection of the data shows that for each plate there are two intensity maxima, one at about J = 16 and the other, except for Ce 1756, at J = 24 to 26. The J = 16 maximum corresponds to an effective rotational temperature of about 300°K, the J = 25 maximum to an effective rotational temperature of about 700°K.

The obvious cause of the double maxima is a cloud layer at some level whose temperature is considerably in excess of 300°K, say at about 350 to 400°K. This cloud cannot of course be CO_2 or H_2O ; and, in order to reflect near-infrared radiation as effectively as it does, must be quite opaque to far-infrared radiation. The cloud, and the gas from which it presumably condenses are undoubtedly of considerable importance in providing part of the greenhouse effect that is necessary to maintain surface temperatures in excess of 700°K.

The Venus spectra from 8 to 12 microns obtained by Sinton and Strong indicate a high cloud layer with cloud-top temperature less than 235°K. This may be the visible cloud top. If so, the Regulus occultation measurements indicate that it is at a pressure of less than a tenth of an atmosphere, that is, less than one per cent of the surface pressure.

The cloud stratification makes Spinrad's estimate of the five per cent abundance of CO_2 by mass a lower limit. How much ot an

underestimate it is will depend on the reflectivity of both cloud layers especially the upper one to λ 7820 radiation.

It should be noted that the rotational temperatures refer only to the sunlit portion of the planet. The phase variation of the centimeter wave radiation indicates a temperature difference of about 100°K between sunlit and dark side. Since the microwave data are linear averages, a larger temperature difference is implied between the sub-solar point and the anti-solar point.

The rotational temperatures, on the other hand, are non-linear averages, weighted towards the higher temperatures. Surface temperatures considerably in excess of 700°K are therefore compatible to the microwave measurements. The strong greenhouse effect necessary to maintain the high surface temperatures on the sunlit side makes it possible for a slow circulation to maintain high surface temperatures on the dark side, even if Venus is in synchronous rotation as indicated by the radar bounce experiments.

We will perform a more thorough analysis of the data, and report the results at a later date. However, the data are only of limited usefulness because of the conditions under which the spectrograms were taken. It is necessary that the measurements be repeated with the spectrograph slit parallel to the terminator and placed at many precise locations on the planet.

REFERENCES

(1) H. Spinrad, *Publ. A. S. P.*, **74**, 187, 1962.

(2) W. M. Sinton and J. Strong, *Ap. J.*, **131**, 470, 1960 (see L. D. Kaplan, *J. Planetary and Space Sci.*, 8, 23, 1961).

(3) F. D. Drake, *Publ. N. R. A. O.*, **1**, 165, 1962.

29. — LES CONDITIONS PHYSIQUES DANS L'ATMOSPHÈRE DE VENUS

D. YA. MARTYNOV
Sternberg Astronomical Institute, Moscow University, U.S.S.R.

La température élevée de la surface de Vénus que l'on obtient par des observations radiométriques est très difficile à expliquer, car il est impossible de comprendre comment un effet de serre si grand ait pu se produire. En effet, pour des températures + 300° — + 400° C le maximum de la radiation planétaire est situé sur des longueurs d'onde proches de 5μ, où le carbone dioxide donne plusieurs bandes d'absorption du côté des ondes courtes (5 μ, 4.28 μ, 3.45 μ) et n'en donne aucune du côté des ondes longues. Mais si la radiation de la planète se produit à T = + 600° C, une part perceptible de cette radiation se trouve déjà dans l'intervalle optique, tandis que l'infrarouge proche du spectre où se concentre le maximum de la radiation ($\lambda = 3.3$ μ) ne sera retenu que par des bandes séparées de CO_2 en quantité modérée.

Seule la vapeur d'eau, en quantité considérable, est capable de retenir de manière essentielle la radiation planétaire dans le domaine indiqué des températures. La température élevée de la surface de Vénus et l'abondance de la vapeur d'eau dans son atmosphère sont indissolublement liées entre elles. Ces deux caractéristiques sont en état de connexion contraire : plus la température s'élève, plus une atmosphère puissante est nécessaire ; mais cette atmosphère puissante sera un obstacle à la pénétration de la radiation solaire, ce qui conduira, comme l'a prévu N. A. Kozyrev, à l'isothermie des couches inférieures de l'atmosphère ; cette isothermie, en présence d'une température aussi élevée de la surface, nécessite une atmosphère plus puissante encore.

Naturellement, si l'on n'admet pas l'existence de la vapeur d'eau dans l'atmosphère de Vénus, mais si on admet en même temps la température élevée de sa surface, on peut créer un modèle

d'éolosphère (Öpik) ou bien émettre une hypothèse de modèle plutonique, selon laquelle un grand courant de chaleur vient des profondeurs de la planète. Mais un obstacle surgira dans les deux cas, car la radiation d'une surface chaude ne pénètre pas au-delà de l'atmosphère. En présence de températures allant à 800-900° K sur la partie éclairée de Vénus, on aurait pu s'attendre à une élévation considérable de l'albedo (assez élevé déjà) de cette planète dans le domaine infra-rouge du spectre, car la radiation propre et suffisamment puissante de la planète doit pénétrer la couche de nuages grâce à la dispersion, lorsqu'elle n'est pas accompagnée d'une grande absorption.

La présence de la vapeur d'eau, observée avec quelque incertitude par Strong, est confirmée par l'image de la polarisation de la couche de nuages de Vénus. Remarquons encore que très peu de matières possibles dans l'atmosphère de Vénus, sont de couleur blanche (sa couleur jaunâtre s'explique bien, d'après Sharonov, par la dispersion de Rayleigh), et des nuages d'eau sont les plus vraisemblables. Cependant la présence de la vapeur d'eau dans l'atmosphère exerce une grande influence sur son régime thermique. En particulier, en présence des températures élevées en question, toute l'eau de la planète doit s'évaporer (à moins qu'il n'y ait des pressions invraisemblablement grandes au fond de l'atmosphère) ; sa recondensation la nuit devient une source capable de soutenir la température élevée de la planète même dans le cas d'une rotation très lente, y compris le cas de rotation et de gravitation synchrones : des mouvements horizontaux puissants dans l'atmosphère transportent alors d'une façon permanente un air humide et chaud sur l'hémisphère sombre de la planète.

Mais en réalité, ces courants atmosphériques horizontaux ne sont pas nécessaires. La même chose se passera, si la pression atmosphérique est la même sur la surface sombre et éclairée. Sur la partie éclairée le gradient adiabatique dans une atmosphère qui est loin d'être saturée de vapeur d'eau est près de 10° km^{-1}, alors que sur la partie sombre où l'atmosphère est saturée de

vapeur d'eau, il est beaucoup moindre. En posant le gradient nocturne égal à $4^{o}.2$ km^{-1} et en admettant que la température de la couche nuageuse pendant le jour est la même que pendant la nuit, tandis qu'à la surface de la planète elle est très différente, on devra admettre que la hauteur de la couche de nuages est aussi différente dans les deux cas ; la différence atteint 10-12 km. Mais comme la hauteur d'une atmosphère homogène est beaucoup plus grande pendant le jour que pendant la nuit, la pression à la surface de la planète sera à peu près la même. Il doit y avoir dans la partie supérieure de l'atmosphère un écoulement perpétuel de gaz chaud et humide vers la partie sombre ; cet écoulement doit être compensé par un afflux de gaz froid saturé et plus dense vers la partie éclairée de la surface. Ces courants peuvent être beaucoup plus calmes et sujets à un effet de latitude.

Il doit exister une différence de régime thermique du côté sombre du matin et du soir, qui croîtrait avec un ralentissement de la rotation de la planète (*). Ces différences ne peuvent cependant être observées avec succès par la méthode bolométrique : pendant le refroidissement nocturne de la planète, la quantité de la vapeur d'eau dans l'atmosphère diminue et elle devient plus transparente pour la radiation thermique de la planète. La répartition spectrale de la radiation infra-rouge de Vénus est seule capable de donner une réponse décisive sur ce point.

Les températures très élevées de Vénus déduites des observations radiométriques sont chargées d'erreurs accidentelles si grandes qu'il est impossible aujourd'hui de parler avec certitude de l'absence des effets de la radiation non-thermique de la planète. Les observations de Kuzmin et de Salomonovitch ont montré qu'il s'ajoute peut-être à la radiation thermique une radiation non thermique perceptible sur des ondes plus longues.

(*) En cas de rotation et de gravitation synchrones la différence disparaît, ainsi que la conception de côté du matin ou du soir.

30. — ON THE ATMOSPHERE AND CLOUDS OF VENUS

CARL SAGAN
The Institute for Basic Research in Science, The Space Sciences Laboratory, and The Department of Astronomy, University of California, Berkeley, California, U. S. A. (*)

ABSTRACT

The microwave spectrum of the dark hemisphere of Venus is flat at a brightness temperature of approximately 600°K for wavelengths longward of 3 centimeters. Shortward of 3 centimeters, the brightness temperature drops to some 350 degrees in the middle millimeter range and eventually reaches 235°K at 10 microns. The spectrum is inconsistent with nonthermal emission from trapped charged particles in a Cytherean Van Allen belt, and an alternative possibility, that the emission arises from free-free transitions of electrons in a dense and extensive ionosphere at electron temperature of 600°K runs into very grave accessory difficulties.

If the centimeter microwave emission from Venus arises from its surface, the radar reflectivities and microwave brightness temperatures give mean darkside surface temperatures of about 640°K. Extrapolations of the phase data to small phase angles indicate mean brightside surface temperatures of about 750°K. If the cloudtop pressures and temperatures are known in both hemispheres, the surface pressures and darkside subadiabatic indices can be derived. A reanalysis of the CO_2 absorption bands near 0.8 and 1.6 μ and of the Regulus occultation data indicates (1) that the same cloud level, at $T_c \simeq 234$°K, is responsible for the reflection and emission throughout the visible and infrared, and (2) that the brightside cloudtop pressure is at least as great as the darkside cloudtop pressure, the most probable values being 0.6 atm and 90 mb respectively.

(*) Now at Harvard University and Smithsonian Astrophysical Observatory, Cambridge 38, Mass., U.S.A.

Even with a small phase effect these cloudtop pressures give surface pressures $\simeq$ 50 atm. The darkside lapse rates are substantially subadiabatic, in contradiction to the Aeolosphere Model. Failure of the Urey equilibrium on Venus results in surface pressures of this order or greater ; and similar values are obtained from the atmospheric structure deduced from Spinrad's measurements of the near infrared CO_2 band at 7820 Å. The altitude of the cloudtops on the dark side is then $\simeq$ 80 km, and is possibly even higher in the bright hemisphere.

The surface pressures and phase effect lead to a sidereal period of rotation which exceeds 170 days, and is quite possibly equal to the period of revolution. For nonsynchronous rotation, the specific heat capacity of the atmosphere controls the nocturnal cooling. There is a smaller contribution from subsurface conduction. For synchronous rotation the atmospheric circulation must supply the radiation emitted to space from the dark hemisphere.

The effect of Rayleigh scattering on a cloudless day on Venus is to yellow the sky and redden the sun. The radiation scattered back to space will also have a yellow cast, and may explain the apparent color of Venus. The color index should therefore be a function of phase. In short visual wavelengths, the surface of Venus cannot be seen from space, even on a cloudless day. The observations of permanent dark markings at these wavelengths possibly represent clouds connected with surface features far below ; they cannot be the surface features themselves. But near infrared photography has the promise of detecting surface markings on Venus.

With current values of the atmospheric pressure at the cloudtops and of the ratio of CO_2 to N_2 in the atmosphere, pressure induced dipole absorption by CO_2 is not capable of producing the required millimeter attenuation. However, a cloud layer in part composed of water droplets can provide the additional attenuation required to explain the microwave spectrum. Clouds with a surface density of water of a few tenths of a gm cm^{-2}, with thicknesses less than thirteen km and with mean densities greater than 0.2 gm m^{-3} are

consistent with a large number of planetary observables. However, Spinrad's most recent attempt to detect water vapor on Venus has led to mixing ratios which are too low for the water cloud model proposed here. If these results are correct, the low brightness temperatures shortward of 3 centimeters must be due to absorption by some as yet unspecified constituent of the atmosphere of Venus.

The high surface temperatures and pressures lead to melting and vaporization of surface material; and to greatly enhanced infrared opacities, facilitating the operation of the Greenhouse Effect on Venus. Direct exploration of the surface of Venus would seem to be a very difficult engineering problem.

31. — RADIO OBSERVATIONS OF VENUS CARRIED OUT ON THE RADIO TELESCOPE OF P. N. LEBEDEV PHYSICAL INSTITUTE.

V. P. BIBINOVA, A. G. KISLYAKOV, A. D. KUZMIN,
A. E. SALOMONOVICH, I. V. SHAVLOVSKY
P. N. Lebedev Physical Institute, Moscow, U. S. S. R.

1. Introduction

As it is well-known, investigations of the Venus intrinsic radio emission can give significant data, which will help in detecting temperature conditions of the planet, the character of its surface, the composition and state of the atmosphere, and also the rotation elements.

First radio observations of Venus were carried out near the inferior conjunction of 1956 at the Naval Research Laboratory (U. S. A.) with the 15 m radio telescope at 3.15 and 9.4 cm [1].

According to the data of these observations, the brightness temperature of Venus turned out to be the same at both wavelengths and equal to $\sim$ 600°K. Observations at 3 cm were repeated near the inferior conjunction of 1958 with the use of the maser [2] and gave a similar result. In 1958 observations at 8.6 mm were performed with the 3 m radio telescope of the Naval Research Laboratory [3]. However, due to a small area of the radio telescope, the brightness temperature of the planet again was measured only near the inferior conjunction. It turned out to be 410 $\pm$ 160°K.

Observations in that range with a larger antenna were started by means of the 22 m radio telescope of the P. N. Lebedev Physical Institute (U. S. S. R.) in 1959 [4]. 17 days after the inferior conjunction, the measured brightness temperature of Venus turned out to be 315 $\pm$ 70°K. The following two months a systematic growth of the brightness temperature with the increase of the sun-lit portion of the planet disk was observed.

Later C. H. Mayer, T. P. Mc Cullough and R. M. Sloanaker [5] communicated about the phase variation of the Venus brightness temperature at 3 and 10 cm.

In order to interpret the obtained data, several models of Venus were put forward [4, 5, 6, 7, 8, 9]. However, the lack of sufficient observational data made it impossible to prefer one of the models, as well as to consider them well-grounded.

In this connection in the period of the inferior conjunction of 1961, a new series of observations of the Venus radio emission was carried out at the 22 m radio telescope of the P. N. Lebedev Physical Institute [10].

2. The Technique of Observations

Observations of 1961 were carried out at four wavelengths : 9.6 cm, 3.3 cm, 8 mm and 4 mm [11]. At all above wavelengths modulation radiometers (*) were used whose preamplifiers were situated near the focus of the parabolic reflector. Conical horns or open ends of waveguides were used as feeds. Calibration of antenna temperatures was made by means of gas discharge noise generators weakly connected with the radiometer inputs (at 9.6 and 3.3 cm) or by means of matched absorbing loads introduced in the waveguides by the distance control system (at 4 and 8 mm). At 9.6 cm observations were performed by the method of the passage of Venus through the directional pattern of the radio telescope fixed in the precalculated position. Adjustment of the electrical axis and measurement of the radio telescope parameters were carried out from the radio sources Cassiopeia A, Cygnus-A and Taurus-A. Flux densities of Taurus-A and Cassiopeia-A were adopted to be respectively, 790.10^{-26} and 1450.10^{-26} w. m.$^{-2}$ c. p. s.$^{-1}$. On the days of clear sky the proper position of the device during Venus passage was also checked up with the optical guide. On the days of obser-

(*) The radiometer used at 4 mm has been developed at the Institute of Radiophysics of the Gorky State University.

vations, from 3 to 15 sequential passages of Venus were carried out with the time interval of 20 min. Besides the calibration by means of the noise generator, in many cases, at the beginning of the observation, radio emission of Virgo-A was recorded.

At 3.3 cm observations were made at an optical visibility of the planet. The planet was tracked in altitude with the aid of an optical guider. In the azimuthal direction the radio-telescope was given the speed alternately somewhat faster and somewhat slower than the azimuthal velocity of the planet motion due to the Earth's diurnal rotation. This resulted in multiple passages of the planet through the directional pattern of the radio telescope antenna. Samples of the recordings are given in Fig. 1. Also the marks corresponding to

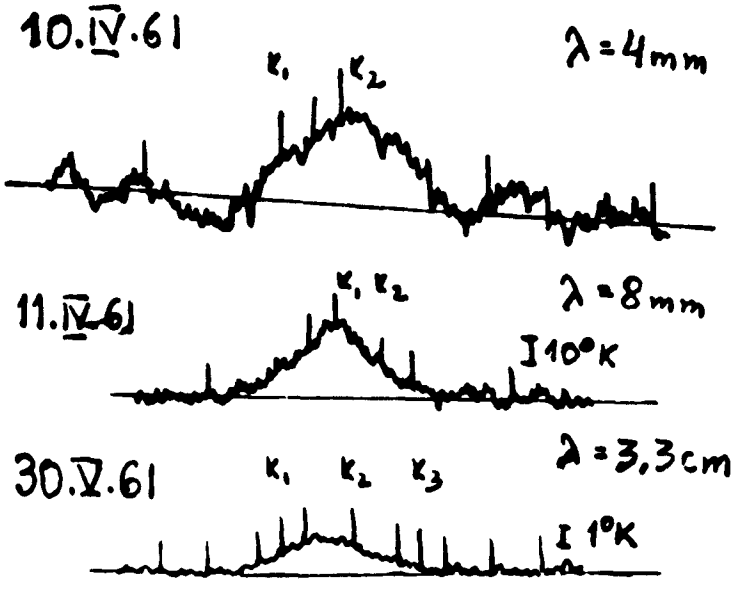

Fig. 1

a definite angular distance in the picture plane were plotted. After several passages the calibration with the noise generator (the effective temperature 18°K) and check-up recording of the passage of Taurus-A were carried out. Adjustment of the radio telescope was made with Cassiopeia-A, determination of the antenna

effective area was made by means of Taurus-A, the flux density of which at this wavelength was adopted to be 600.10^{-26} w. m.$^{-2}$ c. p. s.$^{-1}$. Owing to the fact that the feed of the radiometer at 3.3 cm was shifted from the focus (millimeter feed were in the focal position), the antenna effective area turned out to be somewhat less than in ([12]) and equal to $A_3 = 160 \pm 25$ m^2, and the directional pattern width was equal to $\varphi_{0.5} = 6'.8 \pm 0'.2$.

Observations in the millimeter range were also carried out at optical visibility by the method similar to that applied at 3.3 cm. To exclude errors caused by possible disagreement of the electric axis of the radio telescope and the axis of the optical guide, recordings of Venus passages were made at varied settings of the ocular cross of the guide. At the processing, a series of recordings was used obtained with the installation corresponding to the maximum averaged signal.

Due to the small value of the flux density of radio sources with small angular sizes, determination of radio-telescope parameters at 8 and 4 mm is rather difficult. Therefore, earlier ([13]) at 8 mm the estimate of an effective area of the antenna was made only approximately. The main lobe was measured, but the streying in the side and back lobes was only estimated.

In this work an attempt was made to estimate effective area of the antenna from the cosmic source of radio emission. At the end of the series of Venus measurements, observations of Jupiter were made (apparently, for the first time in the millimeter range) (Fig. 2). The composition of the radiometric temperature (130°K) in the infrared region ([14]) and the brightness temperature of Jupiter in the 3 cm range obtained by us and other observers ([15]) made it possible to take the value 140°K as the brightness temperature of the planet at 8 mm. Using the ratio

$$T_b = \frac{T_A \lambda^2}{A \Omega g}, \qquad (1)$$

where Ω — is the visible solid angle of Jupiter, and g — is the

factor which takes into account the commensurability of the angular dimensions of the source and the directional pattern ([16]), one could estimate the effective area of the antenna at 8 mm — $A_{0,8}$. Some changes $A_{0,8}$ which took place during the period of Venus observations were taken into account in the results of the measurements by introducing the correction factor proportional to the square of the width of the main lobe determined by the records of Venus passages. The antenna effective area at the beginning of the period of observations when the main lobe width was equal to 2′ at the half power level, was found to be $A_{0,8} = 108 \pm 20\ m^2$ that was somewhat less than the value of $A_{0,8}$ estimated before ([13]). The above difference was caused apparently by the inaccuracy of the estimate of streying in side and back lobes made in ([12]).

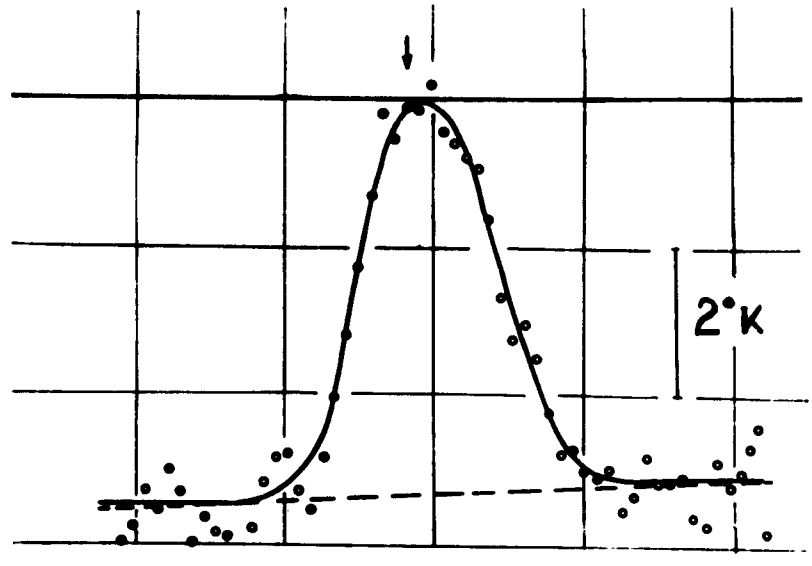

Fig. 2

The greatest difficulties were encountered in determining parameters of the antenna at 4 mm. The main lobe of the pattern was determined by the averaged record of the Venus passage. The width of the main lobe at the half power level was found to be $1'.6 \pm 0'.2$.

The strey factor outside the main lobe was determined by means of the analysis of records of the Sun passage through the antenna pattern (in this manner the value of streying was determined within the Sun angular size) and, also from the results of measurements of the antenna temperatures of the Moon and Sun (in this manner streying outside the solid angle of the Sun (Moon) was determined). In this case the brightness temperatures of the Moon and Sun at 4 mm were taken in accordance with [17].

Thus one could determine the brightness temperature of Venus by comparison with the brightness temperature of the Moon and by estimating the streying outside the solid angles occupied by Venus and the Moon. Attenuation in the Earth's atmosphere, especially significant in the millimeter range, and also the influence of the Earth radiation were taken into account in the process of calibration and further processing of the observation results. Calculation of the brightness temperatures from the measured antenna temperatures was carried out by well-known expression (1).

3. Results of Measurements

Observations at 8 and 4 mm and at 9.6 cm were carried out from the middle of March to the beginning of June. From May 26 to July 10 observations at 3.3 cm were performed.

Measurements at the first three wavelengths corresponded to the variation interval of K- the relative area of the illuminated portion of the planet disk from $K = 0.1$ to $K = 0.007$ at eastern elongations and further from $K = 0.007$ to $K = 0.4$ at western elongations. Measurements at 3.3 cm were carried out at western elongations, in the period when K was changing from 0.33 to 0.6.

The results of measurements at 4 and 8 mm are plotted in Fig. 3 a, b in the form of dependence on K of the brightness temperature $T_{b\varphi}$ averaged over the planet disk. Solid lines in the figures indicate the averaged dependence of $T_{b\varphi}(K)$ obtained by approximation with the least-mean method. Minimum values of the

brightness temperature at those wavelengths were obtained near the inferior conjunction and were equal respectively to 375 ± 75°K and 390 ± 120°K.

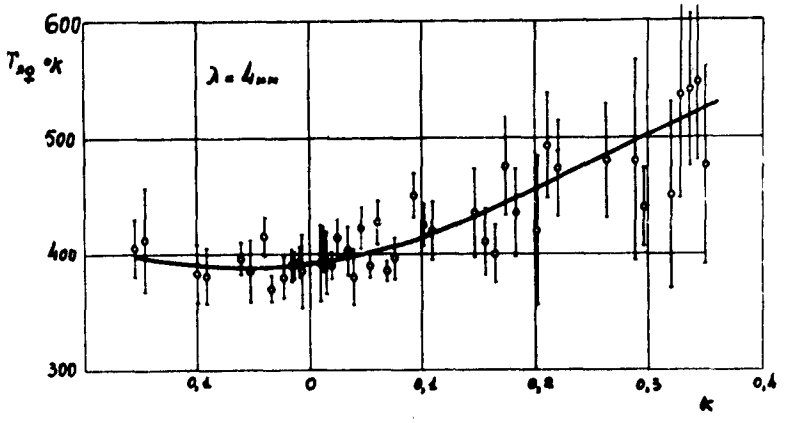

Fig 3a

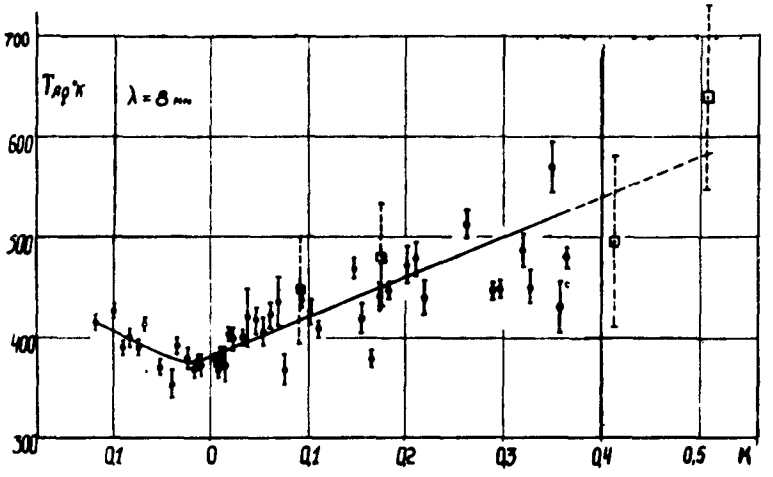

Fig. 3b

The position of the minima does not coincide exactly with the moment of the inferior conjunction, but is somewhat shifted towards the eastern elongations. However, one should note that the above-mentioned shift of the minima is apparently connected

with the inaccurate account of the antenna parameter changes and, therefore requires further checking.

With moving away from the inferior conjunction and the increase of K connected with this, a tendency is revealed towards growth of $T_{b\varphi}$ the brightness temperature averaged over the disk. The mean value of $T_{b\varphi}$ obtained at maximum value of $K = 0.3$—0.4 was found to be $483 \pm 100°K$ and $495 \pm 150°K$ respectively at 8 and 4 mm.

At 3.3 cm the mean value of brightness temperatures measured in the interval $K = 0.33 - 0.6$ was found to be $542 \pm 85°K$. By the growth of K a tendency of the brightness temperature to increase was also detected (Fig. 4).

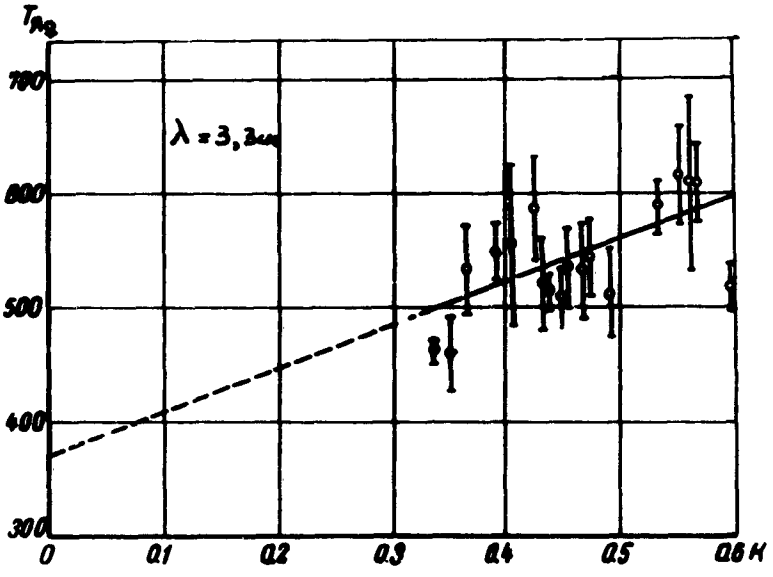

Fig. 4

At 9.6 cm the mean value of the brightness temperature (for the observation period from March 20 to June 1) averaged by the Venus visible disk was 690°K (*).

(*) The systematic error of the brightness temperature measurements caused by inaccurate knowledge of fluxes of the sources assumed as standard ones is estimated as $\pm$ 15 %.

To analyse the observed spread of brightness temperature about this mean value, histograms were plotted (Fig. 5). In connection with the small number of records made on one day, the histograms were constructed from the data of a series of measurements for several days. The histograms have shown that for the majority

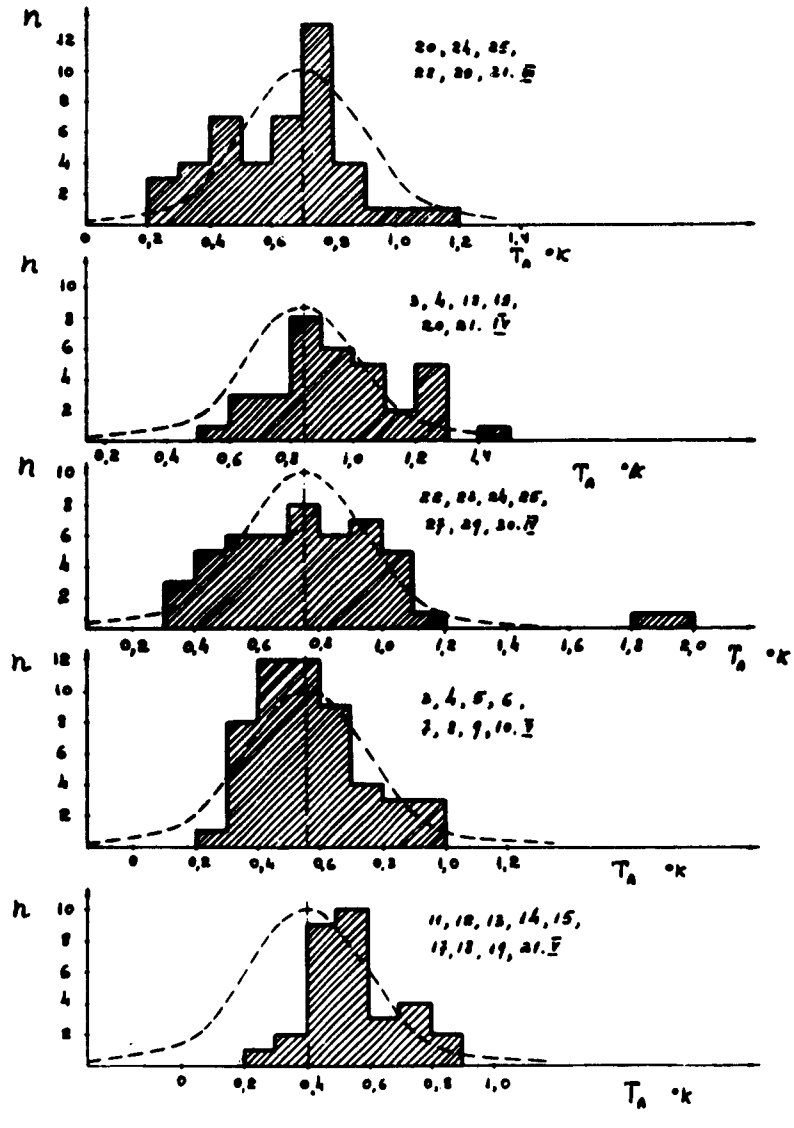

Fig. 5

of days of measurements, the brightness temperatures distribution was close to the Gaussian one near the average temperature $\sim 690^{\circ}$K with a dispersion corresponding to a dispersion of the antenna temperatures of $\sim 0.2^{\circ}$K.

Independently in the period of Venus observations and after it control records of the radio sources of 3 C 270, 3 C 348 (16 NOA) [18] and CTB 74 [19] which intensity are close to that of Venus at 9.6 cm were made. The results of these records carried out on April 1 and 21, 1961 and March 24, 27 and 28, 1962 have shown that the mean square error (dispersion) of a single measurement was within 0.13 — 0.22°K.

The statistical processing of the zero level carried out on the records of Venus passage showed that in the majority of cases, the mean square deflection was also found to be 0.2°K. Thus, for the majority of the days of observation, spread of the obtained brightness temperature of Venus was of the same order as the expected mean square error of the single measurement. Therefore, on those days it seems impossible to determine unambiguously whether the variations of Venus brightness temperature pointed out earlier [20] are real at that wavelength or are caused by the insufficient accuracy of the measurements.

However on two days of observations — April 4 and 23, — the detected brightness temperatures were so high that we were unable to explain them by statistical errors of measurements.

On April 4 three records of the Venus passage were made at $15^{h}00^{m}$, $15^{h}40^{m}$, and $15^{h}48^{m}$ UT. In each of the above-mentioned records the antenna temperature $\sim 1.3^{\circ}$K was obtained, which corresponds to the brightness temperature $\sim 1000^{\circ}$K. However, at the average brightness temperature of 690°K, one should obtain antenna temperatures of 0.9°K. The mean square deviations of the zero level were 0.21°K on that day. The probability that at measuring the temperature of 0.9°K the antenna temperature of 1.3°K was obtained three times one after another as a result of statistical errors, was $1.5.10^{-4}$.

On April 23, increased antenna temperatures were also observed. For instance, at 3^h10^m and 4^h20^m UT the measured antenna temperatures of 1570 and 1660°K. At the mean square deflections of zero level on this day of 0.22°K the probability of receiving the above data as a result of statistical errors was 10^{-5} and 10^{-6} respectively. In addition, on that day also, essential (comparing to dispersion) relatively rapid variations of the Venus antenna temperature took place at measurements which corresponded to the brightness temperature equal to 1570, 980, 1660, 830 and 710°K at 3^h10^m, 3^h40^m, 4^h20^m, 4^h57^m, and at 5^h16^m UT, respectively. Copies of records of the above passages are presented in Fig. 6.

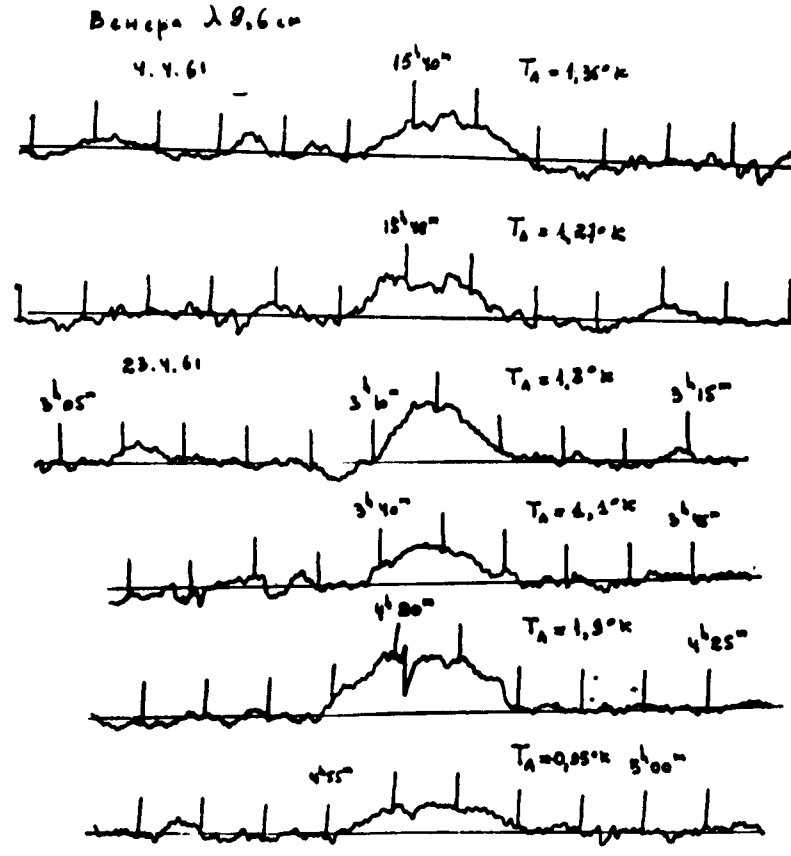

Fig. 6

It is not excluded that the above-mentioned increased temperatures and essential intensity variations are due to a certain systematic error which was not taken into account. Therefore, since the available observation material is not sufficient, the above data require further checking and confirmation.

Thus at 4 and 8 mm the Venus brightness temperature reaches its minimum near the inferior conjunction and is $390 \pm 120°K$ and $375 \pm 75°K$, respectively. The position of the minima does not coincide exactly with the moment of the inferior conjunction but is somewhat shifted towards eastern elongations.

At 3.3 cm the mean value of the brightness temperature in the variation interval of the relative area of the illuminated part of the planet disk $K = 0.33 — 0.6$, where the measurements were carried out was $542 \pm 85°K$.

At all three wavelengths, a tendency was found out towards growth of the brightness temperature with the increase of K.

At 9.6 the value of the brightness temperature averaged for the observation period is 690°K. On April 4 and 23 we observed anomalously high (1000-1500°K) brightness temperatures which we were unable to explain by statistical errors of measurements.

The next paper ([21]) is devoted to the discussion of the results obtained.

REFERENCES

([1]) C. H. Mayer, T. P. McCullough, R. M. Sloanaker, *Astrophys. J.*, **127**, N. 1, I, 1958.

([2]) L. E. Alsop., J. A. Giordmaine, C. H. Mayer, C. H. Townes, *Astr. Journ.*, **63**, 301, 1958.

([3]) D. E. Gibson, R. McEwan, *Radioastronomy*, Paris Symposium, Chicago Univ. Press, 1959.

([4]) A. D. Kuzmin, A. E. Salomonovich, *Astr. Journ.*, **37**, N. 2, 297, 1960.

([5]) C. H. Mayer, T. P. McCullough, R. M. Sloanaker, *Report to the XIII General Assembly URSI*, London, 1960.

([6]) A. H. Barrett, *Astrophys. J.*, **133**, N. 1, 281, 1961.

([7]) D. E. Jones, *Planetary and Space Sci.*, **5**, N. 2, 166, 1961.

(9) C. SAGAN, *Science*, **133**, 849, 1961.

(10) E. ÖPIK, *J. Geophys. Res.*, **66**, 2807, 1961.

(11) P. D. KALACHEV, A. E. SALOMONOVICH, *Radiotechn. and Electronics*, **6**, N. 3, 422, 1961.

(12) A. G. KISLYAKOV, A. D. KUZMIN, A. E. SALOMONOVICH, *Izvestia VUZ, Radiophysics*, **4**, N. 3, 573, 1961.

(13) A. M. KARACHUN, A. D. KUZMIN, A. E. SALOMONOVICH, *Astr. Journ.*, **38**, N. 1, 83, 1961.

(14) A. M. KARACHUN, A. D. KUZMIN, A. E. SALOMONOVICH, *Radiotech. and Electronics*, **6**, N. 3, 430, 1961.

(15) D. H. MENZEL, W. W. COBLENTZ, C. O. LAMPLAND, *Astrophys. J.*, **63**, 177, 1926.

(16) L. E. ALSOP, J. A. GIORDMAINE, C. H. TOWNES, C. H. MAYER, *Astr. Journ.*, **64**, N. 8, 332, 1959.

(17) A. D. KUZMIN, *Radiotech. and Electronics*, **3**, N. 4, 561, 1958.

(18) A. G. KISLYAKOV. *Izvestia VUZ. Radiophysics*, **4**, 3, 433, 1961.

(19) D. O. EDGE, J. R. SHAKESHAFT, W. B. MCADAMS, J. E. BALDWIN, S. ARCHER, *Mem. R. A. S.*, **68**, 37, 1959.

(20) R. W. WILSON, J. G. BOLTON, *Publ. Astron. Soc. Pacif.*, **72**, N. 428, 1960.

(21) A. D. KUZMIN, A. E. SALOMONOVICH, *Astron. Circ.* N. 221, 1961, April 30. *Astr. Journ.*, **38**, N. 6, 1115, 1961.

(22) A. D. KUZMIN, A. E. SALOMONOVICH, This Symposium, 1962.

32. — SOME CONCLUSIONS ABOUT PHYSICAL CONDITIONS ON VENUS ACCORDING TO RADIO ASTRONOMICAL OBSERVATIONS AT P. N. LEBEDEV PHYSICAL INSTITUTE

A. D. KUZMIN, A. E. SALOMONOVICH
P. N. Lebedev Physical Institute, Moscow, U. S. S. R.

1. Introduction

As it is well-known, since the Venus surface is covered with a dense layer of clouds opaque for visible and infrared radiations, optical investigations of the physical conditions on the planet carried out during many tens of years have not yet given any complete information about the temperature and character of its surface, the composition of the atmosphere and even about the period and sense of rotation. As radio waves can penetrate through a cloud layer, one can expect that investigations of the intrinsic radiation of Venus will make it possible to clarify the questions essentially significant for the planet physics.

At P. N. Lebedev Physical Institute of the USSR Academy of Sciences investigations of Venus radiation were started near the inferior conjunction of 1959 (1). Observations were carried out at 8 mm with the 22-meter radio telescope (2). The use of that radio telescope operating at so short a wavelength allowed to observe the planet two months after the inferior conjunction. For the first time it became possible to detect that the brightness temperature averaged over the visible disk of Venus grew with increase of the illuminated part of the planet disk. The existence of phase variation of the averaged brightness temperature was interpreted as an effect of the difference between the brightness temperatures of the illuminated and unilluminated hemispheres of the planet, that in its turn, showed a relatively large period of its rotation (longer than the Earth day).

Later C. H. Mayer. T. P. McCullough and R. M. Sloanaker [3] made also a communication about the existence of phase variation of the Venus brightness temperature at 3 and 10 cm. According to the data of radar investigations of Venus [4, 5] carried out in 1961, the rotation period of Venus is really essentially longer than the Earth day.

As one of the possible reasons for the fact that the brightness temperature at 8 mm measured by us [1] and D. E. Gibson and R. McEwan [6] was found to be considerably lower than at 3 and 10 cm according to the data of Mayer, McCullough and Sloanaker[7], it was pointed to the stronger absorption of shorter waves in the relatively cold atmosphere of Venus. For a quantitative explanation of this difference, A. H. Barrett [8] had to assume the existence of considerable (to 30 atmospheres) pressure on the planet surface, or (at less pressure of 20-10 atmospheres) of the appreciable (1-3%) content of water vapour.

In the greenhouse model put forward by C. Sagan [9] attenuation of radiation in the millimeter range takes place in the cloud layer containing H_2O and CO_2. According to this model, the greenhouse effect causing high temperature of the surface is produced by the atmosphere comprising CO_2 and H_2O.

In the « aeolosphere » model put forward by E. Öpik [10] the undercloud layer is the region of strong winds heating the planet surface owing to friction.

D. E. Jones [11] suggested another mechanism according to which the planet ionosphere, optically thick up to 3 cm, is responsible for radiation at 3 cm and longer wavelengths.

All the above-mentioned models are based on the equality of brightness temperatures of the Venus night side ($\sim 600^{\circ}$K) in the range from 3 to 20 cm.

The lack of observational data made it impossible to prefer one of the above models or even consider them as well-grounded.

2. Results of observations of 1961

In the period of the inferior conjunction of 1961, radio-observations of Venus were continued on a wider scale in P. N. Lebedev Physical Institute of the USSR Academy of Sciences. In order to obtain spectral characteristics, measurements were carried out in a series of millimeter and centimeter ranges. From the middle of March to the beginning of June, observations were performed at 4 and 8 mm and 9.6 cm. Unfortunately since the instruments were not ready to operate we were unable to carry on observations at 3.3 cm. Those measurements were started only on May, 26 and continued to June, 10. The technique of the observations was described in [12],

At 4 and 8 mm minimum values of the brightness temperatures $T_{b\varphi}$ averaged over the planet disk were obtained near the inferior conjunction and were equal to $390 \pm 120^{\circ}$K and $375 \pm 75^{\circ}$K. The position of the minima did not coincide exactly with the moment of the inferior conjunction, but is somewhat shifted towards eastern elongations. It is not excluded, however, that this displacement depends on inaccurate account of the variation in the antenna parameters, and, therefore, it requires confirmation. With the increase of the distance from the inferior conjunction and the growth of K- relative area of the illuminated part of the planet disk, a tendency towards increase of the brightness temperature averaged over the visible disk was found out. At the same time it should be noted that at 8 mm deflections from the regular increase, as a rule, exceed the mean square errors of measurements of average values of $T_{b\varphi}$ obtained day after day. Generally speaking, these deflections can testify the existence of short time variations of the Venus brightness temperature connected apparently with the planet rotation. However, it is more probable, that they are the result of systematical changes of the measurement conditions not taken into account and therefore they cannot be considered yet really significant.

The mean value of $T_{b\varphi}$ obtained at maximum K = 0.3-0.4 at which measurements were carried out, was $495 \pm 150^{\circ}$K and $483 \pm 100^{\circ}$K at respectively 4 and 8 mm.

At 3.3 cm the mean value of the brightness temperature in the interval K = 0.33-0.6 in which measurements were carried out, was $542 \pm 85^{\circ}$K. With the increase of K a tendency towards the growth of $T_{b\varphi}$ was also found out.

At 9.6 cm the mean value of brightness temperature for the observation period from March 20 till June 1, was $690 \pm 100^{\circ}$K.

In connection with large relative errors of measurements it seems impossible at the present time to determine the dependence of $T_{b\varphi}$ on K, and also to decide unambiguously whether the variations of Venus brightness temperature noted earlier in ([13]) are real at this wavelength or depend on the insufficient accuracy of measurements. However, at observations on April 4 and 23, so high brightness temperatures (1000-1500°K) were observed that we were unable to explain them as accidental errors of measurements.

3. Comparison with the Data of Other Radio Astronomical Observations

Before starting to discuss conclusions about the physical conditions on Venus, that one can make from the results of our measurements, it is useful to compare them with the data of other radio observations of the planet.

More correct than the previous ([14]) estimate of antenna parameters of the radio telescope at 8 mm made by us in ([12]) from Jupiter radio emission, makes it possible to correct the value of Venus brightness temperatures measured near the inferior conjunction of 1959 ([1]). If one assumes that in 1959 the effective area of the antenna was the same as estimated in 1961, then recalculation of the antenna temperatures obtained in 1959 for the corresponding values of K gives the values of the brightness temperatures coincid-

ing within the measurement errors, with the values of $T_{b\varphi}$ measured in 1961.

The data by D. E. Gibson and R. McEwan ([6]) are also in a good agreement with the results of our observations and some difference in brightness temperatures can be apparently explained by the difference in methods of determining effective areas of the radio telescope antennas.

Thus, at 8 mm, the brightness temperature on the night side of Venus is $\sim 400^{\circ}$K.

At 3.3 cm the results obtained by us can be compared with the recently published results of similar measurements by C. H. Mayer, T. P. McCullough and R. M. Sloanaker ([3]) carried out in 1958. Since both series of measurements were performed, to our regret, in different intervals of variation of Venus phase, one can compare only with making use of extrapolation to the corresponding intervals. Assuming to a first approximation, that brightness temperatures are constant within the illuminated and unilluminated hemisphere of the planet, we can assume linear (relative to K) dependence of T_b : Venus brightness temperature averaged over the disk. The linear extrapolation of the phase variation communicated in ([3]) to K = 0.47 (the middle of the interval of our measurements in 1961) gives the value $T_{b\varphi} = 760^{\circ}$K. For the same K we obtained $T_{b\varphi} = 545 \pm 60^{\circ}$K. On the other hand, the linear extrapolation of values of $T_{b\varphi}$ measured by us in the interval K = 0.33-0.6 to the value K = 0 carried out by the least-square method, gives $T_{b\varphi} = 372 \pm 75^{\circ}$K. The analogous extrapolation of the data communicated in ([3]) gives $T_{b\varphi} = 470^{\circ}$K.

Thus, at 3.3 cm brightness temperatures of the unilluminated hemisphere of Venus determined by extrapolation, turned out to be rather close to 400-500°K. At the same time, near dichotomy the brightness temperature measured by us was found to be considerably lower than according to the data ([3]). It means that at 3.3 cm the phase variation of Venus brightness temperature is apparently considerably less than it was indicated in ([3]).

The above-mentioned difference of Venus brightness temperatures measured by us in 1961, in ([3]) in 1958 and also in the earlier observations of 1956 ([7]), depends apparently on the inaccuracy of extrapolations, the inexact knowledge of radiation fluxes of the sources assumed as standard, and the difference in calibration methods. At the same time it is not excluded that Venus brightness temperatures indeed differ one from another in different years.

At 9.6 cm the mean value (for the observation interval) of Venus brightness temperature measured by us (690°K) is somewhat larger than that obtained by F. D. Drake ([15]) ($\sim 600^{\circ}$) at 10.0 cm. However, the above difference is within the systematical errors of measurements (15 % in our measurements ([12]) and 8 % in ([15])) and, apparently, depends on the difference in flux densities of the sources adopted as standard at calibration.

Our data do not contradict the small phase variation measured by Drake ([15]), but do not confirm the considerable growth of the brightness temperature with the increase of K communicated by C. H. Mayer, T. P. Mc Cullough and R. M. Sloanaker ([3]).

The above-mentioned anomalously high (1000-1500°K) brightness temperatures of Venus observed by us on April 4 and 23 due to difference in local time cannot be directly compared with Drake's data ([15]) which mentioned the absence of appreciable variations of $T_{b_{\varphi}}$ for the whole interval of observations.

IV. Discussion of the Obtained Results and Some Conclusions about Physical Conditions on Venus

All our results together with the results of other radio astronomical investigations of Venus, make it possible to draw some conclusions about physical conditions on the planet.

1. *Venus temperature conditions*

Dependence of Venus brightness temperature $T_{b_{\varphi}}$ averaged over the disk on the relative area of the illuminated part of the

disk indicated the difference of brightness temperatures of the night and day sides of Venus.

a. *Surface temperature of Venus night side.*

As is well-known, in the general case the brightness temperature of the emitting object is not connected directly with its physical temperature. Only in the case of a thermal mechanism of electromagnetic radiation of an optically thick layer the brightness temperature is equal to the temperature of the emitting body. Therefore, to conclude about the thermal conditions on Venus, first of all one must separate the thermal component of its radiation. For the thermal radiation component of the isothermal and optically thick medium, independence of the brightness temperature on the wavelength is typical (*).

According to the early data of American scientists ([7]) the same brightness temperature of the unilluminated side of Venus of $\sim$ 600°K was obtained at 3 and 10 cm. This gave many authors the grounds to assume that the radiation in those ranges is thermal and to ascribe it to the surface of the planet with the temperature (on the night side) equal to 600°K.

As it was noted above, at 3 cm the extrapolated data give brightness temperature of the unilluminated side of Venus of 400-500°K which is less than in ([7]). However, one should note that the results obtained by means of extrapolation with the presence of relatively large errors of measurement need confirmation by direct measurements. Confirmation of the lowest of the above-mentioned temperatures will show that brightness temperatures of unilluminated side of Venus in 4 mm — 3 cm range are approximately the same. In its turn, it will give reasons to assume Venus radio emission to be chiefly thermal, in that range. However, this will not make possible to decide unambiguously whether the surface or the optically thick (up to 4 mm wavelength ionosphere is responsible

(*) If the reflection factors are the same.

for this radiation. The later assumption is of small probability since it requires that the electron concentration exceeds more than by four orders of magnitude, that of the earth ionosphere.

It is most probable that in the 4 mm — 3.3 cm range, radiation is emitted by the surface or the near to the surface layer of the atmosphere, and that the brightness temperature of this radiation is close to the physical temperature of the unilluminated surface of Venus. In this case one can assume that the surface temperature of the unilluminated side is $\sim 400^{\circ}$K.

On the other hand, if direct measurements at 3 cm in the inferior conjunction give the brightness temperature of $\sim 600^{\circ}$K, it is not excluded that the surface temperature of Venus night side reaches 600°K. (*)

It should be noted that the above temperatures are the result of averaging over the unilluminated side of Venus.

b. *Temperature of Venus Day Side.*

In order to determine the surface temperature of Venus day side, it would be necessary to measure its brightness temperature near the superior conjunction ($K = 1$) at different wavelengths. However, the observations carried on by us continued only three months after the inferior conjunction (to $K = 0.6$) and then, were stopped because of the signal weakening caused by the increase of the distance from Venus.

Therefore, according to the up-to-date data available on radio observations of Venus one cannot yet determine the surface temperature of the day side. It is possible only to make a preliminary estimate of it with the help of extrapolation of the available data to $K = 1$. Such an extrapolation based on the data of our observations at 4 mm, 8 mm and 3.3 cm gives the brightness temperature of the illuminated side ~ 750-800°K. However, besides

(*) In accordance to Mayer, McCullough and Sloanaker's measurements (this symposium) the brightness temperature near inferior conjunction is close to 550°K. Therefore the last assumption seems a more real one.

the thermal component connected with the planet surface, a contribution due to the ionosphere can probably take place. In this case the density of the cytherean ionosphere should be larger on the day side than on the night side of Venus.

The question about the separation of the component depending on the thermal radiation of the surface can be solved only after carrying out additional investigations. At present one can only assume that the surface temperature of the day side of Venus apparently does not exceed 800°K.

2. *Rotation of Venus*

The phase dependence of the brightness temperature averaged over the planet disk, at 4.8 mm and 3.3 cm, established earlier ([1, 3]) and confirmed by present observations makes it possible to conclude that the rotation period of Venus exceeds the Earth day. Indeed, if Venus day were shorter than Earth day, then carrying out, day after day, observations of Venus radiation averaged over the disk, we would not found out monotonous variation of its brightness temperature. The existence of the phase variation speaks in favour of a relatively slow rotation of Venus.

Besides, as it was noted in ([1]), relative observations of the phase variation of Venus brightness temperature at eastern and western elongations make it possible to determine the sense of the planet rotation. One should expect that due to the thermal inertia of the substance of the planet surface layer at equal portions of the illuminated part of its disk, the brightness temperatures averaged over the disk will be different at eastern and western elongations, and that the minimum of the planet brightness temperature will be shifted relative to the point of the inferior conjunction. Indeed, at the direct rotation of the planet, it will face the Earth observer by its morning side (rotation from the unilluminated side to the illuminated one) at eastern elongations and by its evening side (rotation from the illuminated side to the unilluminated one) at western

elongation. Therefore at eastern elongations, already cold dark and not heated yet illuminated parts of the planet will face the Earth's observer. At western elongations the observer will see the heated illuminated and not yet cooled dark parts. It is obvious that at equal relations between areas of the illuminated and unilluminated parts of the visible disk of the planet (equal K) the brightness temperatures averaged over the disk will be lower at eastern elongations (comparing to western elongations), and the brightness temperature minimum will be shifted towards eastern elongations. At the inverse sense of the rotation we shall have an opposite situation.

We carried out observations just near the inferior conjunction at 4 and 8 mm. In both cases, apparently, a shift of the minimum takes place towards eastern elongations that shows the direct rotation of Venus about its axis.

The shift of T_b minimum allows also to point out that the rotation period of Venus cannot be equal to its period of revolution. Indeed, in this case the planet would always face the Sun by one side and its surface would have a stationary distribution of temperatures depending only on the illumination by the Sun. Therefore, at equal phases the brightness temperatures averaged over the visible disk will be the same at western and eastern elongations, and the minimum will take place exactly in the inferior conjunction.

3. *Venus ionosphere*

Since at 10 cm Venus brightness temperature ($\sim$ 600-700°K) is apparently higher than at shorter wavelengths, one can assume that in this range, the medium located above the planet surface is responsible at least for some part of this radiation. The cytherean ionosphere could be such a medium if its optical thickness is close to 1 at 10 cm. In this case the brightness temperature of the planet radiation will be close to the kinetic temperature of electrons in the ionosphere. At shorter wavelengths the ionosphere will become

transparent and the received radiation will be a thermal radiation of the surface and the near-to-surface layer of the atmosphere.

As is well-known a serious difficulty in this model is the mechanism of production and keeping of a rather high electron concentration in the Venus ionosphere necessary to explain the obtained results (at the altitude of the inhomogeneous ionosphere of 100 km it is necessary that $N_e = 5.10^6$ cm^{-3}).

Calculations carried out by Danilov ([16]) for Venus atmosphere consisting chiefly of CO_2 have shown that if the only ionizing factor is solar ultraviolet radiation, then the maximum of the electron density will be 10^4 cm^{-3}. Thus, for the production of $N_e = 5.10^6$ cm^{-3}, additional ionizing factors are necessary.

According to D. E. Jones ([11]), in the case when the Venus magnetic field is 1/30 of the Earth's magnetic field, the necessary ionization can be caused by solar corpuscular streams.

As another possible ionizing factor, one can suggest meteoric fluxes. As is well-known, in the Earth's ionosphere the electron concentration in the meteor tracks reaches $10^{10} - 10^{11}$ cm^{-3} ([17]). However, to obtain the necessary mean electron concentration of 5.10^6 cm^{-3}, it is necessary for the density of those fluxes to be by some orders of magnitude larger near Venus than in the vicinity of the Earth.

If at 10 cm Venus ionosphere has optical thickness close to 1, then one should expect that, at the moments of the increase of the activity of the ionizing factors, the ionosphere will also make an additional contribution to the planet radiation at 3 cm. In this connection, it is interesting to compare the results of the measures of the Venus brightness temperature, in this wavelength range, carried out in different years corresponding to various phases of the 11-years cycle of solar activity.

The surface temperature of the planet and, therefore, the intensity of its thermal radiation cannot apparently change considerably in connection with the decrease of the solar activity. However, one can assume that some portion of the Venus radiation at 3 cm is

generated by its ionosphere, the state of which must be closely connected with the 11-year cycle (*).

Another difficulty of the ionosphere model is its matching to the available data of radar observations ([4,5]) from which it follows that the reflection factor of Venus is ~ 0.1 at 12 and 43 cm. If the optical thickness of the ionosphere is ~ 1 at 10 cm, then at a longer 43 cm wavelength it will be for sure greater than 1 and the observed reflection can take place only from the ionosphere itself.

However to obtain such a reflection, the gradient of the electron concentration in Venus ionosphere must be very large.

To conclude, it should be noted that although the obtained materials allow us to make some considerations about the physical conditions on Venus, at the present time, it is apparently impossible to prefer any available model of the planet. It is possible that the solution of the problem will be found in some combination of these models.

In order to clear up the question, additional measurements in a wavelength range as wide as possible, during a sufficiently large period of observations, are necessary.

REFERENCES

([1]) A. D. KUZMIN, A. E. SALOMONOVICH, *Astr. Journ.*, **37**, N. 2, 297, 1960.

([2]) P. D. KALACHEV, A. E. SALOMONOVICH, *Radiotechn. and Electronics*, **6**, N. 3, 422, 1961.

([3]) C. H. MAYER, T. P. MCCULLOUGH, R. M. SLOANAKER, *Report to the XIII General Assembly URSI*, London, 1960.

([4]) V. A. KOTELNIKOV, *J. Brit. Inst. Radio. Engrs.*, **621**, 293, 1961.

([5]) L. R. MALLING, S. W. GOLOMB, *Journ. of the Brit. Inst. Radio Eng.*

([6]) D. E. GIBSON, P. MCEWAN, *Radioastronomy*, Paris Symposium, Stanford Univ. Press, 1959.

(*) Let us note also that another reason of the annual brightness temperature variation may be the existence on Venus of large regions having different reflection factors (for instance, continents and oceans). At a sufficiently large rotation period in the inferior conjunction of different years, Venus will face the Earth different hemispheres, brightness temperature of which can be different due to difference in irradiative abilities.

(7) C. H. Mayer, T. P. McCullough, R. M. Sloanaker, *Astrophys. J.*, **127**, N. 1, I, 1958.

(8) A. H. Barrett, *Astrophys. J.*, **133**, N. 1, 281, 1961.

(9) C. Sagan, Science, **133**, 849, 1961.

(10) E. Öpik, *J. Geophys. Res.*, **66**, 2807, 1961.

(11) D. E. Jones, *Planetary and Space Sci.*, **5**, N. 2, 166, 1961.

(12) V. P. Bibinova, A. G. Kisliakov, A. D. Kuzmin, A. E. Salomonovich, I. V. Shavlovsky, This symposium, 1962.

(13) A. D. Kuzmin, A. E. Salomonovich, *Astronomical Circular* N. 221, 1961. April 30. *Astr. Journ.*, **38**, N. 6, 1115, 1961.

(14) A. M. Karachun, A. D. Kuzmin, A. E. Salomonovich, *Radiotechnics and Electronics* **6**, N. 3, 430, 1961.

(15) F. D. Drake, *Publ. NRAO*, **1**, N. II, 165, 1962.

(16) A. D. Danilov, *Geomagnetism and Aeronomy*, I, N. 3, 314, 1961.

(17) K. U. Allen, *Astrophysical magnitudes* (Publishing House of Foreign Literature, 1961).

33. — 3.15 CM OBSERVATIONS OF VENUS IN 1961

C. H. MAYER, T. P. McCULLOUGH and R. M. SLOANAKER
Radio Astronomy Branch, U. S. Naval Research Laboratory
Washington, D. C., U. S. A.

A long series of observations of the 3.15 cm radiation from Venus which included the inferior conjunction of April 11, 1961 was made to investigate the dependence of the radio emission on the phase of solar illumination which had been suggested by previous observations (Mayer, McCullough, and Sloanaker, 1958, 1960; Alsop, Giordmaine, Mayer, and Townes 1958, 1959; Kuzmin and Salomonovich 1960). The observations were made using the 50 foot reflector at the Naval Research Laboratory in Washington which was equipped with a superheterodyne radiometer similar to those previously used but with improved sensitivity mainly due to better crystal mixers and a broader bandwidth. The *rms* fluctuation at the output of the radiometer with a two second time constant was 1/4°K. Each day of the observations, a large number of drift scans were made across Venus with on the average about 10 at the proper declination for Venus and the rest at declinations above and below the proper one to check the pointing of the antenna. The intensity scale of the radiometer was calibrated at about 20 minute intervals using an argon discharge noise source which in turn was calibrated against a thermal noise source before the observations were started in March and again after the observations were completed in September. In addition, the overall system calibration was monitored on as many days as possible by observing the radio source Taurus-A.

Observations

The observations are summarized in Figure 1 where daily average antenna temperatures for Taurus-A and Venus are plotted in the upper graph and the corresponding daily values for the apparent blackbody disk temperature of Venus are plotted in the

lower graph. The measurements of Taurus-A showed gradual changes with time of maximum amplitude of about $\pm$ 2-½ percent which were taken to be indications of changes in the overall system calibration or the transmission of the earth's atmosphere and were applied as corrections to the Venus observations. The antenna temperature of Venus increased to a maximum of 3.8°K and reached

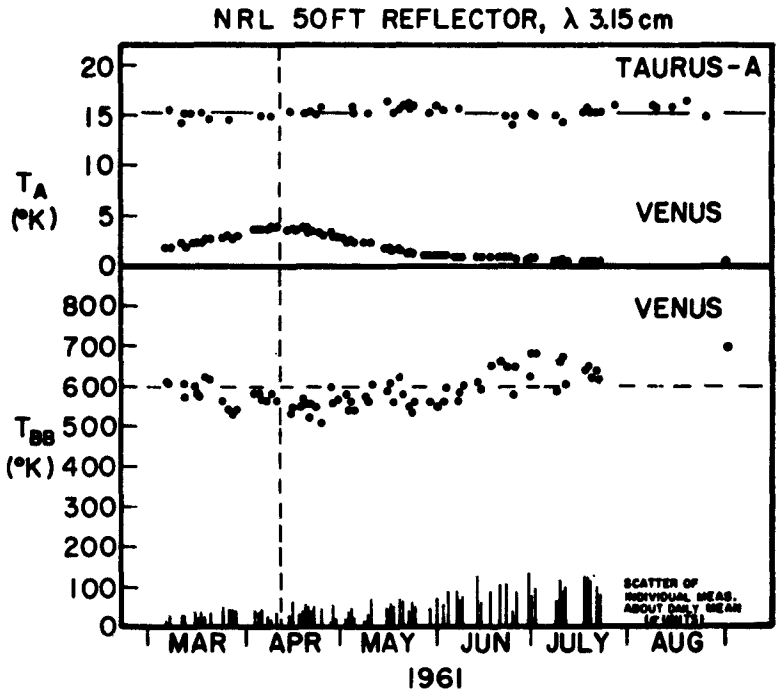

Fig. 1

a level of about 0.5°K near the end of the measuring period. The single point of August 31 corresponds to an antenna temperature for Venus of 0.25°K.

The daily average values of the blackbody disk temperature were corrected for (1) an averaging reduction due to pointing errors of 2 percent, (2) the calculated atmospheric absorption based on average meteorological conditions which was less than 2 percent for 80 percent of the data, (3) a decrease in the gain of the antenna

at altitude angles less than 40 degrees of from 0 to 9 percent maximum, but which affected only 20 percent of the data, (4) the correction derived from the observations of Taurus-A within the range of about $\pm$ 2-1/2 %. The observed scatter of the individual measurements around the daily means are indicated by the bars along the bottom axis. From the radiometer noise level, the antenna temperature, and estimates of other sources of error, a scatter of about 20°K near inferior conjunction and about 100°K in July would be reasonable. The day to day scatter predicted from experimental errors is about 55°K peak to peak near conjunction and about 120°K peak to peak in July. The observed values are close to the predicted experimental scatter both for individual measurements and for day to day averages and indicate little if any short term variation in the observed 3.15 cm emission of Venus.

Phase Dependence of the Blackbody Disk Temperature

The dependence of the apparent blackbody disk temperature on phase angle is illustrated in Figure 2 where the plotted points are the daily average values. A least square fit to these points gives

$$T_{BB} = 636°K + 89°K \cos (i - 12.1°)$$

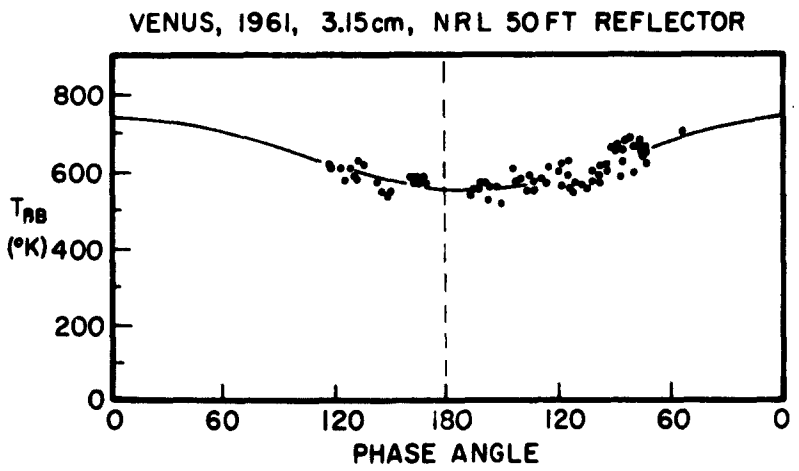

Fig. 2

which corresponds to a minimum blackbody disk temperature at a phase angle 12 degrees after inferior conjunction of 547°K and an extrapolated maximum of 725°K.

The daily average values are not of equal weight because of the change in the measured intensity by a factor of 10 during the observations. To take this into account, an extreme weighting proportional to the square of the intensity was applied to the data. A least square fit to the result gives

$$T_{BB} = 621°K + 73°K \cos (i - 11.7°)$$

which corresponds to a minimum blackbody disk temperature at a phase angle 12 degrees after inferior conjunction of 548°K and an extrapolated maximum of 694°K. For the measured data, the best solution is probably somewhere between the unweighted and the extremely weighted solutions. The probable errors derived from the least square analysis of the weighted data are 5°K for the time average value of 621°K, 6°K for the amplitude of the cosine term of 73°K, and 22 degrees for the phase angle lag after inferior conjunction of 11.7 degrees.

In addition to the uncertainty in the weighting of the data, the main uncertainties in the measured values are thought to be from systematic errors. The principal uncertainty in the time average value is the uncertainty in the effective area of the antenna which has been estimated as about 11 %. This same uncertainty applies to the absolute magnitude of the phase variation. The maximum error in the phase variation caused by a systematic overestimating of weak intensities is estimated to be 2 or 3 percent. This estimate is based first on reductions of the data both by reading individual drift curves and by averaging the drift curves point by point prior to reading, and second on readings of experimentally simulated drift curves of known intensity. The estimated effects of systematic instrumental errors such as non-linearity are negligible.

Our conclusions from the observations are that the 3.15 cm emission of Venus varies with the phase of solar illumination and that the minimum is reached about 12 degrees after inferior con-

junction. The simple solutions found by fitting the first two terms of a Fourier series to the measurements place the probable magnitude of the phase variation between $\pm$ 73°K and $\pm$ 89°K with some preference for the lower value.

Comparison with Previous NRL Observations near a Wavelength of 3 cm

The daily averages of the blackbody disk temperature are compared in Figure 3 with the daily values from previous obser-

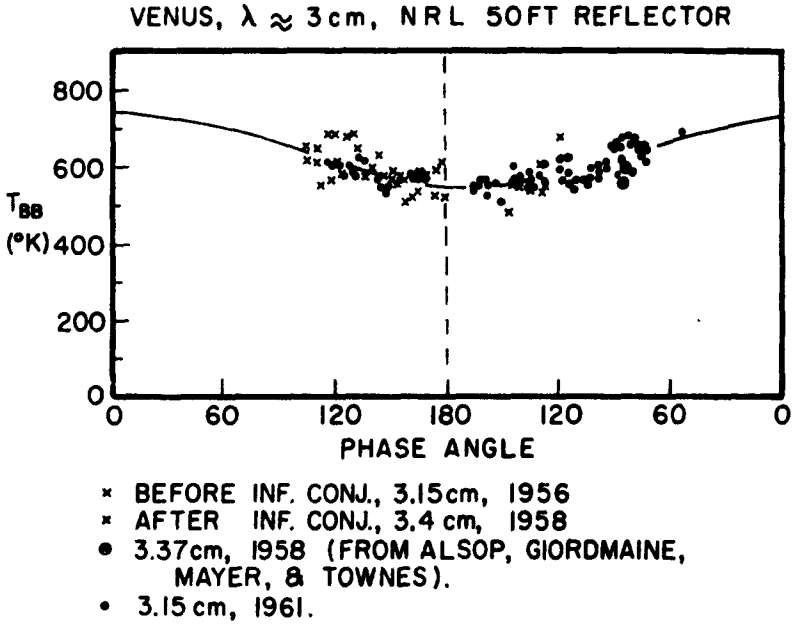

Fig. 3

vations made using the 50 foot reflector at wavelengths near 3 cm in 1956 and 1958. The reproducibility appears good, and there is no apparent evidence in these data for changes in the emission characteristics of Venus from one inferior conjunction to another.

Discussion

Observations at 10 cm wavelength made over the same time interval have been published by F. D. Drake (1962), and the result indicates a small but apparently significant phase variation in the radiation from Venus at this longer wavelength. Drake's solution gives the following result.

$$T_{BB} = 622^{\circ}K\ (9) + 39^{\circ}K\ (12) \cos\ (i - 17^{\circ})$$

The time average radio brightness temperature observed by Drake at 10 cm and that at 3.15 cm from the observations described here agree closely, and as a result there is no significant evidence for a temperature gradient or a difference in emissivity from these results.

The magnitude of the phase variation is much smaller at 10 cm than at 3.15 cm which is consistent with the emission of the longer wavelength at a deeper level as is expected in the absence of ionospheric effects. The minimum of the phase variation is observed after inferior conjunction in both cases, by 12 degrees at 3.15 cm and by 17 degrees at 10 cm, although the uncertainty in the phase angle is rather high. The larger phase lag at the longer wavelength would also be consistent with the emission of the 10 cm radiation at a deeper level than the 3.15 cm radiation. The observation of the minimum after inferior conjunction suggests that the rotation period of Venus is not the same as the orbital period, and that the sense of the rotation is retrograde. The larger phase variation at 3.15 cm than at 10 cm could also be consistent with emission from the ionosphere of Venus, as variations in the ionization would be more evident at the short wavelengths where the medium becomes more transparent, but short time variations might be expected from this same cause.

REFERENCES

ALSOP, L. E., GIORDMAINE, J. A., MAYER, C. H., and TOWNES, C. H., *A. J.*, **63**, 1958.

— *Proc. I. A. U. Symp.* No. 9 — U. R. S. I. Symp. No. 1, ed. R. N. Bracewell (Stanford : Stanford University Press), pp. 69-74, 1959.

DRAKE, F. D., *Publ. Nat. Radio Astron. Obs.* **1**, No. 11, 165, 1962.

KUZMIN, A. D. and SALOMONOVICH, A. E., *A. J.* (U.S.S.R.), **37**, 297, 1960.

MAYER, C. H., MCCULLOUGH, T. P., and SLOANAKER, R. M., *Ap. J.*, **127**, 1, 1958.

— Paper read at the XIIIth General Assembly U. R. S. I., September 5-15, 1960.

DISCUSSION DES COMMUNICATIONS 23 à 33.

E. J. Öpik (23). — A layer of accumulated dust and rubble will provide protection from further erosion. For Mercury, as well as for the moon, the fraction of new eroded mass will be insignificant.

C. Sagan (23). — Dr. Hodge was concerned that the low surface atmospheric pressure on Mercury, detected polarimetrically by Dollfus, was still large enough to prevent substantial micrometeoritic erosion of Mercury. I would like to point out that whatever atmosphere may exist on the sunlit side of Mercury must be absent in the dark hemisphere because of the extremely low temperatures — all gases are probably frozen out. Therefore, the micrometeoritic erosion and redistribution of surface material must occur preferentially on the dark side. In a way, this is unfortunate, because many of us had hoped that the dark side of Mercury would provide an historical record on the interplanetary material in the inner regions of the solar system dating back to the times of origins — with the older material being deepest. If substantial stirring and erosion occurs, this record will not be in the pristine state we would desire.

J. Rösch (24). — To which part of the Saturn rings do your spectrometer tracings refer?

G. P. Kuiper (24). — A square area, on one side, 8″ × 8″ covering rings A, B and C.

H. A. Gebbie, G. Roland, L. Delbouille (24). — Nous croyons utile de présenter ici un spectre infra-rouge de Jupiter tout récemment obtenu au moyen d'un interféromètre de Michelson.

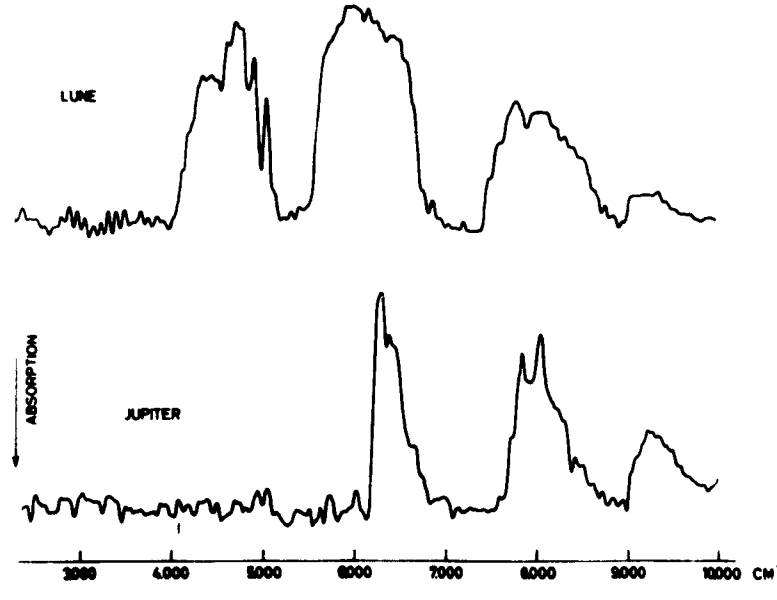

Les observations ont été faites à l'Observatoire de Haute-Provence, dans des conditions expérimentales tout à fait comparables à celles utilisées en 1961 pour l'étude de Venus (H. A. Gebbie, L. Delbouille et G. Roland : *Monthly Notices*, **126**, 497, 1962).

La figure montre un spectre de Jupiter calculé avec une résolution d'environ 40 cm^{-1}, ainsi qu'un spectre de la Lune obtenu la même nuit avec le même équipement. Une comparaison rapide de ces deux résultats met en évidence la très forte absorption de l'atmosphère de Jupiter dans la région de 6000 à 3000 cm^{-1}, et indique une autre région d'absorption vers 6500 cm^{-1}.

Faisons remarquer encore que la quantité de vapeur d'eau présente dans l'atmosphère terrestre au moment de ces deux observations était assez grande (on peut noter l'importance de la bande de H_2O à 8800 cm^{-1} et le bruit non négligeable provenant des fluctuations de l'absorption atmosphérique pendant les mesures, redistribuées sur tout le spectre par l'analyse harmonique). Nous envisageons d'effectuer prochainement d'autres observations par des nuits plus sèches, et permettant d'atteindre une plus haute résolution.

D. H. Menzel (30). — I desagree with Dr. Sagan's suggestion that the yellow color of Venus may be an effect of Rayleigh scattering. It is true that, for an observer near the surface the incident radiation — sky plus direct beam — will be reddened. But this reddening arises from the fact that the missing blue light has been scattered outwards. I concede that, near inferior conjunction, some reddening may occur, but this must be balanced by excess blue near superior conjunction.

C. Sagan (30). — There is a paper by Coulson in which multiple scattering in a Rayleigh atmosphere is considered, and the outgoing radiation computed. The computation is made for an atmosphere of terrestrial mass but for very large zenith angles which give us an idea of the effect of more massive atmosphere. As the effective pathlength increases, the light scattered out of the atmosphere is increasingly reddened.

D. H. Menzel (30). — I have not seen the work Dr. Sagan has referred to, but elementary principles show that it must be wrong. A perfect Rayleigh atmosphere of infinite extent must essentially scatter into space all the incident radiation. It will, therefore, appear white. If the atmosphere is not infinite the blue light will be dispersed in the upper atmosphere. The planet must appear blue in integrated light, though some variation of color with phase may occur.

E. J. Öpik (27) (30). — For more reliable results, extrapolation of the temperature-pressure relation should be made logarithmically, and not linear T versus P, or T versus log P.

C. Sagan (30). — The extrapolation was not made free-hand ; the choice of axes, linear, semi-long, or long does not affect the results. The data point were fit assuming convection equilibrium, and the adiabats were simply continued to the surface.

H. E. Suess (30). — I do not think that the large amounts of CO_2 in the atmosphere of Venus have anything to do with the Urey equilibrium. Relatively large amounts of carbon in the surface material of Venus would explain the absence of O_2 and the high CO_2 pressure. Absence of water makes it probably that sulphur compounds might be contributing to the formation of clouds. Has a search been made for sulphur compound in the atmosphere of Venus?

C. Sagan (30). — The original suggestion that failure of the Urey equilibrium may explain the large amounts of carbon dioxide on Venus was made by Urey a decade ago. The equilibrium partial pressure carbon dioxide on the Earth computed on the assumption that the Urey equilibrium obtains, gives a result which is within about 1 order of magnitude of the observed terrestrial carbon dioxide abundance. For this reason I think it is at least a natural line of attack to assume that the failure of the Urey equilibrium is the cause of the large abundance of CO_2 on Venus. However, I would like to point out that neither the failure of the Urey equilibrium nor Suess' assumption of large amounts of surface carbonaceous material on Venus explain the high partial pressure of nitrogen which are also indicated on Venus. As for sulphur compounds in the Cytherean atmosphere, an unsuccessful search for sulphur dioxide has been made many years ago by Kuiper (G. P. Kuiper, Atmospheres of the Earth and Planets, revised edition, University of Chicago Press, Chicago, Chapter 12, 1952).

A. H. Barrett (30). — What water vapor abundance is required to support clouds of water droplets?

C. Sagan (30). — To explain the millimeter spectrum by water droplets, a total water vapor abundance below the clouds of several tens of gm cm^{-2} are required for an adiabatic lapse rate on the dark side ; of several hundreds of gm cm^{-2} for a half adiabatic lapse rate. The required water vapor mixing ratio is then several orders of magnitude greater than the values obtained by Spinrad.

A. H. Barrett (30). — I would like to caution against drawing conclusions about the temperature on the sunlit hemisphere on the basis of published microwave phase data. The existing data cover a small range of phase angles and sunlit temperatures derived thereby involve a considerable extrapolation. Conclusions that the sunlit temperature may approach 1000° K are based on an unrealistic model consisting of constant, and different, temperatures for the dark and sunlit hemispheres. When these circumstances are coupled with the inherent poor accuracy of radio measurements, the need for extreme care in using these data to define models of Venus is obvious.

C. Sagan (30). — The preceding conclusions depended only on the existence of a moderated phase effect : 50 or 100°K. Such phase effects have been reported by Dieke, by Mayer, and by Kuzmin and Salomonovitch ; Lilley has suggested much greater phase effects. I certainly agree that better observations would be very useful.

G. de VAUCOULEURS (30). — The temperature at the occultation level is $T = 7.0\ \overline{m}$, hence depends on the CO_2 mixing ratio. To what level does your value of 240°K refer?

C. SAGAN (30). — 240° K was not the temperature at the occultation level ; it was the temperature at the cloud top, obtained from the occultation data under the assumption of radiative equilibrium between the two levels. The occultation temperature was about 203° K.

S. I. RASOOL (30). — With regard to the attenuation of microwave radiation by clouds, I had done similar calculations for different thicknesses of water clouds in order to explain the observed relative decrease of radiation from Venus at 8 mm. If Mr. Chairman allows I should like to show a slide to this respect (see figure I).

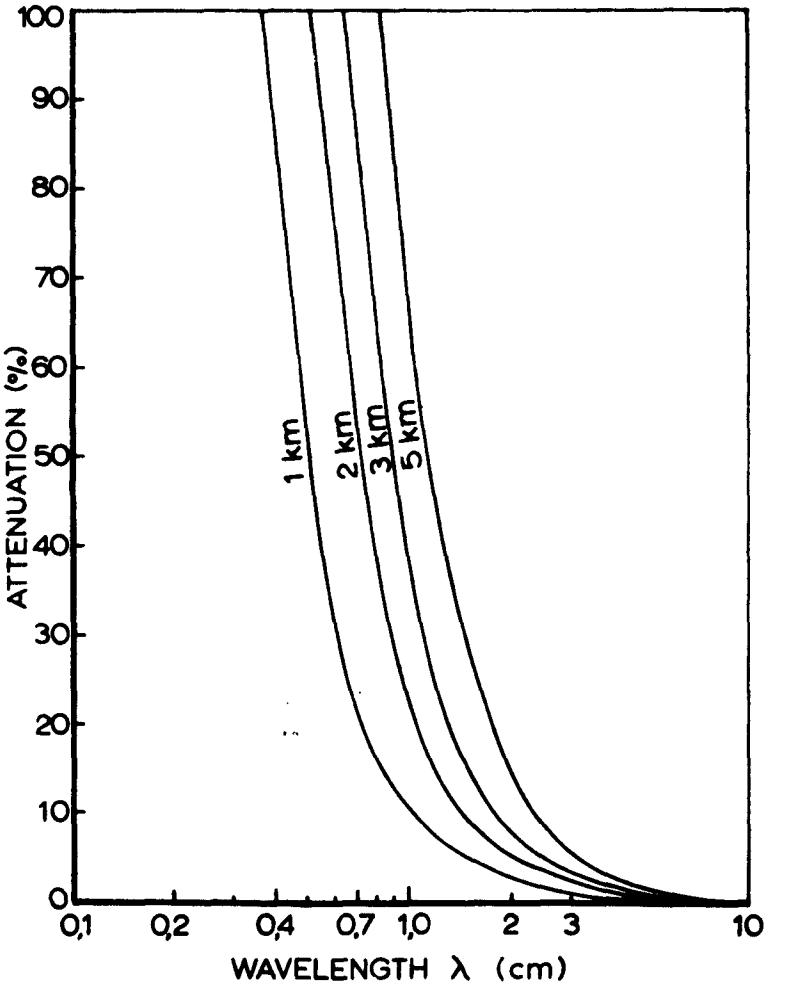

Fig. 1

The attenuation by different cloud thicknesses has been plotted as a function of wavelength. It is seen that a 2 km thick cloud is almost completely transparent to 3 cm radiation, but absorbs about 50 % of the 8 mm radiation. I had therefore estimated the Venus clouds thickness $\sim$ 2 km, which could have explained the observed spectrum of Venus radio temperatures.

Now that observations at 4 mm are also available (see Mayer's review paper) and the temperature at *this wavelength is about the same as at* 8 *mm*, figure I suggests that if the Venus clouds are a terrestrial type, their thickness may be either < 0.5 km or > 4 km. The thicknesses in between would be absorbing the 8 and 4 mm radiation differentially, which will contradict the observations.

F. Link (32). — En ce qui concerne le sens de la rotation directe déduite des mesures radio-astronomiques, l'asymétrie de l'allongement des cornes de Vénus (voir BAC **10**, 114, 1959 ; *A. J.*, **55**, 184, 1949) me conduit à la même conclusion.

E. J. Öpik (33). — A moderate effect of phase in the microwave temperature of Venus, as now proposed, may be an effect of opacity and emission level and need not necessarily contradict the aeolospheric model. Very much larger phase effects formerly suggested by other authors indicate a large margin of uncertainty in the reality of the phase effect.

34. — PRECISION MAPPING OF MARS

G. DE VAUCOULEURS
Department of Astronomy, University of Texas, Austin, Texas and Harvard College Observatory, Cambridge, Mass., U. S. A.

1. Introduction

The need for accurate maps of Mars has been obvious since the beginning of the space age. Within a few years close-up TV photography of the surface of Mars will be attempted by reconnaissance probes of the Mariner series. At present discrepancies of 5 to 10 degrees (*) or more are not uncommon in the areographic coordinates of even well-defined points on different maps. It is clear that such maps of Mars will not meet the requirements of the planetary exploration program a few years hence. In anticipation of this need for a geometrically accurate net of reference points a program for the precision mapping of the surface of Mars was initiated by the author in 1958 at Harvard Observatory under the general direction of D. H. Menzel and with the assistance of R. Wright, C. S. Yü, and Mrs L. Hudson. Since 1960 the program has been continued under the immediate supervision of A. T. Young at Harvard Observatory and by the author assisted by R. Wright, H. Ables, J. Roth, and Mrs. V. Wittasek at the University of Texas. This program has been supported and assisted in various ways since its inception by the Cambridge Research Laboratories, Air Research and Development Command, U. S. Air Force, by the Applied Research Laboratory, General dynamics — Fort Worth, and by the Jet Propulsion Laboratory, California Institute of Technology.

(*) 1 areocentric degree = 60 km at the surface = 0″12 (0″22) in the center of the disk at aphelic (perihelic) oppositions.

2. The Mars Map Project

The Mars Map Project has developed during the past four years in the following four main directions :

1. Preparation of a detailed, critical compilation of published areographic coordinates (visual and photographic) for the oppositions of 1909 to 1954 [1].

2. Preparation of a map and list of areographic coordinates from visual observations at Lowell Observatory during the opposition in 1958 [2, 3].

3. Checks on the basis of the areographic coordinates system (coordinates of pole, rotation period, ellipticity of globe) and study of systematic and accidental errors (zero points, phase effect, definition of stations) [7, 8].

4. Measurement of areographic coordinates on composite enlargements of photographs by W. S. Finsen (Union Observatory 1954, 1956) and by R. B. Leighton (Mount Wilson Observatory 1956).

The following is a summary of the main results to date.

3. Sources of Areographic Coordinates [1]

A total of 49 different sources of areographic coordinates are available for the three cycles of oppositions from 1909 to 1954 during which 21 observers contributed a total of 2,300 values (from over 12,000 independent measurements) for 586 areographic stations (307 from visual observations, 429 from photographic observations, with 150 in common). These were carefully checked by Mr. Wright through a critical study of the original sources. Ref. 1 gives a homogeneous survey of this material with a detailed cross-identification of the points ; it includes a series of 28 maps on transparent paper showing the precise locations of the stations measured by each observer at each opposition (Fig. 1) with extensive notes as to misidentifications, misprints and other errors ; the stations can be

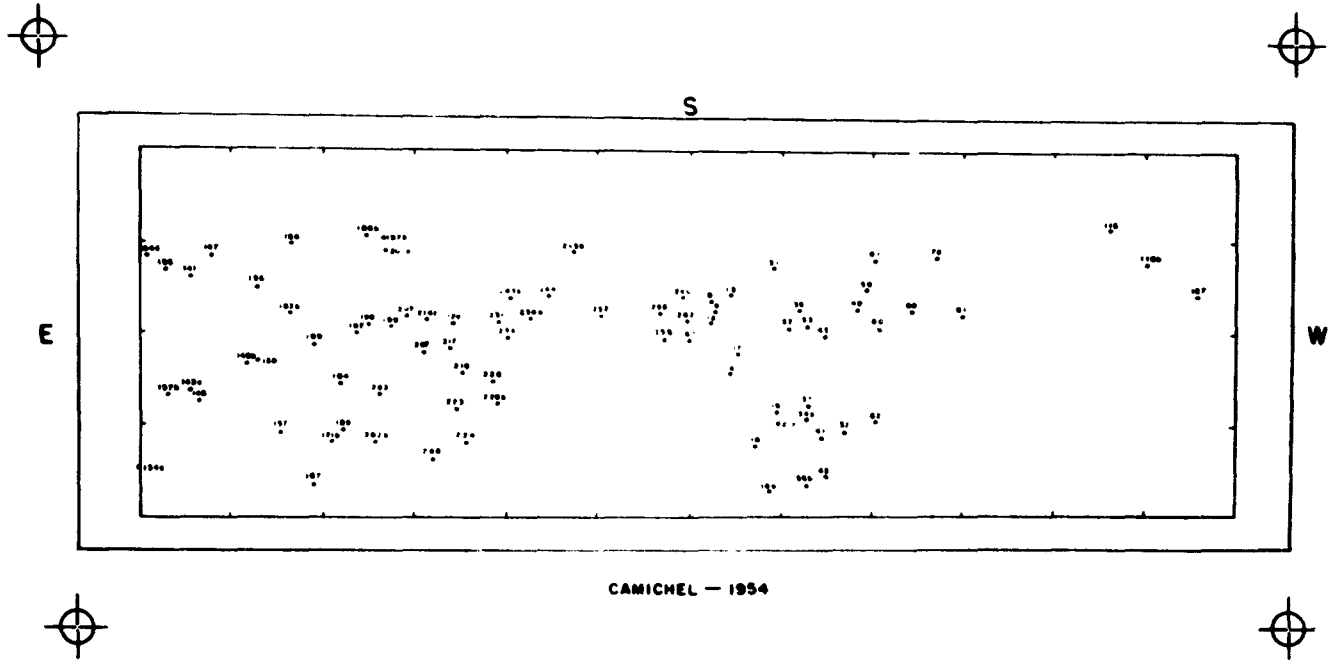

Fig. 1. — Example of stations identification map.

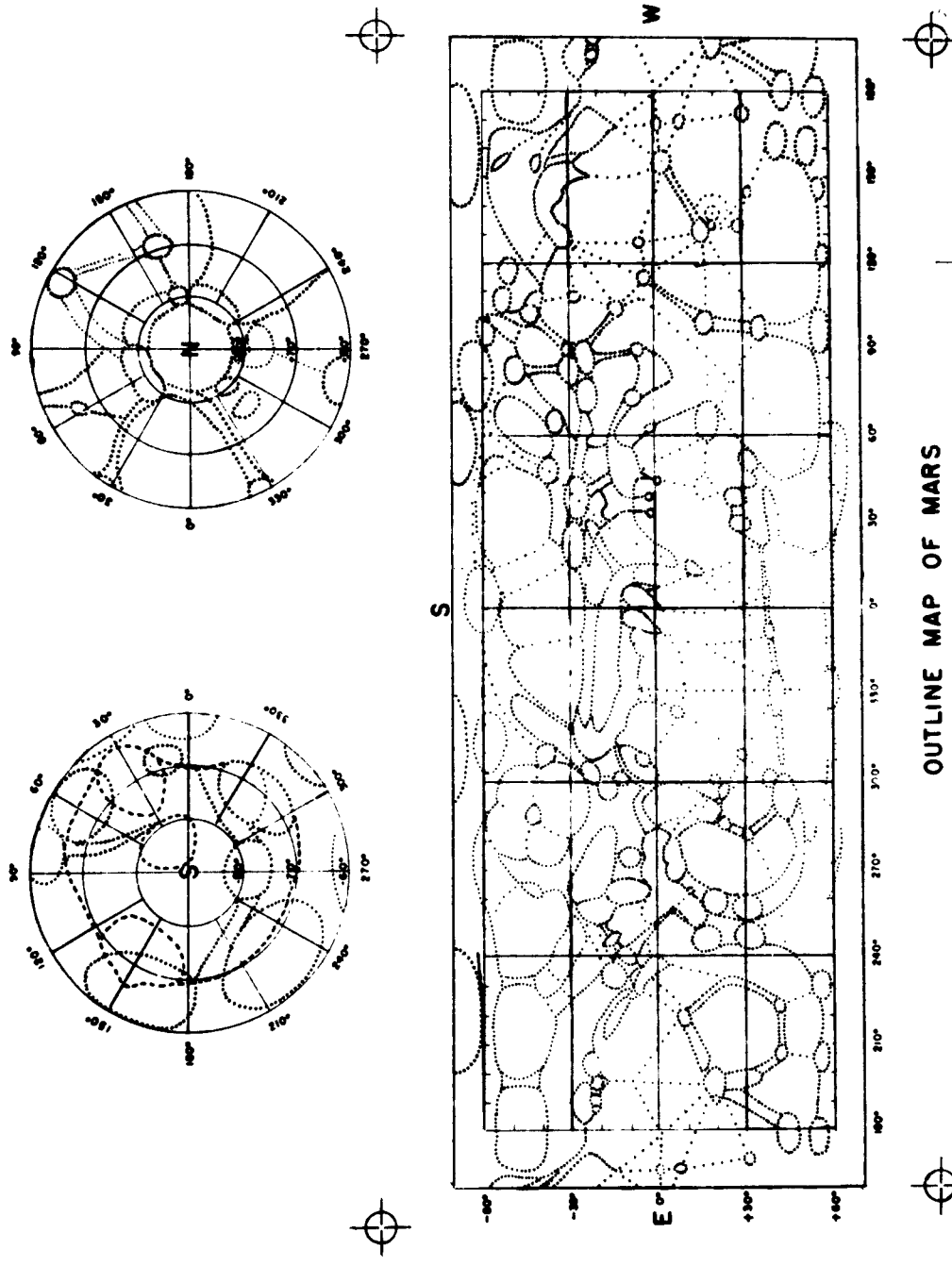

Fig. 2. — Outline map of Mars for stations identification, 1909-1954.

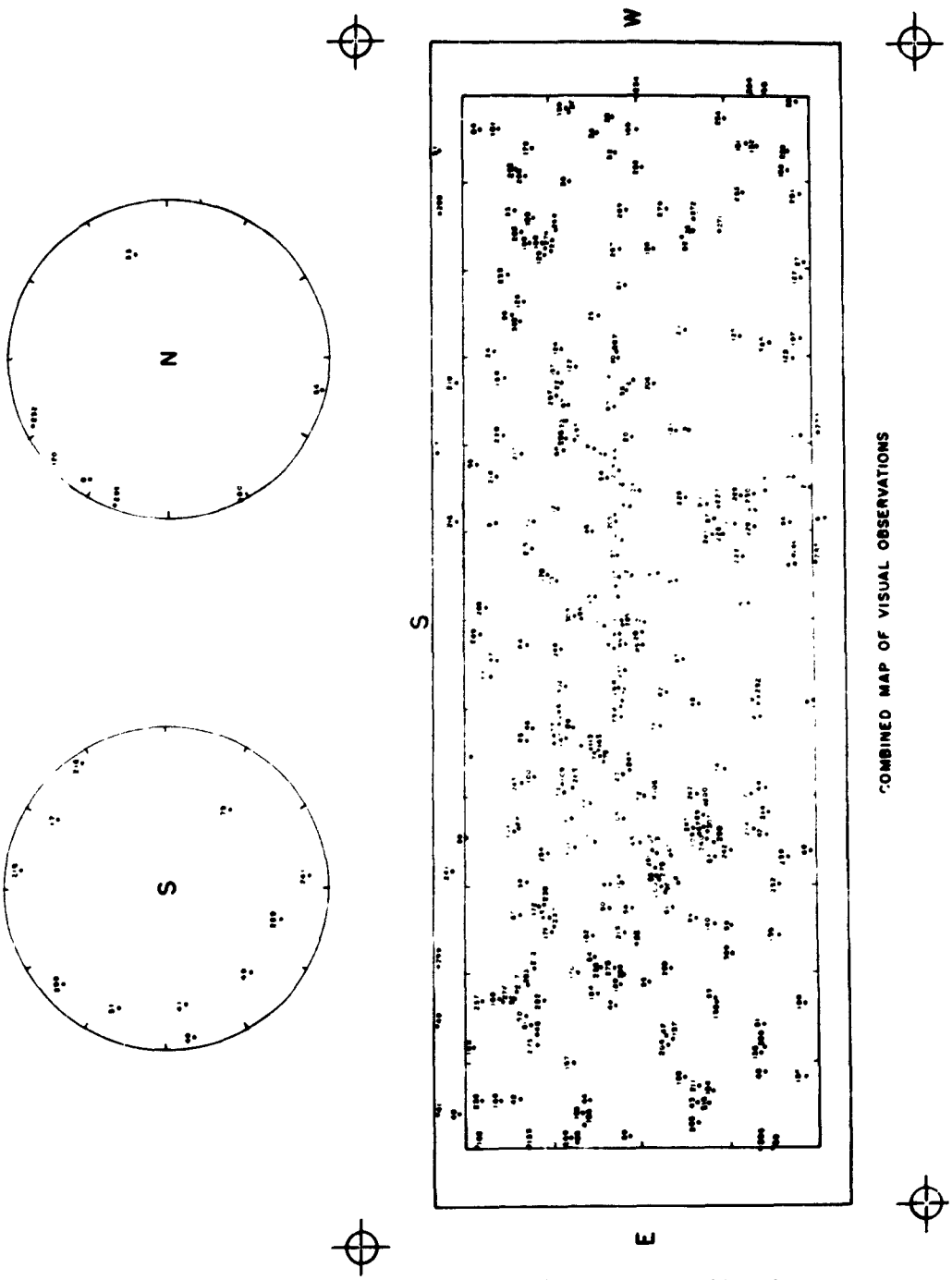

Fig. 3. — Combined map of visual observations, 1909-1954 (307 points).

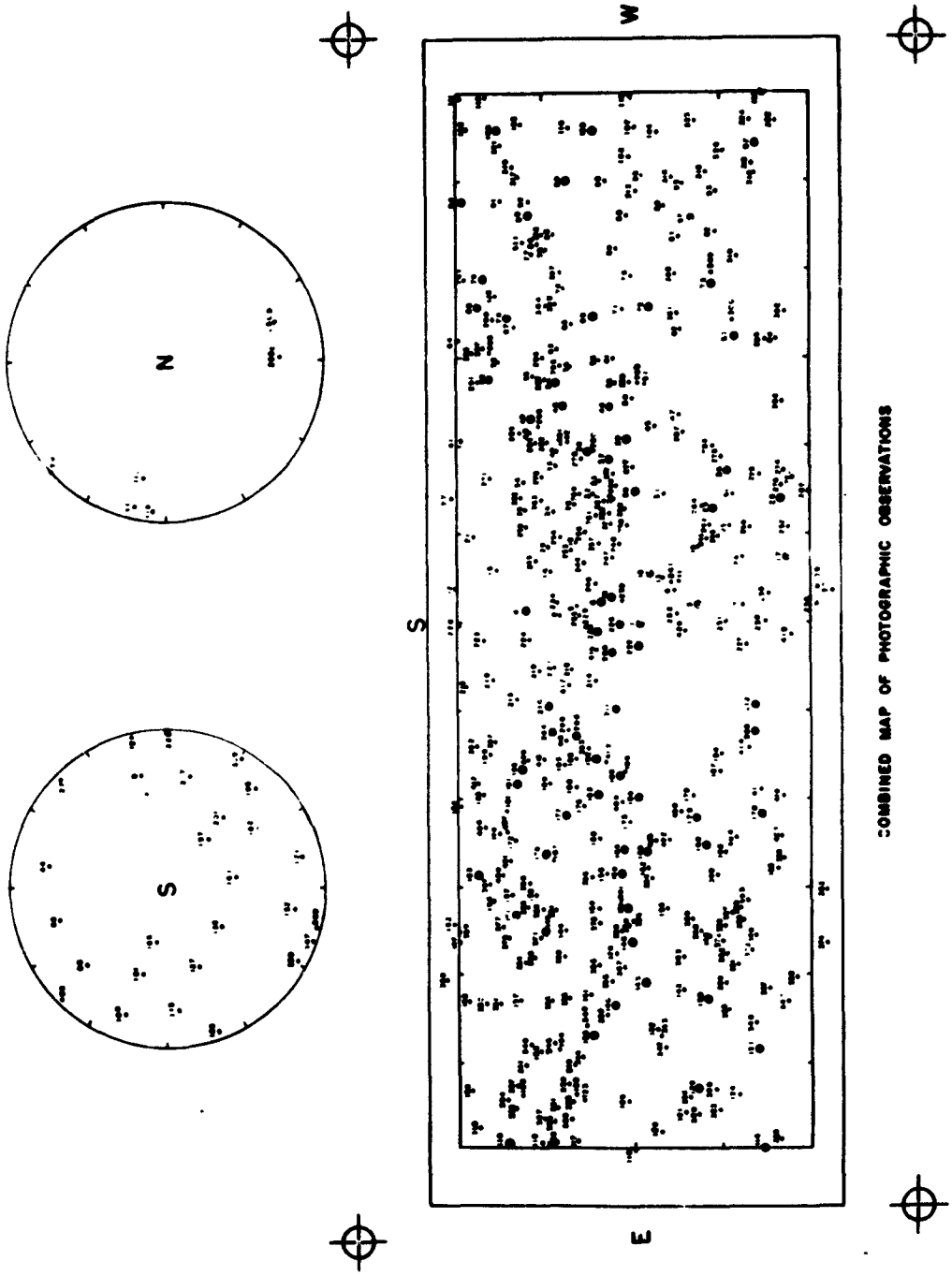

4. — Combined map of photographic observations, 1924-1954 (429 points).

identified by means of an outline map of the topography (Fig. 2) and two combined maps of all well-identified points, one for the visual observations (307 points) and one for the photographic observations (429 points) (Fig. 3, 4). A double-entry table of « Master List Numbers » provides the cross-identification between the individual maps and the combined maps which are all precisely on the same scale. The areographic coordinates themselves and other relevant data have been recorded on IBM punched cards for statistical analysis and future publication.

An extension of the survey of areographic coordinates data to the period 1877-1907 is in progress.

4. Areographic Coordinates and Map for 1958 ([2, 3, 7])

The opposition of Mars in 1958 was observed by the author at Lowell Observatory, Flagstaff, Arizona. Some 32 carefully positioned drawings of the disk were secured between October 4 and November 22, 1958 with the 24-inch refractor generally diaphragmed to 18 or 21 inches and magnifications of 350× to 550× ([2]). Areographic coordinates of 546 points of the surface (Fig. 5) were derived from 2321 coordinate pairs measured on these drawings by Mr. Wright using orthographic coordinate grids prepared by Dr. C. S. Yü, Hood College, Maryland. The reduction of the data recorded on punched cards was made through the courtesy of Drs. A. R. Hibbs and R. Eimer with the IBM 7090 computer of the Jet Propulsion Laboratory. The use of an electronic computer made possible a much more thorough allowance for systematic effects, weights, and other factors than in earlier work. Table 1 gives as an example the output of the machine (2nd approximation) for a typical first-class point (N° 2001 = VML N° 20 = Juventae Fons). The internal probable errors of the adopted mean coordinates (in the system of the 1958 ephemeris ; cf. section 5 below) of well-defined and well-observed points are of the order of $\pm$ 1°0 in longitude and $\pm$ 0°5 in latitude, near the equator ([3]). A comparison of the

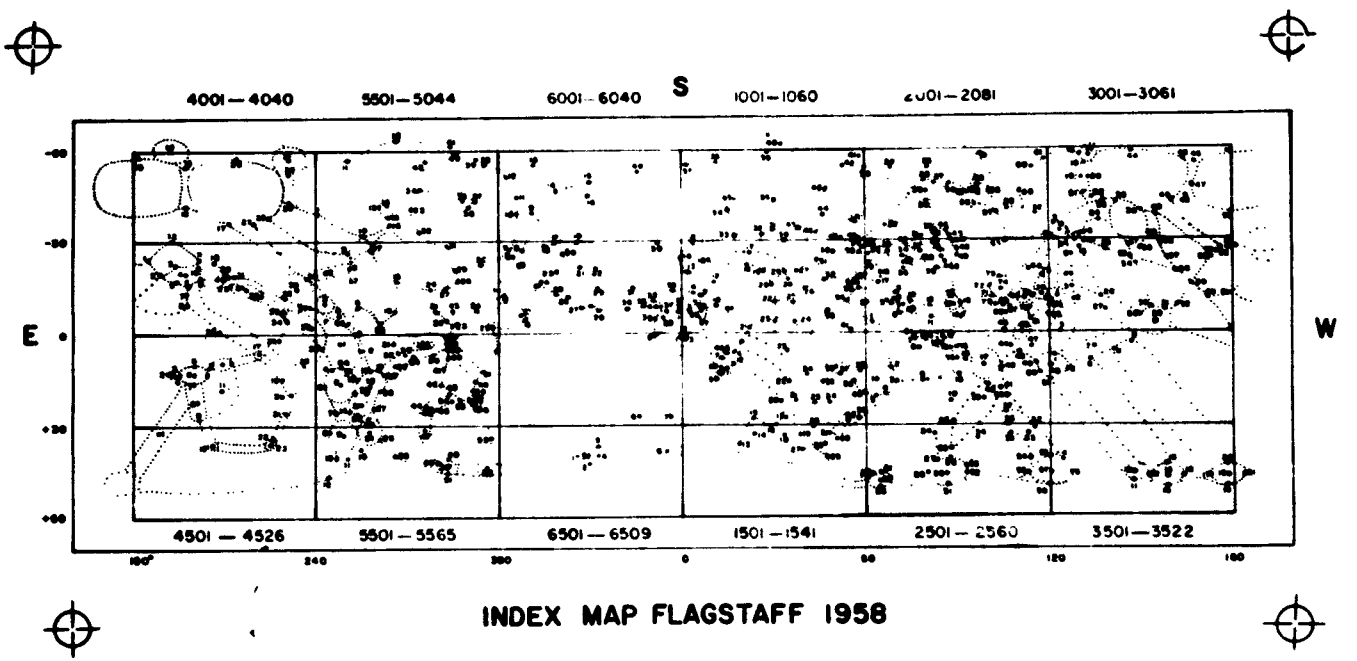

Fig. 5. — Index map of Flagstaff observations, 1958 (546 points).

longitudes derived from drawings and from transits indicates a negligible systematic difference (0°3 ± 0°3 p. e.). A comparison of visual longitudes (corrected for phase effect) in 1939 ([4]) and in 1958 ([7]) tends to support the correction to the (old) ephemeris rotation period derived by Ashbrook in 1953 ([5]) and adopted in the ephemeris since 1960 (cf. section 5 below).

Two maps in Aitoff equal area projection based on the 1958 observations (Fig. 6, 7) were prepared by Mr. J. Roth, using a photometrically checked step scale of « gray » to transfer to the maps the relative brightness or « tone » values of the dark and bright regions. The visual step-values (i. e., relative surface brightnesses on a logarithmic scale) of the various regions were derived from over 1,000 photometric estimates made during the 1958 opposition and previously reduced to a standard system ([6]).

A similar reduction of 4200 coordinate pairs of some 650 points of the surface of Mars measured by Mr. Wright on 73 carefully-positioned drawings made by the author in 1941 at the Péridier Observatory, Le Houga, France is now in progress.

5. Systematic and accidental Errors ([7, 8])

A comparison of existing lists of areographic coordinates discloses quickly that systematic errors are often much larger than the internal (accidental) probable errors. A special effort has been made to estimate the magnitude of these systematic errors and to devise ways of eliminating them as far as possible prior to the setting up of a standard system of areographic coordinates. This investigation is still in progress, but some preliminary results may be listed :

5. 1. *Origin (zero point) of longitudes*

Most observers have adopted the ephemeris system in use from 1909 to 1959 ; a few, however, followed the faulty tradition of placing the center of Sinus Meridiani (or Fastigium Aryn) at 0°.0 ;

a few others used arbitrary origins (e. g., placing Titanum Sinus at 170°.0) [1]. Apparent errors of up to about 3° may arise from this source alone. Provisional mean values of the coordinates of the center of Sinus Meridiani (Visual Master list N° 1) on the new ephemeris system (see below) are $\lambda_1 = 357°.1$, $\varphi_1 = -2°.6$; errors are probably well under 0°.5 in λ and 1° in φ [8].

5. 2. *Coordinates of the pole*

Most visual observers have adopted the ephemeris coordinates $\alpha = 317°.5$, $\delta = +54°.5$ (Eq. 1905.0) derived by Lowell (*M. N.* **66**, 51, 1905) ; a few, however, have used slightly different poles, especially the photographic observers : Trumpler, 315°.77, + 54°.63 (*Lick O. Bull.* **13**, 33, 1927) and Camichel : 316°.48, + 52°.78 [9]. Apparent errors of up to about 1°.5 in the latitudes (and 1° in the longitudes within 60° from the equator) may arise from this source alone. The inherent freedom from systematic errors of Camichel's method and its good agreement with the mean pole of the satellite orbits 316°.60, + 52°.94 derived by Burton (*A. J.*, **39**, 163, 1929) suggests that the ephemeris values should be corrected by about — 1°.0 and — 1°.5 ; the errors of the corrected coordinates $\alpha_c = 316°.55$, $\delta_c = +52°.85$ are probably under 0°.1 [8,10]. A physical ephemeris of Mars for the oppositions of 1877 to 1963 will be computed with these revised elements.

5. 3. *Ellipticity of the globe*

Most visual observers have ignored the ellipticity of Mars, i. e. the difference between areographic and areocentric latitudes. Trumpler has made allowance for an apparent ellipticity of about 1/100 which introduces a maximum difference of 0°.3 at intermediate latitudes ; if the true ellipticity has the dynamical value 1/190 the difference is at present negligible for all practical purposes. The unresolved discrepancy between geometric and dynamical ellipticities makes it advisable to postpone decision [10].

Fig. 6. — Map of Mars based on observations with the 24-inch refractor of Lowell Observatory, Flagstaff, Arizona. Aitoff equal area projection. Central meridian 0°.

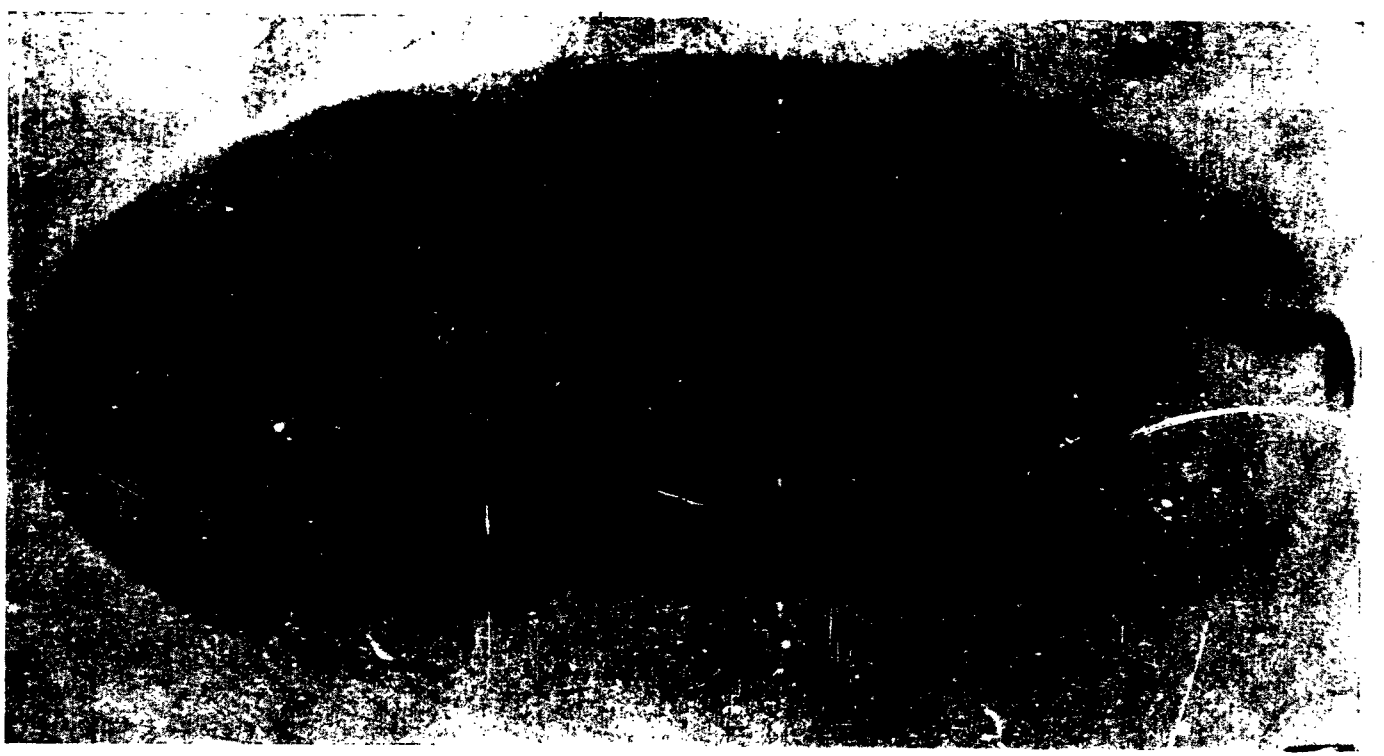

Fig. 7. — Map of Mars based on observations with the 24-inch refractor of Lowell Observatory, Flagstaff, Arizona, in October and November 1958. Aitoff epuel area projection — Central meridian 180°.

5. 4. *Rotation period*

The Ashbrook correction of $+ 0^s.0147 \pm 0^s.0026$ (m. e.) ([5]) to the ephemeris value in use between 1909 and 1959 (P = 24 h 37 m 22.6542 s) has been incorporated in the ephemeris since 1960, thus introducing a discontinuity of $1^o.2$ in the ephemeris longitude of the central meridian. The following correction will reduce longitudes based on the 1909-1959 ephemeris to the new system : $\Delta\lambda_2 = -0^o.0212\,(t - t_0)$, where $(t - t_0)$ is in years and $t_0 = 1909.04$. To it must be added a correction for the difference $\Delta t = \mathrm{ET} - \mathrm{UT}$ between Ephemeris Time and Universal Time, $\Delta\lambda_3 = -0.00406\,(\Delta t - 8.6)$, where Δt is in seconds. The total correction varies almost linearly from $-0^o.02$ to $-1^o.15$ between the oppositions of 1909 and 1958 ([7, 8]).

5. 5. *Phase effect*

Longitudes measured on drawings or photographs are subject to a common systematic error depending on the phase angle in longitude $\Delta A = A_\odot - A_\oplus$, due to the asymmetrical illumination of the disk (invisibility of geometric terminator, irradiation at the limb) ([4]). Systematic errors in excess of $\pm 2^o$ may be introduced by this effect which on several occasions has caused observers to announce prematurely and mistakenly errors of up to 3^o in the ephemeris. To a first approximation the error (measured in degrees of longitude) is independent of latitude $|\varphi| < 60^o$ (there are too few measurable points in the polar regions) and the following correction will reduce the measures to exact opposition :

$$\Delta\lambda_1 = -0.150\,(\Delta A) + 0.11 \times 10^{-3}\,(\Delta A)^3$$

($\Delta A < 0$ before opposition) ([7, 8]). Note that the effect exceeds $0^o.5$ for phases angles as small as 4^o. By analogy, systematic errors of this order of magnitude may be present also in areographic *latitudes* when Mars is not in the plane of the ecliptic. The yearly residuals $\Delta\varphi = \varphi_y - \bar{\varphi}$ of the latitudes measured on photographs by

Camichel ([11]), $\Delta\varphi = +0^{\circ}.2 + 1^{\circ}.0 \cos(\eta - 316^{\circ})$, if η = heliocentric longitude, indicate the presence of an effect of this type, perhaps mixed with small systematic errors due to the effect of the irradiation of the polar caps on the apparent position of the center of the disk ([8]).

5. 6. *Timing and other errors*

The data of some visual observers (especially Fournier) lead to longitudes systematically in error by up to $+2^{\circ}$ and due pro-

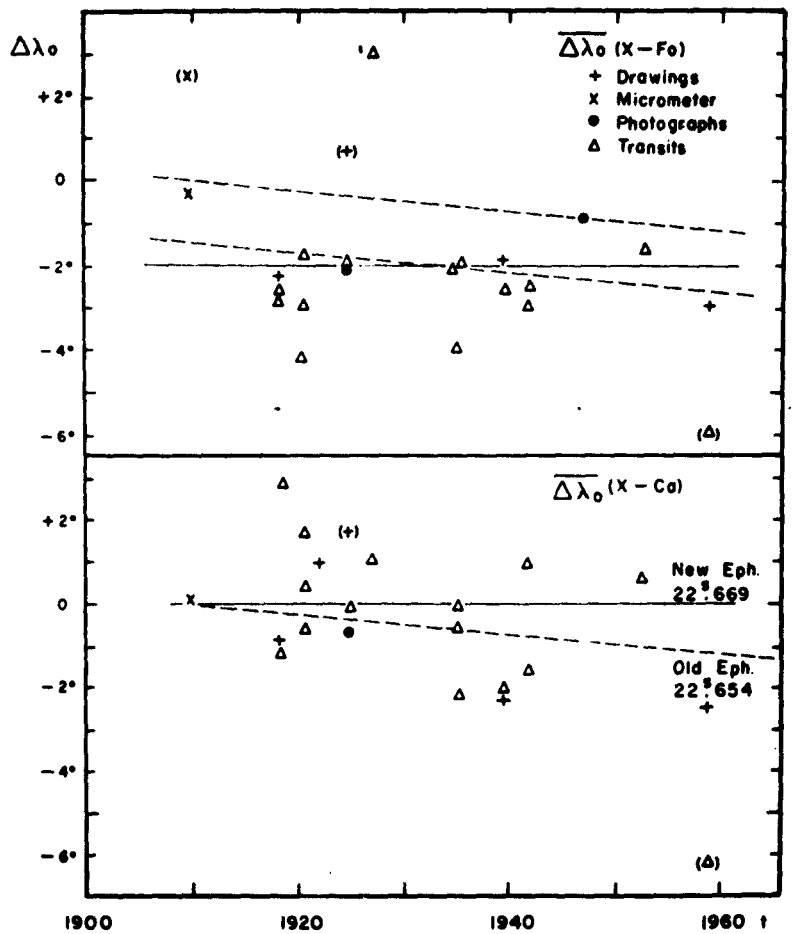

Fig. 8. — Mean longitude differences from provisional mean Fournier system (above) and mean Camichel system (below), all reduced to new ephemeris system, and corrected for phase effects (where applicable).

bably to faulty timing (for instance, if the longitude of the central meridian is computed for the middle of each observing session lasting perhaps 20 to 30 minutes rather than for the middle of the initial period of a few minutes during which the main markings are positioned on the drawing). These errors are disclosed a) by comparison with other observers (visual and photographic), and more directly, b) by comparison with longitudes derived from transits (*). On the other hand, there is good agreement between longitudes from transits and from photographs, thus from 82 transits by 14 observers $\Delta\overline{\lambda_0}$ (transits minus Camichel) = — 0°.02 ; however, the time interval 1909 — 1958 is still too short for a decisive confirmation of the new ephemeris rotation period (22^s.669) as against the old value (22^s.654) (Figure 8).

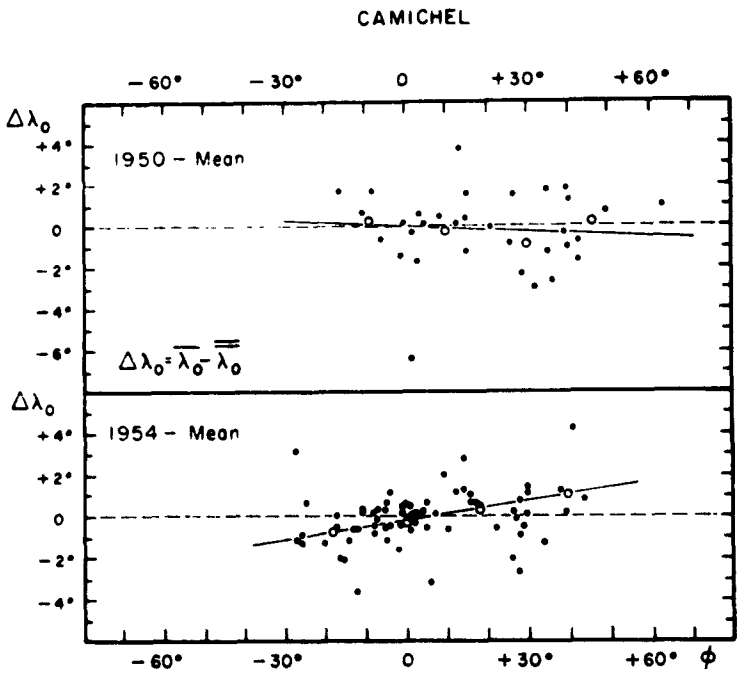

Fig. 9. — Example of systematic longitude differences vs. latitude.

(*) Surprisingly, longitudes derived from timing of transits seem to be free of systematic errors depending on phase angle (Ashbrook draws the opposite conclusion in Ref. 5).

The comparisons are complicated by the fact that in many cases the systematic longitude differences (as well as the latitude differences) depend on latitude (Fig. 9, 10). Hence, a simple separation of errors between the two coordinates does not lead to a satisfactory reduction to a homogeneous system. An application to this problem of new methods of numerical interpolation and mapping developed by R. Gallet and W. Jones at the U. S. Bureau of Standards, Boulder, Colorado, is now under consideration.

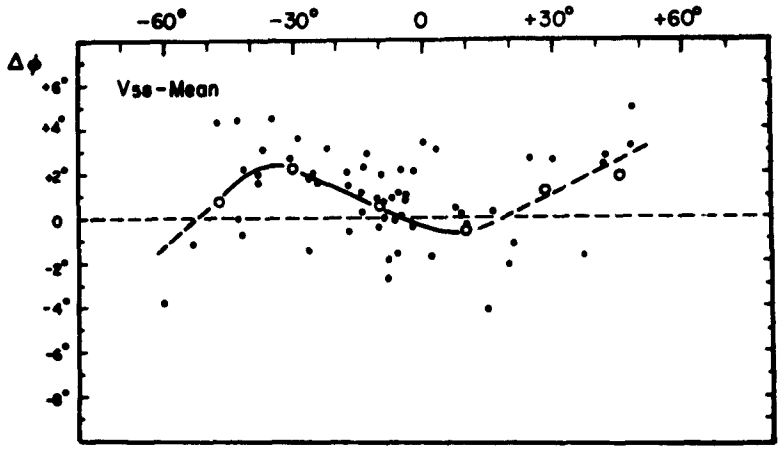

Fig. 10. — Example of systematic latitude differences vs. latitude.

6. Measurement of Composite Photographs

Through the kindness of Dr. W. S. Finsen some 80 enlarged composite positives on film of photographs taken by him in 1954 and 1956 with the 27 ½-inch refractor of the Union (now Republik) Observatory, Johannesburg, South Africa were made available to the Mars Map Project for measurement; some 4,000 coordinate pairs of about 200 points have been measured on these composites by Dr. C. S. Yü and will shortly be prepared for further reduction at Harvard Observatory.

Dr. R. B. Leighton of the California Institute of Technology generously loaned to the Project slightly enlarged black-and-

white color separation negative copies of color films of Mars taken by him in 1956 with the 60-inch reflector of Mount Wilson Observatory. Some of Dr. Leighton's photographs are among the best on record and they show a large amount of fine detail. Out of 14,000 images about 7,000 were selected as suitable for compositing, and from these 740 composite positive transparencies on film (image diameter about 50 mm) were prepared at Harvard Observatory by Mrs. L. Hudson who then measured some 8,000 coordinate pairs of about 300 surface points. This material will be transferred to punched cards in the near future for analysis and reduction ; this phase of the project continues at Harvard Observatory under the immediate direction of Dr. A. T. Young.

REFERENCES

(1) G. DE VAUCOULEURS and R. WRIGHT, « Sources of Areographic Coordinates 1909-1954 » Harvard College Observatory, *Scientific Report* No **2**, *ARDC Contract AF* 19(604)-7461, February, 1961 ; *AFCRL Report* No **257** (1).

(2) G. DE VAUCOULEURS, « Observations of Mars in 1958 », *Sky and Telescope*, **18**, No 9, 484-489, July 1959 ; *Harvard Reprint* II, No 151 (1).

(3) G. DE VAUCOULEURS, « Areographic Coordinates for 1958 », Harvard College Observatory, *Scientific Report* No 4, *ARDC Contract AF* 19(604)-7461, August 1961, *AFCRL Report* No **818** (1).

(4) G. DE VAUCOULEURS, « Commission de la planète Mars. Rapport sur l'opposition de 1939 », *L'Astronomie*, **62**, 153, 217, 268, 1948.

(5) J. ASHBROOK, « A new determination of the Rotation Period of the planet Mars », *The Astronomical Journal*, **58**, 145-155, 1953.

(6) G. DE VAUCOULEURS, « Photometric Observations of Mars in 1941 and 1958 », Harvard College Observatory, *Scientific Report* No **5**, *ARDC Contract AF* 19(604)-3074, August 1960 ; GRD-TN-60-616 (1).

(7) G. DE VAUCOULEURS, « A study of areographic coordinates 1909-1958 » Univ. of Texas, *Report ERR-FW-075 Physics*, December 1960, Convair-Fort Worth Division, General Dynamics Corp (1).

(8) G. DE VAUCOULEURS, « Precision Mapping of the planet Mars », Part 1 of Report on « Research Program in Planetary Astronomy at the University of Texas in 1961 », to Applied Science Laboratory, General Dynamics/Fort Worth, January 1962 (3).

(9) H. CAMICHEL, « Détermination photographique du pole de Mars, de son diamètre et des coordonnées aréographiques », *Bulletin Astronomique, Paris*, **18**, 83-191, 1954 ; **20**, 131-140, 1956.

(10) G. DE VAUCOULEURS, « Interplanetary Navigation Studies : Diameters of Terrestrial Planets », *GCA Technical Report* 61-30-A, *ARDC Contract No AF* 33(616)-7413, July 1961 (5).

---

(1) Copies may be obtained through the U. S. Department of Commerce, Office of Technical Services, Washington 25, D. C. or from Harvard College Observatory, Cambridge 38, Massachusetts.

(2) Copies may be obtained through the Applied Research Laboratory, General Dynamics Corp., Fort Worth, Texas or from the Department of Astronomy, University of Texas, Austin 12, Texas.

(3) Copies may be obtained through the U. S. Department of Commerce, Office of Technical Services, Washington 25, D. C. or from Geophysics Corporation of America, Bedford, Massachusetts.

TABLE 1

Example of Output for point No. 2001 = ML 20 = Juventae Fons

Point 2001 $\overline{Q}_\lambda = 1.2$ $\bar{\lambda}_w = 62°5$ $\Sigma w_\lambda = 3.50$
$\overline{Q}_\varphi = 1.0$ $\bar{\varphi}_w = -3°6$ $\Sigma w_\varphi = 4.51$

λ	δQ_λ	δ_λ	W_λ	φ	δQ_φ	δ_φ	W_φ	Dr.
62.0	—.2	— .5	.48	—4.5	.0	— .9	.70	25
62.0	—.2	— .5	.62	—2.7	.0	.9	.79	26
60.5	—.2	—2.1	.73	—3.1	.0	.5	.85	27
62.9	—.2	.4	.88	—5.6	.0	—2.0	.94	28
68.6	.8	6.1	.27	—3.2	.0	.4	.52	29
62.8	—.2	.2	.51	—1.9	.0	1.7	.71	30

$\sigma(Q_\lambda) = .41$ $\sigma(Q_\varphi) = .00$ $\sigma_\lambda = 1°98$ $\sigma_\varphi = 1°.29$
$E_\lambda = 0°.71$ $E_\varphi = 0°.41$

The entries are as follows :

1st line : Mean value of point definition Q_λ ; weighted mean λ ; sum of weights in λ.

2nd line : Mean value of point definition Q_φ ; weighted mean φ ; sum of weights in φ.

Successive columns give : longitude corrected for phase effect and drawing error in λ, residual of Q_λ, residual of λ, weight w in λ ; latitude corrected for drawing error in φ, residual of Q_φ, residual of φ, weight w in φ ; drawing number.

Last two lines give : standard error of Q_λ, standard error of Q_φ ; standard error of λ, standard error of φ (both for unit weight), probable error of mean λ, probable error of mean φ.

1. Example of machine output for point 1958-2001 = VML 20 = Juventae Fons (p. 66 of Sc. Rep. No. 4).

35. — LA NATURE DE LA SURFACE ET DE L'ATMOSPHÈRE DE LA PLANÈTE MARS D'APRÈS LES DONNÉES PHOTOMÉTRIQUES ET COLORIMÉTRIQUES

V. V. SHARONOV
Observatoire de l'Université de Leningrad, U.R.S.S.

Pendant plusieurs années, le laboratoire d'astronomie planétaire de l'Université de Léningrad, a étudié la répartition de brillance et de couleur sur le disque de Mars, en employant des méthodes visuelles et photographiques [1, 2, 3, 4, 6]. En même temps, on a déterminé l'albedo et la couleur des échantillons des roches ainsi que des régions du paysage terrestre. Les résultats obtenus permettent de tirer quelques conclusions sur la nature de la surface et de l'atmosphère de Mars.

Le problème de la couche violette a une grande importance ; il consiste à expliquer l'invisibilité complète des détails sur les clichés, obtenus dans l'ultraviolet (la valeur de l'albedo ultraviolet étant basse, à peu près 0,1).

On peut arriver à l'obtenir à l'aide d'un des trois modèles suivants :

I. La coloration de la surface est telle que les différences de brillance de ses détails diminuent au fur et à mesure qu'on s'éloigne vers la région ultraviolette du spectre ; c'est pourquoi, dans l'ultraviolet, il suffit d'une couche bien mince d'atmosphère diffusante pour rendre les détails invisibles.

II. Les contrastes de brillance dans l'ultraviolet ne sont pas faibles, mais l'albedo général est si bas (à peu près 0,01) que la brillance de la lumière diffusée, dans une mince couche d'atmosphère, suffit à rendre les détails indiscernables.

III. L'albedo et les différences de brillance dans l'ultraviolet sont normaux, mais l'atmosphère est opaque, l'extinction ayant pour cause l'absorption vraie et non la diffusion. Pour qu'un tel

modèle soit en accord avec les faits observés, il est nécessaire d'admettre qu'au-dessus de la couche absorbante se trouve une couche diffusante, dans laquelle se trouvent les calottes polaires et les nuages bleus, et dans laquelle la diffusion des rayons solaires fait disparaître l'assombrissement au bord du disque, dû à l'absorption dans la couche basse.

Si l'on admet que pour l'atmosphère et le sol de Mars il est permis de prendre des valeurs tout à fait arbitraires pour les paramètres optiques, les trois modèles peuvent s'accorder avec la distribution de brillance et de couleur observée sur le disque de Mars. Mais si l'on part du principe que les modèles les plus vraisemblables sont fondés sur la comparaison de la nature de Mars et celle de la Terre, et selon lesquels il y a analogie relative entre la nature de ces planètes, on sera obligé de préférer le premier modèle.

Pour ces raisons, nous allons supposer que la couleur orange du disque de Mars appartient au sol même de la planète et que le voile violet a pour cause la simple diffusion des rayons solaires dans l'atmosphère, cette diffusion se faisant suivant une loi semblable à celle de Rayleigh. Nous admettons de même que l'absorption vraie dans l'atmosphère est insignifiante, que la densité optique de la couche atmosphérique n'est pas grande, et qu'il n'existe aucune couche violette élevée.

Les travaux de N. P. Barabachov (7), de I. K. Koval (8), de N. N. Sytinskaya (4) et d'autres démontrent qu'un tel schéma correspond bien aux résultats des mesures photométriques faites dans diverses régions du spectre.

D'autre part, il est certain que l'atmosphère de Mars présente un aérosol dont les particules de la phase dispersée, en naissant et en se détruisant, donnent lieu aux changements de densité du voile violet, à l'apparition des nuages bleus, et peut-être, des calottes polaires. Il est possible que ces particules se trouvent concentrées dans les couches basses de l'atmosphère. A cet effet, on peut citer le fait suivant : pendant le développement des brumes

oranges de grande étendue sur Mars en 1956, les nuages bleus et la calotte polaire sud en étaient recouverts (⁸). On peut discuter l'hypothèse selon laquelle l'échauffement de la surface de Mars par le Soleil conduit à l'évaporation de l'eau dont une quantité se trouve dans le sol de la planète. Sortant du sol et pénétrant dans les basses couches de l'atmosphère, (dont la température sur Mars est beaucoup plus basse que celle du sol), la vapeur se condense et forme une brume raréfiée, composée de cristaux de glace très petits ; la diffusion sélective dans un tel milieu est la cause de l'apparition des nuages bleus ou violets dans l'atmosphère.

Il s'ensuit des nombreuses recherches de colorimétrie des régions claires à la surface de Mars que leur coloration rouge-orange est très saturée et seul un très petit nombre de minéraux et de roches terrestres a une coloration aussi intense ; par exemple, la limonite pulvérisée (c'est-à-dire l'ocre ferreuse), le sable et l'argile pigmentés de limonite (⁹). Les données sur l'albedo et la couleur sont représentées dans le tableau 1 ; l'albedo est pris par rapport à la région visuelle du spectre, et la couleur en fonction du « color-excess », c'est-à-dire en fonction de la différence D des indices de couleur de l'échantillon et des rayons solaires. Le système employé pour obtenir les valeurs de D est le même pour les échantillons obtenus au laboratoire et pour les détails de Mars. Les valeurs moyennes sont obtenues en utilisant un grand nombre de mesures de chaque espèce de roches (dans certains cas plus de 100), les échantillons étant pris, autant que possible, dans différents pays.

On peut voir que l'albedo de Mars ressemble à celui de différents matériaux terrestres, tandis que les valeurs élevées de D de la surface de la planète (dépassant 1 pour les régions claires), ne peuvent être semblables qu'aux produits de l'efflorescence pigmentés par la limonite dont la coloration est très saturée. Il est à remarquer que les régions sombres ont aussi une couleur rougeâtre, bien que moins saturée, s'approchant du brun (D = 0,9). Leur couleur verdâtre, souvent indiquée par les observations visuelles, devrait être attribuée à une illusion d'optique provoquée

par le contraste de couleur avec des régions claires de coloration plus intense.

Les observations photométriques nous montrent que la réflexion de la lumière par le sol des régions claires se produit d'après la loi de Lambert. L'explication la plus simple en est que la nappe extérieure de la surface de Mars est composée de poudre ou de poussières colorées en orange par la limonite.

Il est à noter que M. A. Dollfus, ayant fait de nombreuses mesures polarimétriques, est arrivé à des conclusions analogues ([10]). Cette hypothèse est en accord avec les observations des brouillards oranges dont nous avons vu quelques exemples remarquables pendant l'opposition de 1956.

Il est naturel de supposer qu'une nappe continue et uniforme de poussières dans les régions claires de Mars s'est formée grâce aux particularités des processus de l'efflorescence et de l'érosion, pour lesquels l'eau joue un rôle insignifiant, contrairement a ce qu'on voit sur la Terre. Dans des conditions pareilles, il ne se forme pas d'hydrosilicates et pour cette même raison, l'argile ne peut être répandue sur Mars. Les produits de destruction des roches initiales seraient des particules fines du type $CaCO_3$, $MgCO_3$, $FeCO_3$, quelques silicates anhydres, et les particules non décomposées des minéraux des roches ignées, du quartz par exemple, du feldspath, des pyroxènes, des amphiboles, de l'olivine. En l'absence d'eau, la cimentation du matériel clastique n'a pas lieu et celui-ci reste en état de poudre.

Il est à noter que l'idée, suivant laquelle le sol de Mars est formé non par le sable, mais par des particules en état de poussière, des carbonates et de la limonite, se trouverait en accord avec le résultat obtenu par Sinton et Strong ([11]), qui n'ont pas trouvé dans le spectre de Mars la raie d'absorption typique pour le quartz et les silicates (8,9 μ). Il serait très important d'étudier le spectre infrarouge pour les rayons réfléchis par la limonite et les roches colorées par elle.

Il faut encore noter que si le pigment principal à la surface

de Mars est la limonite ou l'hydrogoethite ($Fe_2O_3 + nH_2O$, n étant égal à 1,5 — 5), on est obligé d'admettre la présence d'une quantité quelconque d'eau, car dans le cas où il n'y en aurait pas du tout, la déhydratation de la limonite et sa transformation en goethite ($Fe_2O_3 + H_2O$) et ensuite en hématite (Fe_2O_3) aurait lieu. Puisque sur Mars la température moyenne est partout au-dessous de 0° C, l'eau y sera toujours en état de glace, qui ne peut fondre que dans une mince couche supérieure du sol et seulement pour un temps très court. Mais sans doute, cela suffit pour que la limonite des couches supérieures du sol soit un minéral stable.

La supposition concernant la présence de quelque quantité d'eau, se trouve en accord avec la susdite hypothèse selon laquelle la brume violette et les nuages bleus sont formés dans la zone de contact entre le sol et l'atmosphère.

Plusieurs auteurs ont admis que dans les régions sombres de Mars il doit exister un mécanisme de régénération quelconque qui leur permet de garder leur coloration sombre malgré la sédimentation de la poussière. L'exemple de la nature des déserts terrestres nous montre que cela n'est pas nécessaire, puisque sur la surface de la Terre, il existe des régions de déflation où les produits de l'érosion éolienne sont emportés par les vents, ainsi que des régions de sédimentation et d'accumulation de tels produits. Par analogie, on peut supposer que les régions sombres de la surface de Mars représentent des zones de déflation, tandis que les régions claires représentent des zones d'accumulation de poussières. Dans ce cas, la couleur et les autres propriétés optiques des régions sombres seront déterminées par la couleur des roches initiales, couvertes d'une nappe interrompue de fines poussières ; les roches peuvent être sédimentaires ou ignées.

Les changements saisonniers de leur couleur peuvent être attribués aux changements de l'épaisseur de la nappe de poussières, ainsi que le suppose Kuiper ([12]), et aussi à l'apparition d'une végétation primitive, selon l'opinion de la plupart d'auteurs.

TABLEAU 1

L'albedo et la couleur des objets sur la Terre et sur Mars.

Espèce des matériaux ou des nappes	Albedo r		Couleur D	
	Valeurs extrêmes	Valeur moyenne	Valeurs extrêmes	Valeur moyenne
Le désert argileux	0.15-0.44	0.29	0.24-0.56	0.37
Le désert pierreux	0.15-0.25	0.19	0.28-0.36	0.33
Les sables des déserts	0.14-0.38	0.26	0.26-1.22	0.49
Les sables des plages	0.11-0.30	0.21	0.08-0.50	0.35
Les sables d'origines différentes	0.11-0.40	0.24	0.06-1.14	0.54
Les roches rouges du système de Perm	0.10-0.28	0.17	0.29-0.86	0.61
Les produits ferreux de l'efflorescence	0.08-0.27	0.16	0.28-1.07	0.62
Les minerais de fer paludéen	0.08-0.35	0.15	0.33-1.06	0.73
Limonite opaque	0.05-0.22	0.11	0.00-1.00	0.44
Limonite pulvérisée (ocre)	0.13-0.28	0.18	0.85-1.24	1.01
Le sable de la couche de l'ortstein	0.08-0.23	0.16	0.93-1.31	1.07
Terra rossa	0.10-0.18	0.13	0.93-1.28	1.07
Mars, régions claires	0.17-0.24	0.18	1.03-1.18	1.09
Mars, régions sombres	0.06-0.14	0.10	0.82-0.99	0.89

REFERENCES

(1) L. N. RADLOVA, Photometrical and colorimetrical observations of Mars during the opposition of 1939. *Astron. Journ. of Soviet Union*, 17, 4, 30-36, 1940.

(2) V. V. SHARONOV, Photographic observations of Mars at the opposition of 1939. *Astron. Journ. of Soviet. Union*, 17, 4, 37-39, 1940.

(3) V. V. SHARONOV, The brightness contrasts observed on the surface of Mars. *Poulkovo Observ. Circ.*, 32, 62-73, 1941.

(4) N. N. SYTINSKAYA, The nature of the surface and atmosphere of the planet Mars according to data of absolute photometry. *Comptes Rendus de l'Acad. de Sc. des l'URSS*, 43, 151-154, 1944.

(5) V. V. SHARONOV, « *Vestnik* » *de L'Université de Leningrad*, 13, 19, 187-202, 1958 ; Les résultats des observations pendant l'opposition de Mars en 1956, 123-154, 1959.

(6) V. V. Sharonov, *Bulletin de la commission de physique planétaire*, **2**, 30-35, 1960.

(7) N. P. Barabachov et I. K. Koval, La photométrie photographique de Mars a l'aide des écrans colorés pendant l'opposition de 1956. Edition de l'Université de Kharkov, 530 pages, 1959.

(8) I. K. Koval, *Astron. Journ. of Soviet Union*, **34**, 3, 412-218, 1957.

(9) V. V. Sharonov, *Astron. Journ. of Soviet Union*, **38**, 2, 267-272, 1961.

(10) A. Dollfus, Étude des planètes par polarisation de leur lumière. Thèse. Université de Paris, ser. A, 2869, 70-110, 1955.

(11) W. M. Sinton and J. Strong, *Ap. J.*, **131**, 459-469, 1960.

(12) G. Kuiper, *Ap. J.*, **125**, 307-317, 1957.

36. — LES PROPRIÉTÉS OPTIQUES DE L'ATMOSPHÈRE ET DE LA SURFACE DE MARS DÉDUITES DES OBSERVATIONS PHOTOMÉTRIQUES ET SPECTROPHOTOMÉTRIQUES EFFECTUÉES A L'OBSERVATOIRE ASTRONOMIQUE DE KHARKOV

N. P. BARABASHEV et W. I. EZERSKY,
Observatoire Astronomique, Kharkov, U. R. S. S.

Résumé

L'analyse des résultats des observations photométriques de Mars, effectuées à l'observatoire astronomique de Kharkov (1932-1958), sur la base de la théorie de la diffusion de la lumière dans les atmosphères des planètes, montre que les petites valeurs de la densité optique de l'atmosphère et de l'albedo de la surface sont les plus probables.

Les résultats des observations spectrophotométriques du disque de Mars montrent aussi qu'il n'est pas nécessaire d'adopter des grandes valeurs de la densité optique de l'atmosphère de Mars en lumières bleue et ultraviolette.

37. — SUR L'APPLICATION DE LA PHOTOMÉTRIE DANS LES RECHERCHES DE LA NATURE DE MARS

N. N. SYTINSKAYA
Observatoire de l'Université de Leningrad, U.R.S.S.

Les observations de Mars, faites à l'aide des méthodes visuelles, photographiques et photoelectriques, fournissent la distribution de la brillance sur le disque de la planète pour différentes régions spectrales. Pour l'interprétation ultérieure des résultats de telles observations, il est aisé d'exprimer la brillance sous la forme d'une quantité appelée « l'albedo apparent A_a » et qui représente le rapport de la brillance mesurée B en un point donné du disque, à la brillance B_d d'un diffuseur parfait, orienté normalement aux rayons du Soleil et éloigné de celui-ci d'une distance égale au rayon vecteur de Mars au moment de l'observation :

$$A_a = \frac{B}{B_d} \tag{1}$$

On peut trouver un pareil albedo à l'aide de différentes observations, en faisant, par exemple, une comparaison photométrique entre la brillance du disque de Mars et la brillance des images extrafocales des étoiles. Mais c'est la comparaison de la brillance des parties de la surface de la planète avec la brillance d'un écran diffusant (l'albedo duquel est bien déterminé au laboratoire) qui donne les résultats les plus précis.

On installe l'écran à une distance telle du télescope qu'on puisse en faire la photographie ou le mesurer sans changer la distance focale. Pendant les observations, il doit rester normal aux rayons du Soleil. Puisque dans cette position, il est éclairé non seulement par les rayons directs du Soleil, mais aussi par la lumière diffusée du ciel et des objets terrestres, il est nécessaire d'en mesurer la brillance deux fois : d'abord, pendant l'éclairement total (valeur B_{e1}) et ensuite pendant l'éclairement diffusé seulement (valeur B_{e2}). La différence $B_{e1} - B_{e2}$ représente la brillance déterminée

seulement par l'éclairement direct du Soleil. Si l'on désigne les rayons-vecteurs de Mars et de la Terre par Δ_M et Δ_T, les facteurs de la transparence de l'atmosphère terrestre au moment de l'observation de Mars et de l'écran par P_M et P_e, et les masses d'air correspondantes par F_M et F_e, on peut écrire A_e sous la forme :

$$A_e = A_e \frac{B}{B_{e1} - B_{e2}} \cdot \frac{\Delta_T^2 P_e^{F_e}}{\Delta_M^2 P_M^{F_M}} \qquad (2)$$

On peut trouver des descriptions plus détaillées concernant de telles observations dans un de mes ouvrages précédents (1). Les observations de cette sorte ont été effectuées à l'observatoire de Tachkent en 1939, 1954 et 1956. La méthode de l'écran diffusant a été aussi employée à l'observatoire de Kharkov par N. P. Barabachov et par I. K. Koval (2).

Il est à remarquer qu'en se servant de la photométrie photographique, l'irradiation photographique devient une source dangereuse d'erreurs. Cette irradiation est provoquée autant par le tremblement de l'image, par suite de la turbulence de l'atmosphère, que par la diffusion de la lumière dans l'émulsion de la plaque photographique. A cause de ces effets, la lumière va au-delà des vraies limites de l'image du disque, ce qui peut créer un faux assombrissement au bord du disque là où il n'y en a pas et altérer le vrai assombrissement là où il y en a. C'est pourquoi, en reprenant plusieurs fois de pareilles observations, il est souhaitable d'utiliser ultérieurement un tel procédé ; ainsi, les sources d'erreurs sont réduites au minimum.

La brillance d'un élément quelconque du disque de Mars comprend de la lumière réfléchie par la surface de la planète et de la lumière diffusée dans l'atmosphère. On doit séparer ces deux composantes lors de l'interprétation des résultats des observations photométriques ; ne disposant que de données photométriques, il n'y a aucune possibilité de le faire avec exactitude. C'est pourquoi, il faut, à priori, faire quelques hypothèses arbitraires sur les propriétés de la surface et de l'atmosphère de Mars. A cause de cela, les conclusions finales seront, en quelque sorte, hypothétiques.

Du point de vue des calculs pratiques, il est plus commode de se servir des données pour la vraie opposition, quand l'angle de phase est égal à zéro, et l'angle i d'incidence des rayons solaires, pour chaque point du disque, est égal à l'angle de réflexion ε dans la direction de l'observateur. Comme l'on sait [3], dans ce cas l'albedo A_s peut être exprimé par la formule générale suivante :

$$A_s = r \cos^q i \, e^{-m\tau \sec i} + \varkappa (1 - e^{-n\tau \sec i}) \qquad (3)$$

r étant l'albedo vrai de la surface, q — un paramètre empirique qui est défini par la loi de réflexion de la surface ; τ — l'épaisseur optique de l'atmosphère ; m, n et $\varkappa$ — quelques paramètres déterminés d'après la méthode de calcul de la lumière diffusée.

En appliquant cette formule à l'étude de la nature de Mars, on suppose connues quelques quantités, tandis que les autres sont inconnues ; celles-ci sont obtenues en résolvant plusieurs équations du type (3). Le plus souvent, on prend pour quantités connues A_s, i, m, n et $\varkappa$, il reste alors à déterminer r, q et τ.

Pour avoir les quantités m, n et $\varkappa$ indispensables au calcul, en se servant de la théorie de la diffusion de tel ou tel genre, il est nécessaire de connaître encore quelques propriétés optiques de l'atmosphère, comme par exemple le diagramme de diffusion et le facteur :

$$\Gamma = \frac{\tau_d}{\tau_d + \tau_a} = \frac{\tau_d}{\tau} \qquad (4)$$

où τ_d et τ_a sont les composantes de l'épaisseur optique τ, déterminées par la diffusion pure et l'absorption vraie. Puisque ces données nous sont inconnues, on est conduit à les choisir comme un des éléments du modèle de l'atmosphère adopté pour les calculs [4].

La théorie de la diffusion la plus simple ne tient pas compte de la diffusion d'ordre supérieur et de l'échange de lumière entre la surface et l'atmosphère ; $m = n = 2$ correspond à ce cas. Si, outre cela, le diagramme de diffusion est sphérique, alors $\varkappa = 0{,}0796$, mais s'il correspond à la loi de Rayleigh, $\varkappa = 0{,}188$.

Puisque les valeurs de la brillance ou de l'albedo évaluées à l'aide d'une théorie si primitive, sont toujours inférieures aux

véritables, il est utile de faire usage de méthodes plus précises.

V. G. Fessenkov a proposé, pour compenser le manque de brillance, de prendre dans la formule (3) $m = 1$ et non pas $m = 2$, n restant égal à 2 [5]. A présent, plusieurs savants (Ambartzoumjan [6], Chandrasekhar [7], Sobolev [8] et d'autres) ont élaboré des théories exactes de la diffusion, dans lesquelles ils tiennent compte de l'éclairement de la surface par la lumière diffuse de l'atmosphère, de l'éclairement de l'atmosphère par la lumière réfléchie de la surface et de la diffusion d'ordre supérieur dans l'atmosphère même. Les expressions concernant la brillance sont très compliquées. Cependant, dans les calculs pratiques, on peut les utiliser en se servant de la formule (3).

Il faut, pour cela, calculer pour chaque valeur de l'angle i la valeur de la composante atmosphérique de la brillance ou de l'albedo (y compris la brillance de la surface, définie par la réflexion de l'éclairement diffusé de l'atmosphère) pour les différentes valeurs de la densité optique de la couche atmosphérique τ. Si l'on choisit convenablement les paramètres x et n, on peut représenter empiriquement par le deuxième terme de la formule (3), la dépendance entre cette composante et τ, pour un intervalle particulier de valeurs de τ, supposé exister sur Mars (par exemple, pour $0 < \tau < 0{,}5$). Ces paramètres étant connus, on peut prendre cette formule pour une équation et trouver les valeurs inconnues r, q et τ à la base d'une théorie plus précise.

Il est évident que pour cela il faut avoir les valeurs A_a pour la série de i. On peut le faire en observant la même partie de la surface de Mars à différentes distances du méridien central. Pourtant, cela exige de longues observations pendant toute une nuit, ce qui peut, à son tour, entraîner des erreurs ayant un caractère systématique par suite d'un calcul non complet de l'extinction terrestre. Un procédé plus simple consiste en l'étude de la distribution de la brillance le long du rayon du disque, aux différents points desquels correspondent des valeurs diverses de i. Cependant, en ce cas on est conduit à négliger les différences locales des propriétés de l'atmos-

phère et de la réflexibilité en divers points du disque. Dans les deux cas, il faut partir de l'hypothèse suivante : il n'y a pas de variation diurne dans les propriétés de la surface et de l'atmosphère, c'est-à-dire que les paramètres de (3) ne changent pas avec i.

Dans mes travaux sur l'étude de la nature de Mars par les méthodes photométriques, je partais toujours du schéma d'une atmosphère purement diffusante ($\Gamma = 1$), qui me paraît plus vraisemblable. E. I. Öpik [3], a montré que l'hypothèse d'une atmosphère absorbante peut être aussi en accord avec les résultats des observations, mais alors il faut admettre $q = 0$, ce qui me paraît peu probable. Car à la valeur $q = 0$, il correspond une structure fort rugueuse et très tourmentée. Dans les conditions de l'atmosphère de Mars, ayant des tempêtes de poussière, une pareille structure de la surface peut rester difficilement inchangée, puisque les saillies seront détruites par l'érosion, et les cavités seront remplies de sable ou de poussières.

Le paramètre Γ étant égal à 1, les résultats de la définition de r et q dépendent peu de la méthode de calcul adoptée, parce que, dans ce cas, τ n'est pas grand et la brillance de la lumière diffusée dans l'atmosphère est faible par rapport à la brillance de la surface même. Cependant, les valeurs de τ, d'après des méthodes de calcul diverses, sont très différentes. Par exemple, si on néglige toutes les formes de la diffusion secondaire ($m = n = 2$), τ se trouvera trop élevée, puisque dans ce cas les composantes de la brillance, dues à la diffusion secondaire, seront attribuées à la diffusion atmosphérique du premier ordre, ce qui donne une masse de gaz plus élevée qu'en réalité. Je cite, à titre d'exemple, les résultats d'observations (les données initiales sont présentées dans le tableau 1), obtenus en utilisant d'abord la théorie la plus simple et ensuite une théorie, tenant compte de la diffusion d'ordre supérieur et de l'échange de lumière entre l'atmosphère et la surface. Dans les deux cas, on prend $\Gamma = 1$, le diagramme de diffusion selon la loi de Rayleigh.

Comme on le voit, la différence entre les valeurs de τ est plus que

TABLEAU 1

$\lambda(m\mu)$	380	420		560		630		730	
i		régions sombres	régions claires	régions sombres	régions claires	régions sombres	régions claires	régions sombres	régions claires
0°	0.100	0.114	0.119	0.168	0.184	0.163	0.236	0.161	0.280
10	0.100	0.114	0.119	0.166	0.182	0.161	0.232	0.158	0.272
15	0.100	0.113	0.118	0.163	0.180	0.157	0.227	0.156	0.265
20	0.099	0.112	0.117	0.160	0.174	0.153	0.220	0.152	0.256
23	0.098	0.112	0.117	0.157	0.170	0.150	0.214	0.148	0.249
26	0.098	0.111	0.116	0.155	0.166	0.147	0.209	0.146	0.243
28	0.098	0.110	0.116	0.153	0.164	0.141	0.204	0.143	0.235
31.3	0.097	0.110	0.115	0.150	0.160	0.138	0.196	0.140	0.229
33,5	0.096	0.109	0.115	0.147	0.157	0.135	0.193	0.136	0.222
36,5	0.095	0.109	0.114	0.143	0.151	0.128	0.184	0.130	0.211
41.5	0.094	0.108	0.113	0.137	0.145	0.119	0.119	0.122	0.194
44.5	0.094	0.108	0.112	0.134	0.140	0.115	0.162	0.117	0.183
48.0	0.093	0.107	0.111	0.129	0.135	0.108	0.154	0.111	0.176
51.5	0.092	0.107	0.110	0.125	0.130	0.102	0.145	0.105	0.156
55.0	0.091	0.107	0.109	0.121	0.124	0.098	0.135	0.099	0.144
59.0	0.090	0.106	0.108	0.120	0.119	0.092	0.126	0.093	0.128

TABLEAU 2

Region du Spectre λ $m\mu$	La théorie la plus simple				Une théorie plus précise			
	régions claires	régions sombres	Calottes polaires	τ	régions claires	régions sombres	Calottes polaires	τ
380	0.057	0.057	0.30	0.205	0.051	0.051	0.32	0.145
430	0.092	0.083	0.28	0.175	0.099	0.089	0.30	0.101
560	0.190	0.163	0.28	0.103	0.184	0.159	0.28	0.047
630	0.238	0.160	0.24	0.080	0.236	0.160	0.24	0.031
730	0.283	0.155	0.18	0.051	0.278	0.159	0.18	0.023
q	1.22	1.20	(1.0)	—	1.18	1.04	(1.0)	
D =	0.0506		$P_1 = 225$ mm		D = 0.0147		$P_1 = 171$ mm	
C =	0.0396		$P_2 = 86$ mm		C = 0.0301		$P_2 = 65$ mm	

double. Dans les deux méthodes de calcul, la variation de τ avec λ est moins rapide que dans la loi de Rayleigh en λ^{-4}. Cela s'explique facilement par le fait que l'atmosphère de Mars contient une quantité de grandes particules de poussière en suspension, qui donnent une diffusion neutre. La variation de τ avec λ est bien représentée par la formule de King :

$$\tau = D + \frac{C}{\lambda^4} \tag{5}$$

Le premier terme exprime la diffusion neutre sur les grandes particules ; le second exprime la diffusion moléculaire dans le gaz pur. En admettant que la pression atmosphérique est proportionnelle au paramètre C, on peut par comparaison avec la valeur de C pour l'atmosphère terrestre obtenir la pression atmosphérique P_1 (en mm), à la surface de Mars, mesurée au baromètre à mercure, et la pression $P_2 = 0{,}38\ P_1$ mesurée au baromètre anéroïde.

Le fait que le changement de τ avec la longueur de l'onde ne suit pas la loi de Rayleigh, montre que le diagramme de diffusion ne doit pas être symétrique. C'est pourquoi les résultats les plus

TABLEAU 3

Région du spectre λ $m\mu$	r			τ	
	régions claires	régions sombres	calottes polaires	d'après les mesures des régions claires	d'après les mesures des régions sombres
350	0.064	0.064	0.34	0.117	0.117
430	0.103	0.092	0.31	0.074	0.071
560	0.179	0.159	0.29	0.034	0.034
630	0.235	0.161	0.24	0.028	0.025
730	0.277	0.159	0.18	0.018	0.018
	1.16	1.09	(1.0)		
D = 0.0301			P_1 = 121 mm		
C = 0.0213			P_2 = 46 mm		

corrects seront ceux qui s'obtiennent à l'aide du diagramme de diffusion de forme allongée, correspondant, par exemple, à ce qu'on obtient en moyenne pour toute la couche de l'atmosphère terrestre, d'après les observations de la distribution de la brillance sur le ciel sans nuages.

En faisant le calcul d'après une méthode précise et admettant, comme auparavant, $\Gamma = 1$, nous obtenons les résultats du Tableau 3.

Les valeurs de A_s sont différentes, selon que les régions sont sombres ou claires ; mais leur application conduit à des valeurs égales de τ. C'est une bonne raison pour dire que les valeurs obtenues de τ sont réelles.

REFERENCES

(1) N. N. SYTINSKAYA, Photométrie absolue des objets célestes étendus. Éditions de l'Université de Leningrad, 198 pp., 1948.

(2) N. P. BARABACHOV et I. K. KOVAL, Photométrie photographique de Mars à écrans colorés pendant l'opposition de 1956. Éditions de l'Université de Kharkov, 530 pp., 1959.

(3) N. N. SYTINSKAYA, *Comptes rendus (Doklady) de l'Acad. des Sc. de l'URSS*, 43, 151-154, 1944 ; Comptes rendus de la session scientifique à l Université de Leningrad, 1945, sec. astronomie, 21-41, 1948.

(4) N. N. SYTINSKAYA, « Les résultats des observations de Mars pendant l'opposition de 1956 ». Édition de l'Acad. des Sc. de l'URSS, 114-132, 1959.

(5) B. G. FESSENKOFF, *Astron. Journ. of the Soviet Union*, 21, 6, 257-275, 1944.

(6) V. A. AMBARTSUMIAN, L'astrophysique théorique, Gostechizdat, Moscou, ch. 8, 553-570, 1952.

(7) S. CHANDRASEKHAR, Radiative Transfer, Oxford, 1950.

(8) V. V. SOBOLEV, Le transport du rayonnement dans les atmosphères des étoiles et des planètes. Gostechizdat, Moscou, 1956.

(9) E. I. ÖPIK, *Journ. Geophys. Res.*, 65, 10, 3057-3063, 1960.

38. — SPECTROPHOTOMÉTRIE CONTINUE (entre 6100 et 3200 A) D'UNE RÉGION CLAIRE DE MARS A L'OPPOSITION, ET NATURE DE LA COUCHE VIOLETTE

Pierre GUERIN
Institut d'Astrophysique de Paris, France

Fin décembre 1960, au cours de quatre nuits d'observation, nous avons obtenu, sur deux plaques indépendantes, de nombreux spectres à petite dispersion (longueur totale : 13 mm) du centre du disque de Mars (région claire d'*Arabia*) et d'une étoile (η Cas A) de type spectral (G0V) voisin de celui du Soleil (G1,5V), au moyen du petit spectrographe à châssis oscillant de D. Chalonge, fixé au foyer Cassegrain du réflecteur de 81 cm de l'Observatoire de Haute-Provence. Par comparaison spectrophotométrique de ces spectres, longueur d'onde par longueur d'onde (plus de 40 pointés dans l'intervalle 3167 — 6113 A), nous avons cherché à obtenir, *dans le détail*, la courbe de pouvoir réflecteur de la région martienne visée.

La méthode d'observation et la technique de dépouillement utilisées ont déjà été décrites antérieurement, ainsi que les premiers résultats obtenus [1] [2]. Insistons ici sur la précision de ces mesures, qui tient à plusieurs causes : a) faible longueur des spectres, lesquels sont en outre contigus sur les plaques, ce qui diminue grandement les erreurs locales photographiques ; b) égalité approximative des noircissements à comparer ; c) fort élargissement des spectres, obtenu par l'oscillation du châssis porte-plaque (*), qui ne produit aucune strie et permet l'enregistrement au microphotomètre avec une fente fine et haute, d'où diminution de la granularité ; d) plaques développées à fond, pour réduire l'effet Eberhard ; e) détermination, pour chaque plaque, des courbes de noircissement correspondant à 37 longueurs d'onde différentes ; f) observations de Mars et de η Cas A à des distances zénithales voisines ; g) cor-

(*) L'élargissement obtenu est environ deux fois plus grand dans le rouge que dans l'ultra-violet, ce qui a pour effet de renforcer le noircissement photographique aux courtes longueurs d'onde.

rection différentielle de l'absorption atmosphérique par diffusion Rayleigh et par l'ozone.

Aussi bien nos diverses comparaisons spectrophotométriques de Mars à η Cas A conduisent-elles à des résultats similaires, tant dans l'allure générale que dans le détail. Nous présentons ici (fig. 1) deux de ces comparaisons. Rappelons que les courbes obtenues ont été établies de la façon suivante:

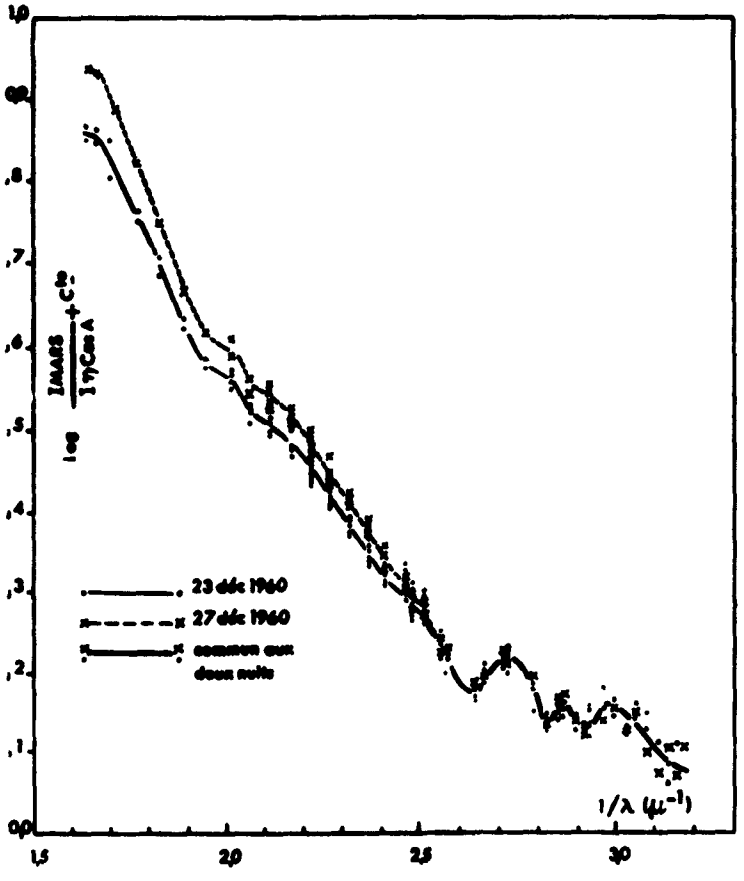

FIG. 1. Deux comparaisons de Mars à η Cas A.

1°. — *Dans l'intervalle spectral 6113 — 4020 Å* ($1/\lambda$ compris entre 1.63 et 2.49), nous avons comparé les intensités en de nombreux points des fonds continus apparents. (Les fonds continus

réels des étoiles G sont inaccessibles avec la faible dispersion utilisée, en raison du très grand nombre de raies fines, noyées dans le grain de la plaque). Nous avons défini les fonds continus apparents selon la même méthode qu'utilise Chalonge pour déterminer les gradients relatifs stellaires, dans le visible et le bleu, au moyen du même spectrographe. Pour rapporter les intensités monochromatiques de Mars à celles du Soleil, c'est-à-dire pour passer de la courbe de la fig. 1 à la courbe de pouvoir réflecteur de Mars, dans l'intervalle spectral considéré, il nous a donc suffi de corriger la première courbe en tenant compte de la valeur, déterminée par Chalonge, du gradient relatif dans le visible (*) de η Cas A par rapport à une étoile de type solaire. Ce gradient est *à peu près* bien connu, mais sa valeur est faible, de sorte que la correction apportée est de toute façon petite.

2°. — *Dans l'intervalle spectral compris entre les raies H et K et l'ultra-violet extrême* (bandes de l'ozone), il n'est plus possible, en revanche, de définir un fond continu apparent : les bandes et les raies visibles (ou plutôt les groupements de raies, compte tenu de la faible dispersion du spectrographe) sont tellement nombreuses et intenses, que nous avons dû comparer entre elles les intensités dans 22 « fenêtres » arbitrairement choisies entre ces bandes ou ces raies. Nous avons ainsi mis en évidence les ondulations de la partie inférieure de la courbe dessinée fig. 1. Ces ondulations se retrouvent sur toutes nos comparaisons de Mars à η Cas A, et ne sont donc pas dues à un effet photographique. La question est de savoir si ce sont de véritables bandes, produites par l'atmosphère martienne, ou au contraire si ces ondulations traduisent seulement la légère différence entre les types spectraux de η Cas A et du Soleil. En effet, bien qu'à première vue, les intensités des raies ultraviolettes apparaissent identiques sur nos spectres de Mars et de η Cas A, il est certain qu'un examen attentif de forts

(*) Chalonge distingue deux gradients dans la région spectrale considérée : le gradient « rouge » et le gradient « bleu ». Le premier n'est différent du second que si l'on compare des étoiles O, B, A, à des étoiles F et G.

agrandissements photographiques de ces spectres montre que certaines bandes ou raies sont légèrement renforcées dans le spectre de Mars (c'est-à-dire dans le spectre solaire), comme il fallait s'y attendre. Cela conduit à penser que le passage du type G0V au type G1,5V pourrait également se traduire par le renforcement, en certaines régions du spectre ultra-violet plus qu'en d'autres, de très nombreuses raies fines non résolues, lesquelles contribueraient à l'intensité dans les pseudo-fenêtres choisies et seraient à l'origine des ondulations observées.

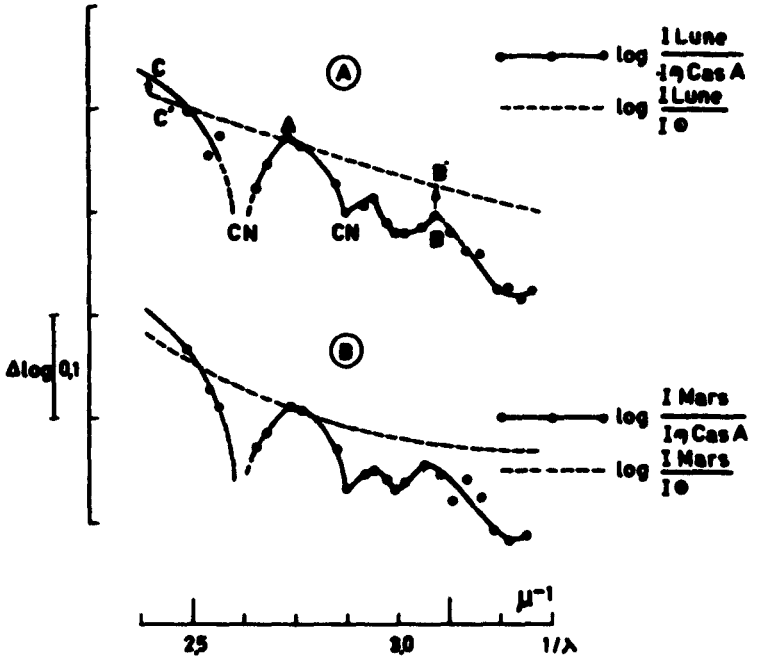

Fig. 2. — Comparaisons ultra-violettes de la Lune et de Mars à η Cas A (trait plein) et au Soleil (pointillé).
Chacune des courbes en trait plein est la moyenne de 4 comparaisons (8 spectres).

Pour trancher la question, nous avons comparé spectrophotométriquement, dans l'ultra-violet, le rayonnement d'une région non luminescente de la Lune à celui de η Cas A, au moyen du même spectrographe. Les spectres furent obtenus en 1962, et la région

lunaire visée fut le centre du cirque Copernic (*), vers la pleine lune. La comparaison de ces spectres a fait apparaître *exactement* les mêmes ondulations ultra-violettes (fig. 2A) que la comparaison de Mars à η Cas A, rappelée pour mémoire sur la fig. 2B. Ce résultat prouve que les ondulations observées *ne sont pas dues* à l'atmosphère de Mars, et infirme donc les conclusions provisoires de nos premières publications ; il apporte en outre une preuve directe de la fidélité et de la sensibilité de nos comparaisons spectrophotométriques.

Dès lors, il est possible d'obtenir la courbe de réflectivité ultra-violette de la région martienne visée en opérant de la façon suivante. Les gradients relatifs « ultra-violets » (au-delà de la limite de Balmer) des étoiles des classes F et G sont établis par Chalonge au moyen de mesures portant sur deux longueurs d'onde seulement (points A et B), qui semblent correspondre à de véritables fenêtres : pour passer du type G0V au type G1,5V (Soleil), il suffit d'opérer le relèvement BB'. Du côté des longueurs d'onde plus grandes que celle de la limite de Balmer, il faut au contraire abaisser la courbe (le point C venant en C'), pour tenir compte de la différence des gradients « bleus » (déjà mentionnée plus haut). Le point A joue ici le rôle de charnière, la différence de discontinuité de Balmer étant négligeable. Puisque l'on ne doit pas s'attendre à observer des bandes d'absorption ou des bandes de luminescence dans le spectre propre de la région lunaire étudiée, la ligne à peine incurvée joignant de façon monotone les trois points C', A et B' traduit la comparaison spectrophotométrique de cette région lunaire au Soleil (c'est-à-dire la courbe de pouvoir réflecteur de Copernic). Les différences d'ordonnées entre cette courbe et la courbe ondulée CAB fourniront les corrections à apporter à la courbe ondulée relative à Mars (fig. 2B) pour obtenir la courbe de pouvoir réflecteur ultra-violet de la planète.

La courbe complète obtenue finalement est représentée fig. 3. Le zéro des ordonnées de cette courbe ne peut évidemment pas

(*) Région lunaire non luminescente, d'après les résultats de Dubois et de Vigroux.

être déduit de nos mesures, mais il est possible de le fixer après coup en tenant compte des mesures absolues publiées par d'autres auteurs. Nous avons utilisé celles de Dollfus, portant sur 8 longueurs d'onde dans le visible, et relatives à un certain nombre de taches claires de Mars à l'opposition (fig. 4).

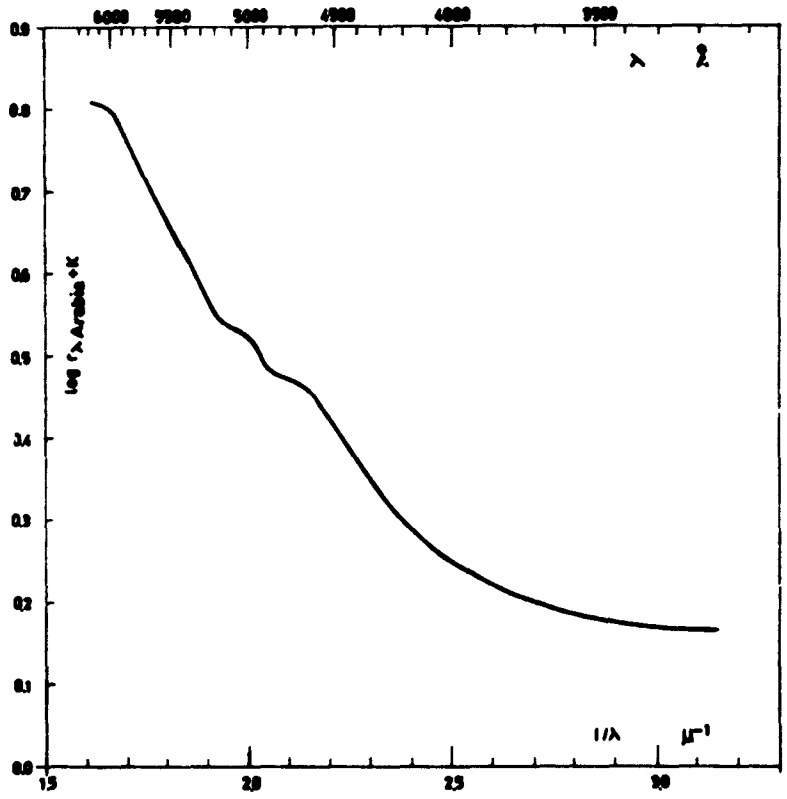

Fig. 3. — Courbe de réflectivité du centre du disque de Mars (*Arabia*) à l'opposition (échelle logarithmique).

Quelles conclusions pouvons-nous tirer maintenant de la courbe obtenue?

En lumière visible, Dollfus a mesuré, au Pic du Midi, la polarisation des taches de Mars peu de temps après nos observations spectrophotométriques, et d'après ces mesures, il semble que l'atmosphère martienne soit restée relativement transparente à

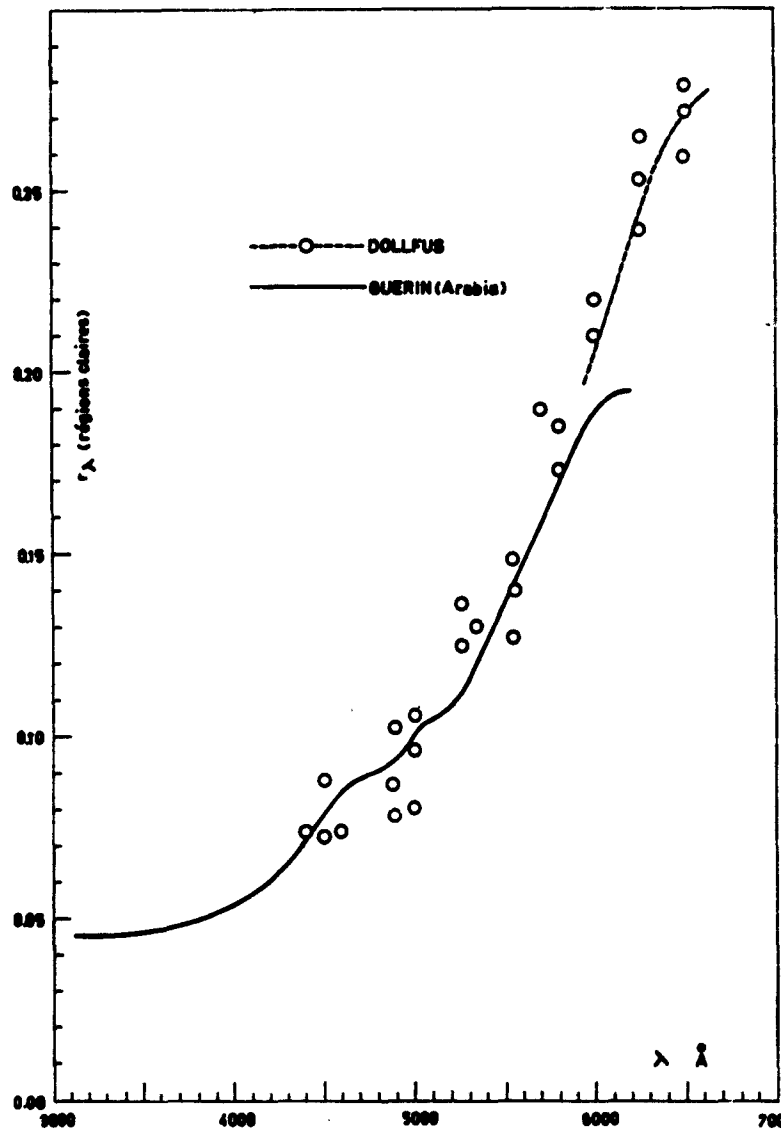

Fig. 4. — Courbe de réflectivité du centre du disque de Mars (*Arabia*) à l'opposition (échelle linéaire), et comparaison avec les mesures de Dollfus dans le visible.

cette époque. Nos mesures de réflectivité d'un désert clair de Mars dans le visible traduisent donc la réflectivité du sol lui-même. Il

serait intéressant de comparer la courbe obtenue à celles que l'on pourrait établir en étudiant divers échantillons de limonite pulvérisée. La spectrophotométrie continue est la seule, en effet, à pouvoir mettre en évidence de légères ondulations comme celles visibles sur les fig. 3 et 4, entre 4600 Å et 5200 Å. Par ailleurs, on remarquera que le sommet de notre courbe s'incurve vers l'horizontale dans le rouge, alors que les mesures de Dollfus, tout comme celles de Vaucouleurs (3), qui atteignent le rouge extrême, ne montrent pas trace d'une telle incurvation. Si celle-ci est réelle, ce n'est donc qu'un accident très localisé de la courbe de réflectivité ; il se peut d'ailleurs que l'incurvation en question soit illusoire et résulte d'une petite erreur systématique dans le repérage des longueurs d'onde ou dans la mesure des noircissements en une région du spectre où la dispersion est très petite et où la sensibilité de la plaque s'annule brusquement.

Dans l'ultra-violet, l'absence totale de bandes d'absorption diffuses ou de bandes de luminescence d'origine martienne permet de rejeter les diverses tentatives d'explication de la couche violette basées sur l'existence de telles bandes. Au moment de nos observations, la couche violette, photographiée sur émulsion orthochromatique avec filtre violet Wratten 34 au foyer coudé du réflecteur de 193 cm de l'Observatoire de Haute-Provence, ne montrait, au centre du disque de Mars, ni « clearing » spectaculaire, ni formations nuageuses claires importantes. On peut en déduire que nos mesures de pouvoir réflecteur de Mars dans l'ultra-violet traduisent la réflectivité de la couche violette « normale ». L'incurvation progressive et régulière de la couche vers l'horizontale, aux courtes longueurs d'onde (*) témoigne en faveur de la diffusion par de petites particules, gouttelettes ou cristaux (4), conformément aux théories classiques (5).

De nouvelles mesures de réflectivité, portant sur les taches claires et les taches sombres de Mars, en particulier au moment d'un

(*) La courbe de réflectivité de la Lune, dans le même domaine spectral (fig. 2A), ne cesse au contraire de décroître avec la longueur d'onde.

grand « clearing » (l'étoile de comparaison choisie étant de type solaire, pour la facilité du dépouillement), seraient cependant nécessaires pour trancher la question de savoir si les « clearings » consistent effectivement en un éclaircissement de la couche violette, laissant voir les taches sombres du sol, ou si, au contraire, les apparences observées sont dues à de simples renforcements du pouvoir diffusant de cette couche au-dessus des déserts clairs, liés principalement, mais non impérativement, à la nature du sol sous-jacent. Il est bien connu, en effet, que de nombreuses grisailles observées en lumière bleue ou violette au moment des « clearings » ne correspondent à aucune tache sombre du sol (*) ; d'autre part, le contraste naturel, dans le visible, des taches sombres de Mars par rapport aux taches claires (déterminé par Dollfus lorsque les mesures polarimétriques indiquent une grande transparence de l'atmosphère martienne jusque dans le bleu) décroît rapidement vers les courtes longueurs d'onde : ce contraste naturel, très faible dans le bleu, l'est sans doute encore plus dans le violet, ce qui peut faire douter que les taches sombres du sol soient clairement discernables dans cette couleur à la faveur de prétendues grandes éclaircies de la couche violette.

(*) Cette remarque a été formulée en particulier par Kuiper (6).

REFERENCES

(1) Guérin P., *Annales d'Astrophysique*, 25, 43, 1961.

(2) Guérin P., *Planetary and Space Science*, 9, 81, 1962.

(3) Vaucouleurs G. de, *Planetary and Space Science*, 2, 26, 1959.

(4) Nat. Bur. Stand., Appl. Math. Series, 4, 1949.

(5) Hess S. L., *Astrophysical Journal*, 127, 743, 1958.

(6) Kuiper G. P., The Solar System, Vol. III, Chap. 16, planche 5, Chicago University Press, 1961.

39. — THE ATMOSPHERE OF MARS

D. H. MENZEL
Harvard College Observatory
Cambridge 38, Mass., U. S. A.

The available data concerning Mars are far too few to permit the development of a definitive model of the atmosphere of that planet. We urgently need new observations. Until now these models are likely to display wide variance. There are, however, a few general conclusions that one can draw concerning the lower atmosphere of Mars, especially the layers responsible for haze and clouds.

I shall not concern myself about the chemical composition of the Martian atmosphere. I suppose that it consists mainly of nitrogen, with a few per cent of carbon dioxide and argon. I shall not object to adding a small amount of molecular oxygen.

I am concerned, however, with water vapor content since that substance is capable of condensing out to form liquid or crystal fogs. The quantity of water in an atmosphere is often expressed as the number of centimeters of precipitable water. And the somewhat vague standard of reference is the amount of water vapor above Mount Wilson on an average clear winter day. We shall not be far wrong if we adopt 1 centimeter of precipitable water as the reference standard.

We may reasonably suppose that about ten times as much water exists on Mars in the solid state as exists in the form of atmospheric vapor. We may further assume that the polar caps occupy about one-tenth of the surface of Mars. Then, if the atmosphere of Mars were to contain the standard reference figure of one centimeter of precipitable water, the depth of accumulated ice or, rather, hoar frost over the poles,would be about 100 times greater, or one meter.

Actually this figure must be much too large. Dunham estimated it as about 1000 times smaller. Hence, if this were so, the depth of

the layer of polar frost would be only a millimeter. I think that Dunham's figure, arrived at without consideration of the curve growth, is perhaps ten times too low. I conclude that the thickness of the layer of polar frost is not more than a few centimeters.

Adopting 0.1 millimeter as the amount of precipitable water in the atmosphere and assuming that it is distributed through one scale height of about 20 km, we calculate a vapor pressure of 5 dynes. This figure is the equilibrium vapor pressure over ice at a temperature of 190°K. The air, of course, may not be saturated, so that higher temperatures are permissible. But, if we are to form an ice fog in an atmosphere of such a low vapor pressure, the temperature of the surrounding air must be less than 190°K. The vapor pressure is very sensitive to small changes in temperature. Lowering the temperature by only 12 degrees will reduce the vapor pressure by a factor of 10. At the theoretical adiabatic gradient for the atmosphere of Mars, a difference of 12 degrees will take place in only 4 kilometers. A layer of ice fog will thus be extremely thin and it will occur in that region of the atmosphere where the temperature ranges between about 180°K to 190°K.

The height of that layer will vary with latitude, season, and time of day. The rarefied atmosphere of Mars would stimulate radiation cooling during the night, with possible formation of a temperature inversion. One may therefore expect under certain conditions a double ice layer, one near the ground and another at higher elevation. Indeed, the white markings often seen on the eastern terminator may well be a layer of frost on the surface of the planet, a thin deposit that quickly sublimes as the day advances.

It is tempting to suppose that the thin layer of crystal fog is responsible for the appearance of the blue image of Mars. A thin layer is necessary to account for the sharp edges of the blue images. And Rayleigh scattering does the rest. Particles some 2×10^{-5} in diameter are indicated. A column of 2×10^{6} particles per cm^2 will give adequate optical depth in the violet and yet be transparent in the visible. This amount of material is extremely small, slightly less

than 10^{-6} grams per cm^2. This is much less than the 10^{-5} grams per cm^2 of precipitable water previously postulated. The discrepancy disappears if we set the cloud layer forming at about 160°K, with a partially saturated atmosphere underneath. And we cannot completely dismiss the possibility that the fog may consist of frozen carbon dioxide.

Now return to other questions related to the atmosphere. The redness of Mars, its low albedo, and the visibility of surface markings in the red and yellow indicate that the total amount of atmosphere is small. Dollfus sets the value of 0.22 in terms of the equivalent scattering power of the earth's atmosphere. And since at least half of this scattering must be attributed to haze, the total atmosphere of Mars must be less than one tenth that of the earth.

Although some scientists have ascribed the red color of Mars to its atmosphere, I see no justification for this hypothesis. Mars is red because its surface is red. The red images show marked darkening to the limb. For this effect I see no explanation but absorption by a low and fairly thick layer of dust. The dust particles must be larger than 1 micron to minimize the Rayleigh scattering. According to Stokes' formula, particles of this size near the surface of Mars would acquire a speed of sedimentation of 3×10^{-2} centimeters per second. A layer three kilometers thick, therefore, would take about 10^7 seconds or about four months to settle out. This slow rate of fall for the absorbing red layer is thus consistent with the permanence of the polar caps and the failure of the dust to cover it.

We have concluded, then, that the atmosphere of Mars contains two layers of particulate matter, a thick layer of large dust particles near the surface and a very thin layer of fine particles above, perhaps well above, the layer of dust. We have implied that this upper layer consists of fine ice crystals. Certainly this suggestion is consistent with the association between the thin atmospheric clouds and the underlying polar caps. The clouds, for example, persist for some time after the solid cap has sublimed. But the

ice crystal hypothesis is not without difficulty. Ice crystals would seem to have a very high reflecting power and should, therefore, lead to a higher violet albedo than that determined for Mars. I should prefer dark absorbing clouds, rather than ice crystals. Smoke would be about right, like the blue smoke from the lighted end of a cigarette, rather than the white smoke from the unlit end. Perhaps the blue clouds consist of very fine dust and their association with the polar regions may be attributed to some effect of atmospheric circulation that causes the particles to concentrate in these areas.

None of these hypotheses accounts satisfactorily for the phenomenon known as « blue clearing », the improved visibility of surface features in blue light near the time of opposition. I have long felt that this « clearing » may arise from improved contrast at the planet's surface, near opposition, when rays of sunlight falling upon a roughened surface can escape from the interstices through which they entered.

I have noticed a similar effect from airplanes flying over desert areas in the south western U. S. The effect is especially pronounced near sunset. The shadow of the plane on the ground is surrounded by a bright halo 2 or 3 degrees in diameter. Within this halo, the details of the surface markings are much more clearly seen than outside of the halo.

This work is related to and has received partial support from National Aeronautics and Space Administration Grant NsG 89-60 with Harvard University.

40. — UPPER ATMOSPHERE OF MARS (*)

JOSEPH W. CHAMBERLAIN (**)
Yerkes Observatory and Department of Geophysical Sciences
University of Chicago, U. S. A.

ABSTRACT

Most of our knowledge of the earth's upper atmosphere is obtained from experiments *in situ* or remote observations that offer fairly direct interpretations. For the other planets neither approach is as yet possible, so indirect, theoretical procedures are required to construct models of their atmospheres. Herein the wide variety of basic physical processes governing the structure of a planetary high atmosphere are set forth, with a view toward obtaining « deductive models » — i. e., models derived theoretically when only the chemical composition and temperature of the lower atmosphere and the incident solar flux are specified (in addition to various physical and astronomical constants).

The procedures are applied to Mars, whose lower and middle atmosphere is already partially understood from earlier work, notably that of R. Goody. The uncertainties involved at various stages in the construction of such a model are emphasized, as are the major differences in physical processes and atmospheric characteristics between Mars and the Earth.

The most significant result is that the CO that must be in the upper atmosphere of Mars should serve as an effective thermostat, keeping the temperature at the escape level (1500 km) from exceeding about 1100°K. This is cool enough for Mars to retain atomic oxygen. Were it not for CO cooling, Mars' upper atmosphere would be so extensive and form such an effective thermal insulation between the upper ionosphere and the heat sink at the mesopause

(*) Complete paper published in the *Astrophysical Journal*, Vol. 136, 582, 1962.

(**) Alfred P. Sloan Research Fellow, 1961-63.

that the temperature would exceed 2000° K. The lifetime for the escape of oxygen is estimated as 10^9 years.

The mesopause is determined by CO_2 radiation. Near the mesopause CO_2 should become dissociated and the free O atoms form a thin layer of O_2; this effect has no analogy on earth. The model ionosphere has considerably smaller densities of ionization than comparable regions in the earth's atmosphere. The E region is split into two distinct portions, with X-rays forming the higher one (E_2) and ultraviolet light ionizing O_2 near the mesopause (E_1). The Martian analogue to the terrestrial F_2 region may not develop a very high electron density, and the entire ionosphere should be depleted at night.

41. — BORD ATMOSPHÉRIQUE DE MARS

F. LINK
Institut Astronomique de l'Académie des Sciences,
Prague-Ondřejov, Tchécoslovaquie

Cette note essaie de répondre en quelque sorte à la suggestion formulée par de Vaucouleurs (1).

« A re-evaluation of the theoretical effect of the atmospheric layer projected beyond the limb should be made for both molecular scattering and plausible assumption on the vertical distribution of turbidity in the atmosphere of Mars. »

qui, en même temps, résume ce que nous nous proposons de développer dans la suite.

Dans un milieu diffusant sans absorption vraie, négligeons la diffusion secondaire et tout autre éclairement sauf celui dû au Soleil. La luminance d'un volume élémentaire du milieu db est liée à la profondeur optique $d\tau$ dans la direction de propagation de la lumière solaire par (2)

$$db = \mathrm{K}\mathrm{E}\, d\tau \qquad (1)$$

où E est l'éclairement solaire de l'élément et K une constante qui prend les valeurs

$\mathrm{K} = \dfrac{1}{4\pi}$ (2) pour la diffusion orthotrope,

$\mathrm{K} = \dfrac{3}{8\pi}$ (3) pour la diffusion moléculaire et pour l'observateur en P regardant dans la direction des rayons solaires.

La luminance db vue du point P sera alors

$$db = \mathrm{K}\mathrm{E}_0 \exp(-2\tau_1)\, d\tau \qquad (4)$$

où τ_1 est la profondeur optique depuis l'entrée M_1 du milieu, E_0 l'éclairement solaire en M_1. La luminance totale dans la direction PM_1 sera alors

$$b = \frac{\mathrm{K}\mathrm{E}_0}{2}[1 - \exp(-2\tau)] \qquad (5)$$

où τ est la profondeur optique totale suivant le rayon.

La dernière relation permet de calculer la luminance du bord de l'atmosphère de Mars lorsque la planète est en opposition si nous connaissons les valeurs de la profondeur optique en fonction de l'altitude minimale h_0 des rayons.

Dans la suite, nous allons considérer d'abord l'atmosphère pure et ensuite quelques modèles simples des couches de poussières. Pour l'atmosphère, nous adopterons les paramètres suivants :

a = 3400 km : le rayon de la planète,

g = 383 cm/sec^2 : l'intensité de la pesanteur,

p_0 = 85 mb (d'anéroide) : la pression au sol,

T = 220° K : la température de l'atmosphère isotherme,

m = 28 : le poids moléculaire de l'air (N_2).

On obtiendra alors dans l'atmosphère isotherme :

$M_0 = \rho_0 H = 1{,}77$ km (6) — la hauteur réduite de l'atmosphère ou la masse d'air au zénith en km d'air de la densité normale.

$H = \frac{kT}{mg} = 17$ km (7) — l'échelle de hauteur, $k = 8{,}3.10^7$.

$\rho_0 = \frac{273}{T}\frac{p_0}{1013} = 0{,}104$ (8) — la densité de l'air au sol exprimée en densité normale de l'air.

$\log \rho = -1{,}02 - 0{,}0255\, h$ (9) — la densité en fonction de l'altitude h exprimée en km

$M = \rho\sqrt{2\pi a H}$ (10) — la masse d'air traversée par les rayons horizontaux passant à l'altitude h_0.

$\tau = AM$ (11) — la profondeur optique suivant ces rayons où A est le coefficient d'absorption apparente calculé à partir de la diffusion moléculaire de la lumière.

Dans la suite nous adopterons les modèles suivants pour l'atmosphère de Mars :

Type	Description	Structure
I	atmosphère pure	formule (9)
II	atm. pure + couche homog.	$h_1 = 0$ km, $h_2 = 30$ km
III	atm. pure + couche homog.	$h_1 = 27$ km, $h_2 = 30$ km
IV	atm. pure + couche homog.	$h_1 = 0$ km, $h_2 = 100$ km
V	atmosphère polluée proportionellement à ρ.	

La profondeur optique dans les cas II et IV sera donnée par la formule

$$\tau = 2t_0\sqrt{\frac{2a}{h_2}}\sqrt{1 - \frac{h_0}{h_2}} \tag{12}$$

et dans le cas III

$$\tau = 2t_0\sqrt{\frac{a}{h_1 + h_2}}\,\frac{\sqrt{h_2 - h_0} - \sqrt{h_1 - h_0}}{\sqrt{h_2} - \sqrt{h_1}} \tag{13}$$

où t_0 est la profondeur optique au zénith.

Dans le cas V, nous supposerons l'atmosphère de Mars remplie de poussières en chute libre dans le milieu résistant atmosphérique. Comme le diamètre des poussières est probablement inférieur à 1 μ (d'après la sélectivité de l'absorption), leur distribution en altitude sera de la même forme que celle de la densité de l'air, sauf dans les couches immédiatement voisines du sol.

La valeur du facteur K dépend du genre de la diffusion ce qui pourrait influencer dans une certaine mesure l'intégration de (4), mais un tel raffinement est provisoirement superflu étant donné le degré d'approximation de nos modèles atmosphériques. Dans la formule (5), nous mettrons donc simplement (2) ou (3).

Nous avons effectué les calculs de τ dans les trois régions spectrales suivantes :

	A	t_0	A' (cas V)
	km^{-1}		km^{-1}
UV 3500 Å	0,0350	0,075	0,0775
VIS 5400 Å	0,00575	0,040	0,0282
IR 7000 Å	0,00205	0,015	0,0105

Les valeurs ci-dessus sont décadiques.

Les figures 1-5 donnent les courbes $\log [1 - \exp (- 2\tau)] = f(h_0)$ calculées pour les cas I-V et les trois régions spectrales ci-dessus. On peut les diviser en deux catégories. Dans la première catégorie nous mettrons les courbes monotones (I et V), tandis que dans la seconde catégorie seront classées les courbes à descente brusque qui marquent le niveau supérieur des couches II, III et IV.

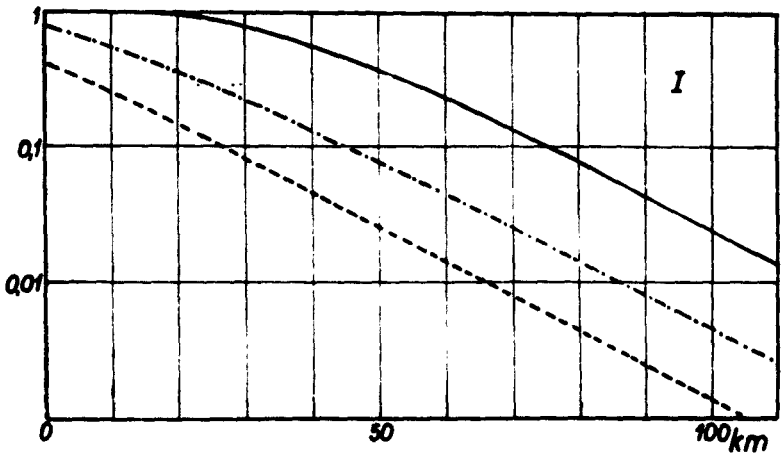

Fig. 1. — Luminance du bord atmosphérique en fonction de l'altitude. Atmosphère pure (cas I) ——— 3500 Å, – – – 5400 Å, ····· 7000 Å.

Sur les courbes monotones, le bord optique sera défini par les propriétés du récepteur qui, directement ou indirectement (sur le cliché), sera en fin de compte l'œil humain. En vertu de la théorie du contraste [2], l'œil place la limite estimée au point d'inflexion de la courbe $\log b = f(h)$. Cela veut dire, par ex., pour le cliché photographique, qu'il faut transformer la courbe $\log b = f(h)$, à l'aide de la courbe de gradation, en une courbe de densité $D = F(h_0)$ dont le point d'inflexion fixe le bord estimé de la planète.

Ainsi, dans l'atmosphère pure (I) ou polluée (V) le bord estimé se trouve plus haut dans l'UV que dans l'IR (fig. 6C en bas). Sa position, fixée par le point d'inflexion de la courbe D et l'extension optique du disque, est un effet mixte d'origine atmosphérique et instrumentale. L'extension est d'autre part plus grande dans l'atmo-

sphère polluée que dans l'atmosphère pure, mais nous ne sommes pas d'accord avec Fessenkov (4) qui a trouvé que l'atmosphère pure ne suffit pas pour donner en UV une extension observable.

Dans l'atmosphère à couche de poussières limitée, le bord optique est donné par la limite supérieure de la couche. Toutefois sur quelques courbes (II et III) en UV, cette limite est peu marquée (fig. 2 et 3) de façon que le bord optique en UV soit le même que

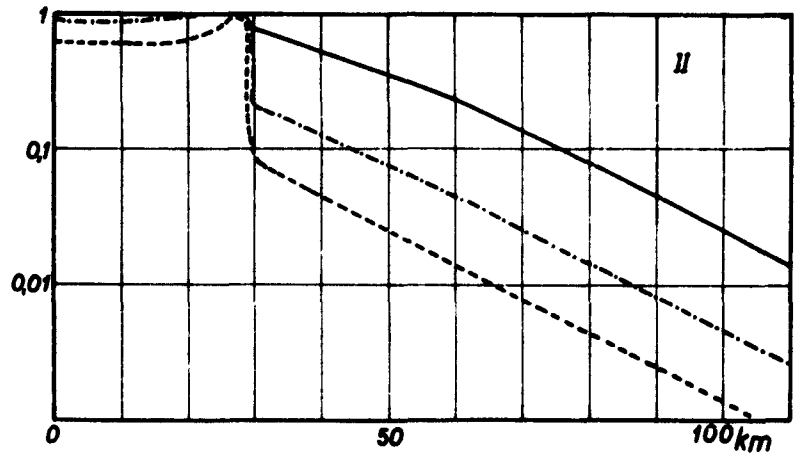

Fig. 2. — Luminance du bord atmosphérique en fonction de l'altitude. Couche mince à l'altitude de 30 km (cas II) dans l'atmosphère pure.

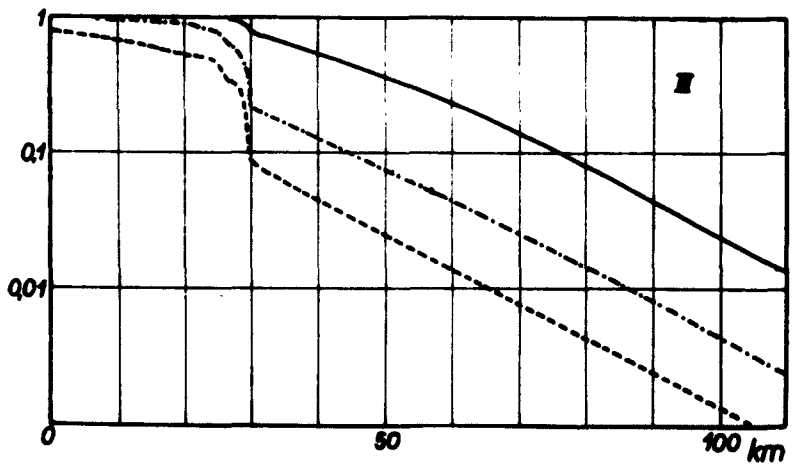

Fig. 3. — Luminance atmosphérique en fonction de l'altitude. Couche épaisse à l'altitude de 30 km (cas III) dans l'atmosphère pure.

dans l'atmosphère pure (I), c'est-à-dire vers 70 km, tandis que dans l'IR il se trouverait à la limite supérieure de la couche vers 30 km.

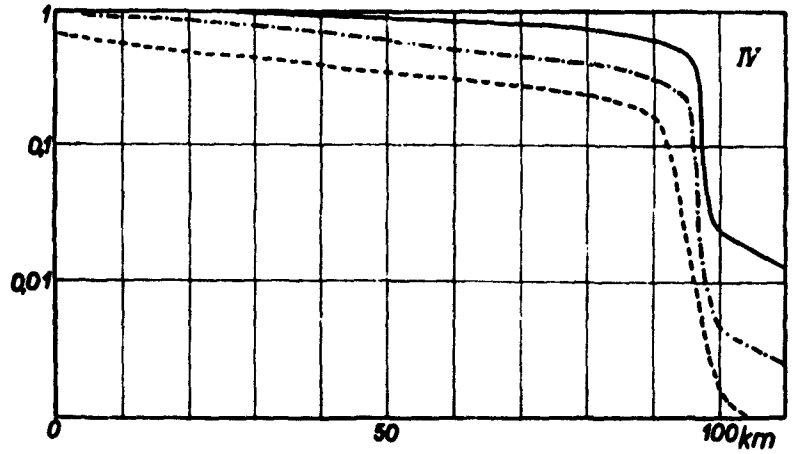

Fig. 4. — Luminance atmosphérique en fonction de l'altitude. Couche épaisse à l'altitude de 100 km (cas IV) dans l'atmosphère pure.

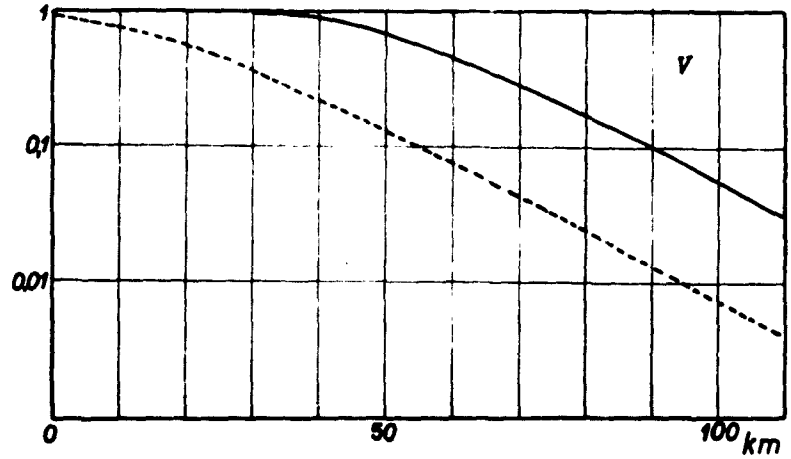

Fig. 5. — Luminance atmosphérique en fonction de l'altitude. Atmosphère polluée proportionellement à la densité (cas V).

En ce qui concerne les observations visuelles où l'œil intervient directement, le phénomène devrait être neutre dans les cas I et V, car la partie rectiligne de la courbe caractéristique de l'œil

est très étendue. Les mesures de Dollfus (v. plus loin) sont de cette nature.

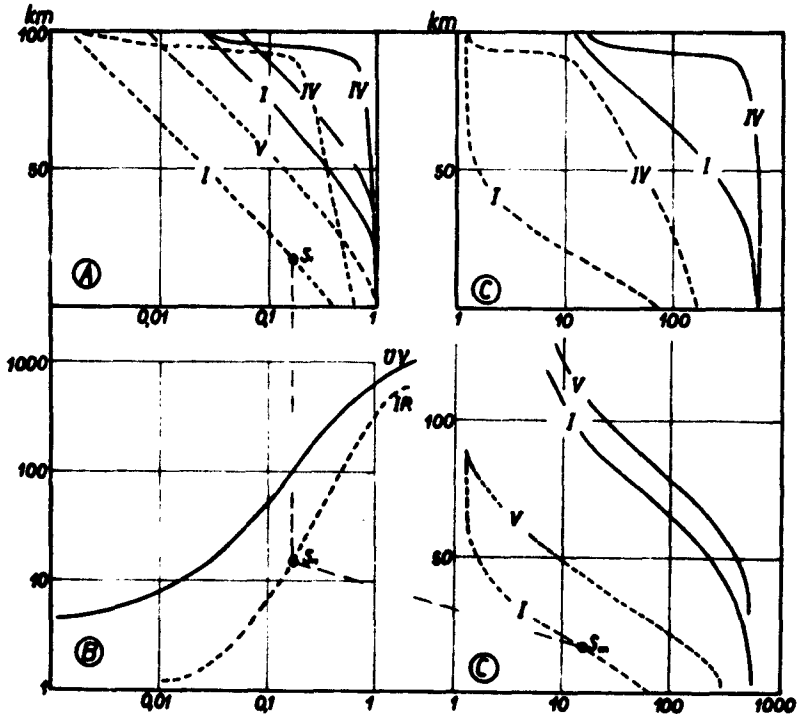

Fig. 6. — Représentation photographique (cas fictif) de la luminance ph. A... quelques courbes reprises des fig. 1, 4, 5. B... courbes de gradation des plaques photographiques. C... densités D de l'image photographique en fonction de l'altitude.

Nous pouvons donc conclure que si les mesures de répartition de la luminance sur le disque semblent prouver l'existence de l'atmosphère polluée de Mars, l'élargissement du bord optique ne demande pas nécessairement que cette pollution soit localisée dans les couches élevées. Dans tous ces problèmes, il ne faut pas perdre de vue que la valeur angulaire de l'élargissement optique est de l'ordre de 1/4″ — donc assez difficilement observable de la Terre. Les conditions seront nettement améliorées quand nous pourrons observer, à l'instar des « cosmonautes » terrestres, l'atmosphère de Mars au cours d'un vol circumplanétaire.

REFERENCES

(1) G. DE VAUCOULEURS, *Physics of the Planet Mars*, p. 305, London 1954.

(2) F. LINK, *Bull. Astr.*, 15, 143, 1950.

(3) A. KÜHL, *Phys. Zeit.*, 29, 1, 1928.

(4) B. FESSENKOV, *Astr. Nachr.*, 228, 25, 1926.

42. — THEORETICAL ESTIMATES OF THE AVERAGE SURFACE AND ATMOSPHERIC TEMPERATURES ON MARS

GEORGE OHRING
Geophysics Corporation of America
Bedford, Mass., U. S. A.

I. AVERAGE SURFACE TEMPERATURE

A. *Introduction*

Of extreme interest to meteorologists and astrophysicists who are involved in planetary atmospheres research is the average surface temperature of the planets. Planetary surface temperature can be derived from both experimental observation and theoretical reasoning. The observational determinations, which work well in the case of a rather tenuous atmosphere such as Mars', are based upon measurements of the planet's emission of infrared radiation ; the theoretical determinations are based largely upon some sort of radiative equilibrium considerations. In the present study we derive estimates, based upon radiative equilibrium considerations, of the minimum and maximum possible value of the average temperature of the Martian surface. These estimates are then compared to some of the thermal emission observations.

B. *Theory*

The average surface temperature of a planet which has an atmosphere that is transparent to long wave radiation can be computed by equating the energy received from the sun to the energy emitted by the planet's surface. The following formula for the temperature of such a planet can be easily derived :

$$T^4 = \frac{(s.c.)\,(1 - A)\,\mu}{4\sigma}, \qquad (1)$$

where T is temperature,

$s.\ c.$ is the solar constant at the earth's distance from the sun,

A is the planetary albedo,

σ is the Stefan-Boltzmann constant,

μ is a dilution factor equal to r_e^2/r_p^2,

where r_e is the mean distance from the earth to the sun, and r_p is the mean distance from the planet to the sun.

If one now introduces into such a planetary atmosphere gases that absorb long wave radiation, a « green-house » effect is created and the average surface temperature will increase above that given by Equation (1). Thus for an atmosphere that is not completely transparent to long wave radiation Equation (1) can be used to derive an estimate of the lowest possible value of the average planetary surface temperature. For the planet Mars the following numerical values can be substituted in Equation (1) :

$A = 0.15$

$\mu = 0.44$

$s.\ c. = 2.0$ cal cm^{-2} min^{-1}

$\sigma = 8.13 \times 10^{-11}$ cal cm^{-2} deg^{-4} min^{-1}

With these substitutions the lowest possible value for the average planetary surface temperature for Mars turns out to be 219° K.

The problem of estimating the maximum possible value of the average Martian surface temperature is more complex. We wish to maximize the greenhouse effect, within reason, in order to obtain a realistic estimate of the maximum surface temperature. The green-house effect depends essentially upon the amount and vertical distribution of absorbing gases, and on the vertical distribution of temperature. The greater the amount of absorbing gases — the more opaque the atmosphere is — the greater will be the green-house effect, and thus the higher will be the surface temperature. In our model (discussed later) we attempt to make realistic estimates of the maximum amounts of carbon dioxide, water vapor and ozone in the Martian atmosphere, and their distribution with height. Once the maximum amount of absorbing gas is fixed we have only to chose a realistic temperature distribution with height,

which would maximize the surface temperature. For simplicity, and for lack of knowledge, we shall assume that the temperature variation with height is linear. This is probably a good approximation in the troposphere of Mars, as it is for the troposphere of the earth, and it is the troposphere rather than the upper atmosphere that contributes most to the radiation fluxes. The question we must now answer is, « What choice of constant lapse rate will produce a maximum green-house effect and thus a maximum surface temperature? » We can answer this question by going through the following qualitative reasoning.

The upward flux of long wave radiation at the top of the Martian atmosphere must balance the incoming solar radiation that is not reflected back to space. This can be written as

$$I_0 (1 - A) = W \qquad (2)$$

where I_0 is the average incoming flux of radiation at the top of the Martian atmosphere,

A is the planetary albedo, and

W is the upward flux of long wave radiation at the top of the atmosphere.

The upward flux W is composed of radiation coming directly from the planet's surface and of radiation emanating from the planet's atmosphere. If the atmosphere is isothermal, the radiation originating in the atmosphere will be at the same temperature as the radiation originating from the surface. Thus, the upward flux will remain constant with height and have a value equal to the black body flux emitted by the surface. The surface temperature of an isothermal atmosphere would then be the same as that computed from Equation (1), i. e. 219° K. If the temperature decreases with height, however, the radiation emitted by the atmosphere would be at a lower temperature than that emitted by the ground. In order that W now balance the incoming radiation, the surface temperature must be higher than 219° K. The greater the lapse rate the greater is the surface temperature in order for balance to occur at the top of the atmosphere. In a planetary

atmosphere the limiting lapse rate is the adiabatic lapse rate and we choose this as the lapse rate that will maximize the green-house effect and hence the surface temperature.

With a given distribution of absorbers and temperature lapse rate, the outgoing radiation, W, is a function only of the surface temperature, and can be written as (Elsasser, 1960 ; Hales et al, 1960)

$$W = \sigma T_s^4 - \int_{T_t}^{T_s} R(CO_2)\, dT - \int_{T_t}^{T_s} R(H_2O)\, dT - \int_{T_t}^{T_s} R(O_3)\, dT \quad (3)$$

$$\text{where } R = \int_{\nu_1}^{\nu_2} \frac{dB_\nu}{dT} (1 - \tau_f)\, d\nu \quad (4)$$

and T_s is surface temperature,

T_t is the temperature at the top of the atmosphere,

B is the black body flux,

τ_f is the flux transmissivity, and

ν is frequency.

R is a function of path length, u, and temperature, T, of the particular gas in question. Tables of R for carbon dioxide, water vapor and ozone have been presented by Elsasser (1960) and expanded by Hales, *et al*, (1960). R for carbon dioxide covers the 15 μ band, R for H_2O covers the 6.3 μ band, the window region, and the rotational band, and R for ozone covers the 9.6 μ band. The integrals in Equation (3) can be evaluated numerically, given the temperature and absorber distribution in the atmosphere. It should be noted that both water vapor and carbon dioxide absorb radiation in the 15 μ band. However, since we are attempting to maximize the green-house effect we shall treat these absorptions independently and make no correction for the overlap.

Equation (2) can now be written as :

$$I_0 (1 - A) + \int_{T_t}^{T_s} R(CO_2)\, dT + \int_{T_t}^{T_s} R(H_2O)\, dT + \int_{T_t}^{T_s} R(O_3)\, dT = \sigma T_s^4 \quad (5)$$

To solve this equation for the surface temperature, T_s, one can assume a value for T_s and perform the integrations on the left side of the equation. Upon adding the incoming radiation to the evaluated integrals, we can compute a second approximation of T_s from Equation (5). This new value is then used to recalculate the integrals and obtain a third approximation, and so on, until a value of T_s is obtained that balances Equation (5). The surface temperature obtained from this model represents an estimate of the maximum possible value of the average surface temperature on Mars.

C. *Green-house model and computational techniques*

The green-house model that we shall adopt is based upon reasonable estimates of the maximum amounts of carbon dioxide, water vapor and ozone in the atmosphere of Mars. Of these three constituents, carbon dioxide is the only one that has definitely been detected in the Martian atmosphere. Grandjean and Goody (1955), in a re-analysis of Kuiper's (1952) near infrared measurements, derive a carbon dioxide content of about 2 % for the commonly accepted surface pressure of 85 mb. We shall simply double this value for our estimate of maximum carbon dioxide content. We shall further assume that all three gases are uniformly mixed with height so that the path lengths are a function only of pressure, and that a linear pressure correction can be applied directly to the path lengths as suggested by Elsasser (1960). With these assumptions and a carbon dioxide content of 4 % the carbon dioxide path length for any pressure thickness is

$$\Delta u_{CO_2} = 86.8 \left(\frac{\bar{p}}{1000}\right) \Delta p \qquad (6)$$

where Δu_{CO_2} is the pressure corrected path length (cm STP) in a layer with mean pressure $\bar{p}$ mb and thickness Δp mb.

Although water vapor has not been detected spectroscopically in the Martian atmosphere, the aqueous nature of the polar caps

indicates that there must be some water vapor present. Dunham (1952), on the basis of spectroscopic observations, derived an upper limit of 0.0015 times the terrestrial amount over Mt. Wilson on an average clear night. This is of the order of 10^{-3} cm of precipitable water with the terrestrial amount of about 0.7 cm prevailing during Dunham's observations. De Vaucouleurs (1954) states that the amount of precipitable water is very likely much less than 4×10^{-2}cm and probably less than 1×10^{-2} cm. We take as our estimate of the maximum water vapor content the value 10^{-3} cm of precipitable water. Assuming a constant mixing ratio with height, the pressure corrected water vapor path length (cm precip. water) for any pressure thickness can be written as

$$\Delta u_{H_2O} = 1.18 \times 10^{-4} \left(\frac{\bar{p}}{1000}\right) \Delta p \tag{7}$$

Ozone also has not been detected in the Martian atmosphere. An upper limit of 0.05 cm has been given by Kuiper (1952) who based his estimate on the failure of attempts to detect ozone by means of absorption spectra. Another estimate of the maximum amount of ozone has been derived by Marmo, *et al*, (1960) who computed the total amount of photochemically produced ozone for an atmosphere that had a maximum possible amount of oxygen. The maximum amount of oxygen is about 2.5 m (Dunham, 1952) and for this oxygen content Marmo, *et al*, computed a value of about 0.15 cm for the total amount of ozone. Using this latter value as our estimate of the maximum amount of ozone on Mars we can express the pressure corrected ozone path lengths (cm STP) as

$$\Delta u_{O_3} = 1.8 \times 10^{-3} \left(\frac{\bar{p}}{1000}\right) \Delta p \tag{8}$$

As discussed previously the adiabatic lapse rate, approximately 3.7 deg/km is to be used in the radiation computations. The surface pressure is taken as 85 mb. In order to evaluate numerically the integrals appearing in Equation (5), the atmosphere is divided into

nine layers of thickness 10 mb, except for the topmost layer, whose thickness is 5 mb. For example the integral for carbon dioxide is written as

$$\sum_{i=1}^{9} R_i \, (\log u_i, \, \overline{T}_i) \, \Delta T_i,$$

where R_i is the R value of the i^{th} layer, which is a function of u_i, the pressure corrected carbon dioxide path length from top of the

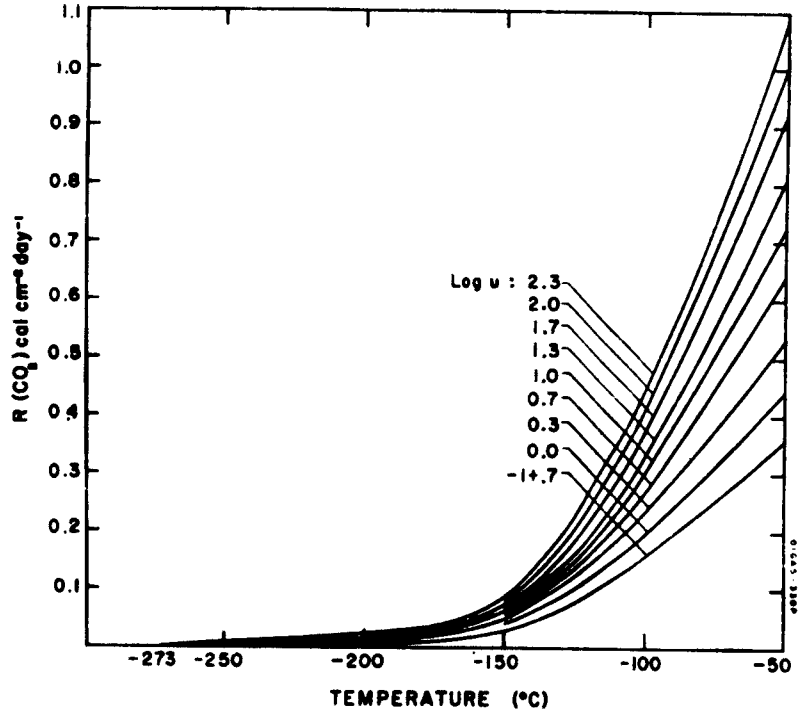

Fig. 1. — Extrapolated values of $R(CO_2)$.

atmosphere to the middle of the layer, and $\overline{T}_i$, the average temperature of the i^{th} layer ; and ΔT_i is the temperature difference between the bottom and top of the i^{th} layer.

Mean temperatures and path lengths for each layer are used to obtain values of the R function from Elsasser's (1960) tables,

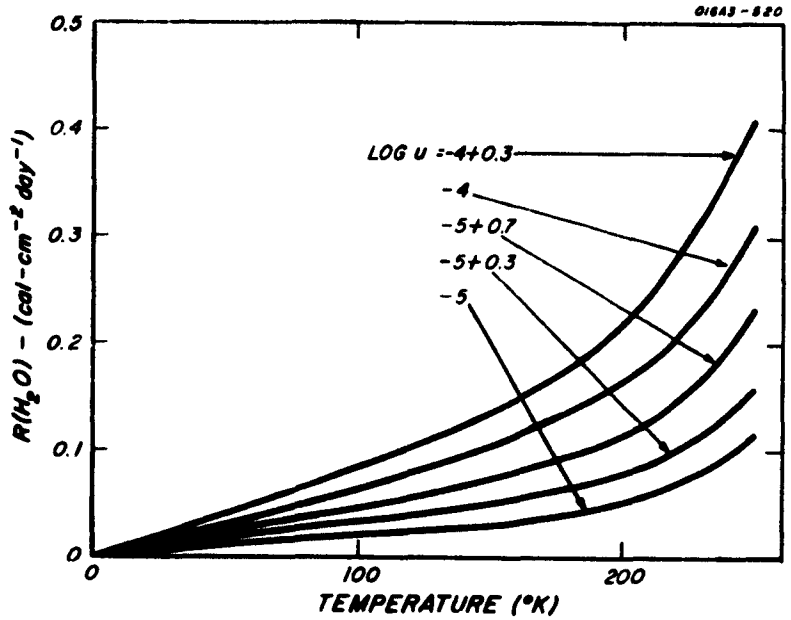

Fig. 2. -- Extrapolated values of $R(H_2O)$.

and the computation is similar in all respects to that suggested by Elsasser except that numerical rather than graphical integration is used. In our model the temperature at the top of the atmosphere is zero K and the temperatures in the upper part of the atmosphere are below 193° K. Since Elsasser's tables of R cover only the range $193 \leqslant T \leqslant 313$, they were extrapolated from 193 K to a temperature of zero K, for selected path lengths, in our computations. The extrapolation to zero degrees K was performed with the knowledge that R at zero degrees is equal to zero (see Equation [4]). As a check on the extrapolation, integrals of the form $\int_0^{193} R\, dT$ at constant path length were evaluated graphically and compared to similar integrals given by Elsasser (1960). Although there may still be some error in the values of R used at temperatures less than 193° K, these will not significantly affect the computations since the contributions of the upper layers to the outgoing radiation are much less than the contributions from the lower layers. Graphs

showing the extrapolated R curves are contained in Figures 1, 2, and 3.

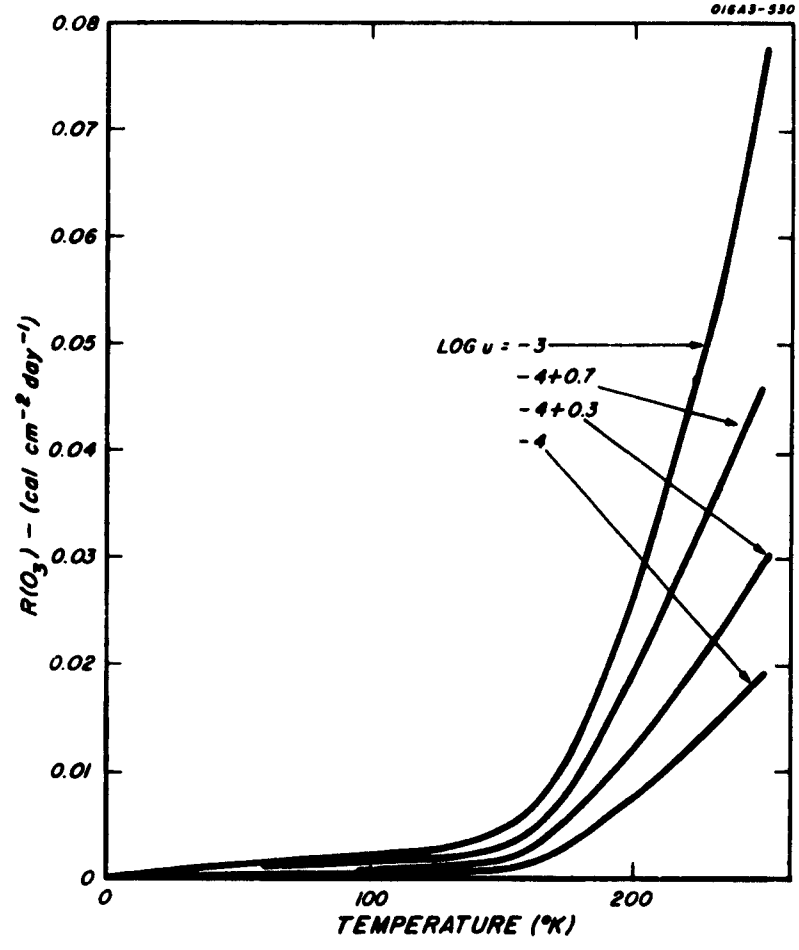

Fig. 3. — Extrapolated values of $R(O_3)$.

D. *Results*

For a solar constant of 2.0 cal cm^{-2} min^{-1} and a dilution factor of 0.44, the average incoming radiation at the top of the Martian atmosphere, I_0, is 317 cal cm^{-2} day^{-1}. With the commonly accepted

value of 0.15 for the Martian planetary albedo the average amount of solar radiation remaining after reflection is

$$I_0 (1 - A) = 269 \text{ cal cm}^{-2} \text{ day}^{-1}.$$

Using this value and the maximum green-house model discussed above, we obtain from Equation (5) a value of T_s equal to 233° K. This temperature is our estimate of the maximum possible value of the average surface temperature on Mars. Comparing 233° K with our previous estimate of 219° K for the minimum possible value, we see that even a maximum green-house effect would raise the surface temperature only about 14° K. This maximum green-house effect can be compared to the average green-house effect for the earth. The temperature of the earth's surface, if it had an atmosphere transparent to long wave radiation, can be computed from Equation (1). With an albedo of 0.35, $\mu = 1$ and a solar constant of 2.0 cal cm^{-2} min^{-1}, Equation (1) yields a temperature of 252° K for the earth. The observed average temperature of the earth is about 288° K, indicating that the *average* green-house effect for the earth is about 36° K, or about 2 1/2 times as large as the maximum green-house effect for Mars.

Of the three gases contributing to the green-house effect, carbon dioxide is by far the most important as can be seen from the following values of the integrals appearing in Equation (5) :

$$\int_{T_t}^{T_s} R(CO_2)\, dT = 57 \text{ cal cm}^{-2} \text{ day}^{-1}$$

$$\int_{T_t}^{T_s} R(H_2O)\, dT = 18 \text{ cal cm}^{-2} \text{ day}^{-1}$$

$$\int_{T_t}^{T_s} R(O_3)\, dT = 4 \text{ cal cm}^{-2} \text{ day}^{-1}$$

This is in contrast to the earth's atmosphere where water vapor is the most important absorber of long-wave radiation.

Another measure of the effectiveness of the green-house is the ratio of outgoing long-wave radiation at the top of the atmosphere

to the long-wave radiation emitted by the surface, which may be termed the infrared transparency of the atmosphere. The lower the infrared transparency, the more effective is the green-house. For average conditions on earth the infrared transparency (based on radiation fluxes computed by London, 1957) is about 57 % ; for our maximum green-house on Mars, the infrared transparency is 77 %.

Based upon our theoretical estimates the true average surface temperature of Mars should lie between 219° K and 233° K. In order to fix the average temperature more accurately, it would be necessary to know the actual amounts and distribution of absorbing gases, and the actual vertical temperature distribution. A sample calculation indicated that the use of the estimated average carbon dioxide concentration — 2 % by volume — rather than a maximum concentration — 4 % by volume — did not affect the outgoing radiation too much. Also the vertical temperature distribution we used cannot be too far from the actual temperature distribution. We therefore suggest that the actual mean temperature is closer to 233° K than to 219° K. In the next section we compare our estimate with some of the observations of Martian temperatures.

E. *Comparison with observations*

The observations of surface temperature on Mars are generally based upon measurements of the planet's thermal emission ; these measurements are usually made during oppositions and therefore refer largely to the sunlit side of the planet. Gifford (1956) has analyzed systematically large numbers of such observations and has derived average latitudinal surface temperature distributions on the noon meridian for each of the four seasons for the latitude range 60° N to 80° S. On the basis of continuity and solar insolation considerations we have extrapolated these curves to the poles ; they are shown in Figure 4, with extrapolations indicated by dashed lines. In order to compute the average planetary surface temper-

ature from these observations we must perform the following operations :

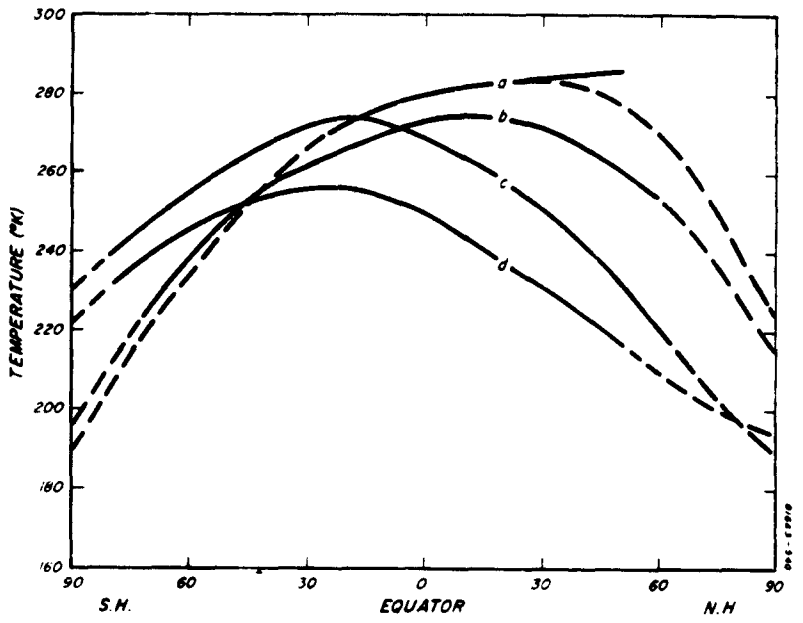

Fig. 4. — Average surface temperature variation along the Martian noon meridian for southern hemisphere seasons (after Gifford, 1956). (a) Winter, (b) Fall, (c) Summer, (d) Spring.

(1) Average the seasonal curves to obtain an average annual curve ;

(2) Subtract from these noon-time temperatures the amplitude of the average diurnal variation of temperature as a function of latitude in order to obtain a mean daily temperature ;

(3) Compute the average planetary surface temperature by weighting the mean temperature at each latitude belt according to the area of the latitude belt.

When the first of these operations is performed the average annual noon curve shown in Figure 5 results. The correction of this curve for diurnal variation is important because such variations are apparently appreciable on Mars. There have been a number

of measurements, mostly in tropical regions, of the variations of Martian surface temperature during the day. Gifford's (1956) analysis of 214 daytime surface temperatures near the Martian equator indicates a diurnal range of about 70° C, which is equivalent to an amplitude of 35° C. De Vaucouleurs (1954), in his book on Mars, suggests an average amplitude of 25°C in the equatorial regions.

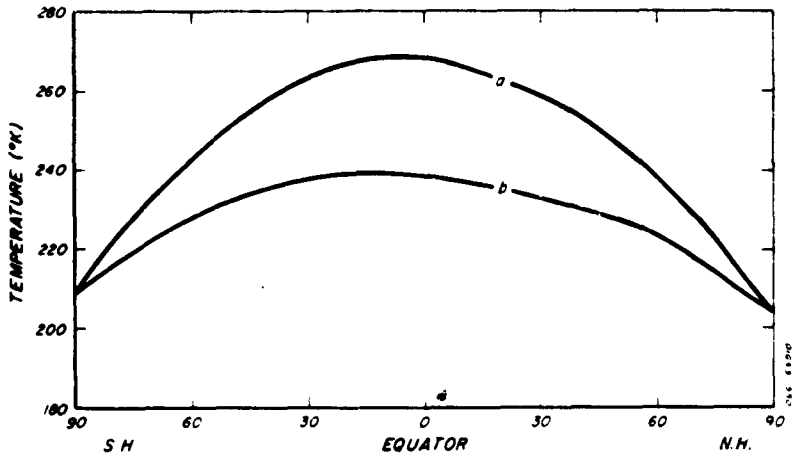

Fig. 5. — Average annual surface temperature as a function of latitude : (a) noon temperatures, (b) mean daily temperatures.

In the recent observations of Sinton and Strong (1960), however, the indicated amplitude is about 45° C or higher. Since the analyses of Gifford and de Vaucouleurs are based upon more data we shall rely on their estimates for the amplitude of the diurnal variation at the equator ; we therefore adopt an amplitude of 30° C in the equatorial regions of Mars. Assuming that the diurnal variation depends only on insolation, we can approximate the latitudinal variation of the amplitude by a simple cosine function

$$a_\varphi = 30 \cos \varphi \qquad (9)$$

where a_φ is the amplitude at any latitude φ. When these amplitudes are subtracted from the noon curve, the average annual curve shown in Figure 5 is obtained. The curve indicates an average equatorial temperature close to 240° K and average polar temper-

ature of between 200° K and 210° K. The average planetary surface temperature can be obtained from a numerical integration of this curve from pole to pole, weighting the temperatures according to surface area as follows :

$$\bar{T} = \frac{1}{2}\int_{-\pi/2}^{\pi/2} T(\varphi) \cos\varphi \, d\varphi \tag{10}$$

where $\bar{T}$ is the average planetary surface temperature, and $\bar{T}(\varphi)$ is the average surface temperature at latitude φ. Upon performing this integration we obtain a value of 233° K for the average Martian surface temperature. Within the scope of the uncertainties involved in obtaining this value, it can be considered to be in reasonable agreement with the computed theoretical range 219° K to 233° K.

II. Average vertical Distribution of Temperature

A. *Introduction*

The average vertical distribution of temperature in a planetary atmosphere is generally controlled by the following processes : (1) radiation, (2) convection, and (3) condensation phenomena. Horizontal eddy transport and advection of heat, though important at various latitudes and seasons, should not affect the *average* vertical temperature distribution. The Martian atmosphere and, to a smaller extent, the earth's atmosphere are largely transparent to solar radiation. Thus, most of the solar energy is not absorbed directly in the atmospheres of these planets but rather at the planetary surfaces. This energy is then transmitted to the atmosphere by infrared radiative and convective transfer. In the earth's atmosphere, but probably not on Mars, the release of heat into the atmosphere by condensation of water vapor accompanies the radiative and convective processes. The combination of these processes in the earth's atmosphere results in an average tropospheric lapse rate of about 6° K/km, which is about 60 % of the lapse rate that

would be produced by dry convection alone : the adiabatic lapse rate. Radiative processes, both short-wave absorption and long-wave emission, if allowed to act alone in the earth's atmosphere would produce a temperature distribution close to adiabatic in the troposphere and close to the observed temperatures in the upper stratosphere (Manabe and Möller, 1961). Thus, in the earth's stratosphere, the controlling processes are principally radiative.

The temperature distribution in the Martian atmosphere is unknown. Present knowledge concerning the Martian atmosphere indicates that condensation phenomena and absorption of solar radiation by the atmosphere can be neglected. The major processes affecting the average vertical temperature distribution in the Martian atmosphere are then infrared radiation and convection. In the present study, we compute the average vertical temperature distribution on Mars on the basis of a simple model which, though primarily a radiative equilibrium model, permits the effect of convection to be considered.

B. *Theoretical formulation*

As stated in the introduction, the important processes controlling the temperature structure of the Martian atmosphere are infrared radiation and convection. If one computes the temperature distribution that would result from radiative transfer alone, one obtains a radiative equilibrium temperature profile. For an atmosphere such as Mars' or the earth's, the infrared radiative equilibrium temperature profile is characterized by extreme convective instability in the lower layers (see, for example, Goody, 1954, de Vaucouleurs, 1954). Because of its instability, such a temperature profile cannot exist ; convection takes place and the temperatures in the lower layers are changed. The new lapse rate is determined by convective equilibrium rather than radiative equilibrium and is equal to the adiabatic lapse rate (in the case of the earth's atmosphere condensation processes further change the prevailing

lapse rate). The height to which convection extends depends upon infrared radiation processes ; convection will extend to that height above which infrared radiation produces a stable lapse rate (Goody, 1954). This level separates a convective troposphere from a radiative equilibrium stratosphere and can be referred to as the tropopause. Simple as this theoretical formulation may be, it does improve upon a theory based upon radiative equilibrium alone in that the effect of convection, if not the actual mechanisms, are included, and it does permit estimates of the height of the tropopause. This formulation has been applied to the Martian atmosphere previously (Goody, 1957) ; however, the surface temperature used, 270° K, is probably about 40° K higher than the average surface temperature (see previous discussion of average surface temperature).

C. *Computational technique*

Our goal is to determine the average temperature structure in the Martian atmosphere on the basis of a convective troposphere lying below a radiative equilibrium stratosphere that is thermally stable. The computations are based upon the initial value method of computing radiative equilibrium temperatures (see Manabe and Möller, 1961). Starting with an initial isothermal atmosphere whose temperature is equal to the average Martian surface temperature, we compute the infrared radiative temperature change rates as a function of height. These rates are then applied to the initial temperature profile in order to obtain a new temperature profile. This process is continued until a temperature profile is obtained for which the radiational rates of temperature change are negligibly small. At each stage of the calculations, however, the temperature profiles are checked for instability ; if any layer has a lapse rate greater than the adiabatic, the temperatures are brought back to the adiabatic curve prior to the next calculation of radiational rates of temperature change. Such instabilities will occur, according to the previous discussion, in the lower layers of the atmosphere. Throughout the computation the surface temperature is held con-

stant. Within the limits of the theoretical formulation, the final temperature profile obtained from these calculations should be representative of the average temperature structure of the Martian atmosphere.

The radiational rates of temperature change were determined from the divergence of the net flux of radiation with height, as computed with the aid of Elsasser's (1960) radiation tables. Carbon dioxide is assumed to be the only important radiating gas, and the 15 μ band of carbon dioxide the only important band. Following Elsasser's notation, the upward and downward fluxes of radiation at any reference level can be written as (see Elsasser, 1960, and Hales, *et al*, 1960).

$$F\uparrow (O) = \sigma T_g^4 - \int_{T_0}^{T_g} R(u,T)\, dT \tag{11}$$

$$F\downarrow (O) = \int_{T_1}^{T_0} R(u,T)\, dT + \int_{0}^{T_1} R(u_1,T)\, dT \tag{12}$$

where

$$R(u,T) = \int \frac{dB_\nu}{dT} [1 - \tau(u)]\, d\nu \tag{13}$$

and $F\uparrow (O)$ and $F\downarrow (O)$ are the upward and downward radiation fluxes at the reference level, σ is the Stefan-Boltzmann constant, T_g is the ground temperature, u is the reduced carbon dioxide path length (increasing upwards and downwards from the reference level), T is temperature, T_1 is the temperature at the top of the atmosphere, T_0 is the temperature at the reference level, u_1 is the reduced carbon dioxide path length from the top of the atmosphere to the reference level, B_ν is the black-body energy per unit spectral interval, and τ is the flux transmissivity. The integral in Equation (11) and the first integral in Equation (12) follow the actual temperature-path-length relationship in atmosphere ; the second integral in Equation (12) is a boundary term ; the integral in Equation (13) extends over the 15 μ carbon dioxide band.

The net flux at any level is given by the difference between the upward and downward fluxes.

$$F_{net}(O) = F\uparrow(O) - F\downarrow(O) \tag{14}$$

The radiational rate of temperature change can be obtained from the vertical divergence of the net flux

$$\frac{\Delta T}{\Delta t} = \frac{g}{c_p}\frac{\Delta F_{net}}{\Delta p} \tag{15}$$

where $\Delta T/\Delta t$ is the radiational rate of temperature change for a layer of pressure thickness Δp, g is the acceleration of gravity, c_p is the specific heat of the atmosphere at constant pressure. With $g = 373$ cm sec^{-2}, $c_p = 0.24$ cal g^{-1} deg^{-1}, ΔF_{net} in cal cm^{-2} day^{-1} and Δp in mb, Equation (15) can be written as

$$\frac{\Delta T}{\Delta t}\left(\frac{\text{deg}}{\text{day}}\right) = 1.55\frac{\Delta F_{net}}{\Delta p} \tag{16}$$

The atmospheric integrals in Equations (11) and (12) are evaluated numerically by dividing the atmosphere into eight layers of thickness 10 mb and one layer (the topmost) of 5 mb. Mean temperatures and path lengths for each layer are used to obtain the values of R from expanded tables of R, which have been computed by Hales, *et al* (1960). As suggested by Elsasser (1960), a linear pressure correction is applied to the path lengths to correct for pressure broadening of the absorption lines.

The Elsasser-Hales tables of R cover the range of temperature from 313° K to 193° K. These tables were extended, for the path lengths applicable on Mars, to a temperature of zero °K. The extrapolation to zero °K was performed with the knowledge that $R(u,T)$ at $T = 0$ is equal to zero. As a check on the extrapolation, integrals of the form $\int_0^{193} R\,dT$ at constant u were evaluated graphically and compared to similar integrals presented by Elsasser (1960). If necessary, the curves were redrawn until good agreement was obtained. Fortunately, the values of R are small at these low temperatures so that the use of extrapolated values should not

seriously affect the final results. The extrapolated values of R for the 15 μ carbon dioxide band are shown in Figure 1.

The second integral in Equation (12), which represents an integration from zero °K to the temperature at the top of the atmosphere, at constant path length, was evaluated graphically from the curves in Figure 1. At the lower boundary, the ground, the temperature was held constant throughout the computations; at the upper boundary, the top of the atmosphere, the temperature was assumed equal to the temperature of the highest layer, which varied during the successive iterations. The radiation fluxes were computed at the top and bottom of each layer and the radiational rates of temperature change were then obtained from Equation (16).

The calculations were stopped when all of the radiational rates of temperature change were equal to or less than 0.1 deg day^{-1}. As a check on the calculations, the same iteration technique was applied to an atmosphere that initially had an adiabatic lapse rate.

D. *Physical model*

A value of 230° K is adopted for the average surface temperature of Mars. This value is based upon the discussion in Section I. The most probable value of surface pressure is about 85 mb (de Vaucouleurs, 1954) and the adiabatic lapse rate is about 3.7°K/km (Kellogg and Sagan, 1961).

In the present calculations, the Martian atmosphere is assumed to be dry and devoid of ozone. The only gas that has been observed spectroscopically in the Martian atmosphere is carbon dioxide. Grandjean and Goody (1955) derive a carbon dioxide content of about 2 %, assuming a surface pressure of 85 mb. This compares to an average carbon dioxide content of 0.03 % by volume in the earth's atmosphere. Assuming that the carbon dioxide is uniformly mixed in the Martian atmosphere, we can write the pressure corrected path length as

$$\Delta u = 43.4 \left(\frac{\bar{p}}{1000}\right) \Delta p \tag{7}$$

where Δu is the carbon dioxide path length in cm STP of a layer of thickness Δp mb and average pressure $\bar{p}$ mb. With this physical model and with the theoretical formulation and computational techniques outlined above, we can now compute the average vertical distribution of temperature in the Martian atmosphere.

E. *Results*

The computed temperature profile and an adiabatic profile are illustrated in Figure 6; the crosses represent temperatures obtained from an atmosphere that is initially isothermal at 230° K, and the circles represent temperatures obtained from an atmosphere that initially has an adiabatic temperature profile and a surface temperature of 230° K. At no level is the difference between the two sets of computed temperatures greater than 5° K. The troposphere extends to a height of about 9 km where it is topped by a tropopause whose temperature is 196° K. Above the tropopause the temperature decreases at an average rate slightly less than adiabatic to about 90° K near 42 km (2.5 mb). This last temperature represents the average temperature of the topmost 5 mb layer of the Martian atmosphere. Also shown in Figure 6 is an approximate representation of the profile computed by Goody (1957) for the same carbon dioxide content but with a surface temperature of 270° K. Goody's computed tropopause is about the same height as ours. Above the tropopause the shapes of both curves are in reasonable agreement up to about 20 mb, but above this level our temperatures decrease more rapidly than Goody's. This discrepancy may be due to a number of factors, including the low height resolution in the upper part of our model atmosphere, the boundary condition we imposed at the top of the atmosphere and the extrapolated R values used at these heights. In any case the major features of both profiles are the same :

(1) An adiabatic troposphere extending to about 9 km ; and

(2) A stratosphere that is stable but with temperature still decreasing with height.

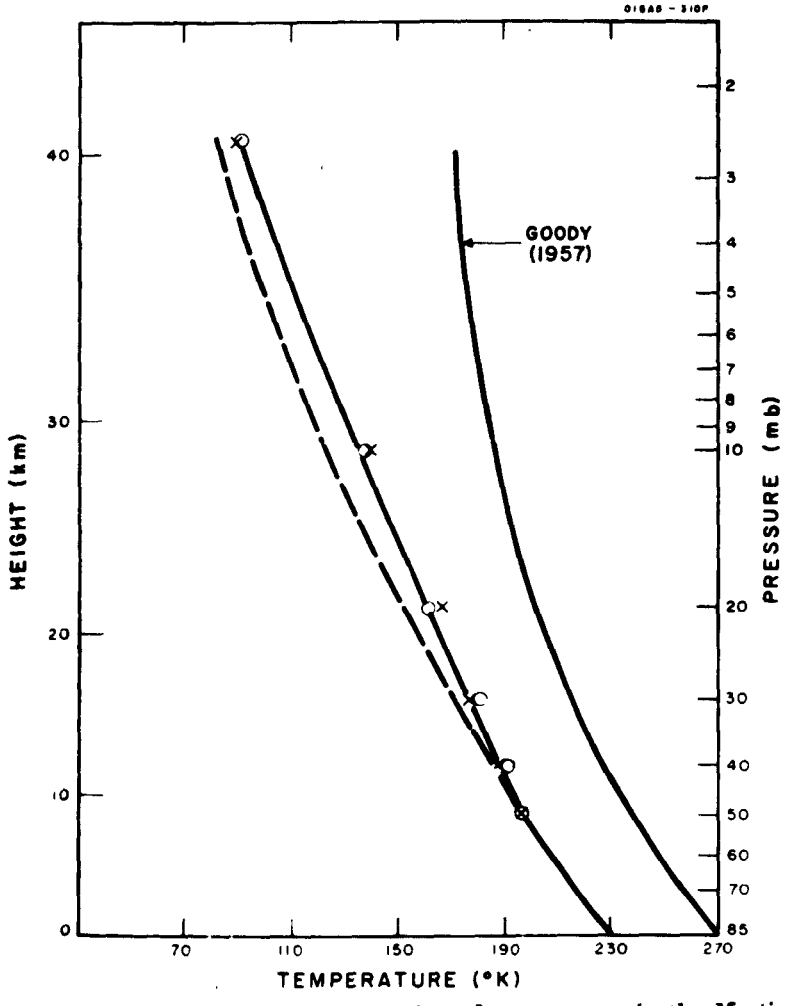

Fig. 6. — Computed vertical distribution of temperature in the Martian atmosphere. — Crosses represent temperatures obtained from an initial isothermal state ; circles represent temperatures obtained from an initial adiabatic state. — Goody's (1957) profile and an adiabatic profile (dashed line) are also indicated.

It is interesting to note that at the low temperatures which we have computed for the 30 to 40 km region, carbon dioxide would condense. Such a condensation might have some connection with the blue haze observed in the Martian atmosphere. However, before we can adopt our estimated temperature distribution with

any degree of certainty we must first ascertain how much water vapor and ozone is actually present in the Martian atmosphere. Ozone especially, if present, would affect the stratospheric temperature distribution through its direct absorption of solar radiation. Thus, the computed temperature distribution should be considered as a tentative estimate of the true temperature distribution. Additional computations should be made as soon as better estimates of the average water vapor and ozone contents become available.

III. Summary

From theoretical computations based upon radiative equilibrium considerations, the average surface temperature of the planet Mars is found to be in the range of 219° K to 233° K.

This is in reasonable agreement with the thermal emission observations which suggest a mean temperature of about 233° K. The computations also indicate that the *maximum* green-house effect on Mars is about 40 % of the *average* green-house effect in the earth's atmosphere, and that carbon dioxide is the most important contributor to the Martian green-house.

The major characteristics of the computed vertical distribution of temperature in the Martian atmosphere are an adiabatic troposphere extending to 9 km, and a stratosphere that is stable, but with temperature still decreasing with height. If ozone is present in the atmosphere additional computations should be made to evaluate its effect on the temperature distribution.

REFERENCES

de Vaucouleurs, G., *Physics of the Planet Mars*. London, Faber and Faber Limited, 365, 1954.

Dunham, T., Spectroscopic observations of the planets at Mount Wilson. *The Atmospheres of the Earth and Planets*, ed. by G. P. Kuiper, University of Chicago Press, 288-305, 1952.

Elsasser, W. M., Atmospheric Radiation Tables. *Amer. Meteor. Soc. Meteorological Monographs*, 4, 23, 43, 1960.

GIFFORD, F., *Ap. J.*, **123**, 154-161, 1956.

GOODY, R. M., *The Physics of the Stratosphere*, Cambridge Univ. Press, 187, 1954.

GOODY, R. M., *Weather*, **12**, 3-15, 1957.

GRANDJEAN, J., and GOODY, R. M., *Ap. J.*, **121**, 548, 1955.

HALES, I. V., WILLIAMS, T. L., HENDERSON, D., Calculation of infrared radiative flux emission of the Earth plus atmosphere at various levels high above the earth, Final Report, Contract AF 19(604)-2418. (ASTIA order number AD-248155), 1960.

KELLOGG, W. W. and SAGAN, C., *The Atmospheres of Mars and Venus*. A Report of the Space Science Board, National Academy of Sciences — Nation Research Council Publication 944, 151, 1961.

KUIPER, G. P., *The Atmospheres of the Earth and Planets*, Univ. of Chicago Press, 343, 1952.

LONDON, J., A study of the atmospheric heat balance. Final Report Contract No. AF 19(122)-165, Dept. of Meteorology and Oceanography, N. Y. U., 99 pp. (ASTIA order number AD-248155), 1957.

MANABE, S. and MOLLER, F., *Monthly Weather Review*, **89**, 503-532, 1961.

MARMO, F., and WARNECK, P., Photochemical processes in the atmosphere of Mars, in Final Report on Laboratory and Theoretical Studies in the Vacuum Ultraviolet for the Investigation of Planetary Atmospheres, Contract NASw-124, (GCA Technical Report No. 61-20-N, available from Geophysics Corporation of America, Bedford, Massachusetts), 1961.

43. — EXTREME MODEL ATMOSPHERE OF MARS (*)

G. F. SCHILLING
The RAND Corporation
Santa Monica, California, U. S. A.

Introduction

When faced with the requirements of designing and building space probes to explore our neighboring planets, the scientific experimenter as well as the engineer must rely on quantitative data rather than best estimates. Mars has been the subject of astronomical observations for centuries, and there can be found in the scientific literature an abundance of material about its atmosphere. Yet an impartial, critical analysis soon reveals that our present reliable, quantitative knowledge of its characteristics is very scarce, indeed.

Consequently, I have recently attempted to compute theoretical models of the atmosphere of Mars on the basis of the very few available, factual data, together with a minimum of assumptions. Distinct from earlier approaches which have resulted in « mean values », these model atmospheres give extreme upper and lower limits for the distribution of pressure, temperature, and density in the Martian atmosphere up to 150 km altitude.

The mathematical method used is essentially one which proved successful in developing model atmospheres of Earth as recently as some twenty years ago, before the advent of sounding rockets and high-altitude balloon measurements. While I believe that this method has indeed yielded reliable data needed for the engineering design of space probes for the exploration of Mars, the spread of values is still very broad, and indicative of our present scarcity of knowledge.

(*) This research was supported in part by the Jet Propulsion Laboratory, California Institute of Technology, under Contract No, N-33561 (NAS 7-100) for the National Aeronautics and Space Administration.

Method of computation

The study took three steps towards a quantitative description of the principal physical parameters of the atmosphere of Mars. First, an attempt was made to derive extreme limits for the permissible ranges of atmospheric temperature, pressure, and density which could prevail near the Martian surface in middle and low latitudes. These limits were derived essentially from past observations of the mass of the Martian atmosphere per unit surface area, and from radiometric observations of the ground temperature, permitting inferences about the range of air temperature close to the ground.

Secondly, the permissible variations with altitude of these limits were computed for a Martian troposphere in convective as well as conductive equilibrium, with isothermal equilibrium above the tropopause. Taken into account were such uncertainties as our knowledge of mass and diameter of Mars (and hence gravitational acceleration) and variation of the intensity of solar radiation from aphelion to perihelion. This method allowed a reasonably confident calculation of probable lower limits up to about 80 km altitude. Reliable upper limits, however, could not be derived in such a rigorous way, primarily because of our practically complete lack of factual knowledge of the composition of the Martian atmosphere.

The third step, consequently, introduced a number of speculative assumptions with regard to the role played by minor constituents, especially CO_2 and ozone. A resultant conjectural model was computed for the case of maximum heating caused by these constituents absorbing solar energy in the Martian atmosphere.

Conclusions

The detailed calculations and the numerical results of the limiting envelopes for three specific model atmospheres are being published elsewhere [1]. Figure 1 is an attempt to combine these

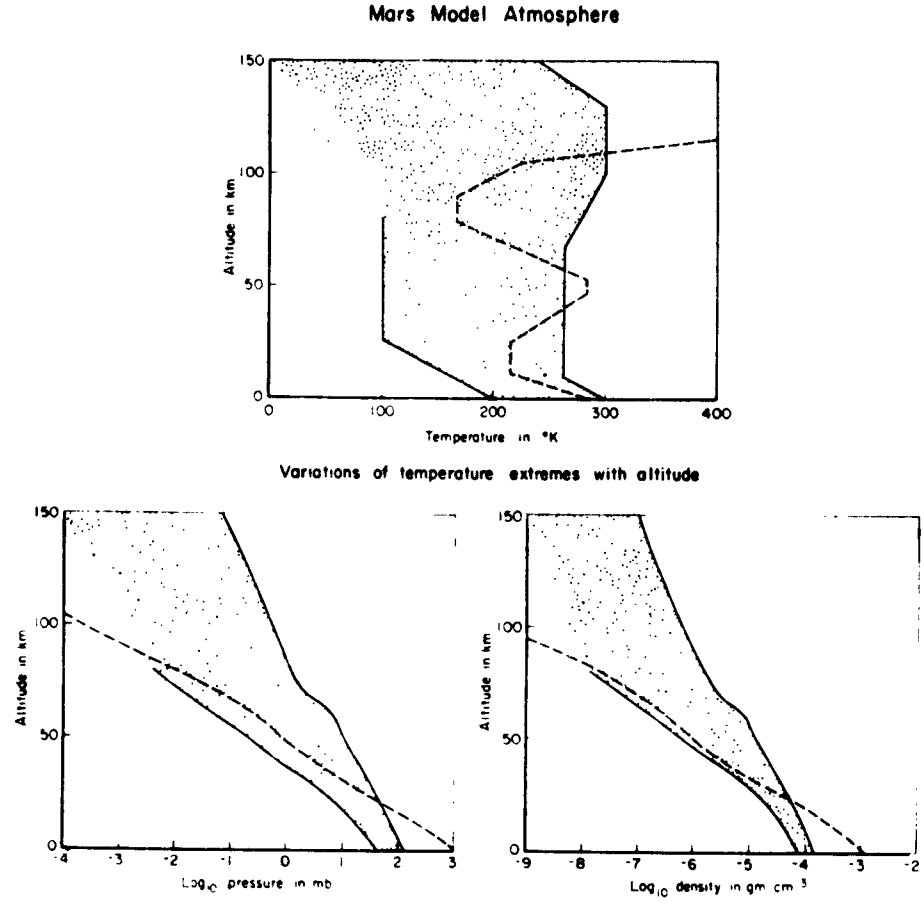

Fig. 1

results in one realistic model atmosphere which gives probable extreme limits for the basic atmospheric conditions which we must expect to prevail on Mars up to altitudes of 150 km. It constitutes a parametric envelope of the extreme values at each altitude; actual conditions over middle and low latitudes should fall between these limits independently of time of day or of season. For purposes of ready comparison, representative mean conditions in the Earth's atmosphere are also shown in the figure. Since above the altitude

of about 130 km, properties will depend so sensitively on the atmospheric composition ([2]), it was felt that computations of reliable limits would be too speculative at this time.

Obviously, the range of values is undesirably broad. Yet it probably reflects more realistically our actual knowledge about the atmosphere of Mars, than do model atmospheres based on « best values » or « most likely conditions ». In the near future we can expect that any single datum obtained by means of space probes or high-altitude balloons will make it possible to narrow these wide limits of possible conditions. Using any of our present factual knowledge, I must hesitate to do so.

REFERENCES

([1]) G. F. Schilling, Limiting Model Atmospheres of Mars, R-402-JPL, The RAND Corporation, Santa Monica, 1962.

([2]) J. W. Chamberlain, Upper Atmosphere of Mars. This symposium, 1962.

44. — ON THE PROBLEMS OF A MARTIAN OZONOSPHERE

H. K. PAETZOLD
Institute of Geophysics and Meteorology,
University of Cologne, Allemagne

In the terrestrial atmosphere, the ozone layer is one of the most interesting atmospheric components. On the other hand, the Martian atmosphere has the most similar features to the terrestrial atmosphere in the solar system. The greatest difference is the certainly extreme low oxygen content, which cannot be greater than 200 cm O_2 (NTP). This suggests the problem of the photochemical ozone formation in a planetary atmosphere with a very low oxygen concentration. The photochemical theory of ozone formation is well known now for the earth so that an extrapolation can be tried for other conditions. The basic photochemical reactions are for the Martian atmosphere :

(1)	O_2	+	$h\nu$		→	O	+	O
(2)	O	+	O_2	+ M	→	O_3	+	M
(3)	O_3	+	$h\nu$		→	O	+	O_2
(4)	O	+	O_2		→	O_2	+	O_2
(5)	O	+	O	+ M	→	O_2	+	M
(6)	CO_2	+	$h\nu$		→	CO	+	O
(7)	CO	+	O	+ M	→	CO_2	+	M

For a relative oxygen concentration $C_{O_2} > 0{,}001$ (*), a simple formula can be held as valid for the main part of a Martian ozonosphere :

$$(8)\quad [O_3] = \text{const}\; C_{O_2}\, \rho\,(h)^{3/2} \sqrt{\frac{1}{\exp(Q/RT)}} \cdot \sqrt{\frac{{}_{O_2}\int \alpha_{O_2}\, I_0\,(h)\, e^{-\tau_{O_2}}\, dh}{{}_{O_2}\int \alpha_{O_2}\, I_0\,(h)\, e^{-\tau_{O_2}}\, dh}}$$

with $\rho\,(h)$: air density
T : air temperature
$I_0\,(h)$: extramartian intensity of the solar light

(*) C_{O_2} means the relative concentration of molecules.

Q : activation energy of the bimolecular reaction (4)

α_{O_2}, α_{O_3} : spectral absorption coefficients for oxygen and ozone

τ_{O_2}, τ_{O_3} : optical thickness

$[O_3]$: number of O_3-Molec./cm³ (**)

In formula (8) only the reactions 1 — 4 are considered. For

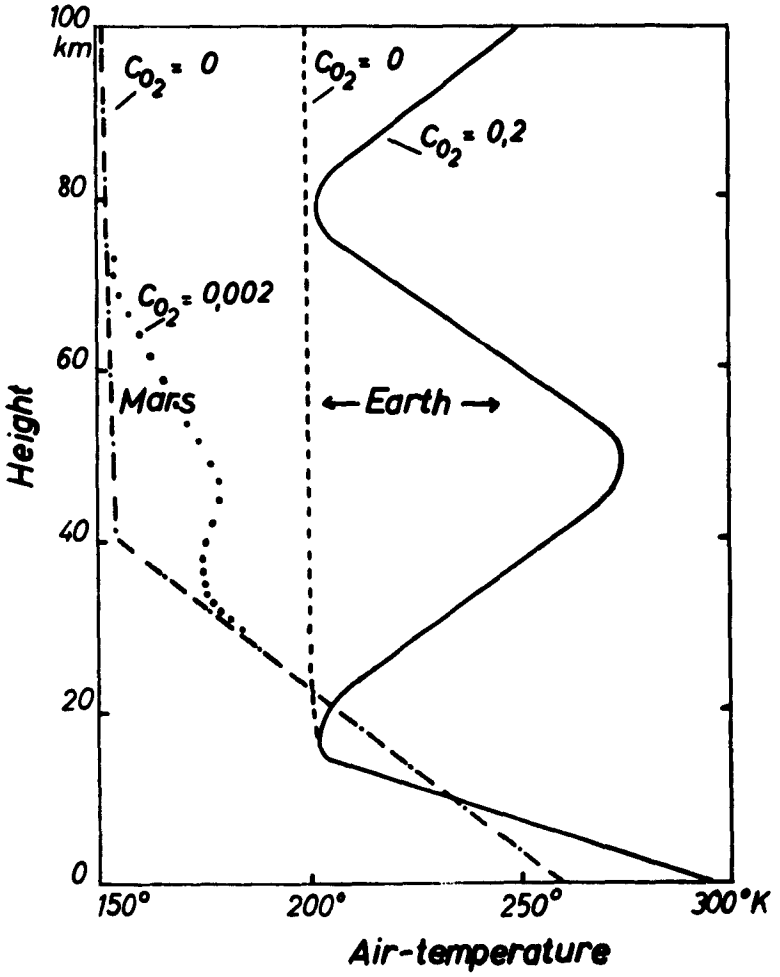

Fig. 1. — Vertical temperature profiles for Earth and Mars

(*) In Fig. 3 and 4 the ozone content $\varepsilon(h)$ is given in cm O_3/km — units $[O_3] = \varepsilon(h) \cdot 10^{-5} N_A$. ($N_A$ = Avogadro's number).

oxygen concentration $C_{O_2} < 0{,}001$ also the reactions 5 — 7 have to be involved. All calculations have been made for a sun elevation of 45°. No effects of atmospheric transport has been considered since its influence does not affect the general features according to our experiences on earth.

For the ozone calculation, the heating effect of the ozone layer itself must be considered since the ozone formation strongly depends on the temperature (Equ. (8)). In Fig. 1 the assumed temperatures are given for an oxygen concentration $C_{O_2} = 0$ and

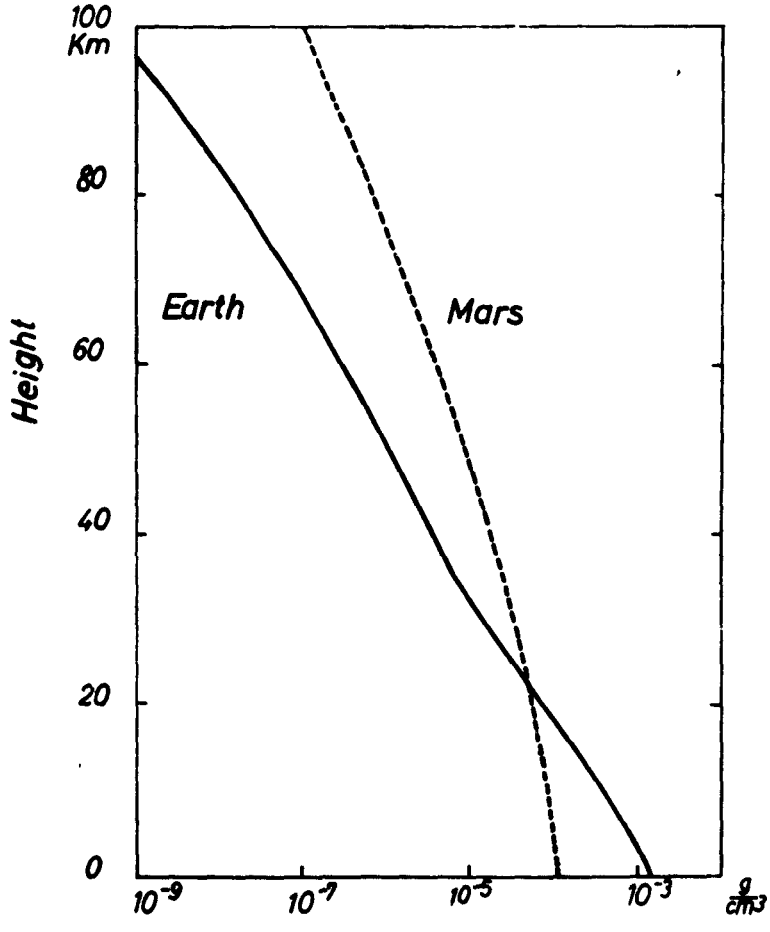

Fig. 2. — Air density profiles

$C_{O_2} = 0{,}002$. Fig. 2 demonstrates the profiles of the air density of Mars and Earth with its crossing in an altitude of about 28 km.

It is very instructive to calculate the ozone profile for the earth with varying oxygen concentration C_{O_2}. From Fig. 3, it can be well seen that also for low oxygen concentrations, an ozone layer exists above an altitude of about 10 km. This is due to the strong dependence of the ozone formation on the air density according to Equ. (8). The same feature is shown by Fig. 4 for Mars. Since the ozone formation does not depend on the absolute intensity

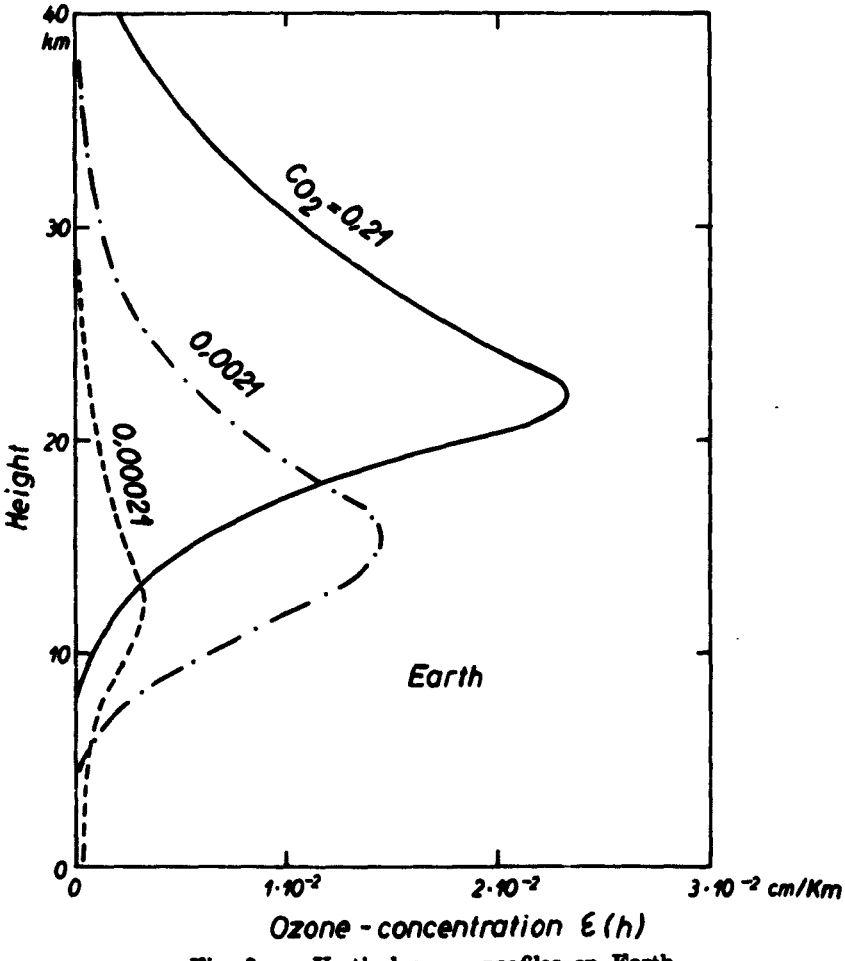

Fig. 3. — Vertical ozone profiles on Earth

of the solar UV-radiation but strongly on the temperature, more ozone is found on Mars than on the Earth for the same oxygen concentration due to the lower air temperature on Mars. As a main result it must be pointed out that also on Mars, an ozone layer should exist high above the planetary surface for oxygen concentration $C_{O_2} > 0{,}001$. This limit for Earth and Mars means that a higher planetary ozone layer should be expected also for a low oxygen concentration until the value of the optical thickness τ_{O_3} of the ozonizing UV-light becomes smaller than the one at the ground.

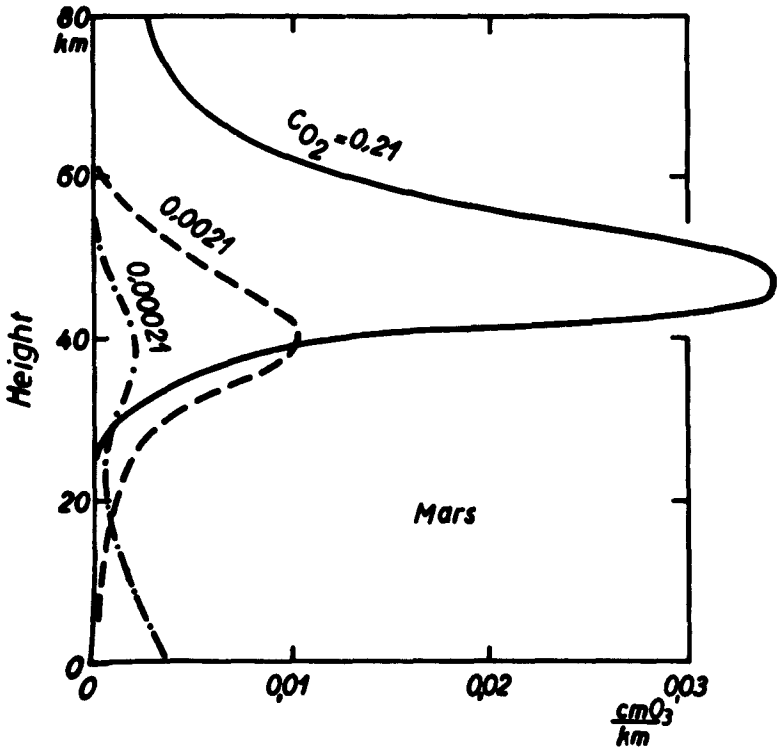

Fig. 4. — Vertical ozone profiles for Mars

Fig. 5 gives the total thickness of the ozone layer for different oxygen concentrations. The most important fact is that the total amount linearly decreases while the oxygen concentration expo-

nentially decreases down to very low values. From these results several interesting conclusions can be made :

First the ozone content can be used as a very sensitive indicator for the oxygen concentration in a planetary atmosphere. From a total ozone layer of 0,01 cm O_3 a Martian oxygen layer of 30 cm O_2 (NTP) must be concluded.

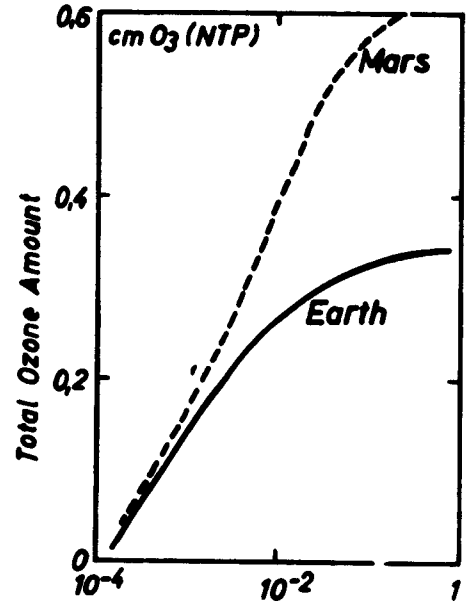

Fig. 5. — Total ozone amount for Earth and Mars

Since according to the existing measurements, a Martian O_3 — layer will not exceed the value above the upper possible oxygen concentration cannot be greater than about 5. 10^{-4} O_2-Mol/Air-Mol. In future, balloon measurements at 40 km altitude should be made to reduce this limit, since at that altitude nine tenth of the terrestrial ozone layer is below the instruments.

Further also for low oxygen concentration a typical circulation should exist in the Martian stratosphere similar to that which is produced by the warm layer due to the O_3-UV-absorption on Earth. In Fig. 1, the warm layer is shown, which results, for an oxygen

concentration of 0,002 on Mars. Since the inclination of the Martian rotation axis to the orbital plane is similar to that of the Earth, such a Martian warm stratospheric layer should produce also a stratospheric pressure gradient from the summer to the winter hemisphere. The resulting zonal winds are demonstrated in Fig. 6 with its typical change from west to east between winter and summer.

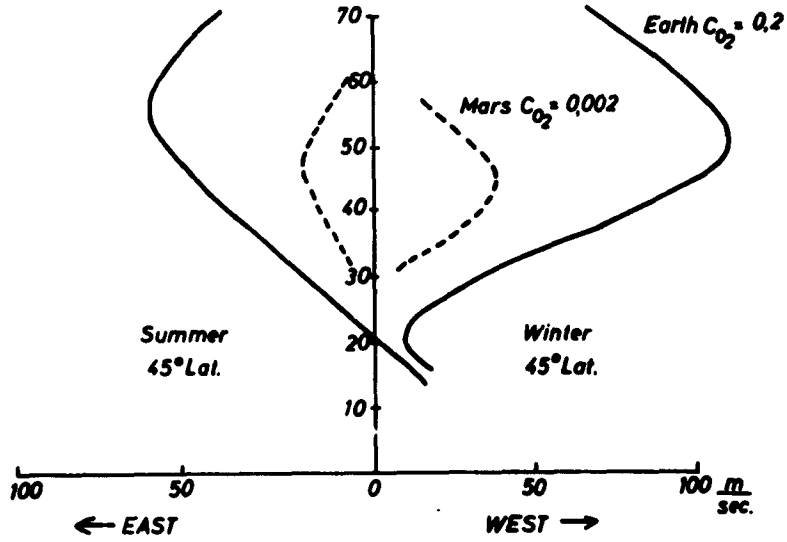

Fig. 6. — Stratospheric wind system.

At least the results above are connected with the existence of oxygen in the Martian atmosphere. It was an old idea that the oxygen has vanished by oxydation of the Martian crust, since one assumed that a Martian ozone layer would be located directly at the planetary surface for a lower oxygen concentration. But this assumption cannot be further held as valid. On the other hand, recent datas of satellites have given a new picture of the exospheric terrestrial temperatures. During daytime they vary between 1900 and 1400°K in the solar cycle. From this, the exospheric temperature may be estimated to be of 1300°K on Mars. But at this temperature the atomic oxygen is not anymore a stable component of

the Martian atmosphere, because a considerable amount of oxygen will escape into space. Nitrogen (molecular weight 28) will be stable also in the Martian atmosphere because its dissociation must be very weak according to the conditions in the terrestrial atmosphere.

The so called lifetime t_e is defined as the time, in the course of which an atmosphere has escaped to $1/e$ of its initial amount. It is given by formula (9)

$$(9)\quad t_e \approx \frac{1}{fM}\frac{1}{\sqrt{m}}\frac{r_c^3}{fmM + RTr_c}(RT)^{3/2}\cdot\exp\left(\frac{2Mf}{r_c}\frac{m}{RT}\right)$$

with m : atomic weight
R : gas constant
f : gravitation constant
M : planetary mass
r_c : lower boundary of the exosphere

For $r_c = 4500$ km and $T = 1300°K$, the escape time t_E results only to $1 \cdot 10^5$ years for atomic oxygen. Regarding the intensity of dissociating solar UV-light and the energy flux heating up the Martian ionosphere and exosphere ($\approx 0{,}3$ erg/cm² sec), it seems possible that during a time of $4 \cdot 10^9$ years, a layer of liquid water of 500 to 1000 meter thickness has been dissociated and evaporated into space. This would explain the lack of water and oxygen on Mars without any additional assumptions. For the solar system a very instructive row follows for the atmosphere of several planets.

Planet	Atmosphere
Great planets	high hydrogen amount
Earth	nearly no hydrogen
Mars	no oxygen and hydrogen
Mercury	no atmosphere
Moon	no atmosphere

This row can be fully explained with our recent knowledge about planetary masses and exospheric temperatures.

DISCUSSION DES COMMUNICATIONS 34 à 44.

E. H. COLLINSON (34) (36). — Dr. Sinton's photographs showing some of the canals would indicate that they may be fine lines after all. I would like to ask whether visual observers at the Pic du Midi or elsewhere see the canals as fine lines.

A. DOLLFUS (34) (36). — Under the best seeing conditions we see them broken up into spots.

W. M. SINTON (34) (36). — Though they may be resolved into spots they are quite narrow and long and whether they can be divided into spots or not they cannot result from a statistical alignment of spots and there must be some physical reason for their existence.

P. GUERIN (38). — Concernant un éventuel renforcement des bandes de l'ozone dans le spectre de Mars, les comparaisons ont été faites dans les « fenêtres » correspondant aux minima d'absorption de l'ozone dans l'extrême ultra-violet. Il eut fallu comparer celle-ci pour mettre en évidence une éventuelle composante martienne. Celle-ci est certainement très faible, si même elle existe, car elle n'apparait pas visuellement sur de forts agrandissements à grand contraste des spectres obtenus. Une étude spectrophotométrique particulière des bandes de l'ozone serait cependant nécessaire pour trancher la question.

E. J. ÖPIK (39). — An interpretation of the blue clearing being observed more often around opposition, as a statistical effect of contrast, has been recently published by Öpik in « Progress in the Astronautical Sciences ». It would follow from a phase law of the solid Martian surface similar to that of the rough surface of the moon. It is gratifying to find independent support from Dr. Menzel for this idea — it makes « a majority of two ».

E. J. ÖPIK (40) (44). — Oxygen will escape more efficiently on the ionized state and its lifetime on Mars will be much shorter than 10^9 years. CO will accumulate. It is a strong radiator and will completely change the radiative and photochemical balance of the Martian upper atmosphere.

A. DOLLFUS (41). — A propos de la variation du diamètre de Mars en lumière bleue et rouge et aux effets de l'atmosphère martienne sur la mesure de ce diamètre, je peux résumer les mesures micrométriques très précises qui ont été réalisées ces dernières années à l'Observatoire du Pic du Midi.

Ces mesures mettent à profit les trois oppositions au voisinage du périhélie de 1954, 1956 et 1958. Elles mettent à profit également la très grande sensibilité du micromètre biréfringent à double image décrit par l'auteur en 1952.

De nombreuses mesures ont été réalisées au cours des trois oppositions précédentes successivement ou simultanément par MM. Camichel, Focas et l'auteur. L'accord entre les mesures des différents observateurs dépasse rarement 0″.04.

Les résultats des mesures du diamètre équatorial *de* et du diamètre polaire *dp* sont les suivants :

Année	de(orange)	dp(orange)	de(bleu)	dp(bleu)	ellipticité	
1954	9″41	9″30	9″38	9″28	0,0118	à 1 U.A.
1956	9″45	9″35	9″48	9″38	0,0117	
1958	9″41	9″29	9″45	9″28	0,0116	
Moyennes	**9″42**	**9″31**	**9″44**	**9″31**	**0,0117**	

La dispersion des mesures en orangé est voisine de 2,5 millièmes seulement ; la précision est celle de l'étalonnage du micromètre, soit 3 millièmes.

On ne décèle aucun écart sensible entre les diamètres mesurés en bleu et en rouge aux regards de la dispersion des mesures. Il faut déduire que la différence des rayons planétaires en bleu et en rouge est inférieure à 27 *km*. Par conséquent le « phénomène de Wright » n'existe pas. Les voiles bleus de l'atmosphère ne sauraient donc être très absorbants.

La correction due à l'atmosphère au bord du disque a été effectuée. Elle vaut environ 35 *km*. On trouve finalement pour le diamètre équatorial : 6 790 *km*, pour le diamètre polaire : 6 710 *km* et pour densité : 4,09.

La valeur de l'aplatissement polaire vaut 0,012 ; il ne peut être attribué à l'atmosphère, mais doit provenir de la surface même de la planète. L'aplatissement dynamique donné par la perturbation séculaire des satellites vaut 0,0051 ; il est donc probable que la constitution interne du globe doit être complexe.

E. J. Öpik (42). — If *maximum* greenhouse effect is considered, shielding by dust (optical thickness 0.25 to 0.5) of outgoing and incoming radiation should not be neglected.

A. Dollfus. — L'objet de ce commentaire est de présenter le travail que vient d'achever le Dr. G. de Mottoni à Gênes (Italie) d'après l'étude des collections de clichés de la planète Mars groupées dans le Centre de Documentation de l'Union Astronomique Internationale à Meudon.

Le Dr. G. de Mottoni a extrait 260 clichés de Mars obtenus pendant l'opposition périhélique de 1956 aux Observatoires du Pic du Midi, de Johannesburg, de Lick, de Bloemfountain, de Stalingrad, de Milan Merate, de Tokyo, du Mont Wilson et de Gênes.

Grâce à cette très importante documentation, le Dr. G. de Mottoni a réalisé par le dessin neuf grandes cartes planisphères en coordonnées polaires centrées sur le pôle Sud martien. Ces cartes découpent en neuf intervalles de temps la période s'étendant entre le 15 juillet et le 15 octobre 1956. La documentation utilisée provient d'Observatoires situés sous des longitudes terrestres diverses, de sorte qu'il devient alors possible de reconstituer l'aspect de la planète Mars sous presque toutes ses longitudes, pour chacune

des cartes précédentes. Chaque carte est accompagnée de reproductions de l'ensemble des clichés photographiques qui ont servi à la constituer ; ces clichés sont rangés radialement au regard de la longitude correspondant à leur méridiens centraux. Grâce à ce très gros travail de dessin et de photographie, particulièrement soigné, on peut observer immédiatement la position et les mouvements des différents nuages portés par l'atmosphère martienne. Le Dr. G. de Mottoni a cherché à reconstituer l'évolution des grandes perturbations anormales qui se sont développées dans l'atmosphère martienne à cette période. En particulier, il a constaté que les grands voiles jaunes apparus en août 1956 se sont produits simultanément et indépendamment en différents points du disque vers la latitude —50° et semblent avoir suivi grossièrement des trajectoires spiralées dans le sens des longitudes croissantes en se rapprochant de l'équateur.

Le Dr. G. de Mottoni a remis au Centre de Documentation planétaire de Meudon les copies de son travail afin de les rendre disponibles pour la consultation.

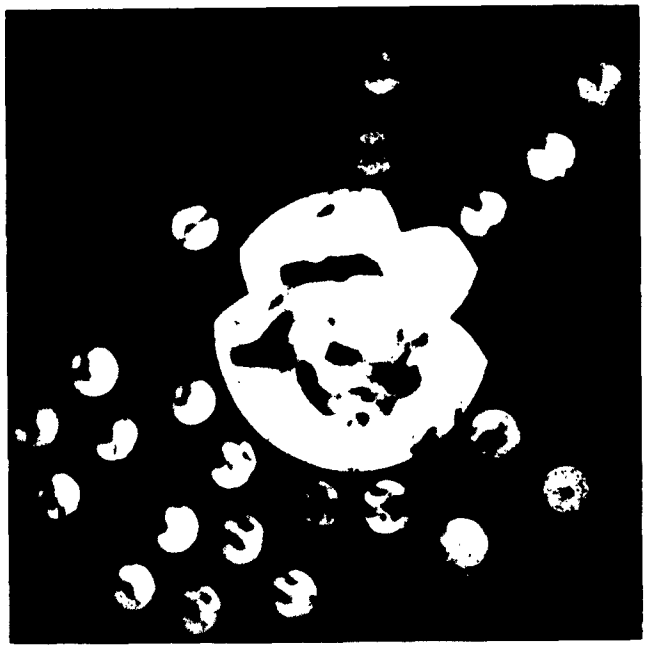

Cartes en coordonnées polaires de l'hémisphère Sud de la planète Mars au moment du développement des grands nuages jaunes apparus en septembre 1956 et montrant l'évolution de ceux-ci.

45. — A SEARCH FOR PERIODICITY IN THE THICKNESS OF JUPITER'S N. E. B. (*)

RONALDO ROGÉRIO DE FREITAS MOURÃO
National Observatory of Rio de Janeiro, Brazil

A distinctive feature of Jupiter's surface is a number of light and dark belts where striking, easily observable changes will occur. Doubtless the activity of those belts is closely bound up with changes occurring in the higher layers of the planet's atmosphere which alone are open to optical observation.

A detailed study of those belts is therefore requisite for any theoretical approach of Jupiter's atmosphere.

Each belt displays as a whole two characteristics, intrinsic factors — its mean zenocentric latitude and its thickness. Either factor allows of micrometric measurement, an operation which — with due allowance for its incidental inaccuracies — provides indexes for the activity of the belts no less than for the irregularities of colour and aspect.

Analyses of zenographic latitude variations of the belts were carried out in 1954 by E. Schoenberg and W. D. Heintz (1), who considered the mean latitude of every individual belt on the planet. Those authors have found a striking periodicity to occur exclusively in the belts N. T. B. and S. E. B., the periods varying around 11 years.

However, a study of the belts from the thickness viewpoint would certainly prove a sounder and closer approach of their activity, and, consequently, of that of the higher layers of the planet's atmosphere.

For the analysis of thickness variations we have drawn on the observations carried out over the past 60 years. A study of these variations has shown the most striking ones to occur in the N. E. B.

(*) This work was sponsored by the National Research Council of Brazil.

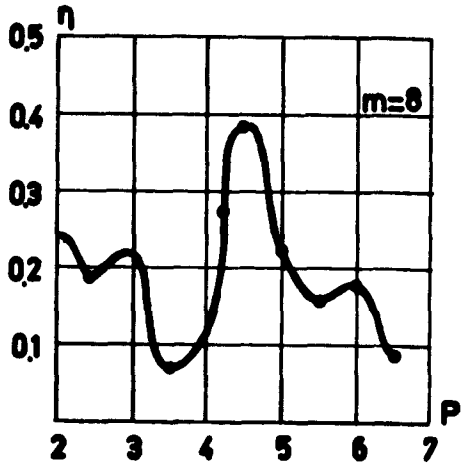

Fig. 1

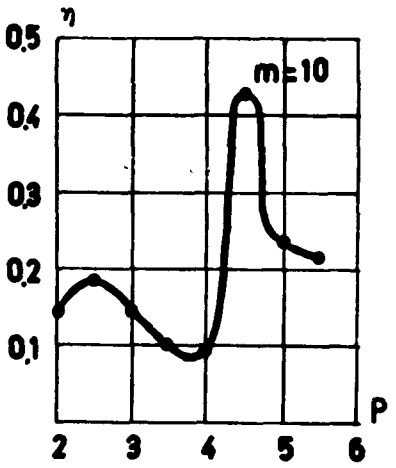

Fig. 2

The enclosed Table presents the values obtained for the Northern and Southern parts and their difference or thickness of belt, including bibliografical reference. A graph covering these observations suggested to us a period of 4 and 6 years. By approaching these values through the Schuster-Whittaker ([10]) research method we have obtained the periodograms in figs. 1 and 2 that suggest the existence of a period of 4.5 years.

A harmonic analysis brought us to the following analytic formula for the N. E. B. thickness variation over a period of 4.5 years :

$$T = 9^{\circ}87 - 1^{\circ}03 \cos u - 0^{\circ}16 \cos 2u - 0^{\circ}44 \cos 3u + 0^{\circ}04 \operatorname{sen} u - 0^{\circ}03 \operatorname{sen} 2u - 0^{\circ}10 \operatorname{sen} 3u$$

$$u = 80^{\circ}\,(t - 1916.96)$$

where t is reckoned in calendar years.

A graphic representation of this function with the mean values can be seen in Fig. 3.

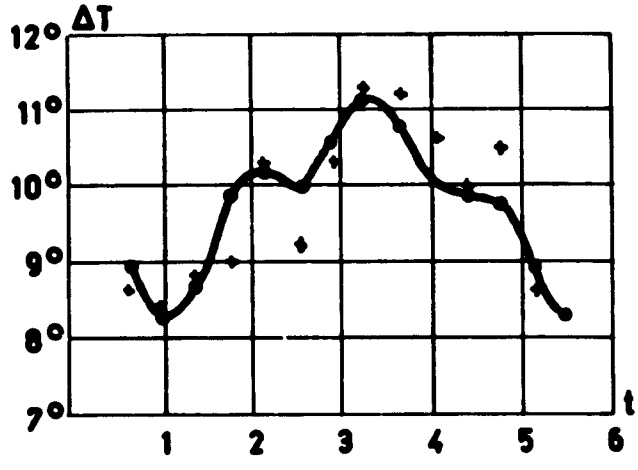

Fig. 3

REFERENCES

(1) H. E. Lan, Mikrometermessungen auf Jupiter, *Astron. Nachr.*, **171**, 260 ; **175**, 228 ; **178**, 194 ; **183**, 56 ; **197**, 62 ; **200**, 237, 1906-1918.

(2) Report of Jupiter Section, *Mem. of the British Astron. Ass.*, 26 ; 27 ; 29 ; 30 ; 32 ; 35 ; 39 and *Journal of the British Astron. Ass.*, 63, 64, 1906-1961.

(3) G. Ruggieri, *Mem. Soc. Astr. Italiana*, **27**, 1, 1958.

(4) E. Reese, *Strolling Astronomer*, **13**, 1959.

(5) T. Cragg, *Strolling Astronomer*, **11**, 1957.

(6) U. Dall'Olmo, *Mem. Soc. Astron. Italiana*, **32**, 1962.

(7) L. M. Barreto R. R. de Freitas Mourão, *Publ. Serv. Astron. Obs. Nac. Rio de Janeiro*, **11**, 1960.

(9) R. R. DE FREITAS MOURÃO-P. MOURILHE SILVA, *Publ. Serv. Astron. Obs. Nac. Rio de Janeiro*, **17**, 1961.

(9) E. SCHOENBERG and W. D. HEINTZ, *Astron. Nachr.*, **282**, 85, 1955.

(10) E. T. WHITTAKER and G. ROBINSON, The Calculus of Observations, London, 1924.

	N. E. B.$_n$	N. E. B.$_s$	T	Observers
1903.8	26.2	8.8	17.4	Lan (1)
4.7	—	9.0		» (1)
5.8	21.5	6.8	14.7	» (1)
6.9	22.4	5.9	16.5	» (1)
5.5	20.4	8.8	11.6	» (1)
8.96	19.8	7.0	12.8	Phillips (2)
9.11	15.2	8.0	7.2	Lan – C. Luplan-Jansen (1)
9.25	20.4	8.8	11.6	Phillips (2)
10.25	14.0	8.2	5.8	» (2)
11.	1.9			» (2)
12.	8.3			» (2)
13.61	20.2	7.9	12.3	» (2)
13.64	18.7	12.1	6.6	Lan (1)
14.58	18.7	7.9	10.8	» (1)
14.59	19.3	8.7	10.5	Phillips (2)
15.65	18.0	7.5	10.5	» (2)
16.50	17.1	7.8	9.3	» (2)
17.67	13.5	6.7	6.8	» (2)
17.89	12.9	5.4	7.5	Thompson (2)
18.79	16.5	8.8	7.7	Phillips (2)
19.02	19.9	6.1	13.8	» (2)
20.40	18.7	8.0	10.7	» (2)
21.29	12.7	6.1	6.6	» (2)
22.32	22.0	7.5	14.5	» (2)
23.56	19.6	6.1	13.5	» (2)
23.34	19.5	8.1	11.4	Peck (2)
24.53	16.6	5.0	11.6	Phillips (2)
24.48	15.5	4.7	10.8	Peck (2)
25.65	13.4	6.1	7.3	Phillips (2)
26.70	13.9	6.1	7.8	» (2)
27.77	17.3	6.0	11.3	» (2)
28.42	18.5	7.6	10.9	» (2)
29.18	20.3	7.7	12.6	» (2)
28.86	16.6	7.3	9.3	» (2)
30.77	14.2	7.0	7.2	Peck (2)
30.83	14.5	6.4	8.1	Phillips (2)
31.17	15.4	6.6	8.8	» (2)

	N. E. B.$_n$	N. E. B.$_g$	T	Observers
31.16	14.0	5.3	8.7	Kellaway (3)
31.50	21.0	6.3	14.7	Phillips (3)
32.50	19.0	6.6	12.4	» (3)
34.50	14.0	6.1	7.9	» (3)
35.50	18.6	6.4	12.2	» (3)
36.50	19.6	7.5	12.1	» (3)
37.59	18.3	4.5	13.8	» (3)
38.49	14.1	8.3	5.8	Peck (3)
38.64	16.4	6.8	9.6	Phocas (3)
38.79	16.0	7.3	8.7	Phillips (3)
38.92	14.6	8.0	6.6	» (3)
39.78	16.3	9.4	6.9	Phocas (3)
40.97	14.0	7.4	6.6	Peck (3)
42.08	20.1	7.1	13.0	» (3)
43.08	20.2	8.0	12.2	» (3)
44.11	13.4	7.4	6.0	» (3)
45.34	19.4	9.0	10.4	» (3)
46.23	19.9	8.7	11.2	» (3)
47.43	19.5	6.8	12.7	» (3)
49.50	17.9	7.0	10.9	» (3)
51.50	14.9	7.5	7.4	Ruggieri (3)
52.84	14.5	7.0	7.4	Ressi (4)
52.95	14.4	7.1	7.3	Ruggieri (3)
54.08	18.6	6.0	12.6	» (3)
56.21	12.0	6.2	5.8	Cragg (5)
57.27	14.9	4.1	10.8	Johnson-Reese (4)
.27	14.0	7.5	6.5	Dall'Olmo (3)
58.22	13.7	6.3	7.4	Botham (3)
34	17.0	4.4	12.6	Dall'Olmo (6)
38	16.2	6.2	10.0	Eastman (4)
48	19.8	5.2	14.6	Newman-Reese (4)
50	19.5	7.9	11.6	Richerds (4)
59.59	17.9	7.6	10.3	Mourão (7)
60.52	20.6	8.8	11.8	» (8)
61.64	15.0	8.6	7.4	Mourão, Mourilhe, Rocha

46. — L'ANNEAU DE COMÈTES ET DE MÉTÉORITES CEINTURANT JUPITER

S. K. VSESSVIATSKY
Université de Kiev, U. R. S. S.

Les observations optiques des planètes telles que Jupiter, Saturne et leurs satellites montrent que des processus éruptifs ou de caractère volcanique se produisent sur ces corps célestes (les tâches blanches, la tâche rouge, les volcans de Reese, les changements sur les surfaces des satellites etc.). Cela se confirme aussi par les éclats de radio-émission, liés aux régions actives de Jupiter.

L'existence des comètes à courte période avec leur origine récente et leur mouvement planétaire montre que les éjections de la matière météorique et des glaces s'opèrent de nos jours, dans les systèmes de Jupiter et de Saturne. Les masses de la matière éjectée, avec des vitesses moins grandes que celles qui produisent les comètes et les corps météoriques aux orbites héliocentriques. n'auront pas la possibilité de quitter la sphère de gravitation et doivent former le système des satellites. On doit donc s'attendre à la naissance des anneaux, composés de fragments comètes-météorites, de particules de cendre et de gaz, circulant dans le plan de l'équateur de la planète. D'accord avec les particularités de leur structure et de leur spectre, les anneaux de Saturne seraient de telle nature.

Les observations des anneaux de Saturne montrent de nombreux changements (les apparitions et les disparitions des divisions et des condensations claires, la luminescence au bord de l'anneau A, le changement de l'éclat de l'anneau C, etc.) (1) qui nous indiquent que l'évolution est rapide et qu'une activité existe encore de nos jours. Les faits des observations démentent l'opinion que les masses éjectées ne peuvent pas acquérir le moment angulaire exigé. Ici, on néglige les éjections des satellites, l'influence du champ magné-

tique de la planète, les chocs mutuels des fragments, l'influence de l'anneau qui existe déjà, l'influence des satellites et d'autres effets. Non seulement l'anneau de Saturne parle en faveur de cela, mais aussi l'existence de l'anneau des particules autour de la Terre, les anneaux de gaz autour de beaucoup d'étoiles non stationnaires.

Se basant sur les données obtenues par O. Struve [2] et sur les observations faites plus tard, on a obtenu l'indication que la ligne moyenne des anneaux s'est approchée de 9 mille kilomètres vers la surface de la planète (0,15 du rayon de la planète). Si cela correspond au centre de la distribution des masses, nous obtenons que la diminution de l'énergie mécanique globale de l'anneau est de 10^{36} ergs. L'énergie a dû se dépenser vu les chocs mutuels des fragments de l'anneau et la résistance du milieu de gaz.

A la lumière de ces données, l'existence de l'anneau comètes-météorites, ceinturant Jupiter, paraît bien probable. En vertu de cela, on a examiné de nombreux dessins de Jupiter et on a fait attention à l'aspect et aux particularités de la bande équatoriale située habituellement au milieu de la zone équatoriale claire de la planète. La bande équatoriale a été enregistrée par les observateurs déjà dès le milieu du siècle passé. Les séries des observations Lohse, Flammarion, Nijland, des membres de l'Association astronomique de la Grande-Bretagne et d'autres, obtenues au cours de plus de 80 ans, ont indiqué que les périodes de visibilité stable de la bande correspondent au temps de la latitude zenographique maximale du Soleil (Dc) et de la Terre (Dt). Cela répond à la supposition que la bande équatoriale de Jupiter est l'ombre de l'anneau ceinturant la planète. Une telle conclusion est confirmée par l'examen de la position de la bande sur le disque et par sa structure non homogène pendant les périodes proches aux petits Dc. D'après les dessins Lohse, Nijland, des observateurs BAA et d'autres, ainsi que d'après les photographies obtenues au télescope Mount Wilson, on a déterminé les positions de la bande relativement au centre du disque (α). Ces positions ont été comparées aux valeurs Dc. Une dépendence certaine a été établie : $\alpha = k\,Dc$; les valeurs

$k = -1.38 \pm 0{,}27$ et $k = -1{,}50 \pm 0{,}3$, dépendent de différents procédés de résolution des équations.

Mais une liaison semblable doit avoir lieu au cas où l'ombre de l'anneau est située dans le plan de l'équateur de la planète.

Les valeurs α et les évaluations de la largeur de la bande équatoriale ($= 2°$, en cas de $Dc = 3°$) donnent la hauteur de l'anneau en limites 1,4 — 1,0 du rayon du Jupiter ; le bord intérieur de l'anneau est à la hauteur 0,6 — 0,3 du rayon.

Les observations avec des grands télescopes peuvent confirmer l'existence de l'anneau hypothétique de Jupiter. Il nous paraît que ce problème peut être résolu à l'aide de trois procédés : 1. Il faut évaluer la position et la largeur de la bande équatoriale ; 2. il faut établir l'existence des anses de l'anneau — dans des conditions analogues elles sont aussi invisibles comme celles de Saturne (petits Dc et Dt) ; 3. il faut évaluer les vitesses de rotation des détails de la bande équatoriale dont on n'aperçoit souvent que des fragments. Si la bande équatoriale est l'ombre, la vitesse angulaire doit être 1,5 — 2 fois plus grande que celle des détails du disque.

La comparaison du noircissement de l'ombre de l'anneau de Saturne au moment de sa disparition et de la bande équatoriale de Jupiter montre que l'éclat des anses de l'anneau de Jupiter peut être quelques dizaines de fois moins grand que l'éclat des anses de Saturne dans des conditions analogues.

REFERENCES

(1) Rev. T. E. R. Phillips, M. N., 69, 39, 1908.
E. E. Barnard, M. N., 69, 621, 1909.

(2) O. Struve, 13, 22, 1852.

47. — A PRELIMINARY SEARCH FOR SHORT-PERIOD H(α) ACTIVITY FROM THE PLANET JUPITER, DURING THE APPARITION OF 1960

J. V. JELLEY (*)
and A. D. PETFORD
The University Observatory, Oxford, England

1. Introduction

The purpose of this contribution is to describe a simple experiment, carried out during the summer of 1960 at the University Observatory, Oxford, to search for possible short-lived H(α) activity from the planet Jupiter which, it was then thought, might occur during the sporadic and intense decameter radio storms. The observatory's 12-inch refractor was kindly put at our disposal by Professor H. H. Plaskett, and the experiment was supported by Sir Basil Schonland and Dr. E. Bretscher of A.E.R.E., Harwell.

It is essential for us to emphasize that this experiment was conceived and carried out at a time when it was felt that any possible optical activity on the planet associated with the decametre radio storms, might also possess the violent burst features characteristic of the radio emissions. We thus had in mind the catastrophic phenomena which had been proposed, namely electrical discharges ([1]), chemical explosions ([2]) and volcanic activity ([3]). It was with these considerations that the experimental technique was geared to look only for short-period activity, with time structure comparable with that familiar to the radio observers, namely $\sim$ 10 m. sec to 1 sec.

However, during the last two years, as a result of the more recent work, particularly by the groups at Boulder ([4]), Florida ([5]) and Yale ([6]), together with increased knowledge of the shorter

(*) Nuclear Physics Division, Atomic Energy Research Establishment, Harwell, Berks.

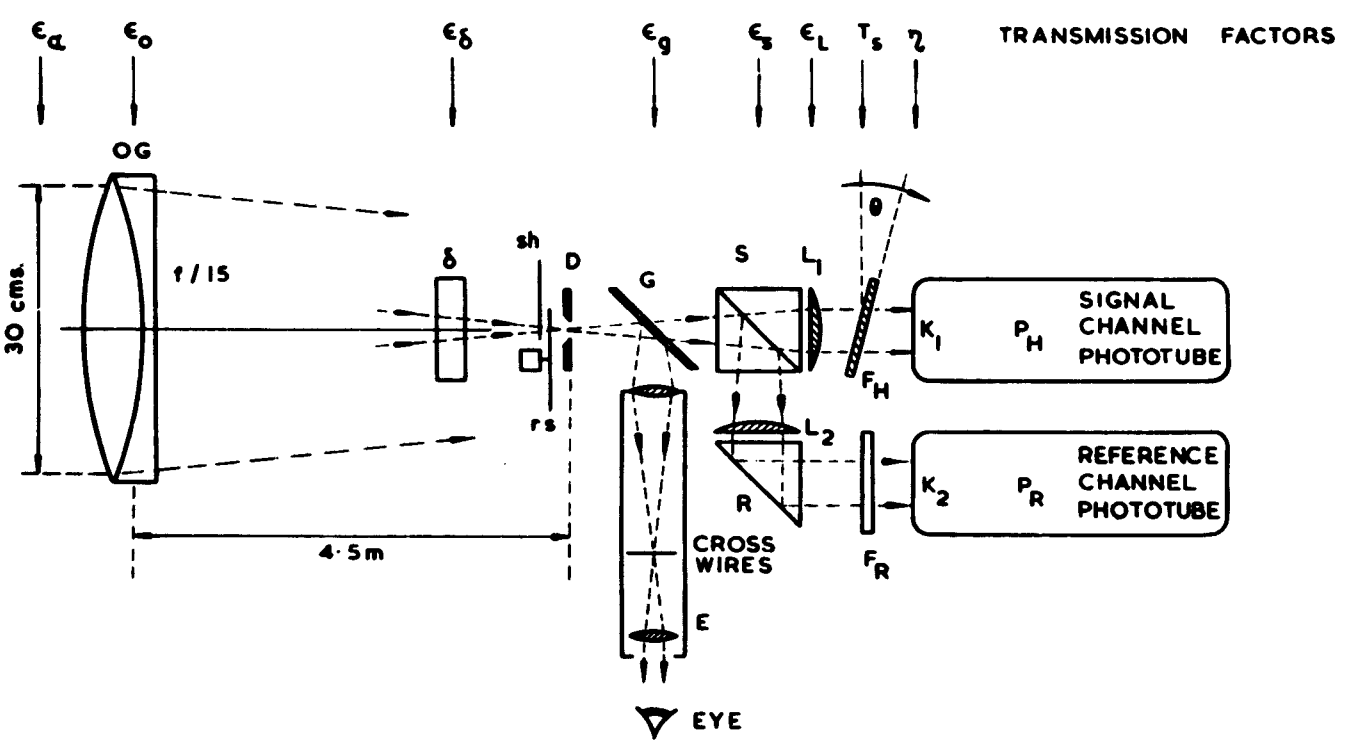

Fig. 1. — The Optical System, showing the essential components with their associated efficiency factors.

wavelength decimetre radiation ([7–12]), it would seem more likely that the radio phenomena are associated with the motion of particles in a magnetic field. It would thus now appear more fruitful to look for phenomena auroral-like rather than discharge-like in character, occuring perhaps in regions of very low gas density and at a considerable altitude above the planet's visible cloud surface.

2. Technique

Optics

The essential features of the two-channel photometer head used in these experiments is shown in Figure 1. Light from the planet's 1 mm diameter image at D is passed to a red-sensitive EMI-Type 9558 phototube P_H (S.20 response) after passing through a 20 Å-wide H(α) interference filter F_H, which could be oriented for tuning purposes. A better-than 15/1 scintillation compensation was achieved by electronically comparing the signal in P_H with that from a second tube P_R which sampled a 700 Å-wide slice of the spectrum for reference purposes, the centre of gravity of the effective response of this channel falling close to the H(α) wavelength, see Figure 2.

The 1 mm diameter primary image of the planet was guided manually by the tilting plate δ, within the field of view of an iris diaphragm D (adjusted to approx. a diameter of 3 mm), by means of the microscope E and an unsilvered glass plate G.

Initially a second interference filter F_R was used in the reference channel, though this was later replaced by a gelatin Wratten filter No. 29. With this second arrangement it was found that when the two channels were set up so that the phototube collector currents were the same, the photoelectron statistical fluctuations were also equalised. With the beam splitter S having a fixed division of the light flux, approx. 48 % in each arm, this condition of equalised photoelectron noise fluctuations leads to the minimum *rms*

noise in the output of the differential amplifier, this noise-level being then $\sim \sqrt{2}$ times the noise in either channel separately.

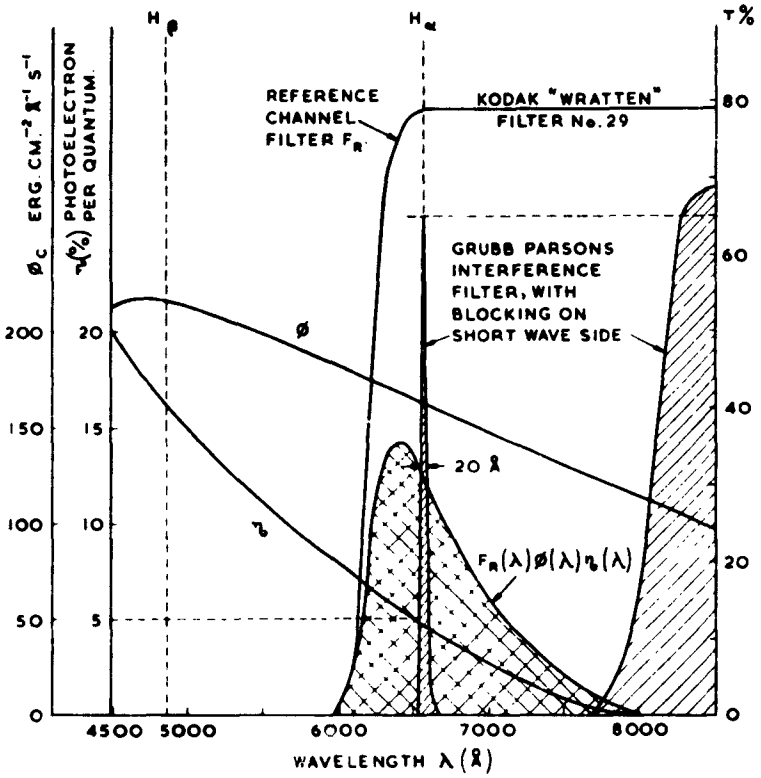

Fig. 2. — Spectral Distributions and Response Curves.
φ ; assumed solar spectrum reflected off Jupiter (Ref 17, page 140).
η ; photocathode quantum efficiency (EMI data).

Electronics

The outputs of the two phototubes pass through integrating networks and D. C. amplifiers, one for each channel, to a differential amplifier whose output in turn was fed to a fast electrolytic paper recorder. The integrating time-constants were adjustable between 15 m. sec and D. C., a value of 45 m. sec being used throughout the experiment. The D. C. amplifiers (Philbrick Research

Type K2-W) had feed-back loops giving an effective gain of 100. The paper recorder responded over a frequency range 50 c. p. s. to D. C. and had a writing speed of 8 cm. min^{-1}. The outputs of the single channels and the differential amplifier were monitored on meters, and the overall gains of the two channels were equalised prior to each run and occasionally during the runs.

Scintillation compensation and filter tuning

Facsimile tracings of recordings are shown in figure 3. Under typical observing conditions, the scintillation intensity fluctuations observed on the two single channels are shown at A and B (of amplitude $\sim$ 15 % peak to peak), while, with both channels in operation and balanced, the compensated output appeared as at C, with an r. m. s. fluctuation level $\pm$ 1 % of the mean light level.

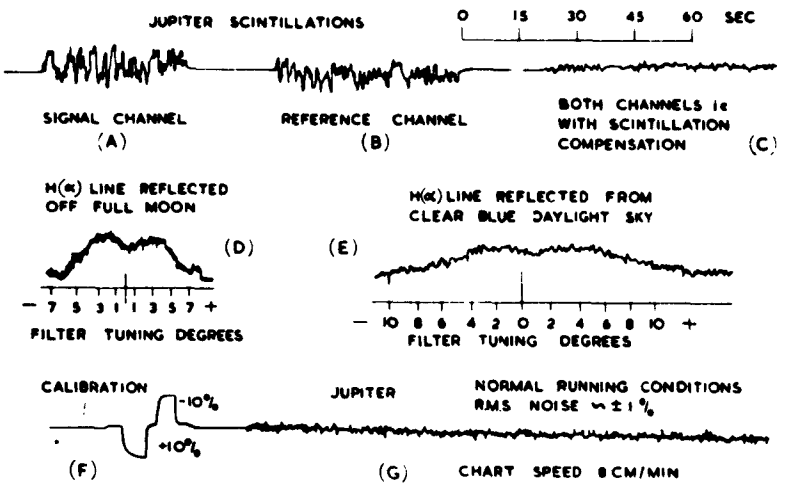

Fig. 3. — Facsimile tracings of recordings.

A & B. Single-channel scintillation fluctuations.
C Residual fluctuations with scintillation compensation.
D Filter tuning on H(α) line reflected off full Moon.
E Filter tuning on H(α) line in blue day-light sky.
F Calibration signals.
G Typical record on normal running conditions.

It was shown, with a steady light source adjusted to give the same collector currents as pertained to runs on the planet itself, that the residual noise shown at C was dominantly photoelectron fluctuation noise ; it thus follows that the scintillation compensation improved the overall limiting sensitivity under the conditions experienced at Oxford, by a factor well in excess of 15. The importance of scintillation compensation cannot be over-emphasised in this type of experiment, for we see from tracings A and B that the scintillations had components in just the frequency regions of interest, that is if we believe there to be any optical activity on the planet with frequency characteristics reported by some for the radio fine-structure ([14, 5, 18]) i. e. up into the millisecond region.

Record G, figure 3 shows a typical recording for 2.5 mins. under normal conditions, with calibration signals at F.

The H(α) filter was « tuned » by three methods. (1) With a hydrogen arc lamp and collimator attached to the inside of the observatory dome, to which the telescope was pointed, (2) on the Fraunhofer C-line, in light reflected from the full Moon, and (3) on the same line reflected from clear blue daylight sky. Examples of (2) and (3) are shown at D and E respectively.

2. Observations and Results

Recordings with the above equipment were made on 14 occasions between June 19th-August 30th (1960) whenever cloud and seeing conditions permitted. The observations ([13]), due to the low altitude and the proximity of buildings, were limited to $\pm$ 2 hours of local meridian transit. The total observing time was 28.5 hours, the useful observing time 19.2 hours, and the total elapsed time 1728 hours ; this represents a fractional observing time of only 1.1 % During these periods no H(α) flashes or short-term flares were observed at the limiting sensitivity of the equipment (see below).

Although generous assistance was provided by various U. S. radio observatories, in an attempt to correlate our observing times

with periods of observed decametre radio activity, difficulties were caused by the limited periods of observations each side the local meridia at the radio sites, and also by the differences between the terrestial longitudes of Oxford and these same radio observatories. The essential points are tabulated below : —

Station	Boulder (Colorado)	Florida (Chile Station)	Yale (Connecticut)
Assistance from	J. W. Warwick	A. G. Smith	H. J. Smith
Longitude	106°W	70°W	73°W
H. A. Local Meridian	± 3 hrs.	±4 hrs (±5hrs)	?
Planet active	1.2% of total time.	5.9% of total time.	Poor conditions (only one certain storm June 19th to August 30th)
Possibility of correlation with Oxford optical observations.	No overlap possible due to terrestial longitude differences.	Overlap possible ; no radio storms occurred however during the Oxford observing periods.	

Although no H(α) bursts were observed, it cannot be concluded definitely that H(α) activity does not exist coincident with the radio storms, at the intensity levels determined by the existing equipment. Nevertheless, it should be realised that recent observations in Australia ([15]) reveal, at least in 1962, that radio storms on 10 Mc/s have been observed on *all* nights.

3. Limiting Sensitivity

The threshold sensitivity is calculated as follows : —

If ΔN is the *observed* r. m. s. photoelectron fluctuation noise

from the output of the difference amplifier, η the photocathode quantum efficiency at H(α), ε the overall optical efficiency of the atmosphere and all components of the optical system, and A is the collecting area of the O. G., then the minimum detectable H(α) flux at the top of the earth's atmosphere will be

$$\varphi_{J_{min}} = (\Delta N/\eta\varepsilon A) \text{ photons/cm}^2 \quad . \quad . \quad . \quad . \quad \text{(i)}$$

for a light flash of duration $\leqslant \tau$, the integration time constant. The minimum detectable H(α) light intensity, at the surface of the planet, J_{min}, will then be :

$$J_{min} = 4\pi d^2\varphi_J \text{ photons} \quad . \quad . \quad . \quad . \quad . \quad . \quad . \quad . \quad . \quad \text{(ii)}$$

where d is the distance of the planet at opposition.

Numerical estimates

From measured phototube collector currents, and an r. m. s. output noise of $\pm$ 1 %, $\Delta N = \pm$ 153 photoelectrons on the H(α) phototube, for τ = 45 m. sec. Allowing $\sqrt{2}$ for the reference channel, ΔN (effective) = $\pm$ 216 photoelectrons.

A = 700 cm² (Oxford 12" OG).
η = 0.05 Ref (16), 150 μA/lumen.
τ = 0.045 secs.
T = 0.6 (60%, Grubb Parsons filter).
$\Delta\lambda$ = 20 Å (Grubb Parsons filter)
ε = 0.092 (see right).
With these figures in (i) we get : —
$\varphi_{J_{min}}$ = 67 H(α) photons/cm²
and, with d = 4.2 AU (Ref (17), p. 155)
= 6.3×10^{13}cm, from (ii)
J_{min} = 3.34×10^{23} H(α) photons
= 1.02×10^{12} joules.

Efficiency estimates
(see figure 1).

At altitude 17°, ref (17), p. 115, atmospheric absorption is 3.4 air masses. At 0.21 mag/air mass, ref (17) p. 116, we get

ε_a = 0.53
ε_φ = 0.89 (45° plate, n = 1.55)
ε_o = 0.80 (estimated)
ε_g = 0.92 (4% at each surface)
ε_s = 0.48 (Grubb Parsons data)
ε_L = 0.92 (4 % at each surface)
T_s = 0.60 (Filter data)
ε (Total) = 0.092

For « flares », of duration longer than the time-constant, i. e. for periods $\sim$ 0.1 sec. to $\sim$ 3 min, the corresponding *rate* of light emission would have to have been $> 2.3 \times 10^{18}$ *watts* to have been detectable, since the power in the source would be $P_{min} = (J_{min}/\tau)$.

4. Future plans

An experiment of a different type has been planned for this summer's opposition (1962) which will be carried out in conjunction with Dr. D. W. Dewhirst at the Observatories, Cambridge, Professor R. O. Redman having generously provided the facilities. It is now planned to look for steady H(α) activity of an auroral character, assuming this to be formed by possible Van Allen particles interacting either with the upper atmosphere of the planet or an exosphere, if such exists around Jupiter. With these considerations in mind, the equipment has been modified for off-limb observations. It consists of a single refrigerated EMI phototube (12 photoelectrons sec^{-1} at — 40°C), a light chopper switching the light between two interference filters at 1 c. p. s., and photon-counting electronics. A siderostat and an $f/12$ 15" O. G. will form the basis of the telescope.

REFERENCES

(1) Burke, B. F. and Franklin, K. L., *J. Geophys. Res.*, **60**, 213, 1955.

(2) Sagan, C. and Miller, S. L., *A. J.*, **65**, 499, 1960.

(3) Gallet, R. M., URSI-US National Comm. 12th General Assembly, *National Acad. Sci. NRC Publication*. **581**, 143, 1958.

(4) Warwick, J. W., *Science*, **132** (3435), October, 1250, 1960. *Annals of the New York Academy of Sciences*, **95**, 39, 1961. This Symposium 1962.

(5) Carr, T. D., Smith, A. G. and Bollhagen, H., *Phys. Rev. Letters*, **5**, 418, 1960. — Carr, T. D., Smith, A. G., Bollhagen, H., Six, N. F. (jr.) and Chatterton, N. E., *Ap. J.* **134**, (1), 105, 1961. — Smith, A. G., this Symposium. — Barrow, C. H., this Symposium.

(6) Smith, H. J., Lasker, B. M. and Douglas, J. N., *A. J.*, **65**, 501, 1960. — Smith, H. J., This Symposium.

(7) Drake, F. D. and Hvatum, S., *A. J.*, **64**, 329, 1959.

(8) Field, G. B., *J. Geophys. Res.*, **64**, 1169, 1959.

(9) Field, G. B., *J. Geophys. Res.*, **65**, 1661, 1960.

(10) Radhakrishnan, V. and Roberts, J. A., *Phys. Rev. Letters*, **4**, 493, 1960.

(11) Morris, D., this Symposium.

(12) Roberts, M. S. and Huguenin, G. R., this Symposium.

(13) JELLEY, J. V. and PETFORD, A. D., *Observatory*, **81**, (922), 104, 1961.

(14) KRAUS, J. D., Proc. I. R. E., **46**, No. 1, 266, 1958.

(15) Reported by A. G. SMITH, this Symposium.

(16) BRADDICK, H. J. J., « Photoelectric Photometry », *Rep. Prog. Phys.*, **23**, 154, 1960.

(17) ALLEN, C. W., Astrophysical Quantities. The Athlone Press, University of London, 115, 116 and 155, 1955.

(18) SMITH H. J. and DOUGLAS, J. N., *A. J.*, **67**, 120, 1962.

48. — ON THE HYDRODYNAMICS OF JUPITER'S ATMOSPHERE

R. HIDE
Massachusetts Institute of Technology, Cambridge 39, Massachusetts, U. S. A.

I. Introduction

The complete specification of any hydrodynamical system requires a knowledge of (a) the physical properties and chemical composition of the fluid one is dealing with, (b) the geometry of the system and (c) the nature and distribution of the energy sources. In addition is required (d) the ability to solve the mathematical equations governing the system. In a « make-believe » world where this knowledge and ability were available, observations of the flow would serve merely as a check on the theoretical calculations.

In dealing with the hydrodynamics of the Earth's atmosphere, since items (a), (b) and (c) can be specified more or less precisely, the most serious difficulties are encountered under item (d). Fortunately, through a judicious combination of observation and theory, significant progress in dynamical meteorology has been made in recent years. Owing to the vast complexity of the problem, this progress has been slow, not always sure, and much remains to be done.

In the case of Jupiter's atmosphere the situation is apparently much worse, since its physical properties and chemical composition are by no means certain, its depth is unknown and what knowledge we possess about energy sources is incomplete. In the absence of any redeeming features, such as some significant observational clues, considerations of the hydrodynamics of Jupiter's atmosphere would be inextricably confined to the realm of day-dream and speculation. Fortunately such clues exist. One of these is the presence of a

strong equatorial current, which moves relative to the rest of the visible surface at 10^4 cm/sec in an eastward direction (*). Another — and the one that we shall pursue in this paper — is the presence of the Great Red Spot (**).

I have already advanced a theory of the Great Red Spot [1] which is capable, evidently, of accounting in a fairly unforced way for its principal properties. In what follows, the essential features of the theory, in its original, simplest, form, will be described briefly, together with a number of subsequent developments. These developments have led not only to further insight into the hydrodynamics of Jupiter's atmosphere, but also give rise to some interesting speculations with regard to Jupiter's deep interior. The details of this work will be published in due course.

It is not immediately obvious why one feature — albeit prominent — should be an early candidate for relatively detailed scrutiny, when the average features of Jupiter's atmospheric motions (« general circulation ») — such as the number of bands displayed by Jupiter's visible surface and the average variation of the rotation rate with latitude, as evinced by the motion of markings on that surface — have not yet been satisfactorily explained [2]. Perhaps this is a matter of personal choice. Certainly it is my experience with this and other work [4] that an indirect approach to problems of this kind can often lead to a valuable interplay between theory, experiment and observation which has no counterpart in the direct approach. Thus, while one of the ultimate goals of any serious study of the hydrodynamics of Jupiter's atmosphere must be a rational theory of its general circulation, this problem is not the central one of this paper.

(*) The rotation periods of Systems I and II are $9^h50^m30^s.003$ and $9^h55^m40^s.632$ respectively [5].

(**) Spinrad discovered recently [3] that according to the Doppler shift of ammonia lines in Jupiter's spectrum, the material giving rise to these lines rotates westward at several kilometres per second relative to the visible surface. The reconciliation of this discovery with other observations is a challenging problem to the hydrodynamicist. It suggests that supersonic « jet streams » may exist in Jupiter's atmosphere, and emphasises the need for the study of the « Spinrad effect » as a function of latitude and time.

II. Principal properties of the Great Red Spot

The principal properties of the Great Red Spot may be summarized as follows : —

(1) Size, position and form
(2) Uniqueness
(3) Long enduring character
(4) Extensive motion in longitude
(5) Very slight motion in latitude
(6) Seeming repul 'on of the South Equatorial Belt and presence of Red Spot Hollow
(7) Interaction with the South Tropical Disturbance
(8) Association with other features of Jupiter's visible surface
(9) Contrast and colour

This list is based on Theodore Phillips's article on Jupiter in the 1929 edition of the Encyclopaedia Britannica ([5]), but with some modifications.

Property 1 : *Size, position and form.* The mean radius R_0 of Jupiter is about 69,000 km. The Great Red Spot is elliptical in shape, having its long axis along zenocentric latitude 22°S, and occupies 30° of longitude and 10° of latitude. Thus it is some 40,000 km long and 13,000 km wide.

Property 2 : *Uniqueness.* Perhaps Phillips excluded this property from his list because it is so obvious. It is, however, a very important property which any acceptable theory must account for.

Property 3 : *Long enduring character.* The apparent permanence of the Great Red Spot amongst the otherwise ever-changing features of Jupiter's surface of dense cloud is the property that has proved most baffling, and which has led to some weird suggestions. There is positive evidence that the Spot has existed since 1831, and since it is likely that the spot reported by Hooke in 1664 (during

the earliest telescopic observations of Jupiter) and the Great Red Spot are one and the same, the age of the Spot is certainly greater than 130 years, and possibly very much greater, perhaps by many orders of magnitude.

Property 4 : *Extensive motion in longitude.* The mean rotation period of Hooke's Spot was $9^h\ 55^m\ 59^s$ in 1664-66 and $9^h\ 55^m\ 54^s$ in 1666-72. That of the Great Red Spot varied irregularly between $9^h\ 55^m\ 31^s$ and $9^h\ 55^m\ 44^s$ during the interval 1831 to 1948 (6). The longitude of the Spot with respect to System II (rotation period $9^h\ 55^m\ 40^s.632$) as given by Smith and Carr include data for the past ten years (7). According to a private communication from Peek, the mean annual period for the years 1950 to 1958 inclusive was $9^h\ 55^m\ 44^s$, 43^s, 43^s, 43^s, 43^s, $42^s.5$, $41^s.5$, $42^s.5$ and 42^s. The corresponding amplitude of the irregular drift in longitude implied by these variable periods is considerable, amounting to over 1000°. Significant accelerations of this motion in longitude occurred in 1880, 1910, 1926 and 1936.

Property 5 : *Very slight motion in latitude.* In contrast to the extensive excursions in longitude undergone by the Great Red Spot, its latitude has hardly varied at all. During the interval 1908 to 1930 the mean latitude of the « centre » of the Spot was — 21.8°, the maximum departure of the « centre » from this position being only 1.5°, although in 1882, one measurement gave — 25.2°. Since the Spot occupies 10° of latitude, which is much greater than these departures, and variations in the appearance of the Spot must introduce uncertainties of the order of a degree in locating the latitude of its « centre », there is no clear evidence that the latitude of the Spot has changed at all.

Property 6 : *Seeming repulsion of South Equatorial Belt and the presence of the Red Spot Hollow.* In longitudes remote from the Great Red Spot, the southern boundary of the South Equatorial Belt is located several degrees south of the northernmost part of the Spot, and the Spot causes an indentation in this boundary.

This indentation is the so-called « Red Spot Hollow ». Short-lived spots in the South Tropical zone tend to be swept around the Great Red Spot, skirting round its northern edge.

Evidently there is seldom anything equivalent to the Red Spot Hollow on the southern side of the Spot, and any successful theory of the Great Red Spot should account not only for the Red Spot Hollow but also for the striking asymmetry manifested by the absence of an indentation on the other side of the Spot.

Property 7 : *Interaction with the South Tropical Disturbance.* In 1901, a conspicuous marking arose in the South Tropical Zone. It occupied the whole breadth of the zone and some tens of degrees of longitude. Its rotation period was somewhat less than that of the Great Red Spot, which it overtook two years later. Although the so-called « South Tropical Disturbance » has subsequently disappeared and then reappeared from time to time, it seems to be a semi-permanent feature of Jupiter's visible surface, which may, according to drawings, have been present as early as 1859. Peek ([6]) has described the interaction between the Great Red Spot and the South Tropical Disturbance, his account being based on observations covering several conjunctions. There is evidence that the S.T.D. propagates from one end of the G.R.S. to the other *at an average speed which is up to ten times the speed at which it approaches and recedes from the G.R.S.*

Property 8 : *Association with other features of Jupiter's visible surface.* This is a somewhat vague property which Phillips included in his list ([5]). Possible features which may turn out to be associated with the presence of the Great Red Spot are the tendency for short-lived spot activity to be a maximum between 5°S and 35°S, and the unsymmetrical rotation with respect to the equator of the visible surface of the planet. In 1915, for example, the northern hemisphere rotated more slowly than the southern hemisphere, average rotation periods for these two regions (excluding the Equatorial Zone with its much shorter period of rotation ($9^h\ 50^m\ 25^s$) than

the rest of the planet) being $9^h\ 55^m\ 42^s$ and $9^h\ 55^m\ 24^s$ respectively.

Several years ago when the existing evidence suggested to some authors that intense radio bursts from Jupiter might be associated with the Great Red Spot, it would have been natural to include this feature here. Now that we have more information about these radio bursts, a *direct* connection between them and the Spot is no longer suspected (7).

Property 9 : *Contrast and Colour.* At times the Great Red Spot is a very conspicuous object, contrasting greatly with its surroundings. On occasions when the outline of the Spot is difficult to discern, the position of the Spot is evinced by the Red Spot Hollow. Evidently, although there have been occasions when either the Spot or the Hollow is invisible, one of these features seems always to be present (6).

The Spot was described as « brick red » when it first came into prominence in 1878 — hence its name — and there is spectroscopic evidence that the Spot is generally redder than its surroundings. However, there have been occasions when observers have given its colour as « faint grey », and others when the Spot, in contrast with the surrounding regions of dense, light grey cloud, was very dark, having no cloud over it. This tendency for cloud to have difficulty in forming over the Spot is noteworthy and may be significant.

III. Previous theories of the Great Red Spot

There have been no previous theories, if by « theory » we mean a model which is based on fewer reasonable *ad hoc* assumptions than there are significant facts to explain. The suggestion that the Spot is due to a floating solid object (a raft) seems to have attracted most attention (6).

Such a suggestion can obviously account for Properties 1 and 3, although the chemical composition of the raft has not been specified.

This is not a trivial objection since the mean density of Jupiter's atmosphere is probably much less than that of nearly all known solids.

The supposition that the object is floating has been considered necessary in order to account for Property 4. One famous textbook of astronomy states effectively that this property demonstrates unequivocally that « the Spot cannot be rooted in anything solid within the planet », and another that it « shows unquestionably that the Spot is floating ». There are at least two logical errors in the arguments leading to this conclusion. First, it has been assumed (implicitly) that the « solid planet » must rotate uniformly, which, as we shall show later, is probably untrue. Secondly, property 5 — very slight *latitudinal* motion of the Spot — does not find a natural explanation in terms of a floating object unless one makes additional assumptions that are apparently so artificial that one could only consider them seriously in the absence of any reasonable alternative approach to the problem ([5]).

IV. Jupiter's internal structure and rotation

The mean density $\bar{\rho}_0$ of Jupiter is 1.34 gm cm^{-3} ([6]). Its moment of inertia I_0 about the rotation axis of the planet is given by

$$I_0 = \alpha_0 \frac{2}{5}\left(\frac{4}{3}\pi \rho_0 R_0^3\right) R_0^2 = 2.2 \times 10^{49} \text{ gm cm}^2 \qquad (1)$$

where $\alpha_0 = 0.6$ and R_0 ($= 6.9 \times 10^9$ cm) is the mean radius of the planet. Since $\alpha_0 = 1$ corresponds to a homogeneous distribution of density, Jupiter is centrally condensed, having a density ρ which is a generally decreasing function of r, the distance from the centre. (The corresponding value of α_0 for the Earth is 0.84).

Although there have been many attempts to determine the composition and internal constitution of Jupiter ([9]), general agreement has not yet been reached, and even if the writer were competent to do so it would take us too far from the main theme of this paper to give a critical discussion here. Without being too

precise about all the details, we shall assume here that Jupiter is almost spherically symmetrical and consists essentially of three regions, namely a central core of mean radius R_c and mean density $\bar{\rho}_c$; an intermediate region which we term « mantle » of mean density $\bar{\rho}_m$ extending out to a mean radial distance R_m, and an atmosphere of mean density $\bar{\rho}_a$ surrounding the mantle and extending somewhat beyond the visible surface of the planet, mean radius R_0.

If the core is liquid and electrically conducting, then this presumably is where the general Jovian magnetic field ([10]) has its origin, the most likely mechanism being a « homogeneous dynamo » type of process ([11]), involving hydrodynamical motions in the core of the order of 1 cm/sec.

Properties of radio bursts on decameter wavelengths from Jupiter have led to the introduction of System III, which rotates with a period of $9^h\ 55^m\ 29.37^s$ and with respect to which the general pattern of radio burst sources has moved only slightly during the past decade ([10, 12]), variations of the rotation period P_R of this pattern amounting to no more than about 0.5 sec. It is likely that irrespective of the details of the mechanism responsible for the radio bursts, the pattern of sources is related to the form of the magnetic field. Hence, if P_c is the instantaneous (spatial) average rotation period of the core, then $P_c = P_R$.

Now consider the rotation period, P_m, of the mantle. Hide ([1]) (Section V below) has suggested that the Great Red Spot is due to a « topographical feature » at the surface of the « solid planet » underlying the atmosphere and has proposed a mechanism by means of which the hydrodynamical effects of this « topographical feature » make themselves manifest at great heights in the atmosphere, thus accounting for Properties 1 and 3 of the Spot. On this model, the motion of the « solid planet » is essentially that of the Great Red Spot.

We shall identify the « mantle » of the present model with the « solid planet » of reference ([1]), « solid » in the sense that any internal motions within the mantle are characterized by time scales of the

order of the age of the Great Red Spot. Thus Properties 4 and 5 imply that while the longitude with respect to its mean motion of any material point in the mantle undergoes extensive changes, variations in latitude are slight.

Because of the tremendous gyroscopic stability of the mantle, the assumption that the motion of the Great Red Spot is that of the mantle makes it possible to reconcile Properties 4 and 5 [1]. From the observed longitude variations, making reasonable assumptions about R_m and ρ_m, it is possible to estimate the order of magnitude of the torque C_m required to account for these variations. Assuming that torques on the mantle applied about an axis in the equatorial plane are no stronger than C_m, it is a simple matter to show that resulting variations in latitude are utterly negligible [1].

The origin of these torques remains to be accounted for. One suggestion is that atmospheric motions may be responsible [1]. Certainly, if the motions of the visible surface are characteristic of the flow at lower levels (see Section VII), and the depth $(R_0 - R_m)$ of the atmosphere is greater than about 1,000 km, angular momentum variations in the atmosphere could be of roughly the same order of magnitude of those of the mantle, even if $R_c/R_0 \ll 1$. One difficulty with this suggestion is that unless $(R_m - R_c) \ll R_0$, it is hard to account for the energy variations of the mantle without invoking what may be an unrealistic rate of energy dissipation in the atmosphere. Another difficulty is the striking difference between P_c and P_m. We have seen that over the decade for which we have information on radio bursts, P_R, the rotation period of the radio-burst source pattern, and hence P_c, has remained within about 0.5 sec. of $9^h\ 55^m\ 29.4^s$. During the same interval of time, the rotation period of the Great Red Spot, and hence P_m, behaved quite differently (see Property 4, Section II). Thus the suggestion that angular momentum transfer from the atmosphere is responsible for the motion of the mantle requires that the core and mantle should be weakly coupled mechanically. This is unlikely unless the electrical conductivity of the lower mantle is very low indeed.

The obvious alternative possibility as to the origin of the torques responsible for the motion of the mantle is that they arise in the core ([10]). The fact that under plausible assumptions the transit time for hydromagnetic waves to cross the core is of the same order of magnitude as the time scale of the longitudinal motions of the Great Red Spot suggests that the mantle and core undergo coupled torsional oscillations, the coupling being due to Jupiter's general poloidal magnetic field. Presumably the hydrodynamical motions in the core which are responsible for the magnetic field can excite these torsional oscillations, although here again detailed calculations are needed.

The fact that P_R has varied only slightly over the past ten years must mean that the time scale associated with hydrodynamical motions in Jupiter's liquid core is at least several decades. When as a result of further radio-astronomical observations we know how P_R varies with time, it will be possible to subject some of the foregoing suggestions to quantitative tests. Unfortunately if the behaviour of P_R over the past ten years has been typical, it may be several decades before P_R has changed sufficiently for any definite conclusions to be reached.

The argument that since there is as yet no evidence that P_R has varied significantly, P_R must be the rotation period of the « solid planet », has been invoked by several workers. Although properties of Jupiter's interior implied by this seductively direct conclusion have not been discussed in detai', it seems from the foregoing discussion that their reconciliation with present knowledge about Jupiter may raise difficulties which are at least as great as, and probably much greater than, those associated with the model adopted in this paper.

V. « Taylor Columns » and the nature of the Great Red Spot

Simple order of magnitude arguments applied to the hydrodynamical equations show that Coriolis forces due to Jupiter's rotation dominate the atmospheric flow. If U is a typical horizontal

relative flow velocity, L a horizontal length characteristic of the flow pattern and Ω is the basic angular velocity of rotation, in the absence of strong frictional effects the extent to which rotation dominates the hydrodynamical flow depends on the Rossby number, $U/L\,\Omega$. Taking $U = 10^2$ cm/sec and $L = 10^9$ cm as typical of the flow in the neighbourhood of the Red Spot, since $\Omega = 1.7 \times 10^{-4}$ rad/sec, $U/L\,\Omega \simeq 10^{-3}$. When $U/L\,\Omega \ll 1$ and effects due to density inhomogeneities can be ignored, according to a theorem due to Proudman and Taylor ([13]) flows which do not change rapidly with time (i. e. insignificant changes in $2\pi / \Omega$ sec.) tend to be two-dimensional, in planes perpendicular to the axis of rotation.

If the Proudman-Taylor theorem holds even approximately in Jupiter's atmosphere, then the effect on the atmospheric circulation of quite a shallow « topographical feature » of the upper surface of the mantle would be attenuated very slowly with direction parallel to the axis of rotation, and thus, contrary to general expectation, such a feature could make its presence manifest at the upper levels of quite a deep atmosphere.

Hide ([1]) has suggested that the atmospheric flow would be unable to surmount a « topographical feature », irrespective of whether it be a « mountain » or a « depression », if its vertical dimension, h, exceeds $\tilde{h}$ given, on certain simplifying assumptions, by

$$\tilde{h} = \alpha\,(R_0 - R_m)\,(U / L\Omega), \qquad (1)(*)$$

where α is a pure number of order unity, $(R_0 - R_m)$ being the depth of the atmosphere. When this criterion is satisfied there will be a column of fluid stretching from the « topographical feature » at the bottom of the atmosphere all the way to the « top » of the atmosphere. In the absence of internal energy sources this column of fluid will be stagnant, partaking only of the motion of the « topographical feature », and virtually no mixing between the fluid within the column and that without will occur.

(*) Equation (1) does not hold when $\tilde{h}$ is so small that friction is no longer negligible (see Section VII).

Effects of this kind were predicted and demonstrated experimentally many years ago by Taylor ([13]), whose qualitative experiments have since been repeated by others ([14]). Ibbetson is now carrying out quantitative experiments to test Hide's criterion for the occurrence of « Taylor columns » (see equation (1)). In these experiments « Taylor columns » are produced by towing a solid object, of height h, horizontally across a cylindrical tank of water of uniform depth which rotates about a vertical axis.

Since $U/L\Omega \simeq 10^{-3}$ for Jupiter, by equation (1) $\tilde{h} \simeq 10^{-3}(R_0 - R_m)$ The depth $(R_0 - R_m)$ of Jupiter's atmosphere is not known. If we postulate that the Great Red Spot is simply the top of a « Taylor column » ([1]) and accept for the moment the simplest form of the theory based on the highly idealized atmosphere assumed above (homogeneous density, etc.) then the column would be parallel to the axis of rotation. Thus the « topographical feature » responsible for the « Taylor column » will be located at a lower latitude than the Spot. A simple geometrical construction serves to show that this sets an upper limit on $(R_0 - R_m)$, which amounts to about $0.04\ R_0$, or 2800 km. Whether this upper limit is significant will depend on the results of a detailed evaluation of the assumptions which underlie it. It is much less than the value of $(R_0 - R_m)$ assumed in reference ([1]), based on an old model of Jupiter's internal constitution. On the other hand, it is comparable with, or somewhat greater than some of the values of $(R_0 - R_m)$ which have been suggested more recently. If we take $(R_0 - R_m) = 1000$ km then $\tilde{h} \simeq 1$ km. Although geometrically this is a very shallow feature, the mechanical stresses in the mantle associated with such a « topographical feature » might be as high as 10^8 or 10^9 dyne/cm^2. If this « feature » cannot be supported elastically, it may be necessary to invoke slow convection in the mantle to account for it, in which case the coefficient of viscosity of the mantle material must exceed about 10^{19} gm cm^{-1} sec^{-1} ([1]).

In order to account for Property 1 (see Section II) it is necessary to postulate that the size, position and form of the Great Red

Spot are more or less directly related to size, position and form of the « topographical feature ». If the « Taylor column » is parallel to the rotation axis then not only is the « topographical feature » located at lower latitudes than the Spot, but the former is more nearly circular than the latter.

Now consider the uniqueness of the Great Red Spot (Property 2 — see Section II). Equation (1) shows that $\tilde{h}$ is *inversely* proportional to L, and since we identify L with the horizontal dimension of a « topographical feature », it is clear that unless we make *a priori* highly unacceptable assumptions about the relationship between h and L for the topographic structure of the mantle-atmosphere interface (e. g. h inversely proportional to L), there is a highly selective effect in which only large horizontal scale features can produce « Taylor columns ». The fact that on the present theory only one « Taylor column » has had a more or less continuous existence over the past few hundred years suggests that the dimensions of the « topographical feature » responsible for the Great Red Spot are close to the critical value, so that smaller « topographical features » would be incapable of producing persistent effects at the level of the visible surface of the planet [1]. Although these arguments do not account completely for the uniqueness of the Great Red Spot they suggest a plausible explanation which could be quite consistent with a mantle-atmosphere interface which is topographically complicated [1].

VI. Flow around the Great Red Spot

The tendency for short lived spots in the South Tropical zone to pass around the Great Red Spot, thus avoiding the Spot itself (see Property 6, Section II), are accounted for in an obvious way in terms of a « Taylor column ».

Although there have been some suggested explanations of the colouring of Jupiter [6, 15], no general agreement has been reached on this matter. Whatever the correct explanation turns out to be, the

contrast between the Great Red Spot and its surroundings (see Property 9) presumably implies that there is little mixing between the Spot and its environment, since molecular diffusion would be negligible over such tremendous distances. This is in accord with the « Taylor column » model.

It is tempting to suggest that the tendency for cloud to have difficulty in forming over the Great Red Spot (see Property 9) is direct evidence for a stagnant region underlying the Spot, indicating a « Taylor column » possessing no internal energy sources. However, according to some authors ([16]), motions within the Spot have been seen occasionally, implying that energy sources may exist either within the « Taylor column », or at its base ([8]).

Now consider the formation of the Red Spot Hollow, and the characteristic asymmetry manifested by the absence of a comparable indentation on the other side of the Spot (see Property 6, Section II). This property suggests that the flow around the « Taylor column » is approximately laminar on the equatorward side and turbulent on the other side. (This turbulence may account for the tendency for short-lived spot activity to be a maximum between 5°S and 35°S (see Property 8).) The flow outside the « Taylor column » in the experiments referred to in Section V exhibits a distinct asymmetry resembling in a striking way the appearance of the Great Red Spot.

Simple theoretical arguments based on vorticity considerations suggest that the effects of the curvature of the planet on the flow around the « Taylor column » in Jupiter's atmosphere (in meteorological parlance β-effects, β denoting the variation with latitude of the vertical component of the basic rotation vector) should not introduce any gross asymmetry into the flow, so that experiments in which curvature effects are absent may have some relevance. Further experimental and theoretical work is obviously needed, of course, and this will be carried out as part of the programme now in progress.

VII. Critique of simplest model

By invoking the presence of a « Taylor column » in Jupiter's atmosphere we have been able to account for most of the properties of the Great Red Spot. This does not prove that a « Taylor column » exists there, so that we must examine quantitatively the assumptions under which the arguments of Section VI can be expected to hold.

These assumptions are essentially that :

(a) the atmosphere is in motion near the mantle-atmosphere interface ; otherwise there would be no interaction with a « topographical feature » ;

(b) the flow can be regarded as slow and steady ;

(c) primary effects of friction can be ignored ;

(d) the fluid can be regarded as homogeneous ;

(e) the fluid can be regarded as incompressible.

In addition, we must assess :

(f) the effect of the curvature of the planet on the conditions for « Taylor columns » to arise.

We have no direct evidence with regard to (a). Stommel and Veronis ([17]) have studied steady convective motion in a stably stratified fluid subject to horizontal temperature variations over the upper surface, when rotation and curvature effects are present, and thus deduced the depth to which the motions generated near the upper surface will penetrate into the fluid. This theoretical study suggests that the « penetration depth » for Jupiter's atmosphere would be $3 \times 10^3 [(R_0 - R_m/\Delta \vartheta/\vartheta]^{1/2}$ cm where $\Delta \vartheta/\vartheta$ is the fractional potential density contrast between the bottom and top of the atmosphere. There is a wide range of plausible values of $(R_0 - R_m)$ and $\Delta \vartheta/\vartheta$ for which this penetration depth is comparable with, or greater than $(R_0 - R_m)$.

Now consider (b). If the motions at depth in Jupiter's atmosphere are comparable in regard to flow velocity, and also in time scale for gross changes to occur, with those at the level of the

visible surface, then the assumption that the flow is slow and steady should be valid.

Turning to (c), frictional forces will be due primarily to eddy viscosity. In the main body of the flow, over length scales of planetary size, friction will be utterly negligible, although frictional effects would be present in the « walls » of a « Taylor column ». If ν_E is the coefficient of eddy viscosity, then the Ekman boundary layer ([18]) at the bottom of the atmosphere, where it meets the mantle, will have thickness of order $(\nu_E / \Omega \sin \theta)^{1/2}$, where Ω is the angular velocity of rotation of the planet and θ is the angle of latitude. The criterion for the occurrence of « Taylor columns » given in Section V (see equation 1) ignores friction, which is evidently legitimate if $(\nu_E / \Omega \sin \theta)^{1/2} \ll h$, i. e. if $\nu_E \ll h^2 \Omega \sin \theta$. (How seriously the latitude dependence has to be taken is not clear; we include it here in order to be conservative.) If $h = 10^5$ cm, $h^2 \Omega$ is of order 10^6 cm^2 sec^{-1}. Since ν_E is not known, we cannot tell whether the « Ekman layer » will submerge the « topographical feature » and thus suppress the « Taylor column ». Values of ν_E ranging from 10 to 10^6 cm^2 sec^{-1} are encountered in the Earth's atmosphere and oceans, ν_E being strongly dependent on many quantities, especially the vertical stability due to density stratification.

We shall consider assumptions (d) and (f) together. Hide ([19]) has treated the theory of the hydrodynamical disturbance due to corrugations of the lower bounding surface of a rotating spherical shell of fluid relative to which there is a zonal current having velocity U_0 in the eastward (x) direction. Assuming (1) the corrugations to be periodic with wavenumbers k_x and k_y in the x and y directions (y directed northwards) and of small amplitude compared with k_x^{-1} and k_y^{-1}; (2) that U_0 is independent of time t, and also of x, y and the upward vertical coordinate z; (3) that the fluid is incompressible; and employing the « β-plane » approximation of dynamical meteorology and oceanography ([20]), it may be shown

that in a certain approximation the disturbance varies in the z direction as exp. $\pm$ Kz, where

$$K^2 =$$

$$(k_x^2+k_y^2)\left(\frac{1-N^2/U_0^2k_x^2}{1-f^2/U_0^2k_x^2}\right)\left(1-\frac{\beta}{(k_x^2+k_y^2)U_0}\,\frac{(1-U_0^2k_x^2/f^2-2iU_0k_y/f)}{(1-U_0^2k_x^2/f^2)}\right). \quad (2)$$

In equation (2) f is the Coriolis parameter, $2\,\Omega \sin\theta$, $\beta \equiv df/dy = 2\,\Omega\cos\theta/R_0$, assumed constant, and N is the « Brunt-Väisälä frequency » ([21]) equal to $[-g\,(d\ln\vartheta/dz)]^{1/2}$, ϑ being the potential density (equal to the actual density ρ in the case of an incompressible fluid). β is proportional to the variation of Coriolis parameter with latitude, and would vanish in the absence of curvature of the planet's surface. N^2 is a measure of the vertical stability due to density stratification.

To simplify the following discussion, consider the case $k_y = 0$, $k_x = k$, corresponding to ridges having their axes transverse to the direction of the basic current. Thus, by equation (2)

$$K^2 = k^2\left(\frac{1-N^2/U_0^2k^2}{1-f^2/U_0^2k^2}\right)\left(1-\frac{\beta}{k^2U_0}\right). \quad (3)$$

In the absence of rotation ($f = 0$), density stratification ($N^2 = 0$) and curvature effects ($\beta = 0$), $K = \pm k$. This corresponds to a disturbance which suffers exponential attenuation with z.

When $N^2 = 0$, $\beta = 0$ but $f \neq 0$, and the Rossby number $U_0k/f \ll 1$, corresponding to strong rotation effects but none due to density stratification and curvature, $K = \pm i\,U\,k^2/f$. Thus, in contrast to the previous case, the disturbance varies harmonically with z, and in the limit of zero Rossby number, the wavelength of the harmonic perturbation is infinite, that is to say, there is no variation with z, which is in keeping with the Proudman-Taylor theorem (see Section V).

When $\beta = 0$ but $N^2/U_0^2k^2 > 1$ and $f^2/U_0^2k^2 > 1$, corresponding to significant effects due to both density stratification and rotation, then K is real, and again we have exponential damping ([22]), showing that vertical density stratification can oppose the tendency of

rotation to favour the propagation of the disturbance to great distances from its region of origin.

Finally, we consider the case $N^2/U_0^2 k^2 > 1$, $f^2/U_0^2 k^2 > 1$ and $\beta/k^2 U_0 > 1$, corresponding to strong effects due to density stratification, rotation and curvature, and we find that K is again imaginary. Thus, when strong curvature effects are also present, the disturbance varies harmonically with z. In the limit of $N^2/U_0^2 k^2 \gg 1$, $f^2/U_0^2 k^2 \gg 1$, $\beta/k^2 U_0 \gg 1$, we have $K = \pm i\,(N/f)\,(\beta/U_0)^{1/2}$.

Typical values of β and U_0 for mid-latitude regions of Jupiter's atmosphere are 10^{-14} cm^{-1} sec^{-1} and 10^2 cm sec^{-1} respectively, so that atmospheric disturbances due to « topographic features » having horizontal dimensions in excess of about 10^9 cm would be influenced by the curvature of the planet. The term $N^2/U_0^2 k^2$ is of the order of $10^4\,\Delta\rho/\rho$, if $\Delta\rho/\rho$ is identified with the fractional potential density contrast over a scale height, and $f^2/U_0^2 k^2 \simeq 10^4$ so that $\pm iK/k \simeq (\Delta\rho/\rho)^{1/2}$. Since $\Delta\rho/\rho$ would be less than unity, possibly by several orders of magnitude, this result suggests that even in the presence of curvature and density stratification, effects analogous to those responsible for « Taylor columns » in a homogeneous fluid may still occur though it is not clear that the effects of « bottom topography » would be propagated parallel to the rotation axis. This conclusion is tentative, since the foregoing theoretical discussion is obviously far from adequate, and must be amplified in the future. The effects of vertical shear in the basic motion ought to be taken into account, but this is a difficult mathematical problem ([23]).

We shall defer discussion of the conditions under which assumption (*e*) — that in treating the hydrodynamics of planetary scale motions the fluid may be regarded as incompressible — until the next section 8, because, as we shall see, compressibility gives rise to novel effects on Jupiter.

Up to this point we have made no mention of terrestrial meteorology. An obvious question is whether « Taylor columns » arise in the Earth's atmosphere. The subject of air-flow over moun-

tains has been studied intensively, both observationally and theoretically ([24]), but so far as I know, nothing as striking as a « Taylor column » has been discussed in this context. Perhaps this is not surprising since the smallest Rossby number for the Earth's atmosphere is as high as 10^{-1}, that is, one or two orders of magnitude greater than the corresponding quantity for Jupiter. The Earth's rotation can exert a stronger control over ocean currents than over atmospheric motions of comparable horizontal scale, the smallest Rossby number for the oceans being much less than 10^{-1}. It would be interesting to look for possible effects of bottom topography on ocean currents. Equation (2) suggests that topographical features greater than 100 km in horizontal extent might produce such effects in spite of stable density stratification. It is noteworthy, perhaps, that there is now some evidence that meanders of the Gulf Stream are influenced by the topography of the bottom of the Atlantic Ocean ([25]).

VIII. Dynamical effects of compressibility in a highly rotating fluid

The details of the interaction between the Great Red Spot and the South Tropical Disturbance (Property 7, see Section II) have not yet been considered. Some time ago I attempted to interpret the rapid acceleration of the South Tropical Disturbance as it moves past the Spot in terms of ordinary Rossby waves ([20, 26]) but Toomre objected to my interpretation and offered an alternative suggestion. He drew to my attention the possibility that compressibility effects might be important in Jupiter's atmosphere and, idealizing the « Taylor column » as a long rigid cylinder ignoring curvature effects and treating the atmospheric flow as uniform at great distances from the « Taylor column », he showed ([27]) that the stream function for the flow can be expressed in terms of modified Bessel functions of the second kind : —

$$\psi = U_0 \tilde{\omega}_0 K_1 (f\tilde{\omega}/a) \sin \varphi / K_1 (f\tilde{\omega}_0/a), \qquad (4)$$

where U_0 is the speed of flow at $\tilde{\omega} = \infty$, $(\tilde{\omega}, \varphi)$ are cylindrical polar coordinates, (the surface of the rigid cylinder being $\tilde{\omega} = \tilde{\omega}_0$,) a is the speed of sound, and, as before, f denotes the Coriolis parameter. When $f\tilde{\omega}_0/a \ll 1$, $\psi = U_0 \tilde{\omega}_0^2 \sin\varphi/\tilde{\omega}$. This is the incompressible case, in which ψ falls off as $\tilde{\omega}^{-1}$. The flow speed in the neighbourhood of the cylinder is not markedly different from U_0. On the other hand, when $f\tilde{\omega}_0/a \gg 1$, $\psi = U_0\tilde{\omega}_0 \sin\varphi\,(\tilde{\omega}_0/\tilde{\omega})^{1/2} \exp[-f(\tilde{\omega} - \tilde{\omega}_0)/a]$, and it may be shown that in these circumstances the fluid undergoes very rapid acceleration in the neighbourhood of the cylinder.

The value of the « rotational Mach number » $f\tilde{\omega}_0/a$ for the flow around the Great Red Spot is about 10. Thus, compressibility effects will not be negligible. However, when $f\tilde{\omega}_0/a = 10$, the theoretical value of the acceleration in the neighbourhood of the cylinder, though considerable, falls somewhat short of the observed acceleration of the South Tropical Disturbance in the vicinity of the Red Spot, suggesting that additional effects may be present. Further theoretical work along these lines is clearly needed.

It is not intuitively obvious that a « rotational Mach number », fL/a, (where L is a length characteristic of the flow in planes perpendicular to the rotation axis) should determine whether compressibility effects will be significant. However, that this is so may be seen as follows : — If the flow is quasi-two-dimensional in planes perpendicular to the rotation axis, and is highly geostrophic (i. e. the order of magnitude U/L of the relative vorticity is much less than f, where U is a typical relative flow speed) dynamical pressure variations are of the order of ρfUL, and associated density variations $\sim \rho fUL/a^2$. The corresponding contribution to the relative vorticity $\sim f(\rho fUL/a^2)/\rho$, which is only small in comparison with U/L when $f^2L^2/a^2 \ll 1$. Otherwise compressibility effects cannot be ignored.

Amongst the many idealizations made by the meteorologist in treating the dynamics of large horizontal scale flow in the Earth's atmosphere, the assumption of incompressibility is hardly the most

serious one (although even here the rotational Mach number can exceed unity when L exceeds 3000 km). f^2L^2/a^2 is of order 10^2 for Jupiter, and should be comparable for Saturn, so that the systematic study of compressibility effects on the hydrodynamics of rotating fluids will, evidently, be a necessary step towards a satisfactory theory of the hydrodynamics of the atmospheres of large, cold, rapidly rotating planets. To my knowledge, this branch of fluid dynamics has hardly been explored and offers exciting prospects in its own right, apart from any possible application to planetary atmospheres.

The theoretical study of so-called « Rossby waves » in an incompressible fluid has clarified certain aspects of the dynamics of the mid-latitude motions of the Earth's atmosphere. Rossby considered the propagation of a small amplitude horizontal disturbance of a uniform wind in an eastward (x) direction, having a speed U_0 relative to the rotating planet ([20, 26]). Assuming that the disturbance varies harmonically with x and t, having wavenumber k and angular frequency w (wavelength $2\pi/k$ and period $2\pi/\omega$), ignoring the effects of horizontal density gradients and making use of the so-called « β-plane approximation » ([20]) it may be shown that

$$\omega = \frac{2\Omega \cos \theta_0}{R_0} \frac{k}{(k^2 + m^2)}, \tag{5}$$

where the flow is supposed to be confined between latitude circles $\theta_1 = \theta_0 - \pi/R_0 m$ and $\theta_2 = \theta_0 + \pi/R_0 m$ ([26, 28]). The phase velocity C_p of these waves (with respect to the basic current) is given by

$$C_p = -\omega/k = -\frac{2\Omega \cos \theta_0}{R_0 (k^2 + m^2)}, \tag{6}$$

and group velocity C_g by

$$C_g = -d\omega/dk = \frac{2\Omega \cos \theta_0}{R_0} \frac{(k^2 - m^2)}{(k^2 + m^2)^2}. \tag{7}$$

The quantity

$$T_D = \left| \frac{2\pi}{k (C_p - C_g)} \right| = \left| \frac{C_p}{k^{-1}} \frac{d(k^{-1})}{dC_p} \right| \frac{2\pi}{\omega} \tag{8}$$

willbearoug h measure of the time required for a disturbance of arbitrary shape and dominant wavenumber k to disperse.

When the width of the basic current, π/m is comparable with or greater than the wavelength $2\pi/k$ of the disturbance, the waves are highly dispersive. The period $2\pi / \omega$ is then of the order of several days for wavelengths in the 10^3 km range, and so is the dispersion time T_D; this is in accord with meteorological observations.

Hide ([29]) has considered the theory of Rossby waves in a compressible fluid and thus shown that provided m is replaced by $\hat{m}$, where

$$\hat{m}^2 = m^2\left(1 + \frac{4\,\Omega^2 \sin^2 \theta_0}{m^2 a^2}\right), \tag{9}$$

equations (5), (6) and (7) still apply. Since π/m is the width of the current, $\pi/\hat{m}$ may be regarded as a « reduced width », the reduction factor being $(1 + 4\Omega^2 \sin^2 \theta_0/m^2 a^2)^{1/2}$. Hence compressibility has two primary effects. It increases both the period of oscillation $2\pi / \omega$, and the « dispersion time », T_D, by factors which, when $k^2 \ll \hat{m}^2$ are $4\,\Omega^2 \sin^2 \theta_0/k^2 a^2$ and $16\,\Omega^4 \sin^4 \theta_0/k^4 a^4$ respectively.

In the case of Jupiter the reduced width, $\pi/\hat{m}$, will differ significantly from the true width, π/m, when $\pi/m \gg 10^9/\sin \theta_0$ cm. The circumference of the planet is 4.3×10^{10} cm, so that there could be disturbances for which compressibility effects are not negligible. Consider such a disturbance at latitude 20° having a wavelength $2\pi/k = 1.2 \times 10^{10}$ cm, which is 0.25 of the length of the latitude circle. The period of oscillation $2\pi / \omega \sim 10^6$ sec and the dispersion time $T_D \sim 5 \times 10^6$ sec. These should be compared with the « incompressible » values of 10^5 sec and 5×10^4 sec respectively.

In lengthening the oscillation period and dispersion time, compressibility has an effect which is comparable qualitatively and quantitatively with that of vertical density stratification ([29]). For simplicity, such effects were excluded from the analysis leading to equations (5) and (9) by supposing the atmosphere to have a uniform density and to be bounded by two horizontal rigid surfaces. Before a realistic comparison of theory with observation can be

attempted, *horizontal* density gradients will also have to be taken into account and the « β-plane » treatment refined by considering the case of a nearly spherical shell of fluid.

Peek has described the behaviour of what he calls the « oscillating spots » in the South Tropical Zone (6) and has given the following expression for the longitude in System II of one of these spots :

$$\lambda = 271^{\circ}.6 - 0.310\,t - 0^{\circ}.0018\,t^2 + 5^{\circ}.30 \exp(-0.018\,t) \sin 5^{\circ}.0\,t$$

where t is in days. According to this expression, the period of oscillation is 72 days or 6×10^6 sec. Two additional observational facts which we must ultimately explain are (*a*) the persistence, for a matter of years, of the South Tropical Disturbance (see Property 7, Section II), and (*b*) the variations in position and width of the dark and light bands on Jupiter, which are also associated with a time scale of years. If these phenomena are not « climatological », then their time scales would have to be commensurate with « meteorological » periods. The highly idealized theoretical model discussed above leads to oscillation periods and dispersion times which are respectively, one and two orders of magnitude longer than the corresponding quantities for an incompressible fluid. Whether more refined theory will yield oscillation periods and dispersion times long enough to account for the observations remains to be seen.

IX. Conclusion

Doubtless the expert dynamical meteorologist will find my approach to the hydrodynamical problems outlined in this paper cavalier in the extreme, and many of the arguments suspect or incomplete. With this in mind, I have attempted to make my suggestions fairly explicit. because only in this way are underlying assumptions made clear. I do not regard these suggestions as final, but merely as working hypotheses which can serve a useful purpose. A number of promising lines of inquiry have emerged, and these must be followed up. Thus and with average luck, we should at

least learn a little about certain novel hydrodynamical processes. With better than average luck we may thus equip ourselves to deal adequately with the hydrodynamics of Jupiter's atmosphere.

Acknowledgements

Numerous astronomers, geophysicists, meteorologists and fluid dynamicists have helped me in a variety of ways, usually by replying to written inquiries or constructively criticizing an unconvincing argument, and I must acknowledge their support and encouragement.

* * *

Mr. B. M. Peek has been particularly helpful.

The work reported in this paper is part of a programme of research on the hydrodynamics of rotating fluids which was initiated by the author several years ago in England, and is now being continued at M.I.T. This programme has received generous support from the Royal Society of London, the British Department of Scientific and Industrial Research and the Geophysics Research Division, Air Force Cambridge Research Laboratories, Office of Aerospace Research, United States Air Force, (Contract AF.61 (052)-216) through its European Office. Current financial support is from the National Science Foundation under Grant No. NSF. G22390 (DSR.9103).

References

(1) Hide, R., *Nature*, **190**, 895-896, 1961.

(2) Lowell Observatory ; Final report on the study of planetary atmospheres. September 30th, 1952. Contract AF. 19(122)-162.

(3) Spinrad, H., Private communication, 1962.

(4) Hide, R., *Quarterly Journal of the Royal Meteorological Society*, **79**, 161, 1953 ; *Philos. Trans. Roy. Soc.*, London, A. **250**, 441-478, 1958.

(5) Phillips, T. E. R., Article on « Jupiter » in Encyclopaedia Britannica, 14th edition, 1929.

(6) PEEK, B. M., « The Planet Jupiter » (Faber & Faber, London), 1958.

(7) SMITH, A. G. and CARR, T. D., *Quarterly Journal of the Florida Academy of Science*, **24**, 185-196, 1961.

(8) SAGAN, C., this symposium, 1962.

(9) WILDT, R., Article in « Planets and Satellites », Volume III of « The Solar System », edited by G. P. Kuiper and Barbara M. Middlehurst, University of Chicago Press, 1961.

(10) GALLET, R. M., Article in « Planets and Satellites », Volume III of « The Solar System », edited by G. P. Kuiper and Barbara M. Middlehurst, University of Chicago Press, 1961.

(11) HIDE, R. and ROBERTS, P. H., Article in Volume IV of Physics and Chemistry of the Earth, Editors Ahrens et al. (Pergamon Press, London), 1961.

(12) BURKE, B. F., Article in « Planets and Satellites », Volume III of « The Solar System », edited by G. P. Kuiper and Barbara M. Middlehurst, University of Chicago Press, 1961.

(13) TAYLOR, G. I., *Proc. Roy. Soc.* A. **104**, 213, 1923.

(14) FULTZ, D., Unpublished.

(15) RICE, F. O., *Scientific American*, « The Chemistry of Jupiter », June, 1956.

(16) FOCAS, J. H., this symposium, 1962.

(17) STOMMEL, H. and VERONIS, G., *Tellus*, **9**, 401-407, 1957.

(18) PRANDTL, L., « Essentials of fluid dynamics », Hafner Publishing Co., New York, 1952.

(19) HIDE, R., « Two dimensional inertial flow in a rotating stratified fluid which is subject to variations of Coriolis parameter ». Unpublished,1960.

(20) ROSSBY, C. G., *J. Marine Res.*, **2**, 1, 1939.

(21) ECKART, C., « Hydrodynamics of oceans and atmospheres », Pergamon Press, London, 1960.

(22) ROBINSON, A. R., *Journ. Fluid Mech.*, **9**, 321-322, 1960.

(23) CHARNEY, J. G. and DRAZIN, P., *J. Geophys. Res.*, **66**, 83-109, 1961.

(24) CORBY, G. A., *Quart. Journ. Roy. Met. Soc.*, **80**, 491, 1954.

(25) WARREN, B. A., « Topographic influence of bottom topography on the path of the Gulf Stream », Ph. D. dissertation, M. I. T., 1962.

(26) ELIASSEN, A. and KLEINSCHMIDT, E., Article on Dynamic Meteorology in Handbuch der Physik, Vol. XLVIII (Springer-Verlag, Berlin, 1956).

(27) TOOMRE, A., « Effect of rotation on two-dimensional flow of a slightly compressible fluid around a long cylinder ». Unpublished, 1961.

(28) HAURWITZ, B., *J. Marine Res.*, **3**, 35, 1940.

(29) HIDE, R., « Rossby waves in a slightly compressible fluid ». Unpublished, 1961.

49. — ON THE NATURE OF THE JOVIAN RED SPOT

CARL SAGAN (*)
The Institute for Basic Research in Science,
The Space Sciences Laboratory, and The Department of Astronomy,
University of California, Berkeley, California, U. S. A.

The Great Red Spot lies in the South Tropical Zone of the atmosphere of Jupiter. At least for the past 130 years it has been localized at approximately the same latitude, centered near — 22° ; it is possibly identical with a feature observed by Hooke and Cassini in 1664-65. The observed motion of the Red Spot is quite remarkable. Since 1879 it has drifted erratically in latitude only some two or three degrees from the mean position ; on the other hand, the Red Spot has drifted in longitude since 1831 some 3529° with respect to System II, or 1080° with respect to the mean motion (v., e. g., Peek, 1958). The curious discrepancy between the motion in latitude and the motion in longitude has important dynamical consequences, and any model of the Red Spot must be prepared to explain these motions.

Until very recently, the only explanation of the drift in longitude has been that the Red Spot is not connected with the surface of Jupiter ; instead, the Red Spot is conceived to be a large object, with a depth comparable to its transverse dimensions (11,000 km wide and 40,000 km long), floating either in a liquid medium (Hough, 1905), or in an « ocean » of highly compressed gases (Wildt, 1939).

One difficulty which immediately arises is the composition of the (presumed) floating Red Spot. The total atmospheric pressure at the visible cloud tops of Jupiter is $\lesssim 5$ atm, and the temperatures there are some 170 to 200°K (Zabriskie, 1962 ; Opik, 1962). Thus, if we are looking down on the top of the floating object itself — and not some extremely thick permanent cloud form above

(*) Now at Harvard University and Smithsonian Astrophysical Observatory, Cambridge, Mass., U.S.A.

a floating object — the Red Spot must be a solid at these pressures and temperatures. Solid hydrogen and helium, are therefore eliminated. The Red Spot cannot be water, ammonia or methane ices, or a mixture thereof, if its depth is small, because its density would then exceed that of the surrounding atmosphere (cf. Wildt, 1961, p. 205). More exotic compositions are rendered unlikely by the failure to detect their precursors in the Jovian atmosphere by spectroscopy. The hypothesis that the Red Spot is a floating object fails to explain two other observables : that there is only one Red Spot, and that the Red Spot is red.

A more critical test of the notion of a floating Red Spot arises from the absence of a drift in latitude. A floating object on a rotating planet will experience the Eötvös-Lambert force, moving it towards the equator. This force arises from the fact that the gravitational potential of a floating object will be proportional to g, the acceleration due to gravity. On a rotating planet, g is least at the equator, and the object tends to move equatorward to minimize its potential energy. For a spherical object of density ρ and radius r, floating in an incompressible medium of density ρ_0, the Eötvös-Lambert force is

$$F_{E-L} \simeq -\left(1 - \frac{\rho}{\rho_0}\right) m \frac{r}{R} g_0 \left(\frac{5}{2} f - e\right) \cos\lambda \,|\sin\lambda| \qquad (1)$$

(cf. Lambert, 1921 ; Jeffreys, 1959). In eq. (1), m is the mass of the floating object, g_0 is the acceleration due to gravity at the equator of the planet of equatorial radius R, e is the planetary ellipticity, λ is the latitude, and

$$f = \omega^2 R / g_0 \qquad (2)$$

where ω is the angular velocity of planetary rotation. The derivation of equation (1) utilizes the Clairaut equation for gravity to first order only.

In general such a floating sphere will experience a viscous damping force ; in the familiar range of pressures and temperatures where the viscosity is independent of pressure, the damping force is given by Stokes' law

$$F_s = 6 \pi \eta v r \qquad (3)$$

where η is the coefficient of viscosity, and v is the velocity of the floating object.

The equation of motion of the sphere is then given by

$$\frac{d^2\lambda}{dt^2} + b\frac{d\lambda}{dt} + c\cos\lambda\,|\sin\lambda| = 0 \tag{4}$$

where

$$b = \mathrm{G}\,\pi\,\eta\,\frac{r}{m} \tag{5}$$

$$c = \left(1 - \frac{\rho}{\rho_0}\right)\frac{r}{\mathrm{R}^2}\,g_0\left(\frac{5}{2}f - e\right). \tag{6}$$

and we have set $v = \mathrm{R}\,(d\lambda/dt)$. The appropriate boundary conditions will be discussed presently. The substitution $x = \cos\lambda$ transforms equation (4) into the useful form

$$\frac{d^2x}{dt^2} + \left[\frac{x}{1-x^2} + b\right]\frac{dx}{dt} - cx^2 + cx = 0 \tag{7}$$

There are several approximations which can now be applied which greatly simplify equation (7) without substantial degradation of the problem in its present application.

We first consider the relative magnitude of the two terms in square brackets in equation (7). With $r \sim 2 \times 10^9$ cm, $m = (4/3)\,\pi\,r^3\,\rho$, $\rho \sim 1$ gm cm^{-3}, and $\eta \sim 10^{-4}$ poises (as, e. g., for liquid hydrogen), we find from equation (5) that $b \sim 10^{-22}$ sec^{-1}. There are no other choices of ρ and η under the preceding assumptions which will increase b very substantially. Consequently, except for very small values of x,

$$\frac{x}{1-x^2} \gg b \tag{8}$$

Small values of x apply only when the Red Spot is very close to the pole of rotation. Since we are only concerned with motions between middle and equatorial latitudes, inequality (8) can be adopted. Thus

the terms involving the coefficient b can be dropped in equations (7) and (4), and the latter equation reduces to

$$\frac{d^2\lambda}{dt^2} + c \cos\lambda \,|\sin\lambda| = 0 \tag{9}$$

This approximation remains valid as long as $b \ll 10^{-10}\ \text{sec}^{-1}$.

We have already mentioned the stability of the Red Spot over the past two centuries. For relatively small movements about $\lambda = -22^\circ$, we set $\cos\lambda\,|\sin\lambda| \approx$ const. ≈ 0.35, and solve the resulting simple differential equation under the boundary conditions that at $t = 0$, $\lambda = \lambda_0$, and $\frac{d\lambda}{dt} = 0$. It then follows that the drift in latitude due to the Eötvös-Lambert force is given by

$$\lambda - \lambda_0 \simeq -0.17\left(1 - \frac{\rho}{\rho_0}\right)\frac{r}{R^2}\, g_0 \left(\frac{5}{2}f - e\right)\tau^2 \tag{10}$$

With $\lambda - \lambda_0 < 10^\circ$ over $\tau > 130$ years, and setting $R = 7.14 \times 10^9$ cm, $r = 2 \times 10^9$ cm, $g_0 = 2.4 \times 10^3$ cm sec^{-2}, $P = 2\pi / \omega = 3.6 \times 10^4$ secs, and $e = 6.2 \times 10^{-2}$, we obtain that the observed drift in latitude is consistent under the preceding assumptions only if

$$1 - \frac{\rho}{\rho_0} < 5 \times 10^{-24} \tag{11}$$

It is, of course, unlikely in the extreme that an object floating in an incompressible fluid should be so close in density to the buoyant medium. The case of a compressible fluid will be discussed presently.

An escape from this conclusion exists if the viscosity of the flotation medium is very high ; as, for example, if the base of the Red Spot were floating in a medium comparable to that in which the terrestrial continents float ($\eta \sim 10^{21}$ poises). Then the first term in equation (4) can be neglected in comparison with the second, and the equation can be integrated with no further approximations as

$$\tau = \frac{b}{c}\, ln \left|\frac{\tan\lambda_0}{\tan\lambda}\right| \tag{12}$$

With the same choices of other parameters as in the previous case,

large values of η lead to quite reasonable values of $1 - \frac{\rho}{\rho_0}$. But it is easy to show that the large viscosities required to explain the small drift in latitude are incompatible with the much smaller viscosities required to explain the large drift in longitude.

The preceding discussion has assumed that $\eta \neq \eta\,(P, T)$. The temperature dependence of the viscosity is ordinarily slight; for $\eta \propto T^n$, n varies from 0.64 for He to 1.09 for NH_3. At very great pressures, however, as are certainly present deep in the atmosphere of Jupiter, eddy resistance carries away momentum, and the viscosity is a strong function of pressure. For some gases, e. g., for CO_2 at 100 atm, $\eta \propto P$. It should also be noted that the derivation of the Stokes force, eq. (3), in effect assumes that $\eta \neq \eta\,(P)$. However, whatever the effect of an increase in the viscosity over the values we have already adopted, it cannot be an effect *differential* in latitude and in longitude. Consequently, the previous conclusions remain unchanged. We conclude that a model Red Spot floating in *any* incompressible fluid is untenable.

If the Red Spot were immersed in a compressible medium, it would sink until the mean density of the Red Spot just equaled the mean density of the surrounding fluid. At first sight this would eliminate the objections to small values of $1 - \frac{\rho}{\rho_0}$ above. Since high densities are achieved below the clouds in the massive Jovian atmosphere, we proceed to consider a solid Red Spot floating in a dense compressible atmosphere.

For convective equilibrium, the difference in density between two atmospheric levels can be expressed as

$$\Delta\rho = \rho_1 \left[1 - \left(1 + \frac{\Gamma}{T_1} \Delta Z \right)^{\frac{1}{\gamma - 1}} \right] \tag{13}$$

where ρ_1 and T_1 are, respectively, the density and temperatures at the reference level, $\Gamma = -g/c_p$ is the dry adiabatic lapse rate, $\gamma = c_p/c_v$ is the ratio of specific heats, and ΔZ is the difference in altitude between the two levels.

The total angular momentum of the model Red Spot will be conserved. Since the mass and latitude of the Red Spot remain constant to first approximation, a change in angular velocity of rotation, $\omega(t)$, will be compensated by a change in the distance $R(t)$ of the Red Spot from the center of Jupiter. The conditions

$$R_1^2 \omega_1 = R_2^2 \omega_2 \tag{14}$$

and

$$R_1 - R_2 = \Delta Z \tag{15}$$

lead to

$$\Delta\bar{\rho} = \bar{\rho}\left\{1 - \left[1 + \frac{\Gamma R}{2T_1}\frac{\Delta\omega}{\bar{\omega}}\right]^{\frac{1}{\gamma-1}}\right\} \tag{16}$$

Equation (16) expresses the change in the mean density of the medium surrounding the Red Spot as a function of the change in angular velocity of the Red Spot.

At substantial depths in the atmosphere of Jupiter, the combination of absorption and scattering in and below the clouds will attenuate all but a very small fraction of the incident solar radiation. Isothermal conditions should be approached in the lower atmosphere, the extent depending on the existence of other energy sources. For an isothermal atmosphere, the analogue of equation(16) is

$$\Delta\bar{\rho} = \bar{\rho}\left\{1 - \exp\left[-\frac{R}{2\bar{H}}\frac{\Delta\omega}{\bar{\omega}}\right]\right\} \tag{17}$$

where $H = kT/mg$ is the scale height of the Jovian atmosphere at these depths. The true situation should lie somewhere between the extremes of eqs. (16) and (17).

During time-intervals of a year, changes in the period of rotation of the Red Spot of 3 or 4 seconds are not unusual (v., e. g., Peek, 1959, pp. 144-145). The mean period of rotation of the Red Spot during the past 130 years is some $9^h\,55^m$. Thus, in the course of a year,

$$\left|\frac{\Delta\omega}{\omega}\right| = \left|\frac{\Delta P_{rot}}{P_{rot}}\right| \sim 10^{-4} \tag{18}$$

For the evaluation of eqs. (16) and (17) through eq. (18), we adopt

$\Gamma = -4\ \mathrm{K^o/km}$, $T_1 = 180^o\ \mathrm{K}$, $\mu = 3.3$, and $\gamma = 4/3$, although any reasonable choices lead to similar numerical results. We find that for both the adiabatic and the isothermal cases,

$$\Delta \bar{\rho} / \bar{\rho} \sim 0.2 \tag{19}$$

i. e., conservation of angular momentum by a model Red Spot floating in a compressible atmosphere demands that, in the course of one year, the Red Spot must move in depth so that the effective density of its flotation medium varies by some twenty per cent. But then the difficulties posed by the Eötvös-Lambert force, and underlined by inequality (11), are still with us.

Another force on a floating object is the Pekeris stress, due to an assumed temperature difference between equator and poles at great depths (Pekeris, 1935). The Pekeris stress is clearly difficult to estimate for Jupiter. Although it is of opposite sign to the Eötvös-Lambert force, it is very doubtful that the magnitude will be at all similar and that an equilibrium could be attained. If it were necessary to save the floating Red Spot at all costs, such an equilibrium might be invoked.

In the preceding discussion, we have adopted as a computational device — it does not affect the character of the results — the assignment of an effective density $\bar{\rho}$ for the flotation medium. Actually, if the thickness of the Red Spot is comparable to its other dimensions, the density of the atmosphere varies by many orders of magnitude between its top and bottom. In such an atmosphere, the bottom of the Red Spot will float near that atmospheric level at which the ambient density equals the mean Red Spot density. Taking the value of cloudtop pressure and temperature and atmospheric structure previously adopted, and $\bar{\rho}_{RS} \sim 1\ \mathrm{gm\ cm^{-3}}$, we find that the base of the Red Spot is only ~ 100 km below the clouds for an isothermal atmosphere, and ~ 1000 km for an adiabatic atmosphere. If the depth of the Red Spot is to be at all comparable to its other dimensions, we require even for an adiabatic atmosphere below the clouds,

$$\bar{\rho}_{RS} > 10\ \mathrm{gm\ cm^{-3}} \tag{20}$$

If the composition of the Red Spot is to reflect cosmic abundances of the elements, the high mean density of inequality (20) must then indicate a high-pressure solid state phase transition.

The possibility that the Red Spot exists in at least two different solid phases was previously raised by Peek (1959 ; pp. 238 *et seq.*) in a not entirely successful attempt to correlate the albedo and angular acceleration of the Red Spot. Here, the phase transition suggests a possible escape from the problem associated with the Eötvös-Lambert latitude drift. At any given moment the Red Spot will be floating so that its mean density and the effective density of the flotation medium are just equal. At some depth below the top of the Red Spot, a phase transition boundary will exist, below which there is a discontinuous increase in the density of the solid. Now, as a consequence of an acceleration in longitude, conservation of angular momentum alters the depth of the Red Spot. If it rises, the phase transition boundary rides downwards within the solid body of the Red Spot, and its mean density decreases ; if it sinks, the boundary rides upwards, and its mean density increases. In either case, the mean density of the Red Spot changes to counterbalance — at least in part — the change in the effective density of the flotation medium caused by the bobbing of the Red Spot. The changes in level required to explain the angular acceleration of the Red Spot by conservation of angular momentum are only some tens of kilometers as can be seen from eqs. (13) and (16), and their isothermal analogues. Thus the rate of Red Spot bobbing will be < 1 mm/sec. It is therefore conceivable that the smooth motion of a pressure-induced phase-transition boundary up and down through the body of the Red Spot could just compensate the density difference between the Red Spot and the medium established by the bobbing, and thereby keep the Eötvos-Lambert drift in latitude within the observed limits. The hypothesis demands that the mean density of the Red Spot, averaged over both phases near the phase transition boundary, be proportional to the first power of the density of the surrounding medium at the

same level. A detailed test of this hypothesis must await a specification of the composition of the Red Spot and of the nature of the phase transition.

The only published alternative to the floating Red Spot model is that of Hide (1962). Hide shows that a topographical discontinuity in the solid surface of Jupiter, which is only a few kilometers high, but which has transverse dimensions comparable to those of the Red Spot, would suffice to produce a stagnant Taylor column extending to the Jovian cloud level. If the column were fixed to a uniformly rotating solid surface, the drift in longitude cannot be explained — in the last century there would have been times when the plateau was in one hemisphere and the column in the other. But if the solid surface rotated nonuniformly (only the system solid body plus atmosphere must conserve angular momentum), then Hide has shown that the drift in longitude, the absence of a drift in latitude, and several other observable dynamic features of the Red Spot are readily explained.

The meteorological hypothesis may also provide a natural explanation for the color of the Red Spot. In the original formulation of the model, the column is stagnant; there is no material exchange between the Red Spot and its surroundings, and very limited exchange between the top and the bottom of the column. However, the recent observations of Focas (1962) provide direct evidence for exchange through the boundaries of the Red Spot. If the meteorological hypothesis is to be preserved, we must require an energy source within the Red Spot column. Then the cell must be convective and will carry to the top of the atmosphere material characteristic of lower depths. It can be also expected to be the seat of thunderstorm activity. In laboratory experiments with simulated Jovian atmospheres, Sagan and Miller (1960) have shown that a variety of simple organic molecules, among them HCN, C_2H_2, C_2H_4, C_2H_6, and CH_3CN, are produced in high yield by electric discharges. Similar molecules should be produced by ultraviolet light in the Jovian atmosphere and should be carried to lower depths.

It is noteworthy that many of the polymerization and interaction products of these molecules are colored red or yellow ; the acetylene polymer cuprene was first suggested in this connection by Urey (1952). It therefore seems possible that the coloration of the Red Spot is due to organic molecules produced there by electrical discharge ; or produced by ultraviolet light in the whole atmosphere, carried to great depths, and then convectively recirculated to the top of the atmosphere in the Red Spot. High dispersion visible spectra, or lower dispersion infrared spectra of the Red Spot would help to check this suggestion.

We conclude that the hypothesis of a floating Red Spot is generally unsatisfactory, unless a particularly favorable solid state phase transition should be operating ; with a wobbly Jovian solid body, the meteorological hypothesis has several satisfactory aspects and is probably to be preferred at the present time.

ACKNOWLEDGEMENT

I am grateful to Dr. R. Hide for several stimulating discussions. This work was supported by grant NsG-126-61 from the National Aeronautics and Space Administration.

REFERENCES

J. H. FOCAS, This symposium.

R. HIDE, This symposium.

G. W. HOUGH, *Pop. Astron.*, **121**, 1905.

H. JEFFREYS, *The Earth*, Cambridge : The University Press, 1959.

W. D. LAMBERT, *Amer. J. Sci.*, 5th Series, **2**, 129, 1921.

E. J. ÖPIK, *Icarus*, **1**, 200, 1962.

B. M. PEEK, *The Planet Jupiter*, London : Faber and Faber, 1958.

C. L. PEKERIS, *Mon. Not. Geol. Soc.*, **3**, 343, 1935.

C. SAGAN and S. L. MILLER, *A. J.*, **65**, 499, 1960.

H. C. UREY, *The Planets*, New Haven : Yale University Press, 1952.

R. WILDT, *Proc. Amer. Philos. Soc.*, **81**, 135, 1939.

R. WILDT, *Planets and Satellites*, G. P. KUIPER and B. M. MIDDLEHURST, eds., Chicago : University of Chicago Press, 1961.

F. R. ZABRISKIE, *A. J.*, **67**, 168, 1962.

50. — OPTICS AND GEOMETRY OF THE MATTER OF SATURN'S RINGS

M. S. BOBROV
Astronomical Council of the USSR Academy of Sciences, U.S.S.R.

Introduction

The system of Saturn's rings is an object of considerable interest not only for planetary physics, but also for meteoric astronomy and for the cosmogony of the solar system.

The present report is a brief review of the results obtained by the author from 1939 to 1962. The majority of the results concerns the B-ring as for this ring the observational data are more complete than for the A- and C-rings.

Optical characteristics of the B-ring and their interpretation

The first important photometric characteristic of the matter of the B-ring is the absolute surface brightness of the most intensive zone in the ansae in an opposition. It may be estimated to 0.62 in units of that of white orthotropic screen normal to incident solar radiation, with probable error of 0.14, or 22 %.

This estimation is based on the stellar magnitude of Saturn without rings in a mean opposition ($+ 0^{m}.89$ in Harvard visual system ; Russell, 1916), on the observed limb darkening of Saturn's disc (Schoenberg, 1921 ; Barabasheff and Semejkin, 1933 ; Sharonov, 1941 ; Barabasheff and Chekirda, 1952 ; Lebedinets, 1957 ; Camichel, 1958) and on the assumption that in opposition the brightness of the B-ring in the ansae is equal to that of the center of Saturn's disc (Schoenberg, 1933).

Another important characteristic is the optical thickness of the ring (for normal beam). Its value is still uncertain, but the results of the 8-magnitude star occultation by this ring (Westfall,

1958) show that it is only slightly greater than that of the A-ring. The latter may be estimated very accurately from the photometry of Dr. Camichel (1958) to 0.5-0.7. So, the optical thickness of the B-ring may hardly exceed 1.0-1.5.

Having the values of these two characteristics and applying to the ring the theory of the multiple light scattering for the flat layer of non-absorbing particles, we may easily show that the diffraction scattering cannot account for the observed high brightness of the ring. Indeed, the computations with the aid of the formulas and tables of the light scattering theory (Sobolev, 1949 ; Chandrasekhar, 1950 ; Chandrasekhar et al., 1952) show that the ring matter reflects backwards (to the Sun) about 3.5 times more radiation than an isotropic white scatterer (Bobrov, 1951). It is approximately ten times more than from a layer of microscopic dielectric spheres with refractive index of 1.33.

On the contrary, the concept of large light-grey particles with very rough surface (Bobrov, 1951, 1952) covered with hoarfrost or snow (Kuiper, 1949, 1957 ; Moroz, 1961) is in very good agreement with this result as well as with the form of the phase curve of the ring. If we adopt the roughness of particles equal to that of the Moon and Mercury, we obtain for the albedo of an individual particle the value of 0.6-0.7 (Bobrov, 1952, 1959).

Geometric thickness of the rings

This characteristic may be obtained from observations at high altitude observatories either at the moment the Earth is crossing the ring-plane or when the Earth it at the dark side of the rings ; in the latter case, an observer may detect the bright line of the edge at the nearest border of the dark side.

Similar conditions were realized in E. C. Slipher's observations on February, 1921, especially on February 20 (Slipher, 1922). The bright edge of the dark side was not detected. In E. C. Slipher's conditions it is evident that the thickness of the rings is less than

2-4 km. Unfortunately the moment of the ring-plane passage by the Earth was missed. If it was not, E. C. Slipher could still see the rings precisely edge-on if they were as thin as 0.5 km. Such favourable conditions did not take place since that time, but the passages of 1965-1966 will be very favourable.

Phase effect of the rings and its interpretation

I should like to remind that the stellar magnitude of the brightness of the A- and B-rings shows a pronounced and non-linear phase effect, the variation of magnitude being the stronger the less is the phase angle α. The full amplitude of the effect has an order of 0.5 magnitude in spite of the fact that the maximum value of the phase angle cannot exceed 6 ½ degrees. As the role of the diffraction scattering is small the phase effect may be interpreted in terms of geometrical optics.

Seeliger (1887, 1893) was the first who developed a theory of purely geometric collective phase effect of macroscopic particles (shadow effect theory) with specia lattention to Saturn's rings. Seeliger's assumption that the Sun may be treated as a point

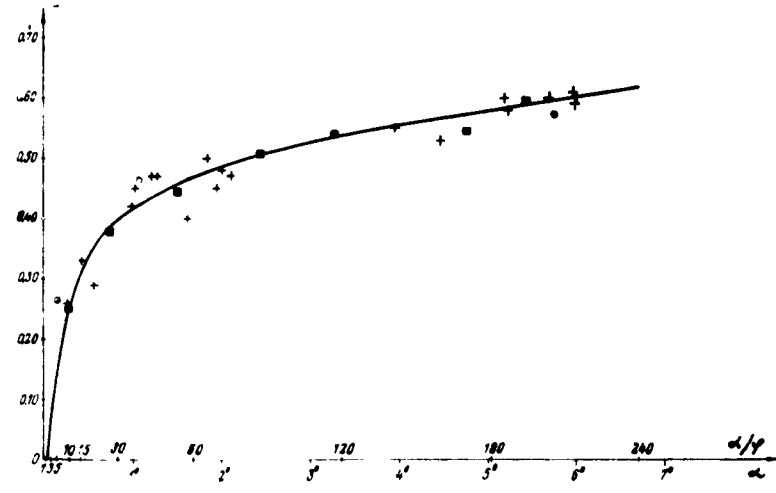

Fig. 1

source led to the disagreement of his theory with observations The improved shadow theory developed by the author (Bobrov, 1940, 1951, 1952, 1954, 1956, 1959, 1960) takes into account finite angular dimensions of the solar disc and the scattering of higher orders. New theoretical phase curve of the B-ring was computed and it was found to be in good agreement with observational data (Bobrov, 1959, see Fig. 1).

Hence the following parameters of the matter of the rings may be obtained : the volume density D has an order of 3.10^{-3}, the total mass of the rings varies from $4.10^{-9}\,M_{\text{ħ}}$ to $4.10^{-7}\,M_{\text{ħ}}$, the average radius of particles ranging from 10 cm to 10 m. It was found that the particles of the B-ring show a strong individual phase effect with the phase coefficient of about $0^{m}.024$ pro 1° of phase. This is an evidence of the fact that the roughness of the particles is greater than that of the Moon and Mercury and is comparable to that of some asteroids, such as Metida, Nioba, Meleta, Tyche, Frigga (see Putilin, 1953).

THE SHADOW EFFECT IN THE CASE WHEN PARTICLES ARE OF UNEQUAL SIZE

The former results were obtained assuming that all the particles were equal in size. A further approximation is a model with particles of unequal sizes (Bobrov, 1961). It was assumed that the radii of particles have a dispersion from ρ_1 to ρ_2 which may be expressed by the equation : $dN = K\rho^{-s}\,d\rho$, dN being the number of particles with radii from ρ to $\rho + d\rho$, K and s-constants. For this model a general formula was derived for b_0/b_{as} as a function of D, τ_0 and s, b_0 and b_{as} denoting the brightness of the ring respectively at opposition ($\alpha = 0$) and at $\alpha = \max$, D being the volume density, τ_0 the optical thickness, and s the exponent in the law of dispersion.

Numerical computations were made for $s = \frac{5}{2}$, 3 and $\frac{7}{2}$, and $\tau_0 = 0.7$ and 1.0. The results may be summarized as follows :

1. If the dispersion interval is wide (i. e. it includes not only macroscopic particles but also fine dust with ρ_1 down to 10^{-4} cm), an agreement with observations (a sufficiently intensive shadow effect) may be obtained only for $s < 3$.

2. The estimations of the volume density D of the B-ring found with the model without dispersion should now be revised. The new values will be higher but likely not more than by one order.

Recommendations for observers

The observational data of Saturn's rings are still incomplete and non-professional. Further observations with big instruments are very desirable. Of special interest are : (a) observations of occultations of stars by rings, (b) observations (including at high altitude observatories) at the moments when the Earth is crossing the ring-plane, and (c) electrophotometry of the phase-effect (rings B and A).

REFERENCES

N. P. Barabashefr and A. T. Chekirda, *Kharkov Obs. Contr.*, **2**, 9, 1952.

N. P. Barabashefr and B. E. Semejkin, *Astron. J. USSR*, **10**, 381, 1933.

M. S. Bobrov, *Astron. J. USSR*, **17**, N. 6, 1, 1940.

— *Doklady Acad. Sci. USSR*, **77**, 581, 1951.

— *Astron. J. USSR*, **29**, 334, 1952.

— *Astron. J. USSR*, **31**, 41, 1954.

— *Astron. J. USSR*, **33**, 904, 1956.

— *Astron. J. USSR*, **36**, 129, 1959.

— *Astron. J. USSR*, **37**, 306, 1960.

— *Astron. J. USSR*, **38**, 669, 1961.

H. Camichel, *Ann. d'Astrophys.*, **21**, 231. 1958.

S. Chandrasekhar, Radiation Transfer, 1950.

S. Chandrasekhar, D. Elbert, A. Franklin, *Astrophys. J.*, **115**, 244, 1952.

G. P. Kuiper, The Atmospheres of the Earth and Planets, 1949.

— *Trans. I. A. U.*, **8**, 213, 1957.

V. N. Lebedinets, *Kharkov Obs. Contr.*, 12, 167, 1957.

V. I. Moroz, *Astron. J. USSR*, 38, 1060, 1961.

I. I. Putilin, Minor Planets (in Russian), 1953.

H. N. Russell, *Astrophys. J.*, 43, 103, 1916.

E. Schoenberg, *Ann. Acad. Sci. Fennicae*, A, 16, 1921.

— *Vierteljaresschr. Astron. Ges.*, 68, 387, 1933.

H. H. Seeliger, *Abh. Bay. Acad. Wiss., II Kl.*, 16, 467, 1887.

— *Abh. Bay. Acad. Wiss, II Kl.*, 18, 1, 1893.

V. V. Shabonov, *Poulkovo Obs. Circ.*, N. 26-27, 37, 1941.

E. C. Slipher, *Popular Astron.*, 30, 8, 1922.

V. V. Sobolev, *Leningrad Univ. Contr., Ser. Math.*, N. 18, 17, 1949.

J. E. Westfall, *J. Brit. Astron. Ass.*, 68, 57, 1958.

51. — PHOTOMÉTRIE DE JUPITER ET DE SATURNE A PARTIR DE CLICHÉS OBTENUS AVEC LA CAMERA ÉLECTRONIQUE

MONIQUE BELLIER, MARIE-FRANÇOISE DUPRÉ, GÉRARD WLÉRICK, JEAN RÖSCH et JACQUES ARSAC
Observatoire de Paris-Meudon et Observatoire du Pic du Midi, France

INTRODUCTION.

Dans le cadre d'une étude des grosses Planètes au moyen de la caméra électronique Lallemand, nous avons obtenu des clichés de Jupiter et de Saturne en septembre 1960 et juillet 1961. Les premiers résultats de cette étude ont été présentés lors du Deuxième Symposium sur les Récepteurs Photoélectriques d'Images (Londres, septembre 1961) et nous appellerons article I cette communication (1) Trois photographies électroniques de Saturne ont été analysées par l'un des auteurs (2) et, à l'heure actuelle, l'étude détaillée de l'ensemble des clichés est assez avancée.

Dans la présente communication, nous nous proposons d'une part de rappeler schématiquement les avantages que présente la photographie électronique système Lallemand pour l'étude des Planètes, d'autre part de signaler quelques résultats nouveaux obtenus à partir des premiers clichés.

Pour la description de la caméra, nous renvoyons aux publications de Lallemand (3), de Lallemand et Duchesne (4) et à deux articles plus récents (5,6).

RAPPEL DES PROPRIÉTÉS DE LA PHOTOGRAPHIE ÉLECTRONIQUE.

1. — Les électrons émis par la photocathode sont enregistrés *directement* dans une émulsion nucléaire, ce qui garantit les performances maximum.

2. — On enregistre *toutes* les informations, en raison des propriétés suivantes :

a. absence de seuil ;

b. rendement élevé et constant : 10 photons donnent un photoélectron, qui donne une trace ([7]) ;

c. réponse linéaire, en raison des deux propriétés précédentes ; la densité est proportionnelle à l'éclairement, au moins aux faibles densités ([6,9]) ;

d. photographie fidèle, en raison de la correspondance exacte entre le point d'émission du photoélectron et sa trace dans l'émulsion.

3. — L'émulsion ne présente pas de voile, et les très faibles densités peuvent se mesurer correctement.

4. — Les trois propriétés précédentes permettent une photométrie précise dans une gamme étendue d'éclairement.

Intérêt de la photographie électronique pour l'étude des Planètes.

En photographie planétaire classique on se heurte aux difficultés suivantes :

a. Poses trop longues avec brouillage des informations par la turbulence atmosphérique.

b. Emploi d'émulsions rapides à grains moyens ou gros (pas assez d'informations enregistrées).

c. Caractéristique défavorable de l'émulsion : si les parties brillantes d'une Planète sont correctement enregistrées, les parties les plus sombres peuvent ne pas être enregistrées du tout.

La photographie électronique permet de surmonter ces difficultés. Dans l'article I, nous avons indiqué les conditions de prise des clichés et de leur analyse : instrumentation photoélectrique et optique, grandeur des images, temps de pose, microphotométrie, etc.

Dans le même article, nous avons présenté deux photographies de Jupiter prises le 9 juillet 1961 et les courbes de variation de la brillance suivant l'axe Nord-Sud de la Planète. Ici nous comparons, figure 1, trois coupes Est-Ouest déduites de l'un de ces clichés.

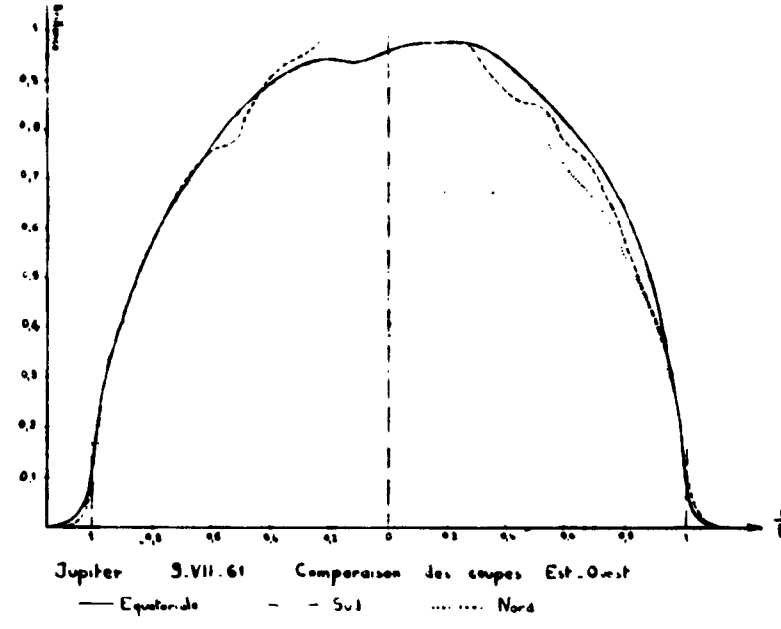

Fig. 1

La première coupe a été faite suivant le diamètre équatorial tandis que les deux autres suivent le milieu des bandes tropicales Nord et Sud. Comme ces diagrammes sont destinés à la mesure de l'assombrissement centre-bord moyen, nous avons omis tous les petits accidents morphologiques bien qu'ils soient caractéristiques de la surface de Jupiter. Seules les variations de brillance à grande échelle ont été conservées. Pour la comparaison, nous avons choisi comme point de référence un point du bord Est où la brillance est les 6/10 de la brillance maximum de la région équatoriale. Les courbes fournissent les résultats suivants :

a. A la longueur d'onde utilisée, $\lambda = 5850$ Å, l'assombrissement est important. Ainsi pour $r/R = 0{,}9$, on trouve : $B_{0,9} \simeq 0{,}45\ B_{max}$.

b. On peut encore mesurer la brillance à $r/R = 0{,}95$ et il est possible de la calculer plus près du bord en faisant une correction tenant compte des diverses causes d'étalement. Nous reviendrons sur ce point lors de l'étude de Saturne.

c. L'assombrissement de la zone équatoriale n'est pas très différent de celui des bandes tropicales. On remarque seulement que, dans le cas présent, la dissymétrie entre les bords Est et Ouest due en majeure partie à la phase, semble un peu plus prononcée pour la zone équatoriale.

Il ressort de cette première analyse que les accidents photométriques de la surface de Jupiter sont si importants qu'il semble souhaitable d'utiliser une autre méthode pour déterminer l'assombrissement centre-bord : on peut, par exemple, prendre une série de photographies de la Planète étalées sur une demi rotation au moins et établir les courbes d'assombrissement de régions bien définies du disque.

Photométrie de Saturne.

Nous avons montré [1,2] que la photographie électronique est bien adaptée à l'étude photométrique des anneaux de Saturne, en particulier du faible anneau de crèpe C. Dans l'article I, nous avons publié plusieurs photographies de cette Planète, une coupe photométrique Est-Ouest et le modèle correspondant pour les anneaux. D'autres coupes Est-Ouest et Nord-Sud ont été établies et analysées [2].

Depuis, il nous a semblé intéressant, à titre expérimental, de déterminer le contenu en information des clichés. En d'autres termes, nous avons cherché quels étaient les plus petits détails significatifs des coupes photométriques. Cette recherche ne présenterait aucune difficulté en l'absence des fluctuations dues à la

granularité et aux défauts de l'ensemble photocathode-émulsion. Heureusement, avec les émulsions à grains fins Ilford C 2 et K 2, les fluctuations sont peu importantes et nous avons pu tracer, avec une approximation suffisante, la courbe moyenne que l'on obtiendrait en l'absence de grain. Nous pensons que les erreurs qui se sont glissées dans le tracé n'altèrent pas sensiblement le résultat.

La planche I présente trois tirages différents du cliché étudié ici et la figure 2 montre la coupe Est-Ouest correspondante. On remarque :

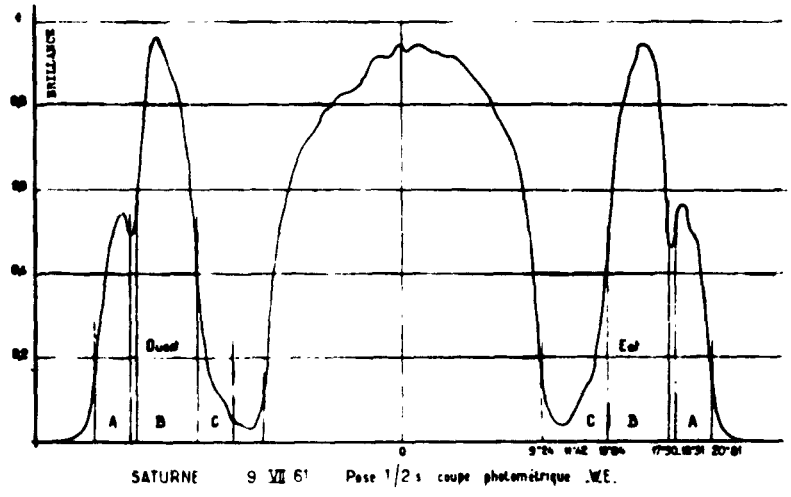

Fig 2

a. La dissymétrie Est-Ouest du disque (phase).

b. La différence de profondeur de la division de Cassini à l'Est et à l'Ouest (qualité différente des images aux points considérés).

c. La présence de plusieurs points d'inflexion en particulier dans la partie intérieure de l'anneau B, à l'Ouest.

A l'extérieur de l'anneau A, les pieds de la courbe correspondent à l'étalement local des images et permettent de déterminer celui-ci

Photographie électronique de Saturne - Pic du Midi — 9 juillet 1961. — Lunette de 60 cm de diamètre F/60 — Plaques Ilford K2 — pose 1/2 sec. 3 tirages sur papier du même négatif original — le tirage le plus blanc montre l'anneau de crêpe.

si on fait une hypothèse sur la répartition de la brillance. Nous avons admis que, à la limite de l'anneau, la brillance passe sans transition d'une valeur finie à une valeur nulle.

Modèle en créneaux. Première méthode.

Grâce à l'hypothèse précédente, nous avons obtenu une fonction d'étalement *moyenne* et admis, en première approximation, sa validité pour l'ensemble de la coupe Est-Ouest. La figure 3 représente cette fonction pour une ligne. Dans un premier calcul,

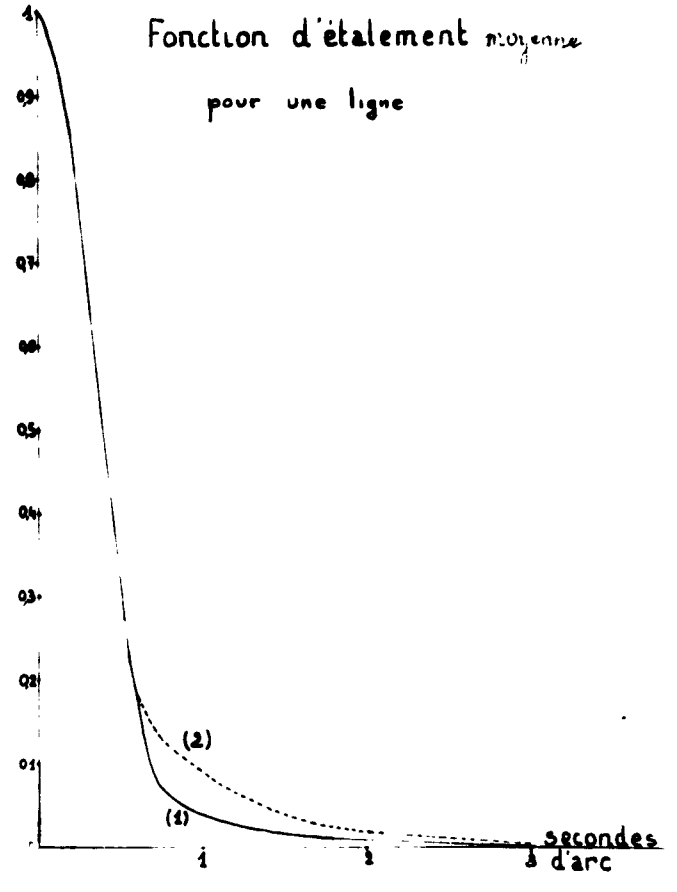

Fig. 3

nous avons utilisé la courbe 1. Par la suite, nous nous sommes servis de la courbe 2, à pied plus étalé. En fait les deux courbes conduisent à des résultats peu différents. L'intégration de la courbe 2 conduit à la courbe de la figure 4 valable pour un demi-plan. Cette dernière courbe doit présenter le même pied moyen que la coupe Est-Ouest de la figure 2.

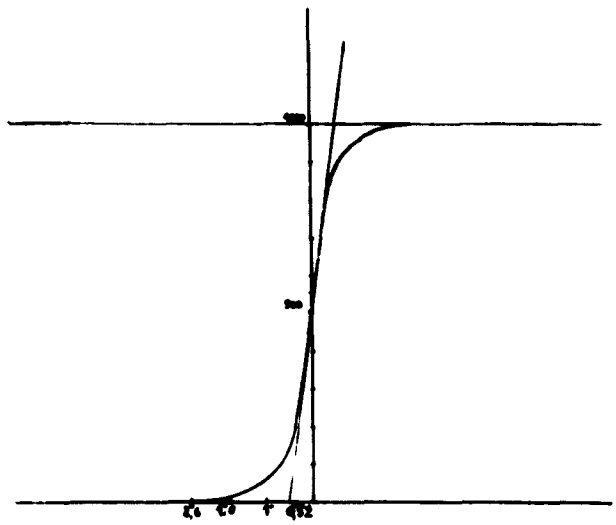

Fig. 4. — Fonction d'étalement pour un demi-plan.

Comme dans l'article I, nous avons établi un modèle en créneaux de la Planète. La méthode consiste à déterminer intuitivement le modèle, à l'étaler et à vérifier a posteriori l'accord avec la coupe photométrique. A défaut, on recommence. Pour le présent travail, nous avons disposé de la calculatrice IBM 650 de l'Observatoire de Paris-Meudon, qui opère un calcul d'étalement en 30 secondes environ. Nous avons pris la largeur du créneau élémentaire égale à 0.″40 et nous avons pensé qu'il était suffisant pour l'étude des anneaux de chercher un modèle présentant la symétrie Est-Ouest.

Le modèle moyen de la figure 5 a les propriétés suivantes :

a. Il représente mal le disque, qui est dissymétrique (phase).

b. L'anneau A peut être décrit par deux créneaux, la partie intérieure étant la plus brillante, comme l'ont noté LYOT ([10]) et DOLLFUS ([11]).

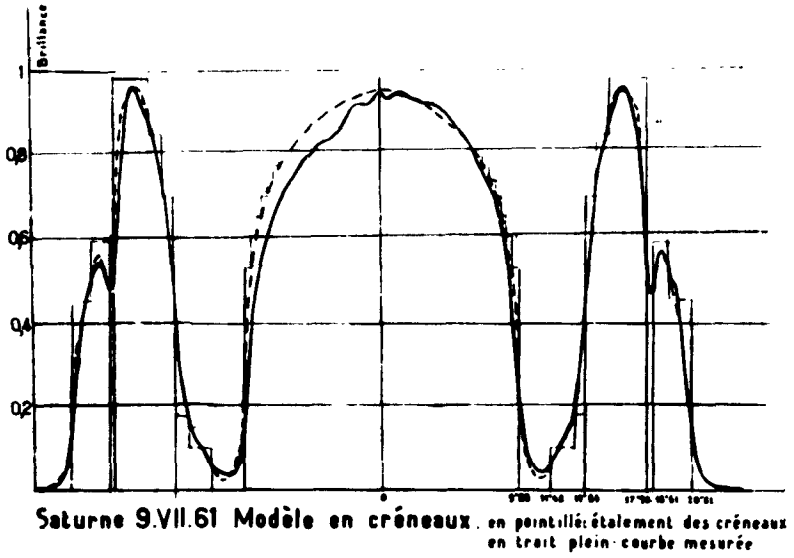

Fig 5

c. L'anneau B est bien représenté par 3 créneaux de largeurs relatives 1/5, 1/5 et 3/5. Leurs séparations correspondent à des divisions mineures prévues par la Mécanique céleste.

d. L'anneau C est constitué par deux créneaux de largeur 2/3 et 1/3 et de brillance 0,10 et 0,18, l'unité correspondant au point le plus brillant du disque. Les calculs étant simples et rapides, nous avons essayé plusieurs modèles pour cet anneau (variation régulière de brillance de 0,10 à 0,15 ; variation régulière de 0,10 à 0,18 avec ou sans division entre B et C ; etc.). Les autres modèles ne donnent pas un accord aussi bon.

MODÈLE EN CRÉNEAUX. DEUXIÈME MÉTHODE.

On pourrait, en appliquant la méthode précédente, construire une succession de modèles représentant de mieux en mieux, après étalement, la courbe expérimentale. Nous avons préféré opérer plus

systématiquement : étant données une courbe expérimentale d'une part, une courbe d'étalement d'autre part, nous avons utilisé une méthode de calcul permettant de restituer, par une suite d'approximations, la courbe correspondant à un étalement nul.

La signification de ce calcul est limitée par les deux points suivants :

1° *Le bruit.* Il reste nécessairement du bruit dans la courbe expérimentale lissée de la figure 2. La restitution qui redonne leur valeur propre aux détails réels crée donc aussi des détails artificiels dûs au bruit.

Ceci conduit à définir un seuil au-dessous duquel on considère, par sécurité, que les détails ne sont pas significatifs et on arrête le calcul de restitution dès que l'écart entre la courbe expérimentale et la courbe restituée puis étalée est inférieur à ce seuil en chaque point. Par suite le problème n'a pas une solution unique. Il existe une série de solutions différant seulement par leur structure fine et le calcul fournit l'une d'elles.

2° *La turbulence atmosphérique.* La photographie électronique des étoiles doubles nous a déjà amené à considérer l'altération des images par la turbulence atmosphérique ([12, 13]). Avec un objectif de 60 cm de diamètre, l'altération instantanée est bien la même pour des directions faisant un angle de 2 à 3″ mais il est peu probable qu'il en soit ainsi pour des directions dix fois plus écartées.

Cependant, les poses sur Saturne ont duré une demi-seconde et ceci conduit par intégration à une altération moins hétérogène. En fait, on constate que l'étalement de l'image est, aux erreurs de dépouillement près, exactement le même aux deux points extrêmes de l'anneau A. Ceci n'est probablement pas entièrement fortuit et par suite on peut espérer que l'étalement a été assez semblable tout le long du diamètre principal de Saturne.

Le programme de calcul a été établi par l'un de nous (J. A.), qui a montré la convergence de la méthode itérative de Van Cittert. Nous avons choisi la valeur 0,5 % comme seuil correspondant au résidu de bruit contenu dans la figure 2 et nous avons utilisé à

nouveau un modèle en créneaux de largeur élémentaire 0''.40. Cette dimension s'est révélée très convenable mais une discussion nous a montré depuis que des créneaux moins larges permettraient une adaptation plus aisée aux variations rapides de brillance de Saturne. Avec la calculatrice IBM 650 le calcul entier dure un peu moins d'une heure.

Les résultats apparaissent sur les figures 6 et 7. La dernière représente la solution correspondant au seuil choisi. Elle a été obtenue après 17 itérations ce qui indique que la convergence n'est pas très rapide. La première qui représente le résultat à un stade intermédiaire, après 8 itérations, montre que la restitution est déjà terminée à ce stade, sauf dans quelques régions à très forte pente telles que la partie intérieure de l'anneau B à l'Ouest ou la division de Cassini à l'Est.

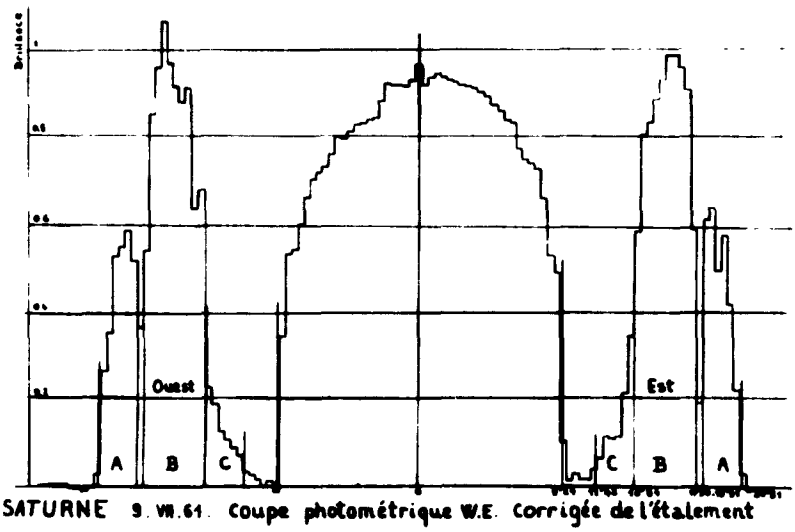

Fig. 6

La figure 7 conduit aux remarques suivantes :

1° Les bords extérieurs de l'anneau A sont assez abrupts. La fonction d'étalement utilisée est donc une bonne approximation de celle qui correspond à l'hypothèse faite.

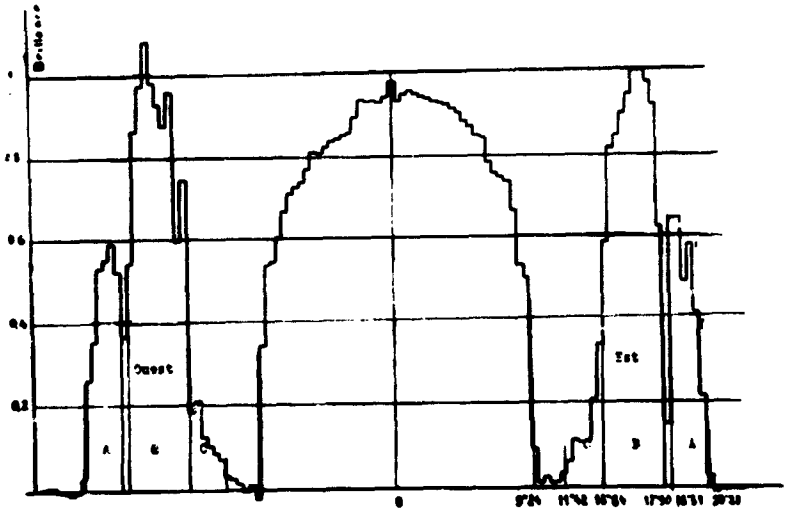

Fig. 7. — Saturne 9.VII.61 Coupe Photométrique W.E.
corrigée de l'étalement. — Solution obtenue après 17 itérations.

2° Pour étudier les dimensions relatives du disque et des anneaux, nous avons pris comme référence la division de Cassini. On voit alors qu'il existe un bon accord avec les positions tirées de l'American Ephemeris, portées en abscisse. Cependant le diamètre équatorial du disque semble un peu plus petit que la valeur admise.

3° L'anneau B à l'Ouest présente deux minima qui sont liés à l'existence de points d'inflexion sur la courbe de la figure 2. Le minimum intérieur a été observé par LYOT ([10]) et par DOLLFUS ([11]) tandis que le deuxième coïncide avec une division faible prévue par la mécanique céleste.

4° A l'Ouest, un minimum très peu profond apparaît à la partie extérieure de l'anneau C, à un endroit où LYOT a observé une division ([10]).

5° A l'Est, l'anneau A présente le renforcement de brillance caractéristique de sa partie interne et un minimum qui correspond sans doute à la série de minima notés par les observateurs visuels.

Ainsi la restitution a fait apparaître de nombreux détails

et il est satisfaisant de constater que tous ces détails coïncident avec des observations visuelles sûres ou avec des prédictions théoriques. Mais on constate aussi qu'elle n'a pas fait apparaître les mêmes structures fines à l'Est et à l'Ouest. En fait, ceci était prévisible. On constate en effet sur la figure 2 que si les côtés Est et Ouest sont absolument semblables dans leurs grandes lignes, ils présentent cependant de petites différences qui après restitution correspondent à des structures assez caractérisées. Le cas de la division de Cassini, dont nous savons par d'autres clichés pris au même moment que la dissymétrie apparente entre l'Est et l'Ouest est due essentiellement à une différence dans l'altération des images, nous incline à penser plus généralement que les dissemblances observées peuvent être, pour une large part, attribuées à de telles variations de l'altération d'un point à un autre.

De petites erreurs de dépouillement ont pu jouer également un rôle. Ainsi la méthode de restitution, à cause de sa puissance même, exige de grandes précautions. Nous pensons l'appliquer ultérieurement avec une précision accrue en utilisant en particulier des images plus grandes pour lesquelles les phénomènes de bruit deviendront encore plus négligeables.

Conclusion.

La photographie électronique des planètes présente les propriétés suivantes :

a. Elle permet d'obtenir des clichés avec des poses suffisamment courtes pour que la turbulence atmosphérique ne brouille pas les informations.

b. Ces clichés, sur lesquels les parties sombres sont aussi bien enregistrées que les parties brillantes, se prêtent bien à une photométrie précise.

c. Ils contiennent beaucoup d'informations et il est possible de mettre en évidence leurs détails fins par une méthode poussée de restitution parce que le niveau de bruit dû au grain est suffisamment faible.

Nous remercions Mademoiselle Ghertzman qui nous a aidés à dépouiller certains enregistrements microphotométriques.

RÉFÉRENCES

(1) G. Wlérick, J. Rösch, M. F. Dupré et M. Bellier, « La photographie électronique des planètes et ses applications photométriques », *Advances in Electronics and Electron Physics*, **16**, 371, Academic Press, 1962.

(2) M. F. Dupré, Photométrie de Saturne à partir de clichés pris avec la caméra électronique (Diplôme d'Études Supérieures, Paris, 1962).

(3) A. Lallemand, *Comptes Rendus*, **203**, 243, 390, 1936.

(4) A. Lallemand et M. Duchesne, *Comptes Rendus*, **233**, 305, 1951 ; **235**. 503 ; **238**, 335, 1954 ; **240**, 1329, 1955.

(5) A. Lallemand, M. Duchesne, G. Wlérick. *Advances in Electronics and Electron Physics*, **12**, 5, Academic Press, New York, 1960.

(6) A. Lallemand, M. Duchesne, G. Wlérick, R. Augarde, M. F. Dupré, *Annales d'Astrophysique*, **23**, 320, 1960.

(7) A. Lallemand, M. Duchesne, L. Goldzahl, J. Duflo et J. Banaigs, *Comptes Rendus*, **248**, 2191, 1959.

(8) P. Vernier, *Bull. Astron. Obs. Paris*, **22**, 83, 1958-59.

(9) M. Duchesne et P. Meallet, *Comptes Rendus*, **254**, 1400, 1962.

(10) B. Lyot, *l'Astronomie*, **67**, 12, 1953.

(11) A. Dollfus dans « *Planets and Satellites* » édité par G. Kuiper & B. Middlehurst, p. 568, University of Chicago Press, 1961.

(12) J. Rösch, G. Wlérick, M. F. Dupré, *Comptes Rendus*, **252**, p. 509, 1961.

(13) J. Rösch, G. Wlérick, C. Boussuge, *Advances in Electronics and Electron Physics*, **16**, 357, Academic Press, New York, 1962.

52. — PRELIMINARY RESULTS CONCERNING THE ATMOSPHERIC ACTIVITY OF JUPITER AND SATURN

J. H. FOCAS
Athens Observatory, Greece

General

With regard to the evolution of the jovian atmospheric phenomena, the following precisions can be made :

— The apparition of brilliantly white and dark matter on Jupiter, is the prominent character of atmospheric activity on this planet.

— The apparent amount of brilliantly white and dark matter gives evidence of the intensity of the atmospheric activity.

— The knowledge of the fine structure of the jovian features allows their classification by forms, brilliancy, dimensions, time of apparition and life time within the cycle of activity and level in the atmosphere.

— The study of the ascending, descending, lateral and vortical motions of brilliant and dark matter, allows conclusions on the dynamics of the jovian atmosphere.

— The manifestations of atmospheric activity are identical for the whole planet irrespectively of the zenographical latitude ; the scale and intensity of the phenomena vary with the zenographical latitude.

— Distribution and motion of the jovian markings as a whole characterize a zonal circulation. Meridian circulation in the cells is evident.

— The total activity on the planet during the last 100 years seems to be stronger in the southern hemisphere.

— The minimum intensity of the total activity for the whole planet seems to follow a 20-22 years cycle.

— The propagation of the activity by starting cycle seems to be effected from 40-45° of zenographical latitude towards the equator ; it changes (opposite) direction in the course of the 20-22 years cycle.

— In the case of Saturn, activity shows propagation from 45-50° of cronographic latitude towards the poles.

Observational data

a. Visual observations and measures taken in the period 1857-1962 by : different observers 1857-1880 ; Lohse, Potsdam 1881-1909 ; British Astron. Assoc. and Lau, 1910-1923 ; S. Plakidis, Athens, 1924-1933 ; J. H. Focas, Athens 1933-1962.

b. Photographs taken by : B. Lyot and H. Camichel (for the most part), Pic-du-Midi 1914-1958 ; J. H. Focas, Athens 1953-1962.

c. Polarimetric observations taken by : B. Lyot, Meudon 1923-1926; A. Dollfus, Pic-du-Midi 1951-1955; J. H. Focas, Athens 1955-1961.

Connection between brilliant and dark matter :

— The white-yellowish zones of Jupiter examined under perfect seeing conditions with a high resolving power show a cumuliform structure of approx. 1 sec. arc size. This is the aspect of the inactive areas and should not be confused with the brilliant spots of a few seconds of arc size, characterizing the disturbed areas.

— The starting stage of the jovian activity is cataclysmic. Paroxysm is manifested by the apparition, on the said cumuliform ground, of brilliantly white spots as isolated units, couples or families ; these spots appear suddenly on one or more points of the atmospheric cells ; for the most part of the cases paroxysm propagates along the axes of the cells oppositely to the direction of rotation of the planet (successive apparition of such spots on increasing longi-

tudes). In some cases the disturbance develops simultaneously either part of a given point of the cell. The life time of these spots varies from a few days to several weeks. The repartition of the energy in the cells seems to be non homogenous. (Fig. I and 2).

— The stage following the paroxysm is marked by the apparition of dark nodes at the following end of the brilliant spots ; dark matter as a rule, follows brilliant matter. The dark nodes are the emanation points of dark filamentary strips. Such strips moving polewards, oppositely to the direction of rotation of the planet, spread along the axes of the cells and result into dark belts. At this initial stage the belts reach their maximum darkening. The longitudinal distribution of dark matter in the cells is closely connected with brilliant matter.

Time elapsed between the apparition of brilliant matter and the formation of the belts, in principle, does not exceed one year (Fig. 3).

— The stage following the formation of the belts is characterized by the apparition by intervals, of brilliant spots in the middle of the dark or semi-dark belts or at their boundaries. Brilliant matter appearing among dark matter provokes a pressional effect and deviation of the latter ; dark belts become suddenly broader when brilliant matter appears along their central axis. Brilliant matter appearing at the boundaries of the belts provokes curvature of the components inwards.

The apparition of bright matter and the resulting deviation of dark matter denote ascending motion of bright matter in the cells.

— In the case of narrow bands, bright spots appear first below the bands, these latter being projected in front of the bright spots ; in their ascending motion the bright spots break the bands up.

— Dark bands are broken up by bright spots being in lateral motion. (Fig. 5 and 6).

— Dark nodes created at the boundaries of brilliant spots are the emanation points of narrow strips of a spiral aspect. Such brilliant spots and strips as a whole characterize a vortex system.

Dark matter being at the vicinity of bright spots in vortical motion is attracted towards the bright spots as by a suction effect.

— Filamentary strips connected with brilliant spots in vortical motion are visible up to the circumpolar areas of Jupiter, more pronounced in the equatorial and adjacent areas, less pronounced in high latitudes due to absorption. Such formations on Saturn, thanks to the favourable inclination of the axis of rotation of this planet, are visible up to the poles.

Strips develop under a screw-like form. Strips created in one hemisphere are sometimes crossing the equator and ride belts in the opposite hemisphere ; they are moving at higher levels than the belts ; proper motion of these items is peculiar.

— Strips characterize an epigenic stage of activity in the cells after maximum.

Strips created at the boundaries of bright spots are deviated and attracted towards new bright spots emerging at their vicinity.

— Evolution of strips is rather slow. Their life-time ranges from a few days to three months.

— Strips remain visible after disappearance of the brilliant spots from which they emanate. They seem to be the residue of decreasing activity.

Strips having vanished by decreasing activity may suddenly become stronger than previously as a result of revival of the activity at the same area of the cell. (Fig. 7 to 12).

— Their fine structure shows that strips consist of discontinued dark blocks ranged a screw-like form.

— The Red Spot or Pseudo-Red Spots show by starting activity an alternation of brilliant and dark matter followed by pressional effects, vertical, vortical and lateral motions ; by decreasing activity they become dark. Their fine structure shows fractional dark masses in motion, vanishing progressively. (Fig. 13 to 23).

— South Tropical Disturbance shows an alternation of bright and dark matter in longitudinal expansion along the axis of the corresponding cell.

— The Red or Pseudo-Red Spots and the South Tropical Disturbance seem to constitute one and the same disturbance phenomenon in the corresponding cell with various manifestations.

— Dark belts or bands after maximum darkening vanish progressively ; blocks of dark matter disappear and the belts take the form of a solenoid with two distinct components ; these components in turn become very faint and narrow ; they remain visible for a long time with intermittent disappearance by localities and vanish progressively as if they were seen through a transparent or semi-transparent medium of increasing thickness ; polarization measured on dark belts shows variation for the same angles of sight of the overlying absorbing atmospheric layer, due to descending motion of the dark matter in the cells. Ascending and descending motions in the cells speak for a meridian circulation.

— The drift of the belts (Fig. 4) of Jupiter in latitude during the period 1875-1961 shows the following periodicities :

Southern hemisphere	*System II*		*Deviation* $(M-m)$
— S. S. T. B.	approx.	12-15 *y.*	approx. 6-8°
— S. T. B.	»	14-16 »	» 3-4
— S. E. B. south edge	»	4-6 »	» 3-4
Equatorial Zone	*System I*		
— S. E. B. north edge	approx.	12-16 *y.*	» 3-4
— N. E. D. south edge	»	12-16 »	» 3-4
Northern hemisphere	*System II*		
— N. E. B. north edge	approx.	3-6 *y.*	» 3-6
— N. T. B.	»	10-14 »	» 3-4
— N. N. T. B.	»	12?	» 4-8

The drift of the belts in latitude seems to be connected with the cycle of activity in the corresponding atmospheric cells ; criteria concerning the meridian circulation in the cells may roughly be established therefrom (Fig. 30).

Cycle of atmospheric activity

— The apparent amount of dark matter is the product of atmospheric activity on Jupiter. Observational material covering approx. nine revolutions of the planet (1857-1961) allows tentative conclusions as regards the cycle as per which the activity in the jovian atmosphere develops. (Figures 24 to 29).

— The minimum total activity for the whole planet is produced according to a 20-22 years cycle. During this cycle, activity in individual cells shows one or two maxima.

— An inversion is shown as regards the intensity of activity in adjacent belts at a given time ; when f. i. the S. T. B. is strong the S. E. B. is faint and vice-versa. The same is noted in the northern hemisphere.

— It seems that by starting cycle the activity propagates from the higher latitudes towards the equator and changes direction during the 20-22 years cycle. In the case of Saturn activity shows propagation from 45-50° latitude towards the pole.

— The total intensity of the activity seems to be slightly higher in the southern hemisphere of Jupiter.

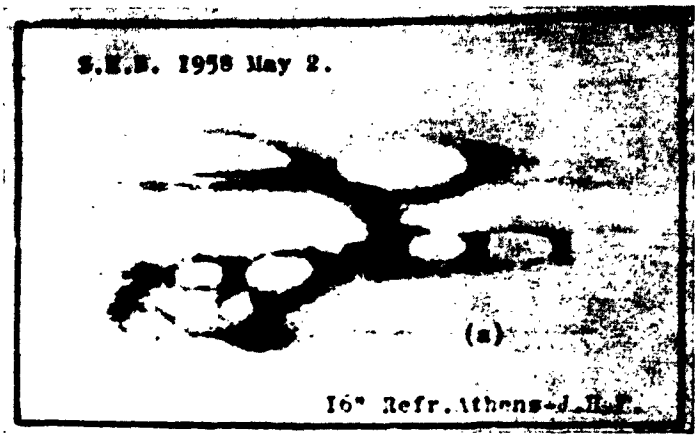

Fig. 1. — Within the remaining faint and narrow components (Fig. 1 a) of the belt of the previous cycle, cataclysmic activity starts.

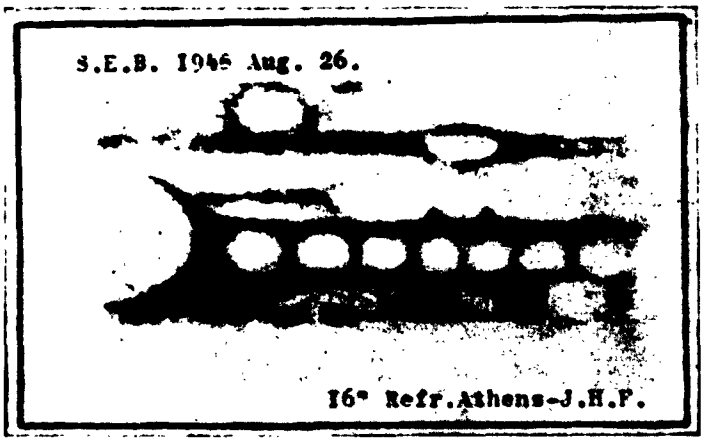

Fig. 2. — Brilliant isolated spots or groups of spots in ascending motion appear along the axis of the belt, followed by dark nodes.

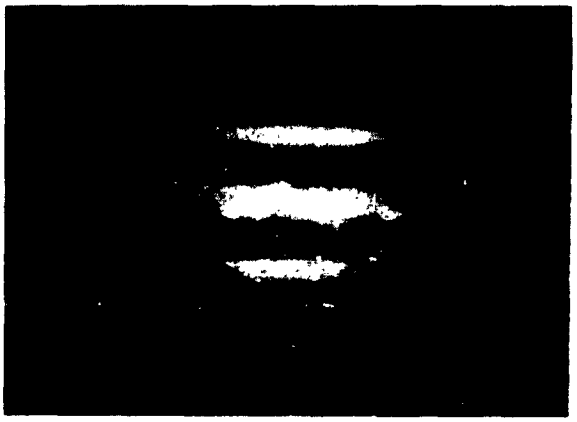

Fig. 3. Strips and blocks of dark matter emanating from dark nodes, moving polewards oppositely to the direction of rotation of the planet, spread along the axes of the cells and form the belts.

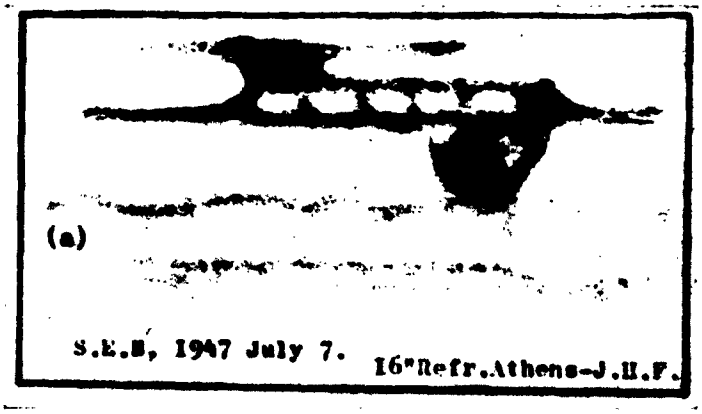

Fig. 4. End of the activity in the S.E.B. (a). There remain traces of the components of the belt. A large bright area in ascending motion appears below the south component of the S.E.B. lying at a higher level.

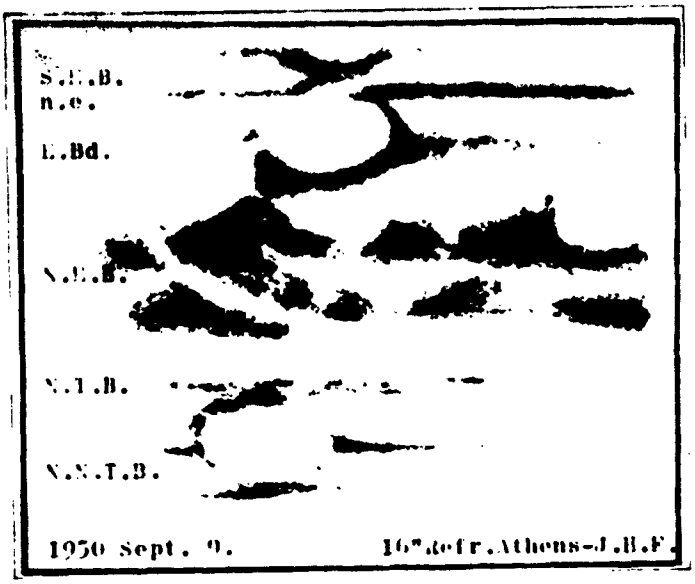

Fig. 5. Brilliant spots in ascending motion broke up the Equatorial Band and the N.N.T.B. Deviation of dark matter as a result of the action of such brilliant spots is obvious.

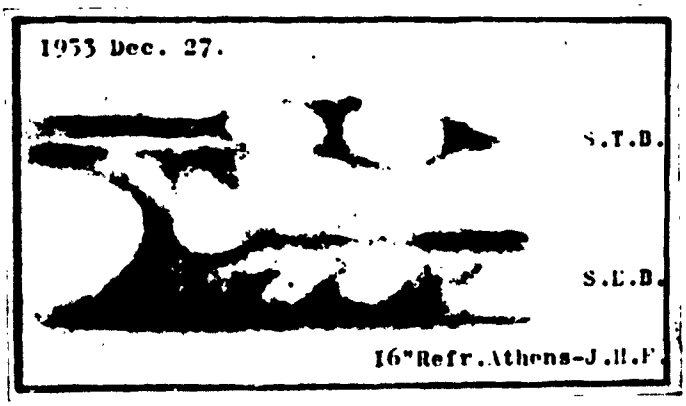

Fig. 6. — Brilliant spots in ascending motion broke up the S. T. B. and the S. E. B. s. e. provoking displacement of dark matter.

JUPITER : EPIGENIC STAGE OF ACTIVITY IN THE CELLS. FORMATION AND EVOLUTION OF DARK FILAMENTARY STRIPS.

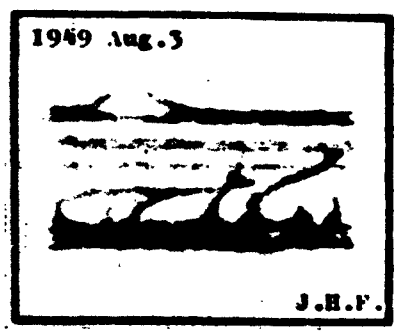

Fig. 7

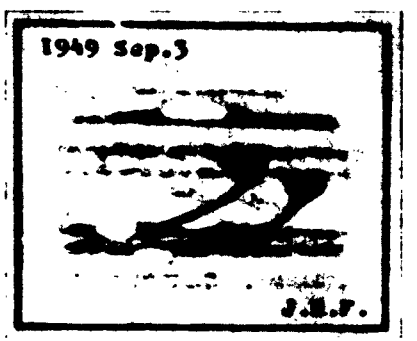

Fig. 8

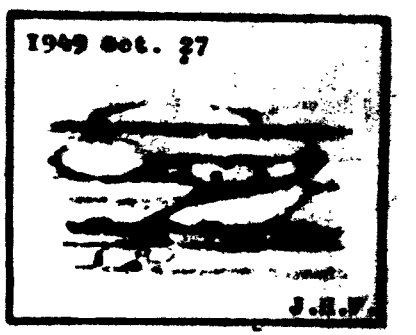

Fig. 9

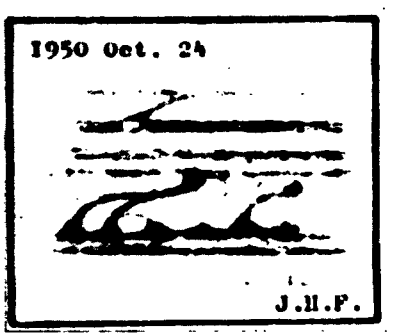

Fig. 10

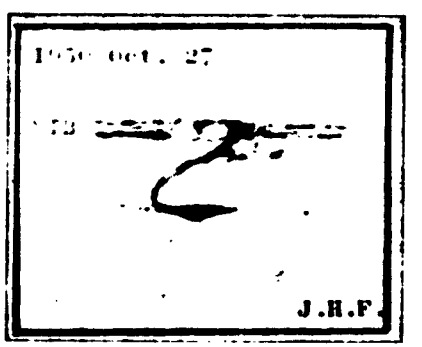

Fig. 11
16″ O. G. Athens

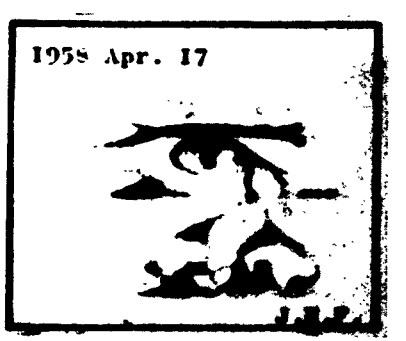

Fig. 12

Fig. 7 to 12

Dark filamentary strips characterize an epigenic stage of activity in the cells (after maximum) ; they are recorded in active areas all over the planet. They emanate from dark nodes following brilliant spots emerging through the dark boundaries of the belts.

Strips develop under a screw like form, cross the equator and occasionally ride belts in the opposite hemisphere, moving at a higher level than the belts.

Strips are shifted over brilliant spots.

Strips remain sometimes visible after disappearance of the brilliant spots and nodes from which they emanate. — Revival of strips is often recorded.

The life-time of the strips ranges between a few days and 3 months.

JUPITER : EVOLUTION OF A PSEUDO-RED SPOT IN THE SOUTH TROPICAL ZONE.
(TYPICAL EVOLUTION OF A CENTRE OF ACTIVITY ON JUPITER).
16″ O. G. Athens — J. H. F.

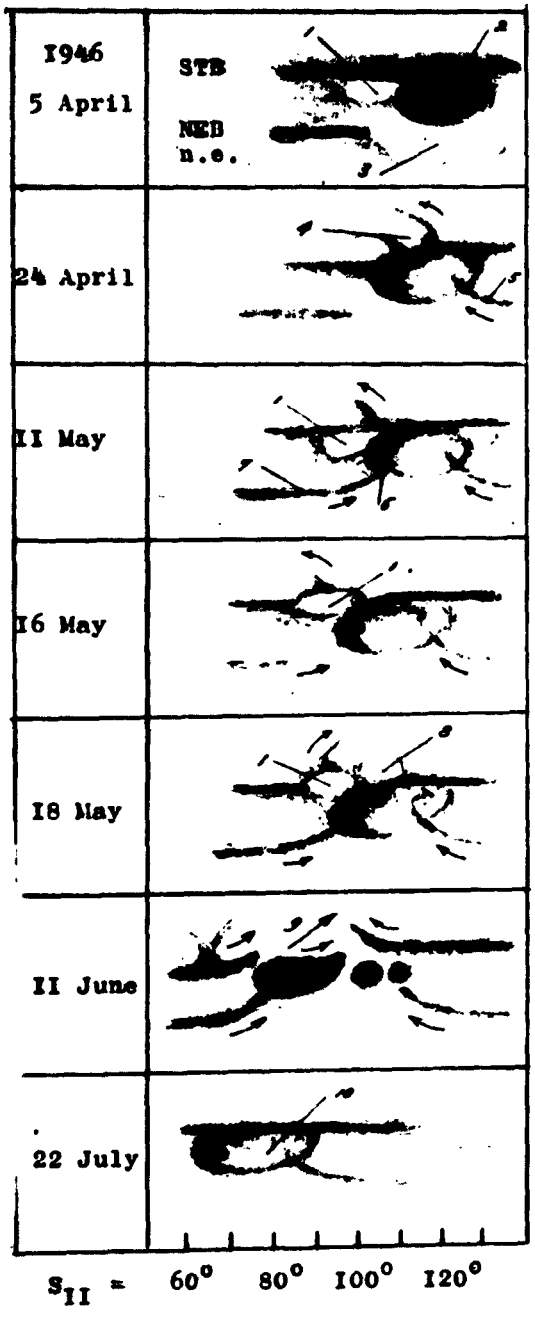

Bright spot (1) is followed by dark matter (2) and a « hollow » is formed.

— Dark filamentary strips (4) in vortical motion appear at the disturbed centre. The S. E. B. s. e. (5 and 7) are attracted towards the disturbed area.

Blocks of dark matter (6) are accumulated close to bright spot (1).

The S. T. B. is broken up by bright spot (1) moving southwards (16 May).

A new bright spot (8) appears close to (1) ; the disturbance centre seems to move in SW direction (18 May).

Fragments of the S. T. B. and S. E. B. s. e. and blocks of the initial dark spot (2), converge towards the disturbance centre (9) moving in S. W. direction. (11 June).

— The activity ceases and the S. T. B. (10) takes its regular aspect again ; dark masses progressively vanishing persist at the place of the disturbance.

Fig. 13

JUPITER : CYCLE (~ 11 YEARS) OF ACTIVITY IN THE RED SPOT'S AREA.
16" REFRACTOR ATHENS.

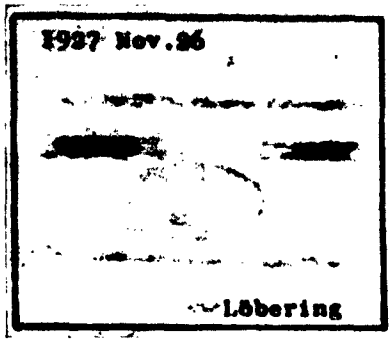

Fig. 14

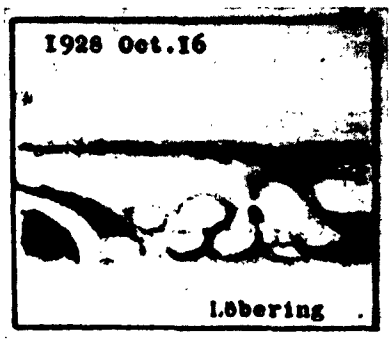

Fig. 15

Fig. 16

Fig. 17

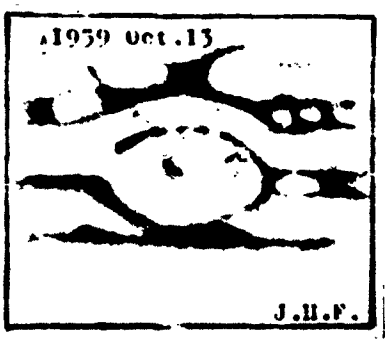

Fig. 18

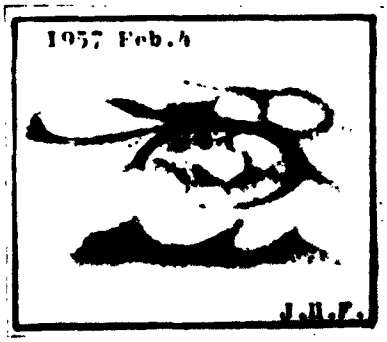

Fig. 19

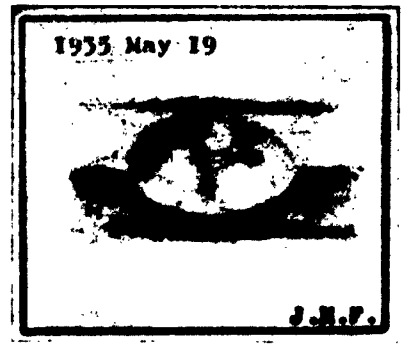

Fig. 20

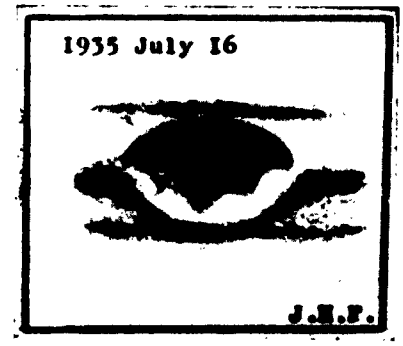

Fig. 21

Fig. 22

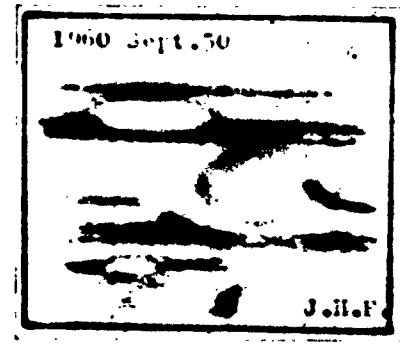

Fig. 23

Fig. 14 to 23

The Red Spot's system is a centre of periodical (approx. II years) activity closely connected with the activity manifested in the corresponding atmospheric cell in which the south edge of the S. E. B. is produced ; it extends symmetrically eitherside of the S. E. B. s. e. (axis of the cell) and shows the typical alternation of brilliant and dark matter characterizing the activity throughout the planet.

By ending activity the R. S. is at limit of visibility or invisible, which is the case for the S. E. B. to (Fig. 14).

By starting activity, at the place of the vanished or disappeared R. S. appear brilliant spots and dark strips converging towards these latter, the S. E. B. being under formation as per the same mechanism (Fig. 15).

The evolution of the activity in the Red Spot's area shows pressional effects permanently on the S. E. B. s. e. (Hollow) and sometimes on the S. T. B. (curvature of the belt, meridian displacement of the centre of gravity of the system Fig. 17, 18, 19) attraction of dark matter towards the disturbed area as by suction effect and vortical motions of dark strips around brilliant spots (Fig. 17, 18, 19 and 23) as well as displacement of blocks of dark matter in the Red Spot (Fig. 20 and 21).

The pinkish-red or rosy aspect of the Red Spot of a rather uniform tonality is the residue of the activity in the area (Fig. 22 and 23).

The manifestations of the activity in the Red Spot's area characterize a long-lived vortex system with peculiar proper motion in longitude. Pseudo-Red Spots (Fig. 24) occasionally appearing in the same atmospheric cell, characterize a rather short lived (a few months) vortex system developing as the classical Red Spot.

(The above aspects belong to different cycles ; they are destined to illustrate roughly the evolution of the activity in the R. S. area during an average cycle).

Fig. 24. — *Minimum activity.* 1943 Dec. 17 — 25″ O. G. Pic-du-Midi B. Lyot

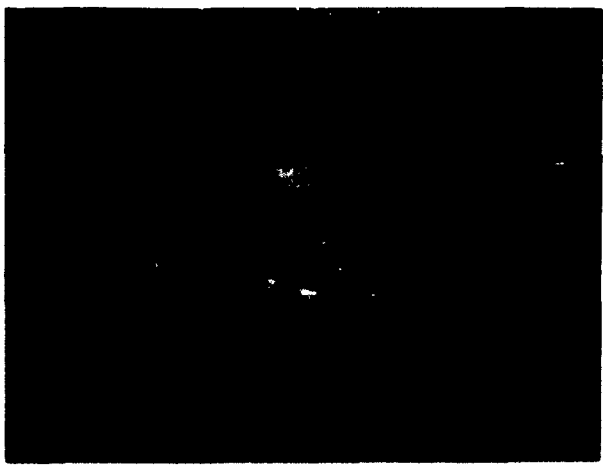

Fig. 25. — *Maximum activity.* 1945 March 20. — 25″ O. G. Pic-du-Midi H. Camichel

Fig. 26. — *Activity approaching minimum.* 1961 August 4. — 25″ O. G. Pic-du-Midi. — M. Marin.

(displacement of the activity in the Equat. Zone. The S. T. B. is attracted towards the southern boundary of the Red Spot)

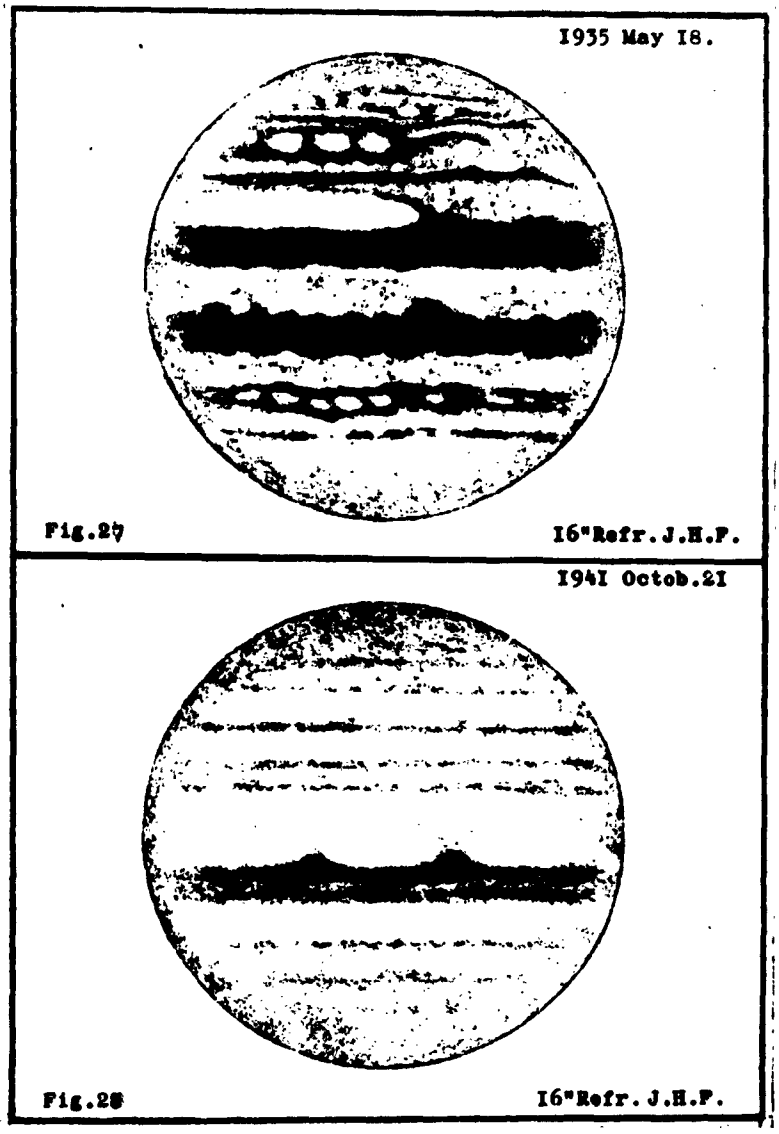

The varying amount of brilliant and dark matter on the planet is a criterium of the intensity of atmosph. activity.

Fig. 26. Maximum activity.

Fig. 27. Minimum activity (whole planet) ; every 20-22 years.

JUPITER : CYCLE OF ATMOSPHERIC ACTIVITY

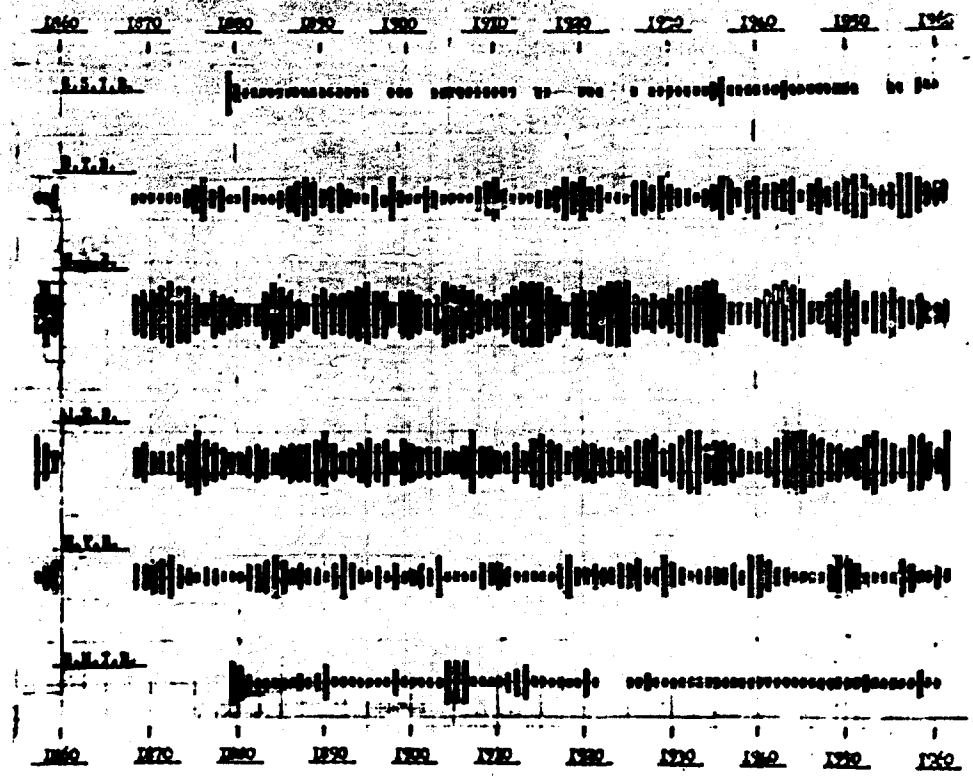

Fig. 29

The above graph is a tentative illustration of the variation of the intensity of the atmospheric activity in the two hemispheres of Jupiter ; it shows roughly the average annual intensity of the belts.

A minimum total activity for the whole planet seems to occur every 20-22 years. During this cycle, the activity in the main atmospheric cells shows one or two maxima. An inversion is noted regarding the intensity of activity in adjacent belts (S. T. B. strong — S. E. B. faint or N. T. B. faint — N. E. B. strong and vice-versa). It seems that by starting cycle the activity propagates from the higher latitudes towards the Equator.

Localization of the activity in the Equatorial Zone has been noted in 1881-1883 (Equatorial Zone including the S. E. B. the N. E. B. being faint) and in 1961-1962 (Equatorial Zone including the N. E. B. the S. E. B. being faint).

JUPITER : DRIFT OF THE BELTS IN LATITUDE

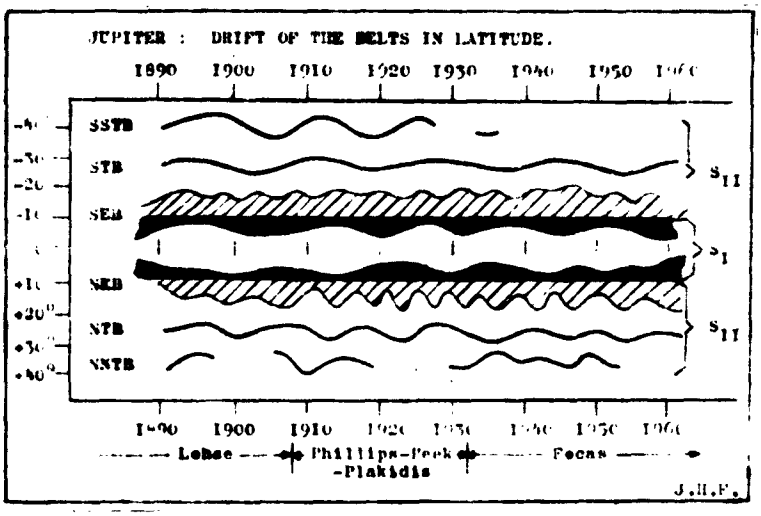

Fig. 30

53. — ON THE SPECTRUM OF SATURN

GUIDO MUNCH
Mount Wilson and Palomar Observatories
Carnegie Institution of Washington, U. S. A.

and

HYRON SPINRAD
Jet Propulsion Laboratory
California Institute of Technology, U. S. A.

It has been recently discovered (Spinrad 1962) that the NH_3 lines observed in the spectrum of the equator of Jupiter have tilts differing significantly from what would be expected from the inclination of the scattered Fraunhofer lines. In order to find out the true nature of this remarkable phenomenon, we have studied the inclination of the Fraunhofer lines and of the CH_4 lines shown by the spectrum of Saturn on plates being taken currently with the Mt. Wilson and Palomar Coudé spectrographs. A Mt. Wilson plate, obtained on May 17, 1962, with the 72 inch camera and a grating with 900 grooves per mm, covers the yellow-red second order with dispersion of 2.85 A/mm. The slit of the spectrograph was placed along the apparent major axis of the ring system, and it is thus the trace of the planet surface with a plane containing the equatorial nodes and a point at $B = +18^\circ$ latitude. Although the plate is somewhat underexposed, repeated independent measures of the *inclinations* $\alpha\,(\odot)$ and $\alpha\,(CH_4)$, of the Fraunhofer lines and of the strongest CH_4 features in the λ 6190 band, with respect to the Fe comparison spectrum or the terrestrial H_2O lines, give

$$\alpha\,(\odot) = 6^\circ 06 \quad \text{and} \quad \alpha\,(CH_4) = 3^\circ 35$$

The relative value of the velocity difference between the material scattering the Fraunhofer spectrum and the CH_4 gas is then

$$\epsilon = 2\,\frac{\alpha\,(CH_4)}{\alpha\,(\odot)} - 1 = 0.10\,(1 \pm 0.6)$$

The probable error here given has been derived from the internal agreement of the various determinations, some made directly

with a reticle-protractor, others by measures of differences in wavelength between the lines at both limbs of the planet.

The Palomar plate, obtained with the 144-inch camera with the slit parallel to the major axis of the ring system and passing approximately through the point $B = +10^{\circ}$ at the central meridian has a dispersion of 3.42 A/mm and a linear scale of $6''.65\ mm^{-1}$. The region of the λ 6190 band of CH_4 in this plate is shown in Figure 1, where it can be seen that many lines appear sharp enough to be measured for wavelength with great accuracy. Several independent determinations of the quantity ϵ defined above, give consistently values very close to 0.1, with a relative probable error around fifty per cent. The actual results of the various measures and description of the procedures followed will be published later. For the time being we wish to point out that, unlike the case of NH_3 in Jupiter, where it was found $\epsilon = -0.3$, the CH_4 layers in Saturn appear to be rotating *faster* than the layers scattering the Fraunhofer spectrum by about ten per cent.

In the course of the preliminary inspection of the two Saturn plates referred to above, two sharp lines, absent in the Fraunhofer spectrum, have been measured at $\lambda\lambda$ 6453.03 and 6367.80 A. These two features should be identified with certainty, with the S(0) and S (1) lines of the 4 — 0 quadrupole rotation-vibration band of molecular hydrogen, as predicted long ago by Herzberg (1938). The inclination of these lines is, within the uncertainty of measurement, half that of the Fraunhofer lines.

REFERENCES

Herzberg, G., *Ap. J.*, **87**, 428, 1938.

Spinrad, H., *Ap. J.* (in press), 1962.

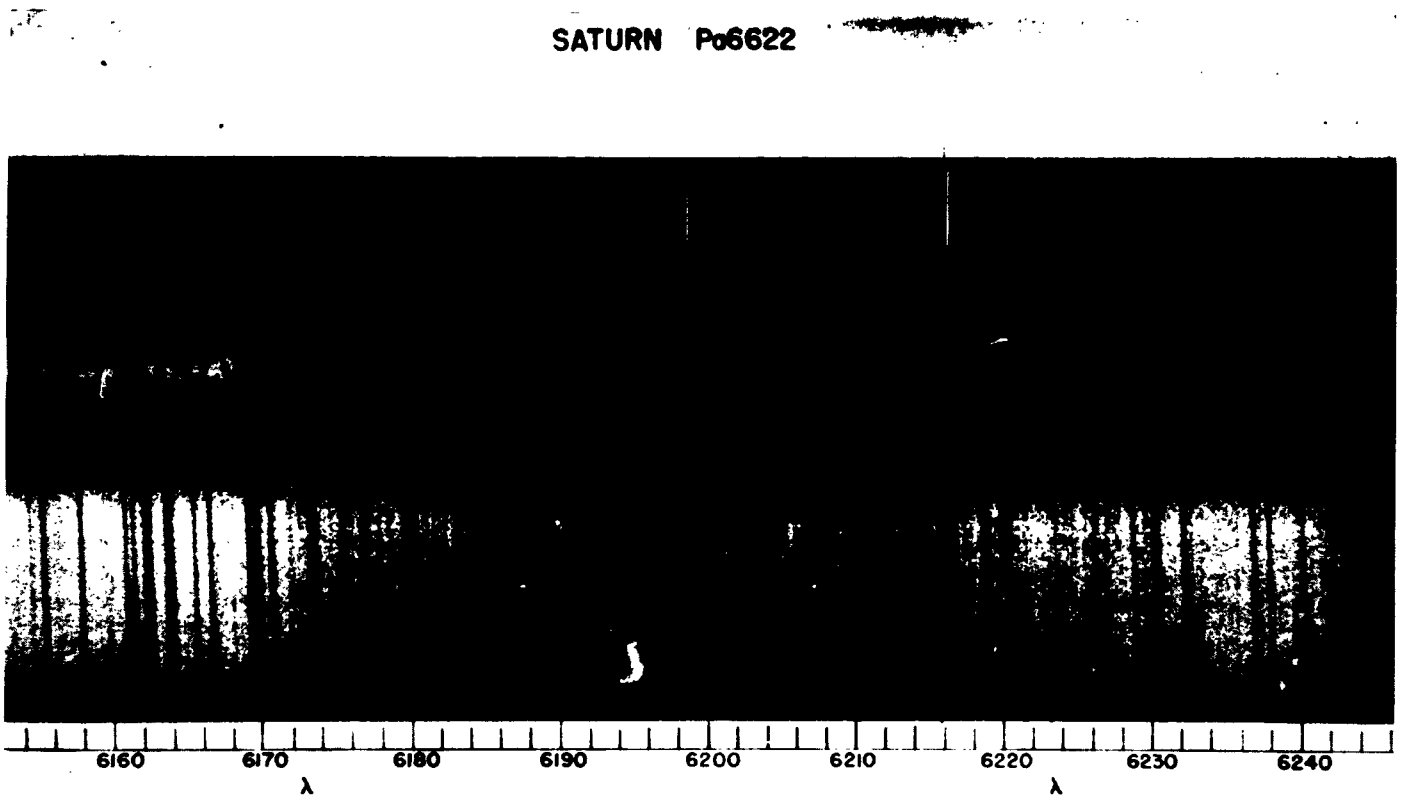
SATURN Po6622
6160
6170
6180
6190
6200
6210
6220
6230
6240
λ
λ

Fig. 1

54. — RESULTS OF RECENT DECAMETER-WAVELENGTH OBSERVATIONS OF JUPITER

ALEX. G. SMITH, T. D. CARR, and N. F. SIX
Department of Physics and Astronomy, University of Florida, U. S. A.
and
Maipú Radioastronomical Observatory, University of Chile

Recently P. A. Sturrock (1962) published a list of no less than five energy sources capable of generating electromagnetic waves in the terrestrial magnetosphere. At the same time, Sturrock discussed a total of seven mechanisms for converting energy from these sources into radiation. The various energy sources and conversion mechanisms are listed in Table 1.

TABLE 1

Mechanisms for the Generation of Planetary Radio Noise

Energy Sources	Conversion Mechanisms
1. Energetic electrons in Van Allen belts	1. Cyclotron or synchrotron radiation
2. Solar wind	2. Plasma oscillations
3. Bursts of energetic particles from the sun	3. Magnetohydrodynamic waves
4. Shock waves of solar origin in the interplanetary medium	4. Acoustic waves
5. Rotational energy of the planet	5. Cerenkov radiation
	6. Travelling-wave amplification
	7. Excitation of whistler modes

There is no apparent reason why this listing should not be equally applicable to the generation of decameter radio noise in the vicinity of Jupiter. It is evident from Table 1 that the number of possible combinations is quite large. In fact, one might be said to have an embarassment of riches. Clearly, if we are to distinguish between all of these sources and all of these mechanisms, it is necessary to examine the details of the radiation with great care.

One important clue is certainly the number and zenographic

distribution of the decameter radio sources on or about Jupiter. In his pioneering work in this field C. A. Shain (1955) recognized only one source. Later Gallet (1961) wrote, « At least four main sources can be distinguished, but a more complex pattern probably exists, made up of weaker sources that cannot be separated... ». In our own publications we have generally referred to three sources, which have been designated by the letters A, B, and C. (Carr et al. 1961). Lately we have been re-examining this question, using computer techniques to combine and smooth all of the available data from our observatories in Florida and Chile in order to obtain the best possible representation of the sources.

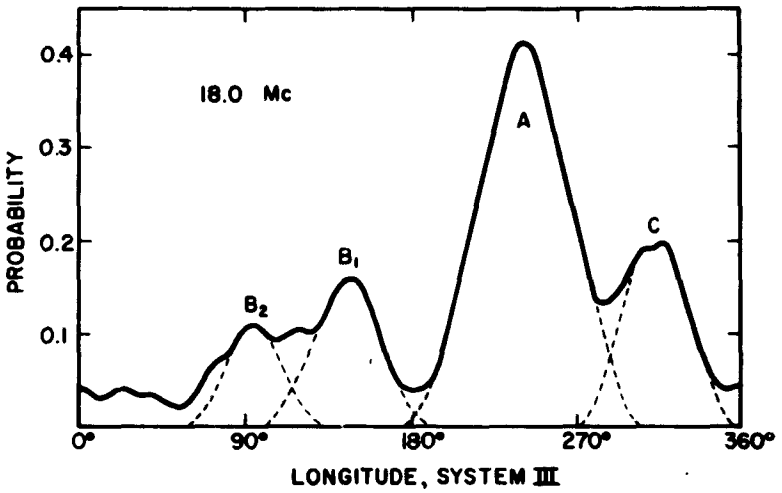

Fig. 1. — Smoothed probability profile for Jovian sources at 18 Mc/s. The longitude system used is the radiofrequency System III (Carr et al 1961).

Although this work is not yet completed, Fig. 1 is typical of the present results. The figure is derived from a histogram in which the probability of receiving 18 Mc/s radiation has been plotted as a function of the longitude of Jupiter's central meridian. A 5° longitude interval was used in the original histogram, and a three-point average has been employed in obtaining the smoothed curved of Fig. 1. The probability peaks, of course, imply the existence of

directional sources at the longitudes of the peaks. One quite persistent feature of the new profiles is that the B source generally appears to be broadened, and in many cases it is at least partially resolved into two peaks. As the dashed curves suggest, there is a strong implication that Gallet's count of « four main sources » was correct. Since most of the theories dealing with the mechanism of the radiation connect the sources with the geometry of Jupiter's magnetic field, it seems possible that not one, but two, magnetic dipoles are involved. It is also significant that in no case is the spacing between the peaks in Fig. 1 very close to 180°, implying that the dipoles are eccentric with respect to the axis of rotation of the planet.

A second clue to the origin of the Jovian radiation is provided

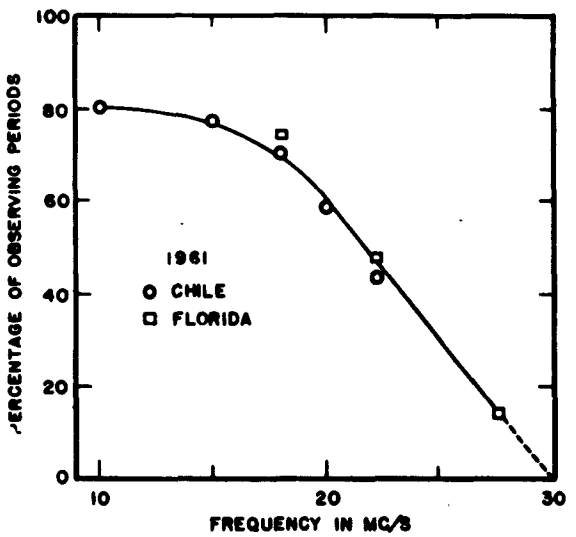

Fig. 2. — Curve showing the percentage of observing periods during which Jovian radiation was received in a three-month period near the middle of the 1961 apparition.

by the variation in its intensity with frequency. Our data indicate that the strongest bursts at 5 Mc/s correspond to a received flux of 10^{-18} w/m²/cps, which is comparable to fairly intense solar bursts. Preliminary estimates based on the 1961 data show that the

intensity declines as the — 3.6 power of the frequency. This spectral index is far smaller than that of the galactic background, which has an index of about — 2.0 in the decameter range. It is also much smaller than the indices of the discrete sources, which generally range from — 0.3 to — 2.2. The latter fact somewhat vitiates the suggestion of the Stroms (1962) that Jupiter is merely focussing upon the earth energy which actually comes from a background of discrete sources.

Fig. 2 shows a simple plot of the percentage of observing periods during which signals were detected at various frequencies by our two observatories. It should be noted that 10 Mc/s signals were observed in a full 80 % of the periods, while 28 Mc/s radiation was, as usual, relatively infrequent. The most striking feature of the curve, however, is the implied sharp cut-off near 30 Mc/s. If the radiation is cyclotron emission from electrons trapped in Jupiter's magnetic field, as we have suggested elsewhere (Smith et al, 1962), this cut-off establishes an upper limit of about 10 gauss for the region of the magnetic field which is ordinarily accessible to the particles. Occasional observations of radiation at slightly higher frequencies can be explained as the result of electrons on unusual trajectories which carry them deeper into the polar magnetic fields.

For a number of years Jupiter observers have been aware of an apparent inverse correlation between sunspot numbers and the general activity of Jupiter in the decameter region. In the past the writers have demonstrated this effect by computing a planet-wide probability of emission, averaged over all longitudes and over an entire observing season (Carr et al. 1961). We have now extended this analysis through the 1961 apparition, which included a full twelve months of observations. As Fig. 3 shows, the new data are consistent with the previous trend. It begins to appear that this negative correlation is more than fortuitous, although it is, of course, desirable to continue the observations throughout an entire sunspot cycle. Several investigators have reasoned that the effect

may be due to the screening action of a Jovian ionosphere which, like that of the earth, increases in density near sunspot maximum. In this connection it is perhaps disappointing that the 22 Mc/s data follow a curve of precisely the same shape as the 18 Mc/s curve. Warwick (1960) has made the ingenious suggestion that interplanetary space itself may become effectively more opaque around sunspot maximum because of the presence of diffusing or scattering clouds of solar plasma.

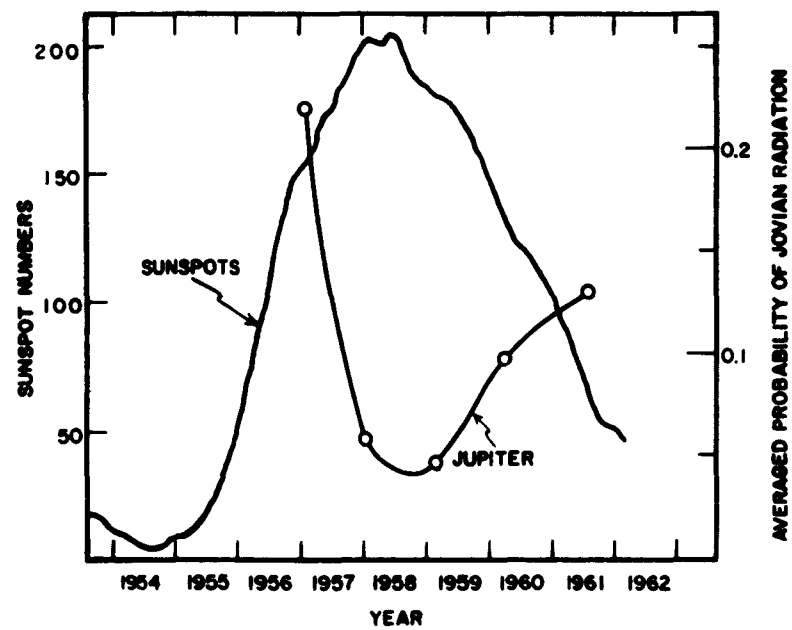

Fig. 3. — Comparison of 18-Mc/s Jovian activity with smoothed Zurich sunspot numbers. (Solar data from Solar-Geophysical Data, Part B, NBS Central Radio Propagation Laboratory, Boulder, Colorado, May 1962).

To these hypotheses we wish to add a further observation. Because of the 7° 11′ inclination of the sun's axis of rotation, as Jupiter circles his orbit the planet is situated first above the northern sunspot belt and then above the southern sunspot belt. Between these extreme positions the planet crosses the plane of the solar equator, a region which is relatively free of spots. Fig. 4

indicates that when Jupiter was extremely active in early 1957 (see Fig. 3) the planet enjoyed maximum exposure to the southern sunspot zone. In 1950 and 1951, at the time of Shain's early observations, when Jovian activity apparently was also at a high level, the planet was experiencing maximum exposure to the northern sunspot zone. At the present time the sub-Jovian point on the solar

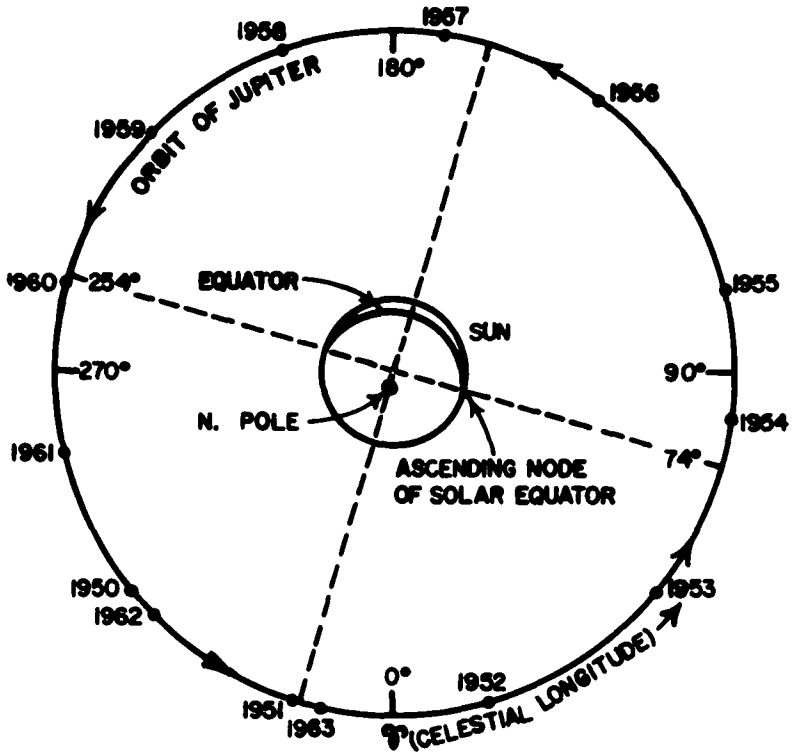

Fig. 4. — Orbital position of Jupiter relative to the inclination of the sun's axis of rotation. The position of Jupiter is shown for January 1 of each year from 1950 through 1963. It is interesting to note that the radio observations now span a complete orbit of the planet.

surface is again moving into the northern sunspot belt, and the Jovian radiation level is once more rising. On the assumption that Jovian activity may be triggered by the emission of relatively narrow, vertical cones of particles from disturbed regions on the

sun, it seems reasonable to suppose that the shape of the curve of Fig. 3 may be determined, at least in part, by the orbital position of the planet relative to the sunspot zones.

During the period immediately following the discovery of the Jovian decameter radiation, J. D. Kraus and R. M. Gallet reported the reception of very short pulses having durations of only a few milliseconds. This type of signal was not heard for a number of years, but in 1961 it began to reappear (Douglas and Smith 1961). During 1962, noise storms composed at least partly of these short pulses have been common. Fig. 5 shows a comparison of several bursts of short pulses with a train of normal pulses. In a loudspeaker the short pulses produce a rapid popping or rasping sound that contrasts strongly with the smooth, swishing noise which characterizes the normal radiation. Recently we have obtained dynamic spectra of a number of bursts of short pulses, and these differ significantly from the spectra of ordinary bursts.

Fig. 6 illustrates the build-up and decay of a normal pulse over a period of about four seconds. The rather smooth envelope of this pulse is typical of many which have been recorded. On the other hand, Fig. 7 shows frames taken from the spectra of two bursts of short pulses which occurred several minutes apart. The striking « saw-tooth » appearance of these spectra is suggestive of harmonics of some highly resonant phenomenon. In several instances a slight frequency drift of individual peaks was evident during a burst. In every case the drift was to lower frequencies at a rate of about 0.1 Mc/*s* per second. The direction of this drift is, of course, reminiscent of the drift of solar bursts, which is attributed to radiation sources rising through a plasma of decreasing density.

In connection with the phenomena shown in Figs. 5, 6, and 7, the reader should be cautioned that the terrestrial ionosphere plays a role of as yet undetermined significance in modifying or even creating certain details of the received radiation (Douglas and Smith 1961, Smith et al 1960). It is not yet possible to present a simple theory which accounts for all of the complexities of the

Jovian decameter radiation. However, cyclotron emission from electrons of solar origin, trapped in a rather complex magnetic field, represents a mechanism which accounts for many of the grosser features of the signals.

Acknowledgements

It is a pleasure to acknowledge the support which this program receives from the Office of Naval Research, the National Science Foundation, and the Army Research Office — Durham. N. E. Chatterton and W. F. Block have contributed significantly to the research effort, while the authors are grateful to H. W. Schrader and W. L. Cain for their assistance in preparing the illustrations.

REFERENCES

Carr, T. D., Smith, Alex. G., Bollhagen, H., Six, N. F., and Chatterton, N., *Ap. J.*, **134**, 105, 1961.

Douglas, J. N. and Smith, H. J., *Nature*, **192**, 741, 1961.

Gallet, R. M., *Planets and Satellites*, ed. G. P. Kuiper and B. M. Middlehurst (Chicago : Univ. of Chicago Press), p. 512, 1961.

Shain, C. A., *Nature*, **176**, 836, 1955.

Smith, Alex. G., Carr, T. D., Bollhagen, H., Chatterton, N., and Six, N. F., *Nature*, **187**, 568, 1960.

Smith, Alex. G., Carr, T. D., and Six, N. F., *Proc. Third Symposium on Engineering Aspects of Magnetohydrodynamics* (New York : Gordon and Breach, in press for December, 1962).

Strom, S. E. and Strom K. M., *A. J.*, **67**, 121 (Abstract), 1962.

Sturrock, P. A., J. Research NBS, **66D**, 153, 1962.

Warwick, J. W., A Comment on Jupiter's Radio Emission at Long Wavelengths in Relation to Solar Activity, presented at Kiruna Symposium on Polar Cap Absorption, August 8, 1960.

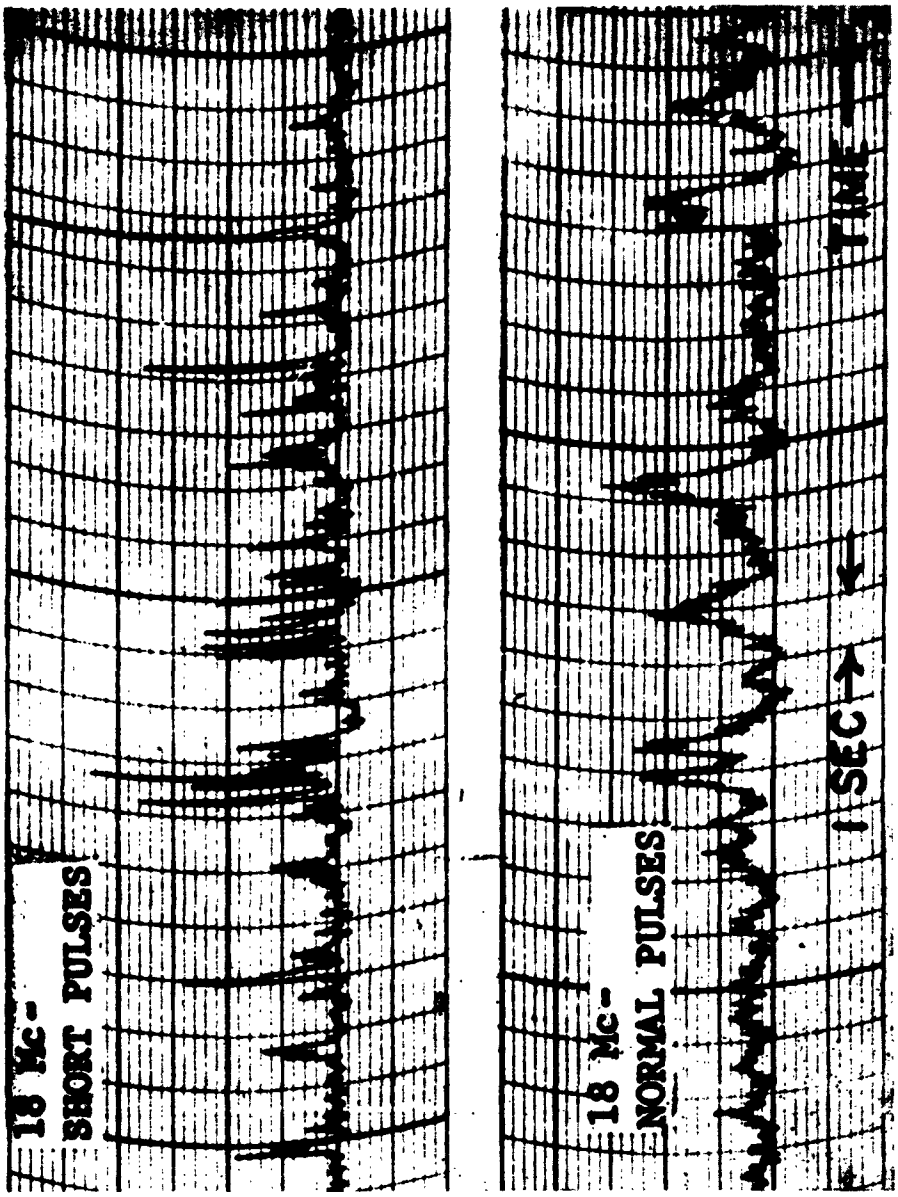

Fig. 5. Comparison of short pulses (above) with normal pulses (below). Each horizontal division represents one second of time. The frequency in both records is 18.0 Mc/s.

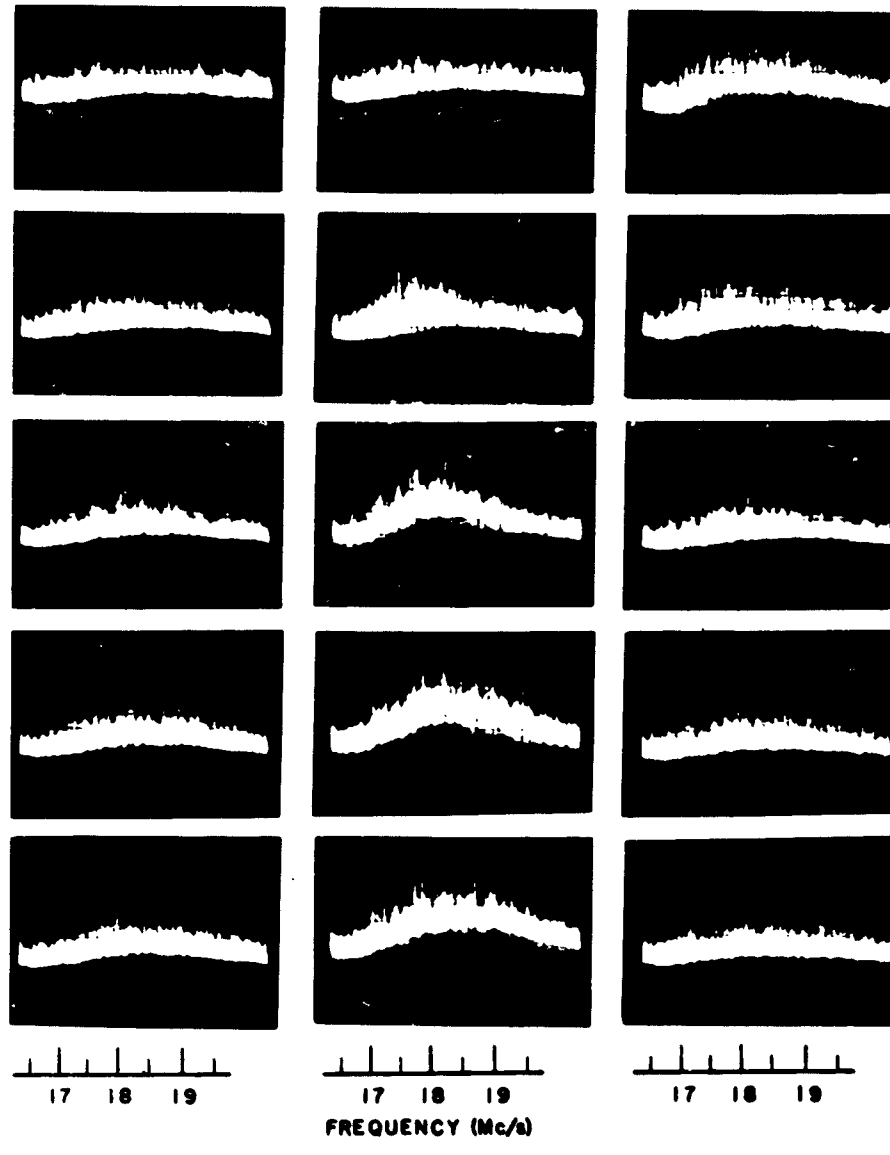

Fig. 6. Dynamic spectrum of a normal pulse. Time increases downward in each colum at the rate of 1.4-second per frame. The deflection in the initial frame (top left) is due to the background of cosmic radio noise from the Galaxy.

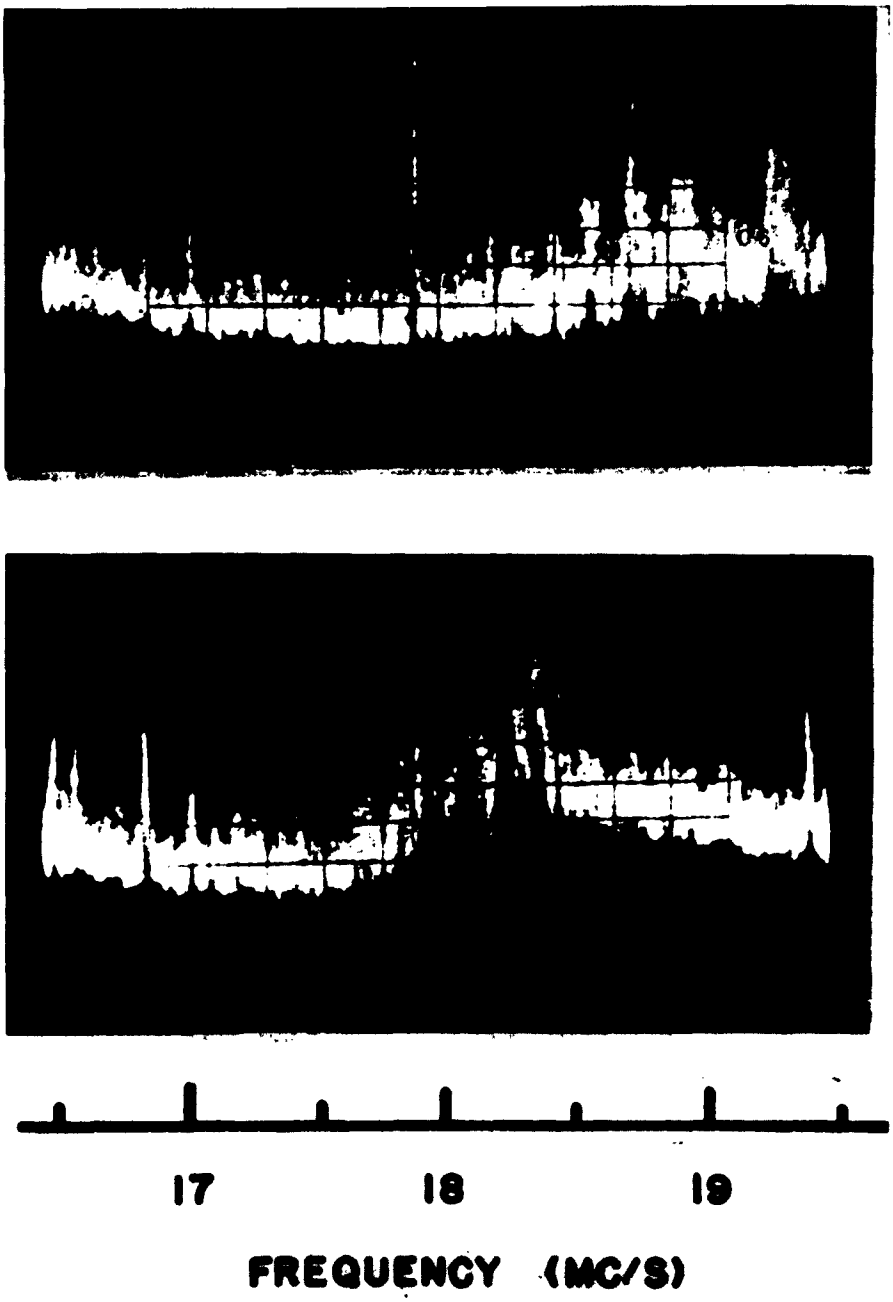

Fig. 7. Individual frames showing spectra of two bursts of short pulses. In the interval between bursts the center of activity has drifted downward nearly 1 Mc/s in frequency. (The narrow lines at 17.9 Mc/s and at the left end of the trace are terrestrial radio stations).

55. — OBSERVATIONS BEARING ON THE MECHANISM OF JOVIAN DECAMETRIC EMISSION

JAMES N. DOUGLAS and HARLAN J. SMITH
Yale University Observatory, U. S. A.

From several current observational and analytical programs of the Yale planetary radio astronomy work, we have selected for summary presentation four results which lead to specific important conditions which must be placed on the Jovian decametric radiation.

1. ROTATION PERIOD AND ITS CONSTANCY

While several workers have reported relatively precise rotation periods derived from limited runs of Jupiter data, Douglas (1960 a, b) has recently published a value for the radio rotation period based on a statistical analysis of all known Jovian noise storms collected by all observers over the interval 1950-1960. This period (now adopted by IAU Commission 40 — see IAU Information Bulletin N° 8, March 1962, p. 4), and the associated Jovian longitude system, bear the designation :

System III (1957.0) : period = $9^h\ 55^m\ 29^s\ 37$
epoch = System II Jan 1. 0, 1957.

The mere existence of so well-defined a period is of course important for understanding the mechanism of emission ; but more particularly it is now relevant to report checks on the accuracy of this published standard value, also to examine it for possible real variations.

The statistical method introduced by Douglas uses as input data only the J. D. times during which Jupiter storms were observed to be active. If one were able to tabulate each observed storm as a function of the corresponding Jovian longitude of central meridian (LCM) at that moment, determined according to the (unknown) true rotation period P_T, and if the distribution of radio emission as

a function of LCM is really asymmetrical, the results generate a non-uniform histogram (cf. Fig. 1) of frequency of events associated with each LCM. Any error in assuming the period will have the effect of assigning storm events to false longitudes, tending to

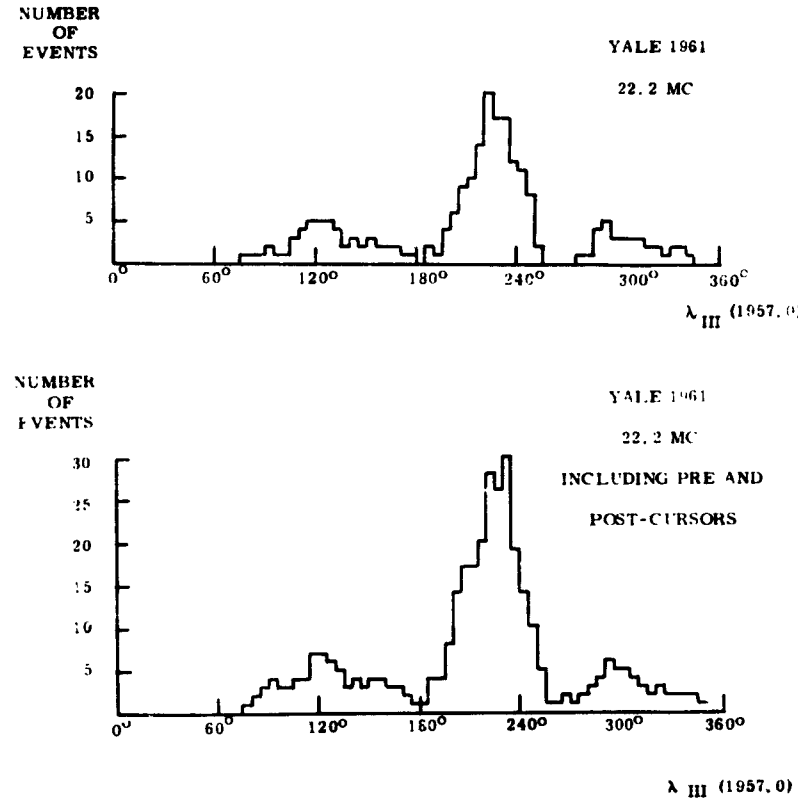

Figure 1. — Histogram of 1961 Yale 22.2 Mc Jupiter noise storm data.

a) Main-storm phases only.

b) Also including weak pre- and post-cursor activity.

disperse histogram peaks into adjacent valleys thus reducing the overall relief. The relief of a histogram is measured by its variance (sum of the squares of its ordinates divided by the number of ordinates). Accordingly, the true rotation period may be estimated by first assuming a range of periods $P_1 \ldots (P_T) \ldots P_n$, and computing the appropriate LCM histogram for each. That period corresponding to

the smoothed maximum of the run of variances of the successive histograms constitutes the best statistical approximation to P_T. Considering that nearly 700 separate storms are now available this program requires substantial time on a large computer; however, the results of such an analysis gave the unambiguous IAU period referred to above, with a standard deviation evaluated in several ways to be about $0^s.16$.

The new conclusions reported here arose from a careful recheck and repunching of all the old input data, during which a number of errors were corrected. Also it was necessary to rewrite the program to fit an IBM 709 computer recently installed at Yale, thus in effect checking the older program. Finally, two additional series of events (Warwick from 1960 and Yale from 1961) have become available; inclusion of these adds important weight to the period determination by extending the time base-line of numerous highly reliable observations through another year.

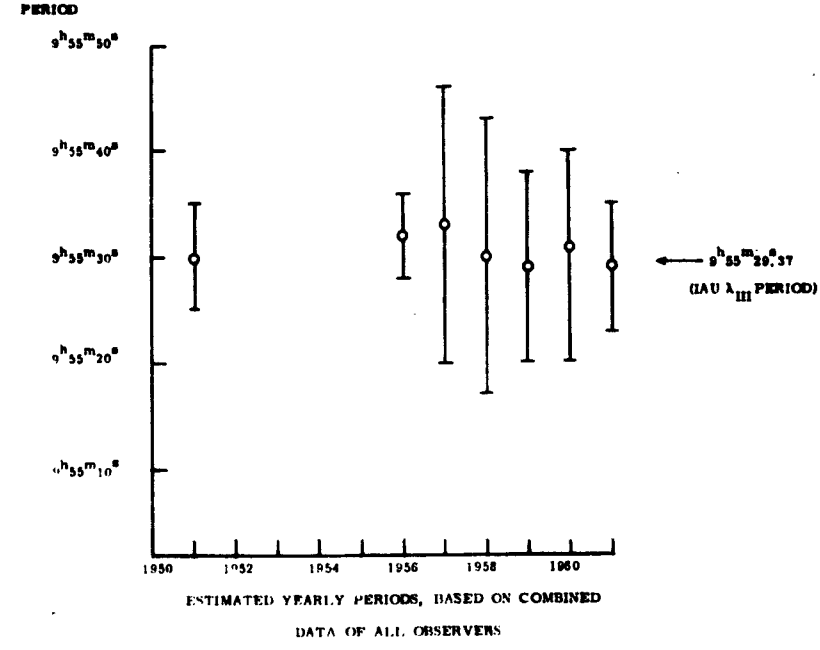

Fig. 2. — Jovian radio rotation periods determined from each year's data separately.

It is pleasant to report that the reanalysis yields the same period as before, to within a small fraction of the quoted standard deviation; there is thus no reason to question that the present System III (1957.0) provides a statistically reliable fit, with a probable error of about $0^s.1$, for all existing data now available to us.

One might still question whether this mean period 1950-1961 may conceal a secular change or significant annual variation. Accordingly the new program was also used to compute an independent period for each year of data (Fig. 2). The estimated standard deviations of the annual periods are much larger than that of the mean because of the relatively short time base-line within each observing season as well as the small number of events in a given year. However, to the limited precision available, Figure 2 (plus other groupings of the data not here reproduced) indicates no systematic period drift greater than about 1 second over the period 1950-1961, also no significant annual fluctuations greater than about $\pm 2^s$ during this time.

A more exhaustive analysis, presenting statistical models and results in detail, is in preparation (Douglas 1963).

2. 1961 Yale data

For several years a portion of our work has been concentrated on obtaining completely unambiguous identification of Jupiter storms with several single-frequency phase-switched interferometers. In 1961 the more or less perfected equipment and the relatively low sunspot number made possible a very strong series of observations on 22.2 Mc. The authors independently judged the records, eliminating doubtful cases, leaving a substantial collection of essentially uncontaminated Jupiter storm data which in turn produced an unusually clean histogram (Fig. 1a) displaying sharp isolation of its three apparent-activity regions (for a similar 22.2 Mc histogram, see Carr et al 1961). During the analysis of the records, in addition to tabulating the usual mainstorm phases of strong

activity (frequently marked by a characteristic abrupt start or stop over only fractions of a minute), we also tabulated separately any instance of the « pre- and post-cursor » activity which often seems to be present but is usually only faintly visible, typically being nearly an order of magnitude weaker than main-storm activity. We rather confidently expected to find that the weak pre- and post-cursor activity would normally violate the histogram of strong events, tending to wash it out severely by filling in the gaps between active regions. Instead, the effect of including this

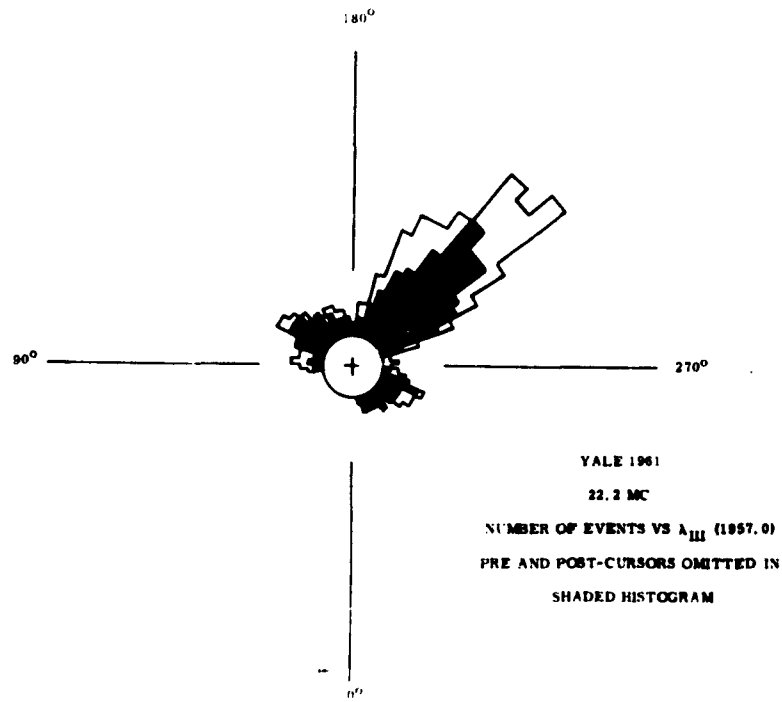

Fig. 3. — Same data as Figure 1, but plotted as a polar histogram (shaded portions refer to main-storm phase ; light portions the pre-and post-cursor activity).

feeble activity (Fig. 1b) proved to be mainly one of supporting the longitudinal distribution shown by the strong activity, with very little filling-in of the quiet longitudes.

Such effects become clearer if the same data, rather than being

plotted on a conventional linear histogram as in Figure 1, are put instead on a polar projection (Fig. 3). In this form it is much easier to appreciate the longitudinal asymmetry of Jovian decametric emission.

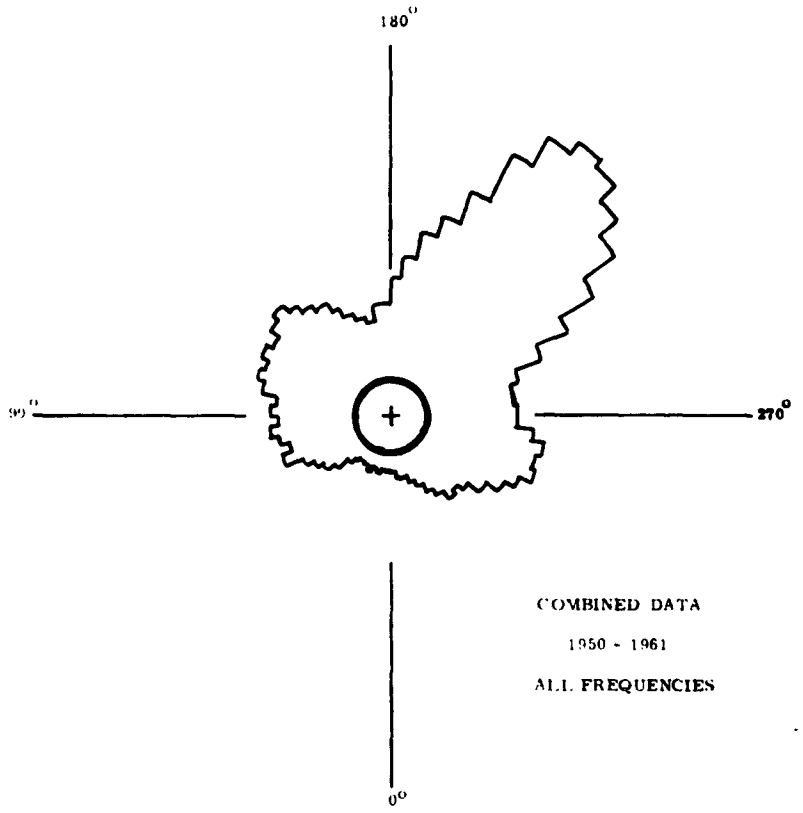

Fig. 4. — Polar Jupiter activity histogram including all data from all observers on all frequencies from 1950 through 1960, plus Yale 1961.

Figure 3 indicates strongly a basically tri-lobed character of the emission, at least around 22 Mc, although it is true that in particular lobe 1 is relatively broad ; as suggested by A. Smith (1962) it may in turn be multiple. Significant changes do appear in the lobe-pattern from year to year, ranging from the near-disappearance of lobe 3 to the occasional suggestion of intermediate minor lobes. Also some presently available data (Carr et al 1961, Warwick 1961 and

1962) indicate that extreme sharpness of lobes tends to wash out in the range of Jupiter storm frequencies below 15 Mc. But Figure 4, a similar histogram which includes all of the available Jupiter data over all years and frequencies, shows that the general tri-lobed aspect of Figure 3 is no accident, even in its 10° tilt of the axis of lobes 1 and 3 with respect to the major lobe 2.

As a second conclusion from Figure 3, comparison of parts (a) and (b) shows that, as seen from the earth, the emission — regardless of whether it is strong or weak — has the same directional characteristics. This suggests the reality of fairly sharp directional containment of the radiation, within which abrupt changes of activity level arise for other reasons (perhaps associated with secondary propagation effects or intrinsic changes in the emitted flux). Effectively the radiation seems to be confined to cones having apparent half-power diameter of the order of 30-40°.

In using any form of Jupiter activity histogram, one must remember that we have no direct observation of the geographical location of the radio source ; a storm is only *associated in phase*, via the LCM, with the specified λ_{III}. The actively emitting region(s) may have a systematically different longitude, as for example above the back side of the planet 180° away from the LCM corresponding to the time of emission. Also there may be three (or more) emitting regions, or perhaps only a single source location having three principal lobes of emission.

But the most interesting conclusion follows in conjunction with Morris and Berge's (1962) recent determination (see also Morris, 1962), using microwave polarization measurements, of the approximate longitude of Jupiter's magnetic pole. Their data indicate for the pole a mean longitude of roughly $208° \pm 10°$ on the System III of Carr et al (1961) which for this purpose differs only insignificantly from the IAU System III (1957.0). The magnetic pole is thus in close alignment with the major lobe (and with the opposite « empty quarter ») centered at $212° \pm 7°$. This is one of the strongest observational facts lending support to Warwick's general

picture of the Jovian decametric radiation being caused by phenomena of an auroral character rather than surface activity of any kind.

3. Polarization anomalies

In 1961 the Yale Bethany Station also brought into operation on 22.2 Mc a complete polarimeter able in principle, with proper calibration, to yield all four Stokes parameters even of the elemental fraction-of-a-second storm bursts. Here we wish merely to report one major finding from the polarization records. Specifically, it has been known since 1956 that the decameter storms are normally right-elliptically polarized, although with occasional appearance of some left-elliptical polarization. Our 1961 records were consistent with this pattern, showing about 97 % of the time the right-elliptical component to predominate strongly (e. g, Fig. 5b).

Violating this normal pattern, on two occasions (June 5.35 and August 7.23, 1961, UT) activity beginning almost exclusively as right elliptical changed during several minutes to almost exclusively left-elliptical, then after about ten minutes switched again smoothly but quickly back to right. Both sources were centered on the principal lobe (perhaps the magnetic pole?), respectively at $\lambda_{III} = 206^{\circ}$ and 231°. Whatever the mechanism invoked (including multiple sources, reflections, or propagation mode-shifts) such well-established anomalies may help to thin the range of acceptable models for the radiation source.

4. Power and energy associated with decameter storms

Several authors (esp. Gallet 1961) have attempted to estimate the powers involved in the decameter storms. Publication of another set of estimates seems to us in order since the time over which well-calibrated observations are available is now longer, and since some

assumptions can now be spelled out more clearly than before. For the past four years the Yale records have included automatic calibration marks such that a source must produce at our antennas a total flux in both polarizations of 6.1 ($\pm$ 25 %) $\times$ 10^{-22} wm^{-2} cps^{-1} in order to cause a deflection equal to the calibration. Since we know the distance of the Jupiter source, computation of the total decametric power radiated depends on three variables : the observed deflections on the charts, the actual emission spectrum, and the true emission cone angle. Serious uncertainty about each of these factors, particularly the last two, permits only an order-of-magnitude final estimate of power.

Considering first the deflections, it is necessary to distinguish between apparent burst intensity and actual storm intensity. The individual bursts of characteristic duration around 1 second, while perhaps in part originating at Jupiter (Douglas and H. Smith 1961), are often so strongly amplitude-modulated by ionospheric diffraction and refraction effects as to be unreliable indicators of power. A typical example of this is provided by Figure 5a, where identical equipment at two stations separated by 100 km indicates the same general pattern of activity plus essential identity of individual burst times — but with ionospheric amplitude modulation inducing gross and random relative changes of intensity at each station. Such effects may also be expected to become more serious toward lower frequencies approaching the critical frequency, rendering the burst or burst-group intensity a questionable basis for spectral studies. Furthermore it is the overall storm activity which sets the basic power and energy requirements, within which even real bursts may only represent perturbations.

With these problems in mind we have chosen to deal with the question of major storm energy, which can be evaluated almost independently of the ionosphere. Figure 5b shows the sort of major storm activity to be discussed here ; note in particular the strong baseline deflection representing integrated power. In our experience, such storms — of typical duration 10 to 100 minutes — have never

shown baseline deflections exceeding twice the calibration ; strong storms are normally of the order of the calibration, and this value is reasonable to adopt as a measure of the integrated 22.2 Mc flux throughout the storm.

The bandwidth and spectrum are more difficult to evaluate. Strong storm activity has been observed over a bandwidth as small as 1 Mc. More typically a 5 Mc bandwidth may be active, while extremely well-developed storms occasionally radiate over much of the spectrum from 5 to 30 Mc (Warwick 1961, 1962). The flux spectral index n may be defined, conventionally, as $S \propto \nu^n$. Since Warwick's swept-frequency equipment is gain-referenced at each frequency to the galactic background, the rather uniform apparent intensity of his spectra as a function of frequency implies a negative index in order to take into account the spectrum of the galaxy itself. The Florida workers (A. Smith 1962), who first called attention to the character of the Jupiter index, suggest that $n \sim -5$ fits at least the strongest bursts observed from 5 to 25 Mc.

Concerning the last major parameter, we have only indirect evidence as to the effective cone angles into which the decameter power is radiated. The duration of a short storm must be accepted as a lowest limit. A more probable value comes from assuming that the lobes of Figures 3 and 4 measure directly that slice of the emission cone which Jupiter's rotation sweeps past the earth, in which case about 60° would seem a reasonable choice for cone half-power diameter. Finally, of course, the upper limit for cone angles would be the case of isotropic emission.

These considerations can now be applied to the problem of the total decametric power radiated from Jupiter. Corresponding to typical strong 22 Mc continuum storms causing deflections of the order of calibration, we require a source at the opposition distance of Jupiter to radiate 2.6×10^2 *w cps*$^{-1}$ *ster*$^{-1}$. Adopting 20 Mc as a maximum momentary emission bandwidth, and a spectral index $n = -1$ for emission into a 60° cone, the total radiated decameter power during strong storms follows as 10^{10} watts, the uncertainty

Fig. 5a.

Jupiter 22.2 Mc total-power tracings (8 June 1962) produced on a common recorder by a set of identical antennas and receivers located respectively at Pomfret, Conn. (upper channel) and Bethany, Conn. (lower channel) separated by 100 km on an ENE line. Timing grid lines on these records are 5^{m} apart.

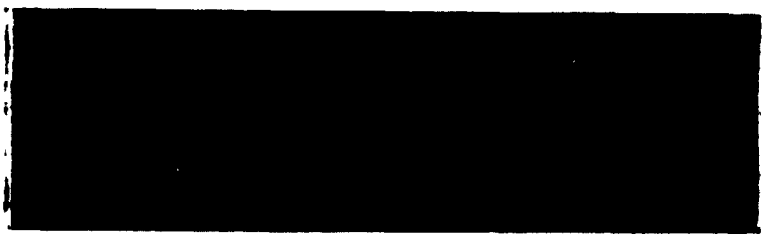

Fig. 5b.

One hour of record showing typical development of 22.2 Mc major Jupiter storm (26 July 1961).

Channel identification, top to bottom : total power left-circular polarization, total power right-circular polarization, phase-switched interferometer with phase-sensitive detection. With time, running from left to right, note first the standard calibration mark, next an isolated early portion of the storm featuring only bursts, then the onset major-storm activity with its pronounced baseline shifts. Note also the customary overwhelming dominance of right-circular polarization.

being at least a factor of 10. Jupiter must thus have a mechanism capable of generating decameter powers of this order at least for times of the order of an hour, and more likely for substantial portions of several days (Douglas and Smith 1963) amounting to a total energy radiated by the entire storm of 10^{30} to 10^{32} erg.

It is still more difficult to estimate Jupiter's averaged continuous decameter R F emission over long periods of time. Keeping to orders of magnitude, emission is detectable roughly 20 % of the time over the range of frequencies considered here (more often at the lowest frequencies), but over periods of a year this activity probably averages only 1 to 10 % of the flux levels discussed above for strong storms. A mean emitted power of the order of 10^8 watts is thus indicated for the decametric spectrum above 5 Mc ; the spectrum below 5 Mc may prove to be the more important component of noise-storm power on the average. It is interesting that the mean decimetric emission also amounts to about 10^8 watts. Although these powers seem large, even a very modest solar breeze should continuously deliver at least 10^{12} watts to the vicinity of Jupiter's magnetosphere.

Support from the National Science Foundation, the National Aeronautics and Space Agency and the Research Corporation for various phases of this work is gratefully acknowledged.

REFERENCES

Carr, T. D., Smith, A. G., Bollhagen, H., Six, N. F., Jr., and Chatterton, N. E., *Ap. J.*, **134**, 105, 1961.

Douglas, J. N., *A. J.*, **65**, 487, 1960a.

— *Thesis*, Yale University, 1960b.

Douglas, J. N. and Smith, H. J., *Nature*, **162**, 741, 1961.

— 1963, in preparation.

Gallet, R. M., *Planets and Satellites* (Ed. G. P. Kuiper and B. M. Middlehurst, University of Chicago Press, Chicago, Ill,), p. 500, 1961.

Morris, D., this symposium.

MORRIS, D., and BERGE, G. L., *Obs. of the Calif. Inst. Tech. Radio Observatory* No. 7, 1961.

ROBERTS, M. S. and HUGUENIN, G. R., this symposium.

SMITH, A. G., this symposium.

WARWICK, J., *Annals of the New York Academy of Science*, **95**, 39, 1961, *Ap. J.*, 1963, in press.

56. — POLARIZATION OBSERVATIONS OF JUPITER AT DECAMETRE WAVELENGTHS

C. H. BARROW
Florida State University, Department of Physics
Tallahassee, Florida, U. S. A.

Radio observations of Jupiter were made at Florida State University in 1961 at frequencies of 18.3, 18.7, 19.5 and 24 mc/s. Crude polarization observations were attempted at 18.3 and 24 mc/s. On three occasions simultaneous observations at these frequencies indicated predominantly right-handed polarization at 24 mc/s, but predominantly random or linear polarization at 18.3 mc/s [1].

A new series of polarization observations has recently been commenced using crossed-Yagi tracking aerial systems at 16, 18, 22, and 26 mc/s. Pending the completion of switching circuitry the aerial manufacturer's phase identification system has, so far, allowed two events to be studied to some extent. A pronounced polarization has yet to be observed at 18 mc/s although right-handed polarization appeared to be present at 22 mc/s.

If the gyrofrequency, or possibly some critical frequency, on Jupiter should be within the frequency range 16-26 mc/s, and there are indications that this may be the case [2], it should be possible to detect this by observing a change in polarization mode from one frequency to another. If, however, the gyrofrequency should be above 26 mc/s, polarization observations at all frequencies should indicate similar modes and it would be necessary to measure axial ratios in order to obtain further information concerning the state of the Jovian magnetic field.

Some eight weeks of observation with a 38 mc/s phase-switching interferometer allowed one small event to be recorded at this frequency.

This work is being supported by the National Aeronautics and Space Administration (Grant Number NSG-224-61).

REFERENCES

[1] Barrow, C. H., *Ap. J.*, **135**, 847, 1962.
[2] Barrow, C. H., *Nature*, **188**, 924, 1960.

57. — POLARIZATION OF THE 2840 MC/S RADIATION FROM JUPITER

D. MORRIS and J. F. BARTLETT
California Institute of Technology Radio Observatory, California, U. S. A.

This paper briefly summarizes measurements made at the Caltech Radio Observatory on the 2840 Mc/s (10.6 cm) radiation from Jupiter. The results are compared with similar measurements made earlier at 960 Mc/s (31 cm) and 1390 Mc/s (22 cm).

The observations were made during the week 14-21 April 1962 with an interferometer of baseline 300 λ E-W. At this antenna separation, Jupiter was unresolved and values were obtained for the total flux, fractional linear polarization and position angle of the electric vector of the radiation. To obtain an adequate signal to noise ratio it was necessary to integrate the fringes for periods of the order of 20 minutes. For this purpose an analogue computer and mechanical integrator were used.

The values so found for the flux and polarization are displayed in Figure 1 as a function of the system III longitude defined by Smith and Carr (1959). Each point is derived from observations extending over $\pm$ 1^h about meridian transit. No circularly polarized radiation greater than 5 % was found.

It is apparent that the position angle of the electric vector shows a variation correlated with Jupiter's rotation. A similar effect was found previously at 1390 Mc/s (Morris and Berge 1962), although in that investigation it had to be assumed that the total flux and fractional polarization were substantially constant during the planet's rotation. On theoretical grounds one can expect variations in the total flux and fractional polarization if the decimeter radiation from the Jovian Van Allen belts is beamed. In addition, as the obscuration of the Van Allen belts by the solid planet varies there will be associated changes in the observed radiation. Within the experimental uncertainties we can detect no systematic varia-

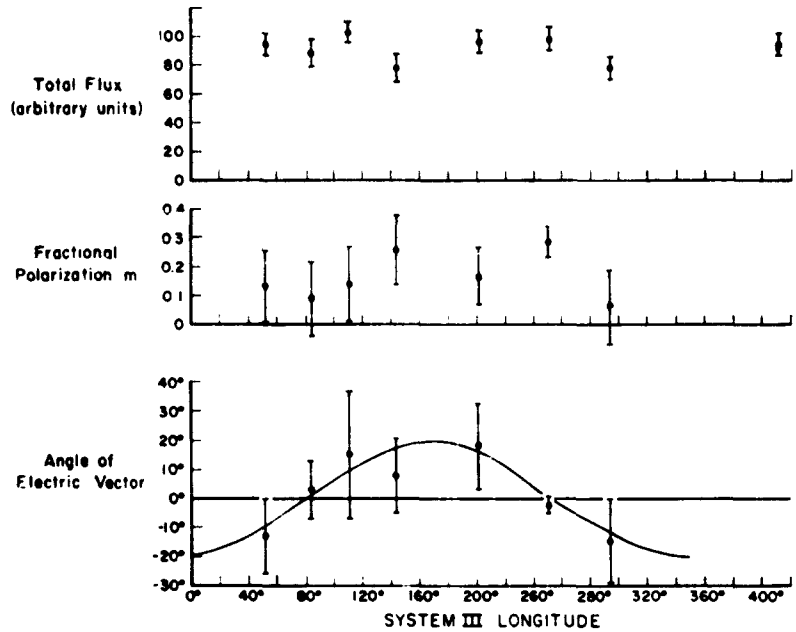

Fig. 1. — Polarization parameters of the 2840 mc/s radiation from Jupiter. Total flux, fractional polarization, and position angle of electric vector measured relative to Jupiter's equator, as a function of System III longitude of the central meridian.

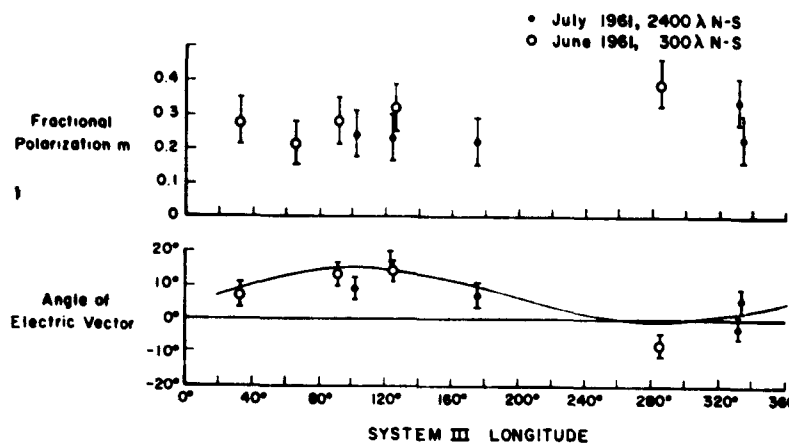

Fig. 2. — Polarization parameters of the 1390 mc/s radiation from Jupiter. Total flux, fractional polarization, and position angle of the electric vector measured relative to Jupiter's equator, as a function of System III longitude of the central meridian.

tion in flux greater than $\pm$ 10 %, nor any change in fractional polarization greater than $\pm$ 0.1.

In Figures 2 and 3 the results of measurements similar to the above, but made earlier at 1390 Mc/s (22 cm) and 960 Mc/s (31 cm), are shown. These observations were also made within $\pm$ 1^h about meridian transit, but on a N-S baseline. The appropriate antenna

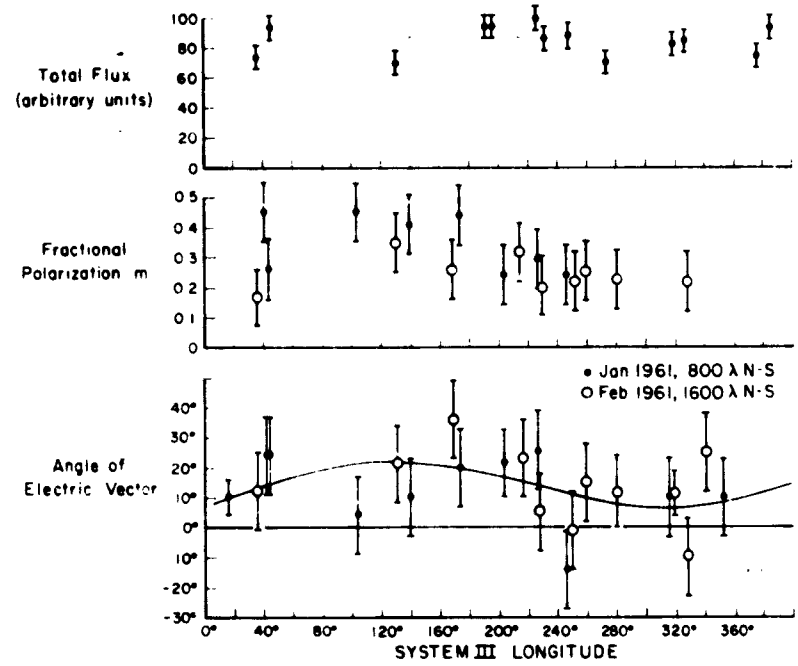

Fig. 3. — Polarization of the 960 mc/s radiation from Jupiter. Fractional polarization, and position angle of the electric vector measured relative to Jupiter's equator, as a function of the System III longitude of the central meridian.

separation is indicated in Figures 2 and 3, and we have assumed in the following that the effects of observing with this resolution are negligible. The measurements at all three frequencies show the same trends and Table I has been compiled as a summary. The 2840 Mc/s flux has been normalized using Broton and Medd's (1960) value for the flux of Cass A with a correction for resolution at 300 λ E-W derived from the measurements of Rowson (1959).

The variation in the position angle of the electric vector has been assumed to be due to a tilt of Jupiter's magnetic axis with respect to its rotational axis together with a time invariant Faraday rotation in the earth's ionosphere. On this basis a least squares analysis yields the full line curve in Figures 1, 2 and 3. The calculated values of the magnetic axis tilt and longitude of the magnetic pole associated with the principal decameter radio source are given in Table I. Within their errors the three sets of measurements yield the same value for the position of the Jovian Magnetic poles.

TABLE 1

Date	f(Mc/s)	Flux*	m%	Magnetic Axis Tilt	Long. III pole
Jan.-Feb. 1961	960	6.7 ± 1.0	33 ± 7	$7°.3 \pm 5°$	$225° \pm {}^{19°}_{45°}$
June 1961	1390	—	—	$9°.0 \pm 3°$	$200° \pm 10°$
June-July 1961	1390	8.2 ± 1.2	28 ± 6	$7°.7 \pm 3°$	$198° \pm 18°$
April 1962	2840	8.3 ± 1.0	20 ± 5	$20° \pm 11°$	$260° \pm 70°$
		$7.0^{**} \pm 1.0$	$23.5^{**} \pm 5$		

It will be seen that the fractional polarization of the radiation shows an apparent variation with frequency. However, this could equally well be a temporal variation and for the same reason we cannot draw any unambiguous conclusion about the spectral index of the radiation. In this connection it is interesting that the 2840 Mc/s disk temperature corresponding to the flux quoted in Table I is $800° \pm 100°$K. Sloanaker and Boland (1961) obtained values of 640°K and 315°K in 1958 and 1959, respectively. They also pointed out that if the discrepancy between their two measurements was to be accounted for by partial linear polarization of the radiation then a very high fractional polarization was required. If we assume that the fractional polarization has remained un-

(*) $\times 10^{-26}$ W/m^2/c/s at 4.0412 A. U.
(**) Corrected for thermal radiation.

changed between 1958 and the present time, Sloanaker and Boland's values can be corrected and become 744°K and 392°K, respectively. Within the experimental errors the larger (1958) disk temperature then agrees with our measurement, but the low (1959) value of 392°K can only be accounted for by a temporal variation in disk temperature or in fractional polarization, or both.

REFERENCES

Broten, N. W. and Medd, W. J., *Ap. J.*, **132**, 279, 1960.

Morris, D. and Berge, G. L., *Ap. J.*, **136**, 276, 1962.

Rowson, B., *M. N.*, **119**, 26, 1959.

Sloanaker, R. M. and Boland, J. W., Proceedings XIII General Assembly of U. R. S. I., p. 524, Publication No. 880 of the National Academy of Science-National Research Council, 1961.

Smith, A. G. and Carr, T. D., *Ap. J.*, **130**, 643, 1959.

58. — THE RADIATION BELT OF JUPITER

M. S. ROBERTS and G. R. HUGUENIN
Harvard College Observatory
Cambridge, Massachusetts, U. S. A.

I. Introduction

The significant aspects of Jupiter's microwave radiation are : a) The flux at decimeter wavelengths is much larger than would be predicted from the measured infrared temperature of about 130°K(1). Equivalent black body disc temperatures derived from these flux measures reach values as high as 40,000°K at 68 cm. b) Measures at 31 and 22 cm (2, 3) and at 21 cm (4) have shown that the radiation is partially polarized in a direction approximately parallel to Jupiter's rotational equator. The equatorial extent of this radiation is about 3 Jovian diameters. c) A positive correlation exists between the flux received from Jupiter and solar activity as measured by sunspot number or 10.7 cm solar flux (5). This correlation has been found only in those observations which were made with the E vector of the antenna system approximately parallel to Jupiter's equator. Items b) and c) above imply that that component of the Jovian decimeter radiation which is polarized is also the component which varies with solar activity.

In anticipation of the discussion to follow, we will find it convenient to separate the Jovian radiation into three components :

Component 1 : The thermal radiation corresponding to an observed temperature of about 130°K.

Component 2 : The nonpolarized, nonthermal radiation which at decimeter wavelengths has a disc temperature of several thousand degrees. Components 1 and 2 may be related but because of the high temperatures found for Component 2 it seems desirable, at present, to distinguish between these two.

Component 3 : The polarized, nonthermal radiation from Jupiter.

II. Observational data

Table I summarizes the observational data for Jupiter. The disc temperatures given in column 2 are equivalent black body

Table I

Summary of Observations

λ cm	T_D °K	S_λ at 5AU $10^{-24} wm^{-2}(c/s)^{-1}$	φ[1]	Avg. 10 cm Solar Flux[2]	Ref.
IR	130				(1)
3.15	140	1.05			(6)
3.15	145	1.05			(6)
3.03	171	1.41			(7)
3.17	173	1.27			(7)
3.36	189	1.27			(7)
3.75	200	1.05			(6)
10.0	622	0.46	74°	108	(9)
10.2	315	0.22	79°	169	(10)
10.3	640	0.44	67°	229	(10)
20.8	3,600	0.61	14°	103	(4)
20.8	2,200	0.37	77°	114	(4)
21.0	2,500	0.42	76°	212	(11)
21.1	4,500[3]	0.74	14°	204	(12)
21.1	3,900	0.65	15°	110	(5)
21.1	4,100	0.68	24°	96	(5)
22.0	2,900	0.43	76°	211	(13)
31	5,500	0.4	77°	214	(14)
68.2	44,000	0.69	14°[4]	201	(15)
68.2	34,000	0.53	15°[4]	215	(15)
68.2	10,000	0.15	14°[4]	159	(15)

1. Average angle between E vector of antenna system and rotational equator of Jupiter. These values are accurate to 1 or 2 degrees. The observations at 3 cm are averages over a range of φ.

2. Averages take into account the difference in synodic rotation period of sun as viewed from Jupiter and the earth.

3. The antenna temperature for Virgo A as adopted in (15) has been corrected.

4. Faraday rotation may significantly alter these values.

temperatures for a source equal in size to the optical dimensions of Jupiter. Column 3 presents the observed fluxes S_λ adjusted to a standard distance of 5 A. U. It should be noted that these fluxes represent the radiation in both planes of polarization for an assumed randomly polarized source. Column 4 gives the angle φ between the E vector of the antenna system and the rotational equator of Jupiter,

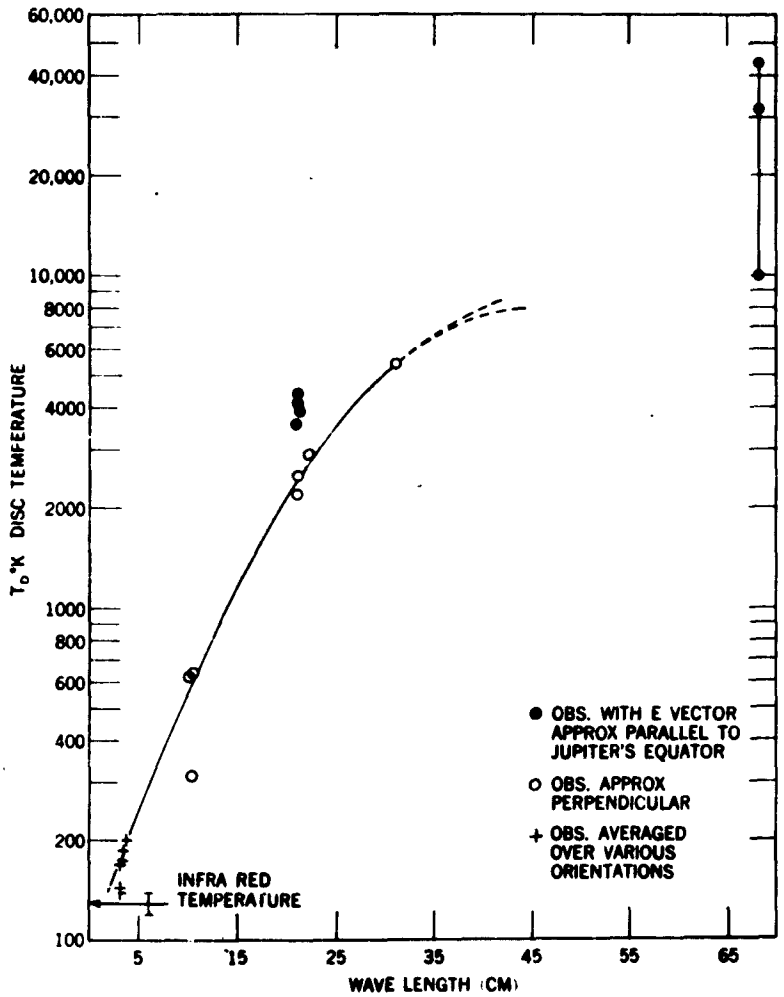

Fig. 1. — Disc temperature as a function of wavelength. The smooth curve represents the spectrum of Component 2. Two possible extrapolations of this spectrum to higher wavelengths are indicated by the dashed lines.

Average values of the 10.7 cm solar flux during the period of observation are given in column 5.

Figure 1 displays the disc temperature T_D as a function of wavelength while Fig. 2 is a plot of the flux as a function of wavelength. An observational uncertainty of the order of 10 % is present in the values of T_D and S_λ. A discordant point occurs at 10 cm where one of the values is about one half of the other two values at this wavelength.

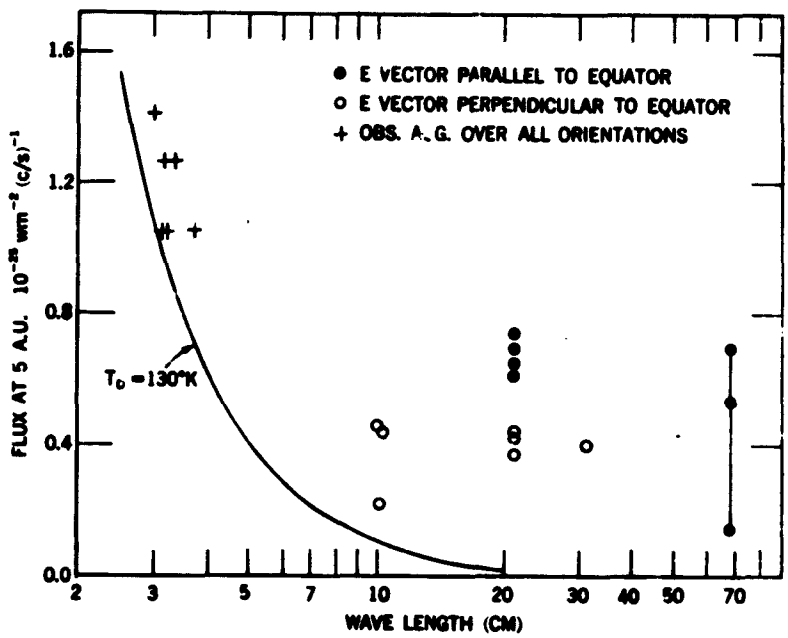

Fig. 2. — Observed flux (adjusted to a distance of 5 A. U.) as a function of wavelength. The contribution to the observed flux from a 130° K source is indicated by the curve. The difference between open and filled circles is due to Component 3 radiation. The lowest flux measure at 68 cm is an upper limit to Component 2 radiation at this wavelength.

As might be expected, those observations which accept only a small fraction of the polarized component of the Jovian radiation, indicated by open circles in both Figs. 1 and 2, are systematically lower than those observations which do measure this component (filled circles). A smooth curve has been drawn through those points

in Fig. 1 which represent observations made of the unpolarized component of the Jovian radiation. This curve, which includes the thermal component of Jupiter (Component 1), represents the energy distribution as a function of wavelength of Component 2. (The contribution of Component 1 merely changes the zero point of the temperature scale.) Two possible extrapolations of this curve are indicated by the dashed lines. The observations at 68 cm were made approximately parallel to Jupiter's equator and therefore include a significant contribution from the polarized radiation. Since Faraday rotation in the earth's ionosphere at this wavelength is quite large, an uncertainty as to the true orientation of the E vector of the antenna system with respect to Jupiter's equator is present. We may use the 68 cm data to place an upper limit of about 10,000°K on the disc temperature, at this wavelength, of Component 2.

The contribution to the observed flux at centimeter wavelengths due to the infrared temperature of 130°K is shown by the curve in Fig. 2. At 10 cm, Component 1 contributes about 25 % of the observed radiation for large φ. We also see from this figure that the flux due to Component 2 is relatively constant to $\lambda \approx 30$ cm and decreases at longer wavelengths, the lowest plotted point at 68 cm representing an upper limit to Component 2 radiation. The difference between observations made parallel to Jupiter's equator and those made perpendicular to the equator represents the radiation due to Component 3. The difference indicated in Fig.2 is artifically large because of the usual procedure in multiplying observed antenna temperatures by a factor of two to account for both planes of polarization in an assumed randomly polarized source. If Component 2 is 100 % polarized at 21 cm, the flux to be attributed to Component 3 should be reduced by one half (for $\varphi = 0°$) from the values (i. e. the differences) indicated in Fig. 2. Smaller amounts of polarization for this component would result in correspondingly smaller reductions in the indicated flux for Component 3.

III. Correlation with solar activity

An analysis for a possible correlation between solar activity and the flux radiated by Jupiter was performed on those data for which sufficient information was available. Several of the solutions are based on unpublished material kindly made available to us by the Naval Research Laboratory and the National Radio Astronomy Observatory. A least squares determination of the regression of Jupiter flux on solar activity of the form

$$\text{Jup. flux} = (m \pm \sigma_m)\left(\frac{\text{10.7 cm solar flux}}{100}\right) + (b \pm \sigma_b) \quad (1)$$

was made for the various sets of 21 cm observations listed in Table I as well as one set of 10 cm data ([10]) and the 31 cm data ([14]). These calculations took into account the different synodic rotation periods of the sun as observed from Jupiter and from the earth and

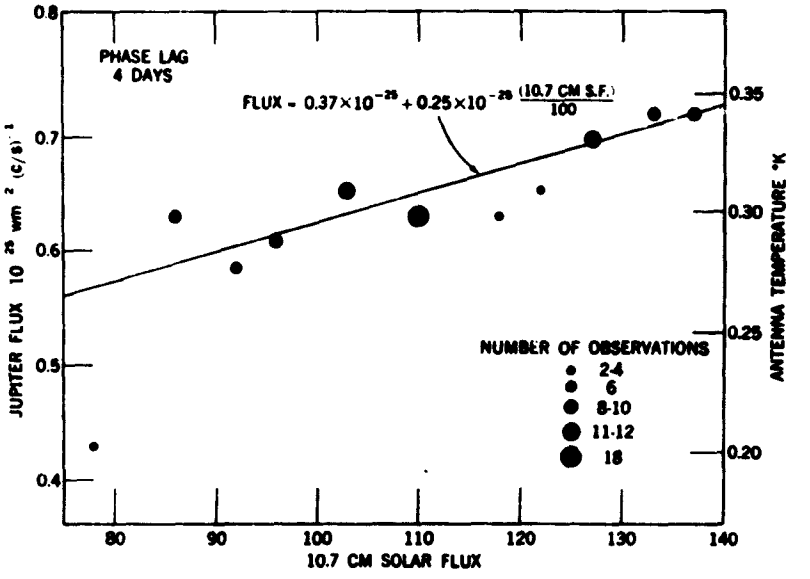

Fig. 3. — Least squares determination of the regression of Jupiter flux (at 1423 Mc) on solar activity. The Jupiter observational data were obtained with a maser radiometer attached to the Harvard 60-foot radio telescope.

were made for a variety of phase lags between solar activity and observed Jupiter flux. An example of one such solution is shown in Fig. 3 where the observational data was obtained in 1961 with a maser radiometer operating at 1423 Mc ([5]). A reproduction of a drift curve observation of Jupiter made with this equipment is

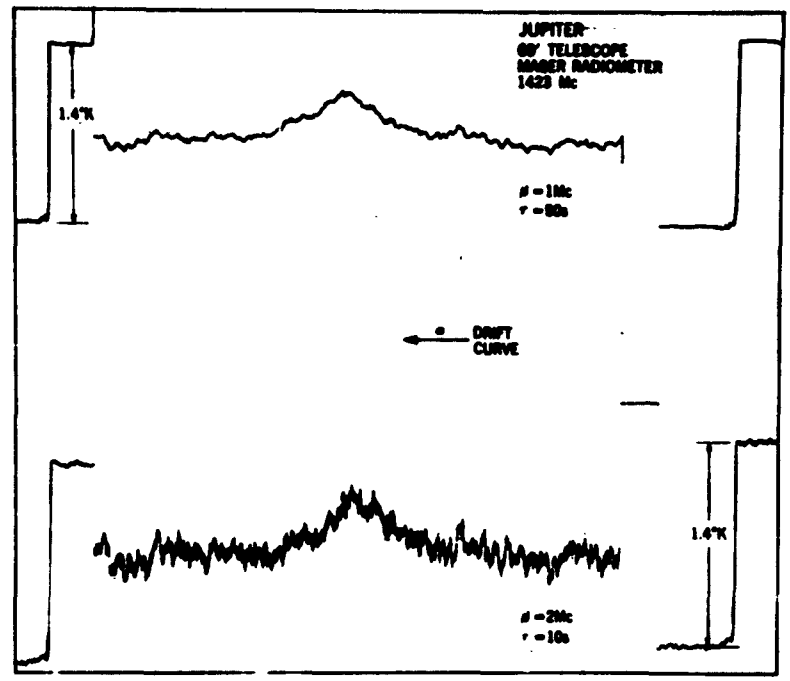

Fig. 4. — Example of drift curve observation of Jupiter obtained with a maser radiometer and 60-foot radio telescope.

shown in Fig. 4. In Fig. 5 we plot the ratio of the slope, as determined by the regression analysis, to the standard error in the determination of the slope, $\frac{m}{\sigma_m}$, as a function of the phase lag. This ratio is highest over a range of phase lags of 2 to 6 days with a peak at 4 days. The smoothly varying nature of this ratio, $\frac{m}{\sigma_m}$, with phase lag is to be expected since the solar activity as measured by 10.7 cm

flux is also a slowly varying quantity from day to day, going through a cycle in the order of one sidereal rotation period of the sun. It is interesting to note in Fig. 5 that the ratio $\frac{m}{\sigma_m}$ is quite high over a large range of values of phase lag ; this range reflects the autocorrelations of Jovian radiation and of solar activity.

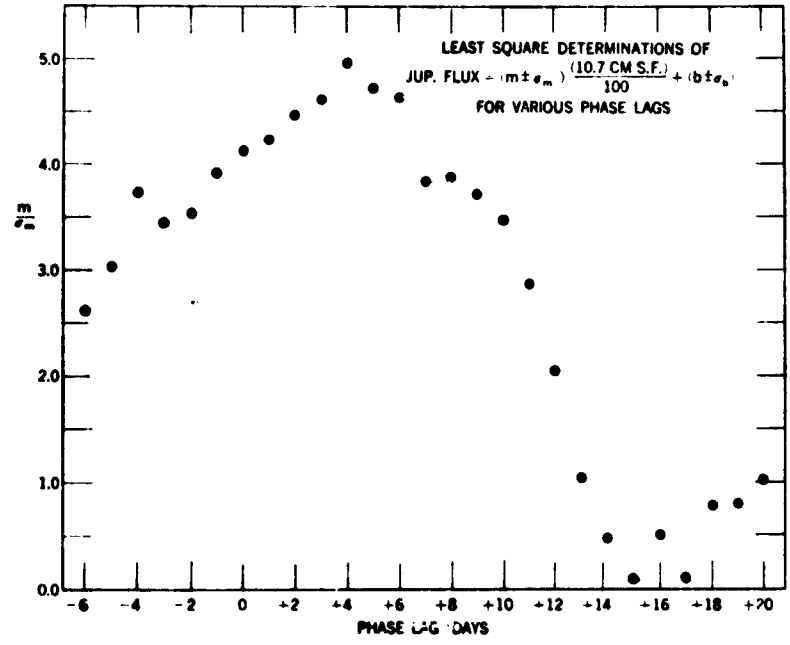

Fig. 5. — The slope of the regression of Jupiter flux on solar activity in terms of the standard error of the determination of the slope *vs* phase lag.

The results of the various least squares determinations for the 21 cm data listed in Table I are shown in Fig. 6. We plot here the average value of the Jupiter flux *vs* the average value of the 10.7 cm solar flux during the period of observations. The filled and open circles represent, respectively, observations in which the E vector of the antenna system was approximately parallel and perpendicular to Jupiter's rotational equator. The length of the line through each point represents the range of solar activity during the period

of observations, while the slope of the line is that obtaincd from the least squares determination. The slope with the largest $\frac{m}{\sigma_m}$ for a phase lag between 2 and 6 days was used in constructing this diagram. The error bar at the end of each of the lines represents the uncertainty in the determination of the slope. The observational uncertainties in the average flux values are about 10 %. The dashed line represents an extension of the well determined solution illustrated in Fig. 3. The regression of Jovian flux on solar activity need

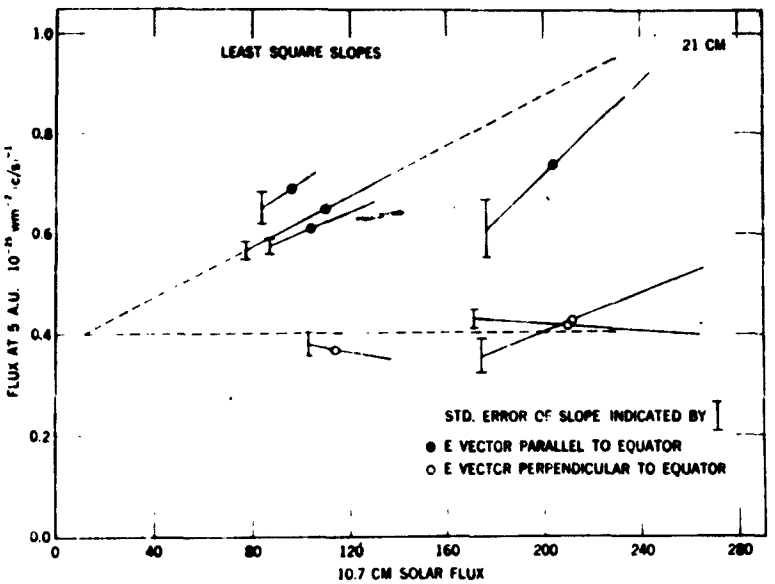

Fig. 6. — The results of the regression analyses on various sets of 21 cm observations. Average values of Jupiter flux and solar flux are plotted as open and filled circles. The length of the solid line through each circle indicates the variation in 10.7 cm solar flux during the period of observation. The standard error of the determination of the slope will yield a range of possible slopes as indicated by the error bars for a line rotated about the plotted average value.

not be linear, and in fact a smaller slope may exist at higher values of solar activity. Physically this would imply a « saturation » of the effect giving rise to the Jovian flux variations.

Within the range of uncertainties mentioned above, we con-

clude that the polarized component of the Jovian radiation is correlated with solar activity while the unpolarized component shows no significant correlation. We see from Fig. 6 that the polarized component will disappear, leaving only the unpolarized component, at very low values of solar activity. This fact together with the polarization characteristics of the two types of radiation are the basis for the delineation of Components 2 and 3. We may thus add another characteristic to the description of Component 3 : its dependence on solar activity.

IV. Origin of Component 3

Because of the polarized, nonthermal nature of Component 3, magneto-bremsstrahlung immediately suggests itself as the mechanism responsible for this component. Following Drake [13], Field [16], and Roberts and Stanley [14], we consider as the basic model high-energy electrons trapped in a Jovian magnetic field. Field [17] has shown that the cyclotron mechanism is unlikely on the basis of the decay time of a monoenergetic injection of electrons into the Jovian magnetic field. Cyclotron radiation may also be excluded by another line of reasoning based on the observational data presented in Section III. From Fig. 6 we see that the polarization of the decimeter radiation increases with increasing solar activity ; cyclotron radiation predicts an opposite result. This follows [19] from Field's polarization curve (Ref. 18, Fig. 4) and the source dimensions and equatorial polarization measured by Morris and Berge [3].

With the elimination of cyclotron radiation we turn to a synchrotron mechanism as the source of Component 3 of Jupiter's radiation. Our task is twofold : (i) to obtain a quantitative picture of the radiation belt responsible for Component 3, and (ii) to account for the formation of such a belt, including its dependence on solar activity, in terms of our current knowledge of the interplanetary medium and the solar wind.

The general theory of synchrotron radiation from electrons trapped in a planetary dipole magnetic field has been considered by Chang ([20, 21]). He derives the appropriate Stokes parameter description of synchrotron radiation from planetary radiation belts. Following Chang's discussion, we shall construct a model of the radiation belt based on the observational data presented in the previous sections. From Fig. 6 we derive the equatorial flux from Component 3 at 21 cm with a 10.7 cm solar flux value of 100 to be

$$S_3^{(E)} \approx 2 \times 10^{-26}\ wm^{-2}\ (c/s)^{-1}$$

It is likely that a polar flux from Component 3 greater than $0.5 \times 10^{-26}\ wm^{-2}\ (c/s)^{-1}$ would have been detected in the solar correlation analyses. We therefore assume that the polar flux is

$$S_3^{(P)} \lesssim 0.5 \times 10^{-26}\ wm^{-2}\ (c/s)^{-1}$$

The resultant polarization of Component 3 at $\lambda = 21$ cm is

$$m_3 = \frac{S_3^{(E)} - S_3^{(P)}}{S_3^{(E)} + S_3^{(P)}} \gtrsim 0.6 \qquad (2)$$

For a polarization of Component 3 of $\gtrsim 0.6$, the polarization of the entire Jupiter source (at 10.7 solar flux, SF, = 100) becomes

$$m_{21} \gtrsim 0.20 \quad (\mathrm{SF} = 100)$$

which is in fairly good agreement with the observed value ([3]) of 0.28 ± 0.06 at 1390 Mc. The size of the decimeter source measured by Morris and Berge ([3]) indicates a polar extent roughly the diameter of Jupiter, and an equatorial size of about 3 Jovian diameters. For the model discussed here, it is assumed that Components 1 and 2 are limited in extent to the visible disc of Jupiter and that Component 3 has an equatorial size of $3\ D_{21}$. To explain the observed polarization of Jupiter and therefore the polarization of Component 3, we find that the north-south extent of the belt is from 0.5 to $0.6\ D_{21}$.

The observational data also yield information as to the characteristic time for the cycle of acceleration and decay of the responsible electrons. This time is of the order of 5 ± 3 days and follows from the width of the correlation *vs* phase lag diagram shown in

Fig. 5 and the corresponding width found in the autocorrelation of the solar 10.7 cm flux over the period of observations.

In summary, the purely observational data yield the following picture of Component 3 at ~ 21 cm.

Size : Equatorial extent $\sim 3\ D_{2\frac{1}{4}}$.

Polarization : $\gtrsim 0.6$

Characteristic time for acceleration (or injection) and decay : $\sim 5 \pm 3$ days

Flux : $2 \times 10^{-26}\ wm^{-2}\ (c/s)^{-1}$ at SF = 100, $\lambda = 21$ cm.

These quantities represent the input data, and may be considered as constraints, for the model. In addition, the following assumptions have been made.

(1) The magnetic field of Jupiter has a dipole configuration for $R \leqslant 3\ R_{2\frac{1}{4}}$.

(2) The equatorial magnetic field at the location of the radiation belt ($3R_{2\frac{1}{4}}$) shall satisfy the condition

$$\frac{B^2\ (3\ R_{2\frac{1}{4}},\ \pi/2)}{8\pi} > nm_pv^2 \qquad (3)$$

where nm_pv^2 is the solar wind pressure at Jupiter's orbit.

(3) The internal pressure of the trapped radiation shall be less than the magnetic pressure of the trapping field, that is :

$$\frac{B^2\ (3\ R_{2\frac{1}{4}},\ \pi/2)}{8\pi} > n_eE. \qquad (4)$$

The relevant Stokes parameters ([20, 21]) for synchrotron radiation are :

$$I(f)dVdf = \frac{CBdVdf}{R^2} \int \rho\ (E,\ a^*)\ F\left(\frac{f}{f_e^*}\right) dE \qquad (5)$$

and

$$Q\ (f)\ dVdf = \frac{-\ CB\ \cos 2\chi\ dVdf}{R^2} \int \rho\ (E,\ a^*)\ F_p\left(\frac{f}{f_e^*}\right) dE \qquad (6)$$

where $I(f)dVdf$ is the total intensity radiated from volume element dV in the frequency range df at f.

$Q(f)dVdf$ is the portion of $I(f)dVdf$ with electric vector parallel to the equator minus the portion of $I(f)dVdf$ with electric vector perpendicular (i. e. parallel to the pole).

B is the magnetic field strength.

R is the distance to the observer.

ρ (E, α^*) $dVdEd\alpha$ is the number of radiating electrons in volume dV with energies in the range dE at E and helix angles in the range $d\alpha$ at α^* where α^* is the angle between the vector magnetic field at dV and the vector to the observer. χ is the angle involved in defining QdV. It is the angle measured clockwise by the observer from a direction coplanar with the equator and at right angles to the line to the observer to the projection of the magnetic field into the plane at right angles to the observer.

f_c is the Schwinger critical frequency corresponding to α^*, i. e. $f^* = LB \sin \alpha^* E^2$ where L is a constant.

$$F\left(\frac{f}{f_c}\right) = \frac{f}{f_c}\int_{f/f_c}^{\infty} K_{5/3}(x)\,dx, \tag{7}$$

and

$$F_p\left(\frac{f}{f_c}\right) = \frac{f}{f_c} K_{2/3}\left(\frac{f}{f_c}\right) \tag{8}$$

The density distribution used for the calculations of this model is based on a monoenergetic electron spectrum, and an isotropic helix angle distribution to the cutoff angle α_E. The cutoff angle α_E corresponds to mirror points consistent with the observed polarization of Component 3. From the spectrum of Fig. 2, the Schwinger critical frequency is chosen to be 3 *k*Mc, which places the frequency of maximum radiation in the decimeter range around 50 to 60 cm. The model, though admittedly crude, is very instructive ; more refined calculations will appear elsewhere ([19]).

Numerically integrating the equations for $I(f)$ and $Q(f)$ with the observational and assumed constraints, the following picture of the Jovian radiation belt emerges :

(1) θ_m, the latitude of the maximum mirror points, of 10°-12°.

(2) α_E, the equatorial cutoff helix angle corresponding to θ_m, of 20°-25°.

(3) An equatorial magnetic field, B ($3R_{2\frac{1}{4}}$, $\pi/2$), at the belt ($3R_{2\frac{1}{4}}$) of 1.75 gauss corresponding to an equatorial field at the surface of Jupiter of 47 gauss.

(4) Electron energies of 10 *Mev* with a corresponding gyroradius, r_E, of 183 meters.

(5) A total number N of electrons participating of 3×10^{35}, or for a belt 0.1 $R_{2\frac{1}{4}}$ in thickness, a density, n_e, of 4×10^{-5} electrons per cm^3. The calculations are for a « thin » belt ; the arbitrarily chosen thickness need only be larger than r_E.

(6) Polarization of Component 3 at 21 cm of 0.64 with a total polarization for Jupiter at 21 cm of 0.21. These values representing recoverable quantities from the input data.

(7) Characteristic time for decay $T_{1/2}$ of 5 days.

(8) The dimensions of the radiation belt are roughly that of a torus with a major radius of $3R_{2\frac{1}{4}}$ and a cross section of 0.1 $R_{2\frac{1}{4}}$ in the equatorial plane and 0.5 $R_{2\frac{1}{4}}$ perpendicular to this plane.

TABLE II

Parameters of Radiation Belt

$T_{1/2}$ Days	$B(3R_{2\frac{1}{4}},\pi/2)$ Gauss	$B(R_{2\frac{1}{4}},\pi/2)$ Gauss	E Mev	N	n_e cm^{-3}	r_E meters
0.1	24	640	2.8	2.10^{34}	3.10^{-6}	3.9
1	5.1	138	6.1	9.10^{34}	1.10^{-5}	39
3	2.5	66	8.8	2.10^{35}	3.10^{-5}	116
5	1.8	47	10	3.10^{35}	4.10^{-5}	183
7	1.4	38	12	3.10^{35}	5.10^{-5}	283
10	1.1	30	13	4.10^{35}	6.10^{-5}	390
100	0.24	6.3	28	2.10^{36}	3.10^{-4}	3,850

We present in Table II the parameters of the radiation belt for various values of $T_{1/2}$ for the range 0.1 to 100 days. The geometric aspects remain the same as those derived above.

From Table II, we see that the equatorial magnetic field, $B(R_{2\frac{1}{2}}, \pi/2)$, required is large compared to the earth but is not unreasonable in size. The total number of high energy electrons N is too large to be supplied directly by the solar wind, i. e. to be transported from the sun to Jupiter. However, *an acceleration by the solar wind of low velocity electrons already present at Jupiter is possible and likely*; such an acceleration has been suggested by Chang ([20, 21]).

The acceleration mechanism active at Jupiter must favor the acceleration of already trapped low-energy electrons to higher energies and flatter helices. The most likely mechanism for producing flat helices and high energies involves the propagation of hydromagnetic waves from the boundary region between Jupiter's magnetosphere and the interplanetary medium. This mechanism could be particularly effective if at Jupiter's orbit ($\sim$ 5 A. U.) the flow of solar plasma broke from laminar flow into turbulence. The correlation of the emission of Component 3 with solar activity is consistent with a solar wind acceleration hypothesis.

The energy radiated by Component 3 for a flux of 2×10^{-26} $w m^{-2}$ $(c/s)^{-1}$ (at SF = 100) over a bandwidth of 3 *kMc* is 2.7×10^{14} ergs/sec. The energy intercepted by Jupiter from the solar wind, assuming 10 protons cm^{-3} travelling at 300 km/sec at the earth ([22]), is 1.4×10^{19} ergs/sec. Thus the efficiency of energy conversion from the solar wind to decimeter radiation need only be of the order of 10^{-5}. The total mass of the radiating electrons is less than one gram.

V. Origin of Component 2

The origin of the Component 2 radiation is more difficult to fix; thermal (including ionospheric free-free transitions) and such

nonthermal mechanisms as a second radiation belt or continual electrical discharges (storms) all encounter difficulties which are compounded by a lack of sufficient observational data. We shall consider here one possible mechanism for accounting for Component 2 : a Jovian ionosphere.

Three quantities are available which will allow us to describe such an ionosphere :

(1) The spectrum of Component 2.

(2) An estimate of Jupiter's equatorial magnetic field (from section IV) and therefore the cyclotron frequency in the ionosphere.

(3) Observations of Jovian decameter radiation to 34 Mc ([22]). We shall assume that this radiation originates below the ionosphere and propagates through this ionosphere in the extraordinary mode (whistler mode).

For decameter radiation of frequency ν to penetrate the ionosphere we require

$$\nu_p < \nu \left(1 + \frac{\nu_H}{\nu}\right)^{1/2} \tag{9}$$

where ν_p is the plasma frequency and ν_H the cyclotron frequency. Adopting ν_H corresponding to a magnetic field $B(R_{2\frac{1}{2}}, \pi/2) = 47$ gauss, the value derived for $T_{1/2} = 5$ days, and an upper limit of $\nu = 50$ Mc we obtain

$$\nu_p < 100 \text{ Mc}$$

The corresponding electron density n is given by

$$\nu_p = 9 \sqrt{n}\, kc, \tag{10}$$

or

$$n_{max} \leqslant 1.3 \times 10^8 \text{ cm}^{-3}.$$

The quantity n_{max} is the maximum electron density in the Jovian ionosphere consistent with circularly polarized decameter radiation. This density is about two orders of magnitude larger than in the earth's ionosphere.

Figure 2 shows a spectrum of Component 2 which, for an ionospheric model, corresponds to an opacity of approximately unity at $\lambda = 20$ cm with a temperature of $\sim 2500^{\circ}$K. The opacity due to free-free transitions in the ionosphere is

$$\tau = 1.1 \times 10^{-22} T^{-3/2} \lambda^2 \int n^2 dz \qquad (11)$$

For $\tau = 1$ at $\lambda = 20$ cm we obtain

$$\int n^2 \, dz = 3 \times 10^{24}$$

Or, for a uniform electron density of $n_{max} \leqslant 1.3 \times 10^6$, $z \geqslant 2.3 \times 10^3$ km. This value, about 5 times larger than the earth's ionosphere, is quite sensitive to the adopted cutoff frequency for decameter radiation.

In general, we require an ionosphere for Jupiter that is both denser and deeper than the earth's. Any complete explanation of such a Jovian ionosphere will have to include a mechanism for maintaining such a large ionosphere. An ionospheric model in addition to explaining Component 2 also possesses the features (and drawbacks)ascribed to it in proposed explanations of Jovian decameter radiation (see e. g. [24, 25]).

VI. Summary and Desiderata

The resumé of the microwave aspects of Jupiter's radiation given in Section I can most simply be interpreted in terms of three separate mechanisms :

1. The thermal radiation

2. A non thermal, non polarized mechanism, e. g. an ionosphere or inner radiation belt.

3. Synchrotron radiation from a radiation belt.

Interestingly enough, an extraterrestrial observer studying the earth's electromagnetic spectrum would arrive at the same general conclusions about the earth.

A high (compared to the earth) but not improbable magnetic field of ~ 50 gauss is required to account for Component 3 radiation. The relativistic electrons responsible for this radiation arise from a hydromagnetic acceleration of trapped low-velocity electrons at Jupiter. The solar wind can supply the energy necessary for the acceleration and, if need be, the necessary number of initially low velocity electrons.

The explanation of Component 2 radiation is more uncertain. If an ionospheric model is to be invoked, this ionosphere will be denser and deeper than the earth's ionosphere. The most serious problem here is the method of maintaining such an ionosphere.

The radio study of Jupiter presents us with a valuable tool for studying the sun, the interplanetary medium, and the problem of radiations belts. To properly evaluate the interrelation of these various parameters, simultaneous observations at different frequencies and polarizations over a solar cycle will be needed. Jupiter also represents an obvious problem for world-wide observations. Even a short period of intensive, round-the-clock observations would be most valuable.

REFERENCES

(1) D. H. Menzel, W. W. Coblentz and C. O. Lampland, *Ap. J.*, 63, 177, 1926.

(2) V. Radhakrishnan and J. A. Roberts, *Phys. Rev. Letters*, 4, 493, 1960.

(3) D. Morris and G. L. Berge, *Obs. of Calif. Inst of Tech. Radio Observatory*, No. 7, 1961.

(4) A. C. Miller and B. L. Gary, Washington meeting, U. R. S. I., 1962, and private communication.

(5) M. S. Roberts, *A. J.*, June 1962 and this paper.

(6) C. H. Mayer, T. P. McCullough and R. M. Sloanaker, *Proc. Inst. of Radio Eng.*, 46, 260, 1958; *Ap. J.*, 127, 11, 1958.

(7) J. A. Giordmaine, L. E. Alsop, C. H. Townes and C. H. Mayer, *A. J.*, 64, 332, 1959.

(8) F. D. Drake and H. I. Ewen, *Proc. Inst. of Radio Eng.*, 46, 53, 1958.

(9) F. D. Drake, Private communication, 1962.

(10) R. M. Sloanaker and J. W. Boland, *Ap. J.*, 133, 649, 1961.

(11) E. F. McClain, J. H. Nichols and J. A. Waak, XIII General Assembly, U. R. S. I., 1960 and private communication.

(12) E. E. Epstein, *Nature*, 184, 52, 1959 and private communication.

(13) F. D. Drake and H. Hvatum, *A. J.*, 64, 329, 1959, and private communication.

(14) J. A. Roberts and G. J. Stanley, *Publ. A. S. P.*, 71, 485, 1959.

(15) F. D. Drake and H. Hvatum, XIII general Assembly, U. R. S. I., 1960, and private communication.

(16) G. B. Field, *J. Geophys. Res.*, 64, 1169, 1959.

(17) G. B. Field, *J. Geophys. Res.*, 66, 1395, 1961.

(18) G. B. Field, *J. Geophys. Res.*, 65, 1661, 1960.

(19) G. R. Huguenin and M. S. Roberts, in preparation.

(20) D. B. Chang, Boeing Scientific Laboratories Document D1-82-0060, 1960.

(21) D. B. Chang, Boeing Scientific Laboratories Document D1-82-0129, 1962.

(22) H. S. Bridge, C. Dilworth, A. Lazarus, E. F. Lyon, B. Rossi and F. Scherb, International Conference on Cosmic Rays and the Earth Storm, Kyoto, Japan, 1961.

(23) J. W. Warwick, *Annals of the New York Acad. of Sci.*, 95, 39, 1961.

(24) R. M. Gallet, in *Planets and Satellites* (ed. G. P. Kuiper and B. M. Middlehurst), (Chicago : Univ. of Chicago Press), p. 500, 1961.

(25) A. G. Smith, *Science*, 134, 587, 1961.

59. — THE RELATION BETWEEN JUPITER'S DECAMETRIC EMISSION AND RADIATION BELTS

JAMES W. WARWICK
High Altitude Observatory Boulder, Colorado, U. S. A.

ABSTRACT

Dynamic spectra of Jupiter's sporadic radio emission show that the longitude profile, above 25 megacycles, consists of two principal sources, one early in longitude, drifting from low to high frequencies, and the other, late in longitude, drifting from high to low frequencies. This pattern is virtually permanent in all spectra obtained over a two-year interval. It can be understood in terms of precipitation of fast (10 kev) electrons out of Jupiter's belts, and down to the surface of the planet along dipole lines of force. There the particles generate emission essentially at the electronic gyro frequency in the local magnetic field. With this interpretation, we may discuss the location and strength of Jupiter's magnetic dipole moment.

60. — SOME DATA ON THE INTENSITY OF METHANE ABSORPTION IN THE ATMOSPHERE OF JUPITER

V. G. TEIFEL
Astrophysical Institute of the Academy of Sciences, KazSSR Alma-Ata, USSR

Observations of the intensity of the absorption band CH_4 6190 A were carried out by the author in 1958-1960 at Alma-Ata. The purpose of these observations was to study the possible changes of the intensity of the band as a function of time and position on the disk of the planet.

The spectrum of Jupiter was photographed by different methods. In 1958 the slit of the spectrograph was set along the equator, along the central meridian and along N-tropical band of a magnified image of Jupiter. The distribution of intensity on the disk, along these directions, in the CH_4 6190 Å and 5430 Å bands of absorption was investigated on the spectrograms.

The entrance slit of the microphotometer cuts out on the negatives regions of the spectrum corresponding to a width of about 36 Å at λ 6200 Å and of about 29.5 Å at λ 5400 Å. The measurements of 75 spectrograms showed that the distribution of intensity along the equator of Jupiter was in accordance with the value $q = 0.79$ [1] of the coefficient of limb darkening. The observed distribution proved to be near the theoretical one for the value of the parameter $\lambda = \frac{\sigma}{\sigma + \varkappa} = 0.97$ ($\varkappa$ — the coefficient of true absorption, σ — the coefficient of scattering in the atmosphere of Jupiter [2]). The distribution of intensity over the disk, within the absorption band, turned out to be completely identical with that in the adjacent regions of the continuous spectrum. This shows that the intensity of the methane absorption band remains constant in any regions of the planet disk. In N-tropical band the intensity of methane absorption does not practically differ from that in the equator. This shows an equality of heights of the upper boundary

of the cloud layer both in dark and bright zones of the visible surface of Jupiter.

These results are in agreement with the previous works of N. T. Bobrovnikoff (3), D. I. Eropkin (4), V. M. Slipher (5) and S. L. Hess (6).

S. L. Hess had found from 30 spectrograms of Jupiter that the greatest difference of intensity of methane absorption from the equatorial zone occurs near 30° latitude. This difference equals — 4 Å in the units of the equivalent widths of the CH_4 6190 Å band.

Our observations (carried out in 1959) of the spectra of different latitude zones of Jupiter from 200 spectrograms showed that the difference in the equivalent widths of the CH_4 6190 Å band for equatorial and temperate planet zone is negligible (table I).

TABLE I

Zone	W_b	σ_w	R_b	σ_R
		±		±
EZ	18.4	1.7	0.210	0.016
NTZ	18.0	1.8	0.202	0.017
STZ	18.1	1.8	0.205	0.017

In this table W_b is the mean value of the equivalent width, σ_w is the mean quadratic error of the determination of W_b, R_b is the depth of the absorption band, σ_R is the mean quadratic error of the determination of R_b.

Thus, these observations confirm the constancy of the methane absorption band intensity in different points of Jupiter's disk. One of the possible explanations of this phenomenon may be the following : the observed intensity of methane absorption band depends on two factors : a) the absorption in the pure gaseous layer of the atmosphere lying over the cloud layer and b) the reduced albedo of the cloud layer in the absorption band due to the decrease

of the value of the parameter λ as a result of the increase of true methane absorption. The absorption in the pure gaseous layer grows towards the edge of the planet disk. The second factor works in the opposite direction because the smaller darkness towards the edge is observed at the smaller values of the parameter λ (7).

At a certain optical thickness of the true gaseous layer in the methane band (at the center of the $\tau_{b_7} = 0.05$) these two factors can compensate each other, and the observed intensity of the CH_4 6190 Å band will remain constant at the transition from the center towards the edge of the disk. The optical thickness of the pure gaseous layer is very small : from 0.0059 at λ 4000 Å to 0.0009 at λ 6500 Å, if we proceed from the composition of the atmosphere of Jupiter according to the model « b » suggested by G. P. Kuiper (8). The full atmospheric pressure on the upper boundary of the cloud layer is about 0.85 — 1.00 atm.

The observations carried out in 1959 and 1960 showed that the intensity of the CH_4 band is somewhat changing from night to night. The average value of W_b for the equatorial zone, in 1959, was 18.4 Å and in 1960, 20.4 Å. The fluctuations of intensity (with discount of possible errors of measurements) proceed within $\pm$ 1 Å and have no marked correlation with the solar activity.

If these fluctuations are real, one may suggest that there are two reasons for changes of the methane absorption with the passage of time on Jupiter : 1. — the photochemical processes (photodissociation of molecules CH_4) affected by the corpuscular and ultraviolet solar radiation, and 2 — the fluctuations of height of the upper boundary of the cloud layer, that cause the changes of linear and optical thickness of the pure gaseous layer of Jupiter's atmosphere. Some dimness can appear in the pure gaseous layer. Its effect can be identical to reason 2.

The computations showed that the life-time of the molecules CH_4, in the field of the solar radiation at the distance of Jupiter, was very large (of order 10 and more days) for a moderate level of radiation. It cannot explain the short-time fluctuations of the intensity of the methane absorption.

The change of heigt of the upper boundary of the cloud layer is more likely to take place. It equals $\pm$ 2 km for the above limits of the fluctuations of the equivalent width of the band CH_4 6190 Å.

To make these results more precise, observations of the distribution of brightness over the disk of Jupiter in bands of CH_4 and NH_3, with the simultaneous determination of the equivalent widths of bands are to be made. The use of interference filters and spectrographs of high dispersion will make it possible to find the small deflections in the distribution of the band intensity over the disk, due to the height of the upper cloud boundary, that is determined by the values of the equivalent widths of the absorption band.

REFERENCES

(1) H. C. Van de Hulst, Atmospheres of the Earth and planets. 2nd ed., Kuiper, 1952.

(2) V. V. Sobolev, *Uspekhi Astronomicheskikh Nauk*, v. VI, 1954.

(3) N. T. Bobrovnikoff, *PASP*, 45, 172, 1933.

(4) D. I. Eropkin, *Circular GAO*, 10, 15-16, 1934.

(5) V. M. Slipher, *MN RAS*, 93, 657, 1933.

(6) S. L. Hess, *Astrophys. J.*, 118, 1, 151-160, 1953.

(7) V. G. Teifel, *Izv. Komissii po fizike planet*, 1, 93-104, 1959.

(8) G. P. Kuiper, Atmospheres of the Earth and planets, 2nd ed, 1952.

B. M. PEEK (49). — As an Advocate of the « floating body » theory I have always been worried by the constancy of the latitude of the Red Spot. I was unaware of the Eötvös-Lambert forces and thought that the object would be resting in neutral equilibrium and should therefore be free to wander at random in latitude.

It was very gratifying to learn of Dr. Sagan's finding that, for the right form of two-phase model, the equator is not the only stable latitude.

R. E. DANIELSON (49). — Is it not possible that the addition of magnetic forces could alter your result, particularly if the bulk of Jupiter is a good electrical conductor?

C. SAGAN (49). — Yes, if the Red Spot is also a good conductor, and the magnetic lines of force are so oriented that drift in latitude is constrained but drift in longitude is permitted, then the observed motions might be explicable on these grounds.

A. DOLLFUS (50). — Au cours des dernières années, j'ai mesuré à l'Observatoire du Pic du Midi, avec un polarimètre à frange de Lyot, la polarisation de la lumière diffusée par l'anneau B de Saturne.

Les mesures donnent des résultats très complexes. Leur analyse montre que l'on peut discriminer dans la polarisation observée deux composantes différentes. Une partie de cette lumière provient de la diffusion directe sur les corpuscules. Cette polarisation reste faible entre les angles de vision 0° et 5° et peut s'interpréter comme provenant d'un dépôt de givre ou de glace, ainsi que l'a proposé le Dr. Kuiper.

Une deuxième composante tantôt radiale et tantôt parallèle à la trajectoire des particules indique nécessairement que les corpuscules qui constituent l'anneau doivent être allongés comme des cigares, éventuellement on pourrait les supposer également striés par de nombreuses incisions parallèles. Il est difficile de discriminer si ces corpuscules sont allongés dans le sens de la trajectoire ou radialement par rapport à la planète. La première position est celle qui résulterait des chocs et frictions internes entre les corpuscules de l'anneau. La deuxième correspond à la position d'équilibre gravitationnel sous l'effet de l'attraction de la planète.

M. S. BOBROV (50). — I suppose that the elongated shape of the particles of Saturn's rings will not change sufficiently the results of the shadow effect theory which is in very good agreement with observations.

F. LINK (52).—Je voudrais bien souligner une certaine parenté entre les périodicités dans la circulation sur Jupiter et celle sur la Terre. C'est sans doute l'activité solaire par l'intermédiaire des radiations corpusculaires ou des rayons X qui contrôle ce genre de phénomènes. En tout cas avant l'introduction de Tiros nous étions assez mal placés pour avoir une vue d'ensemble sur la circulation terrestre en contraste avec Jupiter, où ces résultats peuvent être obtenus sans difficulté.

B. M. PEEK (54). — Considering the rather large standard deviations of your individual years, I am surprised that the probable error of your combined results turns out to be so small. Have you used Schain's actual observations to determine the rotation period for 1951?

H. J. SMITH (54). — Yes.

B. M. PEEK (54). — And your result is exactly what Shain would have obtained, if he had been able to use your computer?

H. J. SMITH (54). — Yes.

M. S. BOBROV (58). — I cannot understand how the shock waves caused in Jupiter's outer atmosphere by solar corpuscular streams may come into it as close as 3 radii of Jupiter. Indeed, for the Earth the respective distance is about 7 Earth radii. In the case of Jupiter we have a weaker energy of solar corpuscular stream and may expect a stronger magnetic field of the planet. Thus, the distance must be sufficiently greater.

M. S. ROBERTS (58). — The radius of the Jovian belt was fixed by the interferometric measures of Jupiter made by the California Institute of Technology group. The magnetosphere is larger; the above radius refers only to the belt, not the entire magnetosphere.

GENERAL CONCLUSIONS

M. MINNAERT
Sterrenwacht « Sonnenborgh », Utrecht, Holland

Among the different branches of astronomy, Planetary Astrophysics during a long time developed rather slowly. In recent years, however, we have watched a real revival of this discipline, which promises to give in a brief delay a wealth of reliable information about celestial bodies, similar to the Earth. This is due to the modern observational techniques, opening new possibilities of investigation ; and also to the stimulus of Space Research, which activated so many parts of Astronomy. To select « The Physics of the Planets » as the subject for our 11th Colloquium was certainly, an excellent choice.

In view of the diversity and abundance of the communications to which we have listened, the customary final résumé may be of some use. We shall try to summarize first the papers of a general character, and then to give a synthetic picture of each of the individual planets. I apologize for many inevitable omissions and even errors, but I hope that this survey will in any case help us to remember some essentials of what we heard in the course of these three days.

Let me then point out in the first place the importance of *international collaboration* for Planetary Physics : Dr. Dollfus told us about the magnificent series of Mars photographs, now collected at Meudon and at the Lowell Observatory ; the cooperation on the Venus clouds is going on ; there have been combined efforts at the moment of a Mercury transit or of a white spot on Saturn. For special purposes standard instruments have been constructed and distributed over different observatories. The precision mapping of Mars is also a cooperative enterprise, in which many observatories are involved.

The theories concerning the *interior of the planets* have plaid a relatively small role in this colloquium. Fortunately we had an

excellent introductory survey of the problems involved. Progress here depends to a great extent on our gradually improving knowledge of the physical constants. It was interesting to notice, how the transfer of heat through a planet, formally treated as a simple problem of conduction, has now proved much more complicate, since the transfer by radiation and the effect of convection currents are found to be of much greater importance.

The *theory of scattering*, applied to planetary atmospheres, is a special field of research, fundamental for the interpretation of many optical observations. We note that progress has been made a. o. in the case of phase functions, sharply peaked in the forward direction, as they are found for haze and clouds. Relatively complicate cases have been treated, as e. g. the transfer of radiation in stratified and in non-grey atmospheres, the case of fluorescence and that of interlocked multiplet lines.

While a more and more perfect theory is thus being developed, allowing to calculate the visible properties of an atmosphere as a function of its composition, it seems that the inverse problem is less hopeful : it will be difficult to derive the vertical structure and elementary properties of an atmosphere from macroscopic optical observations.

Let me also call attention to the theoretical paper on the escape of gases from planetary atmospheres. It was found that in some atmospheres this escape takes place according to the classical theory of Jeans and Spitzer, while in other atmospheres it is limited by the diffusion and becomes a problem of diffusion equilibrium.

Instruments of the most refined design have been applied to the study of the planets. A very useful survey was given of the heat detectors ; note especially the ferro-electric detector $(BaSr)TiO_3$, the modified Golay cell, the cooled Ge bolometer. The electronic camera allows short exposures and measurements over a broad range of brightness, while it has no threshold.

The numerous papers, devoted to *the individual planets*, can perhaps be summarized best by drawing a schematical section of

each of these celestial bodies, and by inserting in this sketch the information, given in the course of the colloquium. We abstain from critical discussions and have only added some question marks, in order to distinguish mere suggestions from direct observational results. In several cases, discrepant opinions have been simply juxtaposed. No attempt has been made to keep the right proportions. A few additional and explanatory notes have been added.

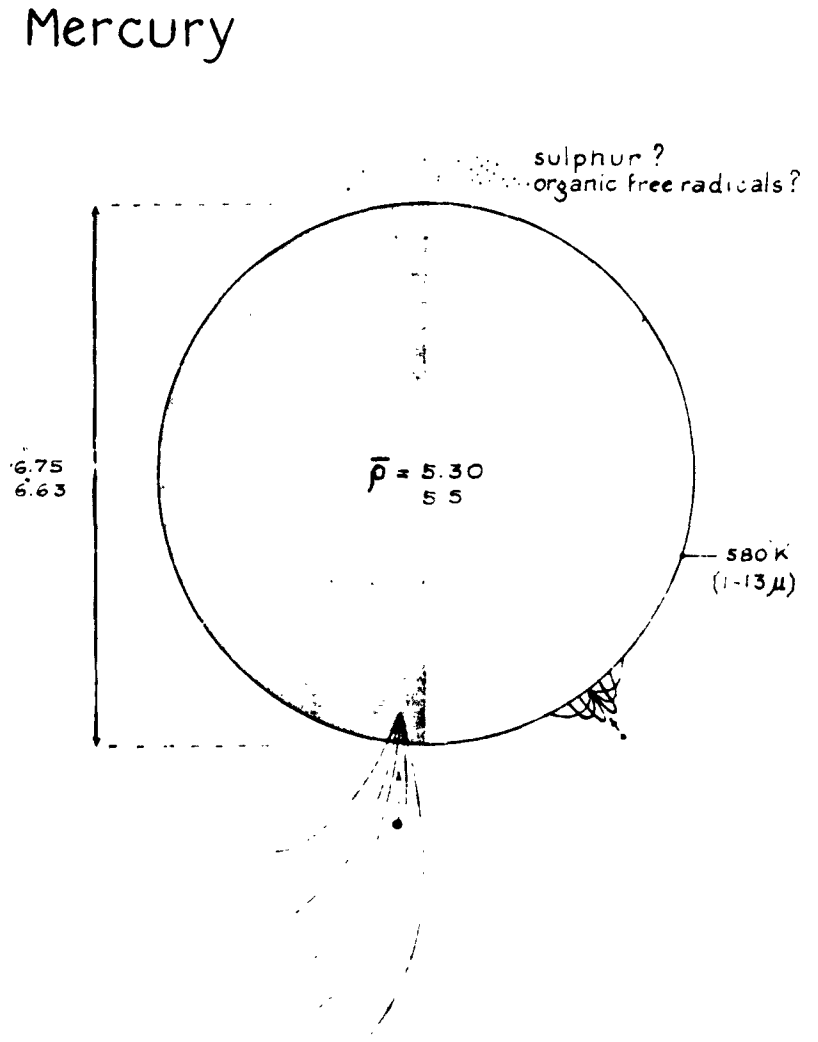

Fig. 1. — Mercury.
Possible erosion by meteoritic bombardment ; formation of a « tail » by radiation pressure (?).

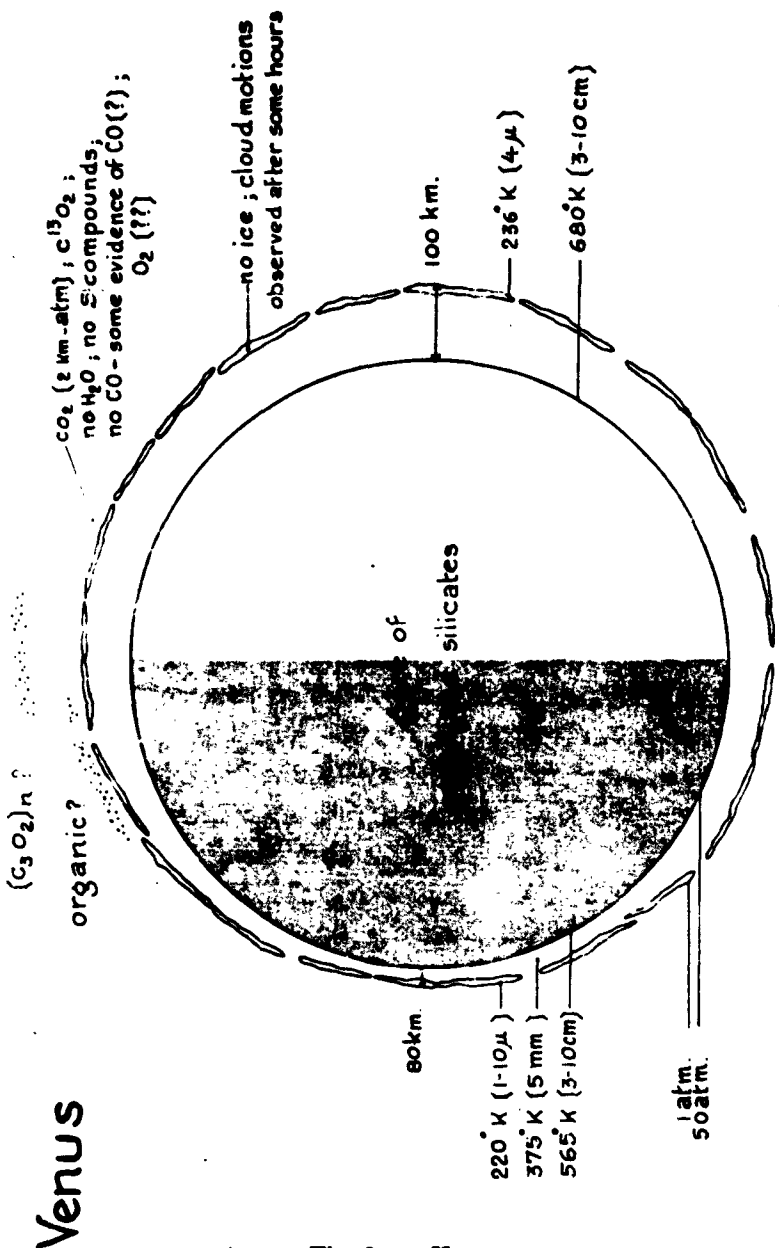

Fig. 2. — Venus

The temperature fluctuation of the surface as a function of phase has now been clearly established (cm waves). It is yet uncertain whether the temperature minimum occurs before or after inferior conjunction. The occurrence of irregular variations in the radiation is dubious. The atmosphere must have a considerable optical depth (water vapour?).
The polarization depends strongly on wavelength.

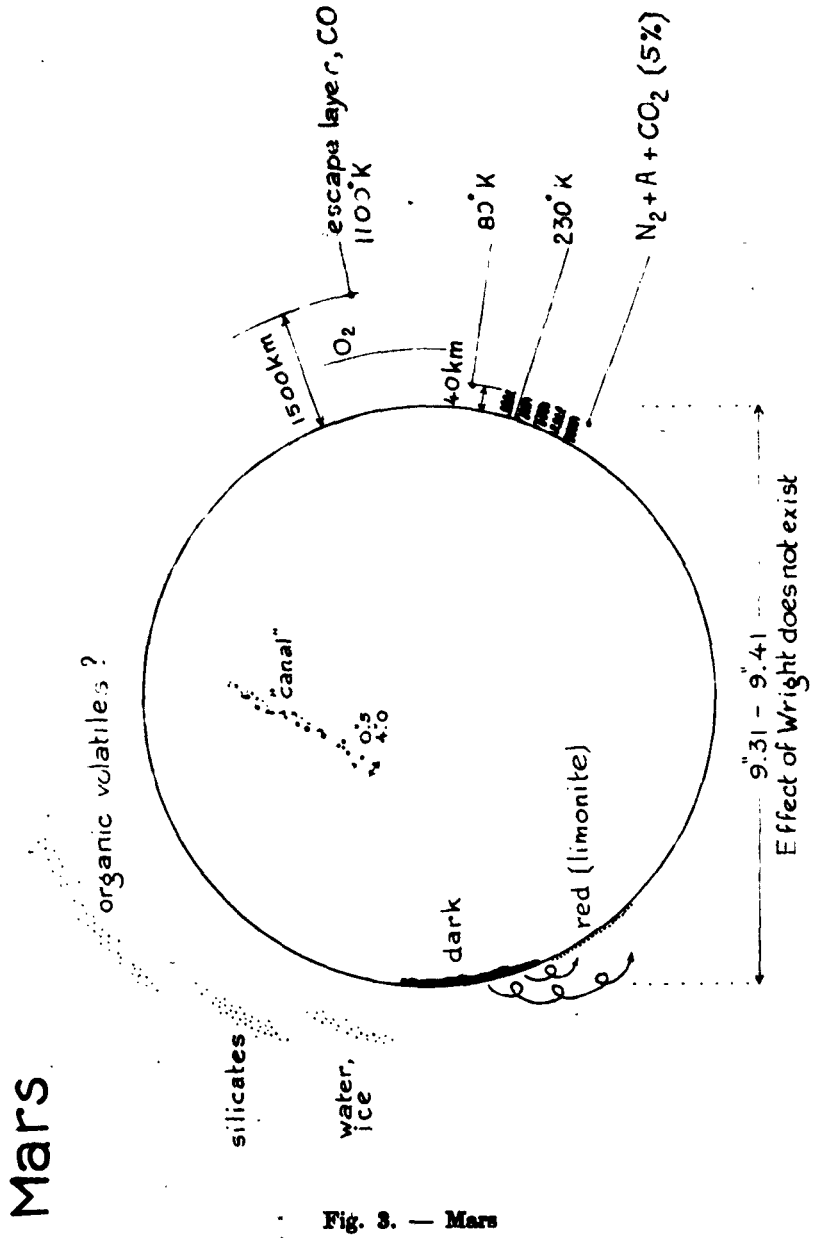

Fig. 3. — Mars

Precision mapping, aiming at 0°1. The coordinates of the poles agree with the poles of the satellite orbits.

A careful spectrophotometric comparison between the radiation of the bright areas with the Sun shows, that their reflectivity increases monotonously with wavelength.

Seasonal effects were studied by photometry and by polarimetry : propagation of darkening waves, alternatively issued from the two poles and propagating with a speed of 35 km per terrestrial day.

Jupiter

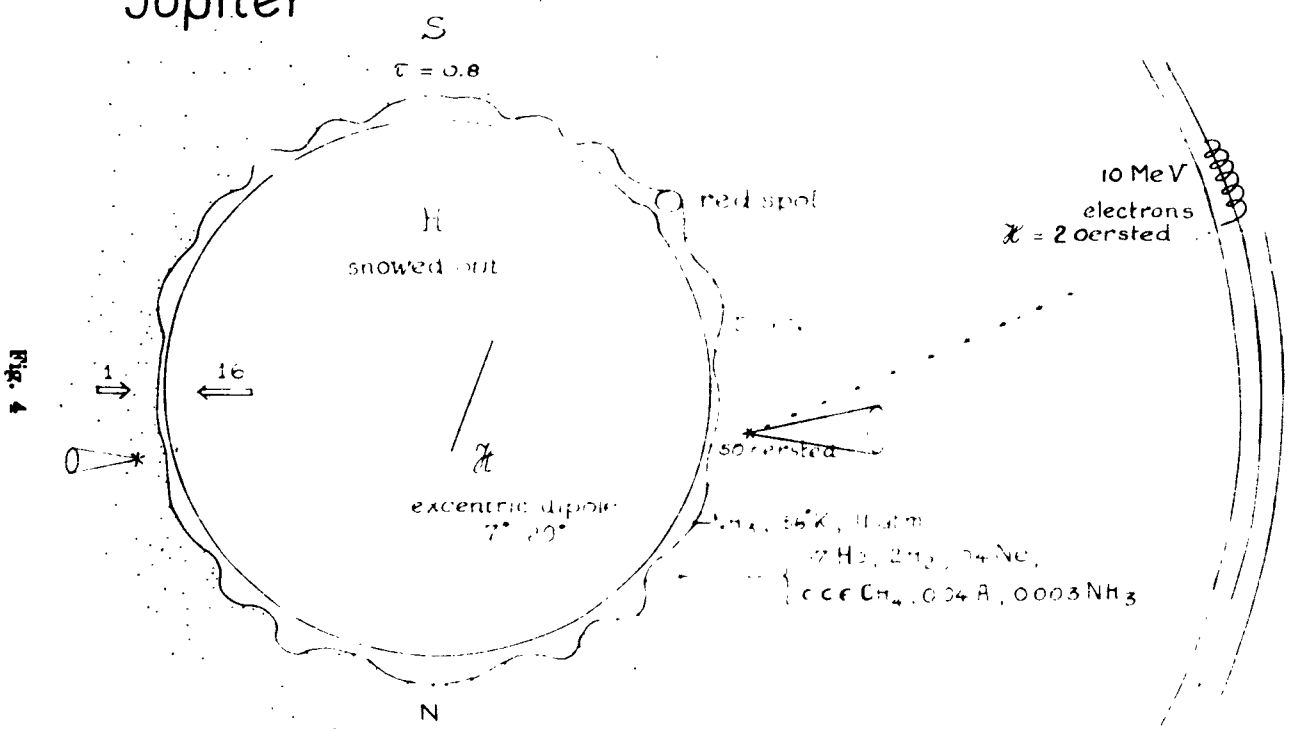

Fig. 4

Fig. 4. — Jupiter

An improved determination of the centre-limb darkening was carried out with the electronic camera. The polarization depends strongly on wavelength.

The activity varies at the same time over the whole planet ; 22 years cycle. Period of 4.5 years in the thickness of the N. equatorial belt.

Radioemission.

Decimeter waves : a) thermal, 130°K ;
b) non thermal, non polarized ;
c) non thermal, polarized, ε equator, positively correlated with solar activity (phase lag = 4^d). Electrons from the solar wind, emitting synchroton radiation in a radiation belt, accelerated by magnetohydr. waves.

Decameter waves (7 MHz — 41 MHz).
Two discrete sources. Period III = $9^h55^m29^s37$ is confirmed. Emission in limited cones. Often right-handed polarization at 24 MHz. No coincidence with Hα activity on the sun. Negative correlation with solar activity.
Electrons, emitting cyclotron radiation in surface magnetic fields.

The hypothesis is put forward, that the same electrons which produce the decimeter waves come down towards the planet and then produce decameter waves.

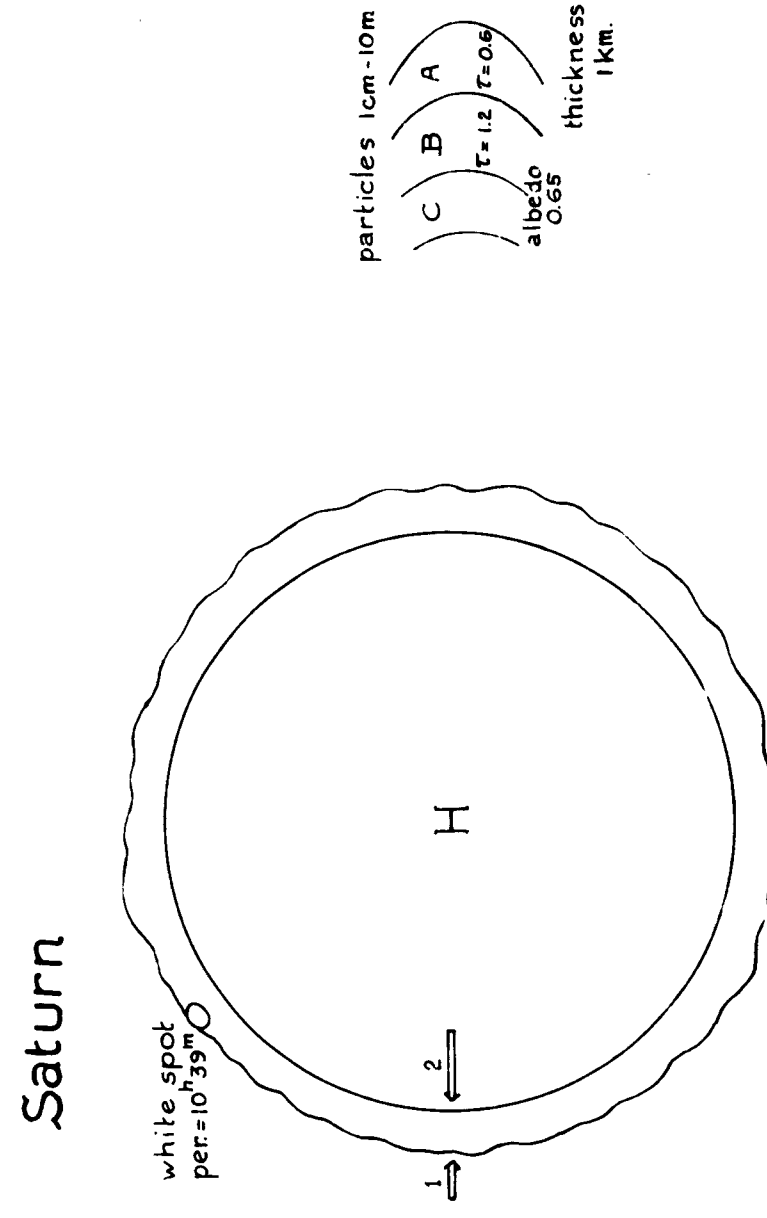

Fig. 5. — Saturn.

The Doppler effect shows, that the rotation of the H_2 layer is normal, while the CH_4 layer rotates quicker.

Determination of the centre-limb darkening and of the photometric profile of the rings with the electronic camera. Improved photometric theory of the rings.

Emission of internal heat, 1.6 times as strong as the incident solar radiation.

Uranus, Neptune

The internal composition is ambiguous ; mainly He, with H and « mud ».

Some interesting spectral features in the Uranus spectrum have not yet been identified.

Emission of internal heat, twice as strong as the incident solar radiation.

Projects

Photo-electric colorimetry of the planets and the moon is undertaken both by the Mt. Wilson and by the Harvard observatories. Differences in the continuum have already been found.

The Princeton University intends to use the 90 cm telescope of Stratoscope II, at an altitude of 24 km, for photography and infrared spectroscopy of the planets ; a resolving power of 0".1 is expected, image stabilization will be better than 1".30.

The Stanford University intends to send a probe near one of the planets, in order to investigate the non-thermal noise, originating in the outer atmospheres under the influence of magnetic fields.

The Berkeley University intends to observe Mars around opposition by means of a rocket with an UV spectrograph and to look for water vapour, organic molecules and minor constituents.

For investigation by means of rockets the following spectroscopic problems are recommended :

resonance lines of H and He ;

molecular lines of CH_3, NH_2 and especially CH_2 at high resolution ;

microwave spectra as a function of altitude ; either resonance lines, or non-resonant absorption, originating under high pressure.

This review of suggestions and projects for the future concludes our résumé.

It is most interesting to see, how astronomers started by using the methods, so successfully applied in stellar astrophysics, and how they gradually extended them to the planets. Characteristic features, however, of planetary studies are the methods of topography, of photometry, and the investigation of the solid body, which had to be especially developed.

From the numerous papers, presented at this colloquium, we may conclude that great progress has been achieved, though our knowledge is still very incomplete. Let us set to work !

We cannot conclude our colloquium without expressing our most cordial thanks to Professor Swings and his collaborators for the organization of this most interesting meeting. This refers as well to the truly scientific spirit with which they have selected the subject, as to the perfect organization, in which Mrs. Boumaz-Crespin certainly had a great part. We also feel grateful to the city and the University of Liège, which provided a delightful setting. And we express the hope that these colloquia will go on for many years, contributing to the progress of astrophysics by giving to the participants a rich, up to date information and new inspiration for future work.

IMPRIMERIE GEORGE MICHIELS, S. A., 6 RUE DE LA PAIX, LIÈGE

PRINTED IN BELGIUM